



A11106 262723

83-2742 (R)

REFERENCE

NIST
PUBLICATIONS

Photonuclear Data - Abstract Sheets 1955 - 1982 Volume IX (Nickel - Gallium)

U.S. DEPARTMENT OF COMMERCE
National Bureau of Standards
National Measurement Laboratory
Center for Radiation Research
Gaithersburg, MD 20899

August 1985



U.S. DEPARTMENT OF COMMERCE
NATIONAL BUREAU OF STANDARDS

QC
100
456
83-2742
1985

NBSIR 83-2742

PHOTONUCLEAR DATA - ABSTRACT SHEETS
1955 - 1982
VOLUME IX (NICKEL - GALLIUM)

E. G. Fuller, Henry Gerstenberg

U.S. DEPARTMENT OF COMMERCE
National Bureau of Standards
National Measurement Laboratory
Center for Radiation Research
Gaithersburg, MD 20899

August 1985

U.S. DEPARTMENT OF COMMERCE, Malcolm Baldrige, *Secretary*
NATIONAL BUREAU OF STANDARDS, Ernest Ambler, *Director*

TABLE OF CONTENTS

Table of Contents	i
Introduction.	1
Nickel (Natural).	3
Nickel (A=58)	61
Nickel (A=60)	115
Nickel (A=61)	177
Nickel (A=62)	183
Nickel (A=64)	205
Copper (Natural).	215
Copper (A=59)	325
Copper (A=60)	329
Copper (A=61)	333
Copper (A=63)	337
Copper (A=65)	401
Zinc (Natural).	435
Zinc (A=64)	461
Zinc (A=66)	507
Zinc (A=67)	531
Zinc (A=68)	535
Zinc (A=70)	551
Gallium (Natural)	555
Gallium (A=66).	563
Gallium (A=69).	567
Gallium (A=71).	577
Definitions of Abbreviations and Symbols.	585

Photonuclear Data-Abstract Sheets 1955-1982

I. Introduction

As used in connection with this collection of data-abstract sheets, the term photonuclear data is taken to mean any data leading to information on the electromagnetic matrix element between the ground state and excited states of a given nuclide. The most common types of reactions included in this compilation are: (e, e') , (γ, γ) , (γ, γ') , (γ, n) , (γ, p) , etc. as well as ground-state particle capture reactions, e.g. (α, γ_0) . Two reactions which fit the matrix element criterion are not included in the compilation because of their rather special nature. These are heavy particle Coulomb excitation and the thermal neutron capture reaction (n, γ_0) . While the energy region of particular interest extends from 0 to 150 MeV, papers are indexed which report measurements in the region from 150 MeV to 4 GeV. Most of the experiments listed are concerned with the excitation energy range from 8 to 30 MeV, the region of the photonuclear giant resonance.

The hierarchical grouping of the photonuclear data-abstract sheets within the file is by: 1. Target Element, 2. Target Isotope, and 3. by the Bibliographic Reference Code assigned to the paper from which the data on the sheet were abstracted. In this file, colored pages are used to mark the beginning and end of the sheets for each chemical element. A brief historical sketch of the element is given on the divider sheet marking the start of each section; the information for this sketch was derived from references such as the Encyclopaedia Britannica. In those cases where the sheets for a given element make up a major part of a volume, colored pages are also used to delineate sections pertaining to the individual isotopes of the element. Each of the sections of the file, as delineated by two colored divider sheets, represents a 27 year history of the study of electromagnetic interactions in either a specific nuclide or a specific element.

The data-abstract sheets are filed under the element and/or isotope in which the ground-state electromagnetic transition takes place. For example, the abstract sheet for a total neutron yield measurement for a naturally occurring copper sample would appear in the elemental section of the copper file. On the other hand, a measurement of the ^{62}Cu 9.73 minute positron activity produced in the same sample by photons with energies below the three-neutron separation energy for ^{65}Cu (28.68 MeV) would be filed with the sheets for ^{63}Cu . Similarly a measurement of the ground-state neutron capture cross section in ^{12}C would be filed under ^{13}C while the corresponding ground-state alpha-particle capture cross section would be filed under ^{16}O .

At the end of this volume there is a master list of the abbreviations that have been used in the index section of the abstract sheets. The listings are those used in the final published index, Photonuclear Data Index, 1973-1981, NBSIR 82-2543, issued in August 1982 by the U. S. Department of Commerce, National Bureau of Standards, Washington, DC 20234. In some cases two notations are entered for the same quantity. The second entry is the abbreviation that was used in one or more of the earlier published editions of the index.

NICKEL

Z=28

An alloy of nickel called packfong was used by the Chinese long before the metal was known in Europe. A heavy, reddish brown ore, often found covered with green spots or stains, was used in Germany to color glass green; the miners called the substance Kupfernickel meaning copper demon. The ore resembled copper in color but yielded a brittle unfamiliar product that caused the copper miners considerable trouble.

Axel Fredrik Cronstedt was the first to discover nickel; he worked as a metallurgist in the Swedish Bureau of Mines. In 1751 Cronstedt was investigating a new mineral from the cobalt mines and placed a piece of iron in an acid solution of the ore expecting to see a copper deposit on it. To his great surprise, he was unable to secure a deposit of any kind—the ore nicolite contained no copper. Further work yielded the metal. After studying the physical, chemical and magnetic properties of the metal, he announced in the Memoirs of the Stockholm Academy that he had discovered a new metal.

Method Li(p,γ) source; nuclear emulsions; G-M counter; Cu⁶³(γ,n) reaction;
flux calibration

Ref. No.	EGF
55 D ₈ 1	

Reaction	E or ΔE	E ₀	Γ	∫σ dE	Jπ	Notes
Ni (γ,p)	17.6					<p>Monitor in terms of counts on G-M counter which had been calibrated in terms of Cu⁶³(γ,n)Cu⁶² (absolute counting and effective σ Li = 7.75 X 10⁻²⁶ ± 15% cm² given by Shimizu; Mem of Un. Kyoto <u>25</u>, 194 (1949))</p> <p>Plates used to detect protons Li σ = 8±4 X 10⁻²⁶ cm²</p>

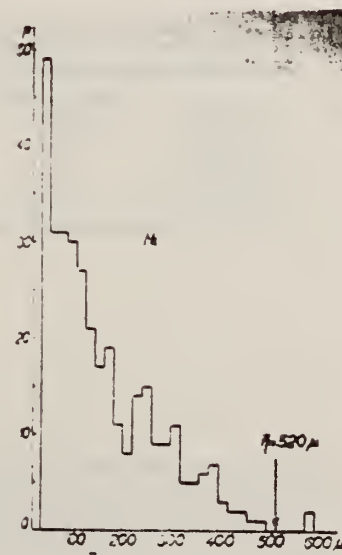


FIG. 2.

ELEM. SYM.	A	Z
Ni		28
REF. NO.		
55 Jo 1		NVB

METHOD

Synchrotron; ZnS counter; ion chamber

REACTION	RESULT	EXCITATION ENERGY	SOURCE		DETECTOR		ANGLE
			TYPE	RANGE	TYPE	RANGE	
G,P	RLY	THR - 65	C 65		SCI-D	14 - +	DST

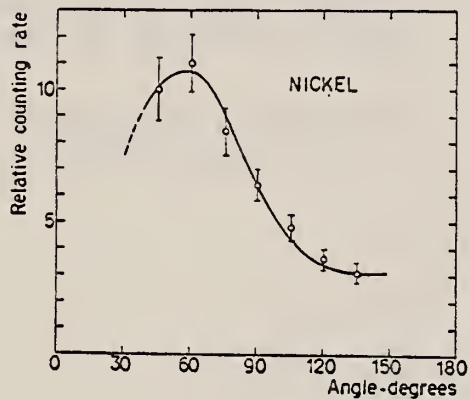


Fig. 5. The angular distributions of protons with an energy above 14 Mev.

TABLE I. Target thickness and the constants a and b in the angular distribution curve $a + (\sin\theta + b \sin\theta \cos\theta)^2$.

Element	Target thickness mg/cm ²	a	b
Carbon	182	0.32	0.80
Aluminum	274	0.58	1.35
Nickel	352	0.94	1.45
Molybdenum	295	0.62	2.00

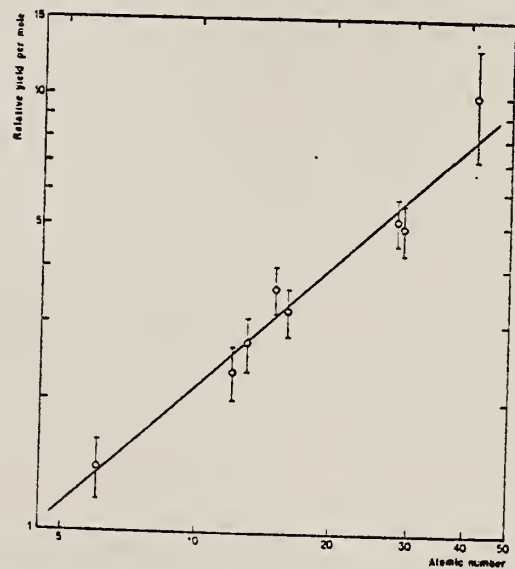


Fig. 10. The relative yield per mole for protons above 14 Mev as a function of the atomic number.

Method
Betatron; photon scattering; NaI spectrometer

Ref. No.
56 Fu 1
NVB

Reaction	E or ΔE	E_0	Γ	$\int \sigma dE$	$J\pi$	Notes
Ni(γ, γ)	Bremss. 4-40					<p>Detector at 120°.</p> <p>Cross sections given here are 13% too high due to erroneous $\cos \beta$ factor in denominator of Eq. 5. [See footnote 8 in Phys. Rev. <u>106</u>, 993 (1957)].</p>

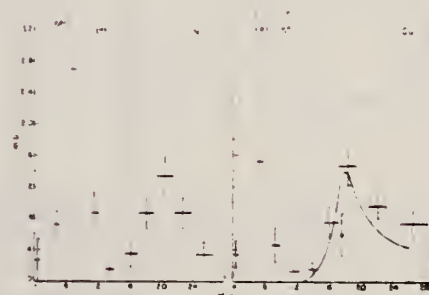


FIG. 5. The elastic scattering cross sections for Ni and Cu. The point at 17.6 Mev is that of Stearns.⁴ The solid curve superimposed on the Cu data is the scattering cross section calculated from the dispersion relation by substituting for $\sigma_e(E)$ in Eq. (7) the γ, n cross section multiplied by the ratio of the total particle yield to the neutron yield.⁴ The open circles on the vertical axis indicate the magnitude of the Thomson cross section for Z free protons scattering coherently.

Elem. Sym.	A	Z
Ni		28

Method	Ref. No.	
Li (p, γ) source, 480 kev protons.	56 Ha 1	EGF

Reaction	E or ΔE	E_0	Γ	$\int \sigma dE$	$J\pi$	Notes
(γ, xn)	14.8 17.6	6-17.6				Average Li cross section is <u>28</u> mb; cross section with detector response weighted for low energy neutrons, <u>25</u> mb. Assumed ratio 17.6/14.8 = 1.7. Calculated cross section at 14.8 and 17.6 MeV assuming cross section curves measured at Pennsylvania and Saskatchewan (refer Table I).

TABLE I. Cross sections for photoneutron emission induced by the lithium gamma rays. The results are compared with previous data.

Element	Present cross-section data		Data of McDaniel <i>et al.</i> ^a	Betatron data					
				Pennsylvania		Saskatchewan		$\sigma_{14.8}^b$	$\sigma_{17.6}^b$
	Counter Group A	Counter Group B		$\sigma_{14.8}^c$	$\sigma_{17.6}^c$	$\sigma_{14.8}^d$	$\sigma_{17.6}^d$		
⁵⁵ Fe	38 mb	33 mb	37 mb			60 ^f mb	0.5	23 mb	47 mb
⁵⁷ Co	49	49	47	60 ^e mb	0.5	95 ^f	0.5	30	60
⁵⁸ Ni	28	25	23			40 ^e	0.7	22	32
⁶³ Cu	64	61	55±12			95 ^f	0.6	45	75
⁶⁵ Zn	48	45	48			90 ^f	0.7	32	51
¹⁰⁷ Ag	175	170	135			240 ^f	1.0	175	177
¹¹⁶ Sn	200	190	180						
¹⁸¹ Ta	355	360	260	350 ^d	1.3	420 ^e	2.3	420 ^d	320 ^d
¹⁸⁷ W	365	355	325					550 ^d	240 ^d
¹⁹⁷ Au	330	295		315 ^e	1.7	480 ^f	1.9	460	255
²⁰⁰ Hg	365	340	290						
²⁰⁸ Pb	310	295	250	320 ^e	1.6	440 ^f	2.5	400 ^d	250 ^d
²⁰⁹ Bi	305	280	250	270 ^d	2.6	550 ^f	2.4	500 ^d	260 ^d

^a See reference 3.

^b Average of 14.8- and 17.6-Mev cross sections weighted with relative intensities of the lithium gamma-ray lines.

^c See reference 24.

^d R. Nathans, Ph.D. thesis, University of Pennsylvania, 1954 (unpublished).

^e J. Halpern (private communication).

^f See reference 23.

^g See reference 32.

^h Separate cross sections at 14.8 and 17.6 Mev as obtained from Group A data and 14.8/17.6 betatron cross-section ratios.

ⁱ Obtained using 14.8/17.6 cross-section ratio from Pennsylvania betatron data.

^j Obtained using 14.8/17.6 cross-section ratio from Saskatchewan betatron data.

Method 30.5 MeV Bremss. synchrotron; emulsions; ion chamber monitor

Ref. No.	
56 Le 1	EGF

Reaction	E or ΔE	E_0	Γ	$\int \sigma dE$	$J\pi$	Notes
(γ, p)	Bremss.					Assuming shape for $\sigma(\gamma, p)$ [Halpern and Mann, Phys. Rev. <u>83</u> , 370 (1951)] gives peak $\sigma(\gamma, p) = 9.0 \times 10^{-26} \text{ cm}^2 \pm 30\%$. At $E_\gamma = 25.5 \text{ MeV}$ ratio of proton yields Ni/Cu = $1.76 \pm 10\%$.
	21.5					
	25.5					
	28.0					
	24.0					

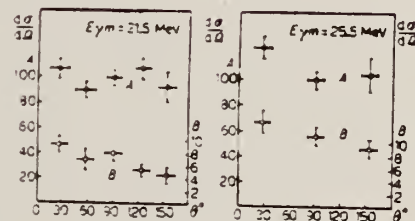


Figure 7: Angular distribution of photoprotons from nickel. $d\sigma/d\Omega$ relative cross section: A, for $e_p \geq 3 \text{ MeV}$ protons; B, for $e_p \geq 10 \text{ MeV}$ protons. The cross section for the angle $\theta = 90^\circ$ is taken equal 100.

REF. E. B. Bazhanov, Iu. M. Volkov, A. P. Komar, L. A. Kul'chitskii
and V. P. Chizhov
Dokl. Akad. Nauk SSSR 113, 65 (1957)
Soviet Phys. Dokl. 2, 107 (1957)

ELEM. SYM.	A	Z
Ni		28
REF. NO.		
57 Ba 2		EGF

METHOD

REACTION	RESULT	EXCITATION ENERGY	SOURCE		DETECTOR		ANGLE
			TYPE	RANGE	TYPE	RANGE	
G, XP	SPC	THR - 85	C	85	TEL-D	15-60	DST

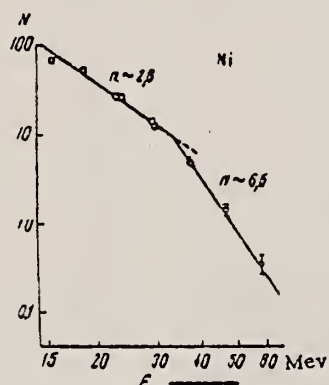


Fig. 1. Energy distribution of photoprotons from Ni. The vertical axis gives the number of protons in a 1 Mev interval per monitor unit, plotted in arbitrary units. Only the statistical errors are indicated.

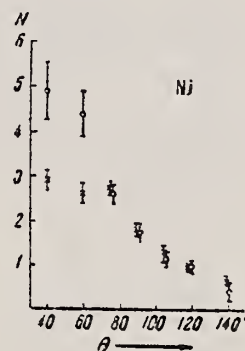


Fig. 3. Angular distributions of photoprotons from Ni. The crosses represent 20-33 Mev protons; the open circles represent 33-65 Mev protons. The errors are statistical.

REF.

F. Bobard, G. Boulegue, and P. Chanson
Compt. Rend. 244, 1761 (1957)

ELEM. SYM. A Z

Ni

23

METHOD

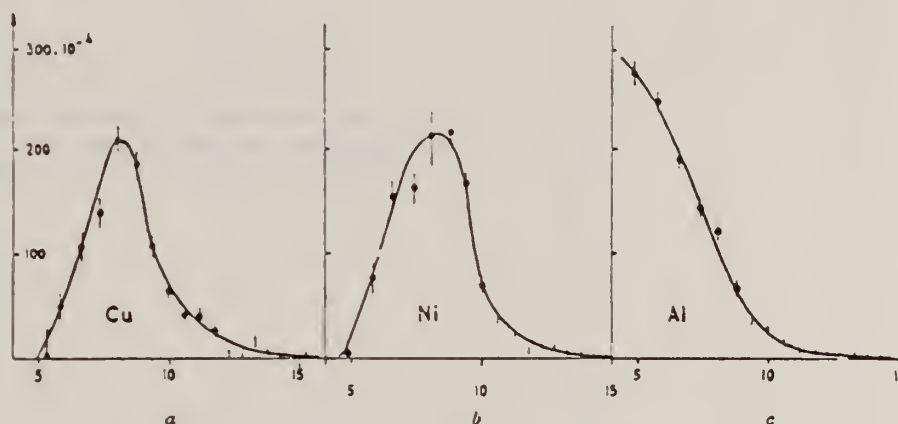
REF. NO.

57 Bo 1

EGF

REACTION	RESULT	EXCITATION ENERGY	SOURCE		DETECTOR		ANGLE
			TYPE	RANGE	TYPE	RANGE	
G,A	SPC	THR - 30	C	31	EMU-D	5-15	DST

Yield per milligram per roentgen Cu 0.86, Ni 0.99, Al 1.15 for 30.5 MeV bremsstrahlung.

Fig. 2. — Nombre de particules α /mg/stéradian/Röntgen/intervalle de 1 MeV.

Method 17.5 MeV Bremss.; proton yield; angular distribution; emulsion

Ref. No.	EGF
57 Sp 1	

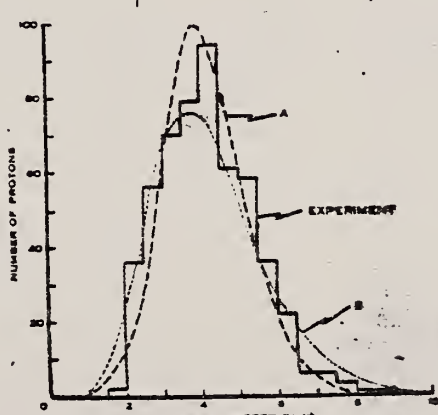
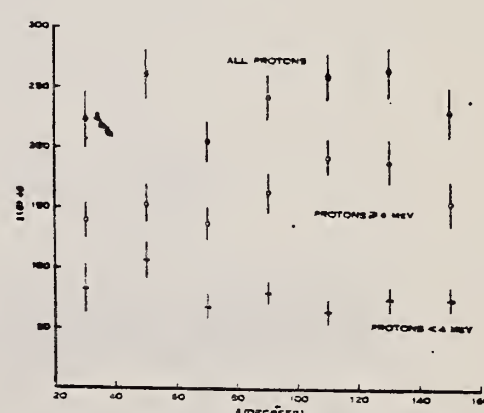
Reaction	E or ΔE	E_0	Γ	$\int \sigma dE$	$J\pi$	Notes
Ni(γ, p)	Bremss. 17.5					<p>In Figure 1:</p> <p>----- Coulomb barrier = 6.9 MeV and residual level density $\sim e(6E^{1/2})$; corresponds to mean temperature of 0.9 MeV.</p> <p>..... Barrier = 5.6 MeV; level density $\sim e^{1.04E}$; same as θ as above.</p>
<div style="display: flex; justify-content: space-around;">   </div>						

Fig. 1.—Energy distribution of photoprotons ejected from nickel by 17.5 MeV bremsstrahlung.

Fig. 2.—Angular distribution of photoprotons from nickel.

E. B. Bazhanov, Iu. M. Volkov, and L. A. Kul'Chitskii
 J. Exptl. Theoret. Phys. (USSR) 35, 322 (1958)
 Soviet Phys. JETP 35, 224 (1958)

Ni

28

METHOD

REF. NO.

58 Ba 6

EGF

REACTION	RESULT	EXCITATION ENERGY	SOURCE		DETECTOR		ANGLE
			TYPE	RANGE	TYPE	RANGE	
G,XP	SPC	THR - 85	C	85	TEL-D	13 - 40	DST

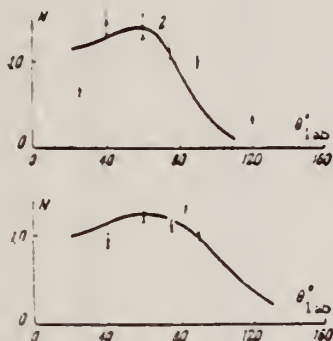


FIG. 4. Angular distributions of photoprotons from Ni. The solid curves give the results of calculation. Only statistical errors are shown. 1) $E_p = 13.7-21.5$; 2) $E_p = 21.5-33.3$ Mev.

Method	Betatron; alpha yield; nuclear emulsion	Ref. No. 58 To 2	NVB
--------	---	---------------------	-----

Reaction	E or ΔE	E_0	Γ	$\int \sigma dE$	$J\pi$	Notes
Ni(γ, α)	Bremss. 22					Yield = 3.9×10^4 alpha/mole/roentgen

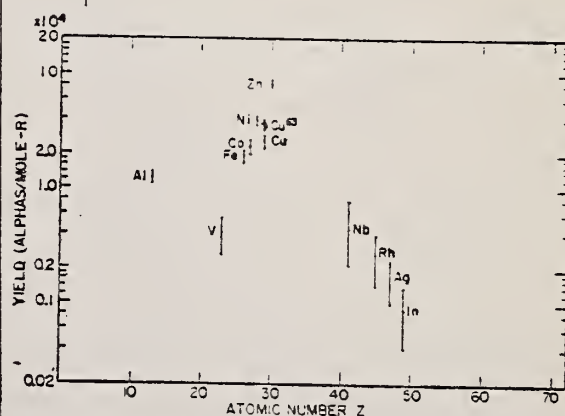


FIG. 8. Photo-alpha yields plotted against atomic numbers for the exposures of the survey.

Ref. V.P. Chizhov
Zhur. Eksp. i Teoret. Fiz. 38, 809 (1960)
Soviet Phys. JETP 11, 587 (1960)

Elem. Sym.	A	Z
Ni		28

Method 90 MeV Bremsstrahlung; scintillator counter telescope

Ref. No.	JHH
60 Ch 1	

Reaction	E or ΔE	E_0	Γ^-	$\int \sigma dE$	$J\pi$	Notes
Ni (γ, p)						Energy Range of particles detected: E_d - 15.5-30 MeV E_p - 15.5-30 MeV E_t - 17-30 MeV Ratios: $\sigma(\gamma, d)/\sigma(\gamma, p)$ } at $\theta = 90^\circ$ $\sigma(\gamma, t)/\sigma(\gamma, d)$
Ni (γ, d)						
Ni (γ, t)						

FIG. 1. Ratio of $\sigma(\gamma, d)$ to $\sigma(\gamma, p)$ cross sections for various elements of energies 15.5-30 MeV at $\theta = 90^\circ$. The solid curve shows the calculated ratio by the G.M. multiplicity model.



TABLE I

Element	$100\sigma_{\gamma, p}$	Element	$100\sigma_{\gamma, p}$	Element	$100\sigma_{\gamma, p}$	Element	$100\sigma_{\gamma, p}$
Li	30 ± 4	Si	10 ± 4	Sn	10 ± 4	In	10 ± 4
B	10 ± 4	Ni	10 ± 4	Pb	10 ± 4	Ta	10 ± 4
C	10 ± 4	Fe	10 ± 4	U	10 ± 4	Au	10 ± 4

Ref. K. Reibel, A.K. Mann
Phys. Rev. 118, 701 (1960)

Elem. Sym.	A	Z
Ni		28

Method γ 's from $F^{19}(p,\gamma)$ reaction; protons from Vande Graaff; Na I.

Ref. No.	JHH
60 Re 1	

Reaction	E or ΔE	E_0	Γ	$\int \sigma dE$	$J\pi$	Notes
(γ, γ)	$E_\gamma \sim 7$					$\langle \bar{\sigma} \rangle (E_p = 2.05 \text{ MeV}) = 0.20 \pm 0.02 \text{ mb}$

METHOD

Betatron; fast neutron yield, angular distribution; Si threshold detector; ion chamber

REF. NO.

61 Ba 2

NVE

REACTION	RESULT	EXCITATION ENERGY	SOURCE		DETECTOR		ANGLE
			TYPE	RANGE	TYPE	RANGE	
G,XN	ABY	THR-22	C	22	THR-I	5--	DST

In Table 4:

$\bar{\sigma}$ = average cross section of detector
weighted with neutron spectrum

\bar{n} = neutrons/100 roentgen/mole

$$W(\theta) = a_0 \sum_{n=1}^{\infty} (1 + A_n P_n(\cos \theta))$$

TABLE IV

I Element	II a_0	III a_1	IV a_2	V $(\bar{\sigma}\Phi) \times 10^{10}$	VI $\Phi_{\text{total}} (22 \text{ MeV}) \times 10^9$	VII $\Phi_{\text{fast}} / \Phi_{\text{total}}$
Vanadium	245 (1±0.06)	0.01±0.08	-0.09±0.10	6.05	0.21	0.12
Chromium	164 (1±0.03)	0.04±0.04	-0.05±0.05	4.05	0.17	0.10
Manganese	308 (1±0.02)	0.07±0.03	-0.09±0.04	7.61	0.25	0.12
Iron	200 (1±0.03)	0.05±0.04	-0.17±0.05	4.91	0.18	0.11
Cobalt	390 (1±0.02)	0.08±0.03	-0.22±0.04	9.63	0.26	0.15
Nickel	145 (1±0.05)	0.07±0.07	-0.23±0.06	3.52	0.12	0.12
Copper	347 (1±0.02)	0.05±0.03	-0.29±0.06	8.57	0.30	0.12
Arsenic	432 (1±0.03)	0.11±0.04	-0.24±0.05	11.91	0.33	0.15
Rubidium	638 (1±0.05)	0.13±0.06	-0.14±0.08	15.75		
Strontium	409 (1±0.03)	0.10±0.06	-0.17±0.05	10.10		
Yttrium	290 (1±0.10)	0.08±0.12	-0.12±0.15	7.10		
Silver	590 (1±0.04)	0.10±0.06	-0.22±0.08	14.57	0.87	0.07
Cadmium	905 (1±0.02)	0.02±0.02	-0.26±0.03	22.35		
Iodine	1133 (1±0.03)	0.04±0.04	-0.29±0.05	27.99	1.42	0.08
Barium	1048 (1±0.04)	0.10±0.06	-0.38±0.08	25.89		
Lanthanum	1595 (1±0.02)	0.02±0.03	-0.42±0.04	39.40	1.04	0.15
Cerium	1310 (1±0.05)	0.05±0.06	-0.39±0.08	32.50		
Dysprosium	1652 (1±0.03)	0.04±0.10	-0.34±0.13	40.80		
Tantalum	1558 (1±0.02)	0.04±0.03	-0.22±0.04	38.48	2.50	0.06
Tungsten	1365 (1±0.02)	-0.07±0.03	-0.24±0.04	33.71		
Mercury	1345 (1±0.02)	0.04±0.03	-0.31±0.04	33.22		
Lead	2274 (1±0.01)	0.02±0.02	-0.42±0.03	56.17	2.72	0.08
Bismuth	2162 (1±0.02)	0.05±0.03	-0.45±0.04	53.40	3.36	0.06
Thorium	3031 (1±0.04)	0.06±0.05	-0.32±0.07	74.87		
Uranium	4630 (1±0.02)	0.05±0.03	-0.17±0.04	114.36		

$(\bar{\sigma}\Phi) = 2.47 \times 10^9$ e.m.u./roentgen. Errors are standard errors due to counting statistics only.

REF.

M. Masuda

J. Phys. Soc. 16, 1801 (1961)

ELEM. SIM. A

Ni

28

METHOD

REF. NO.

Betatron; proton angular distribution; ZnS scintillator

61 Ma 2

REACTION	RESULT	EXCITATION ENERGY	SOURCE		DETECTOR		ANGLE
			TYPE	RANGE	TYPE	RANGE	
G,XP	RØX	8 - 21	C	18,21	SCI-I	1 - 10	DST

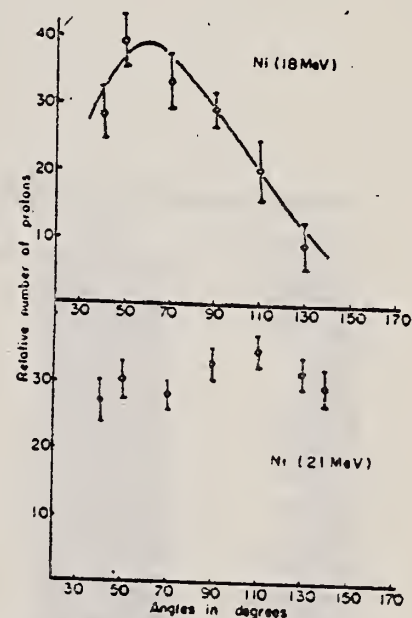


Fig. 7. Angular distribution of photo-protons from nickel. The results of the least square to fit the experimental plots with 18 MeV bremsstrahlung are described with the form,
 $1 + 6.0 \sin^2 \theta (1 + 0.87 \cos \theta)^2$.

REF. J. Miller, C. Schuhl, C. Izara
J. Phys. Radium 22, 529 (1961)

ELEM. SYM.	A	Z
Ni		28

METHOD Positron annihilation; total photonuclear cross section;
NAI, BF₃

REF. NO.	
61 Mi 1	NVB

REACTION	RESULT	EXCITATION ENERGY	SOURCE		DETECTOR		ANGLE
			TYPE	RANGE	TYPE	RANGE	
G.G	ABX	8-15	D	8-15	NAI-I	8-15	DST

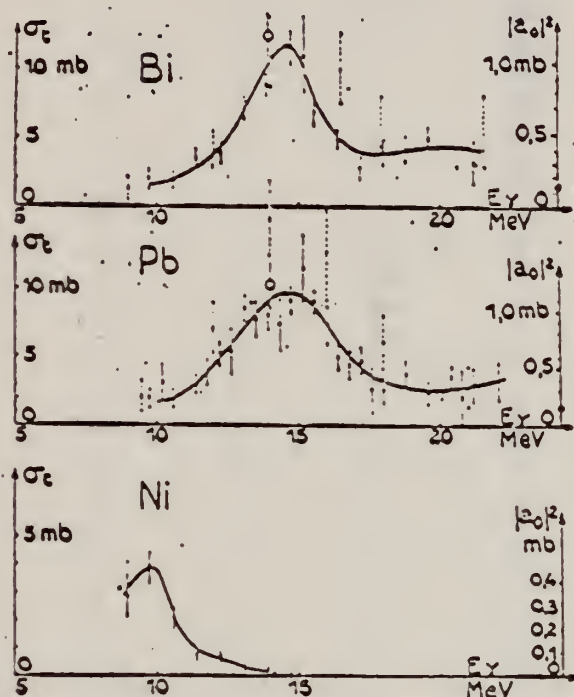


FIG. 8. — Section efficace totale de diffusion élastique et module au carré de l'amplitude de diffusion vers l'avant. Cas de Ni, Pb et Bi.

Cercles vides : module au carré des amplitudes de diffusion absorptive calculées à partir des sections efficaces $\sigma(\gamma, n) + 2\sigma(\gamma, 2n) + \sigma(\gamma, np) + \dots$ (seule la première réaction intervient vers 14 MeV).

Cercles pleins : limites $(Ze^2/Mc^2)^2$ de la section efficace de diffusion à haute énergie. En réalité, à cause des interactions mésoniques des nucléons et de l'incertitude sur la limite à haute énergie de la diffusion, il vaudrait mieux parler de la section efficace de diffusion vers l'avant au delà de la résonance géante et avant le seuil photomésonique ; on peut montrer que l'expression

$$(Ze^2/Mc^2)^2 (1 + 0.8x)^2$$

où x est la fraction de force d'échange entre nucléons, est mieux appropriée.

En pointillés : résultats de Fuller et Hayward.

Method 25 MeV betatron; photon scattering; NaI(Tl) spectrometer;
ion chamber.

Ref. No.	
61 To 1	NVB

Reaction	E or ΔE	E_0	Γ	$\int \sigma dE$	$J\pi$	Notes
$^{60}\text{Ni}(\gamma, \gamma)$	Bremss. 5-12	9.8				Detector at 120° Table II from J. Phys. Soc. Japan <u>18</u> , 17-22 (1963)

Table II. The summary of the cross sections and the threshold energies.

Element	E_{\max} (MeV)	$E_{th}(\gamma, p)$ (MeV)	$E_{th}(\gamma, n)$ (MeV)	$\frac{\sigma(\gamma, \gamma)}{\sigma_{po}(\gamma, \gamma)}$	$\frac{\sigma(\gamma, p)}{\sigma_{po}(\gamma, p)}$	$\frac{\sigma(\gamma, n)}{\sigma_{po}(\gamma, n)}$
Al	8.3	8.27	13.07	0.04	0.02	
S	8.5	8.8	15.07	0.02	0.06	
Si	12.0	11.59	17.18	0.12	0.05	
K	7.0	6.39	13.09	0.04	0.07	
Ca	8.0	8.34	15.73	0.05	0.07	
Ni58		7.91	11.93			
60	9.8	9.53	11.39	0.09	0.15	
Cu63		6.12	10.83			
65	7.5	7.46	9.92	0.07	0.11	
Cd	7.5	~9.5	~9.3	0.18		0.50
Sn	7.5	~9.8	~9.2	0.75		0.63
Pb	7.2	~7.5	~7.5	1.00		1.00
Bi	8.0	3.7	7.4	1.00		1.00

Table II. The correction of the energy scale.

Energy in Ref. 1 Should be read

4.0 MeV	3.3 MeV
6.0	5.5
8.0	7.7
10.0	9.9
12.0	12.1
14.0	11.3

References

- 1) E. G. Fuller and E. Hayward: Phys. Rev. **101** (1956) 692.
- 2) see E. Segre: *Experimental Nuclear Physics*, vol. 1, p. 346.
- 3) J. S. Levin and D. I. Hughes: Phys. Rev. **101** (1956) 1328.
- 4) K. Reibel and A. K. Mann: Phys. Rev. **113** (1960) 701.

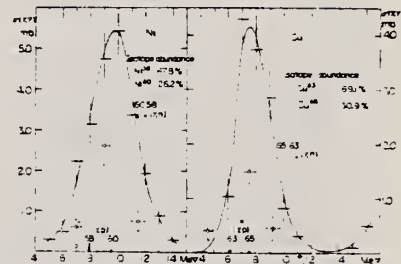


Fig. 7. The elastic scattering cross sections of photons. \cdots : data from Fuller and Hayward¹⁾. \square : data from the experiment using the monochromatic γ -rays⁴⁾.

(a): $\sigma(\gamma, \gamma)$ by Ni. The arrows indicate the positions of the (γ, p) and (γ, n) threshold energies of ^{58}Ni and ^{60}Ni .

(b): $\sigma(\gamma, \gamma)$ by Cu. The arrows indicate the positions of (γ, p) and (γ, n) threshold energies of ^{63}Cu and ^{65}Cu .

Ref. G. Ben-David (Davis); B. Huebschmann

Phys. Letters 3, 87 (1962)

Elem. Sym.	A	Z
Ni		28

Method
(n, γ) reaction - NaI(Tl)

Ref. No. 62Be2	BG
-------------------	----

Reaction	E or ΔE	E_0	Γ	$\int \sigma dE$	$J\pi$	Notes
(γ, γ)	discrete energies in the range 5.44- 8.997	7.64				σ (total) (mb) 1.5 Fe Detector at 135°

REF. W. Sebaoun J. Phys. Radium <u>23</u> , 989 (1962)						ELEM. SYM. Ni		A 28		Z 28	
METHOD Proton cross section; CSI; Cu ⁶³ (γ ,n) reaction						REF. NO. 62 Se 2				NVB	
REACTION		RESULT	EXCITATION ENERGY	SOURCE		DETECTOR				ANGLE	
				TYPE	RANGE	TYPE		RANGE			
G,P		ABX	15, 18	D	15, 18	SCI-I				0	
			(14.8, 17.6)	(14.8)	(17.6)						

$\sigma = 43 \pm 5$ mb, assuming $\sigma [\text{Cu}^{63}(\gamma, n)] = 82 \pm 8$ mb.

Ref. M. Kregar, B. Povh
Nuclear Phys. 43, 170 (1963)
Erratum in Nuclear Phys. 47, 528 (1963)

Elem. Sym.	A	Z
Ni		28

Method Betatron; α yields; spectra; solid state detectors; NBS chamber monitor.

Ref. No.	JHH
63 Kr 1	

Reaction	E or ΔE	E_0	Γ	$\int \sigma dE$	$I\pi$	Notes
Ni (γ, α)	Bremss. 21 30					

Fig. 2. The x-particle spectrum from Ni taken at 90 and 21 MeV betatron energy by 5000 Ω cm counter.

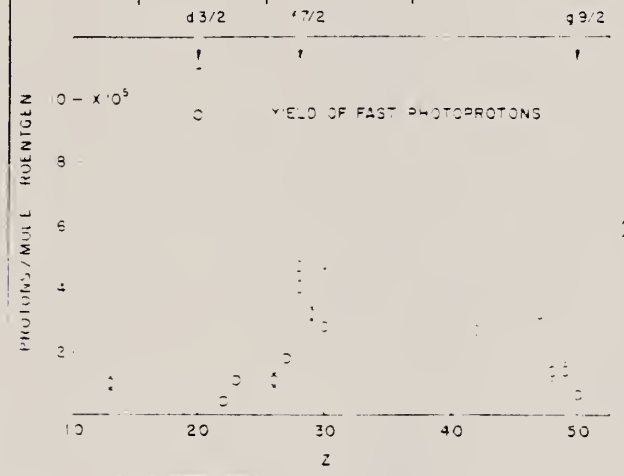
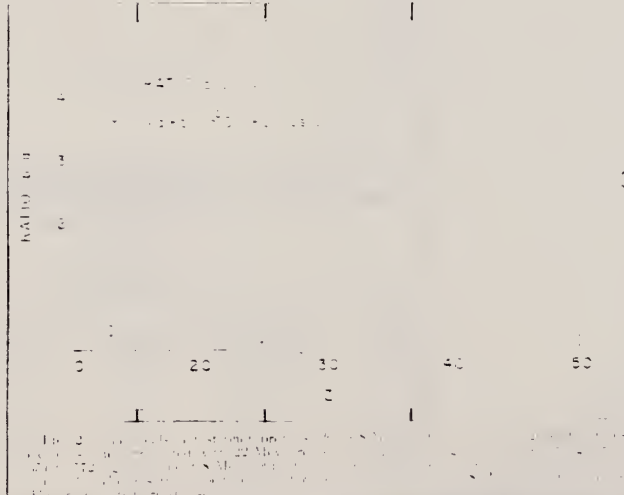
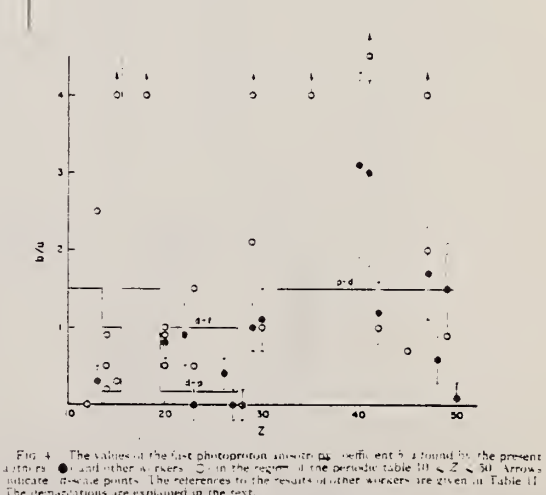
Fig. 4. The x-particle spectrum from Cd taken at 90 and 21 MeV betatron energy by 5000 Ω cm counter.

TABLE I
Relative yields

Element	21 MeV		30 MeV	
	Number of alphas	Relative yield at 90	Number of alphas	Relative yield at 90
Ni	1209	40	536	13
Cu	1124	13	590	7
Fe	1108	4.5	653	1.7
V	172	1	563	1
Cd	176	0.7		

Method Betatron; proton yield; angular distribution; scintillator;
ion chamber.

Ref. No.
63 Mi 5
NVB

Reaction	E or ΔE	E_0	Γ	$\int \sigma dE$	$J\pi$	Notes
Ni(γ , xp)	Bremss. 22					<p>Angular distribution: $Y(\theta) = a + b \sin^2 \theta (1 + p \cos \theta)^2$ where $a = 99 \pm 10$; $b = 1 \pm 2$; and $b/a = 0.0 \pm 0.2$.</p> <p>Yield ($E_p > 8$ MeV): $(4.4 \pm 0.5) 10^5$ protons/mole-r</p> <p>Yield ($3.7 < E_p < 14$): $(34 \pm 3) 10^5$</p>
 <p>YIELD OF FAST PHOTOPROTONS</p> <p>PROTONS / MOLE R</p> <p>10 - x 10⁵</p> <p>8</p> <p>6</p> <p>4</p> <p>2</p> <p>10 20 30 40 50</p> <p>Z</p> <p>2</p>						
 <p>YIELD OF FAST PHOTOPROTONS</p> <p>PROTONS / MOLE R</p> <p>10 - x 10⁵</p> <p>8</p> <p>6</p> <p>4</p> <p>2</p> <p>10 20 30 40 50</p> <p>Z</p> <p>3</p>						
 <p>b/a</p> <p>4</p> <p>3</p> <p>2</p> <p>1</p> <p>10 20 30 40 50</p> <p>Z</p>						

Method
Betatron; deuteron spectrum; nuclear emulsion

Ref. No.	NVB
63 Ya 2	

Reaction	E or ΔE	E ₀	Γ	∫σdE	Jπ	Notes
Ni(γ, d)	Bremss. 25.5					Detectors at 90°.

Table I. Ratios of the yield of photodeuterons to that of photoprotons.

Element	Ni	Cu	Sn	Sb
Angle of observation	90°	90°	126°	54°, 90° and 126°
Number of events examined	161	168	171	99
Number of photodeuterons estimated	3	10	7	4
Yield ratio	~0.02	0.06±0.04	0.04±0.02	~0.04

REF.	B. Arad (Huebschmann), G. Ben-David (Davis), I. Pelah, Y. Schlesinger Phys. Rev. <u>133</u> , B684-700 (1964)	ELEM. SYM.	A	Z
		Ni		28
METHOD	Reactor, (n, γ) reactions source	REF. NO.	64 Ar 1	NVB

REACTION	RESULT	EXCITATION ENERGY	SOURCE		DETECTOR		ANGLE
			TYPE	RANGE	TYPE	RANGE	
G,G	ABX	8	D	8	NAI-D		DST
		(7.639)		(7.639)			

Angular correlation measurement at 90° , 135°

J,WIDTH

gives $\frac{W(135^\circ)}{W(90^\circ)} = 1.7 \pm 0.1$, indicating $J = 1$.

Level width $\Gamma_0 = (3.28_{-0.50}^{+0.70})/u$ MeV, where u = fractional isotopic abundance.

TABLE III. Effective cross sections.

γ source	Energy (MeV)	Element	Protons	Scatterer	Neutrons	$\langle\sigma_{\gamma\gamma}\rangle$ (mb)	Notes
Hg	5.44	Hg	80	116, 118, 119, 120, 121, 122, 124		128	
Cl	6.12	Pr ¹⁴¹	59	82		103	a
V	6.508	Sn	50	62, 64-70, 72		14	
Co	6.690	Pr ¹⁴¹	59	82		2.7	a
Co	6.867	Nd	60	82, 83, 84, 85, 86, 88		22	
Al	6.98	Pb ²⁰⁸	82	126		2900	b
Cl	6.98	Pb	82	124, 125, 126		346	a
Ti	6.996	Bi ²⁰⁹	83	126		1560	b
Cu	7.01	Sn	50	62, 64-70, 72		1000	b
Ti	7.149	Pb ²⁰⁸	82	126		1000	b
Co	7.201	Pb ²⁰⁸	82	126		25	
Mn	7.261	Pb ²⁰⁸	82	126		25	a
Fe	7.285	Pb ²⁰⁸	82	126		4100	a
V	7.305	Pb ²⁰⁸	82	126		12.5	
Hg	7.32	Pb	82	124, 125, 126		5500	c
Fe	7.639	Ni	28	30, 32, 34, 36		10.5	d
Fe	7.639	Pr ¹⁴¹	59	82		10	d
Cr	8.499	Cu	29	34, 36		24.4	
Cr	8.881	Pr ¹⁴¹	59	82		9.3	
Ni	8.997	Sm	62	82, 85-88, 90, 92		2.8	

* A large error could be introduced in the cross-section values because of large differences in line intensities quoted by Bartholomew and Higgs and by Groshev *et al.* (Ref. 6).

^b Because of the low counting rate, thick scatterers were used, which will introduce a systematic error in estimating $\langle\sigma_{\gamma\gamma}\rangle$ for resonances having a high nuclear cross section.

^c The cross section was evaluated assuming the gamma intensity to be 0.02 photons per 100 captured neutrons (see text).

^d Reference 6 gives the 7.639 line of iron capture gamma rays as a single line. However, a recent paper by Fleoiger, Kand, and Segel [Phys. Rev. 125, 2031 (1962)] reports two different lines of equal intensities having energies of 7.647 and 7.533 MeV. The present experiment cannot resolve an energy difference of 14 keV, therefore, there is no possibility of deciding which line is responsible for the scattering.

ELEM. SIM.		
Ni		28
REF. NO.	64 Ba 4	egf

METHOD					REF. NO.	egf	
					64 Ba 4		
REACTION	RESULT	EXCITATION ENERGY	SOURCE		DETECTOR		ANGLE
			TYPE	RANGE	TYPE	RANGE	
G,XN	ABX	10-27	C	10-27	BF3-I		4PI

540 65 BA3 SAME DATA

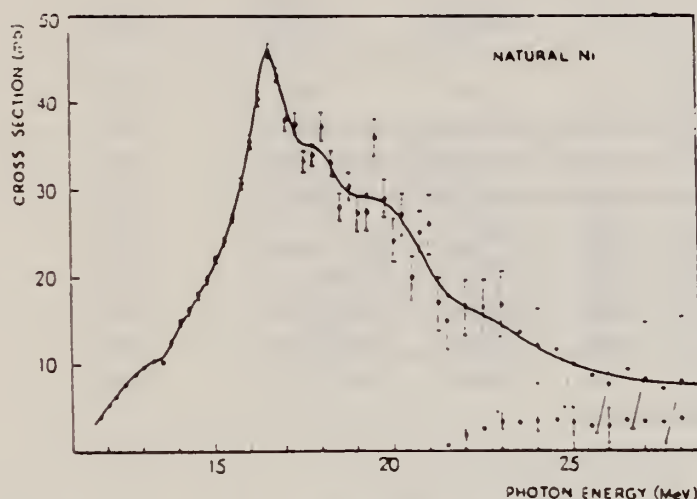


Fig. 2. — $\sigma(\gamma, 2n)$ for Ni of natural isotopic abundance. The circles represent the values for $\sigma(\gamma, 2n)$ calculated (for $a = 6.5 \text{ MeV}^{-1}$) in the approximation of the equality of thresholds for the reaction $\sigma(\gamma, n)$ and $\sigma(\gamma, 2n)$ for Ni^{58} and Ni^{60} .

REF.

G. Baciú, C. Molino, B. Minetti, L. Pasqualini, G. Piragino
 Stud. Cercetari Fiz. 16, 903 (1964)

ELEM. SYM.

A

Z

Ni

28

METHOD

REF. NO.

64 Ba 5

egf

REACTION	RESULT	EXCITATION ENERGY	SOURCE		DETECTOR		ANGLE
			TYPE	RANGE	TYPE	RANGE	
G,XN	ABX	12-28	C	12-28	BF3-I		4PI

Tabela 2
 $Ni^{58}(\gamma, Tn)$

E_0 (MeV)	σ_0 (mb)	Γ (MeV)	Δ (MeV)	E_1 (MeV)	E_2 (MeV)	$\int_{E_1}^{E_2} \sigma dE$ (mb MeV)
13,2	6,0	1,1	0,6587	12,3	13,8	5,13
14,65	27,0	1,2	0,71856	13,6	15,6	28,74
16,9	53,0	1,8	1,0778	15,2	18,5	88,57
18,7	51,0	1,0	0,5988	17,8	19,6	46,96
20,4	44,0	1,4	0,8383	19,8	21,5	54,24

$$\int_{E_1}^{E_2} \sigma dE = 223,64 \text{ mb. MeV}$$

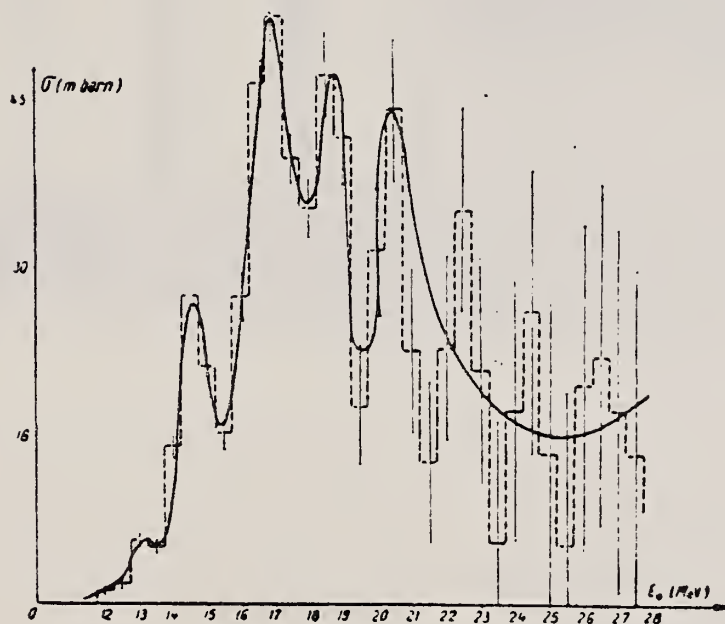


Fig. 2

Synchrotron; $C^{12}(\gamma, n)$ monitor

REACTION	RESULT	EXCITATION ENERGY	SOURCE		DETECTOR		ANGLE
			TYPE	RANGE	TYPE	RANGE	
G.K.N.	ABV	THR - 80	C	80	BF3-I		4 PI

Table 1

Element	Yield (36) eV cm ² mol MeV	60 NZ/A (mb MeV)	$\frac{\sigma}{Z}$ 0	$\frac{\sigma}{Z}$ 0	$\frac{\sigma}{Z}$ 0	E_m (MeV)	σ_m (mb)
^{24}Cr	63×10^{-5}	777	1.01	2.1	0.53	18.5	97
^{25}Mn	102×10^{-5}	813	1.52	2.33	0.65	19.5	114
^{26}Fe	63×10^{-5}	822	0.58	2.46	0.60	17.5	75
^{27}Co	59×10^{-5}	873	1.03	1.82	0.59	17.5	92
^{28}Ni	44×10^{-5}	879	0.55	1.07	0.51	13.5	56
^{29}Cu	95×10^{-5}	947	1.06	2.99	0.53	17.5	98
^{30}Zn	58×10^{-5}	975	0.94	1.63	0.56	17.5	86
^{31}Ga	100×10^{-5}	1034	1.29	2.13	0.59	17.5	131
^{32}Ge	109×10^{-5}	1084	1.35	2.29	0.59	17.5	153
^{33}As	127×10^{-5}	1109	1.22	2.13	0.56	17.5	127

$$\frac{\sigma}{Z} = \frac{\int_0^{30} \sigma(\gamma, xn) dE}{60 \text{ NZ/A}}$$

Table 2

Element	maximum yield ($\times 10^{-5}$)	$\sigma_{-1}(\text{Th})$	$\sigma_{-1}(\text{Th}) \times \frac{3}{4\pi} \frac{A^2}{Z^2} \left(\frac{A-1}{NZ} \right)^2$
^{12}C	4.0	3.54	2.13
^{16}O	5.2	4.55	1.92
^{23}Na	10.6	11.00	2.49
^{27}Al	10.0	8.81	1.73
^{28}Si	11.6	9.95	1.85
^{32}S	10.3	17.36	2.32
^{36}S	9.5	8.55	1.97
^{39}K	10.3	17.30	2.61
^{40}Ca	10.1	12.63	1.92
^{54}Cr	86	61.6	3.56
^{55}Mn	103	76.1	2.96
^{56}Fe	71	80.3	2.53
^{57}Co	94	63.5	2.94
^{58}Ni	46	34.2	1.89
^{60}Cu	102	72.3	2.96
^{62}Zn	93	65.7	2.63
^{61}Ga	140	93.3	3.21
^{62}Ge	150	101.3	3.36
^{63}As	151	99.3	3.13

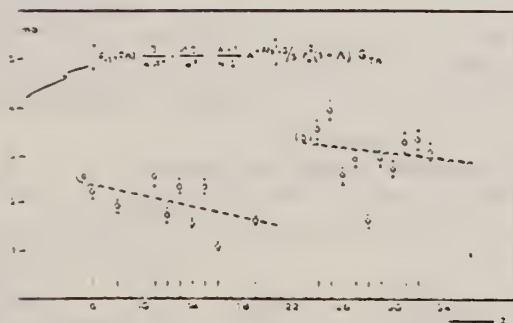


Fig. 2. Bremsstrahlung weighted cross sections, $\sigma_{-1}(\text{Th})$, conveniently normalized, versus Z.

REF.

M. Giannini, P. Oliva, D. Prosperi and S. Sciuti
Nuovo Cimento 34, 1116 (1964)

ELEM. SYM.

A

Z

Ni

28

METHOD

Reactor; Fe(n, γ)

REF. NO.

64 Gi 1

NVB

REACTION	RESULT	EXCITATION ENERGY	SOURCE		DETECTOR		ANGLE
			TYPE	RANGE	TYPE	RANGE	
G.G	NØX	8	D	8	NAI-D		135
		(7.64)		(7.64)			

WIDTH

TABLE I.

Source-scatterer	Energy (MeV)	$\langle\sigma_{rs}(300)\rangle$ (Barn)	$\bar{\sigma}_{rs}(300)$ (Barn)	$\frac{\langle\sigma_{rs}(100)\rangle}{\langle\sigma_{rs}(300)\rangle}$	$\Gamma_{\gamma 0}/\Gamma$	$\Gamma_{\gamma 0}$ (eV)	δ (eV)
$^{57}\text{Fe}-^{208}\text{Pb}$	7.28	5.62 ± 0.15	17.5 ± 1.5	1.004 ± 0.006	0.84 ± 0.08	0.73 ± 0.05	4.8 ± 0.3
$^{57}\text{Fe}-^{62}\text{Ni}$	7.64	0.375 ± 0.006	≤ 5	0.338 ± 0.011	0.71 ± 0.07	0.15 ± 0.02	11.0 ± 0.5
$^{57}\text{Fe}-^{114}\text{Cd}$	7.64	0.287 ± 0.006	4.1 ± 1.8	1.116 ± 0.015	0.11 ± 0.06	0.22 ± 0.02	≤ 1
$^{28}\text{Al}-^{208}\text{Pb}$	6.98	1.29 ± 0.06	22.1 ± 2.7	1.002 ± 0.012	0.30 ± 0.07	0.86 ± 0.10	11.5 ± 2.5

Cross sections based on assumed $1 + \cos^2\theta$ distribution.

METHOD

Betatron

REF. NO.

64 Sc 1

JOC

REACTION	RESULT	EXCITATION ENERGY	SOURCE		DETECTOR		ANGLE
			TYPE	RANGE	TYPE	RANGE	
G.A.	SPC	THR - 33	C	33	SCD	4 - 13	90

ABS YIELD

TABELLE 1
Meßdaten und Ergebnisse

	Ti	Ni	Cu	Nb
Targetdicke (mg/cm ²)	2.08	1.52	9.90	8.87
Bestrahlungsdauer (h)	52.5	55.5	18.0	84.5
Registrierte Teilchenanzahl (4 ≤ E _γ ≤ 12.6 MeV)	1861	2376	2333	1987
Lage des Maximums E _{max} der Energieverteilung (MeV)	6.4	8.2	8.5	11
Halbwertsbreite des Maximums (MeV)	2.8	2.8	4.0	3.5
Mittlerer Energieverlust im Target bei E _γ = E _{max} (MeV)	0.4	0.25	1.7	1.1
Ausbeute in μb/MeV *)	22 ± 3.5	45 ± 7	23 ± 3.5	5.5 ± 0.8

*) Vgl. Bemerkung *) in Tabelle 2.

TABELLE 2
Vergleich der Ergebnisse verschiedener Autoren

E _γ (MeV)	Ti	Ni	Cu	Nb
<i>Ausbeute (10³ × N_γ/Mol. r)</i>				
Boulègue 31		58.7	50.8	
Diese Arbeit *) 32.5	48 ± 7	98 ± 15	50 ± 7.5	12 ± 1.8
Toms und McElhinney 21.5		39.4	26	4.6 b)
<i>Relative Ausbeute</i>				
Boulègue 31		1	0.87	
Kregar und Povh 30		1	0.54	
Diese Arbeit 32.5	0.49 ± 0.08	1	0.51 ± 0.08	0.12 ± 0.02
Toms und McElhinney 21.5		1	0.66	0.12 b)

*) Die Fehlerangaben beinhalten auch die Unsicherheit in der Absoluteichung der Intensität des γ-Strahles.

b) Dieser Wert wurde aus nur 14 beobachteten Ereignissen bestimmt.

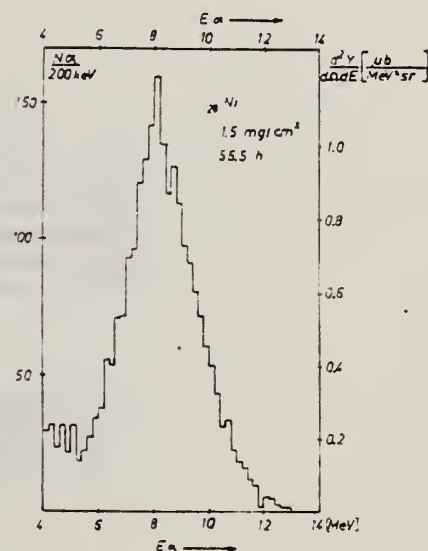


Abb. 1. Die erhaltenen Energie-Spektren der Photoalphateilchen aus Ti, Ni, Cu und Nb.

REF.	G. Baciú, G. C. Bonazzola, B. Minetti, C. Molino, L. Pasqualini and G. Piragino Nuclear Phys. <u>67</u> , 178 (1965)			ELEM. SYM.	A	Z
				Ni		28
METHOD	NBS Monitor			REF. NO.	65 Ba 3	
	[Page 1 of 2]				EGF	
REACTION	RESULT	EXCITATION ENERGY	SOURCE		DETECTOR	
			TYPE	RANGE	TYPE	RANGE
G,XN	ABX	THR - 28	C	10-30	BF3-I	4PI

TABLE 2
Cross sections for Co, Ni, Cu and Ga

	E_m (MeV)	σ_m (mb)	$\int_0^x \sigma(E) dE$ (mb · MeV)	Ref.
Co ⁵⁸	16.9	130	750(24)	^{a)}
	16.75 19	110 103	709(25)	^{a)}
	17.5	68	725 ± 72(28)	^{a)}
	16.5 19	82 80	701 ± 91(29)	¹²⁾
	16.5 19	72 74	657 ± 89(28)	this work
			537 ± 34(24)	this work
			445 ± 48(24)	^{a)}
Ni	16.5	50	340(24)	¹¹⁾
	16.5	46 ± 1	313 ± 48(28)	this work
			276 ± 25(24)	this work
Ni ⁵⁸	18.5	60	330(24)	¹³⁾
		30	180(24)	^{a) 13)}
	20.5	21	160(24)	¹³⁾
	19.0	32	220 ± 30(32)	¹⁴⁾
Ni ⁶⁰	16.5	85	440(± 20 %)(24)	^{b)}
Cu	19.5	120	870(20)	^{a)}
			904(27)	¹²⁾
	17.2	126	930(27)	¹²⁾
	17	90	450 ± 15(19,6)	¹⁷⁾
	16.75	71 ± 7	745 ± 74(28)	¹²⁾
	17.0	86 ± 2	733 ± 105(28)	this work
			451 ± 18(20)	this work
Ga	16.5	115 ± 3	947 ± 98(28)	this work

σ_m is the peak value of the cross section, E_m is the peak energy and $\int_0^x \sigma(E) dE$ is the integrated cross section. The upper limit of the integration is indicated in parentheses.

^{a)} Value obtained subtracting the (γ , 2n) reaction contribution from the $\sigma(\gamma, Tn)$.

^{b)} Value obtained by subtracting the Ni⁵⁸(γ , n)Ni⁵⁷ reaction contribution from the $\sigma(\gamma, Tn)$ for natural nickel corrected for the (γ , 2n) reaction contribution.

11) J. Goldenberg and L. Katz, Can. J. Phys. 32 (1954) 49

12) L. Katz and A. G. W. Cameron, Can. J. Phys. 29 (1951) 518

13) J. P. Roalswing, R. N. H. Haslam and D. J. McKenzie, Can. J. Phys. 37 (1959) 607

14) J. H. Carver, and W. Tuchinetz, Proc. Phys. Soc. 73 (1959) 585

REF.

G. Baciú, G. C. Bonazzola, B. Minetti, C. Molino, L. Pasqualini
and G. Piragino
Nuclear Phys. 67, 178 (1965)

ELEM. SYM.

Ni

28

METHOD

NBS Monitor

[Page 2 of 2]

REF. NO.

65 Ba-3

EGF

REACTION	RESULT	EXCITATION ENERGY	SOURCE		DETECTOR		ANGLE
			TYPE	RANGE	TYPE	RANGE	

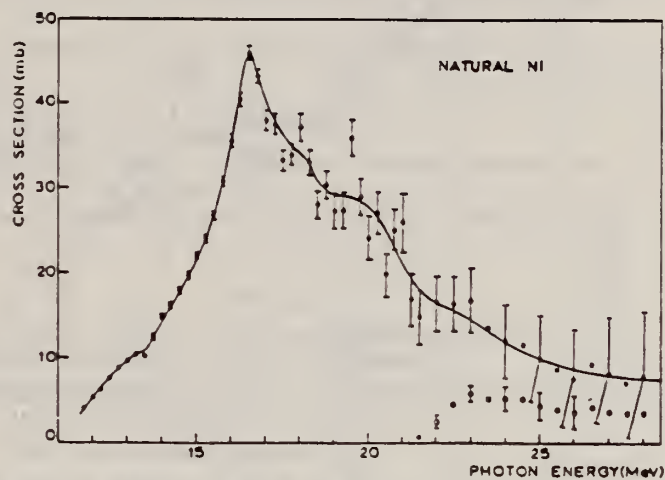


Fig. 2. The solid line represents the average of data points of the total cross section $\sigma(\gamma, Tn)$ for natural nickel. The open circles represent the $\sigma(\gamma, 2n)$ calculated by taking $a = 6.5 \text{ MeV}^{-1}$ and assuming that the (γ, n) and $(\gamma, 2n)$ reaction threshold have the same values for Ni^{58} and Ni^{60} .

REF.

M. Giannini, P. Oliva, D. Prosperi and S. Sciuti
Nuclear Phys. 65, 344 (1965)

ELEM. SYM. A Z

Ni

28

METHOD

Source: n-capture γ 's from Fe.

REF. NO.

65 G1 1

EGF

REACTION	RESULT	EXCITATION ENERGY	SOURCE		DETECTOR		ANGLE
			TYPE	RANGE	TYPE	RANGE	
G,G/	RLY	8	D	8	NAI-D	8	135

Inelastic branching ratio

$$I(E_Y = 5.59) \approx 0.47 I(7.64)$$

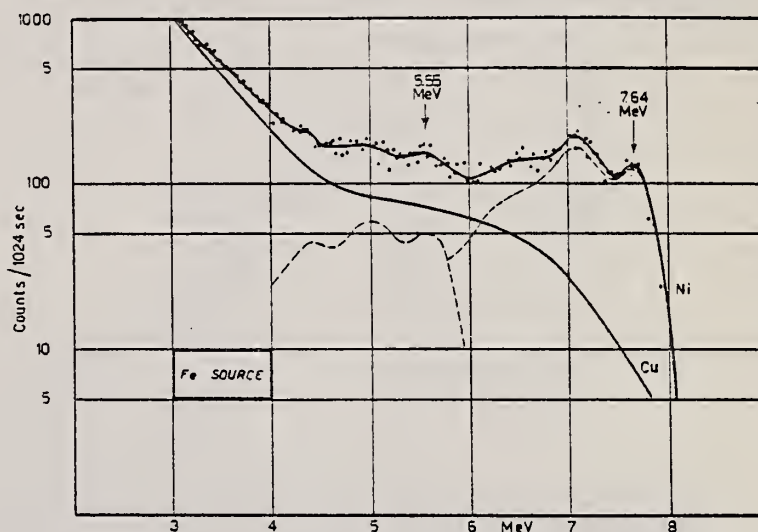
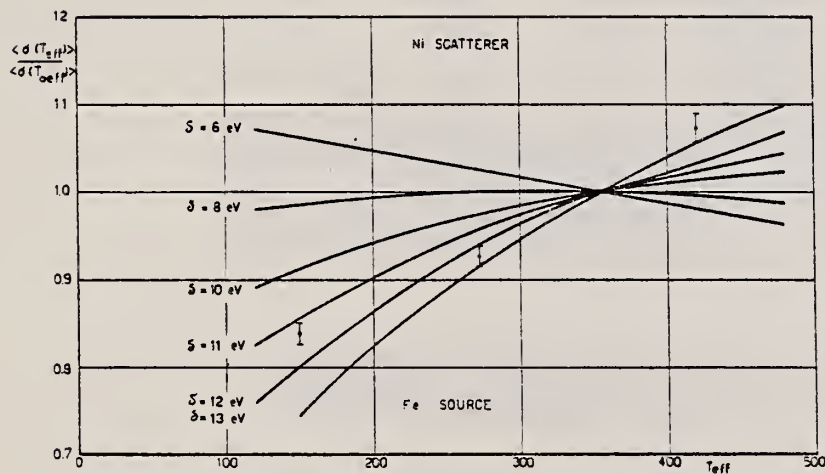
Fig. 3. Spectra of γ -rays scattered by Ni and Cu targets.

Fig. 7. Fe-Ni resonance.

REF.

J.M. Wyckoff, B. Ziegler, H.W. Koch, and R. Uhlig
Phys. Rev. 137, B576-94 (1965)

ELEM. SYM. A

N1

28

METHOD

Synchrotron; ion chamber monitor

REF. NO.

65 Wy 1

NVB

REACTION	RESULT	EXCITATION ENERGY	SOURCE		DETECTOR		ANGLE
			TYPE	RANGE	TYPE	RANGE	
G,MU-T	ABX	10-35	C	90	SCI-D		4PI

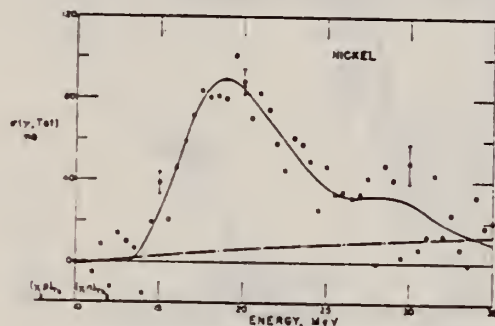
59

FIG. 25. Nickel total photonuclear cross section.

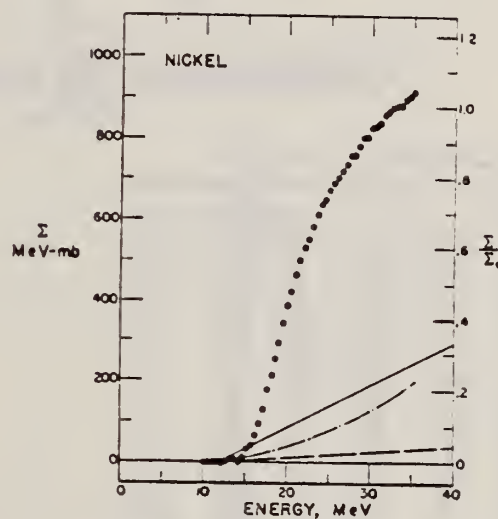


FIG. 26. Nickel total photonuclear cross section integrated over energy.

REF.

I. Bergqvist, B. Lundberg, L. Nilsson and N. Starfelt
Phys. Letters 19, 670 (1966)

ELEM. SYM.

Ni

A

Z

28

METHOD

Van de Graaff

REF. NO.

66 Be 1

EGF

REACTION	RESULT	EXCITATION ENERGY	SOURCE		DETECTOR		ANGLE
			TYPE	RANGE	TYPE	RANGE	
N,G	SPC	16	D	7	NAI-D	8-18	

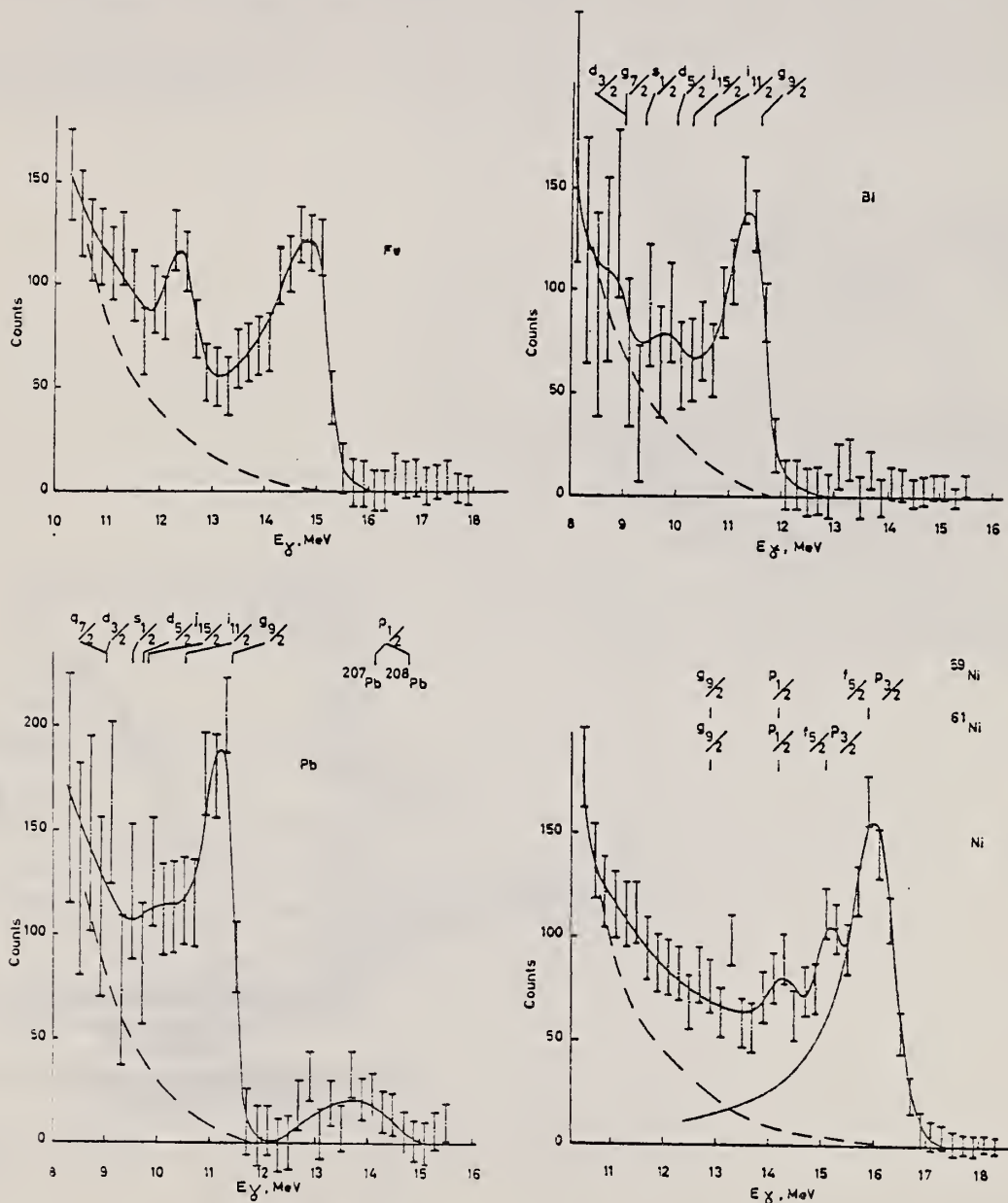


Fig. 1. Gamma-ray spectra emitted in the capture of 7.4 MeV neutrons. The dashed line is the spectrum calculated for the decay of a compound nucleus. The dot-dashed line is the response function of the gamma-ray spectrometer for 16.0 MeV γ rays. Single-particle states as determined from (d,p) reactions are shown.

ELEM. SYM.	A	Z
Ni		28
REF. NO.		
66 Be 3		
JDM		

METHOD

Nuclear Resonance Scattering using N,G reactions.

REACTION	RESULT	EXCITATION ENERGY	SOURCE		DETECTOR		ANGLE
			TYPE	RANGE	TYPE	RANGE	
G,G	RLX	5 - 10	D	5 - 10	NAI-D	5 - 10	135

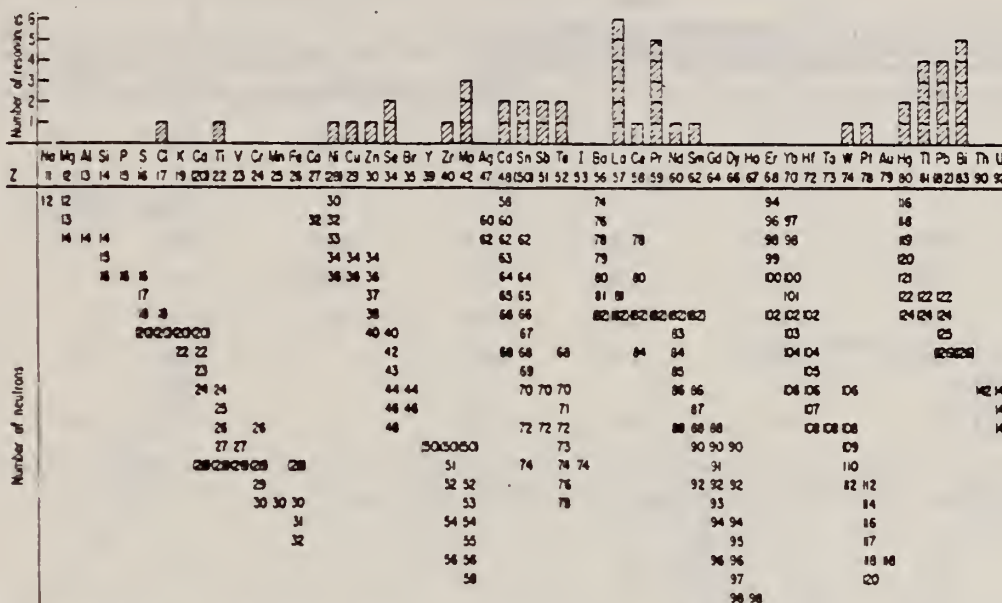


FIG. 3. Histogram of distribution of observed resonances among the different targets. The atomic number is given directly beneath the chemical symbol followed by the neutron numbers of the naturally occurring isotopes. Magic numbers are shown in brackets.

TABLE III. List of effective cross sections.

Scatterer	Energy (MeV)	Gamma source	σ (mb)	Scatterer	Energy (MeV)	Gamma source	σ (mb)
Sm ¹⁴⁴	8.997	Ni	100	Sn	7.01	Cu	110
Pr ¹⁴¹	8.881	Cr	9	Nd	6.867	Co	30
La	8.532	Ni	6	Pr ¹⁴¹	6.867	Co	3
Te	8.532	Ni	3 ^a	Te	6.7	Ni	...
Cu	8.499	Cr	24	La	6.54	Ag	12
Zr	8.496	Se	3050	Cl	6.474	Co	110
Zn	8.119	Ni	13	Mo	6.44	Hg	25 ^a
Se	7.817	Ni	50	La	6.413	Ti	72
Se	7.76	K	90	Mo	6.413	Ti	10
Sb	7.67	V	...	Ti	6.413	Ti	25
Cd	7.64	Fe	40 ^b	W	6.3	Ti	...
Ni	7.64	Fe	7 ^c	Sh	6.31	Hg	6 ^e
Pr ¹⁴¹	7.64	Fe	12 ^c	Ti	6.31	Hg	2 ^e
Ti	7.64	Fe	370 ^e	Sn	6.27	Ag	75
La	7.634	Cu	7	Pb ²⁰⁸	6.15	Gd	...
Mo	7.634	Cu	11	Te	5.8	Ni	...
Bi ²⁰⁹	7.634	Cu	4	La	6.12	Cl	35
Te	7.528	Ni	66 ^d	Pr ¹⁴¹	6.12	Cl	110
Bi ²⁰⁹	7.416	Se	100	Pt	5.99	Hg	40 ^a
Bi ²⁰⁹	7.300	Ag	80 ^a	Ti	5.99	Hg	5 ^e
Pb ²⁰⁸	7.285	Fe	4100	Pb ²⁰⁸	5.9	Sr	...
Cl	7.283	Fe	34	Ce	5.646	Co	17
Pr ¹⁴¹	7.185	Se	80	Bi ²⁰⁹	5.646	Co	55
Ti	7.16	Cu	120	Ph ²⁰⁴	5.53	Ag	70
La	7.15	Mn	50	Hg	5.44	Hg	75 ^e
Bi ²⁰⁹	7.149	Ti	2000	Hg	4.903	Co	385

^a High-energy component of a complex spectrum.
^b A broad scattered spectrum with no observable peak structure.
^c There are actually two lines of energies 7.647 and 7.633 MeV having equal intensities in the iron capture gamma spectrum. The cross section has therefore been corrected, although there is no possibility at present of deciding which line is responsible for each resonance.
^d Is probably an independent level in the complex spectrum of Ni γ rays on Te.
^e Rough estimate.
^f May be inelastic component from 7.528 level in Te.
^g The relative line intensities in this case are due to Groshev and co-workers.
^h No line is known for the source at this energy.
ⁱ Difficult to resolve among the many source lines present at this energy.

REACTION	RESULT	EXCITATION ENERGY	SOURCE		DETECTOR		ANGLE
			TYPE	RANGE	TYPE	RANGE	
G, A	SPC	THR-31	C	31	SCD-D	3-14	130

TABLE 1
Experimental data and results

Element	Mg	Al	S	Ni	Cu	Zn	Error (%)
target thickness (mg/cm ²)	0.81	1.54	0.80	2.50	2.68	3.00	5 ^a)
dose (r)	6190	25400	23200	3880	5840	4220	10
yield absolute (10 ³ /mole · r) for $E_m > 3.16$ MeV	0.61	0.93	1.46	1.65	0.92	2.42	11 ^a)
yield relative to Ni	0.36	0.56	0.88	1	0.55	1.43	5 ^a)
$Y_{\gamma, 2}/Y_{\gamma, \text{tot}}$ (%)	9.6	11.4	12.4	7.0	3.2	^b)	
nuclear temp. θ (MeV)	1.43	1.48	1.46	1.04		0.91	10
level density parameter a (MeV ⁻¹)	5.1	4.8	4.9	8.6		10.8	10

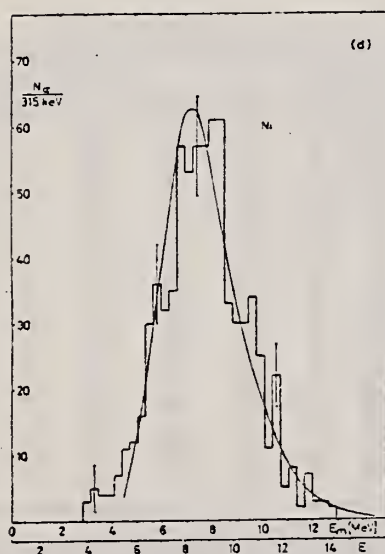
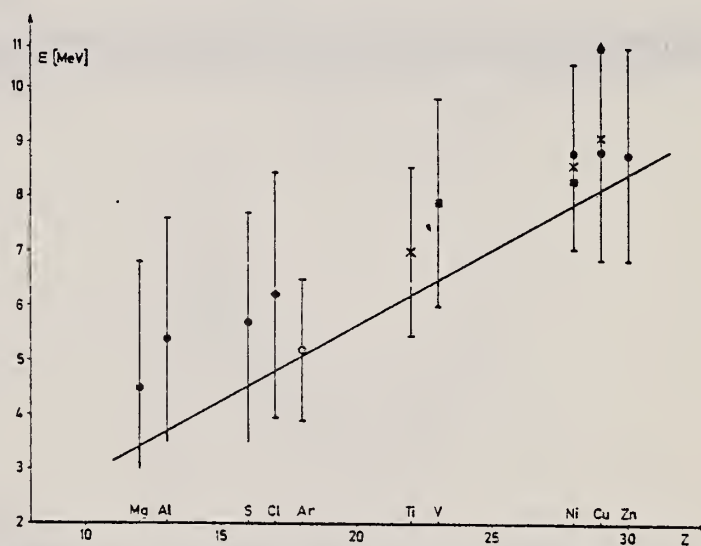
^a) For S, the error of the target thickness has been 10 %, of the absolute yield 14 % and of the relative yield 10 %.^b) For Zn $\sigma_{\gamma, \text{tot}}$ is not known.

Fig. 3d-e. Photoalpha spectra of Ni and Zn. Notations as in fig. 3a-c.

Fig. 3f. Statistical plot of the measured spectra. The straight lines are drawn to give the best fit.

Fig. 4. Position of the peaks in different photoalpha spectra plotted against Z of the target nuclei. \times : Scheer *et al.*¹⁰), \blacksquare : Kregar and Povh⁹), \blacktriangle : Meneghetti and Vitale⁴), \blacklozenge : Erdős *et al.*¹), \circ : Komar *et al.*⁷), \bullet : this work. The signs show the position of the maximum, the bars give the widths at half maximum. The curve shows the height of the Coulomb barrier.

REF. S. M. Hussain and K. G. McNeill
Can. J. Phys. 45, 2851 (1967)

ELEM. SYM.	A	Z
Ni		28
REF. NO.		EGF
67 Hu 2		

REACTION	RESULT	EXCITATION ENERGY	SOURCE		DETECTOR		ANGLE
			TYPE	RANGE	TYPE	RANGE	
G,N	ABY	THR-22	C	22	THR	4-	DST

YIELD AT $E_0 = 22 \text{ MeV}$
 $^{28}\text{Si}(n,p)$ ACTIVATION BY PHOTONEUTRONS

FIG. 3. The yields of fast photoneutrons from various elements as measured in the present work and by Baker. The present results have been normalized to Baker's measurements for lead.

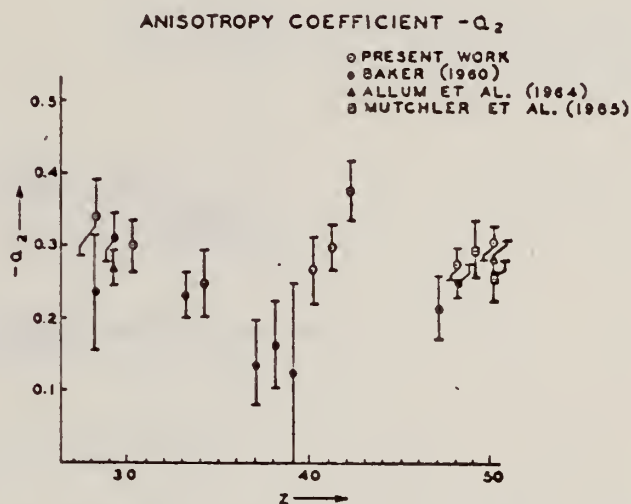
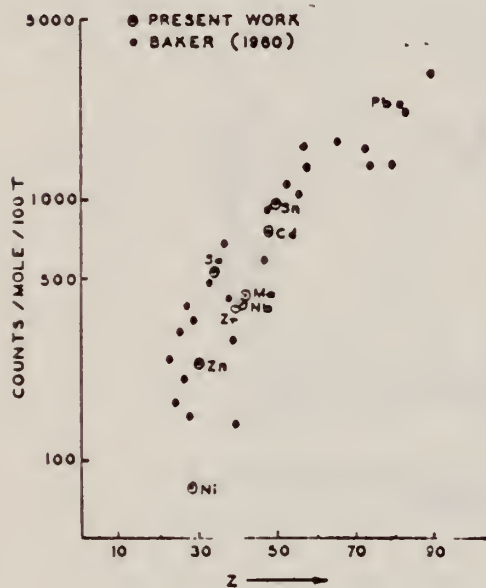


FIG. 2. The anisotropy coefficients a_2 in the formula $W(\theta) = a_0(1 + a_1P_1 + a_2P_2)$, obtained in the present work, and those obtained by other workers in the same part of the Periodic Table.

TABLE I

Element	a_0^*	a_1	a_2
Nickel	77 (1.0±0.05)	0.14±0.04	-0.31±0.06
Zinc	236 (1.0±0.04)	0.06±0.03	-0.30±0.04
Selenium	525 (1.0±0.05)	0.10±0.04	-0.25±0.05
Zirconium	380 (1.0±0.05)	0.03±0.04	-0.27±0.05
Niobium	392 (1.0±0.03)	0.04±0.02	-0.30±0.03
Molybdenum	410 (1.0±0.03)	0.05±0.03	-0.41±0.04
Cadmium	755 (1.0±0.02)	0.05±0.01	-0.28±0.02
Tin	955 (1.0±0.02)	0.05±0.02	-0.30±0.02
Lead	2274 (1.0±0.02)	0.06±0.02	-0.48±0.02

*For comparison purposes the experimental value of a_0 for Pb has been normalized to coincide with that obtained by Baker and McNeill (1961) and is the yield per mole per 100 roentgen. All other values of a_0 have also been quoted with the same normalization.

REF.

P. Kneisel, A. Goldmann and H. v. Buttler
Z. Physik 199, 440 (1967)

ELEM. SYM.

A

Z

Ni

28

METHOD

Linac

REF. NO.

67 Kn 1

JDM

REACTION	RESULT	EXCITATION ENERGY	SOURCE		DETECTOR		ANGLE
			TYPE	RANGE	TYPE	RANGE	
G,T	RLY	THR-49	C	36,49	ACT-I		4PI

Tabelle. Zusammenstellung der Meßergebnisse

	$E_m = 36,2 \text{ MeV}$	$E_m = 49,2 \text{ MeV}$
$Y[\text{Ni}(\gamma, t)]/Y[\text{C}(\gamma, n)\text{C}^{11}]$	$(2,2 \pm 0,2) 10^{-3}$	$(4,6 \pm 0,4) 10^{-3}$
$Y[\text{Pd}(\gamma, t)]/Y[\text{C}(\gamma, n)\text{C}^{11}]$	—	$(6,1 \pm 1,0) 10^{-3}$
$\sigma_y[\text{Ni}(\gamma, t)]$	$(4,0 \pm 0,4) \mu\text{barn}$	$(10,5 \pm 1,0) \mu\text{barn}$
$\sigma_y[\text{Pd}(\gamma, t)]$	—	$(13,8 \pm 2,3) \mu\text{barn}$

REF. S. Costa, C. Manfredotti, L. Pasqualini, F. Ferrero
Nuovo Cimento 54B, 344 (1968)

ELEM. SYM.	A	Z
Ni		28

METHOD

REF. NO.

68 Co 3

egf

REACTION	RESULT	EXCITATION ENERGY	SOURCE		DETECTOR		ANGLE
			TYPE	RANGE	TYPE	RANGE	
G, XN	ABX	11- 34	C	11- 34	BF3-I		4PI

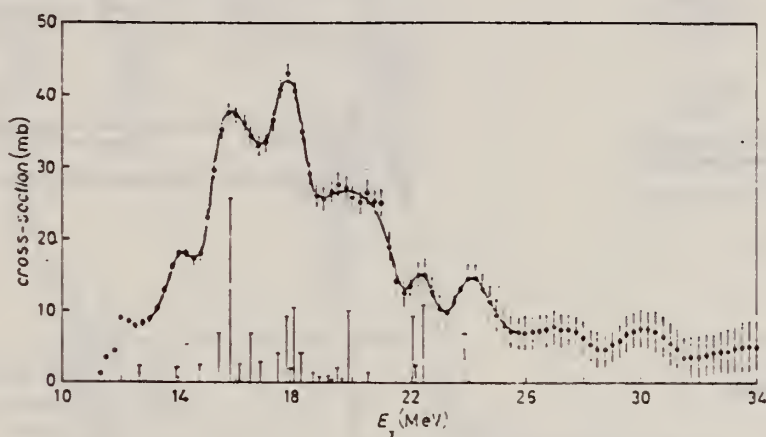


Fig. 1. - Experimental photoneutron cross-section in natural Ni. The vertical bars represent the dipole strengths predicted by the theory (see text).

ELEM. SYM.	A	Z
Ni		28
REF. NO.		HMG
68 Fi 1		

METHOD			SOURCE		DETECTOR		ANGLE
REACTION	RESULT	EXCITATION ENERGY	TYPE	RANGE	TYPE	RANGE	
G, XN	ABX	11-25	C	11-25	BF3-I		4PI

TABLE II. Results.

Nickel [without $(\gamma, 2n)$ correction]			
σ_m (mb)	E_m (MeV)	σ_{int} (MeV mb)	Reference
41.9 ± 0.4	15.9	$291.1 \pm 11(24)^a$	This work
46 ± 1	16.5	$276 \pm 25(24)^a$	15
Silver [with $(\gamma, 2n)$ correction]			
181 ± 1	16.3	$1254(24)^{a,b}$	This work
240 ± 17	16.0	$1600(21)^{a,b}$	16 ^c

^a The numbers in parenthesis are the upper limits of integration for σ_{int} .
^b Reference 16 gives the cross section of Ag^{107} .
^c No errors are given with these quantities because of the uncertainty in the neutron multiplicity correction.

¹⁴ D. B. Thomson, Phys. Rev. 129, 1649 (1963).

TABLE III. Integrated partial cross sections up to 24 MeV for the natural nickel, Ni^{58} and Ni^{60} .

	$\int \sigma_{ab} dE$ (MeV mb)	$\int \sigma(\gamma, n) dE$ (MeV mb)	$\int \sigma(\gamma, p) dE$ (MeV mb)	$\int \sigma(\gamma, p) dE / \int \sigma(\gamma, n) dE$
Natural	650 ^a	290	360	1.2
Ni^{58}	180 ^b	440 ^b	2.4	
Ni^{60}	570	160	0.28	

^a Taken from Ref. 18.

^b Taken from Ref. 21.

²¹ J. H. Carver and W. Turchinets, Proc. Phys. Soc. (London) 73, 585 (1959).

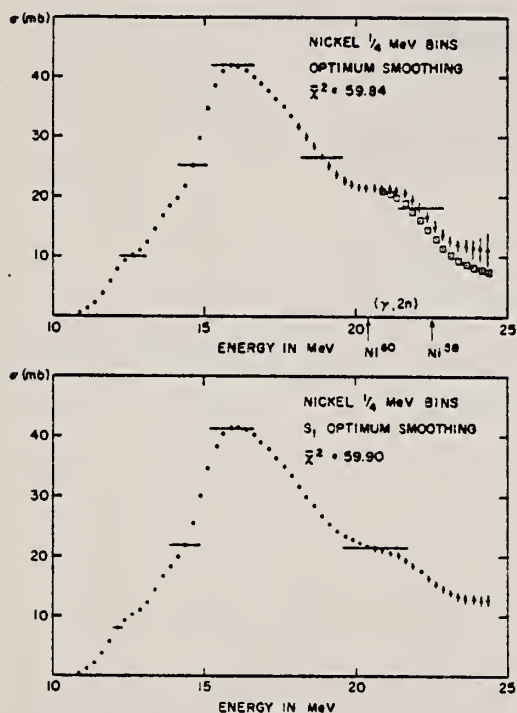


FIG. 1. Least-structure solutions for natural nickel. Upper curve: optimum smoothing using S_2 [Eq. (3b)]; lower curve: optimum smoothing using S_1 [Eq. (3a)].

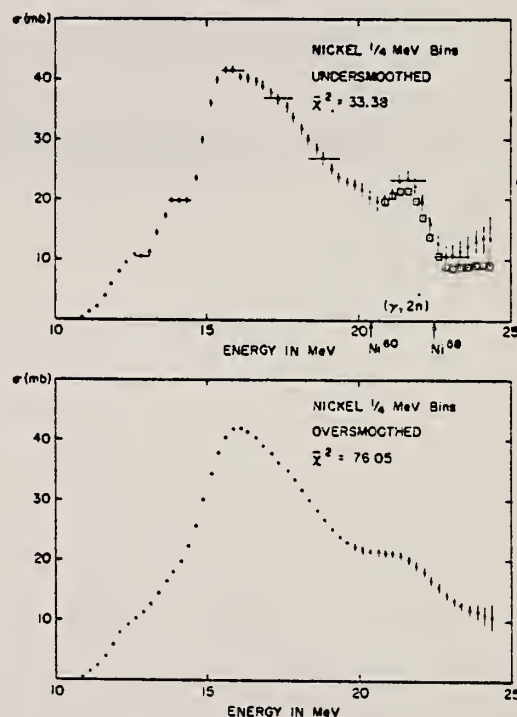


FIG. 2. Least-structure solutions for natural nickel. Upper curve: undersmoothed solution, $\chi^2 = 33.38$; lower curve: oversmoothed solution, $\chi^2 = 76.05$.

REF.

R. Garfagnini and G. Piragino
Nucl. Phys. A122, 49 (1968)

ELEM. SYM.

A

Z

Ni

28

METHOD

REF. NO.

68 Ga 1

egf

REACTION	RESULT	EXCITATION ENERGY	SOURCE		DETECTOR		ANGLE
			TYPE	RANGE	TYPE	RANGE	
$^{68}\text{Ga}, \text{XN}$	SPC	THR-85	C	85	CCH	1-15	135

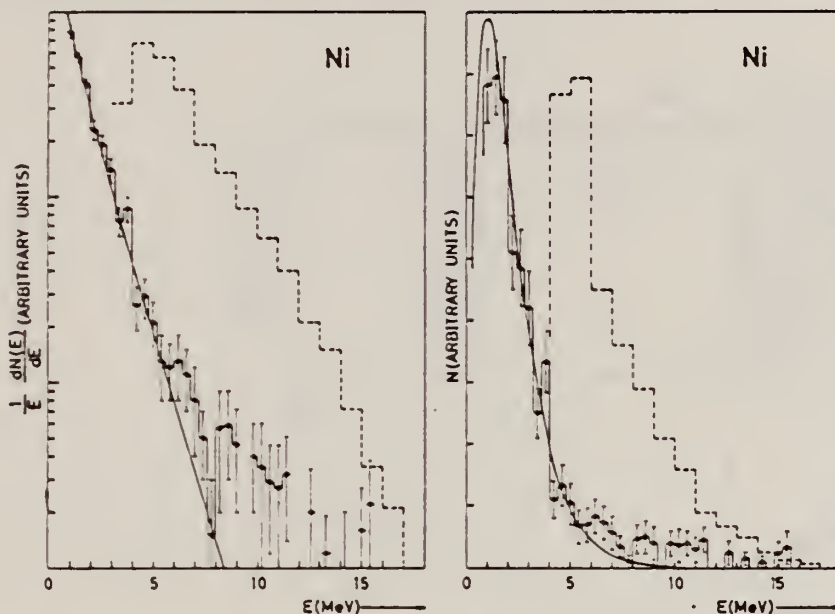
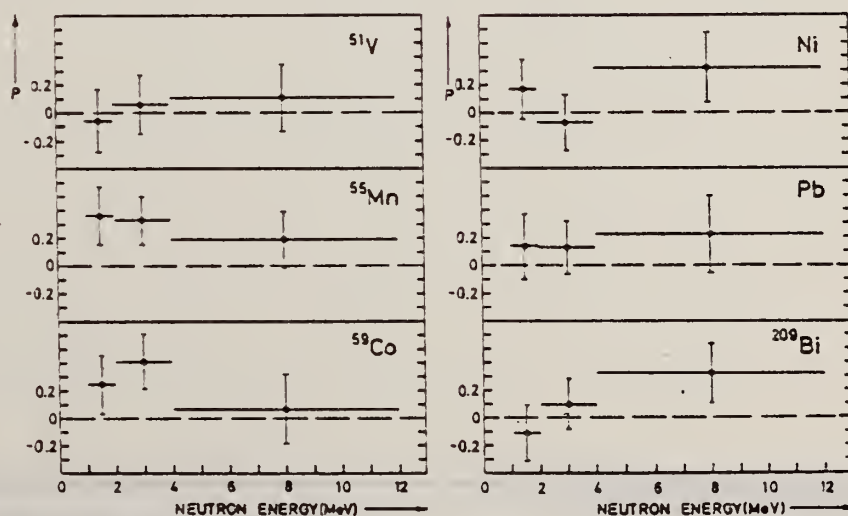


Fig. 6. Energy spectrum of photoneutrons from natural nickel compared with the spectrum of photoneutrons for $E_{\gamma \text{ max}} = 23$ MeV of ref. ¹⁴ (dashed histogram) and with the evaporation-model prediction (full line). The normalization used is described in the text.

²⁸E. Lejkin, R. Osokina and B. Ratner,
Nuovo Cim. Suppl. 3, 105 (1965).



PHI Fig. 7. Polarization of photoneutrons from ⁵¹V, ⁵⁵Mn, ⁵⁹Co, natural Ni, natural Pb and ²⁰⁹Bi.

REF.

K. Min and T. A. White
 Phys. Rev. Letters 21, 1200 (1968)

ELEM. SYM.	A	Z
Ni		28
REF. NO.		
68Mi 1		egf

METHOD

REACTION	RESULT	EXCITATION ENERGY	SOURCE		DETECTOR		ANGLE
			TYPE	RANGE	TYPE	RANGE	
G,XN	ABX	THR- 24	C	10- 24	BF3-I		4PI

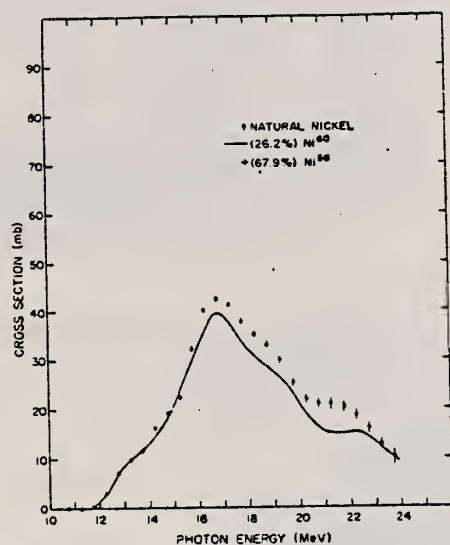


FIG. 2. Photoneutron cross section of natural nickel and the sum of Ni^{60} and Ni^{58} contributions.

ELEM. SYM.		
Ni		23
METHOD	REF. NO.	
	69 Ce 1	egf

REACTION	RESULT	EXCITATION ENERGY	SOURCE		DETECTOR		ANGLE
			TYPE	RANGE	TYPE	RANGE	
G.G	NOX	6-8	D	6-8	SCD-D	0-8	DST

TABLE 5
Energies and relative intensities of elastic and inelastic γ -transitions scattered from Ni

$E_{\gamma}(\text{keV})$	$I_{\gamma}(\text{rel})$	$I_{\gamma}(\text{rel})^a$	$E_{\gamma}(n, \gamma)_{Fe}^b$	$I_{\gamma}(n, \gamma)_{Fe}^b$
604 \pm 2	21.0 \pm 0.6	23 \pm 8	inel. trans.	
6266 \pm 4	3.0 \pm 0.5		elastic trans.	3.5
			$E_{\gamma}(n, \gamma)_{Fe} = 6269 \pm 8^b$	
6470 \pm 4	5.2 \pm 0.5	8 \pm 2	inel. trans.	
6977 \pm 4	3.5 \pm 0.8		elastic trans.	
7646	73.8 \pm 6.0	69 \pm 8	elastic trans.	32
			$E_{\gamma}(n, \gamma)_{Fe} = 7646 \pm 1^b$	

^a) Ref. ⁶).

^b) Ref. ¹¹).

REACTION	RESULT	EXCITATION ENERGY	SOURCE		DETECTOR		ANGLE
			TYPE	RANGE	TYPE	RANGE	
G,XN	SPC	11-85	C	85	CCH-D		135

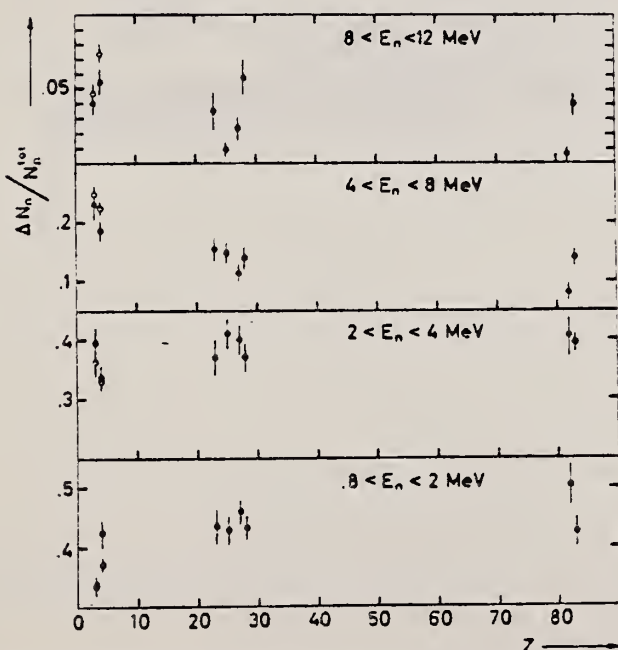


Fig. 1. - Percentage of the photoneutrons emitted at 135° in the respective energy interval as a function of Z , by a γ -ray bremsstrahlung beam with $E_{\gamma \max} = 85$ MeV. The open circles represent the values obtained at 90° for ^7Li and ^9Be .

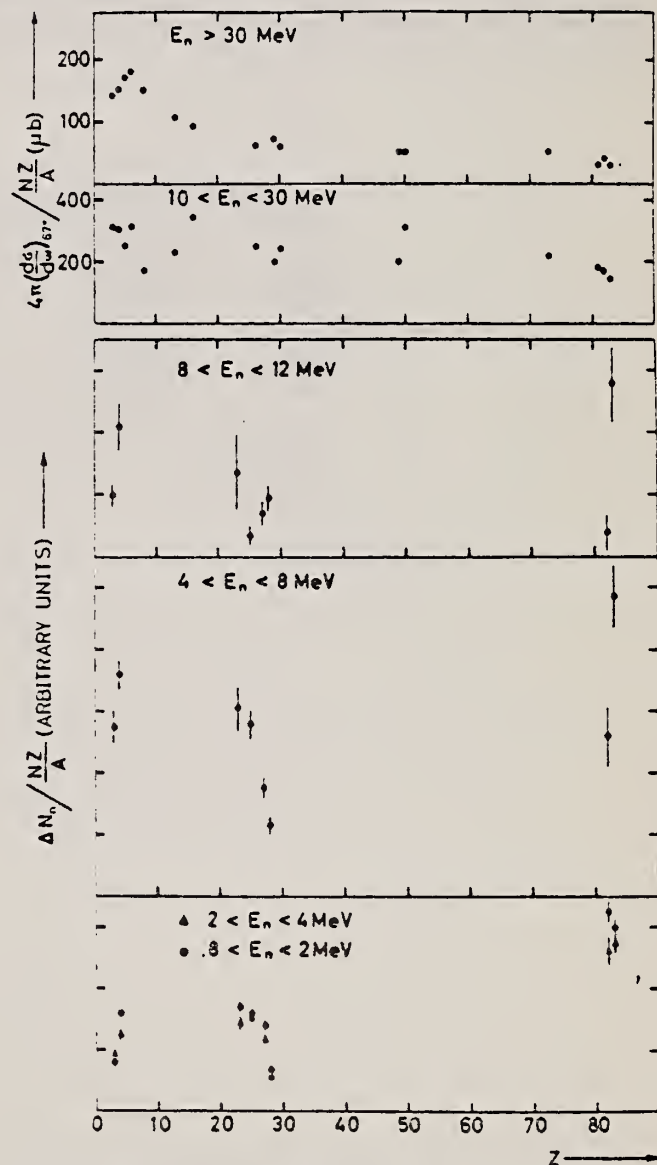


Fig. 2. - Number of photoneutrons emitted at 135° , normalized to the sum rule factor NZ/A , as a function of Z . In the upper part is reported the effective cross section divided by NZ/A for photoproduction of fast neutrons by 55-85 MeV bremsstrahlung photons as deduced by Kaushal *et al.* [1].

¹N. N. Kaushal *et al.*, Phys. Rev. **175**, 1330 (1968).

REF.			ELEM. SYM.			A	Z
Yu. P. Antuf'ev, V. L. Agranovich, V. G. Ganenko, V. S. Kuz'menko, I. I. Miroshnichenko, and P. V. Sorokin Yad. Fiz. <u>12</u> , 1143 (1970); Sov. J. Nucl. Phys. <u>12</u> , 627 (1971)			Ni				28
METHOD			REF. NO.				
			70 An 5				hmg
REACTION	RESULT	EXCITATION ENERGY	SOURCE		DETECTOR		ANGLE
			TYPE	RANGE	TYPE	RANGE	
E, p	RLY	90-999	C	999	TEL-D	80-265	DST

999 = 1140 MEV

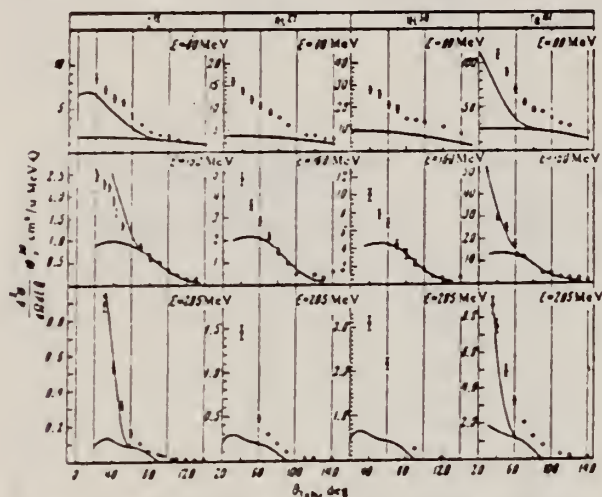


FIG. 1. Angular distributions of protons with energies of 80, 160, and 285 MeV produced from C^{12} , Al^{27} , Ni , and Ta^{181} nuclei by photons with maximum energy 1140 MeV. Only the statistical errors are shown.

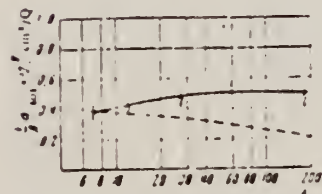


FIG. 3

FIG. 3. Total cross section for proton production per nucleus $E_{\gamma \text{ max}} = 1140 \text{ MeV}$. Dashed curve - theory from ref. 11.

¹¹K. S. Kölbig and B. Margolis, Nucl. Phys. B6, 85 (1968).

ELEM. SYM.	A	Z
Ni		28
REF. NO.		
71 Me 1		egf

METHOD		
--------	--	--

REACTION	RESULT	EXCITATION ENERGY	SOURCE		DETECTOR		ANGLE
			TYPE	RANGE	TYPE	RANGE	
G,F	ABY	THR-900	C	300-900	FRG-I		4PI

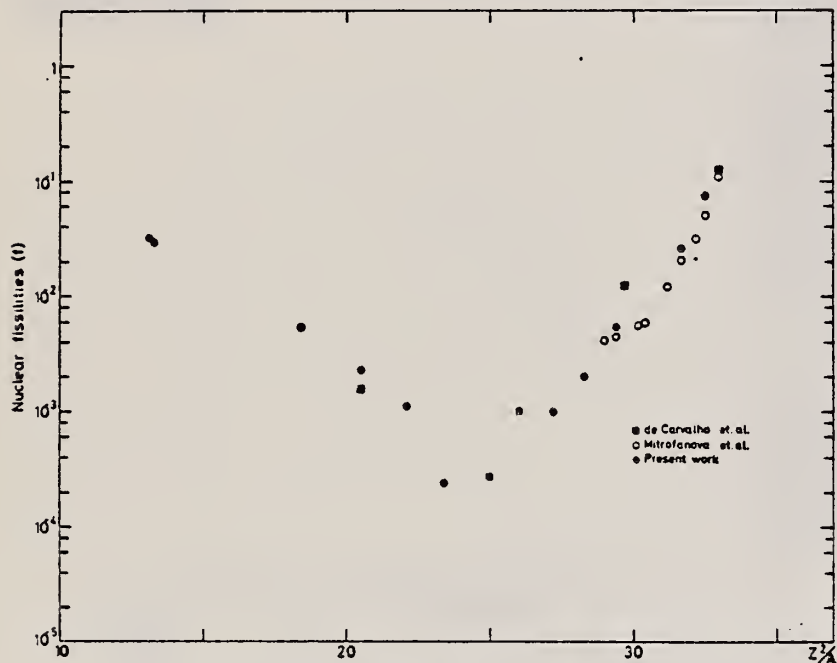


Fig. 2. Nuclear fission cross sections as a function of Z^2/A .

TABLE I

The constant fission cross sections above the threshold

Element	σ_f (cm ²)	Element	σ_f (cm ²)
Pb	$(5.0 \pm 0.2) \times 10^{-27}$	La	$(1.1 \pm 0.1) \times 10^{-29}$
Au	$(1.7 \pm 0.1) \times 10^{-27}$	Sn	$(4.3 \pm 1.1) \times 10^{-29}$
Ta	$(3.3 \pm 0.2) \times 10^{-28}$	Ag	$(8.4 \pm 2.0) \times 10^{-29}$
Yb	$(1.2 \pm 0.2) \times 10^{-28}$	Mo	$(1.7 \pm 0.4) \times 10^{-28}$
Ho	$(5.5 \pm 0.3) \times 10^{-29}$	Cu	$(6.6 \pm 1.2) \times 10^{-28}$
Gd	$(5.3 \pm 0.8) \times 10^{-29}$	Ni	$(5.8 \pm 0.1) \times 10^{-28}$
Nd	$(1.3 \pm 0.2) \times 10^{-29}$		

[over]

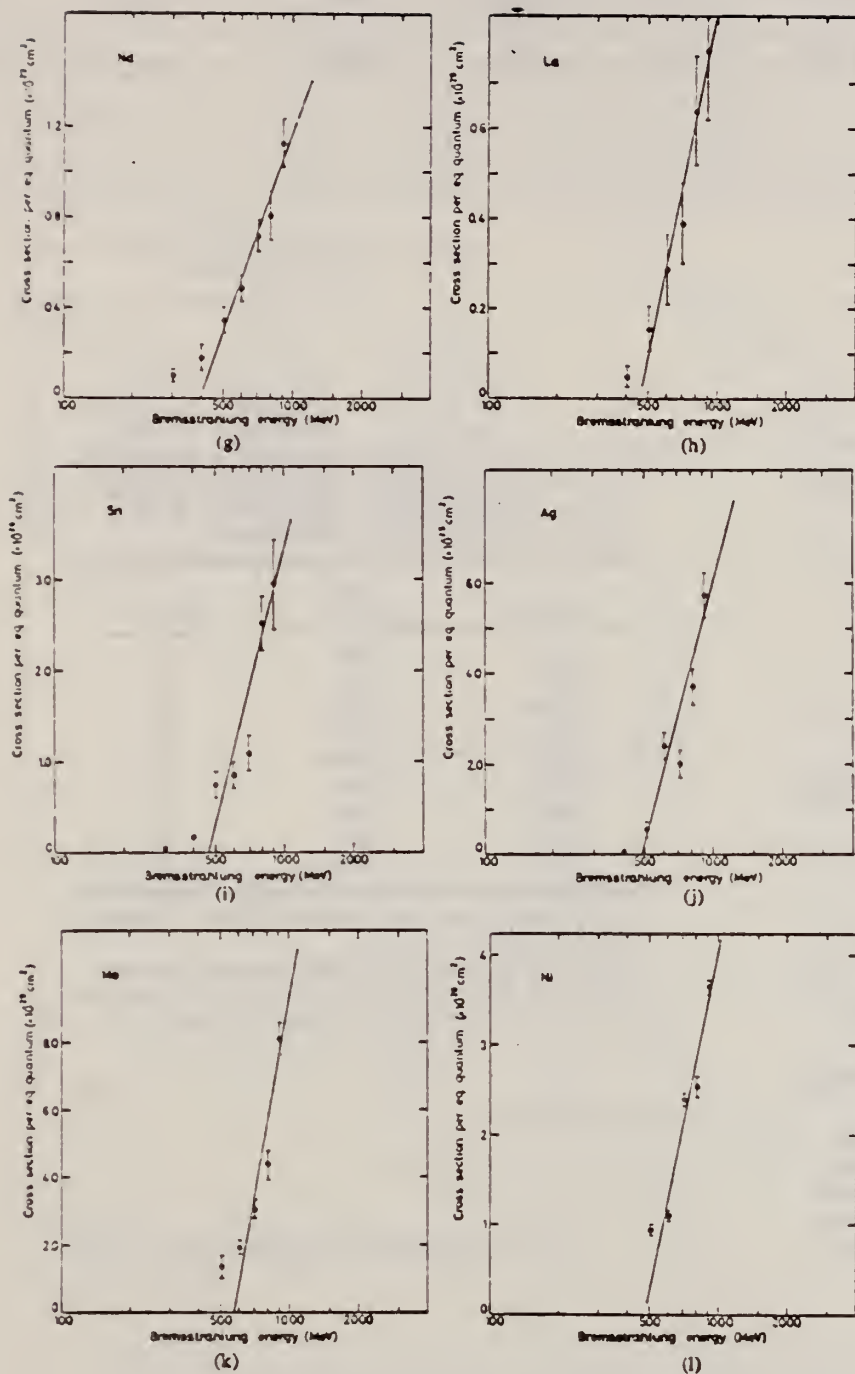


Fig. 1. Cross sections per equivalent quantum $\sigma_q(E)$ as a function of $\log E$.

REACTION	RESULT	EXCITATION ENERGY	SOURCE		DETECTOR		ANGLE
			TYPE	RANGE	TYPE	RANGE	
E, E/	ABX	0-240	D	500	MAG-D		60

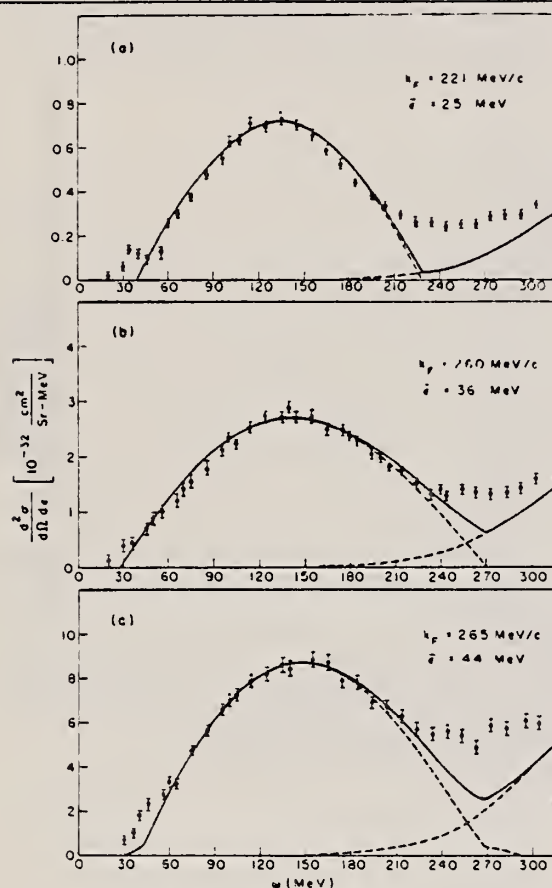


Table 1. Nuclear Fermi momentum h_F and average nucleon interaction energy $\bar{\epsilon}$ determined by least-squares fit of theory to quasielastic peak.

Nucleus	h_F (MeV/c) ^a	$\bar{\epsilon}$ (MeV) ^b
${}^3\text{Li}^6$	169	17
${}^6\text{C}^{12}$	221	25
${}^{12}\text{Mg}^{24}$	235	32
${}^{20}\text{Ca}^{40}$	251	28
${}^{28}\text{Ni}^{58.7}$	260	36
${}^{39}\text{Y}^{89}$	254	39
${}^{50}\text{Sn}^{118.7}$	260	42
${}^{73}\text{Ta}^{181}$	265	42
${}^{82}\text{Pb}^{208}$	265	44

^aThe fitting uncertainty in these numbers is approximately ± 5 MeV/c.

^bThe fitting uncertainty in these numbers is approximately ± 3 MeV. Simple estimates for $\bar{\epsilon}$ give numbers in reasonable agreement with those in the table.

Fig. 1. Cross sections $d^2\sigma/d\Omega d\epsilon$ versus electron energy loss $\omega = \epsilon_1 - \epsilon_2$ for inelastic scattering of 500-MeV electrons at 60° from (a) carbon, (b) nickel, and (c) lead. Solid lines are the results of the Fermi-gas calculation with the nuclear parameters indicated on the figure.

REF.

N. A. Keller and D. B. McConnell
Can. J. Phys. 50, 1554 (1972)

ELEM. SYM.

A

Z

Ni

28

METHOD

REF. NO.

72 Ke 4

hmg

REACTION	RESULT	EXCITATION ENERGY	SOURCE		DETECTOR		ANGLE
			TYPE	RANGE	TYPE	RANGE	
G,A	RLY	6-32	C	32	SCD-D		DST

TABLE 3 Observed angular distribution parameters for
32 MeV electron energy

Element	A_0	A_1/A_0	A_2/A_0
Ti	7.03 ± 0.15	0.073 ± 0.052	-0.286 ± 0.073
V	2.58 ± 0.06	0.037 ± 0.042	-0.126 ± 0.069
Fe	10.22 ± 0.30	0.006 ± 0.043	-0.333 ± 0.072
Co	6.80 ± 0.20	0.022 ± 0.048	$+0.016 \pm 0.077$
Ni	15.95 ± 0.49	0.051 ± 0.048	-0.213 ± 0.074
Cu	8.37 ± 0.28	0.076 ± 0.056	-0.035 ± 0.081
Zn	17.87 ± 0.61	0.004 ± 0.045	-0.270 ± 0.073
Ag	0.39 ± 0.01	0.115 ± 0.049	$+0.093 \pm 0.074$

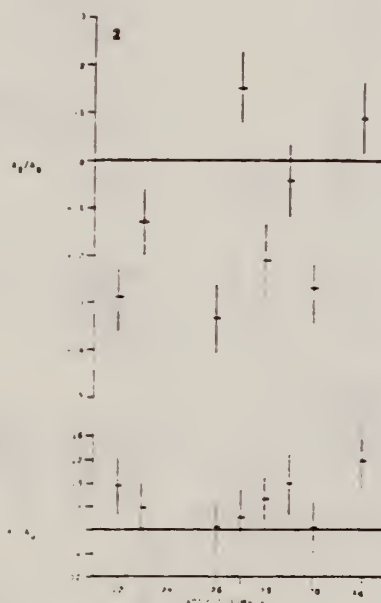


FIG. 2. Angular distributions for 32 MeV electron energy

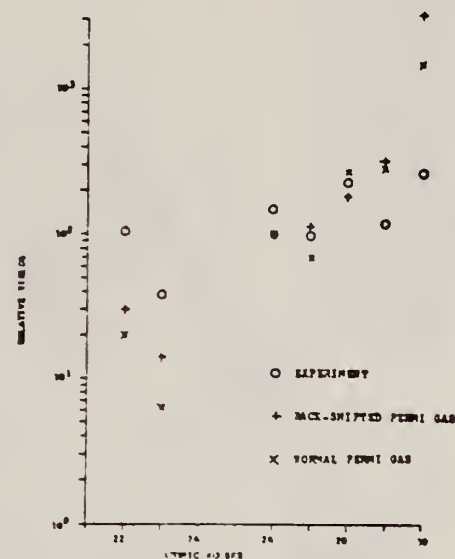


FIG. 13. Experimental and theoretical relative photo-alpha yields for 32 MeV electron beam energy.

REF.			ELEM. SYM.		A	Z
R.F. Barrett, J.R. Birkelund, B.J. Thomas, K.S. Lam, and H.H. Thies Nucl. Phys. <u>A210</u> , 355 (1973)			Ni			28
METHOD			REF. NO.			
			73 Ba 20			egf
REACTION	RESULT	EXCITATION ENERGY	SOURCE		DETECTOR	
			TYPE	RANGE	TYPE	RANGE
G ₂ N	NOX	THR- 27	C	10- 27	RF3-I	4PI

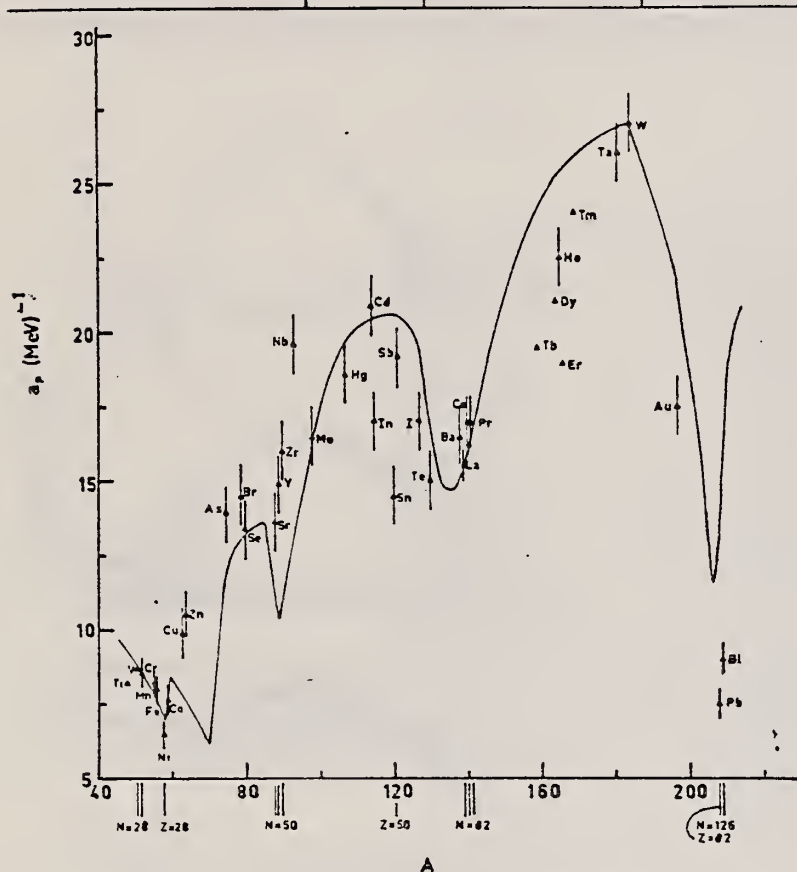


Fig. 12. Experimental values of the level density parameter a_p (Fermi gas formula plus pairing correction) versus atomic number A . The continuous curve is a least-squares fit to the data of a theoretical calculation from Newton ¹⁵.

- 1 H. Baba and S. Baba, Japan Atomic Energy Research Institute report JAERI-1183 (1969).
- 2 H. Baba, Nucl. Phys. A159, 625 (1970).
- 15 T.D. Newton, Can. J. Phys. 34, 804 (1956).

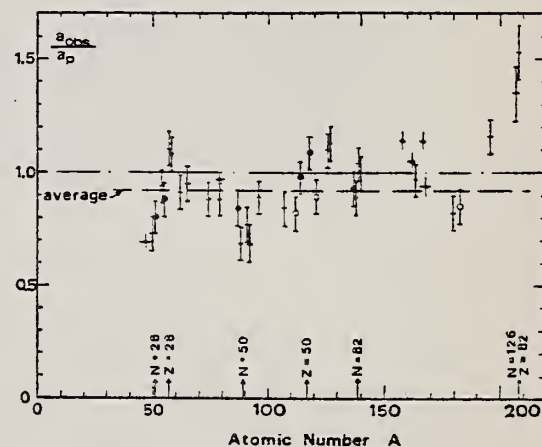


Fig. 15. Ratio a_{obs}/a_p versus atomic number A . Here a_{obs} is the level density parameter taken from the neutron resonance work of refs. ^{1,2}, and a_p is the level density parameter derived from the present (γ, n) work. Filled circles represent points where nuclei in the neutron resonance and in the (γ, n) experiment were the same. Open circles represent points where the respective nuclei were approximately matched. Triangles represent points which are based on measurement of neutron mean energies at two bremsstrahlung energies only.

(over)

TABLE 3

Comparison of experimental and theoretical data on nuclear level densities with Fermi gas formulae, and comparison of nuclear level density parameters from (γ, n) and n-resonance absorption experiments

Target	N (residual nucleus) ^{a)}	Goodness of fit ^{b)} no with p.c. p.c.	$\bar{E}_n(24)$ (MeV) ^{c)}	T (MeV) ^{d)}	a_p (MeV ⁻¹) ^{e)}	a_{nR} (MeV ⁻¹) ^{f)}	a_{nR}/a_p
Ti ^{g)}	23 8%		1.93		8.1- ^{4.7} Ti	6.41- ^{4.7} Ti	0.79
	24 8%						
	25 73%						
	26 5%						
	27 5%						
V ^{g)}	27 100%		1.96		8.7- ^{5.0} V	6.35- ^{5.1} V	0.73
Cr	25 4%	P	1.89		8.6- ^{5.1} Cr	6.9- ^{5.1} Cr	<u>0.80</u>
	27 84%						
	28 10%						
	29 2%						
Mn	29 100%	V.P.	2.1		8.2- ^{5.4} Mn	7.82- ^{5.6} Mn	0.94
Fe	27 6%	F	1.96		8.0- ^{5.5} Fe	7.06- ^{5.5} Fe	<u>0.88</u>
	29 92%						
	30 2%						
Co	31 100%	P	2.12		7.7- ^{5.3} Co	8.35- ^{5.6} Co	1.08
Ni (Z = 28)	29 68%	V.P.	2.04	1.4	6.5- ^{5.7, 7.2} Ni	7.19- ^{5.9} Ni	1.10
	31 26%						
	32 1%						
	33 4%						
	35 1%						
Cu	33 69%	V.P.	1.78	1.0	9.8- ^{6.2} Cu	8.90- ^{6.4} Cu	0.91
	35 31%						
Zn	33 49%	F	1.61		10.5- ^{6.4, 4} Zn	10.0- ^{6.7} Zn	0.95
	35 28%						
	36 4%						
	37 19%						
As	41 100%	V.P.	1.44		14.5- ^{7.4} As	12.81- ^{7.6} As	0.88
Se ^{g)}	41 9%		1.39		13.3- ^{7.8} Se	12.8- ^{7.8} Se	<u>0.97</u>
	42 8%						
	43 24%						
	45 50%						
	47 9%						
Br	43 45%	V.P.	1.41		14.5- ^{7.9} Br	12.69- ^{8.0} Br	0.88
	45 49%						
Sr	47 10%	F	1.31		13.6- ^{8.7} Sr	11.4- ^{8.7} Sr	<u>0.84</u>
	48 7%						
	49 83%						

^{a)} Neutron numbers and abundances of respective residual nuclei in (γ, n) experiments.

^{b)} These give an assessment of the goodness of fit of a calculated E_n versus E_0 curve to the observed data, using the Fermi gas level density formula both without and with pairing corrections.

^{c)} Bremsstrahlung photon neutron mean energies \bar{E}_n for peak bremsstrahlung energy $E_0 = 24$ MeV.

^{d)} Nuclear temperature from fit with constant-temperature formula.

^{e)} Level density parameter a_p derived from the present (γ, n) experiment, using a Fermi gas formula plus pairing correction, and corresponding residual nucleus (the atomic weight shown is the weighted average of atomic weights of the respective isotopes present).

^{f)} As column 7, but using data on n-resonance absorption from refs. ^{1, 2}.

^{g)} Measurements of $\bar{E}_n(E_0)$ for these nuclei were made only for $E_0 = 21, 23$ and 24 MeV.

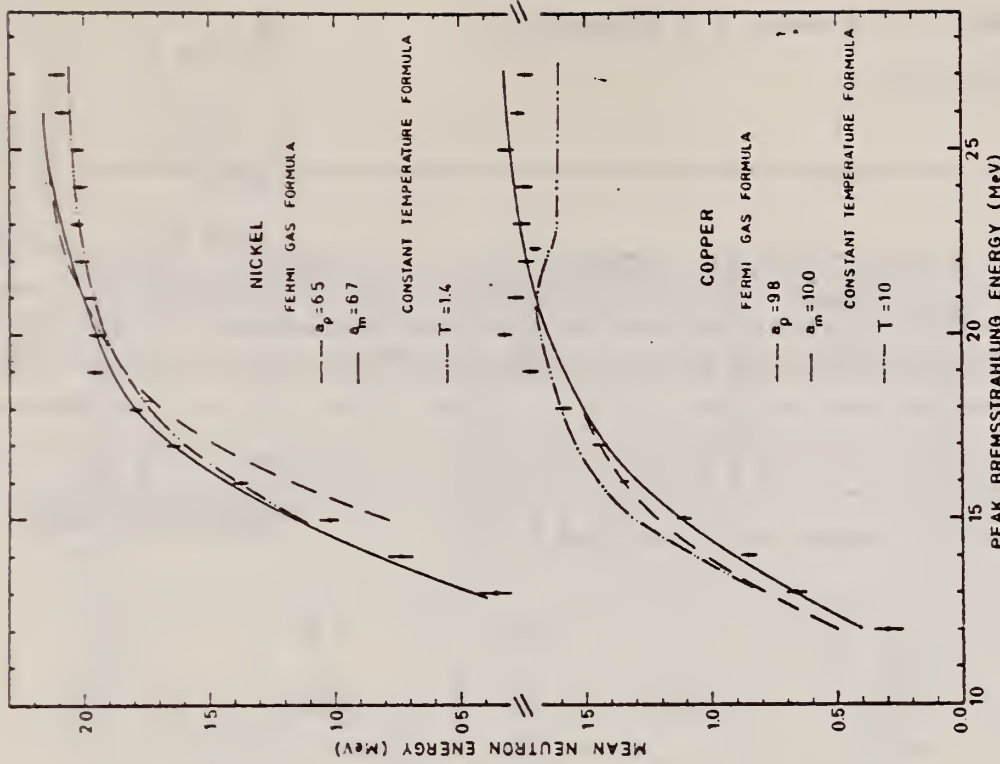


Fig. 6. Same as fig. 5, for nickel and copper.

ELEM. SYM.	A	Z
Ni		28
REF. NO.		
74 Wh 3		hmg

METHOD

REACTION	RESULT	EXCITATION ENERGY	SOURCE		DETECTOR		ANGLE
			TYPE	RANGE	TYPE	RANGE	
E, E/	ABX	0-300	D	500	MAG-D		60

QUASIELASTIC SCAT

See further analysis of this data in reference 79Zil

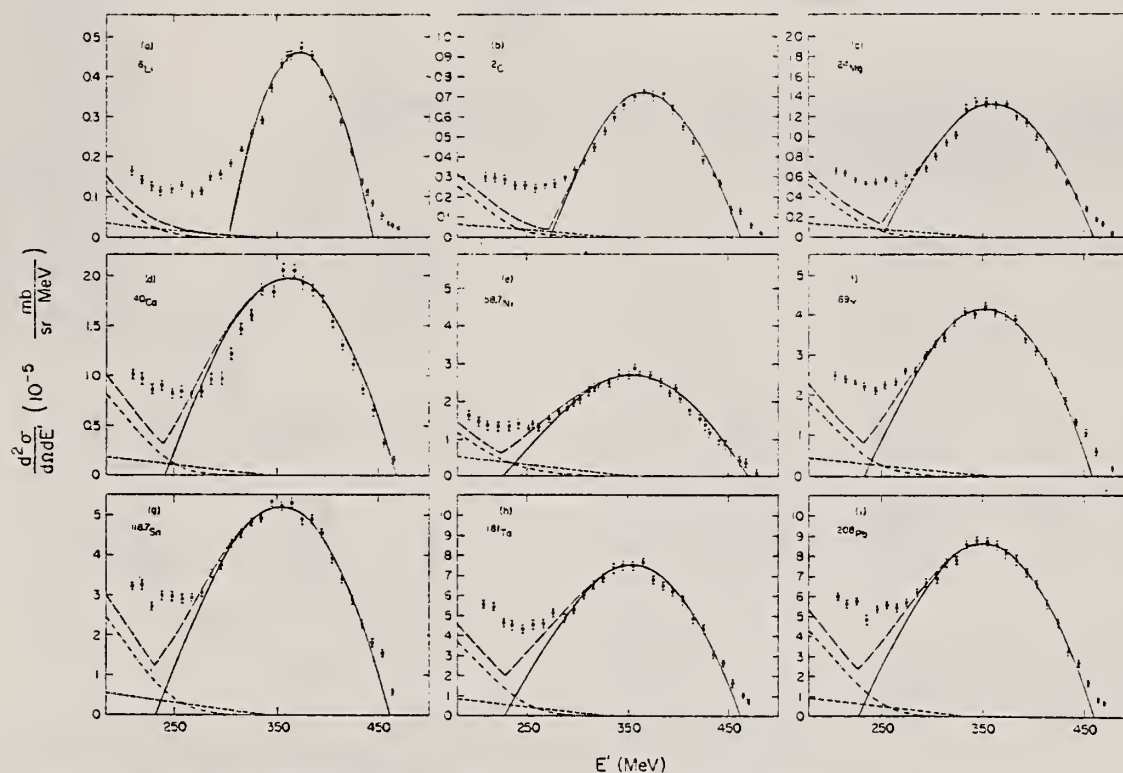


FIG. 1. The measured quasilastic peaks; the errors on the data points do not include an over-all 3% normalization uncertainty. The solid curve is a fit by the Fermi-gas model which yielded k_F (in MeV/c) and $\bar{\epsilon}$ (in MeV) as follows: (a) ^6Li (169, 17); (b) ^{12}C (221, 25); (c) ^{24}Mg (235, 32); (d) ^{40}Ca (249, 33); (e) ^{58}Ni (260, 36); (f) ^{89}Y (254, 39); (g) $^{118.7}\text{Sm}$ (260, 42); (h) ^{181}Ta (265, 42); (i) ^{208}Pb (265, 44). The fitting uncertainty in k_F is ± 5 MeV/c and in $\bar{\epsilon}$ it is ± 3 MeV. The small-amplitude dashed curve is the s-wave π -production contribution, the dot-dashed curve is the isobar excitation, and the large-amplitude dashed curve is the total result.

(over)

TABLE I. Proton-normalized and radiative-corrected cross sections $d^2\sigma/d\Omega dE' = (N \pm \Delta N) \times 10^{-28}$ in mb/sr MeV, for $E = 500$ MeV and $\theta = 60^\circ$.

E' (MeV)	^6Li			^{12}C			^{21}Ne			^{40}Ca			^{58}Ni			^{89}Y			^{110}Sn			$^{180.35}\text{Pt}$			^{208}Pb		
	N	ΔN	n	Λ	$\Delta\Lambda$	n	N	ΔN	n	N	ΔN	n	N	ΔN	n	N	ΔN	n	N	ΔN	n	N	ΔN	n	N	ΔN	n
460.0	1.79	0.19	7	3.83	0.42	7	1.22	0.17	6	1.71	0.19	6
474.0	1.02	0.13	7
470.0	1.72	0.18	7	5.75	0.52	7	1.55	0.15	6	3.90	0.29	6	5.85	0.41	6
464.0	2.19	0.29	7	1.46	0.11	6	1.91	0.17	6	2.72	0.15	6	4.48	0.33	6	5.68	0.37	6	8.32	0.71	6	7.09	0.67	6	7.00	0.68	6
460.0	2.96	0.30	7	1.20	0.09	6	2.58	0.19	6
454.1	5.02	0.47	7	9.31	0.71	7	2.36	0.20	6	1.20	0.17	6	7.00	0.41	6	1.07	0.05	5	1.85	0.09	5	1.70	0.11	5	2.31	0.11	5
450.0	8.92	0.47	6	1.03	0.05	5	1.83	0.09	5
444.3	8.68	0.58	7	1.26	0.07	6	4.11	0.25	6	6.67	0.27	6	1.02	0.05	5	1.33	0.05	5	2.77	0.14	5	2.74	0.12	5
440.0	1.11	0.06	6	2.59	0.13	6	5.23	0.26	6	3.43	0.16	5	3.24	0.13	5
434.2	1.32	0.06	6	2.99	0.11	6	5.50	0.26	6	8.71	0.35	6	1.19	0.05	5	1.90	0.07	5	2.27	0.09	5	3.14	0.15	5	3.34	0.14	5
430.0	1.40	0.07	5	2.11	0.08	5	2.77	0.11	5
424.3	2.12	0.08	6	3.75	0.15	6	7.31	0.29	6	1.12	0.04	5	1.54	0.08	5	2.31	0.09	5	2.88	0.12	5	4.43	0.18	5	4.74	0.19	5
414.4	2.88	0.12	6	1.75	0.19	6	8.78	0.35	6	1.32	0.05	5	1.78	0.10	5	2.88	0.11	5	3.40	0.14	5	4.98	0.20	5	5.64	0.23	5
404.5	3.51	0.14	6	5.46	0.22	6	1.02	0.04	5	1.56	0.06	5	2.09	0.08	5	3.09	0.12	5	3.90	0.16	5	5.89	0.24	5	6.57	0.26	5
400.0	6.25	0.25	6	1.09	0.04	5	2.35	0.09	5	3.34	0.13	5	4.29	0.17	5	6.56	0.27	5	7.00	0.28	5
394.7	4.16	0.17	6	6.32	0.26	6	1.15	0.05	5	1.75	0.07	5	2.22	0.09	5	3.41	0.14	5	4.50	0.18	5	0.29	0.25	5	7.25	0.29	5
385.7	4.55	0.18	6	7.09	0.28	6	1.21	0.05	5	1.86	0.07	5	2.51	0.10	5	3.91	0.16	5	4.88	0.19	5	6.30	0.26	5	7.88	0.32	5
374.9	4.76	0.19	6	6.97	0.28	6	1.33	0.05	5	1.91	0.08	5	2.72	0.11	5	4.02	0.16	5	4.88	0.19	5	6.87	0.28	5	8.19	0.33	5
365.0	4.56	0.18	6	7.28	0.29	6	1.32	0.05	5	2.08	0.08	5	2.69	0.10	5	4.01	0.16	5	5.34	0.21	5	7.77	0.31	5	8.61	0.34	5
360.0	4.50	0.18	6	6.61	0.28	6	1.32	0.05	5	2.88	0.11	5	4.11	0.16	5	5.69	0.23	5	7.92	0.33	5	8.42	0.34	5
355.2	4.35	0.17	6	6.97	0.28	6	1.36	0.05	5	2.08	0.08	5	2.69	0.11	5	4.23	0.17	5	5.22	0.21	5	7.51	0.30	5
345.3	3.68	0.15	6	6.51	0.26	6	1.35	0.05	5	1.85	0.07	5	2.72	0.11	5	4.02	0.16	5	5.37	0.21	5	7.59	0.30	5	8.83	0.35	5
335.4	2.90	0.12	6	5.91	0.24	6	1.29	0.05	5	1.87	0.08	5	2.48	0.10	5	4.08	0.16	5	4.92	0.19	5	7.44	0.29	5	8.68	0.35	5
325.5	2.59	0.10	6	5.21	0.21	6	1.05	0.04	5	1.61	0.07	5	2.48	0.11	5	3.78	0.15	5	4.83	0.19	5	6.93	0.28	5	7.81	0.31	5
320.0	2.35	0.09	5	3.34	0.14	5	4.53	0.18	5
315.7	2.16	0.10	6	4.43	0.18	6	9.41	0.38	6	1.47	0.06	5	2.26	0.09	5	3.43	0.14	5	4.34	0.17	5	6.61	0.26	5	7.76	0.31	5
305.8	1.84	0.09	6	4.79	0.15	6	8.61	0.32	6	1.23	0.05	5	2.03	0.08	5	3.27	0.13	5	4.32	0.17	5	6.11	0.24	5	6.92	0.28	5
300.0	1.97	0.08	5	3.11	0.12	5	4.03	0.16	5
295.9	1.55	0.09	6	3.38	0.14	6	6.77	0.29	6	9.97	0.40	6	1.80	0.07	5	3.02	0.12	5	3.74	0.15	5	6.38	0.22	5	6.73	0.27	5
285.9	1.50	0.09	6	2.96	0.14	6	6.64	0.31	6	9.73	0.39	6	1.72	0.07	5	2.00	0.13	5	3.55	0.15	5	4.92	0.23	5	6.30	0.29	5
276.2	1.14	0.08	6	2.64	0.13	6	6.01	0.32	6	8.35	0.41	6	1.50	0.07	5	2.64	0.13	5	3.10	0.15	5	6.22	0.24	5	5.73	0.30	5
260.3	1.08	0.08	6	2.61	0.11	6	5.32	0.33	6	8.57	0.43	6	1.31	0.08	5	2.37	0.14	5	2.72	0.16	5	4.62	0.26	5	5.51	0.31	5
260.0	1.39	0.08	5	1.95	0.13	5	2.94	0.18	5
256.4	1.28	0.09	6	2.41	0.15	6	5.71	0.35	6	8.33	0.45	6	1.27	0.08	5	2.27	0.14	5	2.87	0.18	5	4.57	0.28	5	5.63	0.33	5
246.0	1.20	0.09	6	2.55	0.16	6	5.47	0.36	6	8.55	0.48	6	1.39	0.09	5	2.14	0.14	5	2.95	0.19	5	4.33	0.28	5	5.40	0.35	5
230.7	1.15	0.10	6	2.54	0.16	6	5.18	0.38	6	8.71	0.51	6	1.34	0.09	5	2.24	0.15	5	3.02	0.20	5	4.35	0.30	5	4.90	0.34	5
226.8	1.27	0.11	6	2.88	0.19	6	5.62	0.42	6	8.72	0.51	6	1.29	0.10	5	2.29	0.16	5	2.73	0.20	5	4.57	0.30	5	5.88	0.37	5
210.9	1.43	0.14	6	2.91	0.21	6	6.35	0.49	6	9.81	0.56	6	1.31	0.10	5	2.38	0.17	5	3.28	0.22	5	5.42	0.36	5	6.70	0.38	5
207.0	1.60	0.16	6	2.94	0.21	6	6.59	0.52	6	1.02	0.06	5	1.13	0.11	5	2.51	0.18	5	3.24	0.22	5	5.58	0.37	5	6.11	0.40	5
197.2	1.78	0.17	6	3.42	0.24	6	7.01	0.59	6	1.59	0.12	5	2.77	0.20	5	3.43	0.24	5	5.67	0.38	5	5.99	0.41	5

V. Emma, S. Lo Nigro, C. Milone
Nucl. Phys. A257, 438 (1976)

ELEM. SYM.	A	Z
Ni		28
REF. NO.		
76 Em 2		egf

REACTION	RESULT	EXCITATION ENERGY	SOURCE		DETECTOR		ANGLE
			TYPE	RANGE	TYPE	RANGE	
G, F	ABY	THR-999	C	999	TRK-I		4PI

TABLE 1

Measured values of σ_q at $E = 1000$ MeV and deduced values of σ_k assumed constant from E_0 to 1000 MeV

999 = 1 GEV

Element	Z^2/A	σ_q (mb)	E_0 (MeV)	σ_k (mb)
Bi	32.96	12.3 ± 0.6	200	7.6 ± 0.6
Pb	32.45	5.4 ± 0.4	220	3.6 ± 0.3
Tl	32.10	4.1 ± 0.3	230	2.8 ± 0.3
Au	31.68	2.0 ± 0.15	240	1.4 ± 0.2
Pt	31.18	1.1 ± 0.08	255	$(8 \pm 0.7) \times 10^{-1}$
Re	30.21	$(3.7 \pm 0.3) \times 10^{-1}$	280	$(2.9 \pm 0.3) \times 10^{-1}$
W	29.78	$(3.5 \pm 0.3) \times 10^{-1}$	290	$(2.8 \pm 0.3) \times 10^{-1}$
Ta	29.45	$(3.3 \pm 0.3) \times 10^{-1}$	300	$(2.7 \pm 0.3) \times 10^{-1}$
Hf	29.04	$(1.7 \pm 0.2) \times 10^{-1}$	310	$(1.4 \pm 0.2) \times 10^{-1}$
Yb	28.31	$(1.3 \pm 0.1) \times 10^{-1}$	330	$(1.2 \pm 0.1) \times 10^{-1}$
Tm	28.18	$(7.5 \pm 0.8) \times 10^{-2}$	335	$(6.8 \pm 0.8) \times 10^{-2}$
Ho	27.21	$(3.6 \pm 0.4) \times 10^{-2}$	355	$(3.5 \pm 0.4) \times 10^{-2}$
Dy	26.80	$(2.6 \pm 0.3) \times 10^{-2}$	360	$(2.5 \pm 0.3) \times 10^{-2}$
Tb	26.58	$(2.5 \pm 0.3) \times 10^{-2}$	370	$(2.5 \pm 0.3) \times 10^{-2}$
Gd	26.04	$(1.6 \pm 0.2) \times 10^{-2}$	380	$(1.7 \pm 0.2) \times 10^{-2}$
Sm	25.56	$(1.3 \pm 0.2) \times 10^{-2}$	390	$(1.4 \pm 0.2) \times 10^{-2}$
Nd	24.96	$(9.2 \pm 0.9) \times 10^{-3}$	405	$(1 \pm 0.1) \times 10^{-2}$
Ce	24.00	$(8 \pm 0.9) \times 10^{-3}$	420	$(9 \pm 1) \times 10^{-3}$
La	23.39	$(8.4 \pm 0.9) \times 10^{-3}$	430	$(1 \pm 0.1) \times 10^{-3}$
Sb	21.36	$(1.2 \pm 0.2) \times 10^{-2}$	460	$(1.5 \pm 0.3) \times 10^{-2}$
Te	21.19	$(8.8 \pm 1) \times 10^{-3}$	465	$(1.2 \pm 0.2) \times 10^{-2}$
Sn	21.06	$(1.3 \pm 0.2) \times 10^{-2}$	465	$(1.7 \pm 0.3) \times 10^{-2}$
Cd	20.49	$(1.7 \pm 0.3) \times 10^{-2}$	470	$(2.2 \pm 0.4) \times 10^{-2}$
Ag	20.47	$(2 \pm 0.3) \times 10^{-2}$	470	$(2.6 \pm 0.4) \times 10^{-2}$
Zn	13.76	$(2 \pm 0.4) \times 10^{-1}$	515	$(3 \pm 0.6) \times 10^{-1}$
Cu	13.44	$(2.4 \pm 0.5) \times 10^{-1}$	515	$(3.6 \pm 0.8) \times 10^{-1}$
Ni	13.35	$(2.4 \pm 0.5) \times 10^{-1}$	510	$(3.6 \pm 0.8) \times 10^{-1}$
Fe	12.10	$(3 \pm 0.6) \times 10^{-1}$	510	$(4.4 \pm 0.9) \times 10^{-1}$

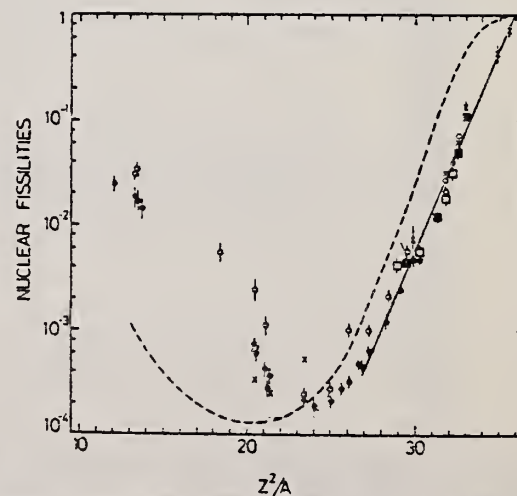
4. A.V. Mitrofanova et al.
Sov. J. Nucl. Phys. 6,
512 (1968).

7. T. Methasiri et al., Nucl.
Phys. A167, 97 (1971).

12. J.R. Nix et al., Nucl. Phys.
81, 61 (1966).

20. N.A. Perfilov et al., JETP
(Sov. Phys.) 14, 623 (1962);
Proc. Symp. on the physics &
chemistry of fission, Salzburg
1965, vol. 2 (IAEA) Vienna,
1965, p.283.

Fig. 2. Nuclear fissilities as a function of Z^2/A . Experimental points: solid circles represent our data; squares, the data from ref. 4); open circles, the data from ref. 7); and crosses, the data from (p,f) experiments²⁰). The straight line is the best fit calculated from our data for $Z^2/A > 26$. The dashed curve is the curve VI calculated by Nix and Sassi¹²).



REF. V.G. Vlasenko, V.A. Gol'dshtein, A.V. Mitrofanova, V.I. Noga,
Yu.N. Ranuuk, V.I. Startsev, P.V. Sorokin, Yu.N. Telegin
Yad. Fiz. 23, 504 (1976)
Sov. J. Nucl. Phys. 23, 265 (1976)

ELEM. SYM.	A	Z
Ni		28

METHOD

REF. NO.	
76 V1 1	hmg

REACTION	RESULT	EXCITATION ENERGY	SOURCE		DETECTOR		ANGLE
			TYPE	RANGE	TYPE	RANGE	
$E, E/$	ABX	100-500	D	1* 2	MAG-D		DST

*E IN GEV, 1.2, 1.36

Elastic electron scattering has been used to measure the total hadronic cross sections for absorption of photons with energy 100-500 MeV by nuclei of C, Al, Ni, Mo, and W. The results obtained are compared with calculations carried out in the impulse approximation.

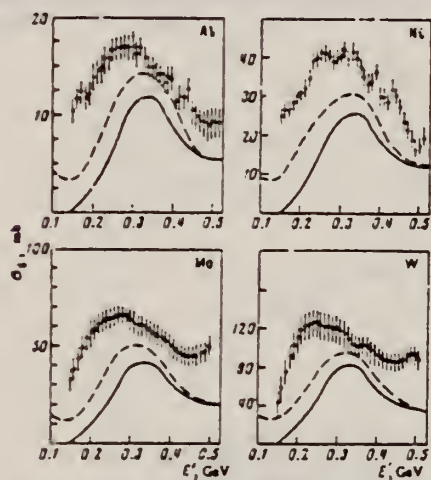


FIG. 5. Total hadronic cross sections for absorption of photons by nuclei.

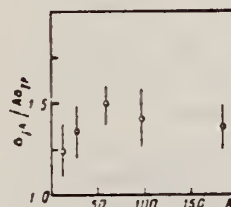


FIG. 6. The ratio $\sigma_t/A\sigma_p$ as a function of A for $h=0.32$ GeV.

ELEM. SYM.	A	Z
Ni		28
REF. NO.		
79F12		hg

METHOD					
REACTION	RESULT	EXCITATION ENERGY	SOURCE		ANGLE
			TYPE	RANGE	
E,A	SPC	UKN	D	120	DST

This paper presents energy spectra of α particles emitted following the bombardment of ^{27}Al , ^{58}Ni , ^{92}Mo , ^{94}Mo , and ^{197}Au with 120-MeV electrons, together with α -particle angular distributions from ^{197}Au and ^{58}Ni for $E_\alpha = 30$ and 50 MeV. The data are compared with preequilibrium exciton-model and statistical-model calculations. It is concluded that few-step processes are dominant in the production of α particles with energies above 20 MeV.

PREEQUILIB A EMISS

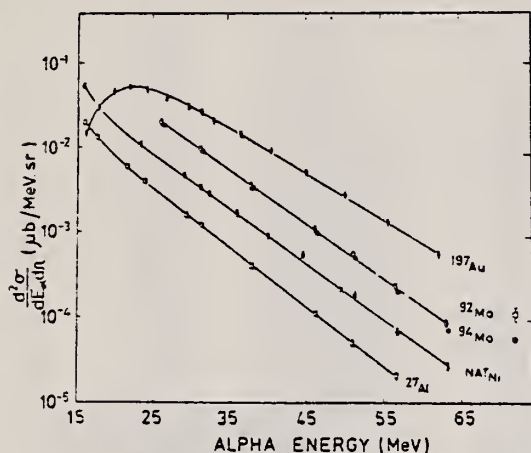


FIG. 1. α -particle energy spectra at $\theta_\alpha = 30^\circ$, for $E_e = 120$ MeV. Errors shown are the sum of statistical and systematic contributions. The solid lines are a guide to the eye.

TABLE I. Temperatures corresponding to the preequilibrium component of the (e, α) reaction, derived from energy spectra at $\theta_\alpha = 30^\circ$ for $E_e = 120$ MeV.

Target	Temperature ^a (MeV)
^{27}Al	5.3
^{58}Ni	5.5
^{92}Zn	5.4
^{92}Mo	5.6
^{94}Mo	5.4
^{197}Au	6.1

^aError is ± 0.2 MeV.

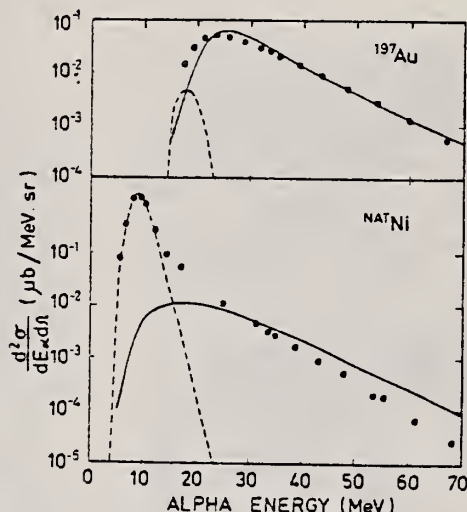


FIG. 2. α -particle energy spectra at $\theta_\alpha = 30^\circ$, for $E_e = 120$ MeV. The solid circles are experimental points. The solid lines are the results of preequilibrium exciton-model calculations and the dashed lines are the results of statistical calculations neglecting photon absorption above $E_\gamma = 33$ MeV.

(over)

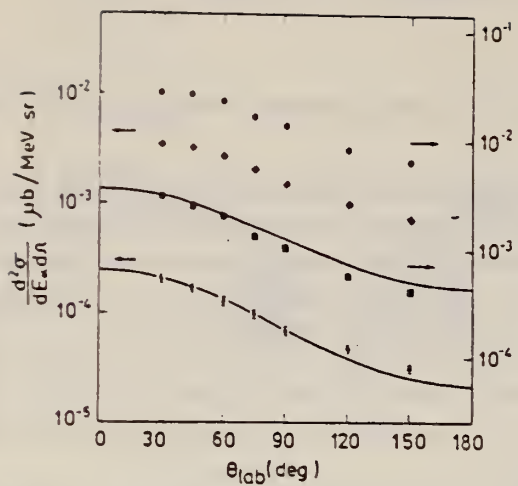


FIG. 3. α -particle angular distributions at $E_p = 120$ MeV for ^{137}Au (shown as circles for $E_\alpha = 30$ MeV and squares for $E_\alpha = 50$ MeV) and ^{226}Nl (shown as diamonds for $E_\alpha = 30$ MeV and stars for $E_\alpha = 50$ MeV). The solid lines are the result of simple kinematic calculations described in the text. The sum of statistical and systematic errors is shown where it exceeds the size of the points.

ELEM. SYM.	A	Z
Ni		28
REF. NO.		
80 Mc 6	hg	

METHOD			SOURCE		DETECTOR		ANGLE
REACTION	RESULT	EXCITATION ENERGY	TYPE	RANGE	TYPE	RANGE	
E,A	ABX	28-120	D	28-120	MAG-D		DST
G,A	ABY	6-120	C	28-120	MAG-D		DST

Abstract. New data on electron- and bremsstrahlung-induced 8 MeV α -particle emission from Ni are shown to be consistent with statistical decay of the excited nucleus. This result is in marked disagreement with a recent analysis of a similar experiment but in good agreement with (α, α') coincidence experiments.

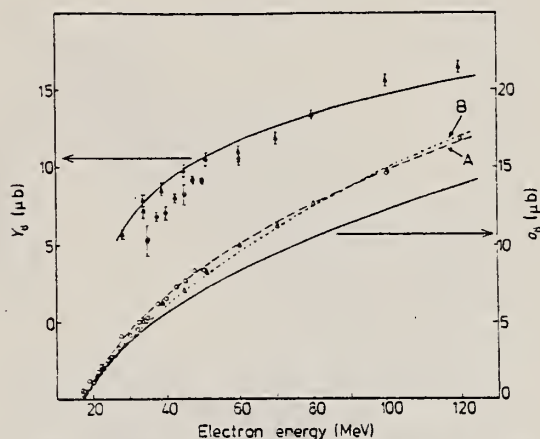


Figure 1. Excitation functions for electron- (open symbols) and bremsstrahlung- (closed symbols) induced yields of 7.5-8.5 MeV α particles from natural nickel. Statistical uncertainties are shown or are smaller than the size of the symbols; the systematic uncertainties are $\leq 7\%$. The triangles show the present data and the circles represent the equivalent data derived from the results of Wolyneć *et al* (1979) normalised to the present radiator thickness of 0.169 g cm^{-2} . The full curves result from folding the bremsstrahlung and E1 virtual photon spectra with the (γ, α) cross section of figure 2. The broken curve A is the result of multiplying the E1-only calculation by a factor of 1.2, while the broken curve B is the result of including a 10% EWSR E2 contribution.

Ni
A=58

NICKEL
Z=28

Ni
A=58

Ni
A=58

J.H. Carver, W. Turchinets
Proc. Phys. Soc. 73, 585 (1959)

Ni

58

28

METHOD

Synchrotron; proton, neutron cross sections; radioactivity

REF. NO.

59 Ca 4

NVB

REACTION	RESULT	EXCITATION ENERGY	SOURCE		DETECTOR		ANGLE
			TYPE	RANGE	TYPE	RANGE	
G,P	ABX	12 - 32	C	12 - 32	ACT-I		4PI
G,N	ABX	12 - 32	C	12 - 32	ACT-I		4PI
G,NP 741+	ABX	12 - 32	C	12 - 32	ACT-I		4PI

$$\frac{\int_0^{32} \sigma(\gamma, p) dE}{\int_0^{32} \sigma(\gamma, n) dE} = 2.35 \pm 0.20$$

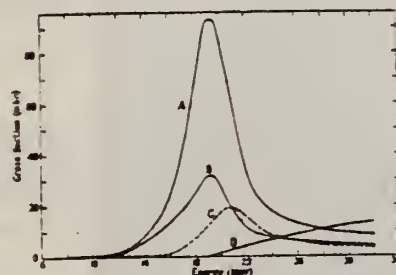
741

Figure 2. Excitation functions for the photodisintegration of nickel: A, $^{60}\text{Ni}(\gamma, p)$; B, $^{60}\text{Ni}(\gamma, n)$; C, $^{60}\text{Ni}(\gamma, p)$; D, $^{60}\text{Ni}(\gamma, np + \gamma, 2n)$.

Table 2

(1)	(2)	(3)	(4)	(5)
$^{60}\text{Ni}(\gamma, n)$	0.032	4.4	19.0	0.22 ± 0.03
$^{60}\text{Ni}(\gamma, p)$	0.093	4.2	19.5	0.52 ± 0.09
$^{60}\text{Ni}(\gamma, pn + \gamma, 2n)$	0.013	—	> 32	$> 0.10 \pm 0.02$
$^{60}\text{Ni}[(\gamma, n) + (\gamma, p) + (\gamma, pn) + (\gamma, 2n)]$	0.125	4.8	19.5	0.84 ± 0.10
$^{60}\text{Ni}(\gamma, p)$	0.019	5.2	22	0.13 ± 0.02

(1) Reaction; (2) σ_{max} (barns); (3) $\Gamma(\frac{1}{2}\sigma_{\text{max}})$ (MeV); (4) $E_{\sigma_{\text{max}}}$ (MeV);

(5) $\int_0^{32} \sigma dE$ (MeV barns).

Elem. Sym.	A	Z
Ni	58	28
Ref. No. 59 Ro 2		
EH		

Method 24 MeV betatron; neutron yield; proportional flow counter; r chamber

Reaction	E or ΔE	E_0	Γ	$\int \sigma dE$	$J\pi$	Notes
$Ni^{58}(\gamma, n)$	Bremss. 24	20.5	$\Gamma_{1/2}$ 7.2 MeV	$\int_0^{24} = 0.20 \text{ MeV-b}$		$\sigma_n = 29 \text{ mb}$ (Katz-Cameron method)
		20.5	8.0 MeV	$\int_0^{24} = 0.16 \text{ MeV-b}$		$\sigma_n = 21 \text{ mb}$ (Penfold-Leiss method)

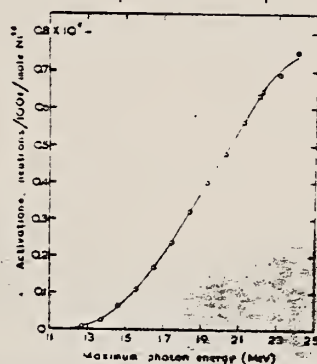


Fig. 2. Activation values for the reaction $Ni^{58}(\gamma, n)Ni^{57}$ as a function of maximum photon energy.

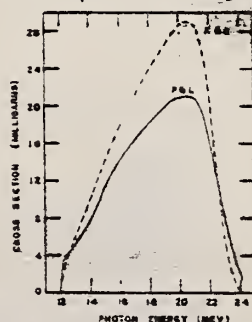


Fig. 3. Cross-section curves for the reaction $Ni^{58}(\gamma, n)Ni^{57}$ as a function of photon energy. Curve marked K and C: photon difference method; curve marked P and L: modified spectrum method.

TABLE I
Yield and cross-section data for the reaction $Ni^{58}(\gamma, n)Ni^{57}$

Reference	Yield at 22 Mev, n/100 r mole	Ratio of yields, $[Cu^{64}(\gamma, n)Cu^{63}] / [Ni^{58}(\gamma, n)Ni^{57}]$	E_{max} Mev	σ_n mb	$\Gamma_{1/2}$ Mev	$\int \sigma dE$ Mev-barn
Roalsvig and Kerner (1959)	1.04×10^6					
Roalsvig et al. (1961)	1.42×10^6	2.2 at 22 Mev	18.5	50	4.8	0.38
Roalsvig and Cameron (1961)			18.5	54	5.8	0.34
Roalsvig and Cameron (unpublished)	(0.63×10^6)		18.5	50	4.8	0.18
Roalsvig et al. (1959)		3.4 at 22 Mev				
Betatron (1959)		3.3 at 20 Mev				
Roalsvig et al. (1961)			18.0	32	4.1	0.23 (to 32 Mev)
Present work	6.82×10^5	2.3 at 22 Mev	21.0*	22	7.3	0.23
			20.5*	21	6.0	0.16

*For natural element.

*Katz and Cameron's method.

*Penfold and Leiss' method.

Method Linac; \checkmark Čerenkov counter telescope

Ref. No.	JHH
61 Cr 1	

Reaction	E or ΔE	E_0	Γ	$\int \sigma dE$	$J\pi$	Notes
(e^-, e^-')	183	1.45			2^+	Measured γ transition rates: $\Gamma_m = (1.56 \pm 0.2) 10^{12} \text{ sec}^{-1}$; (E2); $G = \Gamma_m / \Gamma_{sp} = 14.3 \pm 1.9$
		2.50			4^+	$\Gamma_m = (0.7 \pm 0.21) 10^4 \text{ sec}^{-1}$; (E4) $G = \Gamma_m / \Gamma_{sp} = 2.2 \pm 0.66$
		3.20			2^+	$\Gamma_m = (2.58 \pm 0.94) 10^{13} \text{ sec}^{-1}$; (E2); $G = \Gamma_m / \Gamma_{sp} = 4.45 \pm 1.6$
		3.51			4^+	$\Gamma_m = (2.92 \pm 0.66) 10^5 \text{ sec}^{-1}$; (E4); $G = \Gamma_m / \Gamma_{sp} = 2.50 \pm 0.57$
		4.50			3^-	$\Gamma_m = (5.95 \pm 0.83) 10^{10} \text{ sec}^{-1}$; (E3); $G = \Gamma_m / \Gamma_{sp} = 13.2 \pm 1.8$
		7.55			4^+	

[Γ_{sp} = single-particle estimate of the γ transition rate.]

Fits $R_0 = 1.20$ fermi except for 4.50 MeV level (1.11 fermi).

Table IV. Vibrational parameters for the levels in the even-even nuclei in the present experiment. $B(E2)$ is the reduced transition probability, B_0 and C_0 are the mass transport and the effective surface tension parameters of the harmonic-oscillator approximation to the nuclear surface energy. B_{theor} is the value appropriate to a hydrodynamic model, B_0^{theor} is the theoretical value of B_0 for a multipole order λ . R_0 is the nuclear radius ($R_0 = R_0^{\text{theor}}$ for $\lambda = 1, 2, 3$).

Nucleus	E MeV	$B(E2)$ MeV ²	B_0 MeV ²	B_{theor}	B_0^{theor}	C_0 MeV ²	B_0^{theor}/C_0
12 Ni	1.45	14.3 ± 1.9	60.5 ± 9	4.16	16.7 ± 2.2	145 ± 19	0.745 ± 0.097
	3.2	4.43 ± 1.6	106 ± 18	4.16	25.6 ± 9.2	1070 ± 340	0.407 ± 0.15
	1.33	17.1 ± 2.1	62.2 ± 7.5	3.96	16.45 ± 2.0	110 ± 14	0.792 ± 0.095
13 Ni	4.50	11.2 ± 1.8	103 ± 14	4.45	23.2 ± 3.2	2090 ± 290	0.401 ± 0.056
	4.95	15.9 ± 2.5	58.5 ± 14	4.01	19.1 ± 3.1	1430 ± 230	0.494 ± 0.074
	5.1	4 ± 1.8	144 ± 34	4.61	11.2 ± 2.4	1700 ± 475	0.324 ± 0.077
	2.60	30.8 ± 11	280 ± 105	23.8	11.7 ± 4.2	1890 ± 700	0.495 ± 0.18
14 Ni	2.30	2.2 ± 0.66	6140 ± 1800	5.96	470 ± 260	$3.34 \pm 1.2 \times 10^9$	0.0791 ± 0.024
	3.31	1.5 ± 0.37	1196 ± 270	6.96	17.20 ± 4.0	$1.49 \pm 0.33 \times 10^9$	0.15 ± 0.035
	2.30	1.02 ± 0.09	3400 ± 620	5.54	494 ± 44	$2.12 \pm 0.40 \times 10^9$	0.104 ± 0.02
	5.1	4.95 ± 0.74	1230 ± 145	5.54	180 ± 20	$1.20 \pm 0.40 \times 10^9$	0.115 ± 0.019
15 Ni	4.50	36.6 ± 12	495 ± 100	24.7	20.0 ± 5.5	$9.34 \pm 3.1 \times 10^9$	0.327 ± 0.11

See McMillan et al. reference 37 for theoretical values.

Ref 15: Data on the decay schemes are taken principally from Nuclear Data Sheets National Academy of Sciences - National Research Council (U.S. Government Printing Office, Washington, D.C. 1959)

Ref 37: Crut, Sweetman, Wall - Nuclear Phys. 17, 655 (1960).

METHOD

REF. NO.

Van de Graaff; resonance fluorescence

64 50 : NVE

REACTION	RESULT	EXCITATION ENERGY	SOURCE		DETECTOR		ANGLE
			TYPE	RANGE	TYPE	RANGE	
G.G	LFT	1-3	C	1 - 3	NAI-D		100
		(0.5 - 3.0)		(0.5 - 3.0)			

ABI

TABLE 1
 Cases of observed resonance fluorescence

Nucleus multipol.	State (MeV)	Spin	Γ_0/Γ	$T(gw\Gamma_0^2/\Gamma^2)^{-1}$ (sec).	Mean lifetime T BCW (sec)	Mean lifetime T other (sec)	Ref.	Γ_0/Γ_w BCW
Ni ⁵⁸	0.00	0 ⁺						
E2 ₁	1.45	2 ⁻	1	$19 \pm 6 \times 10^{-14}$	$62 \pm 20 \times 10^{-14}$			16

REF. S. Costa, F. Ferrero, S. Ferroni and R. Malvano
Proc. Paris Conference 1034 (1964)

ELEM. SYM.	A	Z
Ni	58	28

METHOD	REF. NO.
100 MeV synchrotron	64 Co 3 JDM

REACTION	RESULT	EXCITATION ENERGY	SOURCE		DETECTOR		ANGLE
			TYPE	RANGE	TYPE	RANGE	
G,N	ABX	THR-80	C	10-80	BF3-I		4PI

TABLE

ELEMENT	Yield (36 MeV) $\left(\frac{\text{n. cm}^2}{\text{mol. MeV}} \right) \times 10^8$	Σ_0^{30}	Σ_0^{80}	$\Sigma_0^{30} / \Sigma_0^{80}$	σ_{-1} (mb)
²⁴ Cr	83	1.21	2.1	0.58	62
²⁵ Mn	108	1.52	2.33	0.65	76
²⁶ Fe	63	0.88	1.46	0.60	50
²⁷ Co	89	1.03	1.82	0.59	64
²⁸ Ni	44	0.55	1.07	0.51	34
²⁹ Cu	95	1.06	1.99	0.53	72
³⁰ Zn	88	0.94	1.68	0.56	66
³¹ Ga	130	1.29	2.18	0.59	94
³² Ge	139	1.35	2.29	0.59	101
³³ As	137	1.22	2.18	0.56	100

$\Sigma = \frac{A}{60 NZ} \int_a^b \sigma(E) dE$ is the integrated cross section measured in units of the classical dipole $60 NZ/A$ mb. MeV.

REF.			ELEM. SYM.	A	Z
M. Masuda, M. Kondo, S. Takeda, M. Okumura, and J. Ookuma J. Phys. Soc. Japan <u>19</u> , 2339 (1964)			Ni	58	28
METHOD			REF. NO.		
			64 Ma 2		EGF

REACTION	RESULT	EXCITATION ENERGY	SOURCE		DETECTOR		ANGLE
			TYPE	RANGE	TYPE	RANGE	
G,XP	SPC	THR- 22	C	22	SCD-D	3 - 9	

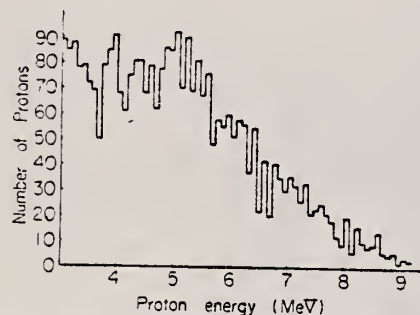


Fig. 2. Energy spectrum of emitted protons from nickel foil irradiated by 22 MeV brems-strahlung.

REF. M.A. Duguay, C.K. Bockelman, T.H. Curtis, and R.A. Eisenstein
Phys. Rev. Letters 17, 28 (1966)

ELEM. SYM.	A	Z
Ni	58	28

METHOD
Linac

REF. NO.	JDM
66 Du 1	

REACTION	RESULT	EXCITATION ENERGY	SOURCE		DETECTOR		ANGLE
			TYPE	RANGE	TYPE	RANGE	
E, E/	FMF	1	D	45 - 65	MAG-D		DST

Table I. Reduced transition probabilities $B(E2)$ and transition radii R_{tr} for the first excited states of the even Ni isotopes.

Isotope	Level energy (MeV)	J^π	$B(E2, 0^+ \rightarrow 2^+)$ ($e^2 F^4$)		R_{tr} (F)
			Ref. 12	Present work	
Ni ⁵⁸	1.452	2 ⁺	720 ± 10%	620 ± 14%	5.35 ± 10%
Ni ⁶⁰	1.332	2 ⁺	910 ± 9%	776 ± 12%	5.23 ± 12%
Ni ⁶²	1.172	2 ⁺	830 ± 9%	770 ± 12%	5.23 ± 10%

METHOD

REF. NO.

67 Du 1

HMG

REACTION	RESULT	EXCITATION ENERGY	SOURCE		DETECTOR		ANGLE
			TYPE	RANGE	TYPE	RANGE	
$E, E/$	FMF	1-5	D	45-65	MAG-D		DST

TABLE II. Reduced radiative transition probabilities and transition radii.

$B(EL)$, SEP ISOTPS

E2 Transitions*					
Excitation energy (MeV)	$B(E2, 0^+ \rightarrow 2^+)$ ($e^2 F^4$)	$B(E2, 0^+ \rightarrow 2^+)$	β_2	R_{12} (F)	
Ni ⁵⁸ 1.452	657 ± 11	10	0.177 ± 0.003	5.51	
3.034	83 ± 3	1	0.063 ± 0.002	5.51	
3.26	153 ± 15	2	0.085 ± 0.008	5.51	
Ni ⁶⁰ 1.330	845 ± 9	12	0.197 ± 0.002	5.55	
Ni ⁶² 1.172	877 ± 11	12	0.197 ± 0.001	5.59	

E3 Transitions*					
Excitation energy (MeV)	$B(E3, 0^+ \rightarrow 3^-)$ ($e^2 F^6$)	$B(E3, 0^+ \rightarrow 3^-)$	β_3	R_{13} (F)	
Ni ⁵⁸ 4.480	$18\,600 \pm 520$	13	0.203 ± 0.005	6.05	
Ni ⁶⁰ 4.038	$28\,100 \pm 640$	19	0.241 ± 0.006	6.09	
Ni ⁶² 3.75	$20\,100 \pm 540$	13	0.197 ± 0.005	6.11	

* The errors quoted for $B(EL)$ assume the liquid-drop model for the transition charge density and are purely statistical in nature. The estimate of error from dependence on the parameters of this charge density are $\pm 15\%$ for both $B(EL)$ and R_{12} . See text.

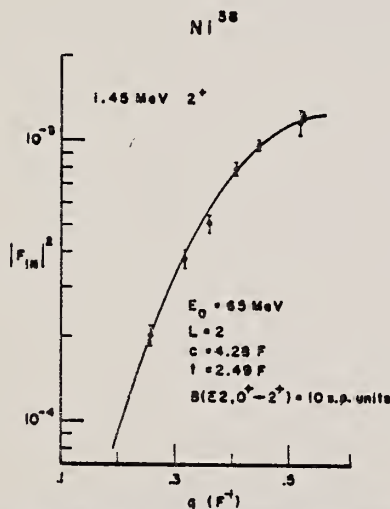


FIG. 19. The theoretical and experimental $|F_{in}|^2$ versus q for the Ni⁵⁸ 1.45-MeV 2^+ state. The solid curve is the $|F_{in}|^2$ calculated by Code GBROW using the strict hydrodynamic model ($c_{tr}=c$; $k_{tr}=0$). The best fit to the data is obtained by a least-squares analysis.

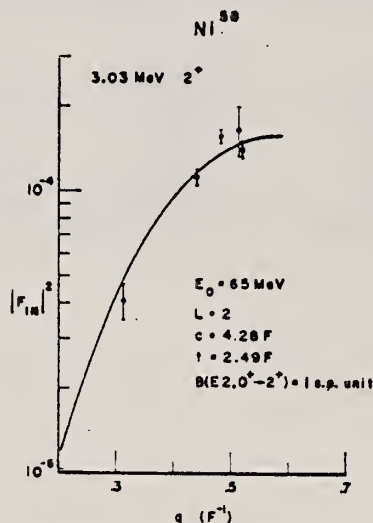


FIG. 20. The theoretical and experimental $|F_{in}|^2$ versus q for the Ni⁵⁸ 3.03-MeV 2^+ state. The solid curve is the $|F_{in}|^2$ calculated by Code GBROW using the strict hydrodynamic model ($c_{tr}=c$; $k_{tr}=0$). The best fit to the data is obtained by a least-squares analysis.

METHOD

[Page 2 of 2]

REF. NO.	
67 Du 1	HMG

REACTION	RESULT	EXCITATION ENERGY	SOURCE		DETECTOR		ANGLE
			TYPE	RANGE	TYPE	RANGE	

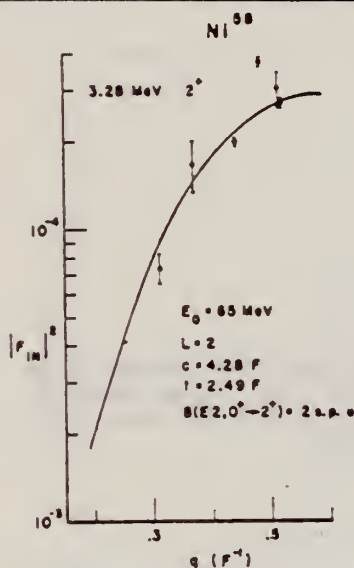


FIG. 21. The theoretical and experimental $|F_{in}|^2$ versus q for the Ni^{58} 3.26-MeV 2^+ state. The solid curve is the $|F_{in}|^2$ calculated by code GBROW using the strict hydrodynamic model ($c_s = c$; $k_r = l$). The best fit to the data is obtained by a least-squares analysis.

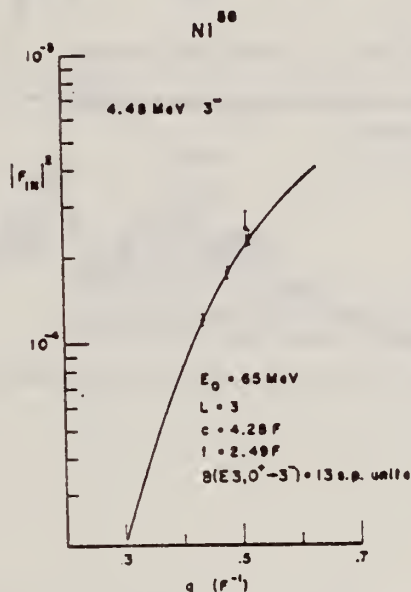


FIG. 22. The theoretical and experimental $|F_{in}|^2$ versus q for the Ni^{58} 4.48-MeV 3^- state. The solid curve is the $|F_{in}|^2$ calculated by Code GBROW using the strict hydrodynamic model ($c_s = c$; $k_r = l$). The best fit to the data is obtained by a least-squares analysis.

REF. B. I. Goryachev, B. S. Ishkhanov, I. M. Kapitonov, I. M. Piskarev,
V. G. Shevchenko, and O. P. Shevchenko
ZhETF Pis. Red. 8, 76 (1968)
JETP Letters 8, 46 (1968)

ELEM. SYM.	A	Z
Ni	58	28
REF. NO.		hmg
68 Go 4		

METHOD

REACTION	RESULT	EXCITATION ENERGY	SOURCE		DETECTOR		ANGLE
			TYPE	RANGE	TYPE	RANGE	
G,XN	ABX	12- 25	C	7-30	BF3-I		4PI

$$\sigma_{\text{int}}(30 \text{ MeV}) = 380 \pm 30 \text{ MeV-mb.}$$

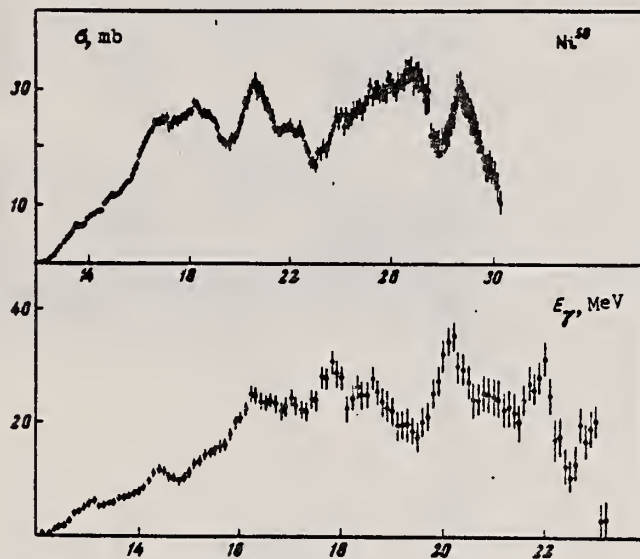


Fig. 1. Effective cross section of the reaction $\text{Ni}^{58}(\gamma, \text{Tn})$. Upper figure - analysis in steps of 1 MeV, lower - in steps of 0.5 MeV.

REF. K. Min and T. A. White
Phys. Rev. Letters 21, 1200 (1968)

ELEM. SYM.	A	Z
Ni	58	28

METHOD	REF. NO.
	68 Mi 1

REACTION	RESULT	EXCITATION ENERGY	SOURCE		DETECTOR		ANGLE
			TYPE	RANGE	TYPE	RANGE	
G. XN	ABX	12- 24	C	10-25	BF3-I		4PI

17

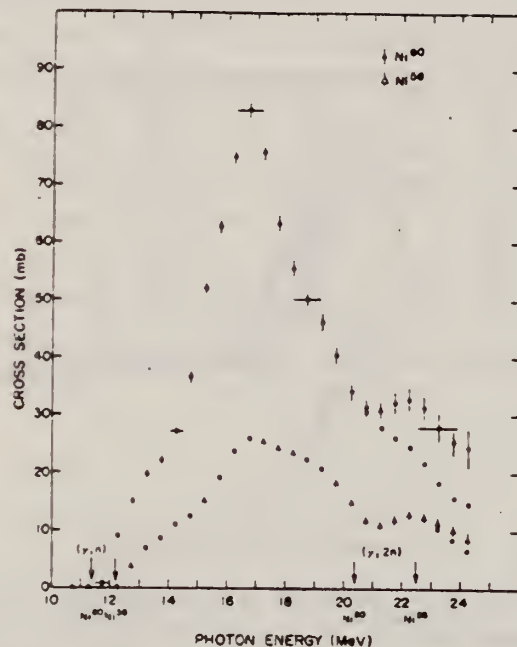


FIG. 1. Photoneutron cross sections of Ni^{60} and Ni^{58} . The corrected values for $(\gamma, 2n)$ process are shown by circles.

Table I. Integrated (γ, n) cross sections up to 25 MeV.

Isotope	Integrated cross section (MeV mb)
Ni^{58}	185 ± 3
Ni^{60}	482 ± 12
Natural nickel	283 ± 6
$(0.262) \text{Ni}^{60} + (0.679) \text{Ni}^{58}$	252 ± 4
Ratio of integrated cross section, $\text{Ni}^{60}/\text{Ni}^{58} = 2.6$	

REF. V. D. Afanas'ev, N. G. Afanas'ev, I. S. Gul'karov, G. A. Savitskii,
V. M. Khvastunov, N. G. Shevchenko and A. A. Khomich
Yad. Fiz. 10, 33 (1969)
Sov. J. Nucl. Phys. 10, 18 (1970)

ELEM. SYM.	A	Z
Ni	58	28

METHOD

REF. NO.

69 Af 1

egf

REACTION	RESULT	EXCITATION ENERGY	SOURCE		DETECTOR		ANGLE
			TYPE	RANGE	TYPE	RANGE	
E, E/	FMF	1,4	D	150,225	MAG-D		DST

1,4 = 1.45, 4.45 MEV

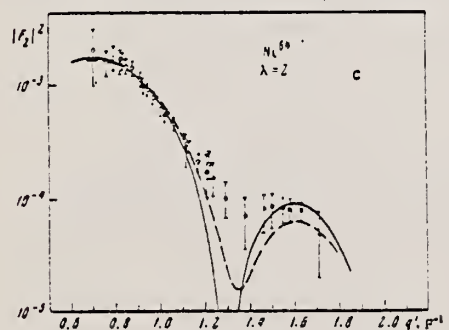
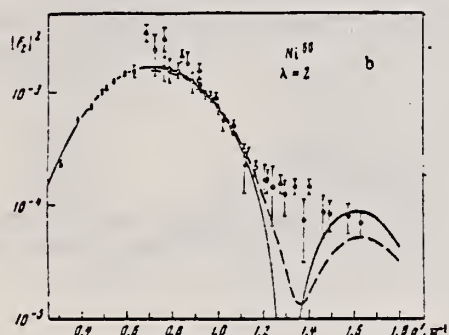
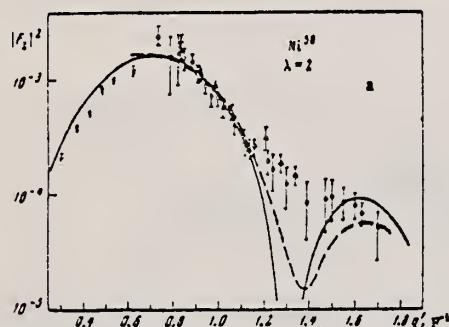


FIG. 2. Form factors for E2 transitions in nickel isotopes: a—Ni⁵⁸, b—Ni⁶⁰, c—Ni⁶⁴. Solid curves—Helm's model, dashed curves—high-energy approximation. Points: O, ●—our data for 150 and 225 MeV, ▲—Stanford data [9], X—Yale data [10].

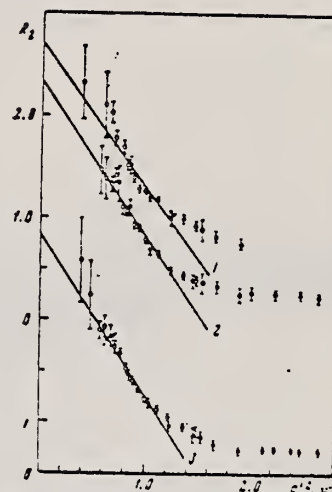


FIG. 3. R_λ as a function of q^2 for E2 transitions. Straight lines: 1—Ni⁵⁸ (the points and straight line are raised by 0.5), 2—Ni⁶⁰, 3—Ni⁶⁴ (the points and straight line are lowered by 1.0). Points: O—150 MeV, ●—225 MeV.

Table II. Reduced probabilities of quadrupole transitions in the isotopes Ni^{58,60,64}

Iso- tope	π , MeV	J^π	$B(E2), e^2 \text{fm}^4$				G_1	Theory		Data of other authors	
			Helm's model	High energy approximation	Model- independent method	Average		[1]	[2]	$B(E2)$	Reference
Ni^{58}	1.45	2^+	560 ± 56	544 ± 11	519 ± 62	554	4.4	340	200	800 650 650 535 + 750	[1] [2] [3] [4]
Ni^{60}	1.33	2^+	603 ± 55	602 ± 40	605 ± 54	603	4.8	430	460	1100 910 845 1250 785 + 1200	[1] [2] [3] [4] [5]
Ni^{64}	1.32	2^+	650 ± 65	661 ± 53	640 ± 58	650	4.8	1430	640	470	[1]

[over]

Table III. Reduced probabilities of octupole transitions in the isotopes $Ni^{58,60,64}$

Isotope	E, MeV	J^π	$B(E3), e^2F^4$			G_3	Data of other authors	
			Helm's model	Model-independent method	Average		$B(E3)$	Reference
Ni^{58}	4.45	3^-	13500 ± 1450	13020 ± 780	13400	10	18 600 27 000 14 600	[10] [10] [10]
Ni^{60}	4.04	3^-	13300 ± 1800	13910 ± 830	13600	9	24 100 35 000 19 100	[10] [10] [10]
Ni^{64}	3.55	3^-	15000 ± 1800	17000 ± 1400	16500	9.4		

Table IV. Transition radii and parameters of the vibrational model of the nucleus for E2 and E3 transitions in $Ni^{58,60,64}$

Isotope	$I_i \rightarrow I_f$	R_{trans}		C_3 , MeV	$B\lambda_3$, MeV-sec 10^3	$B\lambda$, ($B\lambda$) _{h.d.}	μ_3^2
		Our result	[fm]				
Ni^{58}	0-2	4.95 ± 0.21	5.51	173 ± 19	82 ± 9	20.0 ± 2.2	0.115 ± 0.004
	0-3	5.13 ± 0.11	6.05	1520 ± 130	77 ± 8	17 ± 2	0.101 ± 0.006
	0-2	4.92 ± 0.15	5.55	153 ± 17	86 ± 9	20 ± 2.2	0.148 ± 0.008
Ni^{60}	0-3	5.24 ± 0.10	6.09	1500 ± 130	92 ± 8	18.5 ± 1.8	0.097 ± 0.005
	0-2	4.94 ± 0.15	—	145 ± 18	83 ± 9	17.5 ± 1.7	0.150 ± 0.009
	0-3	5.31 ± 0.11	—	1160 ± 130	92 ± 12	17.1 ± 2.2	0.102 ± 0.006

* ($B\lambda$)_{h.d.} is the oscillation parameter of the nucleus, obtained with a hydrodynamical model.

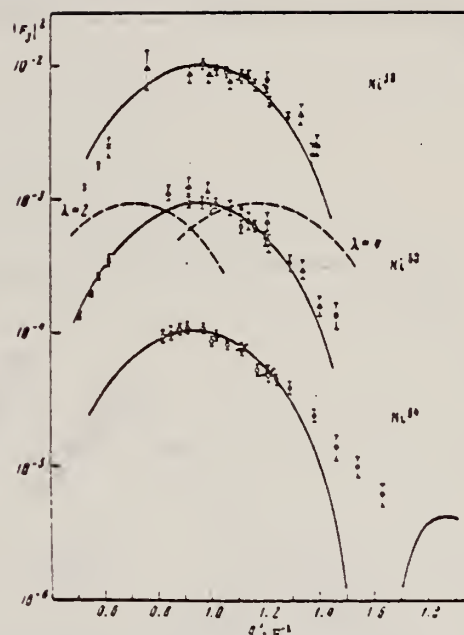


FIG. 4. Form factors for E3 transitions in the isotopes Ni^{58} (the experimental data and curve are multiplied by 10), Ni^{60} , Ni^{64} (the experimental data and curve are divided by 10). The solid curves represent the form factor calculated by Helm's model with $\lambda = 3$, and the dashed curves the form factor calculated by the same model for $\lambda = 2$ and $\lambda = 4$. Points: O and O - our data for 150 and 225 MeV, A - Stanford data [7], X - Yale data [10].

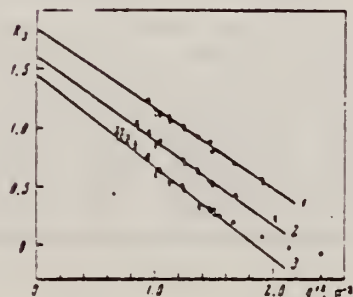


FIG. 5. Analysis of E3 transitions by the model-independent method. Straight lines: 1 - Ni^{58} (the data and straight line have been raised by 0.5) 2 - Ni^{60} , 3 - Ni^{64} (the data and straight line have been lowered by 0.5). Points: O - 150 MeV, O - 225 MeV.

REF. B.I. Goryachev, B.S. Ishkhanov, I.M. Kapitonov, I.M. Piskarev,
V.G. Shevchenko, and O.P. Shevchenko
Yad. Fiz. 10, 252 (1969)
Sov. J. Nucl. Phys. 11, 141 (1970)

ELEM. SYM.	A	Z
Ni	58	28

METHOD

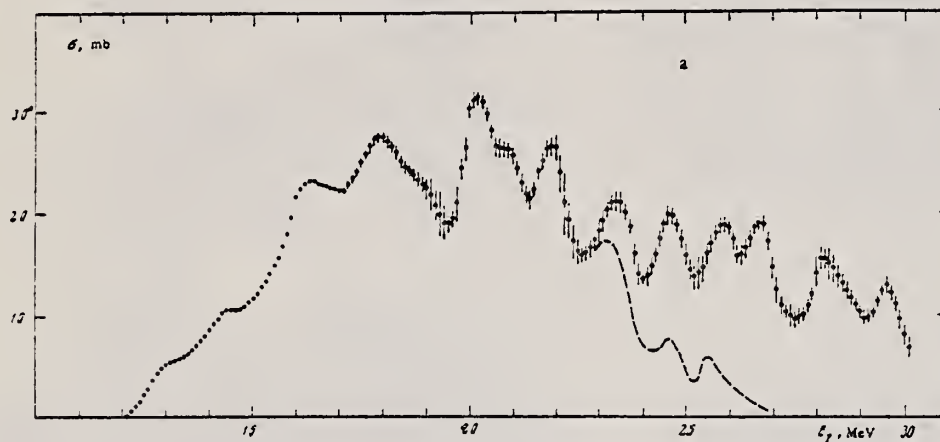
REF. NO.

69 Go 2

hmg

REACTION	RESULT	EXCITATION ENERGY	SOURCE		DETECTOR		ANGLE
			TYPE	RANGE	TYPE	RANGE	
G,XN	ABX	12-30 (12.2-30)	C	12-30	BF3-I		4PI

278



$$\int_{15}^{30} \sigma dE = 310 \pm 30 \text{ MeV mb}$$

FIG. 1. Cross section of the photoneutron reaction for Ni^{58} (a) and Ni^{60} (b). The dashed line shows the cross section of the reaction (γ, n) above the threshold of two-neutron emission, obtained from our data on the basis of the statistical theory.

I. S. Gul'karov, N. G. Afanas'ev, V. M. Khvastunov, N. G. Shevchenko,
V. D. Afanas'ev, G. A. Savitskii, A. A. Khomich
Yad. Fiz. 9, 478 (1969)
Sov. J. Nucl. Phys. 9, 274 (1969)

ELEM. SYM.	A	Z
Ni	58	28
REF. NO.	69 Gu 1	
	hmg	

REACTION	RESULT	EXCITATION ENERGY	SOURCE		DETECTOR		ANGLE
			TYPE	RANGE	TYPE	RANGE	
E.E/	ABX	10-30	D	199	MAG-D		40
				(198.9)			

See paper for summary of other data.

FMF

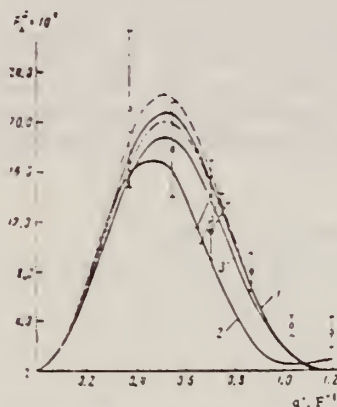


FIG. 2. Giant-resonance form factor as a function of momentum transfer. Points: O—data for Ni^{60} , X—for Ni^{64} , □—for Ni^{58} . The dashed curve, curve 1, and the dot-dash curve were calculated from formula (2) for the nuclei $Ni^{58,60,64}$ respectively, with $k = 19$ MeV. Curve 3 was calculated from the same formula for Ni^{60} with $k = 21$ MeV. Curve 2 is a calculation according to the Goldhaber-Teller collective model.

Table I. Absolute differential cross sections for inelastic scattering of electrons with excitation of the giant resonance in nickel isotopes

Nucleus	θ , deg	E_0 , MeV	q , F^{-1}	q^2 , F^{-2}	$d\sigma/d\Omega$, cm^2/sr	$F_g^2 (\times 10^{-3})$
^{60}Ni	30	198.7	0.245	0.301	$(2.72 \pm 0.70) \cdot 10^{-28}$	2.11 ± 0.63
	30	197.1	0.247	0.303	$(1.73 \pm 0.81) \cdot 10^{-28}$	1.78 ± 0.78
	30	197.6	0.242	0.293	$(7.54 \pm 1.55) \cdot 10^{-29}$	1.12 ± 0.23
	30	197.9	0.240	0.288	$(2.14 \pm 0.50) \cdot 10^{-28}$	0.80 ± 0.15
	30	198.1	0.270	1.029	$(5.22 \pm 1.03) \cdot 10^{-28}$	0.36 ± 0.08
^{58}Ni	30	201.0	1.125	1.154	$(1.51 \pm 0.81) \cdot 10^{-28}$	0.51 ± 0.13
	30	198.9	0.245	0.293	$(8.08 \pm 1.35) \cdot 10^{-29}$	1.22 ± 0.20
^{64}Ni	33	149.7	0.050	0.702	$(4.44 \pm 0.36) \cdot 10^{-28}$	1.42 ± 0.27

Note. The limits of integration of the spectra are from 10 to 30 MeV.

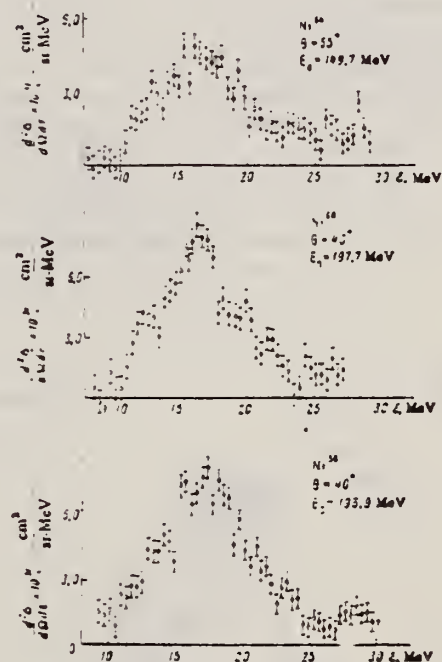


FIG. 3. Energy spectra of electrons inelastically scattered by the isotopes $Ni^{60,64,58}$. All three spectra were measured at the same value of momentum transfer.

ELEM. SYM.	A	Z
Ni	58	28
REF. NO.	69 Ow 1	
	egf	

REACTION	RESULT	EXCITATION ENERGY	SOURCE		DETECTOR		ANGLE
			TYPE	RANGE	TYPE	RANGE	
G,XN	ABX	12-25	C	12-25	BF3-I		4PI

191

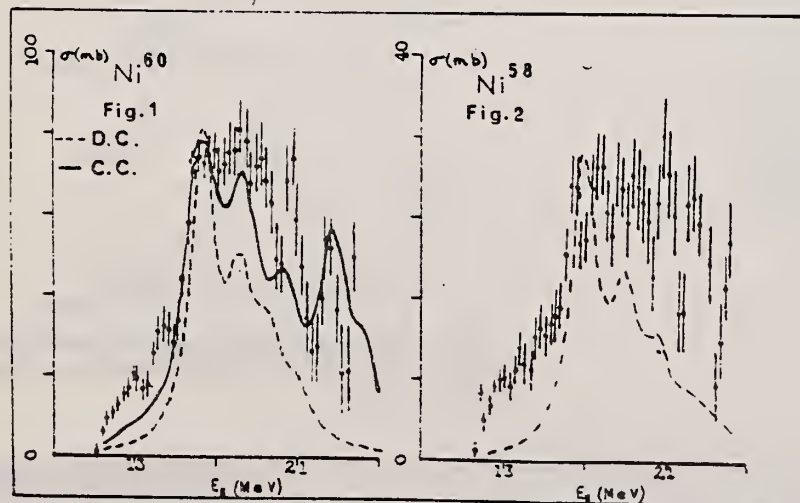
RESULTS OF THE VIBRATIONAL SPLITTING OF THE GIANT DIPOLE RESONANCE
D.G. Owen, E.G. Muirhead and B.M. Spicer, School of Physics, University of Melbourne, Parkville, Victoria 3052, Australia.

The photoneutron yield curves for ^{58}Ni and ^{60}Ni have been measured in 1/4 MeV steps from threshold to 24 MeV, the neutrons being detected in a Halpern-type BF_3 counter system. The cross sections were obtained from the yield curves by the Leiss-Penfold matrix inversion method. A correction, based on the statistical theory of nuclear reactions, has been made for multiple neutron emission. The derived cross sections are shown in figures 1 and 2.

The dotted curves on the Figure are the fits to the dipole spectrum, using Lorentz line shapes, and based on the dynamic collective model of the giant resonance (Huber, priv. comm. 1967), in which quadrupole surface vibrations are coupled to the dipole vibration. The poor fit at low energies is attributed to neglect of single particle effects.

Also shown in figure 1 is the result of the collective correlations calculation for ^{60}Ni (Seaborn, Drechsel, Arenhovel and Greiner, Phys. Lett. 23 (1966) 576). Here the surface vibrations are coupled to particle-hole dipole states, not just the dipole state. This calculation for the closed-subshell nucleus ^{60}Ni yields the result shown in the full curve of figure 1. The agreement with experiment is very much improved, indicating the importance of including single particle effects.

The similarity of low energy spectra for ^{58}Ni and ^{60}Ni , coupled with the fact that the same single particle states are filled in the ground state, leads to the expectation that the giant resonance structure will be similar for the two isotopes. This is in fact observed.



REF. B.S. Ishkhanov, I.M. Kapitonov, I.M. Piskarev, V.G. Shevchenko,
and O.P. Shevchenko
Yad. Fiz. 11, 485 (1970)
Sov. J. Nucl. Phys. 11, 272 (1970)

ELEM. SYM.	A	Z
Ni	58	28

METHOD	REF. NO.	
	70 Is 4	hmg

REACTION	RESULT	EXCITATION ENERGY	SOURCE		DETECTOR		ANGLE
			TYPE	RANGE	TYPE	RANGE	
G, P	ABX	8-30	C	8-30	SCD-D	1-	UKN
		(8.2-30)		(8.2-30)			

We measured the photoproton cross sections for the nuclei Cr^{52} , Ni^{58} , and Ni^{60} from the threshold to 30 MeV. We registered protons with energy larger than 1 MeV. A number of maxima were obtained in the cross sections. The values of the integral cross sections for Cr^{52} , Ni^{58} , and Ni^{60} are equal respectively to 240, 570, and 320 MeV-mb. The anomalously large cross section for the production of photoprotons for Ni^{58} , and also the shift of the centers of gravity of the photoproton cross sections towards higher excitation energies relative to the photoneutron cross sections in the case of Cr^{52} and Ni^{60} , can be attributed to the influence of analog states.

PROB 90 DEGREES

743+
1069

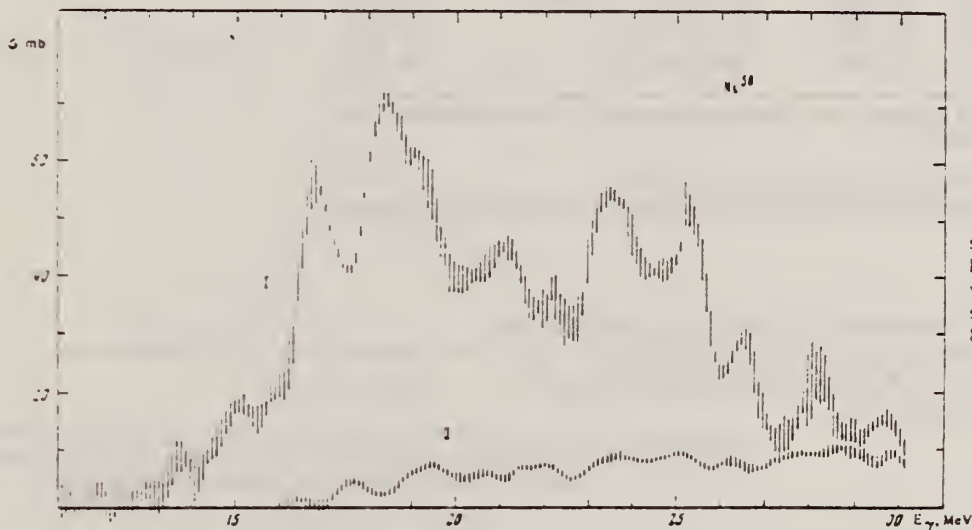


FIG. 2. Photoproton cross sections for Ni^{58} . Cross section I has been obtained for protons with $E_p > 1$ MeV and the cross section II for protons with $E_p > 8$ MeV.

Integral characteristics of the photoproton cross sections σ_p , of the photoneutron cross sections σ_n , and of the total absorption cross sections $\sigma_\gamma = \sigma_n + \sigma_p$

Nucleus	$\int_0^{30} \sigma_n dE_\gamma$	$\int_0^{30} \sigma_p dE_\gamma$	$\int_0^{30} \sigma_\gamma dE_\gamma$	$\sigma_0(N, Z, A)$	$\frac{\sigma_p}{\sigma_\gamma}$	$\frac{\sigma_n}{\sigma_\gamma}$	$\frac{\sigma_p}{\sigma_\gamma}$
	MeV-mb	MeV-mb	MeV-mb	MeV-mb			
Cr^{52}	730 ± 60	210 ± 50	970 ± 110	775	0.25	23.5 ± 3.1	23.5 ± 3.1
Ni^{58}	310 ± 30	570 ± 60	880 ± 90	870	0.95	21.0 ± 1.1	21.0 ± 1.1
Ni^{60}	620 ± 70	210 ± 50	930 ± 100	890	0.15	20.7 ± 3.3	20.7 ± 3.3

Note: The parentheses contain the integral cross sections of the photoproton reactions for protons with energy $E_p > 8$ MeV

REF. F. R. Metzger
Nucl. Phys. A158, 88 (1970)

ELEM. SYM.	A	Z
Ni	58	28

METHOD	REF. NO.	
	70 Me 3	egf

REACTION	RESULT	EXCITATION ENERGY	SOURCE		DETECTOR		ANGLE
			TYPE	RANGE	TYPE	RANGE	
G,G	LFT	1-4	C	4	SCD-D	1-5	DST
		(4.1)				(<4.5)	

6 LEVELS

TABLE 1

The direct results of the resonance scattering experiments on ^{58}Ni described in this paper are listed in the fourth column

E_{level} (MeV)	I^π	Γ_0/Γ	Γ_0^2/Γ (meV)				Total width Γ (meV)	
			res. scatt.	res. scatt.	inelastic elec. scatt.	Doppler shift ^{a)}		
1.453	2 ⁺	1.00 ^{a)}	0.67 ± 0.06	0.67 ± 0.06	0.69 ± 0.10	0.72 ± 0.09		
3.038	2 ⁺	0.41 ^{a)}	1.56 ± 0.34	9.3 ± 2.3	8.4 ± 1.3	11.5 ± 1.6		
3.263	2 ⁺	0.62 ^{a)}	5.3 ± 0.8	13.8 ± 2.2	14.7 ± 2.2	18.3 ± 2.6		
3.593	1 ^(±)	0.69 ^{a)}	4.6 ± 0.8	9.7 ± 2.1		13.7 ± 3.5		
3.898	2 ⁺	0.22 ^{b)}	2.1 ± 0.9	43 ± 19		19.9 ± 2.4		
4.108	2 ⁺	0.50 ^{c)}	1.0 ± 0.6	4.0 ± 2.5		7.0 ± 1.1		

To arrive at the widths listed in column 5, the branching ratios given in the third column were used.

^{a)} Taken from table 4 of ref. ⁴⁾.

^{b)} See ref. ³⁾.

^{c)} Average of the two branching ratios listed in table 3 of ref. ³⁾.

^{d)} To simplify the tabulation, the asymmetrical errors given in ref. ³⁾ were replaced by symmetrical errors.

³⁾ M.C. Bertin, N. Benczer-Koller, G.G. Seaman and J.R. MacDonald, Phys. Rev. 183 (1969)964.

⁴⁾ D.M. Van Patter, R.N. Horoshko and H.L. Scott, Nucl. Phys. A137 (1969)353.

ELEM. SYM.		
Ni	58	28
REF. NO.	70 Ow 1	
	egf	

REACTION	RESULT	EXCITATION ENERGY	SOURCE		DETECTOR		ANGLE
			TYPE	RANGE	TYPE	RANGE	
G.XN	ABX	11-24	C	10-24	BF3-I		4PI

274†

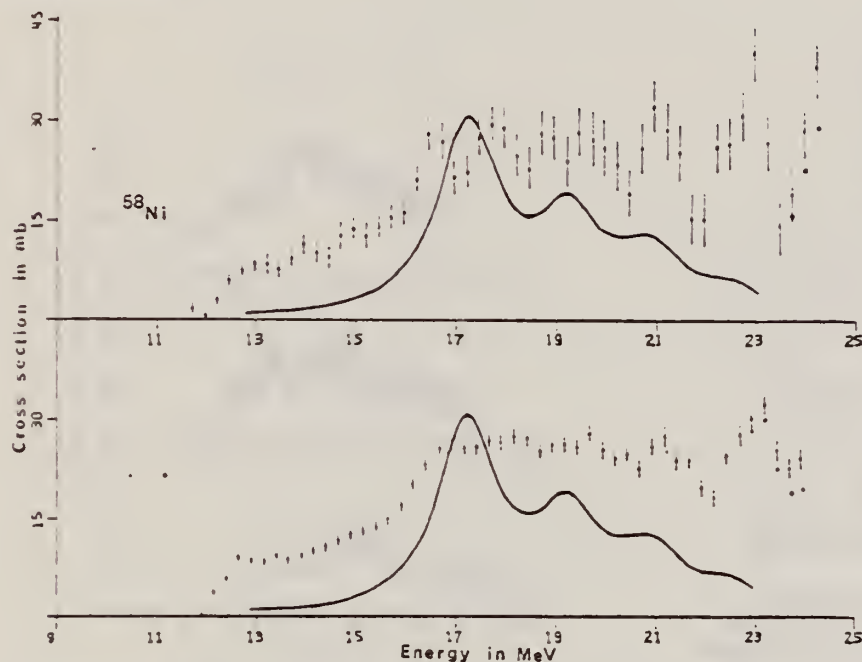


Fig. 2. The $^{58}\text{Ni}(\gamma, xn)$ cross section analysed in (top) 0.5 and (bottom) 1.0 MeV bins. The errors shown represent the total experimental uncertainty for each point. The continuous curve is the shape of the ^{58}Ni photo-absorption cross section predicted by Hüber ^a).

^a M. G. Huber, private communication (1967).

REF. Yu. P. Antuf ev, V.L. Agranovich, V.B. Ganenko, V.S. Kuz menko,
I.I. Miroshnichenko, and P.V. Sorokin
Yad. Fiz. 14, 898 (1971)
Sov. J. Nucl. Phys. 14, 502 (1972)

ELEM. SYM.	A	Z
Ni	58	28
REF. NO.		
71 An 2		hmg

METHOD

REACTION	RESULT	EXCITATION ENERGY	SOURCE		DETECTOR		ANGLE
			TYPE	RANGE	TYPE	RANGE	
G, XD	ABX	107-999	C	999	MAG-D		DST

999 = 1.14 GEV

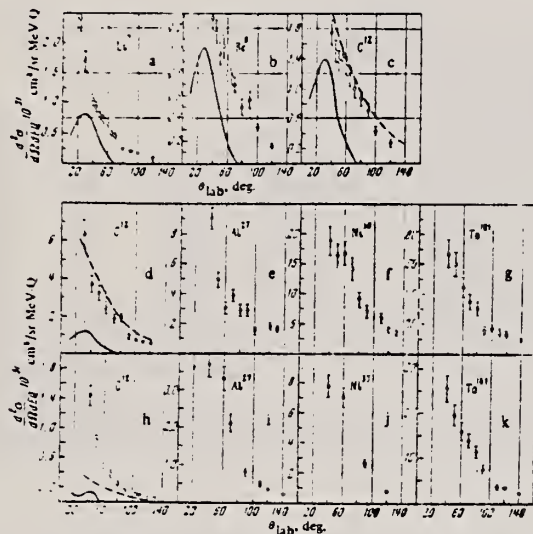


FIG. 1. Angular distributions of deuterons in (γ , d) reactions in nuclei for $E_0 = 620$ MeV (a-c) and $E_0 = 1140$ MeV (d-k). The statistical errors are shown. a-g—angular distributions of deuterons with energies of 90 MeV, h-k—with energy 160 MeV.

REF.

K. Shoda, M. Sugawara, T. Saito, H. Miyase, A. Suzuki, S. Oikawa,
and J. Uegaki
Picns-72, 321 Sendai

ELEM. SYM.	A	Z
Ni	58	28
REF. NO.		
72 Sh 10		hvm

METHOD

REACTION	RESULT	EXCITATION ENERGY	SOURCE		DETECTOR		ANGLE
			TYPE	RANGE	TYPE	RANGE	
G,P	ABX	13- 24	C	13- 24	MAG-D		90

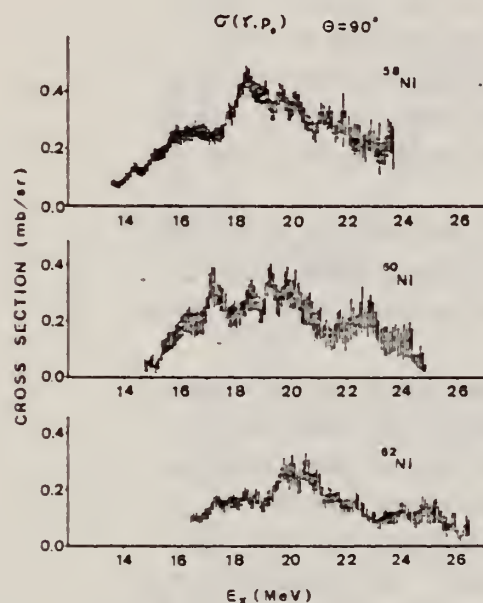
I A STATES

Fig. 10 The (γ, p_0) cross sections of Ni isotopes obtained from proton spectra by the $(e, e'p)$ reaction.

ELEM. SYM.	A	Z
Ni	58	28
REF. NO.		hmg
73 Fu 4		

METHOD					REF. NO.	
					73 Fu 4	
REACTION	RESULT	EXCITATION ENERGY	SOURCE		DETECTOR	
			TYPE	RANGE	TYPE	RANGE
G,N	ABX	12- 34	D	12-34	BF3-I	4PI
G,2N	ABX	22- 34	D	22- 34	BF3-I	4PI

The photoneutron cross section for ^{58}Ni is interesting both because it is anomalously small and because much structure has been observed in previous experiments.¹⁻⁴ We have measured the cross sections, with rather high resolution, for the first time with nearly monoenergetic photons from in-flight annihilation of positrons from the new Livermore electron-positron linac. The experimental method employed was similar to that used in a number of earlier experiments⁵ by the Livermore group. The ^{58}Ni content of the target sample was 99.89%. The photon energy resolution varied smoothly from about 50 keV at 10 MeV to approximately 90 keV at 35 MeV.

The experimental results are shown in Fig. 1. The error bars shown are statistical only. In addition there are several sources of systematic uncertainty which could introduce an overall error of up to about 10% in the region of the giant resonance peak, and perhaps 40% at 35 MeV.

The total photoneutron cross section reaches a peak of about 25 mb in the neighborhood of 18 MeV, and exhibits considerable structure which persists well above 20 MeV. Our data are generally in good agreement with the magnitude of the peak cross sections obtained in previous experiments²⁻⁴ but disagree on the details of the observed structure. The $(\gamma,2n)$ cross section, which has been measured here for the first time, is small (generally $\lesssim 1$ mb) and appears to vanish by about 33 MeV. The integrated total photoneutron cross section, up to 33.5 MeV, is 286 MeV-mb, while the integrated $(\gamma,2n)$ cross section is 7.7 MeV-mb.

The distribution of strength in the cross section, up to 25 MeV, is in good qualitative agreement with particle-hole calculations of the E1 transition strengths;⁶ however, considerable cross section appears to lie above the region of the calculated dipole strength. Comparison of our data with those of Carver and Turchinets¹ implies that most of the high-energy cross section results from the (γ,pn) reaction.

† Work performed under the auspices of the U. S. Atomic Energy Commission.

* Deceased

- 1 J. H. Carver and W. Turchinets, Proc. Phys. Soc. (London) 73, 585 (1959).
- 2 K. Min and T. A. White, Phys. Rev. Letters 21, 1200 (1968).
- 3 B. I. Goryachev, B. S. Ishkhanov, I. M. Kapitonov, I. M. Piskarev, V. G. Shevchenko, and O. P. Shevchenko, Sov. J. Nucl. Physics 11, 141 (1970) [Yad.Fiz. 10, 252 (1969)].
- 4 D. G. Owen, E. G. Muirhead, and B. M. Spicer, Nucl. Phys. A140, 523 (1970).
- 5 B. L. Berman, J. T. Caldwell, R. R. Harvey, M. A. Kelly, R. L. Bramblett, and S. C. Fultz, Phys. Rev. 162, 1098 (1967).
- 6 Y. Tanaka, Prog. Theor. Phys. 46, 787 (1971).

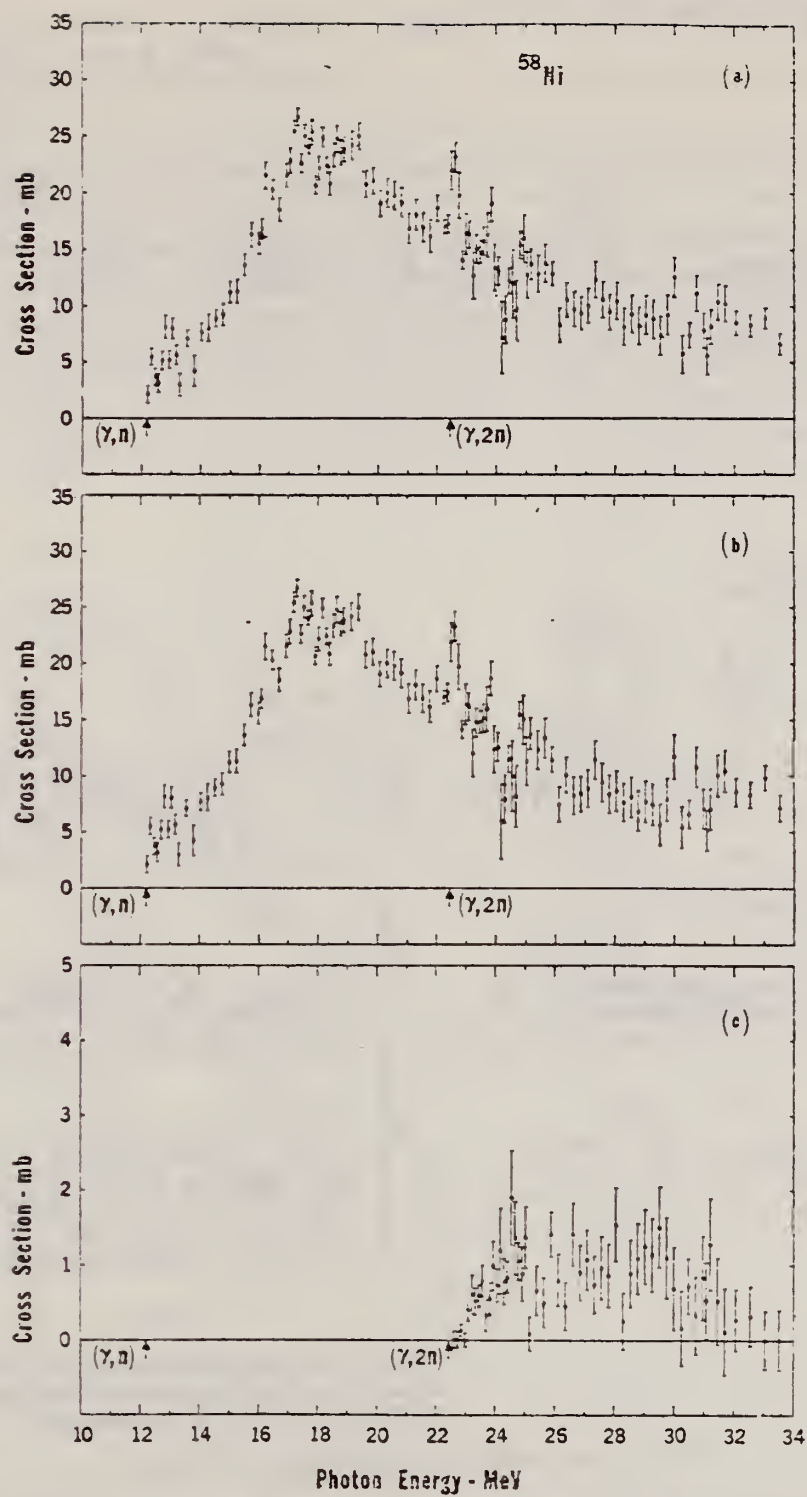


Figure 1. Photoneutron cross sections of ^{58}Ni . Thresholds are indicated by arrows.
 (a) Total photoneutron cross section: $\sigma[(\gamma, n) + (\gamma, pn) + (\gamma, 2n)]$;
 (b) $\sigma[(\gamma, n) - (\gamma, pn)]$; (c) $\sigma(\gamma, 2n)$.

REF.

K. Itoh, M. Oyamada, and Y. Torizuka
Phys. Rev. C7, 458 (1973)

ELEM. SYM.	A	Z
Ni	58	28
REF. NO.		
73 It 1		hmg

METHOD

REACTION	RESULT	EXCITATION ENERGY	SOURCE		DETECTOR		ANGLE
			TYPE	RANGE	TYPE	RANGE	
E, E/	FMF	0- 7	D	183,250	MAG-D		82

See 69To3.

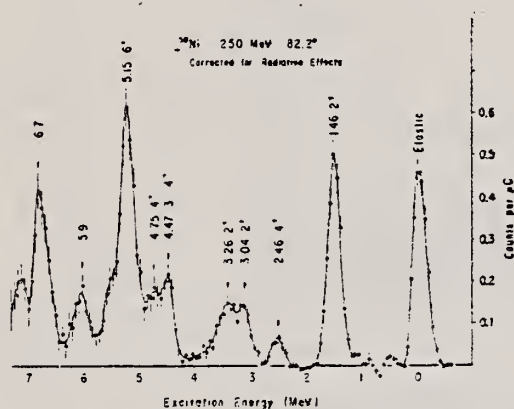
LEVEL AT 5.15 MEV

FIG. 1. The spectrum of ^{58}Ni for inelastic electron scattering obtained at 250 MeV and 82.2° indicates a prominent peak at 5.15 MeV.

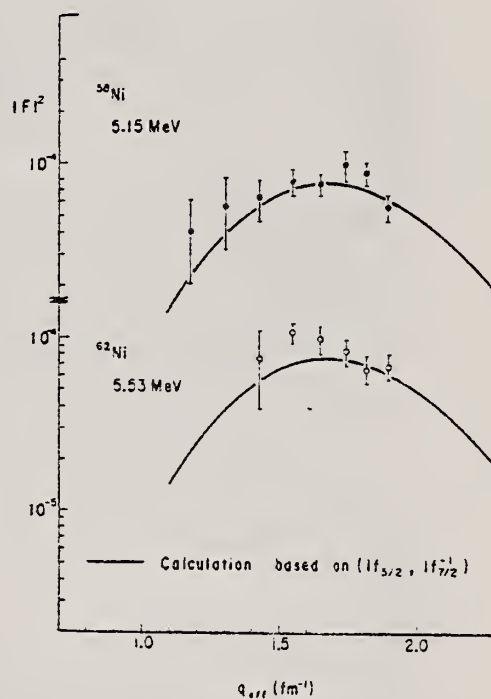


FIG. 2. The experimental form factors for the 6^+ states compared with the theoretical form factors calculated for the $(1f_{5/2}, 1f_{7/2}^{-1})$ configuration.

H. Miyase, S. Oikawa, A. Suzuki, J. Uegaki, T. Saito,
M. Sugawara, and K. Shoda
PIONS-73, Vol. I, p. 553 Asilomar

ELEM. SYM.	A	Z
Ni	58	28
REF. NO.		hmg
73 Mi 7		

REACTION	RESULT	EXCITATION ENERGY	SOURCE		DETECTOR		ANGLE
			TYPE	RANGE	TYPE	RANGE	
E, P	ABX	14- 26	D	0 - 26	MAG-D		DST

736+
737

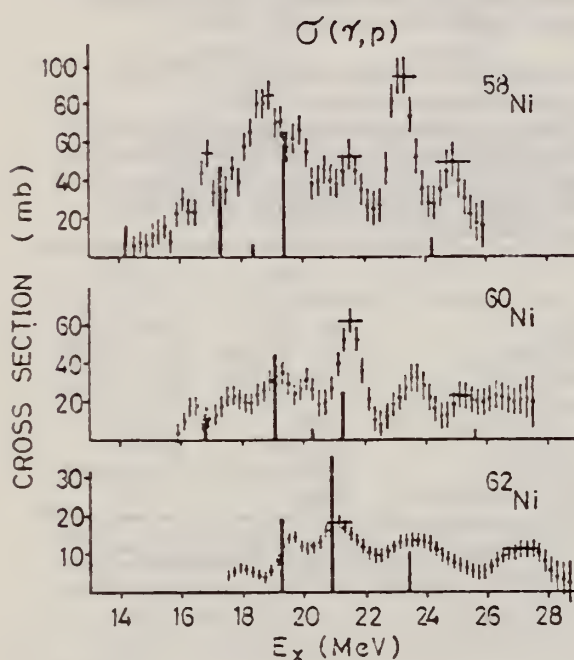


Fig. 1

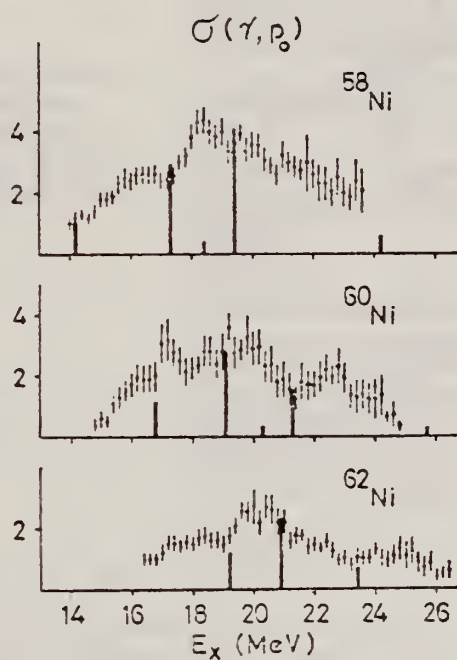


Fig. 2

Table 1 Experimental and theoretical results

Nucleus	T ₀	$\int \sigma_n^3$ (mb-MeV)	$\int \sigma_p$ (mb-MeV)	$\int \sigma_n + \int \sigma_p$ (mb-MeV)	$\frac{\int \sigma_p}{\int \sigma_n + \int \sigma_p}$	$\frac{ c_> ^2}{ c_< ^2 + c_> ^2}$
⁵⁸ Ni	1	310±30	480±100	790±130	0.61	0.45
⁶⁰ Ni	2	620±50	210±80	830±130	0.25	0.27
⁶² Ni	3		110±25			0.17

REF.

ELEM. SYM.	A	Z
Ni	58	28
REF. NO.		
74 Fu 3		hmg

METHOD

REACTION	RESULT	EXCITATION ENERGY	SOURCE		DETECTOR		ANGLE
			TYPE	RANGE	TYPE	RANGE	
G,N	ABX	12- 34	D	12- 34	BF3-I		4PI
G,2N	ABX	22- 34	D	22- 34	BF3-I		4PI

SEP ISOTOPES

522+

TABLE II. Integrated photoneutron cross sections and related quantities from the data of the present experiment. The definitions used in this table are

$$\sigma_{\text{int}} \equiv \int_{E_{\text{thr}}}^{E_{\gamma}^{\text{max}}} \sigma dE_{\gamma}, \quad \sigma_{-1} \equiv \int_{E_{\text{thr}}}^{E_{\gamma}^{\text{max}}} E_{\gamma}^{-1} \sigma dE_{\gamma},$$

where E_{thr} is the threshold energy (see Table I) and E_{γ} is the photon energy; the quantity (γ, Sn) is defined in Ref. 17. Errors on the integrated cross sections are dominated by the systematic errors as discussed in Sec. III of the text.

	⁵⁸ Ni	⁶⁰ Ni
E_{γ}^{max}	33.5 MeV	33.5 MeV
$\sigma_{\text{int}}(\gamma, Sn)$	286 MeV mb	704 MeV mb
$\sigma_{\text{int}}(\gamma, 2n)$	7.65 MeV mb	72.2 MeV mb
$\sigma_{\text{int}}[(\gamma, n) + (\gamma, pn)]^a$	278 MeV mb	632 MeV mb
$\sigma_{\text{int}}(\gamma, 2n)/\sigma_{\text{int}}(\gamma, Sn)$	0.027	0.103
$\sigma_{-1}(\gamma, Sn)$	13.8 mb	35.6 mb
$\sigma_{-1}(\gamma, Sn)$	0.700 mb MeV ⁻¹	1.90 mb MeV ⁻¹
$\sigma_{\text{int}}(\gamma, Sn)/60(NZ/A)$	0.329	0.786

^a This quantity was obtained by subtracting $\sigma_{\text{int}}(\gamma, 2n)$ from $\sigma_{\text{int}}(\gamma, Sn)$; direct integration of the single-photoneutron cross sections gave the same values to within 0.5%.

TABLE IV. Comparison of integrated total photoneutron cross sections $\sigma_{\text{int}}(\gamma, Sn)$ with those from previous experiments.

Reference	E_{γ}^{max} (MeV)	⁵⁸ Ni (MeV mb)	⁶⁰ Ni (MeV mb)
This experiment	30	256	643
Ref. 6 (Moscow)	30	310	620
This experiment	25	204	537
Ref. 5 (Virginia)	25	185	482

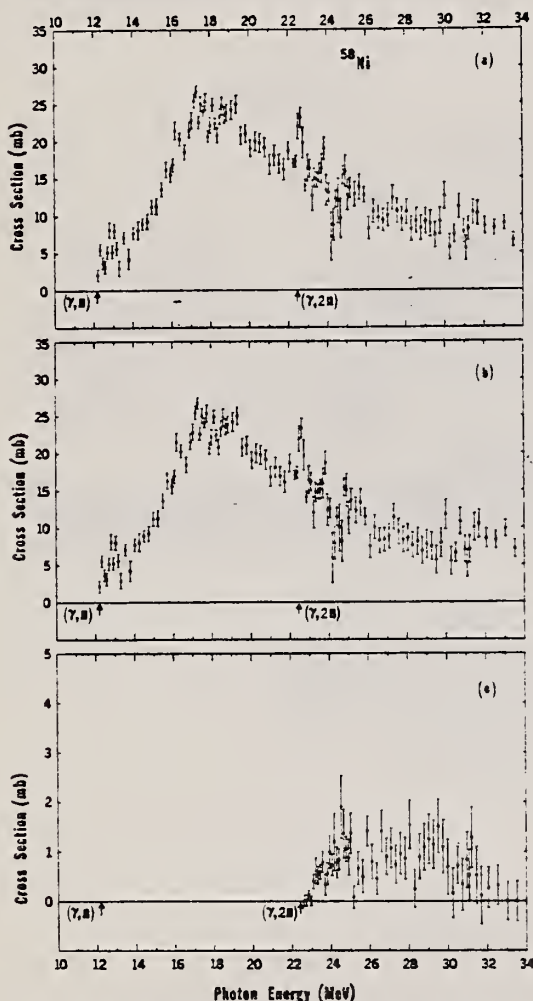


FIG. 2. Measured photoneutron cross sections for ⁵⁸Ni: (a) $\sigma(\gamma, Sn)$ (see Ref. 17); (b) $\sigma[(\gamma, n) + (\gamma, pn)]$; (c) $\sigma(\gamma, 2n)$.

(over)

TABLE III. Energies (MeV) at which peaks appear in the (γ, Sn) cross sections of ^{58}Ni and ^{60}Ni . The energies listed are those at which peaks or shoulders exist in the cross section. Actual resonance energies might be slightly different.

Peak No. ^a	^{58}Ni	^{60}Ni
1	12.3	12.6
2	12.8	13.7
3	13.1	14.4
4	13.6	15.1
5	14.2	15.5
6	15.7	16.3
7	16.3	17.0
8	17.3	17.7
9	17.7	18.8
10	18.2	19.6
11	18.6	21.2
12	19.3	22.1
13	22.6	24.5
14	23.8	
15	24.9	
16	25.7	

^a We have included in the tabulations only the more well-defined peaks (or shoulders). In addition there are possible broad peaks at approximately 20.7, 27.8, and 30.9 MeV in ^{58}Ni , and at 23.5, 26.1, 27.5, and 30.3 MeV in ^{60}Ni , but the data are not sufficiently detailed to make a more definitive judgment about these.

TABLE V. Integrated total photon absorption cross sections and related quantities from the combined data of the present experiment and Ref. 7. The (γ, Xp) cross sections of Ref. 7 have been used rather than those of Ref. 8 because the former extend over a wider energy range; in their mutually inclusive energy range (see Figs. 5 and 6) the integrated cross sections from the two (γ, Xp) measurements agree to within 2% for ^{58}Ni and 10% for ^{60}Ni , the values derived from the data of Ref. 8 being the larger in both cases. The total photon absorption cross section $\sigma(\gamma, \text{total})$ is assumed to be equal to $\sigma(\gamma, \text{Sn}) + \sigma(\gamma, Xp)$; that is the photon-scattering cross section is assumed to be negligible and double counting, owing to the presence of $\sigma(\gamma, pn)$ in both $\sigma(\gamma, \text{Sn})$ and $\sigma(\gamma, Xp)$, is ignored. The latter effect is reasonably compensated for, however (see footnote a).

	^{58}Ni	^{60}Ni
$E_{\gamma \text{ max}}$	33.5 MeV ^a	33.5 MeV ^a
$\sigma_{\text{int}}(\gamma, \text{total})$	850 MeV mb	1025 MeV mb
$\sigma_{-1}(\gamma, \text{total})$	41.3 mb	48.7 mb
$\sigma_{-2}(\gamma, \text{total})$	2.09 mb MeV ⁻¹	2.62 mb MeV ⁻¹
$\sigma_{\text{int}}(\gamma, \text{total}) / (60NZ/A)$	0.98	1.10
$\sigma_{-1}(\gamma, \text{total}) / A^{4/3}$	0.18	0.21
$\sigma_{-2}(\gamma, \text{total}) / A^{5/3}$	0.00264	0.00286

^a The (γ, Xp) data extend only to 30.1 MeV for ^{58}Ni and 30.5 MeV for ^{60}Ni ; above these energies we have used the (γ, Sn) cross section only. Since much of the high-energy cross section probably comes from the (γ, pn) process, the error introduced is probably small and might very well compensate for the double counting of the (γ, pn) cross section below 30 MeV.

5

K. Min and T.A. White, Phys. Rev. Lett. 21, 1200 (1968).

6

B.I. Goryachev, B.S. Ishkhanov, I.M. Kapitonov, I.M. Piskarev, V.G. Shevchenko, and O.P. Shevchenko, Yad. Fiz. 10, 252 (1969); Sov. J. Nucl. Phys. 11, 141 (1970).

7

B.S. Ishkhanov, I.M. Kapitonov, I.M. Piskarev, V.G. Shevchenko, and O.P. Shevchenko, Yad. Fiz. 11, 485 (1970); Sov. J. Nucl. Phys. 11, 272 (1970).

8) K. Shoda, private communication; see also H. Miyase, S. Oikawa, A. Suzuki, J. Uegaki, T. Saito, M. Sugawara, and K. Shoda, in Proceedings of the International Conference on Photonuclear Reactions and Applications, Asilomar, March, 1973, ed. by B.L. Berman (Lawrence Livermore Laboratory, Livermore, 1973), p.553.

17

In our reaction notation we have essentially adopted the convention used by E.G. Fuller, H.M. Gerstenberg, H. Vander Molen, and T.C. Dunn (NBS SP-380, 1973) wherein (γ, Sn) represents the sum of all neutron-producing reactions, (γ, Xp) denotes total proton yield, etc. We use (γ, pn) to represent either the (γ, np) or (γ, pn) reaction since experimentally the two are indistinguishable.

REF. V. V. Varlamov, V. S. Ishkhanov, I. M. Kapitonov,
Zh. L. Kocharova, I. K. Pevtsova, I. M. Piskarev,
and O. P. Shevchenko
Yad. Fiz. 21, 457 (1975); Sov. J. Nucl. Phys. 21, 239 (1975)

ELEM. SYM.	A	Z
Ni	58	28

METHOD

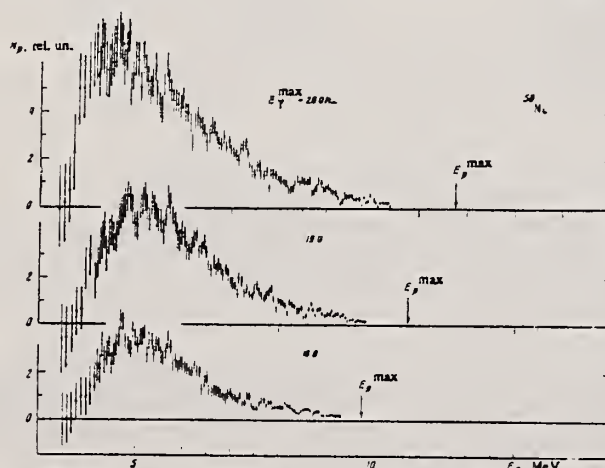
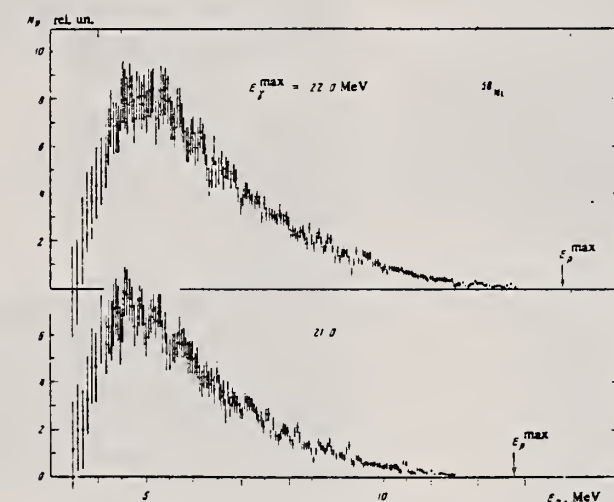
REF. NO.

75 Va 1

hmg

REACTION	RESULT	EXCITATION ENERGY	SOURCE		DETECTOR		ANGLE
			TYPE	RANGE	TYPE	RANGE	
G,P	SPC	8- 22	C	18- 22	SCD-D		UKN

Photoproton spectra have been measured for five different values of bremsstrahlung end-point energy with the purpose of investigating the decay characteristics of giant dipole resonance states in the nucleus ^{58}Ni .



Energy distributions of photoprotons from the nucleus ^{58}Ni , obtained for different bremsstrahlung endpoint energies E_{γ}^{max} .

REF.

C. O. Wene
Z. Phys. A272, 77 (1975)

ELEM. SYM.

A

Z

Ni

58

28

METHOD

REF. NO.

75 We 4

egf

REACTION	RESULT	EXCITATION ENERGY	SOURCE		DETECTOR		ANGLE
			TYPE	RANGE	TYPE	RANGE	
G, P	ABX	18	D	18	SCD-D		90

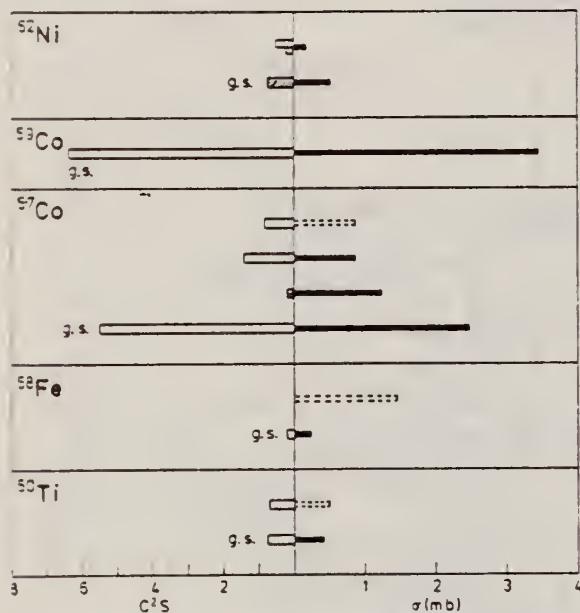
18 = 17.6 MEV

Fig. 5. Correlation between the spectroscopic factors and the cross-sections measured in this work. Open staples indicate $C^2S = 3$ pick-up and cross hatched staples $C^2S = 1$ pick-up. Dashed staples indicate that the cross section is uncertain due to the subtraction of a large background

Table 2

Daughter nucleus	Level		σ^a (mb)
	(MeV)	J^π	
^{44}Ca	0	0^+	$\leq 0.2^b$
	1.16	2^+	$\leq 0.5^b$
^{53}Ti	0	0^+	0.41 ± 0.05
	2.68	4^+	$(0.5)^c$
^{58}Fe	0	0^+	0.23 ± 0.08
	3.24?	$0^+?$	$(1.5)^c$
^{57}Co	0	$7/2^-$	2.5 ± 0.2^d
	1.76	$3/2^-$	1.2 ± 0.3
	1.90	$7/2^-$	0.9 ± 0.2
	2.31	$7/2^-$	$(0.9)^c$
^{59}Co	0	$7/2^-$	3.5 ± 0.8
^{62}Ni	0	0^+	0.51 ± 0.09
	1.18	2^+	0.2 ± 0.1

^a The quoted errors are only those due to counting statistics.^b Confidence level 95%.^c Uncertain because of large background.^d $\sigma = 2.4$ mb from [43].

43. Miyase, H., Oikawa, S., Suzuki, A., Uegaki, J., Saito, T., Sugawara, M., Shoda, K.: The photoproton reactions of Ni-isotopes. In: Proc. Int. Conf. Photonnuclear Reactions and Applications, Vol. I, p. 553. Livermore, USA 1973 (see Ref. 13)

REF. I. A. Grishaev, N. I. Lapin, G. D. Pugachev Yad. Fiz. 24, 335 (1976) Sov. J. Nucl. Phys. 24, 175 (1976)			ELEM. SYM.	A	Z
			Ni	58	28
METHOD			REF. NO.		
			76 Gr 3		hmg
REACTION	RESULT	EXCITATION ENERGY	SOURCE		ANGLE
			TYPE	RANGE	
G,PI+	SPC	150-500	C	500	DST
G,PI-	SPC	150-500	C	500	DST

The energy spectra of charged photopions from ⁵⁴Fe, ⁵⁶Fe, and ⁵⁸Ni targets irradiated with bremsstrahlung of maximum energy 500 MeV have been measured at photopion-emission angles of 30, 60, 90, 120, and 150° in the lab system over the kinetic-energy range from 15 to 80 MeV. Isotope effects are found in the π⁻ yields at 30, 60, and 90°. At all angles and energies, the π⁺ yields are the same for all three targets within the experimental error.

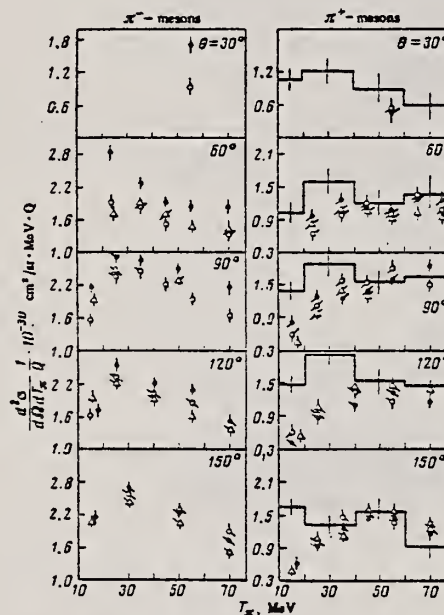


FIG. 1. Energy spectra of charged photopions from ⁵⁴Fe, ⁵⁶Fe, and ⁵⁸Ni targets (open circles, black circles, and tri-angles, respectively) at E₀=500 MeV. The error bars represent statistical errors. The histograms on the π⁺-meson plots represent the results of cascade-model calculations for ⁵⁶Fe.

REF.	R.A. Lindgren, W.L. Bendel, E.C. Jones, Jr., L.W. Fagg, X.K. Maruyama, J.W. Lightbody, Jr., S.P. Fivozinsky Phys. Rev. C14, 1789 (1976)			ELEM. SYM.	A	Z
				Ni	58	28
METHOD				REF. NO.	76 Li 6	
					hmg	
REACTION	RESULT	EXCITATION ENERGY	SOURCE		DETECTOR	
			TYPE	RANGE	TYPE	RANGE
E, E/	ABX	9- 11	D	40- 75	MAG-D	
Using inelastic electron scattering, several isobaric analog 1^+ states between 9 and 13 MeV excitation in ^{58}Ni and ^{60}Ni have been found. They are identified as components of the $T_0 + 1$ giant M1 state in $^{58,60}\text{Ni}$.						

4 M1 STATES

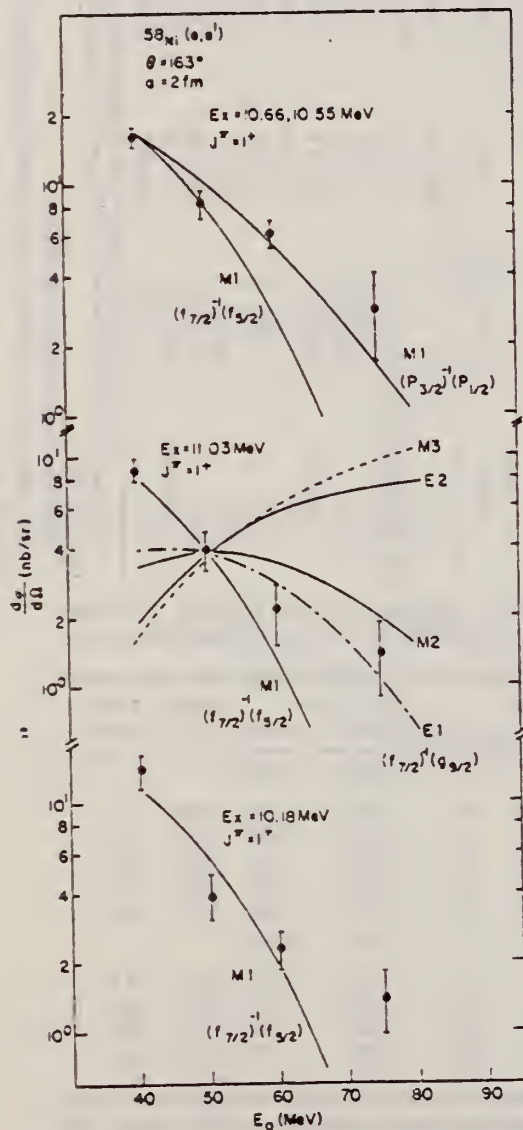


FIG. 7. Comparison of measured cross section with DWBA predictions plotted as a function of E_0 for states $E_x \geq 10$ MeV.

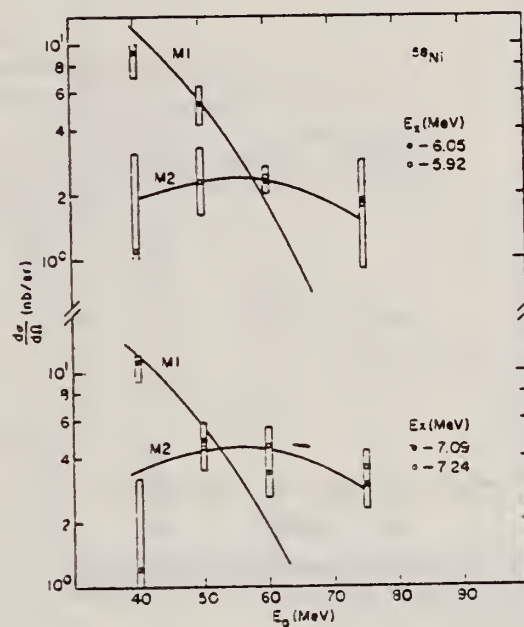


FIG. 9. Decomposition of the differential cross section at $\theta = 160^\circ$ for the partially resolved $E_x = 5.92$ and 6.05 MeV and $E_x = 7.09$ and 7.24 MeV states as a function of E_0 , the incident electron bombarding energy. The data are shown compared to M1 and M2 DWBA calculations.

(over)

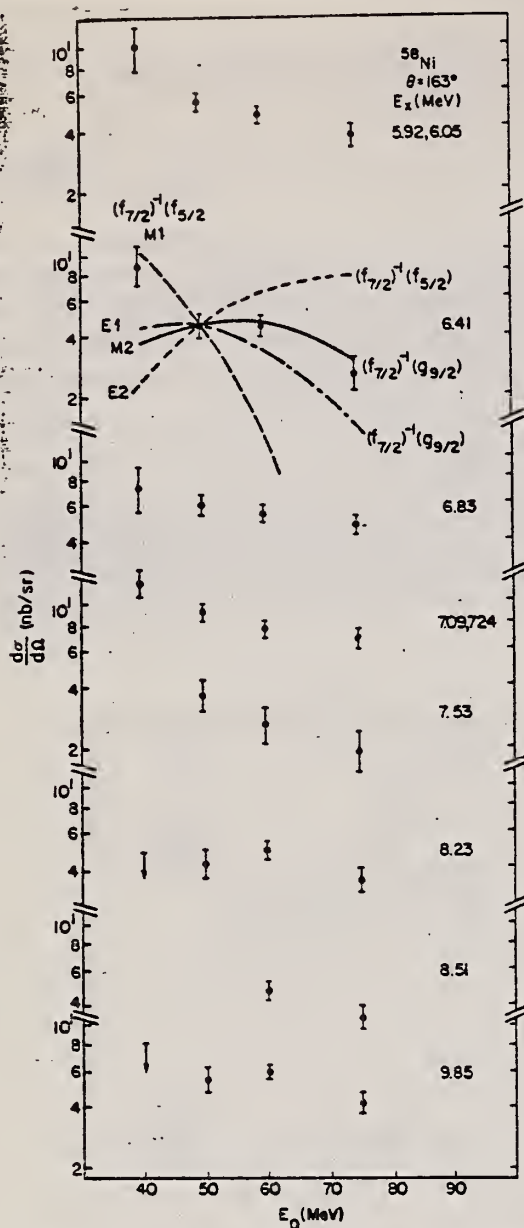


FIG. 8. Comparison of measured cross section with DWBA predictions plotted as a function of E_0 for states in the range $9.8 \geq E_x \geq 5.50$ MeV.

TABLE I. Averaged measured excitation energies and differential cross sections at $\theta = 163^\circ$ at four incident electron bombarding energies for levels in ^{58}Ni .

E_x (MeV) (Ave)	E_0 (MeV)	$d\sigma/d\Omega$ (nb/sr)
1.46	40.2	75.1
4.46	49.5	60.0
5.92, 6.05	60.0	41.8 \pm 2.9
6.41	75.1	21.1 \pm 4.4
6.83		12.3 \pm 0.6
7.09, 7.24		3.7 \pm 0.5
8.23		2.5 \pm 0.5
8.51		4.7 \pm 0.5
9.85		6.7 \pm 0.7
10.55, 10.66		8.0 \pm 0.7
11.03		2.0 \pm 0.4
		3.5 \pm 0.5
		3.5 \pm 0.5
		4.3 \pm 0.5
		1.4 \pm 0.5
		2.9 \pm 1.2
		0.9 $\leq d\sigma/d\Omega \leq 1.9^c$

^a Two background extremes were chosen and then averaged to get the peak cross section (see Fig. 4).

^b Estimated cross section (see Fig. 1).

^c The upper limit is the sum of the two possible peaks and the lower limit is just one of them (see Fig. 4).

TABLE II. Measured excitation energies, J^π assignments, and reduced M1 transition probabilities for levels in $^{58,60}\text{Ni}$.

E_x (MeV) Exp ^a	J^π	E_x (MeV) Predicted ^b	E_x (MeV) Parent	$B(M1)$ (μ_N^2) ^c	$\Gamma(M1)$ (eV) ^d
^{58}Ni		^{58}Ni	^{58}Co		
9.35	(1 ⁺)	9.37	1.05	(0.32) ^e	(3.4) ^e
10.13	1 ⁺	10.25	1.43	0.59	7.2
10.55	1 ⁺	10.55	1.73	0.21	3.0
10.66	1 ⁺	10.68	1.86	0.41	5.7
11.03	1 ⁺	11.06	2.24	0.36	5.6
^{60}Ni		^{60}Ni	^{60}Co		
11.9	1 ⁺	11.87	0.74	0.46	8.9
12.3	1 ⁺	12.34	1.21	0.28	5.6
13.1	(1 ⁺)	13.11	1.98	≤ 0.06	≤ 1.5
13.4	(1 ⁺)	13.35	2.22	≤ 0.06	≤ 1.6
13.9	(1 ⁺)	13.84	2.71	≤ 0.06	≤ 1.8

^a Energy uncertainty is ± 0.04 MeV in ^{58}Ni and ± 0.1 MeV in ^{60}Ni .

^b To get predicted energy in ^{58}Ni add 8.82-MeV to excitation energies in ^{58}Co and for ^{60}Ni add 11.13 MeV.

^c M1 strength uncertainty is estimated to be about $\pm 25\%$ for individual levels.

^d $\Gamma(M1) = 0.0115 E_x^3 B(M1)$.

^e Tentative M1 identification (see text).

B.S. Ishkhanov, I.M. Kapitonov, V.G. Shevchenko, V.I. Shvedunov
and V.V. Varlamov
Nucl. Phys. A283, 307 (1977)

ELEM. NO.	A	Z
Ni	58	28
REF. NO.		egf
77 Is 1		

REACTION	RESULT	EXCITATION ENERGY	SOURCE		DETECTOR		ANGLE
			TYPE	RANGE	TYPE	RANGE	
G,P	NOX	12 - 32	C	18-32	SCD-D		90

DECAY BRANCHING

TABLE 3
The proton decay probabilities in the various channels

Initial states (MeV)		Final states (MeV)				
		$0(1f_{7/2})$	≈ 1.5	$3.3(1d_{3/2})$	$6.2(2s_{1/2})$	$9.6(1d_{5/2})$
^{58}Ni	11.0-16.0		≈ 100			
	16.8	10	10	80		
	18.4	5	20	75		
	19.1	5	20	25	50	
	21.0		10	20	70	
	23.3			10	30	60
	25.2					x
	25.5					x
	27.3					x
^{60}Ni	11.0-16.0		≈ 100			
	16.4	20	10	70		
	18.6	20	10	70		
	20.4	5	5	40	50	
	23.3	5	5	10	50	30
	25.8, 26.6, 27.5				x	

REF.			J. Mougey, M. Bernheim, A. Bussiere, A. Gillebert, Phan Xuan Ho, M. Priou, D. Royer, I. Sick, G. J. Wagner Nucl. Phys. <u>A262</u> , 461 (1976)			ELEM. SYM.	A	Z
						Ni	58	28
METHOD						REF. NO.		
						76 Mo 5		egf
REACTION	RESULT	EXCITATION ENERGY	SOURCE		DETECTOR		ANGLE	
			TYPE	RANGE	TYPE	RANGE		
E,E/P	ABX	8* 80	D	497	MAG-D		53	

*MISSING ENERGY

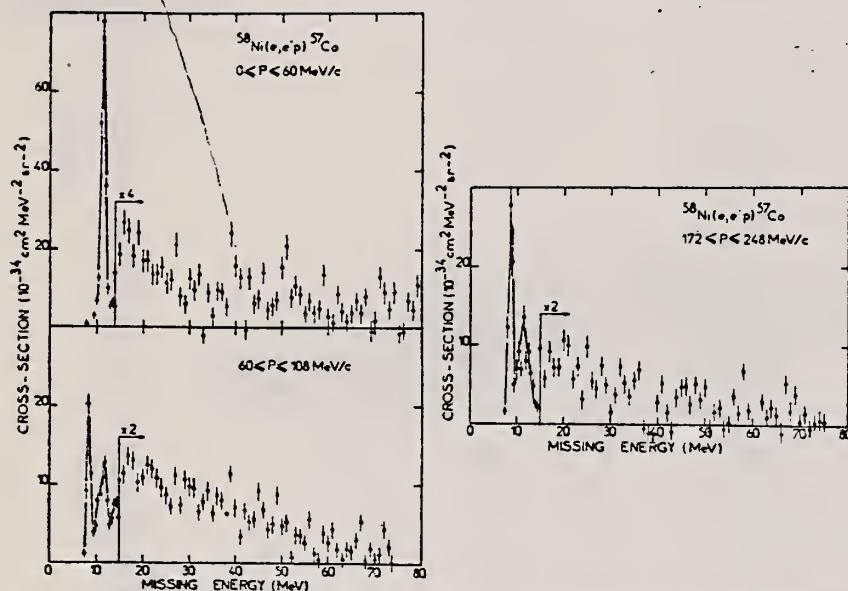


Fig. 15. Missing energy spectra from $^{58}\text{Ni}(e,e'p)^{57}\text{Co}$; (a) $0 \leq P \leq 60$ MeV/c, (b) $60 \leq P \leq 108$ MeV/c and (c) $172 \leq P \leq 248$ MeV/c.

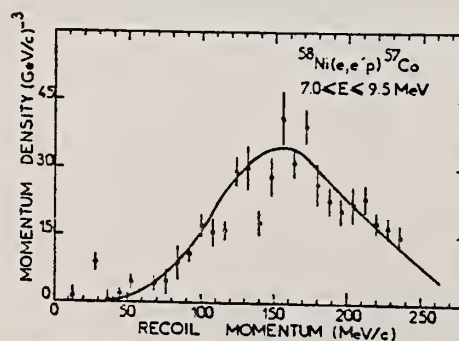


Fig. 16. Momentum distribution from $^{58}\text{Ni}(e,e'p)^{57}\text{Co}$ for $7 \leq E \leq 9.5$ MeV. The solid line represents the DWIA calculation.

REF. R.A. Lindgren, J.B. Franz, W.J. Gerace, R.S. Hicks, A. Hotta,
D. Huse, G.A. Peterson, R.C. York, C.F. Williamson and
S. Kowalski
Phys. Rev. Lett. 41, 1705 (1978)

ELEM. SYM.	A	Z
Ni	58	28
REF. NO.		
78 Li 3		rs

REACTION	RESULT	EXCITATION ENERGY	SOURCE		DETECTOR		ANGLE
			TYPE	RANGE	TYPE	RANGE	
E, E/	FMF	5	D	120-264	MAG-D		DST

Transverse (E6) and longitudinal (C6) cross sections for the excitation of the $J^\pi = 6^+$, $E_x = 5.125$ MeV state in ^{58}Ni were measured by means of inelastic electron scattering. The deduced isoscalar component of the particle-hole wave function is found to be two orders of magnitude greater in amplitude than the isovector. This implies that the particle-hole isospin is relatively pure $\tau = 0$ and is not significantly mixed with $\tau = 1$.

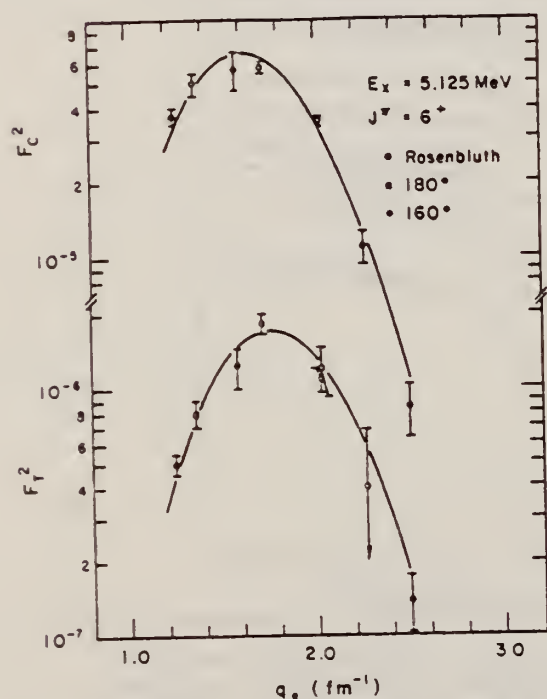


FIG. 2. The extracted transverse and longitudinal form factors compared with calculations described in text.

TABLE I. A tabulation of our measured cross sections for the 5.125-MeV state for various energies and angles that were used to deduce the transverse and longitudinal form factors.

E_0 (MeV)	θ (deg)	q (fm^{-1})	q_0 (fm^{-1})	$d\sigma/d\Omega$ (nb/sr)
189.6	120	1.64	1.71	3.41 ± 0.11
228.1	120	1.97	2.04	1.35 ± 0.03
251.1	120	2.17	2.24	0.40 ± 0.04
120.4	160	1.17	1.25	0.41 ± 0.04
131.1	160	1.28	1.36	0.60 ± 0.11
153.2	160	1.50	1.58	0.64 ± 0.03
167.0	160	1.64	1.72	0.57 ± 0.02
200.4	160	1.97	2.05	0.92 ± 0.07
221.5	160	2.13	2.26	0.067 ± 0.008
242.6	160	2.39	2.47	0.017 ± 0.003
131.1	180	1.30	1.38	0.20 ± 0.02
195.2	180	1.95	2.03	0.13 ± 0.02

METHOD

REF. NO.

78 Ma 10

hg

REACTION	RESULT	EXCITATION ENERGY	SOURCE		DETECTOR		ANGLE
			TYPE	RANGE	TYPE	RANGE	
G,N	ABY	12-68	C	30-68	ACT - I		4PI
G,PN	ABY	20-68	C	30-68	ACT - I		4PI
G,2N	ABY	22-68	C	30-68	ACT - I		4PI

Analysis is made of reactions interfering with photon activation analysis procedures.

The activation yield curves have been presented for a number of photoneuclear reactions in the energy range from 30 to 68 MeV, in order to evaluate quantitatively the interferences due to competing reactions in multi-element photon activation analysis. The general features of the yields as functions of both target mass number and excitation energy were elucidated from the data obtained, discussion being given on the results in terms of the reaction mechanism.

Simultaneous neutron activation due to appreciable neutron production from the converter and surrounding materials has also been studied, and, finally, the magnitudes of interferences in real multi-element analysis were given in the form of their energy dependences.

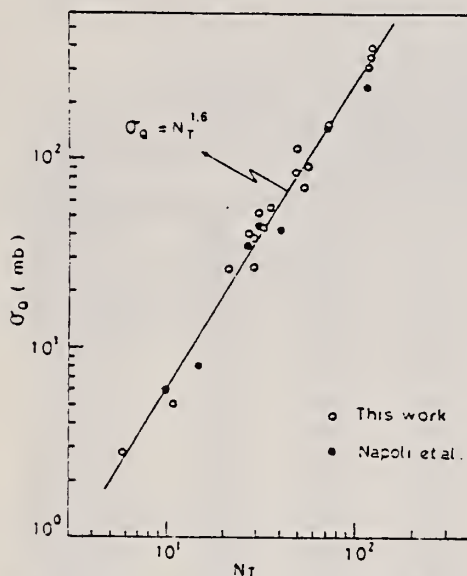


Fig. 2. Yield per equivalent quanta versus target neutron number.

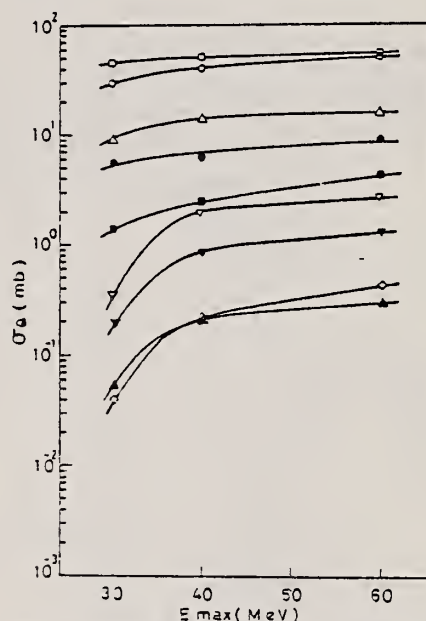


Fig. 6. Activation yield curves for the reactions on Co, Ni and Cu.

○ $^{59}\text{Co}(\gamma, n)^{58}\text{Co}$, ● $^{59}\text{Co}(\gamma, 2n)^{57}\text{Co}$, △ $^{58}\text{Ni}(\gamma, n)^{57}\text{Ni}$,
▽ $^{58}\text{Ni}(\gamma, pn)^{56}\text{Co}$, ▼ $^{50}\text{Ni}(\gamma, pn)^{49}\text{Co}$, ▲ $^{58}\text{Ni}(\gamma, 2n)^{56}\text{Ni}$,
□ $^{63}\text{Cu}(\gamma, n)^{62}\text{Cu}$, ■ $^{63}\text{Cu}(\gamma, 2n)^{61}\text{Cu}$, ◇ $^{62}\text{Cu}(\gamma, xn)^{58}\text{Co}$.

(over)

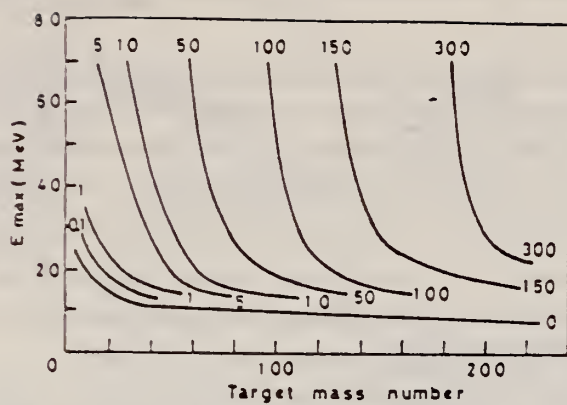


Fig. 9 Yields of the (γ, n) reactions as a function of bremsstrahlung maximum energy and target mass number. The numerical values in the figure are yields per equivalent quanta in mb.

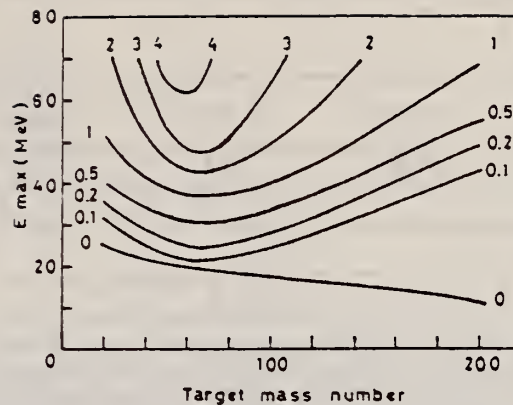


Fig. 11. Yields of the (γ, pn) reactions as a function of bremsstrahlung maximum energy and target mass number. The numerical values in the figure are yields per equivalent quanta in mb.

REF. L. Meyer-Schutzmeister, R.E. Segel, K. Raghunathan, P.T. Debevec, W.R. Wharton, L.L. Rutledge, and T.R. Ophel Phys. Rev. C <u>17</u> , 56 (1978)			ELEM. SYM.	A	Z
			Ni	58	28
METHOD			REF. NO.		
			78 Me 1		hmg
REACTION	RESULT	EXCITATION ENERGY	SOURCE		ANGLE
			TYPE	RANGE	
A,G	ABX	13- 19	D	7- 14	NAI-D

The reaction $^{54}\text{Fe}(\alpha,\gamma)^{58}\text{Ni}$ has been studied for $7.6 \leq E_\alpha \leq 12.8$ MeV. Seventeen angular distributions have been measured in this energy region making it possible to separate the $E2$ strength from the $E1$ strength. The $E1$ cross section reaches a maximum at about the expected energy. A compact $E2$ resonance was observed which agrees quite well with the one measured by inelastic α scattering, with a peak cross section at about 16 MeV and a width of ~ 3 MeV(half width at half maximum). The observed $E1$ strength equals 0.9% of the isospin allowed $E1$ sum rule. The measured $E2$ strength, however, equals 4.3% of the isoscalar $E2$ sum rule, which is about the same as the fraction of the total $E1$ strength in ^{58}Ni excited by proton capture. Assuming only statistical processes and applying the Hauser-Feshbach formula to calculate the total γ absorption from the measured particle-capture cross sections leads to the conclusion that the (α,γ) reaction exciting the isoscalar giant quadrupole resonance and the (p,γ) reaction exciting the giant dipole resonance must have direct components.

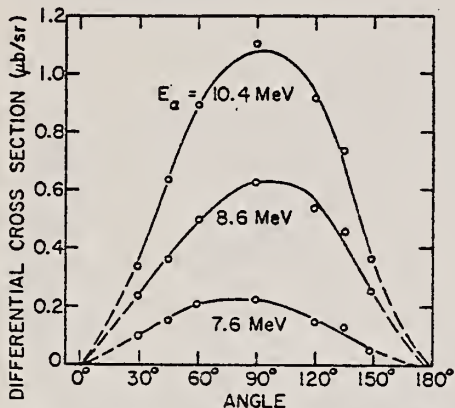


FIG. 2. Angular distributions of the $^{54}\text{Fe}(\alpha,\gamma)^{58}\text{Ni}$ reaction.

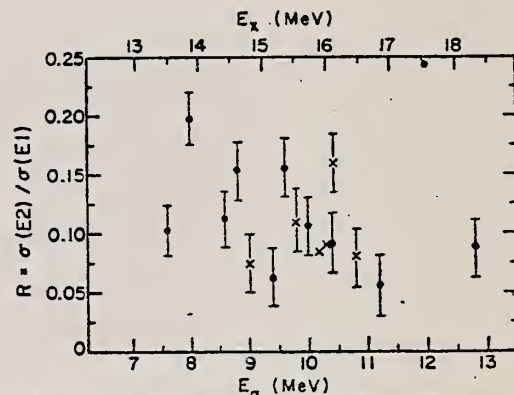


FIG. 3. The ratio $R = \sigma(E2)/\sigma(E1)$ as function of energy. The estimated error is indicated. Crosses indicate angular distribution measurements with only three angles.

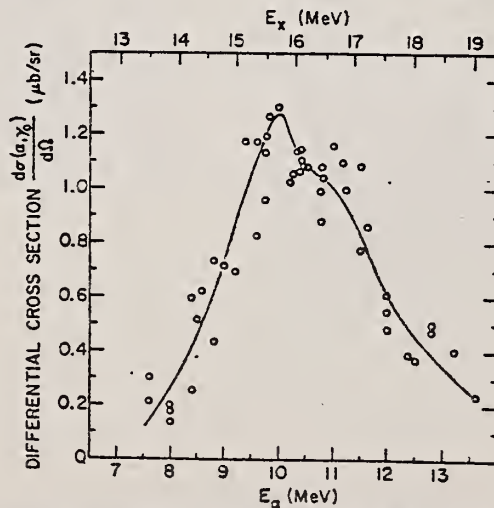


FIG. 4. Differential cross section of the $^{54}\text{Fe}(\alpha,\gamma)^{58}\text{Ni}$ reaction as function of energy. The measurements have been made at 90° for the incoming α beam.

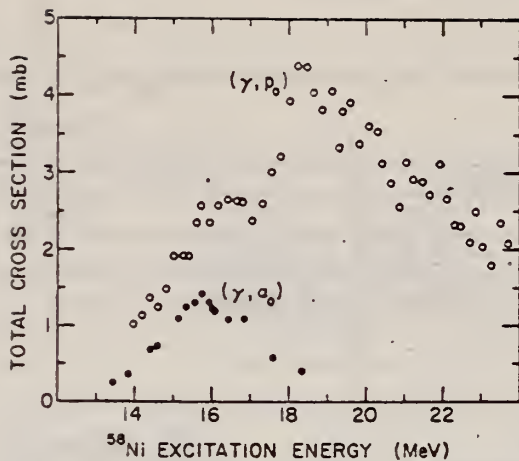


FIG. 7. The cross section of the $^{58}\text{Ni}(\gamma, \alpha_0)$ is presented as function of the excitation energy in ^{58}Ni . The small contribution of the GQR is subtracted. For comparison the cross section of the $^{58}\text{Ni}(\gamma, p_0)$ (see Ref. 6) is shown.

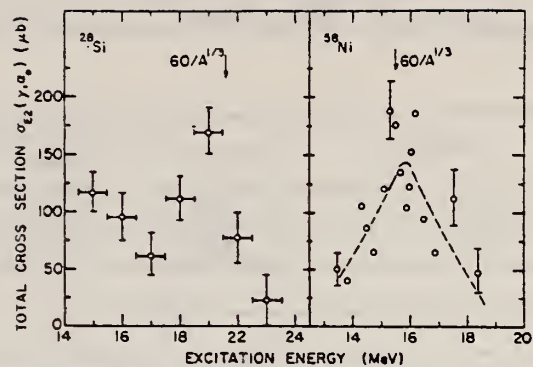


FIG. 8. The cross section of the $^{58}\text{Ni}(\gamma, \alpha_0)$ reaction exciting only the GQR is shown as function of the energy. For comparison an older measurement of the reaction $^{28}\text{Si}(\gamma, \alpha_0)^{24}\text{Mg}$ (Ref. 7) had been partially reanalyzed for a more detailed extraction of the $E2$ strength.

TABEL I. Determination of absolute cross sections of the $^{54,56}\text{Fe}(\alpha, \gamma_0)^{58,60}\text{Ni}$ reactions by using the known reactions $^{12}\text{C}(p, \gamma_0)^{13}\text{N}$ and $^{54}\text{Co}(p, \gamma_0)^{55}\text{Ni}$ for normalization (see text).

Reaction	E_α (MeV)	θ (deg)	Target thickness (mg/cm ²)	$d\sigma/d\Omega$ (μb/sr) normalized to	
				$^{12}\text{C}(p, \gamma_0)^{13}\text{N}$ ^a	$^{54}\text{Co}(p, \gamma_0)^{55}\text{Ni}$ ^b
$^{54}\text{Fe}(\alpha, \gamma_0)^{58}\text{Ni}$	10.0	90	1.1	1.3 ± 0.2	1.2 ± 0.2
$^{56}\text{Fe}(\alpha, \gamma_0)^{60}\text{Ni}$	10.0	90	1.0	0.56 ± 0.15	0.53 ± 0.15

^aReference 12.

^bReference 13.

⁶H. Miyase, S. Oikawa, A. Suzuki, J. Uegaki, T. Saito, M. Sugawara, and K. Shoda, in Proceedings of the International Conference on Photonuclear Reaction and Applications, Asilomar, March 1973, edited by B.L. Berman (Lawrence Livermore Laboratory, Livermore, 1973), Vol. 1, p. 553.

⁷L. Meyer-Schutzmeister, Z. Vager, R.E. Segel, and P.P. Singh, Nucl. Phys. **A108**, 180 (1968)

¹²F.S. Dietrich, M. Suffert, A.V. Nero, and S.S. Hanna, Phys. Rev. **168**, 1169 (1968)

¹³E.M. Diener, J.F. Amann, P. Paul, and S.L. Blatt, Phys. Rev. C **3**, 2303 (1971)

REF. Yu.M. Volkov, A.I. Agnat'ev, G.A. Kolomenskii, E.F. Lakovichev,
E.D. Makhnovskii, A.V. Nadtochii, V.V. Popov, V.P. Fominenko,
V.P. Chizkov
JETP Lett. 30, 59 (1979)
Pis'ma Zh. Eksp. Teor. Fiz. 30, 67 (1979)

ELEM. SYM.	A	Z
Ni	58	28
REF. NO.		hg
79 Vo 4		

METHOD			REF. NO.		hg
REACTION	RESULT	EXCITATION ENERGY	SOURCE		ANGLE
			TYPE	RANGE	
E,P	ABX	12-35	D	12-35	UKN
E,A	ABX	12-35	D	12-35	UKN

Cross sections have been measured for $Ni^{58}(e,e'p)$ and $Ni^{58}(e,e'\alpha)$ reactions. Virtual photon spectra calculated in the distorted wave Born approximation have been used to analyze the experimental results. An electric quadrupole ($E2$) giant resonance has been found which decays principally by the emission of α -particles.

VIRT PHOTON ANAL

PACS numbers: 24.30.Cz, 25.30.Cg, 27.40. + z

TABLE I.

$Ni^{58}(\gamma, p)$			$Ni^{58}(\gamma, \alpha)$		
$\int_0^{30} \sigma(E_\gamma) dE_\gamma$ MeV-mbarn	multi- polarity	ω_0 MeV	Γ MeV	$\int \sigma(E_\gamma) dE_\gamma$ MeV-mbarn	S %
539 ± 33	$E1$	19.1 ± 1.0	4.6 ± 0.4	15.9 ± 2.3	1.8 ± 0.3
$570 \pm 60 [4]$	$E2$	16.0 ± 1.0	2.5 ± 0.5	5.4 ± 1.4	47 ± 12

(over)

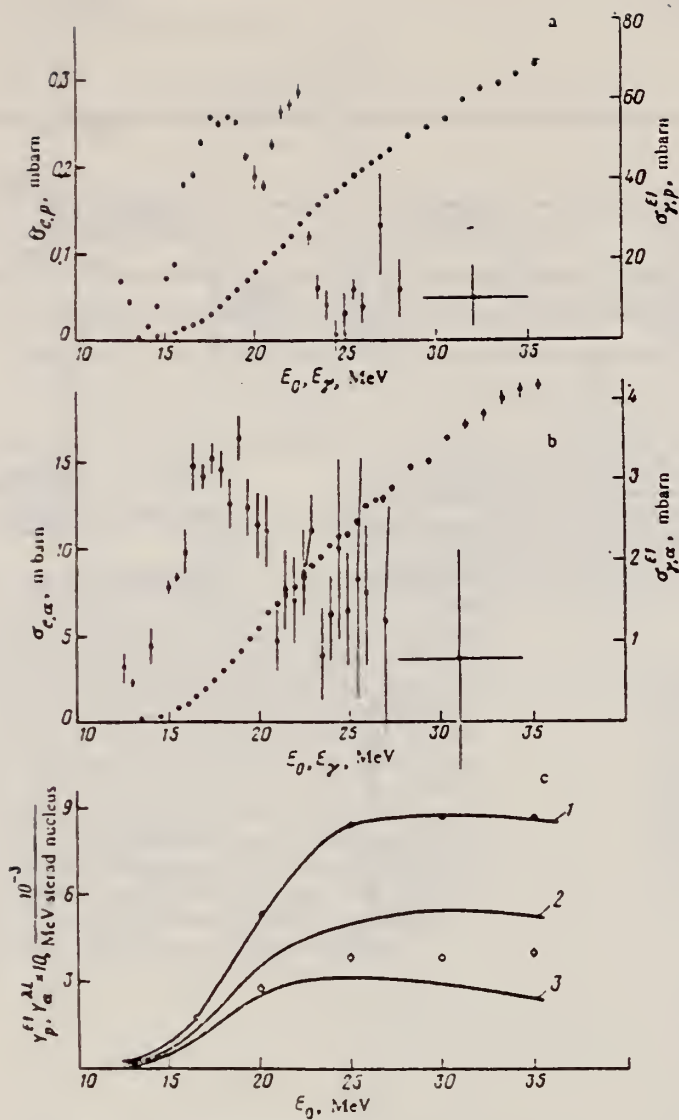


FIG. 1. a—Cross section for the $\text{Ni}^{58}(e,e'p)$ reaction (circles) and the $\text{Ni}^{58}(\gamma,p)$ reaction under the assumption that all the transitions are $E1$ transitions (squares); b—same as Fig. 1a, but for the $\text{Ni}^{58}(e,e'\alpha)$ and $\text{Ni}^{58}(\gamma,\alpha)$ reactions, c—measured emission of protons (dark circles) and α -particles (open circles) correspondingly in the $\text{Ni}^{58}(\gamma,p)$ and $\text{Ni}^{58}(\gamma,\alpha)$ reactions. Curves 1 and 2 are the expected emission respectively of protons and α -particles under the assumption of $E1$ transitions. Curve 3 is the same as curve 2, but under the assumption of $E2$ transitions. The measured proton emission is normalized to curve 1 at an arbitrary point.

ELEM. SYM.	A	Z
Ni	58	28
REF. NO.		
79 Wo 3		hg

METHOD

REACTION	RESULT	EXCITATION ENERGY	SOURCE		DETECTOR		ANGLE
			TYPE	RANGE	TYPE	RANGE	
E, XP	ABX	8-50	D	16-50	MAG-D		4PI
E, XA	ABX	6-50	D	16-50	MAG-D		4PI

The (e, p) and (e, α) cross sections for targets of ^{58}Ni , ^{60}Ni , and ^{62}Ni have been measured in the electron energy range 16–50 MeV. They have been analyzed using the distorted-wave Born-approximation E1 and E2 virtual-photon spectra. Protons are emitted primarily following E1 absorption but α emission results from a combination of E1 and E2 absorption. The E2 isoscalar giant resonance decays predominantly by α emission for these nuclei.

(E, XP) VIRTUAL PHOTON G, XP

(E, XA) VIRTUAL PHOTON G, XA

See also 80 Wo 1

TABLE I. Resonance parameters for $\sigma_{\gamma, p}$.

Nucleus	E_x (MeV)	Γ (MeV) ^a	$\int_0^{30} \sigma dE$ (MeV mb)	SR ^b (%)
^{58}Ni	19.2 ± 0.5	6.5 ± 1.3	738 ± 40	85 ± 5
^{60}Ni	18.5 ± 0.5	9.2 ± 1.8	304 ± 20	34 ± 2
^{62}Ni	21.0 ± 0.5	5.8 ± 1.0	140 ± 10	15 ± 1

^a Γ is the full width at half maximum.

^bSR stands for sum rule; the E1 SR equals $60 NZ/A$ MeV mb.

TABLE II. E1 components in the (γ, α) reaction.

Nucleus	E_x (MeV)	Γ (MeV) ^a	$\int_0^{30} \sigma dE$ (MeV mb)	SR ^b (%)
^{58}Ni	18.3 ± 0.5	6 ± 1	15.3 ± 1.3	1.8 ± 0.2
^{60}Ni	21.5 ± 1.0	6 ± 1	18.5 ± 1.4	2.1 ± 0.2
^{62}Ni	18.3 ± 1.0	5 ± 1	4.8 ± 0.6	0.5 ± 0.1

^a Γ is the full width at half maximum.

^bE1 SR equals $60 NZ/A$ MeV mb.

TABLE III. E2 components in the (γ, α) reaction.

Nucleus	E_x (MeV)	Γ (MeV) ^a	$\int_0^{30} \sigma dE$ (MeV mb)	SR ^b (%)
^{58}Ni	16.5 ± 0.5	4.2 ± 1.0	10.4 ± 0.7	56 ± 4
^{60}Ni	16.0 ± 0.5	3.7 ± 0.3	6.9 ± 0.4	52 ± 3
^{62}Ni	16.8 ± 0.5	4.5 ± 1.0	5.1 ± 0.4	28 ± 2

^a Γ in the full width at half maximum.

^bE2 SR equals $0.22 Z^2/A^{1/2} \mu\text{b/MeV}$.

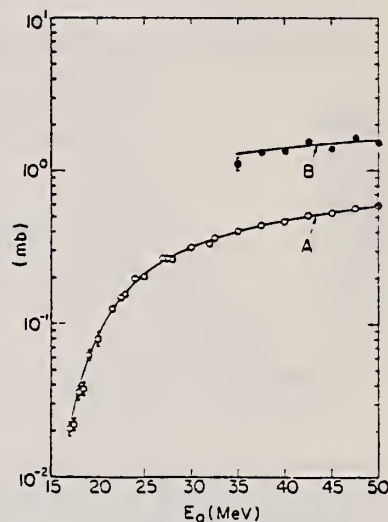


FIG. 2. The cross section for the production of protons, $\sigma_{e,p}(E_0)$, when electrons of total energy E_0 are incident on a ^{62}Ni target (open circles). The closed circles represent the yield of protons obtained when a 0.217-g/cm^2 Ta foil was placed in the incident electron beam. Curve A is predicted using 1.26 times the (γ, p) cross section of Ref. 6 along with the E1 virtual-photon spectra in Eq. (1). Curve B is obtained by taking into account the radiator thickness according to Eq. (2).

(over)

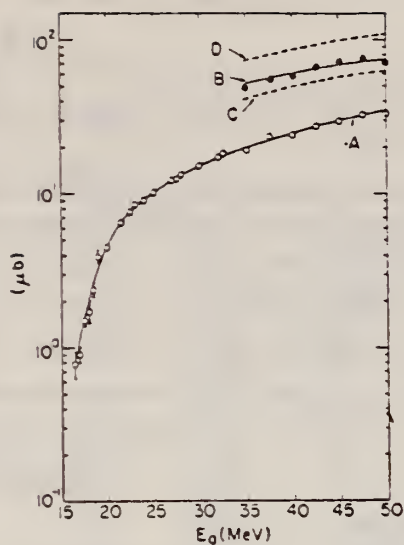


FIG. 3. The measured $\sigma_{e,\alpha}(E_0)$ (open circles) for ^{58}Ni as a function of total incident electron energy, E_0 . The closed circles represent the electrodisintegration plus photodisintegration yield obtained when the 0.217-g/cm^2 tantalum foil was interposed in the incident electron beam. Curve A is the best fit to the data obtained by using the $E1$ and $E2$ virtual-photon spectra in Eq. (1) along with the two resonance lines whose parameters are given in Tables II and III. Curve B is the corresponding result with the radiator in, obtained using Eq. (2). Curve D was predicted using the best $E1$ fit to the data, a 22-MeV-wide resonance. Curve C was predicted using the best $E2$ fit to the data. This figure is intended to show that both $E1$ and $E2$ components are necessary to explain the (e, α) cross section.

METHOD

REF. NO.

80 Ar 11

hg

REACTION	RESULT	EXCITATION ENERGY	SOURCE		DETECTOR		ANGLE
			TYPE	RANGE	TYPE	RANGE	
G, SPI	ABY	THR-999	C	999	ACT-I		4PI

Yield of $(\gamma, n)/(\gamma, p) = 2.77 \pm 0.22$

999=4.5 GEV

New data are presented on the photodisintegration of the enriched isotopes ^{58}Ni and ^{54}Ni under bombardment by photons with maximum energy 4.5 GeV. The isotope effect in photonuclear reactions with formation of residual nuclei is investigated. The experimental yield values are compared with theoretical calculations by Rudstam's formula. In the results we observe a systematic shift of the experimental disintegration yields in comparison to the calculated values. An exponential dependence is found for the ratios of the yields of the residual nuclei from the ^{58}Ni target to the yields of the same nuclei from ^{54}Ni as a function of the third projection of the isotopic spin of the product nucleus, and an exponential dependence is found for the ratios of the experimental yield values to the theoretical values as a function of the difference of the third projections of the isotopic spins of the target nuclei and the residual nuclei.

PACS numbers: 25.20. + y, 27.50. + e

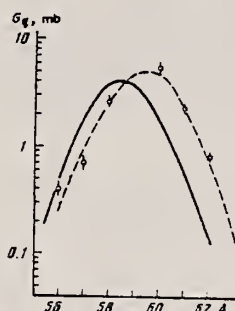


FIG. 1. Distributions of independent yields of Co residual nuclei in mass number. The solid curve is a calculation with Eq. (1), and the dashed curve has been drawn from the experimental points.

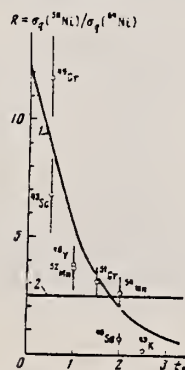


FIG. 3. Ratio of yields of identical residual nuclei from two isotopes of the target nuclei as a function of the third projection of the isotopic spins of the residual nuclei. Curve 1 is the function $15 \exp(-t_3)$, and curve 2 is calculated with Eq. (1).

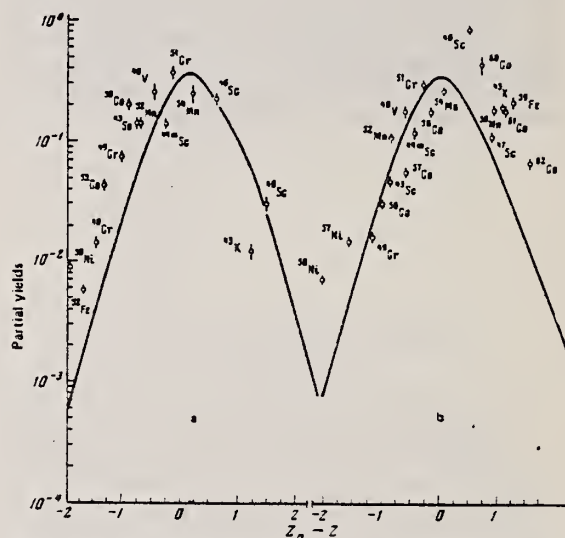


FIG. 2. Charge-dispersion curves of residual nuclei from targets of ^{58}Ni (a) and ^{54}Ni (b).

(over)

TABLE II.

Residual nucleus	^{58}Ni target			^{58}Ni target			Type of yield	t_3
	$\sigma_{\text{exp}}, \text{mb}$	$\sigma_{\text{theo}}, \text{mb}$	$\frac{\sigma_{\text{exp}}}{\sigma_{\text{theo}}}$	$\sigma_{\text{exp}}, \text{mb}$	$\sigma_{\text{theo}}, \text{mb}$	$\frac{\sigma_{\text{exp}}}{\sigma_{\text{theo}}}$		
^{58}Ni	0.81 ± 0.01	0.162	5.16				I	4
^{59}Ni	2.01 ± 0.15	0.5022	4.16				C	3.5
^{60}Ni	5.5 ± 1	1.6247	3.38				I	3
^{61}Ni	2.6 ± 0.1	0.987	0.65	0.146 ± 0.02			I	2
^{62}Ni	1.0 ± 0.1	1.672	0.604	16.5 ± 1	1.066	9.35	C	1.5
^{64}Ni	0.58 ± 0.01	0.9656	1.26	8.1 ± 0.4	1.2965	6.255	C	1
^{66}Ni	-	0.408	-	1.7 ± 0.1	0.2497	6.81	C	0.5
^{67}Ni	0.29 ± 0.03	0.0974	2.987	17.2 ± 1	0.251	68.1	I	1
^{68}Ni	0.15 ± 0.03	0.01528	9.816	0.5 ± 0.03	0.0358	13.97	I	0
^{69}Fe	1.3 ± 0.2	0.2625	6.85	-	-	-	I	3.5
^{70}Fe	-	0.016788	-	0.135 ± 0.01	0.0383	3.52	I	0
^{71}Mn	1 ± 0.05	0.4075	2.453	-	-	-	C	3
^{72}Mn	1.6 ± 0.2	1.706	0.39	3.8 ± 0.4	5.23	0.7267	I	2
^{73}Mn	0.47 ± 0.01	0.3916	1.71	1.36 ± 0.1	1.042	2.12	C	1
^{74}Mn	0.2 ± 0.03			0.85 ± 0.07				
^{75}Cr	1.1 ± 0.1	0.942	1.1677	3.15 ± 0.3	2.5077	1.33	C	1.5
^{76}Cr	0.063 ± 0.006	0.187	0.721	0.67 ± 0.03	0.214	3.175	C	0.5
^{77}Cr	-	0.0167	-	0.13 ± 0.01	0.037	3.513	C	0
^{78}V	0.15 ± 0.04	0.2053	1.524	1.7 ± 0.15	0.7516	2.26	C	1
^{79}Se	-	0.0233	-	0.07 ± 0.02	0.0524	1.336	I	3
^{80}Se	0.44 ± 0.03	0.078987	1.772	-	0.187	-	C	2.5
^{81}Se	0.91 ± 0.09	0.2004	4.54	0.53 ± 0.05	0.493	1.075	I	2
^{82}Se	0.13 ± 0.02	0.2008	-	0.32 ± 0.03	0.186	-	I	1
^{83}Se	0.053 ± 0.005	0.0631	0.8399	0.32 ± 0.05	0.143	2.24	C	0.5
^{84}K	0.09 ± 0.009	0.0209	4.306	0.011	0.015	0.24	I	2.5

Note. σ_{exp} and σ_{theo} are respectively the experimental and theoretical yield values; t_3 is the third projection of the isospins.

ELEM. SYM.	A	Z
Ni	58	28
REF. NO.		
80 Pi 2		hg

REACTION	RESULT	EXCITATION ENERGY	SOURCE		DETECTOR		ANGLE
			TYPE	RANGE	TYPE	RANGE	
E, E/	ABX	7-40	D	102	MAG-D		DST

The cross section for electron scattering from the isotopes ^{58}Ni and ^{60}Ni has been measured with electrons of 102 MeV at scattering angles of 45, 60, 75, 90, and 105° between 3 and 50 MeV excitation energy. Resonances or resonancelike structures at approximate excitation energies of (7-8) MeV, 13 MeV, (16-17) MeV, (18-19) MeV, 27 MeV, 32 MeV, and 40 MeV were classified on the basis of their momentum transfer dependence and discussed in the framework of the shell model. Difficulties in the extraction of the cross section and model dependencies of the interpretation are discussed.

BEL

NUCLEAR REACTIONS $^{58}\text{Ni}(e, e')$ and $^{60}\text{Ni}(e, e')$, $E_0 = 102$ MeV. Measured $d^2\sigma/d\Omega dE_x$, bound and continuum states (giant resonances). Deduced multipolarity, reduced matrix element $B(E\lambda)$, sum rule exhaustion of giant resonances, total width of continuum and clustered states.

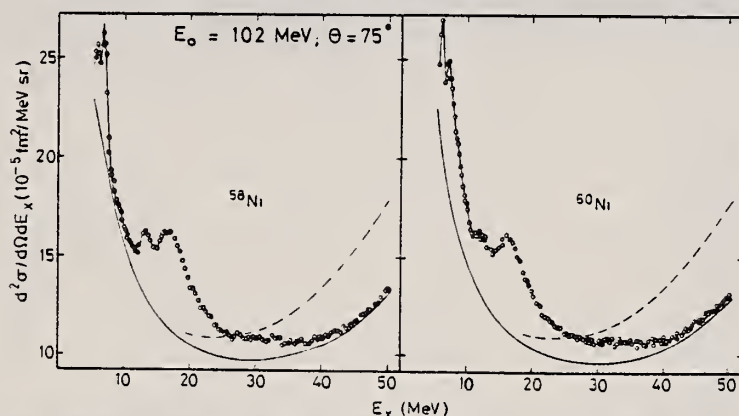


FIG. 4. Comparison of spectra of 102 MeV electrons scattered at 75° from ^{58}Ni and ^{60}Ni . The cross section for ^{60}Ni has been renormalized so that the highest and lowest points in both plots are equal. The spectra were taken with 10 points/MeV but have been reduced for graphical purposes. The broken line is the calculated radiation tail. For demonstration purposes we have subtracted the ghost peak at 8 MeV from the data for ^{58}Ni , but not for ^{60}Ni ; the difference is clearly visible. Note the suppressed zero.

TABLE III. Strength of $E1$ components in the present work. The resonance parameters shown were used to approximate the $E1$ strength distribution for the χ^2 fit. As evident from Fig. 8, where mainly $E1$ contributes, the $E1$ strength function is reasonably well described. The $E1$ strength extracted from the resonances, corresponding to integration to infinity, adds up to approximately 110% of the classical $E1$ sum rule. For ease of comparison, we also give the sum rule strength found by integration from 10 to 30 MeV, 94 ± 10 and $87 \pm 10\%$ for ^{58}Ni and ^{60}Ni , respectively. The table and Fig. 8 also show that the peak strength is shifted to lower excitation energy by going from ^{58}Ni to ^{60}Ni . Although the gross shift is in agreement with the isospin coupling model^{1,37} we do not think it is a sufficient basis for a claim of observed isospin splitting. The average excitation energy, weighted with the $E1$ strength function between 10 and 30 MeV, in contrast, remains virtually unchanged.

^{58}Ni					^{60}Ni				
E_x (MeV)	Γ (MeV)	B (fm ²)	$R\gamma^a$	R_∞^b	E_x (MeV)	Γ (MeV)	B (fm ²)	$R\gamma^a$	R_∞^b
13.1 \pm 0.3	1.4 \pm 0.5	0.4	2.3	2.5 \pm 1	12.65 \pm 0.3	1.5 \pm 0.4	0.9	4.5	5 \pm 1
16.2 \pm 0.3	2.5 \pm 0.5	1.5	10.5	11 \pm 2	16.6 \pm 0.4	2.75 \pm 0.5	2.5	16.5	18 \pm 4
18.3 \pm 0.5	4.5 \pm 0.5	7.3	54	62 \pm 7	19.5 \pm 0.5	6.0 \pm 1.0	7.4	51	63 \pm 8
22.0 \pm 1.0	6.0 \pm 1.0	3.3	27	34 \pm 8	23.5 \pm 1.5	6.0 \pm 1.5	1.9	15	19 \pm 4
			94	110 \pm 11				87	105 \pm 10

^a $\int_{10}^{30} (dB/dE_x)(dE_x/EWSR 100)$.

^b $E_x B(E1)/EWSR 100$.

TABLE VI. Comparative measurements of ^{58}Ni and ^{60}Ni for the $E2$ resonance.

^{58}Ni			^{60}Ni			Ref.	Method
E_x (MeV)	Γ (MeV)	R^a	E_x (MeV)	Γ (MeV)	R^a		
16.4 \pm 0.3	4.9 \pm 0.2	55 \pm 15	16.6 \pm 0.3	5.0 \pm 0.4	63 \pm 15	17	(α, α')
16.5 \pm 0.5	4.2 \pm 1.0	56 \pm 4	16.0 \pm 0.5	3.7 \pm 0.8	52 \pm 3	32	(e, α)
16.2 \pm 0.3	4.5 \pm 0.4	65 \pm 10	16.3 \pm 0.3	4.5 \pm 0.4	55 \pm 10	Present work	(e, e')

^a $R = E_x B(E2)/EWSR(E2, \Delta T = 0)$.

(OVER)

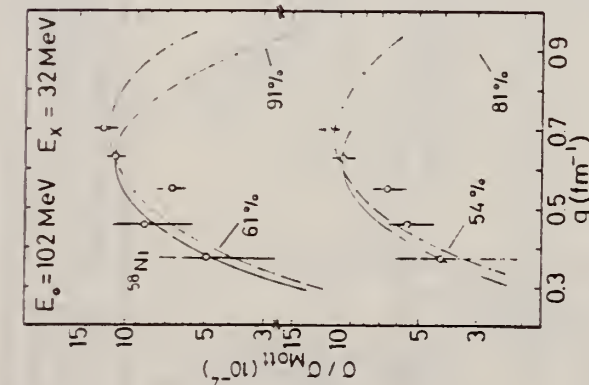


FIG. 14. Comparison between experimental and DWBA cross sections for resonance at 32 MeV. An E2 assignment is preferred, but other multipolarities (not taken into account) could contribute. The Goldhaber-Teller model leads to the higher strength; this strength might be regarded as an upper limit. The Myers-Swiatecki model (broken line) assumed $\alpha = 1$ (see text for definition). Extension of the Myers-Swiatecki model by Kodama to higher multipolarities gives values for α ranging from 0.12 to 0.44. Thus the sum rule values given in the figure for the MS model should be regarded as lower limits. The dependence of the experimental points on the momentum transfer suggest the possibility of more than one multipolarity contributing. This possibility was not investigated due to the accuracy limitations at this high excitation energy.

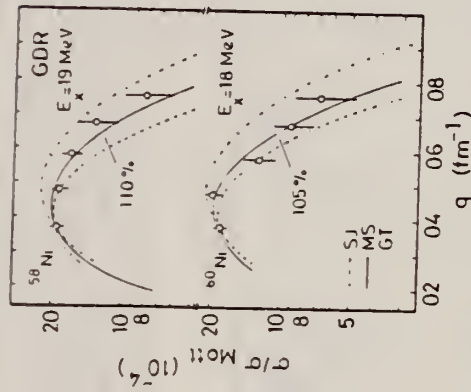


FIG. 9. Comparison between experimental and calculated cross sections for the models of Fig. 8. The curves were normalized to go through the point with the lowest momentum transfer, because this is the one with the least model dependence and the most accurate one. The Myers-Swiatecki model is somewhat favored by this comparison; however, the difficulties with the simultaneous fit of several resonances between 15 and 19 MeV, as discussed in the text, should be noted.

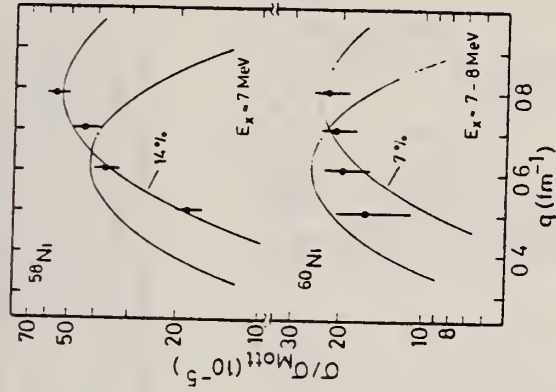


FIG. 11. Comparison of experimental cross sections for a state (group of states?) at 7 MeV in ^{58}Ni and a group of states between 7 and 8 MeV in ^{60}Ni with DWBA calculations. The ^{58}Ni data follow an E3 form factor quite well, but the ^{60}Ni data, which carry only half of the ^{58}Ni strength, may include an E2 or E1 contribution.

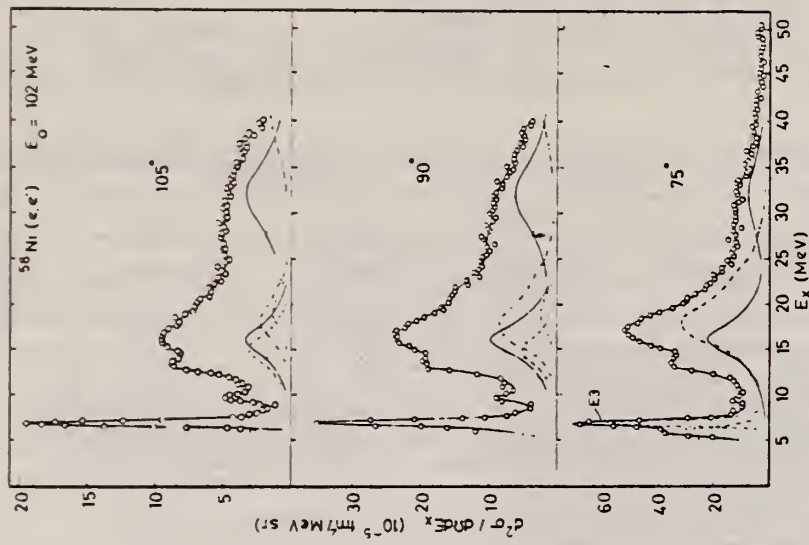


FIG. 5. Comparison of inelastic electron spectra for ^{58}Ni scattered at 75°, 90°, and 105°. The typical feature of higher multipolarities (E3 and E4) becoming more pronounced as compared to E1 and E2 with higher momentum transfer are most clearly visible for the E3 states at 7 and 13 MeV. The solid lines represent E2, the dotted lines E3, the broken lines E4, and the broken-dotted lines E1. For more details concerning assumptions about multipolarities and their possible interplay the text should be consulted. The tail of the resonance at 40 MeV (broken line) for 90° and 105° has been taken from the ^{60}Ni measurements (Fig. 6) because the ^{58}Ni data extended only to about 40 MeV.

REF.	Yu.M. Volkov, A.I. Ignat'ev, G.A. Kolomenskii, E.F. Lakovichev, E.D. Makhnovskii, A.V. Nadtochii, V.V. Popov, V.P. Fominenko, V.P. Chizhov Sov. J. Nucl. Phys. 32, 306 (1980) Yad. Fiz. 32, 595 (1980)			ELEM. SYM.	A	Z
				Ni	58	28
METHOD				REF. NO.		
				80.Vo 2		hg

REACTION	RESULT	EXCITATION ENERGY	SOURCE		DETECTOR		ANGLE
			TYPE	RANGE	TYPE	RANGE	
E, P	ABX	8-35	C	12-30	TEL-D		DST
E, A	ABX	6-35	C	12-30	TEL-D		DST

Cross sections have been measured for the reactions $^{58,60}\text{Ni}(e,e'p)$ and $^{58,60}\text{Ni}(e,e'\alpha)$ in the electron-energy range 12-35 MeV. For analysis of the experimental results we used virtual photon spectra calculated in the DWBA. At energies $E_\gamma = 16.0 \pm 1.0$ MeV for ^{58}Ni and $E_\gamma = 15.6 \pm 1.0$ MeV for ^{60}Ni we have observed giant electric-quadrupole resonances which decay mainly by α -particle emission. The integrated cross sections for the reactions $^{58}\text{Ni}(\gamma, \alpha)$ and $^{60}\text{Ni}(\gamma, \alpha)$ due to E2 transitions are respectively 5.4 ± 1.4 and 6.0 ± 3.0 mb-MeV, which amounts to $47 \pm 12\%$ of the total strength of isoscalar E2 transitions for ^{58}Ni and $56 \pm 28\%$ for ^{60}Ni . The integrated cross sections for these same reactions due to E1 transitions are 15.9 ± 2.3 and 16.9 ± 4.8 mb-MeV, which amount to $1.7 \pm 0.3\%$ of the value given by the sum rule for electric-dipole transitions for ^{58}Ni and $1.8 \pm 0.5\%$ for ^{60}Ni . The measured integrated cross sections for the reactions $^{58,60}\text{Ni}(\gamma, p)$ are 539 ± 33 and 300 ± 20 mb-MeV.

PACS numbers: 25.30.Cg, 24.30.Cz, 27.40.+z, 27.50.+e

VIRT PHOTON ANALYSIS

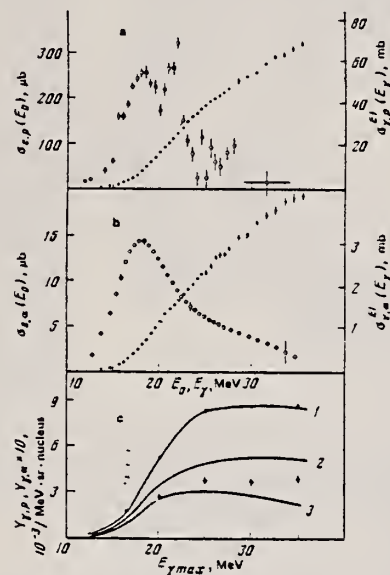


FIG. 2. Cross sections of the reactions $^{58}\text{Ni}(e,e'p)$ (solid points) and $^{58}\text{Ni}(\gamma, p)$, calculated on the assumption that only E1 transitions are excited (hollow points)—a; b—the same but for the reactions $^{58}\text{Ni}(e,e'\alpha)$ and $^{58}\text{Ni}(\gamma, \alpha)$; c—measured yields of protons (solid points) and α particles (hollow points) in the reactions $^{58}\text{Ni}(\gamma, p)$ and $^{58}\text{Ni}(\gamma, \alpha)$. Curves 1 and 2 respectively are the expected yields of protons and α particles obtained on the assumption that only E1 transitions are excited; curve 3 is the same as curve 2 but on the assumption that only E2 transitions are excited. The proton yield has been normalized to curve 1 at an arbitrary point.

TABLE I.

Nucleus	Reaction (γ, p) $\int \sigma(E_\gamma) dE_\gamma$ MeV · mb	(e, γ, α) reaction				
		Multipolarity	E_R , MeV	Γ , MeV	σ_{int}^{E1} , MeV · mb	SAL, %
^{58}Ni	539 ± 33 570 ± 60 [11]	E1 E2	19.1 ± 1.0 18.0 ± 1.0	4.6 ± 0.4 2.5 ± 0.5	15.9 ± 2.3 5.4 ± 1.4	1.7 ± 0.3 47 ± 12
^{60}Ni	300 ± 20	E1 E2	18.0 ± 1.0 15.6 ± 1.0	3.3 ± 1.0 2.4 ± 0.8	16.9 ± 4.8 6.0 ± 3.0	1.8 ± 0.5 56 ± 28

L. Moyer-Schützmeister et al., Phys. Rev. C17, 56 (1978). 78 VU-1

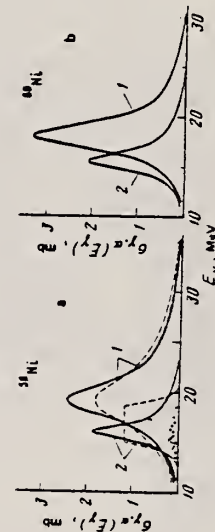


FIG. 5. Resonance curves 1 and 2 (respectively $\sigma_{E1}^{58}(E_\gamma)$ and $\sigma_{E2}^{58}(E_\gamma)$) of the reaction $^{58}\text{Ni}(\gamma, \alpha)$ obtained as the result of an analysis of experimental data. The solid curves are the result of a fit by two Lorentz curves, and the dashed curves are for a fit in which $\sigma_{E2}^{58}(E_\gamma)$ has the form of a rectangle; the points show the cross section $\sigma_{E1}^{58}(E_\gamma)$ of the reaction $^{58}\text{Ni}(\gamma, \alpha)$ from Ref. 2 (a); b—Lorentz curves of $\sigma_{E1}^{60}(E_\gamma)$ (1) and $\sigma_{E2}^{60}(E_\gamma)$ (2) for the reaction $^{60}\text{Ni}(\gamma, \alpha)$.

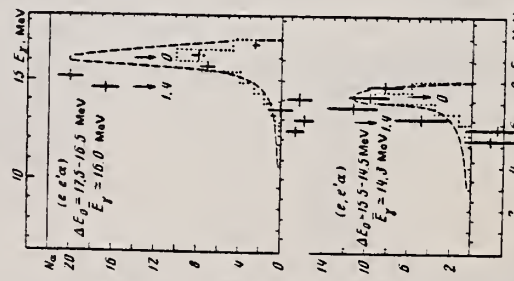


FIG. 6. Difference energy distributions of α particles in the reaction $^{58}\text{Ni}(e, e'\alpha) ^{54}\text{Fe}$. The arrows indicate the α -particle energies corresponding to transitions to the ground state (0) and the first excited state ($E_x^* = 1.4$ MeV) of the ^{54}Fe residual nuclei. The dashed curve is the effective difference spectrum of virtual photons absorbed by the ^{58}Ni nucleus; the histogram gives the theoretical contribution of transitions to the ^{54}Fe ground state.

ELEM. SYM.	A	Z
NI	58	28

METHOD	REF. NO.
	80 Wo 1

ANGLE
hg

REACTION	RESULT	EXCITATION ENERGY	SOURCE		DETECTOR		ANGLE
			TYPE	RANGE	TYPE	RANGE	
E, XP	ABX	8-50	D	16-50	MAG-D		DST
E, XA	ABX	6-50	D	16-50	MAG-D		DST

The (e,p) and (e,α) cross sections for targets of ⁵⁸Ni, ⁶⁰Ni, and ⁶²Ni have been measured in the electron energy range 16-100 MeV. They have been analyzed using the distorted-wave Born approximation E1 and E2 virtual photon spectra. Protons are emitted primarily following E1 absorption but α-emission results from a combination of E1 and E2 absorption.

NUCLEAR REACTIONS ^{58,60,62}Ni(e,p) and ^{58,60,62}Ni(e,α); measured $\sigma(E_0, E_x, 48^\circ)$, $\sigma(E_0, E_x, 90^\circ)$, $\sigma(E_0, E_x, 132^\circ)$; obtained $\sigma(e, p)$, $\sigma(e, \alpha)$; deduced $\sigma_{T,p}^{E1}(E)$, $\sigma_{T,\alpha}^{E1}(E)$, $\sigma_{T,\alpha}^{E2}(E)$.

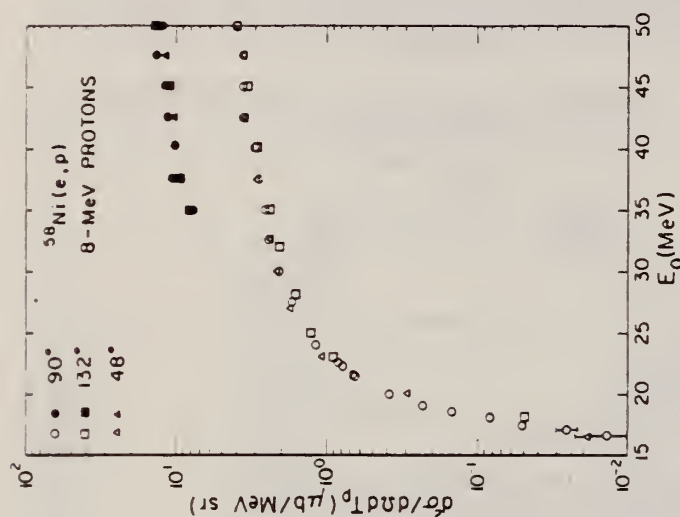


FIG. 4. The differential cross section $d^2\sigma/dT_p d\Omega$ for the production of 8 MeV protons from ⁵⁸Ni as a function of total incident electron energy E_0 . The data were taken at three angles: 132° (squares), 90° (circles), and 48° (triangles). The upper points refer to the yields resulting from electro plus photodisintegration when a 0.217 g/cm² Ta foil is interposed in the electron beam.

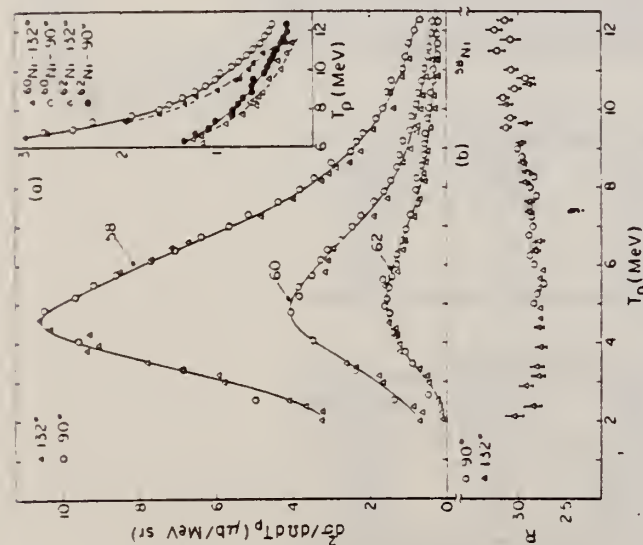


FIG. 3. (a) The proton spectra $d^2\sigma/dT_p d\Omega$ measured at 90° and 132° when 50 MeV electrons are incident on targets of ⁵⁸Ni, ⁶⁰Ni, and ⁶²Ni. The insert shows the tails of the energy spectra for ⁵⁸Ni and ⁶²Ni where the protons are slightly forward peaked. (b) The ratio of the number of protons produced by electro plus photodisintegration in ⁵⁸Ni to the number produced by electrodisintegration alone. This ratio was determined by placing a 0.217 g/cm² Ta radiator in the beam 7.6 cm ahead of the ⁵⁸Ni target.

(over)

(E,XP) VIRTUAL PHOTON G,XP
(E,XA) VIRTUAL PHOTON G,XA

1. Measurement also made at 100 MeV

2. Assumptions:
For photons: $\frac{d\sigma}{dr}(\theta) = \text{constant}$

For alphas:

$$\frac{d\sigma}{dr}(\theta) = \sigma(90^\circ) [A(E_0) + B(E_0) \sin^2 \theta]$$

A(E₀), B(E₀) determined empirically

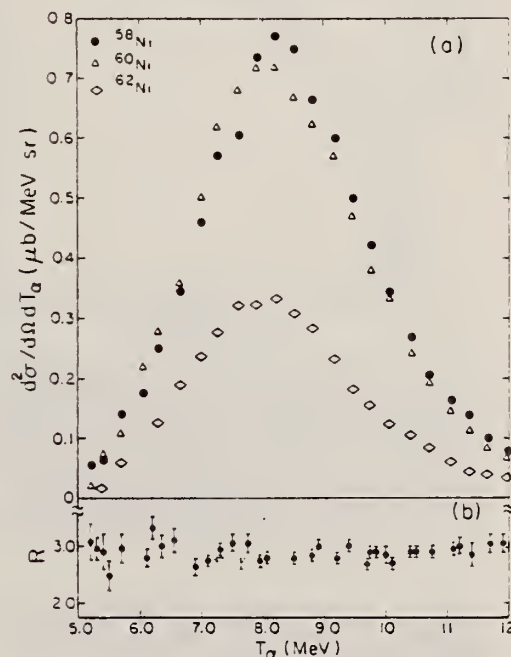


FIG. 2. (a) The α spectra $d^2\sigma/dT_\alpha d\Omega$ measured at 90° when 50 MeV electrons are incident on targets of ⁵⁸Ni, ⁶⁰Ni, and ⁶²Ni. (b) The ratio of the number of α particles produced by electro plus photodisintegration in ⁵⁸Ni to the number produced by electrodisintegration alone. This ratio was obtained by placing a 0.217 g/cm² Ta radiator in the beam ahead of the ⁵⁸Ni target.

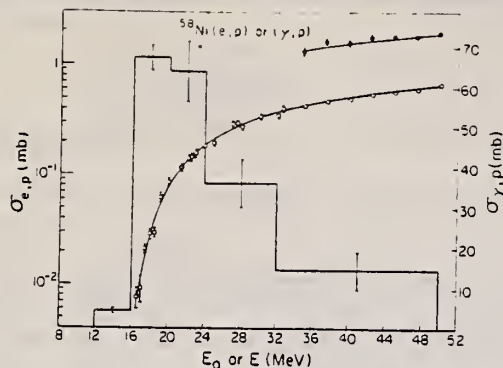


FIG. 5. The cross section (left-hand scale) for the production of protons $\sigma_{e,p}(E_0)$ when electrons of total energy E_0 are incident on a ^{58}Ni target (open circles). The closed circles represent the yield of protons obtained when a 0.217 g/cm^2 Ta foil was interposed in the incident electron beam. The latter have been corrected for the changes in geometry produced by the multiple scattering of the electrons in the radiator. The lines drawn through the points result from folding the histogram, representing the (γ, p) cross section (right-hand scale), with the E1 virtual photon spectrum in Eq. (1) and using the Davies-Bethe-Maximon cross section in Eq. (2).

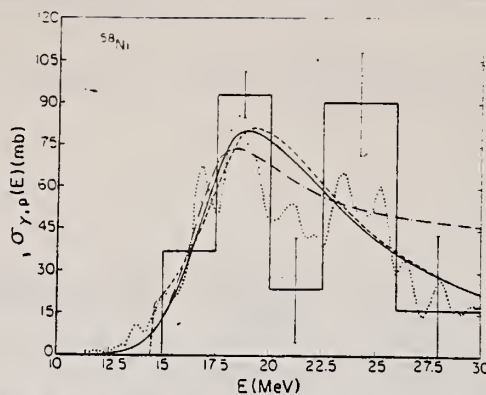


FIG. 6. Various (γ, p) cross section shapes that fit the $^{58}\text{Ni}(e, p)$ data when combined with the E1 virtual photon spectrum in Eq. (8). Here only the electrodisintegration data below 30 MeV have been used. The dotted curve represents the data of Ref. 17 multiplied by 1.22. The dashed curve is a Lorentz line having a smaller width below the resonance energy than above and truncated near 15 MeV. The solid curve has a Gaussian shape below and a Lorentz shape above the resonance energy. The dot-dashed curve is a Gaussian below the resonance energy and a Lorentz line plus a constant above. The histogram with 2.5 MeV bins roughly reproduces the structure in the measured (γ, p) cross section.

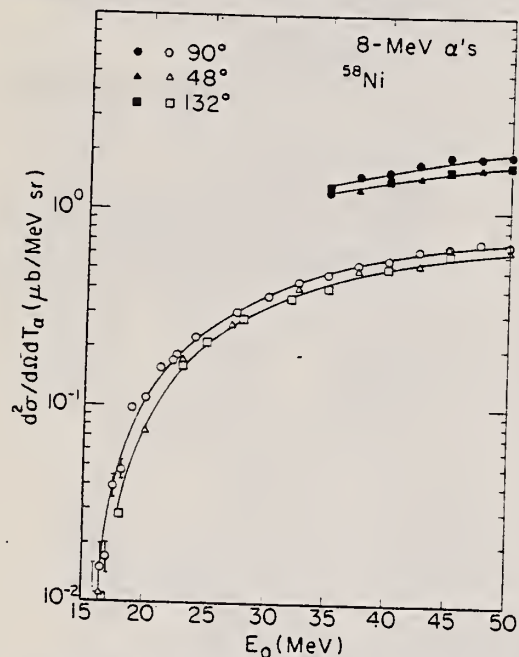


FIG. 9. The differential cross section $d^2\sigma/d\Omega dT_\alpha$ for the production of 8 MeV α particles from ^{58}Ni as a function of total incident electron energy E_0 . The data were taken at three angles: 90° (circles), 48° (triangles), and 132° (squares). The upper points refer to the yields resulting from electro plus photodisintegration when a 0.217 g/cm^2 tantalum radiator was interposed in the incident electron beam. The curves drawn through the points are merely to guide the eye.

TABLE IV. Percentage of the E1 and E2 sums in the α channel. E1 sum: 60 NZ/A MeV mb . E2 sum: $0.22 Z^2 A^{-1/3} \mu\text{b/MeV}$. E2 bin: 14–20 MeV. Upper limits of the integrals = 50 MeV.

Nucleus	E1		E2	
	Schiff	D-B-M	Schiff	D-B-M
^{58}Ni	4.3 ± 0.5	6.0 ± 0.6	24 ± 3	15 ± 3
^{60}Ni	4.4 ± 0.7	5.4 ± 0.7	24 ± 4	15 ± 4
^{62}Ni	2.4 ± 0.3	2.9 ± 0.3	10 ± 2	6 ± 2

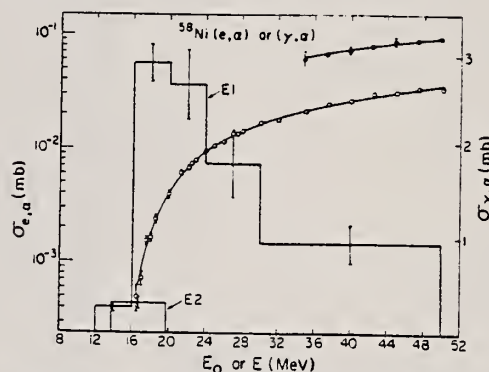


FIG. 11. The $^{58}\text{Ni}(e, \alpha)$ (open circles) cross section (left-hand scale) corrected yield (closed circles) obtained with radiator in. The curves through the points result from combining the histograms, representing the E1 and E2 (γ, α) cross sections (right-hand scale), in Eqs. (1) and (2) with the E1 and E2 virtual photon spectra and making use of the Davies-Bethe-Maximon cross section.

TABLE V. $\sigma_{e,p}$ at 100 MeV.

Nucleus	$\sigma_{e,p}(\text{meas})$ (mb)	$\sigma_{e,p}(\text{calc})$ (mb)	$\sigma_{e,p}(\text{corr})$ (mb)
^{58}Ni	1.15 ± 0.02	1.10	0.98
^{60}Ni	0.50 ± 0.01	0.47	0.42
^{62}Ni	0.24 ± 0.01	0.22	0.19

TABLE VI. $\sigma_{e,\alpha}$ at 100 MeV.

Nucleus	$\sigma_{e,\alpha}(\text{meas})$ (mb)	$\sigma_{e,\alpha}(\text{calc})$ (mb)	$\sigma_{e,\alpha}(\text{corr})$ (mb)
^{58}Ni	0.069 ± 0.002	0.084	0.063
^{60}Ni	0.063 ± 0.002	0.081	0.060
^{62}Ni	0.033 ± 0.001	0.036	0.027

REF K. Ackermann, K. Bangert, U.E.P. Berg, G. Junghans, R.K.M. Schneider,
R. Stock, K. Wienhard
Nuc1. Phys. A372, 1 (1981)

ELEM. SYM.	A	Z
Ni	58	28
REF. NO.		hg
81 Ac 11		

METHOD

REACTION	RESULT	EXCITATION ENERGY	SOURCE		DETECTOR		ANGLE
			TYPE	RANGE	TYPE	RANGE	
G.G	LFT	6 - 10	C	6 - 10	SCD-D		DST

Abstract: Nuclear resonance fluorescence measurements on ^{58}Ni with bremsstrahlung and Ge(Li) detectors were performed to search for bound state dipole excitations. Ten levels with ground state decay widths larger than 0.3 eV have been observed in the energy region between 6 and 10 MeV for which precise excitation energies, spins and lifetimes are reported. The measured transition probabilities are compared with theoretical estimates of E1 and M1 strength in ^{58}Ni . Since the $^{58}\text{Ni}(\gamma, \gamma)$ cross sections were determined relative to strong transitions in ^{208}Pb , the results of a separate $^{208}\text{Pb}(\gamma, \gamma)$ measurement are also presented.

10 LEVELS

E NUCLEAR REACTIONS $^{58}\text{Ni}(\gamma, \gamma)$, $^{208}\text{Pb}(\gamma, \gamma)$, $E < 10$ MeV; measured E_x , $\sigma(\theta)$; deduced lifetimes, spins. Enriched targets.

TABLE 2
Results from the $^{58}\text{Ni}(\gamma, \gamma)$ experiment

E_x (keV)	$I_f(90^\circ)$ $I_f(125^\circ)$	J	Γ_0^a (eV)	τ^b (fs)
6030 ± 3	0.97 ± 0.31	1	0.33 ± 0.12	$1.99^{+0.14}_{-0.53}$
7051 ± 3	0.70 ± 0.23	1	0.69 ± 0.26	$0.95^{+0.53}_{-0.26}$
7710 ± 3	1.05 ± 0.44	1	0.49 ± 0.20	$1.34^{+0.93}_{-0.39}$
8240 ± 3	0.66 ± 0.09	1	2.96 ± 0.46	$0.22^{+0.04}_{-0.03}$
8682 ± 3	0.95 ± 0.26	1	1.16 ± 0.40	$0.57^{+0.30}_{-0.15}$
9193 ± 3	1.20 ± 0.48	1	1.01 ± 0.40	$0.65^{+0.43}_{-0.19}$
9368 ± 3	0.80 ± 0.31	1	1.26 ± 0.48	$0.52^{+0.32}_{-0.14}$
9557 ± 3	1.38 ± 0.54	1	1.53 ± 0.61	$0.43^{+0.29}_{-0.12}$
9670 ± 3	0.83 ± 0.28	1	1.91 ± 0.69	$0.34^{+0.19}_{-0.09}$
9843 ± 5	2.84 ± 1.79	2	0.88 ± 0.38	$0.70^{+0.76}_{-0.24}$
		1	1.79 ± 0.91	$0.37^{+0.38}_{-0.12}$

^{a)} $\Gamma_0, \Gamma = 1$ assumed.

^{b)} $\tau = \hbar/\Gamma$

ELEM. SYM.	A	Z
Ni	58	28
REF. NO.		
81 Br 2		hg

METHOD					
REACTION	RESULT	EXCITATION ENERGY	SOURCE		ANGLE
			TYPE	RANGE	
E,N	ABX	40,80	D	40,80	4PI
G,N	ABY	12-80	C	40,80	4PI

σ_e , σ_p ratios, F values and ^{57}Ni production rates are measured with 40 and 80 MeV electron beams as a function of the Z value and thickness of bremsstrahlung converters.

NI 57 PROD. RATES

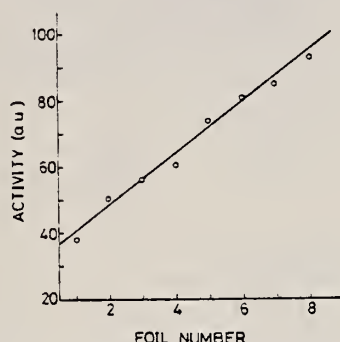


FIG. 1. ^{57}Ni activities (arbitrary units) of a stack of 8 Ni foils irradiated with 80 MeV electrons.

	σ_e (mb)	σ_p (mb)	σ_e/σ_p
40 MeV	0.21	8.0	38
80 MeV	0.28-0.38	13.4-14.0	48-37

TABLE 2. Activities (μCi) of Ni foils (0.1 mm) after 1 h irradiation using 50 μA electrons

(a) EVA, thin converters, no deflecting magnet ($f = 1$) ^a								
40 MeV				80 MeV				
Converter (mm)	None ^b	Ni	Ta	Pt	None ^b	Ni	Ta	Pt
0.0	20				45			
0.1				20				50
0.2			40	30			80	100
0.7		50				110		
1.0			130					

(b) EVA, standard converters					
Thin 15	Middle 10	Thick 1	Thin 55	Middle 45	Thick 7

(c) MEA (LECH-half), thin W-converters with deflecting magnet					
Converter (mm)	f^2		f^2		
0.05	4 ^d	0.44	12		0.81
0.125	6	0.24	16		0.57
0.25	7 ^d	0.14	19 ^d		0.37
0.50	9 ^d	0.09	26 ^d		0.25

TABLE 1. F values for the $^{58}\text{Ni}(e,e'n)^{57}\text{Ni}$ reaction^a

Radiator thickness (mm)	Radiator					
	40 MeV			80 MeV		
	Ni	Ta	Pt	Ni	Ta	Pt
0.1			3.1			3.6
0.2		4.2	3.4		3.2	3.5
0.6	4.0			4.8		
1.0		3.4				
Mean	3.6 ± 0.2			3.8 ± 0.4		

^a F is a measure for the ratio of activities produced by bremsstrahlung and by electrons. Its definition is given in the text.

^a f is the "Ausbeute Faktor".⁽¹⁾

^b No converter was used, the given activities are mainly produced by the $^{58}\text{Ni}(e,e'n)^{57}\text{Ni}$ reaction.

^c Except for the thin and middle converters used at 80 MeV, the converters are thick enough to stop all the electrons.

^d Calculated, see text.

Ni
A=60

Ni
A=60

Ni
A=60

Method Radioactive source; photon scattering; NaI spectrometer

Ref. No.	
56 Me 2	NVB

Reaction	E or ΔE	E_0	Γ	$\int \sigma dE$	$J\pi$	Notes
$\text{Ni}^{60}(\gamma, \gamma)$	1.33	1.33			<div>2 (excited)</div> <div>0 (ground)</div>	Mean life: $\tau = (1.1 \pm 0.2) 10^{-2} \text{ sec.}$

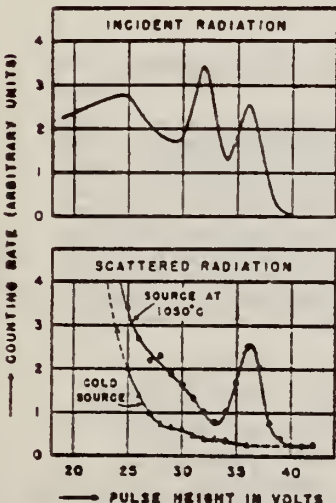


FIG. 2. Resonance fluorescence in Ni^{60} . The pulse-height distribution of the incident radiation (top) clearly shows two peaks corresponding to the 1.17-Mev and the 1.33-Mev gamma rays emitted in the decay of Co^{60} . The scattered radiation with the gaseous source consists mainly of 1.33-Mev resonance radiation, indicating that this gamma ray is the one leading to the ground state of Ni^{60} .

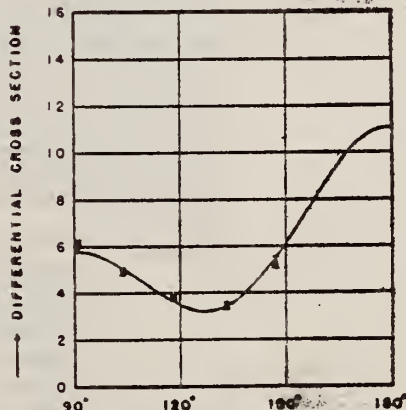
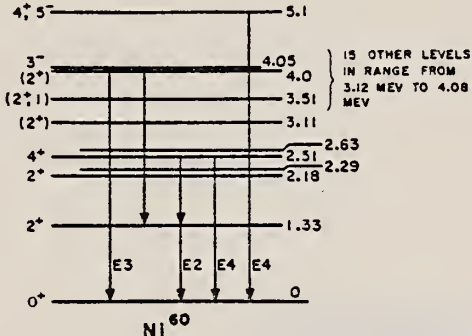


FIG. 3. Angular distribution of the resonance radiation from the 1.33-Mev level in Ni^{60} . The solid line represents the theoretical angular distribution for an excited state with spin 2 and a ground state with spin 0, corrected for the finite angular resolution. The differential cross section is given in arbitrary units.

Elem. Sym.	A	Z
Ni	60	28
Ref. No.		
61 Cr 1		JHH

Method Linac; Cerenkov counter telescope

Reaction	E or ΔE	E_0	Γ	$\int \sigma dE$	$J\pi$	Notes
(e^-, e^-')	183	1.33 2.50 4.05 5.1			2^+ 4^+ 3^-	Measured γ transition rates, Γ_m : $\Gamma_m = (1.27 \pm 0.15) 10^{12} \text{ sec}^{-1}$; (E2); $G = \Gamma_m / \Gamma_{sp} = 17.1 \pm 2.1$. $\Gamma_m = (1.3 \pm 0.24) 10^4 \text{ sec}^{-1}$; (E4); $G = \Gamma_m / \Gamma_{sp} = 3.62 \pm 0.67$ $\Gamma_m = (3.64 \pm 5.8) 10^{10} \text{ sec}^{-1}$; (E3); $G = \Gamma_m / \Gamma_{sp} = 3.62 \pm 0.67$ $\Gamma_m = (7.78 \pm 2.0) 10^{10} \text{ sec}^{-1}$; (E3); $G = \Gamma_m / \Gamma_{sp} = 7.8 \pm 2.0$ $\Gamma_m = (1.58 \pm 0.24) 10^7 \text{ sec}^{-1}$; (E4); $G = \Gamma_m / \Gamma_{sp} = 4.9 \pm 0.73$ $\Gamma_m = (4.66 \pm 1.5) 10^3 \text{ sec}^{-1}$; (E5); $G = \Gamma_m / \Gamma_{sp} = 27.2 \pm 8.7$
 <p>FIG. 15. Energy-level diagram for Ni^{60}. (See caption for Fig. 13.) A number of levels have been omitted from the diagram (see reference 16).</p> <p>FIG. 13. In this and the following four figures are shown portions of the energy-level structures of the nuclei investigated in the present experiment. The information is, for the most part, taken from reference 15. The γ-ray transitions shown are those whose decay rates were determined directly in the present experiment or inferred from a knowledge of the γ-ray branching ratios in de-excitation of the nucleus. The spin and parity of each level are shown at the left, where known, and the energy of the excited states in Mev on the right. The best assignments of the transition multipolarities are indicated. This figure shows the energy-level structure of Ni^{60}.</p>						
Ref 15:	Data on the decay schemes are taken principally from Nuclear Data Sheets, National Academy of Sciences, National Research Council (U.S. Government Printing Office, Washington, D.C., 1959)					
Ref 16:	Mazari et al - Phys. Rev. <u>107</u> , 365 (1957).					
Ref 37:	Crut, Sweetman, Wall - Nuclear Phys. <u>17</u> , 655 (1960).					

Fits $R_0 = 1.20$ fermi except 5.1 MeV level (1.1 fermi).

[Γ_{sp} = single-particle estimate of the γ transition rate.]

Table IV. Vibrational parameters for the levels in the even-even nuclei in the present experiment; $B(E)$ is the reduced transition probability, B_0 and C_0 are the mass transition and the effective surface-tension parameters of the harmonic oscillator approximation to the nuclear surface energy, B_{hyd} is the value appropriate to a hydrodynamic model; β_2 is the distortion parameter of a nucleus of multipole order 2, and R is the nuclear radius ($R = R_0 A^{1/3}$ for $R_0 = 1.20$ fm).

Nucleus	Excitation Energy (MeV)	$B(E)$ (MeV)	B_0 (MeV)	C_0 (MeV)	β_2	R (fm)
Ni ⁶⁰	1.45	14.3 ± 1.9	99.5 ± 9	4.15	16.7 ± 2.2	145 ± 19
	3.2	4.45 ± 1.6	106 ± 34	4.16	25.6 ± 9.2	1070 ± 390
	1.33	17.1 ± 2.1	65.2 ± 7.3	3.96	16.4 ± 2.0	116 ± 14
Ni ⁶²	4.30	13.2 ± 1.4	103 ± 14	4.45	23.2 ± 3.2	2090 ± 290
	4.03	15.9 ± 2.5	98.5 ± 14	4.61	19.2 ± 3.1	1430 ± 230
	5.1	7.8 ± 1.8	144 ± 34	4.61	31.2 ± 7.4	1700 ± 475
	2.60	30.8 ± 11	280 ± 105	23.8	11.7 ± 4.2	1890 ± 300
Ni ⁶⁴	2.50	2.2 ± 0.66	6140 ± 1900	6.96	870 ± 260	$3.84 \pm 1.2 \times 10^4$
	3.51	2.3 ± 0.37	1196 ± 270	6.96	1730 ± 400	$1.46 \pm 0.33 \times 10^4$
	7.20	3.65 ± 0.69	3400 ± 550	6.94	494 ± 34	$2.12 \pm 0.40 \times 10^4$
	5.1	4.95 ± 0.74	1230 ± 185	6.84	130 ± 270	$5.30 \pm 0.48 \times 10^4$
Pb ²⁰⁸	4.30	36.6 ± 12	495 ± 160	24.7	20.0 ± 6.3	$9.34 \pm 3.1 \times 10^4$

* See McDevitt et al., reference 37.
* Present notation is 2A.

REF. M.A. Duguay, C.K. Bockelman, T.H. Curtis, and R.A. Eisenstein
Phys. Rev. Letters 17, 28 (1966)

ELEM. SYM.	A	Z
Ni	60	28

METHOD	REF. NO.	
Linac	66 Du 1	JDM

REACTION	RESULT	EXCITATION ENERGY	SOURCE		DETECTOR		ANGLE
			TYPE	RANGE	TYPE	RANGE	
E, E/	FMF	1	D	45-65	MAG-D		DST

Table I. Reduced transition probabilities $B(E2)$ and transition radii R_{tr} for the first excited states of the even Ni isotopes.

Isotope	Level energy (MeV)	J^π	$B(E2, 0^+ \rightarrow 2^+)$ ($e^2 F^4$)		R_{tr} (F)
			Ref. 12	Present work	
Ni ⁵⁸	1.452	2 ⁺	720 ± 10%	620 ± 14%	5.35 ± 10%
Ni ⁶⁰	1.332	2 ⁺	910 ± 9%	776 ± 12%	5.23 ± 12%
Ni ⁶²	1.172	2 ⁺	830 ± 9%	770 ± 12%	5.23 ± 10%

REF. R. B. Begzhanov and A. A. Islamov
 J. Nucl. Phys. (USSR) 5, 483 (1967)
 Sov. J. Nucl. Phys. 5, 339 (1967)

ELEM. SYM.	A	Z
Ni	60	28

METHOD

REF. NO.	
67 Be 5	HMG

REACTION	RESULT	EXCITATION ENERGY	SOURCE		DETECTOR		ANGLE
			TYPE	RANGE	TYPE	RANGE	
G,G	LFT	1.0	D	1.0	NAI-D		120

$$\tau_Y = (9.0 \pm 1.8) \cdot 10^{-13} \text{ sec. } 1.33 \text{ MeV}$$

METHOD

REF. NO.	
67 Du 1	HMG

REACTION	RESULT	EXCITATION ENERGY	SOURCE		DETECTOR		ANGLE
			TYPE	RANGE	TYPE	RANGE	
$E, E/$	FMF	1-5	D	45-65	MAG-D		DST

TABLE II. Reduced radiative transition probabilities and transition radii.

$B(EL)$, SEP ISOTPS

E2 Transitions ^a					
Excitation energy (MeV)	$B(E2, 0^+ \rightarrow 2^+)$ ($e^2 F^2$)	$B(E2, 0^+ \rightarrow 2^+)$	β_2	R_{E2} (F)	
Ni ⁶⁰ 1.452	657 ± 11	10	0.177 ± 0.003	5.51	
3.034	83 ± 3	1	0.063 ± 0.002	5.51	
3.26	153 ± 15	2	0.085 ± 0.008	5.51	
Ni ⁶² 1.330	845 ± 9	12	0.197 ± 0.002	5.55	
Ni ⁶⁴ 1.172	877 ± 11	12	0.197 ± 0.001	5.59	

E3 Transitions ^a					
Excitation energy (MeV)	$B(E3, 0^+ \rightarrow 3^-)$ ($e^3 F^3$)	$B(E3, 0^+ \rightarrow 3^-)$	β_3	R_{E3} (F)	
Ni ⁶⁰ 4.480	15 600 ± 520	13	0.203 ± 0.005	6.05	
Ni ⁶² 4.038	28 100 ± 640	19	0.241 ± 0.006	6.09	
Ni ⁶⁴ 3.75	20 100 ± 540	13	0.197 ± 0.005	6.11	

^a The errors quoted for $B(EL)$ assume the liquid-drop model for the transition charge density and are purely statistical in nature. The estimate of error from dependence on the parameters of this charge density are ±15% for both $B(EL)$ and R_{EL} . See text.

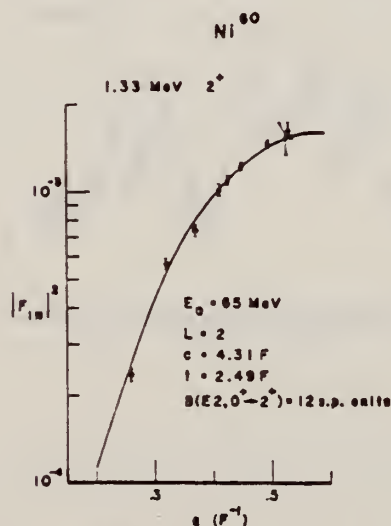


FIG. 23. The theoretical and experimental $|F_{12}|^2$ versus q for the Ni⁶⁰ 1.33-MeV 2⁺ state. The solid curve is the $|F_{12}|^2$ calculated by Code GROW using the strict hydrodynamic model ($c_{12} = c$; $k_{12} = t$). The best fit to the data is obtained by a least-squares analysis.

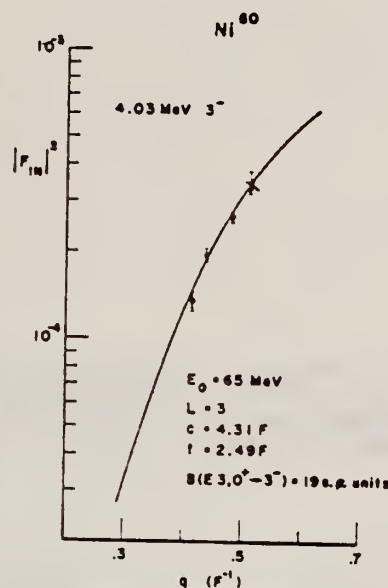
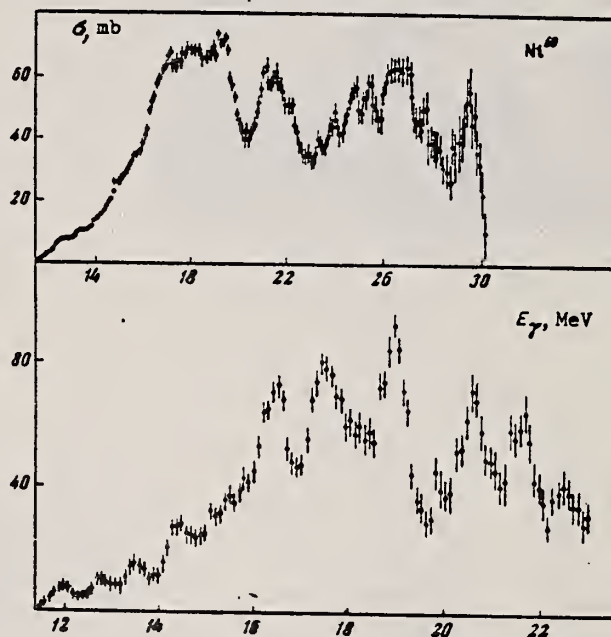


FIG. 24. The theoretical and experimental $|F_{12}|^2$ versus q for the Ni⁶⁰ 4.03-MeV 3⁻ state. The solid curve is the $|F_{12}|^2$ calculated by Code GROW using the strict hydrodynamic model ($c_{12} = c$; $k_{12} = t$). The best fit to the data is obtained by a least-squares analysis.

REF. B. I. Goryachev, B. S. Ishkhanov, I. M. Kapitonov, I. M. Piskarev, V. G. Shevchenko, and O. P. Shevchenko ZhETF Pis. Red. <u>3</u> , 76 (1968) JETP Letters <u>8</u> , 46 (1968)			ELEM. SYM. A Z		
			Ni 60		28
METHOD			REF. NO.		
			68 Go 4		hmg
REACTION	RESULT	EXCITATION ENERGY	SOURCE		ANGLE
			TYPE	RANGE	
G,XN	ABX	11- 30	C	7-30	4PI

$\sigma_{int}(30\text{ MeV}) = 800 \pm 50\text{ MeV}\cdot\text{mb.}$

Fig. 2. Effective cross section of the reaction $\text{Ni}^{60}(\gamma, \text{Tn})$. Upper figure - analysis in steps of 1 MeV, lower - in steps of 0.5 MeV



REACTION	RESULT	EXCITATION ENERGY	SOURCE		DETECTOR		ANGLE
			TYPE	RANGE	TYPE	RANGE	
G, XN	ABX	11- 25	C	10-25	BF3-I		4PI

21

Table I. Integrated (γ, n) cross sections up to 25 MeV.

Isotope	Integrated cross section (MeV mb)
Ni ⁵⁸	185 ± 3
Ni ⁶⁰	482 ± 12
Natural nickel	283 ± 6
(0.262) Ni ⁶⁰ + (0.679) Ni ⁵⁸	252 ± 4
Ratio of integrated cross section, Ni ⁶⁰ /Ni ⁵⁸ = 2.6	

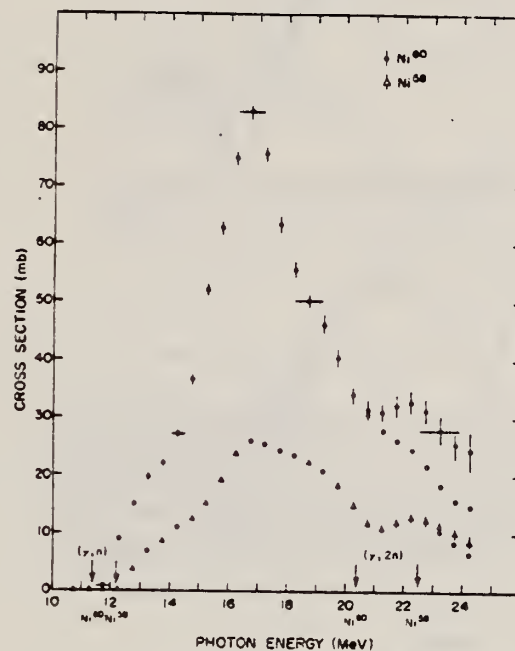


FIG. 1. Photoneutron cross sections of Ni⁶⁰ and Ni⁵⁸. The corrected values for $(\gamma, 2n)$ process are shown by circles.

REF. V. D. Afanas'ev, N. G. Afanas'ev, I. S. Gul'karov, G. A. Savitskii,
V. M. Khvastunov, N. G. Shevchenko and A. A. Khomich
Yad. Fiz. 10, 33 (1969)
Sov. J. Nucl. Phys. 10, 18 (1970)

ELEM. SYM.	A	Z
Ni	60	28
REF. NO.		
69 Af 1		egf

METHOD

REACTION	RESULT	EXCITATION ENERGY	SOURCE		DETECTOR		ANGLE
			TYPE	RANGE	TYPE	RANGE	
E, E/	FMF	1,4	D	150,225	MAG-D		DST

1,4 = 1.33, 4.04 MEV

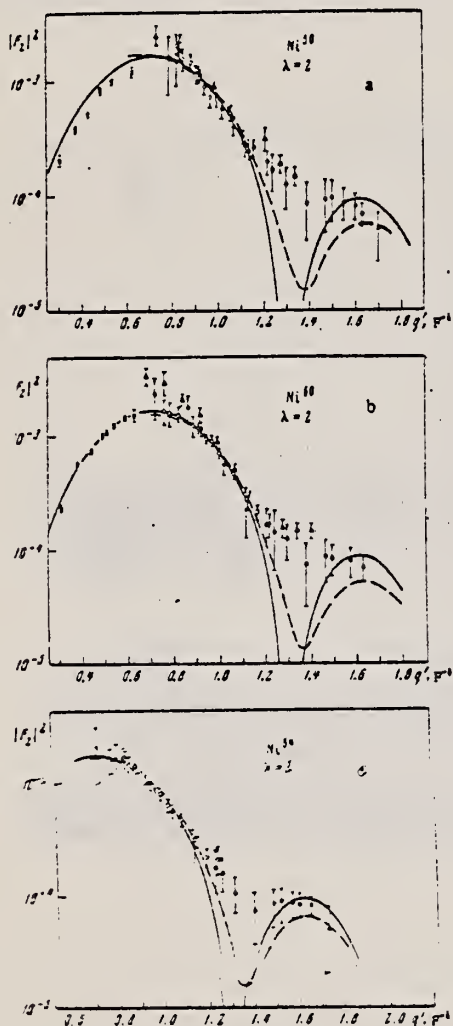


FIG. 2. Form factors for E2 transitions in nickel isotopes: a—Ni⁵⁸, b—Ni⁶⁰, c—Ni⁶⁴. Solid curves—Helm's model, dashed curves—high-energy approximation. Points: O, ●—our data for 150 and 225 MeV, ▲—Stanford data [9], X—Yale data [10].



FIG. 3. R_λ as a function of q^2 for E2 transitions. Straight lines: 1—Ni⁵⁸ (the points and straight line are raised by 0.5), 2—Ni⁶⁰, 3—Ni⁶⁴ (the points and straight line are lowered by 1.0). Points: O—150 MeV, ●—225 MeV.

Table II. Reduced probabilities of quadrupole transitions in the isotopes Ni^{58,60,64}

Iso- tope	E, MeV	J ^π	B(E2), e ² fm ⁴				σ _r	Theory		Data of other authors	
			Helm's model	High energy approximation	Model- independent method	Average		[1]	[2]	B(E2)	Reference
Ni ⁵⁸	1.45	2 ⁺	560 ±56	594 ±11	510 ±42	554	8.4	340	200	800 620 657 580 515, 750	[1] [1] [10] [9] [9]
Ni ⁶⁰	1.33	2 ⁺	603 ±55	602 ±40	606 ±54	603	8.4	800	600	1100 910 845 1250 796, 1280	[1] [1] [10] [9] [9]
Ni ⁶⁴	1.32	2 ⁺	650 ±65	661 ±53	640 ±53	650	8.0	1400	800	870	[1]

[over]

Table III. Reduced probabilities of octupole transitions in the isotopes $\text{Ni}^{58,60,64}$

Isotope	E, MeV	J ^π	D(E3), e ³ F ⁶			G _A	Data of other authors	
			Helm's model	Model-independent method	Average		B(E3)	Reference
Ni^{58}	4.45	3 ⁻	13900 ±1450	13020 ±780	13100	10	18 600 27 000 14 600	[10] [9] [11]
Ni^{60}	4.04	3 ⁻	13300 ±1800	13910 ±830	13600	9	23 100 35 000 19 100	[10] [9] [11]
Ni^{64}	3.55	3 ⁻	16000 ±1800	17000 ±1400	16500	9.4		

Table IV. Transition radii and parameters of the vibrational model of the nucleus for E2 and E3 transitions in $\text{Ni}^{58,60,64}$

Isotope	I _i - I _f	R _{trans}		C ₀ , MeV	$\frac{B\lambda}{h^2}$, MeV·sec	$\frac{B\lambda}{(B\lambda)_{h.d.}}$	β_{λ}^2
		Our result	[10]				
Ni^{58}	0-2	4.85 ±0.21	5.51	173 ±19	82 ±9	20.0 ±2.2	0.115 ±0.004
	0-3	5.13 ±0.11	6.05	1520 ±130	77 ±8	17 ±2	0.101 ±0.006
Ni^{60}	0-2	4.92 ±0.15	5.55	153 ±17	86 ±9	20 ±2.2	0.118 ±0.018
	0-3	5.24 ±0.10	6.09	1500 ±130	92 ±8	13.5 ±1.8	0.097 ±0.005
Ni^{64}	0-2	4.94 ±0.15	—	145 ±16	83 ±9	17.3 ±1.9	0.150 ±0.010
	0-3	5.34 ±0.11	—	1160 ±130	92 ±12	17.1 ±2.2	0.105 ±0.016

^a(Bλ)_{h.d.} is the oscillation parameter of the nucleus, obtained with a hydrodynamical model.

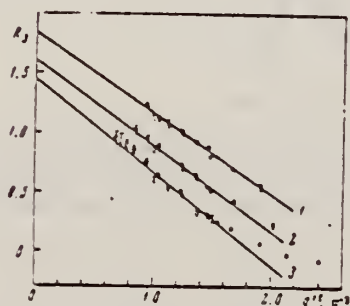


FIG. 5. Analysis of E3 transitions by the model-independent method. Straight lines: 1— Ni^{58} (the data and straight line have been raised by 0.5) 2— Ni^{60} , 3— Ni^{64} (the data and straight line have been lowered by 0.5). Points: ○—150 MeV, ●—225 MeV.

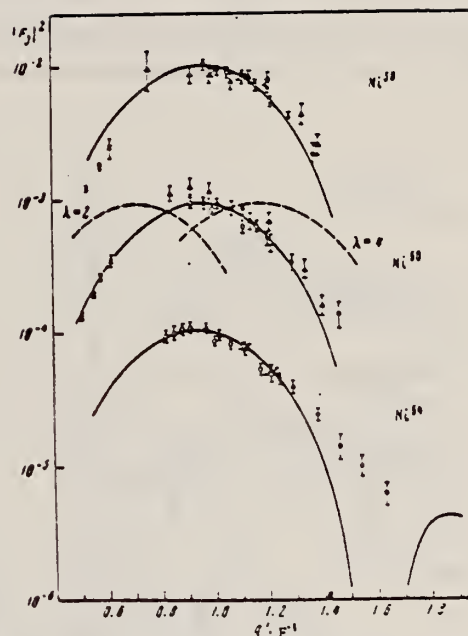


FIG. 4. Form factors for E3 transitions in the isotopes Ni^{58} (the experimental data and curve are multiplied by 10), Ni^{60} , Ni^{64} (the experimental data and curve are divided by 10). The solid curves represent the form factor calculated by Helm's model with $\lambda = 3$, and the dashed curves the form factor calculated by the same model for $\lambda = 2$ and $\lambda = 4$. Points: ○ and ●—our data for 150 and 225 MeV, ▲—Stanford data [9], X—Yale data [10].

REF. B.I. Goryachev, B.S. Ishkhanov, I.M. Kapitonov, I.M. Piskarev,
V.G. Shevchenko, and O.P. Shevchenko
Yad. Fiz. 10, 252 (1969)
Sov. J. Nucl. Phys. 11, 141 (1970)

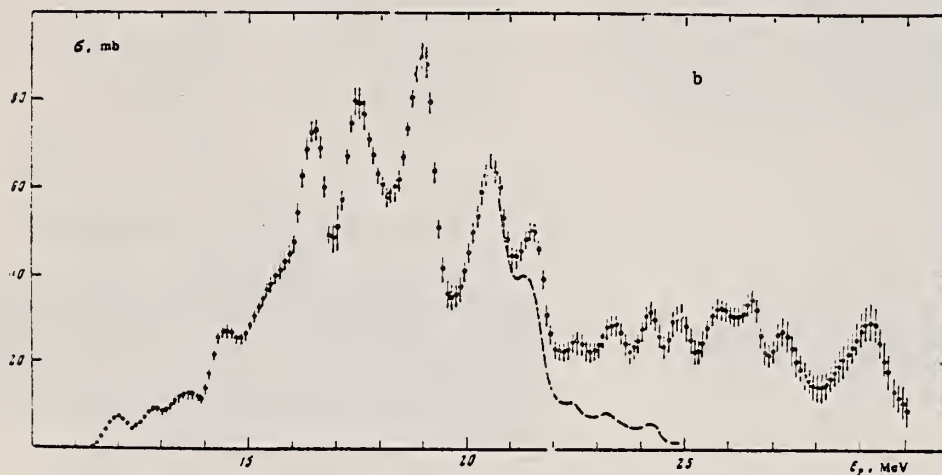
ELEM. SYM.	A	Z
Ni	60	28

METHOD	REF. NO.	
	69 Go 2	hmg

REACTION	RESULT	EXCITATION ENERGY	SOURCE		DETECTOR		ANGLE
			TYPE	RANGE	TYPE	RANGE	
G, XN	ABX	11-30	C	11-30	BF3-I		4PI
		(11.4-30)					

537

FIG. 1. Cross section of the photoneutron reaction for Ni^{58} (a) and Ni^{60} (b). The dashed line shows the cross section of the reaction (γ, n) above the threshold of two-neutron emission, obtained from our data on the basis of the statistical theory.



$$\int_{0}^{30} \sigma dE = 620 \pm 50 \text{ MeV mb}$$

ELEM. SYM.		
Ni	60	28
REF. NO.	69 Gu 1	hmg

REACTION	RESULT	EXCITATION ENERGY	SOURCE		DETECTOR		ANGLE
			TYPE	RANGE	TYPE	RANGE	
E, E/	ABX	10-30	D	199	MAG-D		DST
				(198.5)			

See paper for summary of other data.

FMF

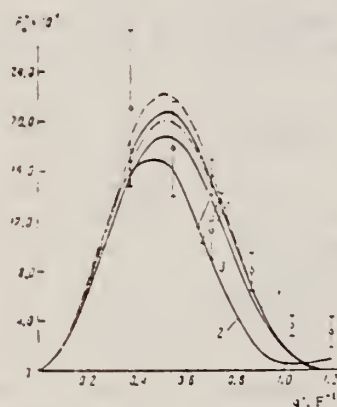


FIG. 2. Giant-resonance form factor as a function of momentum transfer. Points: \circ —data for Ni^{60} , \times —for Ni^{64} , \square —for Ni^{58} . The dashed curve, curve 1, and the dot-dash curve were calculated from formula (2) for the nuclei $\text{Ni}^{58, 60, 64}$ respectively, with $k = 19$ MeV. Curve 3 was calculated from the same formula for Ni^{60} with $k = 21$ MeV. Curve 2 is a calculation according to the Goldhaber-Teller collective model.

Table I. Absolute differential cross sections for inelastic scattering of electrons with excitation of the giant resonance in nickel isotopes

Nucleus	θ , deg	E_0 , MeV	q , F^{-1}	q' , F^{-1}	$d\sigma/d\Omega$, cm^2/sr	$F_2^2 (\times 10^{-4})$
Ni^{60}	20	198.7	0.765	0.736	$(2.52 \pm 0.10) \cdot 10^{-28}$	2.11 ± 0.03
	30	199.1	0.767	0.738	$(3.79 \pm 0.81) \cdot 10^{-28}$	1.78 ± 0.25
	40	197.6	0.762	0.743	$(7.5 \pm 1.25) \cdot 10^{-28}$	1.12 ± 0.23
	50	197.9	0.816	0.800	$(2.14 \pm 0.50) \cdot 10^{-28}$	0.80 ± 0.15
	60	199.1	0.970	1.029	$(5.29 \pm 1.63) \cdot 10^{-28}$	0.36 ± 0.08
Ni^{64}	70	201.9	1.125	1.194	$(1.21 \pm 0.41) \cdot 10^{-28}$	0.31 ± 0.13
	80	198.9	0.983	0.961	$(8.08 \pm 1.55) \cdot 10^{-28}$	1.23 ± 0.20
Ni^{58}	85	149.7	0.650	0.702	$(4.14 \pm 0.50) \cdot 10^{-28}$	1.43 ± 0.27

Note. The limits of integration of the spectra are from 10 to 30 MeV.

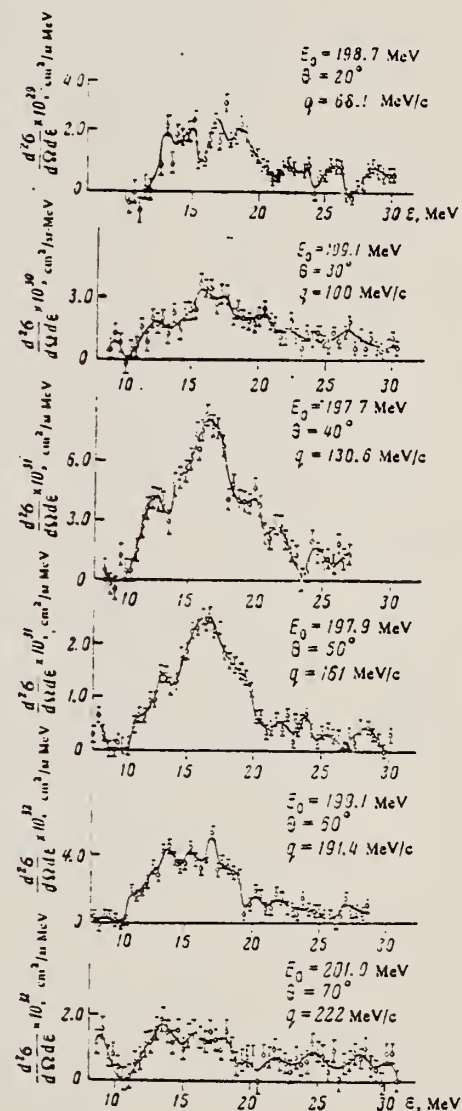


FIG. 1. Energy spectra of electrons inelastically scattered by Ni^{60} , obtained after subtraction of the radiation tail from the elastic and inelastic peaks. ϵ is the excitation energy. The curves through the experimental points have been drawn visually.

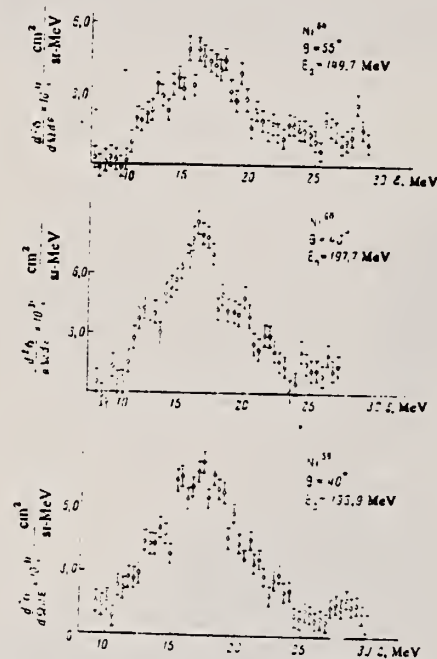


FIG. 3. Energy spectra of electrons inelastically scattered by the isotopes $Ni^{64,60,58}$. All three spectra were measured at the same value of momentum transfer.

EL. NO.	A	Z
Ni	60	28
REF. NO.	69 Ow 1	
	egf	

REACTION	RESULT	EXCITATION ENERGY	SOURCE		DETECTOR		ANGLE
			TYPE	RANGE	TYPE	RANGE	
G,XN	ABX	12-25	C	12-25	BF ₃ -I		4PI

190

MEASUREMENTS ON THE VIBRATIONAL SPLITTING OF THE GIANT DIPOLE RESONANCE

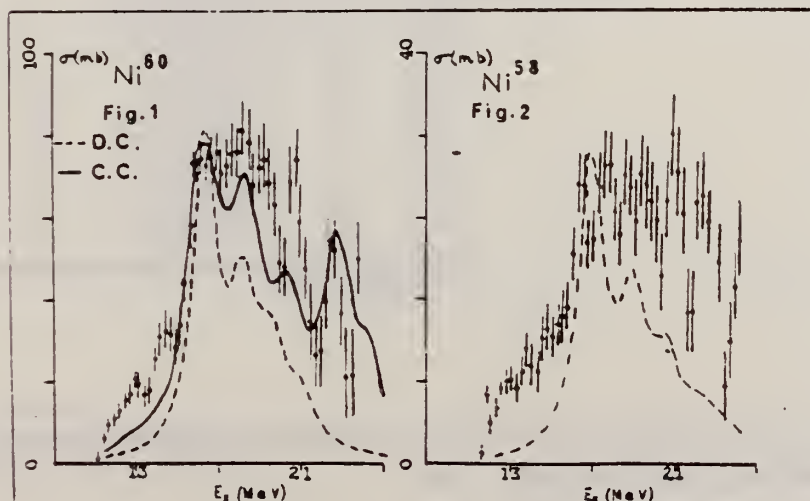
D.G. Owen, E.G. Muirhead and B.M. Spicer, School of Physics, University of Melbourne, Parkville, Victoria 3052, Australia.

The photoneutron yield curves for ⁵⁸Ni and ⁶⁰Ni have been measured in 1/4 MeV steps from threshold to 24 MeV, the neutrons being detected in a Halpern-type BF₃ counter system. The cross sections were obtained from the yield curves by the Leiss-Penfold matrix inversion method. A correction, based on the statistical theory of nuclear reactions, has been made for multiple neutron emission. The derived cross sections are shown in figures 1 and 2.

The dotted curves on the figures are the fits to the dipole spectrum, using Lorentz line shapes, and based on the dynamic collective model of the giant resonance (Huber, priv. comm. 1967), in which quadrupole surface vibrations are coupled to the dipole vibration. The poor fit at low energies is attributed to neglect of single particle effects.

Also shown in figure 1 is the result of the collective correlations calculation for ⁶⁰Ni (Seaborn, Drechsel, Arenhovel and Greiner, Phys. Lett. 23 (1966) 376). Here the surface vibrations are coupled to particle-hole dipole states, not just the dipole state. This calculation for the closed-subshell nucleus ⁶⁰Ni yields the result shown in the full curve of figure 1. The agreement with experiment is very much improved, indicating the importance of including single particle effects.

The similarity of low energy spectra for ⁵⁸Ni and ⁶⁰Ni, coupled with the fact that the same single particle states are filled in the ground state, leads to the expectation that the giant resonance structure will be similar for the two isotopes. This is in fact observed.



METHOD

(Page 1 of 3)

REACTION	RESULT	EXCITATION ENERGY	SOURCE		DETECTOR		ANGLE
			TYPE	RANGE	TYPE	RANGE	
$E_e E_p$	FME	0-8	D	183,250	MAG-D		DST

B(EL), J-PI

TABLE I. Inelastic form factors for ^{60}Ni at the incident energy of 183 MeV.

E_e (MeV)	J^π	35°	45°	55°	$10^4 F ^2$ 65°	75°	85°	95°
1.33	2 ⁺	15.8±0.9	19.5±0.10	14.7±0.71	4.16±0.17	0.58±0.11	0.55±0.22	1.22±0.13
2.16	2 ⁺	0.83±0.50	0.50±0.15	0.43±0.12	0.023±0.06	0.045±0.03	0.038±0.01	
2.50	4 ⁺		0.70±0.17	1.18±0.13	1.35±0.13	1.60±0.28	1.14±0.24	0.47±0.12
3.13	4 ⁺		0.20±0.14	0.23±0.12	0.37±0.07	0.37±0.08	0.40±0.08	
3.67	4 ⁺	0.18±0.14	0.24±0.07	0.62±0.12	0.69±0.07	0.89±0.19	1.03±0.24	0.41±0.12
4.04	3 ⁻	4.25±0.17	8.48±0.24	10.3±0.05	7.97±0.19	4.58±0.32	2.35±0.21	0.49±0.12
4.85	(2 ⁺ , 4 ⁺)	1.18±0.23	1.70±0.34	1.16±0.23	0.90±0.11	0.73±0.13	0.64±0.12	0.33±0.09
5.05	4 ⁺ , 6 ⁺		0.82±0.08	1.4±0.13	1.91±0.18	2.29±0.24	2.46±0.22	2.19±0.21
5.05	6 ⁺				0.22±0.18	0.50±0.24	1.10±0.20	
6.20	3 ⁻	1.29±0.15	1.45±0.08	1.78±0.17	1.35±0.14	0.92±0.14	0.50±0.10	0.44±0.18
6.85	(2 ⁺ , 5 ⁻)	0.83±0.12	1.21±0.07	1.20±0.15	1.25±0.12	0.82±0.13	0.84±0.13	0.78±0.13
7.05	3 ⁻	1.04±0.12	1.33±0.08	1.49±0.14	1.21±0.13	1.24±0.16	0.70±0.13	0.53±0.10

TABLE II. Inelastic form factors for ^{60}Ni at the incident energy of 250 MeV.

E_e (MeV)	J^π	66.3°	72.1°	$10^4 F ^2$ 77.4°	82.2°
1.33	2 ⁺	1.33±0.12	1.44±0.12	1.55±0.15	1.11±0.13
2.16	2 ⁺				
2.50	4 ⁺	0.62±0.06	0.21±0.04		
3.13	4 ⁺	0.25±0.04	0.12±0.02	0.52±0.16	
3.67	4 ⁺	0.60±0.06	0.27±0.05	0.30±0.05	
4.04	3 ⁻	0.58±0.06	0.16±0.03	0.27±0.05	0.30±0.05
4.85	(2 ⁺ , 4 ⁺)				
5.05	4 ⁺ , 6 ⁺	2.15±0.17	1.52±0.10	1.27±0.10	0.99±0.13
5.05	6 ⁺	1.33±0.17	1.12±0.10	1.11±0.10	0.95±0.13
6.20	3 ⁻				
6.85	(2 ⁺ , 5 ⁻)	0.54±0.15	0.41±0.15	0.41±0.18	0.28±0.14
7.05	3 ⁻				

TABLE III. Summary of spins, parities, and reduced transition probabilities in ^{60}Ni extracted from present (e, e') reaction.

E_e (MeV)	J^π	B(EL) (e ² F ² L)	G(B/B _{exp})	R(F) ^a
1.33	2 ⁺	(7.66±0.77)×10 ⁸	11.0	4.73
2.16	2 ⁺	(1.5±0.4)×10 ¹	0.2	4.50
2.50	4 ⁺	(1.50±0.30)×10 ⁸	4.8	4.96
3.13	4 ⁺	(3.09±0.62)×10 ⁸	1.0	4.73
3.67	4 ⁺	(5.67±1.13)×10 ⁸	1.8	4.62
4.04	3 ⁻	(1.65±0.25)×10 ⁸	11.1	4.73
4.85	(2 ⁺)	(5.0±1.0)×10 ¹	0.7	4.73
4.85	(4 ⁺)	(4.38±0.88)×10 ⁸	1.4	4.73
5.05	4 ⁺	(1.22±0.24)×10 ⁸	3.9	4.73
5.05	6 ⁺	(1.54±0.46)×10 ⁸	11.6	4.73
6.20	3 ⁻	(2.20±0.33)×10 ⁸	1.5	4.50
6.85	(2 ⁺)	(3.88±0.58)×10 ¹	0.6	4.73
6.85	(5 ⁻)	(3.53±0.88)×10 ⁸	5.5	4.96
7.05	3 ⁻	(2.17±0.33)×10 ⁸	1.5	4.50

^a g is assumed to be 0.95 F.

[OVER]

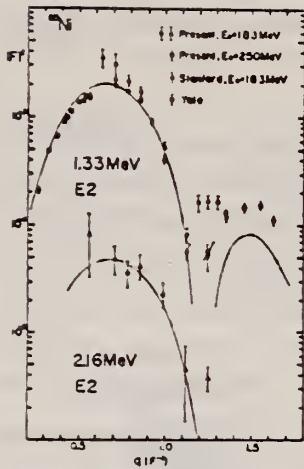


FIG. 5. Experimental $|F|^2$ versus q for the 1.33- and 2.16-MeV excitations in ^{60}Ni . Solid curves are reproduced using Eq. (2) in the text. The experimental data of Stanford and Yale for 1.33-MeV level are also plotted for comparisons.

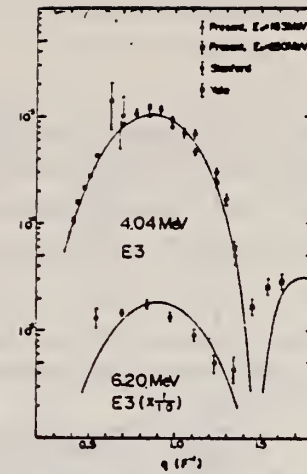


FIG. 6. Experimental $|F|^2$ versus q for the 4.04- and 6.20-MeV excitations. See caption to Fig. 5.

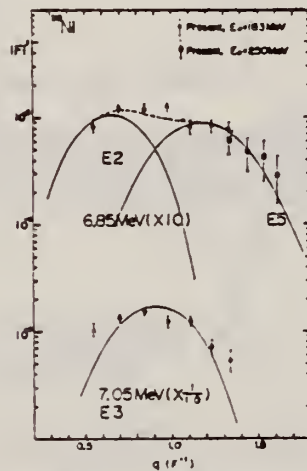


FIG. 7. Experimental $|F|^2$ versus q for the 6.85- and 7.05-MeV excitations. The $|F|^2$ of 6.85-MeV excitation were decomposed tentatively to $E2$ and $E5$ components using the theoretical curves predicted by Eq. (2) in the text.

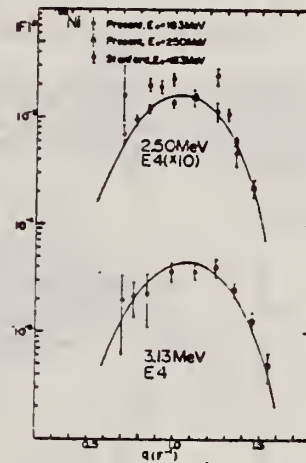


FIG. 8. Experimental $|F|^2$ versus q for the 2.50- and 3.13-MeV excitations. See caption to Fig. 5.

REF.	Y. Torizuka, Y. Kojima, M. Oyamada, K. Nakahara, K. Sugiyama, T. Terasawa, K. Itoh, A. Yamaguchi, and M. Kimura Phys. Rev. <u>185</u> , 1499 (1969)			ELEM. SYM.	A	Z	
				Ni	60	28	
METHOD				(Page 3 of 3)		REF. NO.	
						69 To 3	hmg
REACTION	RESULT	EXCITATION ENERGY	SOURCE		DETECTOR		ANGLE
			TYPE	RANGE	TYPE	RANGE	

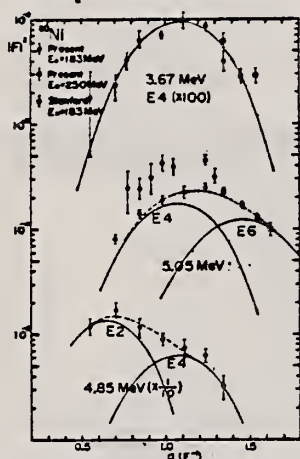


FIG. 9. Experimental $|F|^2$ versus q for the 3.67-, 4.85-, and 5.05-MeV excitations. The $|F|^2$ of 5.05 MeV were decomposed to $E4$ and $E6$ by the help of theoretical curves of Eq. (2) in the text. The $|F|^2$ of 4.85 MeV are tentatively decomposed to $E2$ and $E4$ as mentioned above.

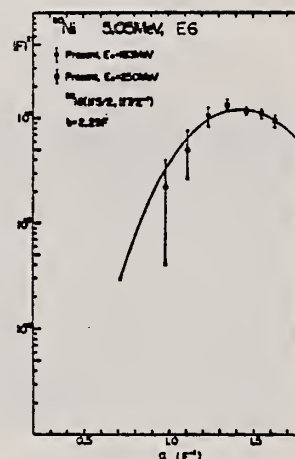


FIG. 10. Experimental $|F|^2$ of 6^+ state at 5.05 MeV. The solid curve is calculated $|F|^2$ of a 6^+ state in ^{60}Ni , assuming a configuration of $(1f_{7/2}, 1f_{7/2}^{-1})$, where oscillator length parameter was taken as $b = 2.29$ F. See the text.

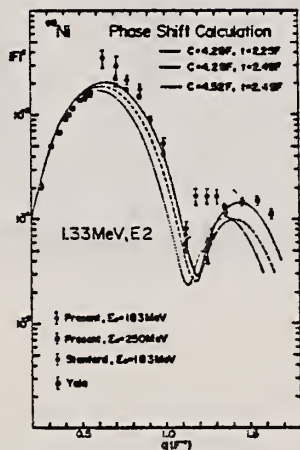


FIG. 11. Theoretical and experimental $|F|^2$ versus q for the 1.33-MeV (2^+) state. The theoretical curves were calculated by the Duke program of distorted-wave analysis (see Ref. 23) using three sets of parameters.

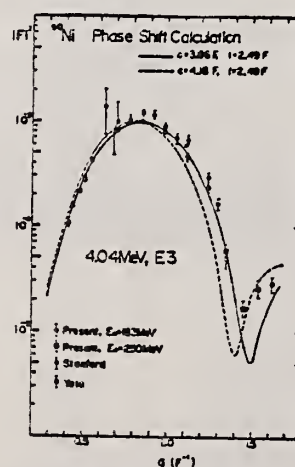


FIG. 12. Theoretical and experimental $|F|^2$ versus q for the 4.04-MeV (3^-) state. The curves were calculated by the Duke program.

REF. B.S. Ishkhanov, I.M. Kapitonov, I.M. Piskarev, V.G. Shevchenko,
and O.P. Shevchenko
Yad. Fiz. 11, 485 (1970)
Sov. J. Nucl. Phys. 11, 272 (1970)

ELEM. SYM.	A	Z
NI	60	28

METHOD	REF. NO.	
	70 Is 4	hmg

REACTION	RESULT	EXCITATION ENERGY	SOURCE		DETECTOR		ANGLE
			TYPE	RANGE	TYPE	RANGE	
G, P	ABX	9-30	C	9-30	SCD-D	1-	XXX
		(9.5-30)		(9.5-30)			

XXX PROB 90

1070+
1071

We measured the photoproton cross sections for the nuclei Cr^{52} , Ni^{58} , and Ni^{60} from the threshold to 30 MeV. We registered protons with energy larger than 1 MeV. A number of maxima were obtained in the cross sections. The values of the integral cross sections for Cr^{52} , Ni^{58} , and Ni^{60} are equal respectively to 240, 570, and 320 MeV-mb. The anomalously large cross section for the production of photoprotons for Ni^{58} , and also the shift of the centers of gravity of the photoproton cross sections towards higher excitation energies relative to the photoneutron cross sections in the case of Cr^{52} and Ni^{60} , can be attributed to the influence of analog states.

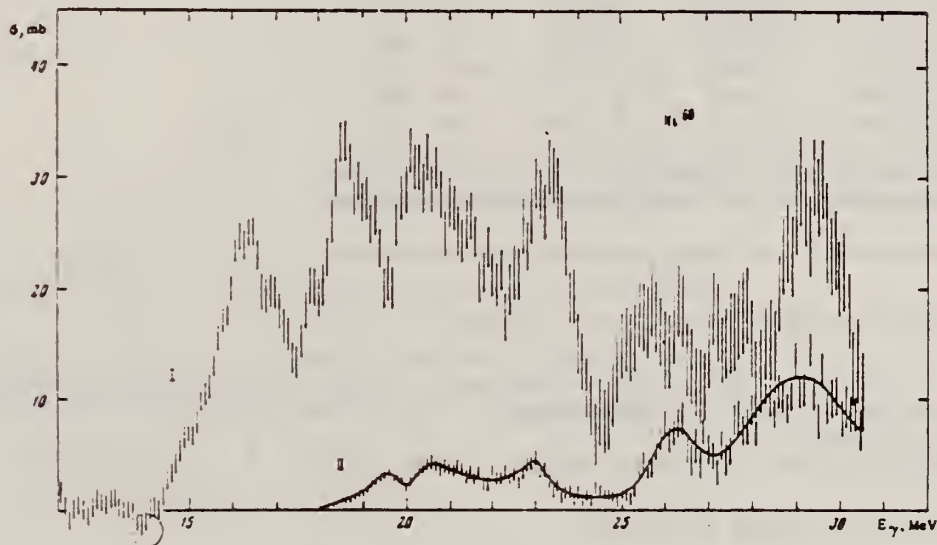


FIG. 3. Photoproton cross sections for Ni^{60} . The cross sections I and II were obtained for protons with $E_p > 1$ MeV and $E_p > 8$ MeV, respectively.

Integral characteristics of the photoproton cross sections σ_p , of the photoneutron cross sections σ_n , and of the total absorption cross sections $\sigma_\gamma = \sigma_n + \sigma_p$

Nucleus	$\int_0^{30} \sigma_p dE$	$\int_0^{30} \sigma_n dE$	$\int_0^{30} \sigma_\gamma dE$	$^{60}(NZ,A)$	$\frac{\int_0^{30} \sigma_p dE}{\int_0^{30} \sigma_\gamma dE}$	$\frac{\int_0^{30} \sigma_n dE}{\int_0^{30} \sigma_\gamma dE}$
	MeV-mb	MeV-mb	MeV-mb			
Cr^{52}	7.0 ± 0.6	210 ± 50	970 ± 110	775	0.25	21.1 ± 0.3
Ni^{58}	310 ± 30	570 ± 60	880 ± 90	870	0.65	21.0 ± 0.4
Ni^{60}	820 ± 50	120 ± 50	940 ± 100	895	0.31	21.3 ± 0.3

Note. The parentheses contain the integral cross sections of the photoproton reactions for protons with energy $E_p > 3$ MeV.

REF. F. R. Metzger
Nucl. Phys. A158, 88 (1970)

ELEM. SYM.	A	Z
Ni	60	28

METHOD

REF. NO.

70 Me 3

egf

REACTION	RESULT	EXCITATION ENERGY	SOURCE		DETECTOR		ANGLE
			TYPE	RANGE	TYPE	RANGE	
G,G	LFT	1-4	C	4	SCD-D	1-5	DST
		(4.1)				(<4.5)	

6 LEVELS

TABLE 3

The direct results of the resonance scattering experiments on ^{60}Ni described in this paper are listed in the fourth column

E_{level} (MeV)	I^{π}	Γ_0/Γ (%) error)	Γ_0^2/Γ (meV) this experiment	Γ_0 (meV)	Γ (meV)
1.333	2 ⁺	1.00 (<1)	0.61 ± 0.08	0.61 ± 0.08	$0.61 \pm 0.08^a)$
3.124	2 ⁺	0.096 ^{b)} (5)	0.07 ± 0.10	0.8 ± 1.1	8 ± 11
3.194	1 ⁺	0.16 ^{b)} (4)	0.63 ± 0.20	3.9 ± 1.3	25 ± 8
3.269	2 ⁺	0.15 ^{b)} (8)	<0.5	<4	<32
4.008	2 ⁺	0.31 ^{b)} (39)	3.2 ± 0.5	10 ± 4	33 ± 19
4.020	1 ⁺	0.54 ^{b)} (15)	11.1 ± 1.5	21 ± 4	39 ± 10

To arrive at the widths listed in columns 5 and 6, the branching ratios given in the third column were used. The errors quoted for the partial and total widths include the uncertainties in these branching ratios.

^{a)} Average of the value reported in ref. ⁷⁾ and of four values of different groups summarized in table 1 of ref. ⁶⁾.

^{b)} Taken from ref. ⁶⁾.

^{c)} A much more accurate value, $\Gamma = 0.63 \pm 0.01$ meV, has recently been reported ¹⁵⁾.

⁶⁾ F. Rauch, D.M. Van Patter and P.F. Hinrichsen,
Nucl. Phys. A124 (1969) 145.

⁷⁾ E.J. Hoffman and D.G. Sarantites, Phys. Rev.
181 (1969) 1597.

¹⁵⁾ F.R. Metzger, Nucl. Phys. A148 (1970) 362.

ELEM. SYM.	A	Z
Ni	60	28
REF. NO.		
70 Ow 1		egf

REACTION	RESULT	EXCITATION ENERGY	SOURCE		DETECTOR		ANGLE
			TYPE	RANGE	TYPE	RANGE	
G.XN	ABX	11-24	C	10-24	BF3-I		4PI

275

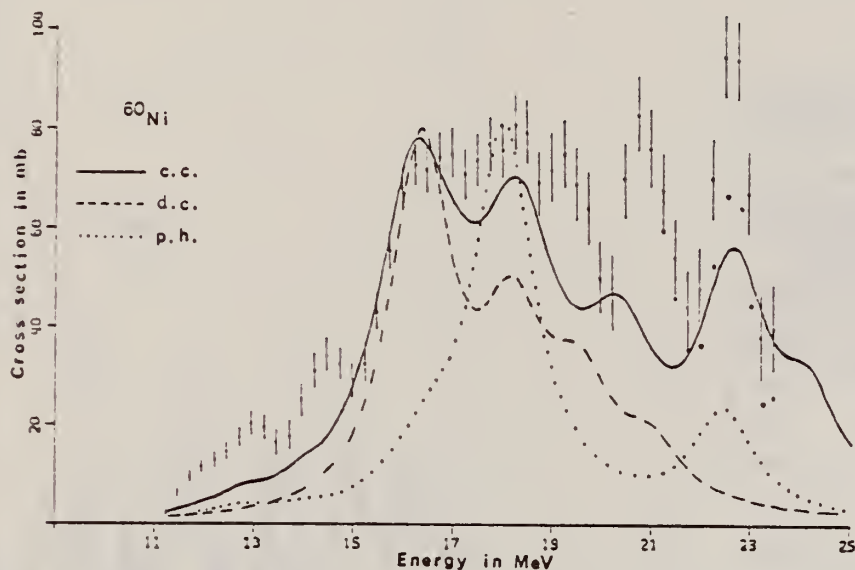


Fig. 3. The $^{60}\text{Ni}(\gamma, xn)$ experimental cross section is contrasted with the theoretical photo-absorption cross sections predicted by the collective correlations (c.c.) calculation, the dynamic collective model (d.c.) and the particle-hole calculation (p.h.) all as taken from ref. ⁴).

⁴D. Drechsel, J. B. Seaborn and W. Greiner,
Phys. Rev. 162B, 983 (1967).

REF.

V.G. Tikhonov, V.G. Shevchenko, V.Ya. Galkin et al.
Ser. III. Fiz. Astron. 11, 208 (1970)

ELEM. SYM.	A	Z
Ni	60	28
REF. NO.		
70 Tl 2		egf

METHOD

REACTION	RESULT	EXCITATION ENERGY	SOURCE		DETECTOR		ANGLE
			TYPE	RANGE	TYPE	RANGE	
G,XN	RLY	12-30	C	12-30	BF3-I		4PI

No data given for ^{51}V , ^{59}Co , ^{58}Ni .

59772 DETERMINATION OF PHOTONUCLEAR REACTION CROSS SECTIONS. Tikhonov, A. N.; Shevchenko, V. G.; Galkin, V. Ya.; (and others). Vestn. Mosk. Univ., Ser. III. Fiz. Astron.; 11: No. 2, 208-14 (Mar-Apr 1970). (In Russian).

An operative system for the automatic handling of data is described for the determination of photonuclear reaction cross sections with a 35-MeV betatron. The system provides for fully automatic processing of experimental data as accumulated in the analyzer all the way to obtaining the cross section of a photonuclear reaction. Bremsstrahlung which is generated at the target of the betatron passes through a collimator and then impinges on the desired material. The neutrons thus produced are recorded by a BF₃ detector using a paraffin moderator. The pulses are sent to the memory of a pulse-height analyzer. This system is illustrated with data from (γ,n) reactions with the nuclei ^{51}V , ^{59}Co , ^{58}Ni , and ^{60}Ni . (K.S.W.)

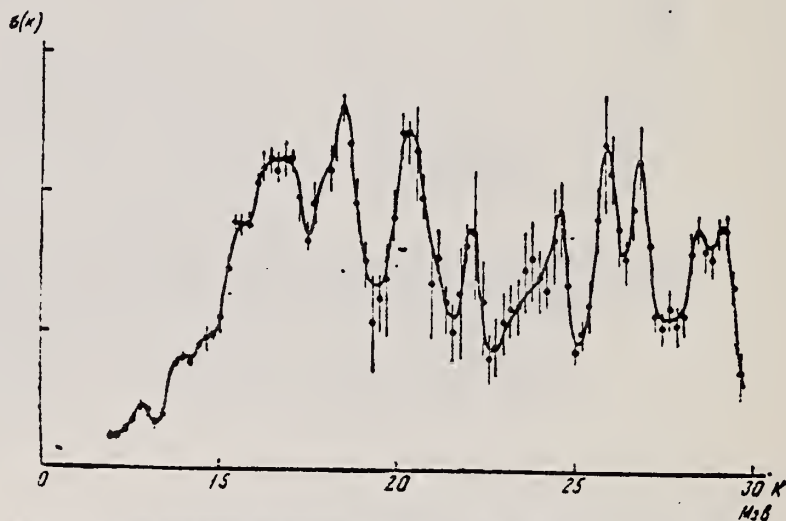


Рис. 3. Сечение фотонейтроной реакции на Ni^{60} , полученное в результате автоматической обработки экспериментальных данных

REACTION	RESULT	EXCITATION ENERGY	SOURCE		DETECTOR		ANGLE
			TYPE	RANGE	TYPE	RANGE	
P, G	ABX	13-23	D	4-14	NAI-D		DST
				(4.4-13.0)			

221+

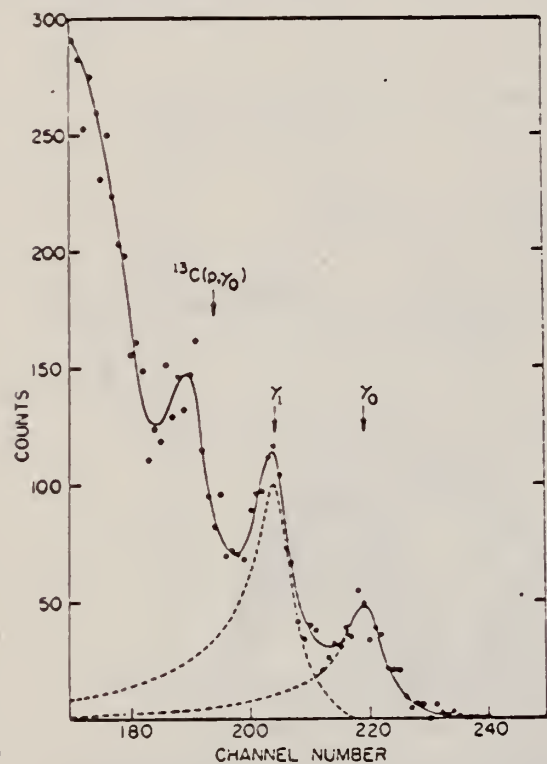


FIG. 1. Spectrum of high-energy γ rays from radiative capture of protons by ^{59}Co . Only the region of the pulse-height spectrum which corresponds to $E_\gamma > 13$ MeV is shown. The 7.6-MeV bombarding energy results in 17.00- and 15.67-MeV γ rays from the ground-state (γ_0) and first-excited-state (γ_1) transitions, respectively. The next lower peak is due to transitions to a group of higher excited states in ^{60}Ni . Also indicated is the position at which γ rays from the reaction $^{13}\text{C}(p, \gamma)^{14}\text{N}$ would appear. The dashed lines indicate the contributions from the γ_0 and γ_1 transitions obtained by fitting the data as described in the text.

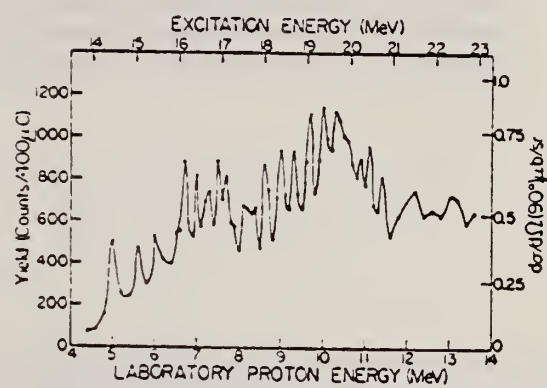


FIG. 2. Excitation function for the reaction $^{59}\text{C}(p, \gamma_0)-^{60}\text{Ni}$. The solid line is intended merely to guide the eye. The uncertainty associated with each data point is $\pm 10\%$ of the yield.

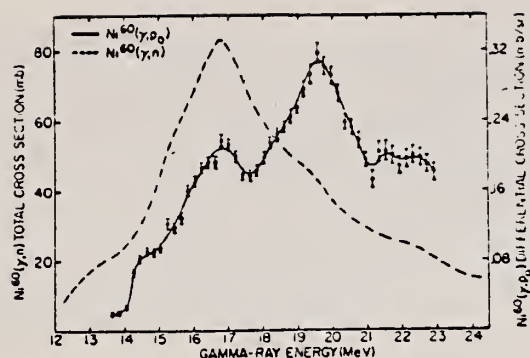


FIG. 3. Excitation functions for the reactions $^{59}\text{Ni}(\gamma, p)^{59}\text{C}$ at 90° , obtained by detailed balance from the data of Fig. 1 averaged over a 600-keV interval, and $^{60}\text{Ni}(\gamma, n)^{60}\text{Ni}$ obtained from Ref. 23. Note the different cross-section scales for the two reactions. Above the $^{60}\text{Ni}(\gamma, 2n)$ threshold, the photoneutron data have been corrected for multiple neutron emission to yield the $^{60}\text{Ni}(\gamma, n)$ cross section. The indicated error bars were obtained from the averaging procedure. The solid line through the $^{60}\text{Ni}(\gamma, p)$ data points is drawn to guide the eye.

²³K. Min and T.A. White, Phys. Rev. Letters 21, 1200 (1968).

The radiative-capture reaction $^{59}\text{Co}(p, \gamma)^{60}\text{Ni}$ has been studied for proton energies from 4.40 to 13.60 MeV. Cross-section and angular-distribution data were measured with a large anticoincidence-shielded NaI(Tl) detector. The yield curve for ground-state capture shows two broad peaks, at ^{60}Ni excitations of 16.6 and 19.6 MeV; these are interpreted as the T_{-} and T_{+} components of the giant dipole resonance. The results of a detailed calculation ignoring isospin effects do not adequately explain all of the observations; a simple 1p-1h calculation using eigenfunctions of T describes the results quite well. The first-excited-state-capture yield curve is similar to the ground-state curve, shifted in energy by ~ 300 keV. The data suggest that most of the observed strength in the giant dipole resonance based on the first excited state of ^{60}Ni is concentrated in 2^{-} states.

J. W. Lightbody Jr.
Phys. Letters 38B, 475 (1972)

Ni

60

28

METHOD

REF. NO.

72 L1.1

egf

REACTION	RESULT	EXCITATION ENERGY	SOURCE		DETECTOR		ANGLE
			TYPE	RANGE	TYPE	RANGE	
$E, E/$	FMF	1-3	D	60-120	MAG-D		DST

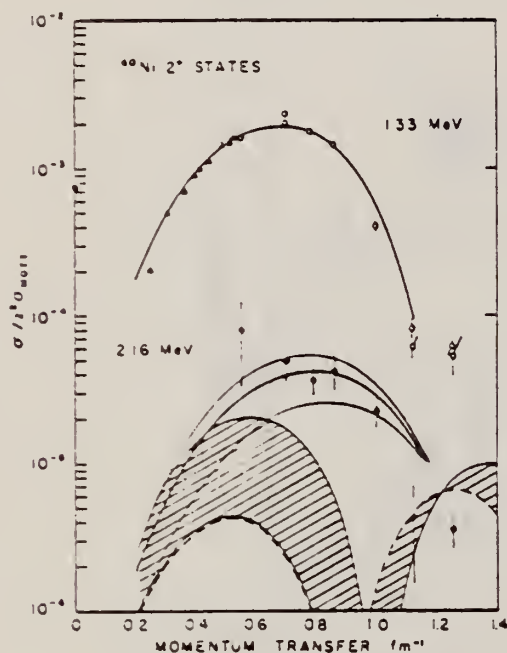
1.33, 2.16 MEV

Fig. 1. Electron scattering form factors for the lowest two 2^+ states in ^{60}Ni . Solid lines were calculated using a best fit admixture and phase. The dashed line represents the harmonic two-phonon form factor. The shaded and cross-hatched regions were determined by using admixtures which fit the measured BR for $\phi = \pi$ and 0, respectively.

REF.

K. Shoda, M. Sugawara, T. Saito, H. Miyase, A. Suzuki, S. Oikawa,
and J. Uegaki
PICNS-72, 321 Sendai

ELEM. SYM.	A	Z
Ni	60	28
REF. NO.		
72 Sh 10		hvm

METHOD			SOURCE		DETECTOR		ANGLE
REACTION	RESULT	EXCITATION ENERGY	TYPE	RANGE	TYPE	RANGE	
G,P	ABX	15- 25	C	15- 25	MAG-D		90

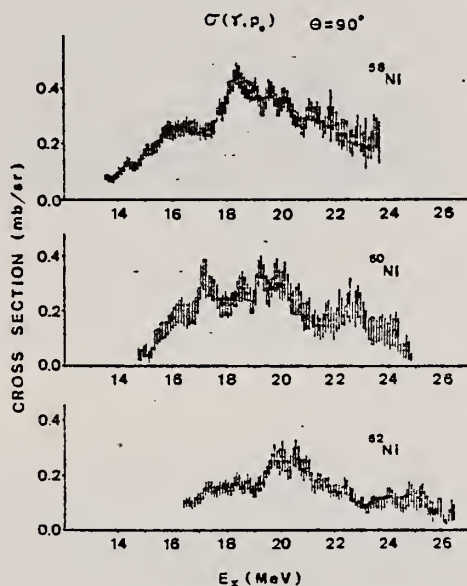
I A STATES

Fig. 10 The (γ, p_0) cross sections of Ni isotopes obtained from proton spectra by the $(e, e'p)$ reaction.

REF

D. Branford, G.S. Foote, R.A.I. Bell, D.C. Weissner,
F.C.P. Huang and R.B. Watson -
PICNS-73, Vol.II, p.943 (1973) Asilomar

ELEM. SYM.	A	Z
Ni	60	28
REF. NO.		egf
73 Br 7		

METHOD

REACTION	RESULT	EXCITATION ENERGY	SOURCE		DETECTOR		ANGLE
			TYPE	RANGE	TYPE	RANGE	
G,A	ABX	14- 22	D	16	NAI-D		DST

NO ANG DST DATA

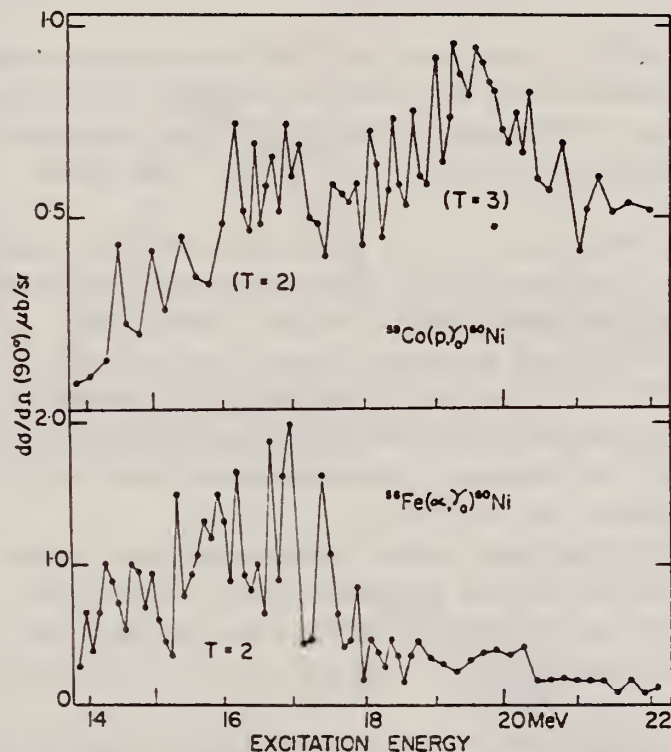


Fig. 1. Excitation functions for radiative capture reactions leading to ^{60}Ni GDR

Table 1. Preliminary Results with Relative Errors; Absolute Errors $\approx 30\%$

Reaction	$\int \sigma(\gamma_0, \alpha_0) dE$ mb. MeV	$\int \sigma(\gamma_1, \alpha_0) dE$ mb. MeV	Excitation Energy (MeV)
$^{40}\text{Ar}(\alpha, \gamma)^{44}\text{Ca}$	1.4 ± 0.3	0.42 ± 0.08	15.5
$^{48}\text{Ti}(\alpha, \gamma)^{52}\text{Cr}$	3.0 ± 0.6	0.48 ± 0.10	17.0
$^{56}\text{Fe}(\alpha, \gamma)^{60}\text{Ni}$	7.8 ± 1.5	1.52 ± 0.30	16.0

ELEM. SYM.	A	Z
Ni	60	28
REF. NO.		
73 Fu 6		hmg

METHOD					
REACTION	RESULT	EXCITATION ENERGY	SOURCE		ANGLE
			TYPE	RANGE	
G,N	ABX	11- 34	D	11- 34	4PI
G,2N	ABX	19- 34	D	19- 34	4PI

As in the case of ^{58}Ni ¹ we report, in this paper, the first high-resolution measurement of the ^{60}Ni photoneutron cross sections with nearly monoenergetic photons from in-flight annihilation of positrons. The experimental details, including resolution and systematic uncertainties, are the same as those in the ^{58}Ni work.¹ The target sample enrichment was 99.79% ^{60}Ni .

Our experimental results are shown in Fig. 1. The total photoneutron cross section reaches a peak value of about 75 mb just above 16 MeV. There is some structure evident, superimposed on the general shape of the giant resonance, which is somewhat less prominent than that observed in ^{58}Ni ; it does not agree in detail with the structure observed in previous experiments²⁻⁴ on ^{60}Ni performed with bremsstrahlung photons. The magnitude of the peak cross section observed in this and previous experiments²⁻⁴ are in reasonably good agreement, however. The integrated total photoneutron cross section is 705 MeV-mb, about 2.5 times as large as that for ^{58}Ni .

Unlike the ^{58}Ni case, the ^{60}Ni ($\gamma,2n$) cross section forms a significant fraction of the total in the region above 20 MeV, although it appears to drop to nearly zero at 33 MeV. The statistics are sufficiently good that definite structure can be discerned in the cross section. The integrated ($\gamma,2n$) cross section is 73 MeV-mb, almost an order of magnitude larger than in the ^{58}Ni case.

As in the case of ^{58}Ni , the measured cross section is in qualitative agreement, up to about 25 MeV, with the distribution of dipole strength calculated by Tanaka.⁵ The collective correlations calculation of Seaborn, *et al*⁶ appears to provide some additional dispersion of the dipole strength to higher energies, yet there still appears to be too much experimental cross section above 25 MeV to be explained by the shell-model calculations done thus far.

[†] Work performed under the auspices of the U. S. Atomic Energy Commission.

* Deceased

1 S. C. Fultz, R. A. Alvarez, B. L. Berman, P. Meyer: preceding paper.

2 K. Min and T. A. White, Phys. Rev. Letters 21, 1200 (1968).

3 B. I. Goryachev, B. S. Ishkhanov, I. M. Kapitonov, I. M. Piskarev, V. G. Shevchenko, and O. P. Shevchenko, Sov. J. Nucl. Physics 11, 141 (1970) [Yad. Fiz. 10, 252 (1969)].

4 D. G. Owen, E. G. Muirhead, B. M. Spicer, Nucl. Phys. A140, 523 (1970).

5 Y. Tanaka, Prog. Theor. Phys. 46, 787 (1971).

6 J. B. Seaborn, D. Drechsel, H. Arenhovel, W. Greiner, Phys. Lett. 23, 576 (1966).

(over)

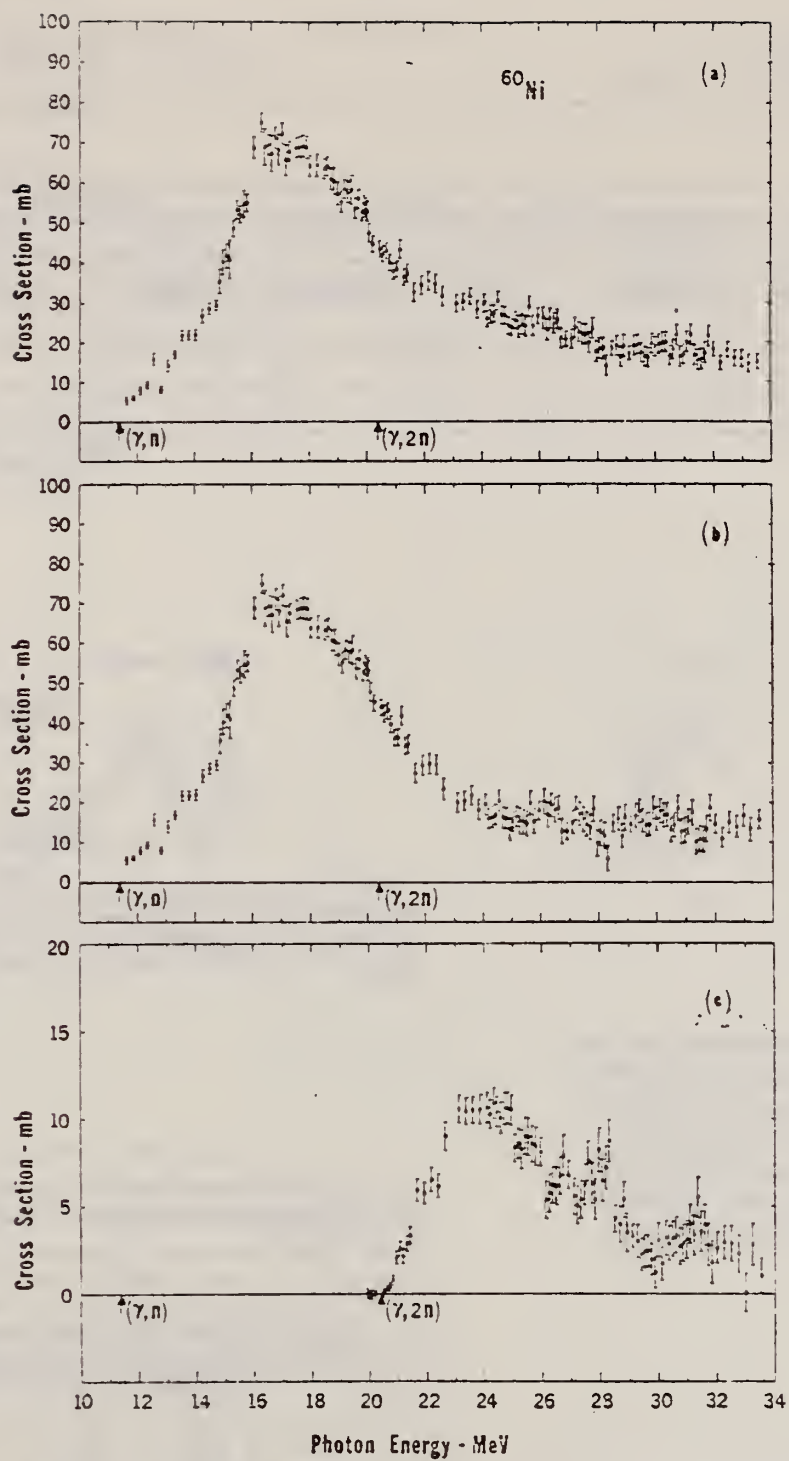


Figure 1. Photoneutron cross sections of ^{60}Ni . Thresholds (see Ref. 7) are indicated by arrows. (a) Total photoneutron cross section: $\sigma[(\gamma,n) + (\gamma,pn) + (\gamma,2n)]$; (b) $\sigma[(\gamma,n) + (\gamma,pn)]$; (c) $\sigma(\gamma,2n)$.

REACTION	RESULT	EXCITATION ENERGY	SOURCE		DETECTOR		ANGLE
			TYPE	RANGE	TYPE	RANGE	
E, E/	SPC	10- 30	D	198-201	MAG-D		DST

FMF/13.0, 16.3 MEV

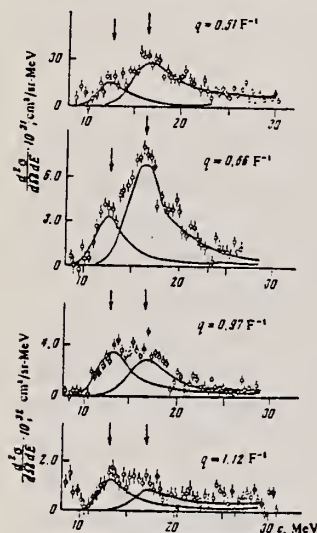


FIG. 1

FIG. 1. Energy spectra of electrons inelastically scattered by Ni^{60} , obtained after subtraction of the radiation tail from the elastic and inelastic peaks. The arrows show the locations of the peaks of the two resonances. With increasing q the contribution from the resonance at 13.0 ± 0.3 MeV increases, and while that from the 16.2 ± 0.2 MeV resonance decreases.

FIG. 2. Form factors for the giant E1 and E2 resonances as a function of effective momentum transfer q' . Points: \bullet — 13.0 ± 0.3 MeV, \circ — 16.3 ± 0.2 MeV. Curves: 1—calculation of E1 resonance form factor in terms of dynamic collective theory, [6] 2—in Helm's model, [7] 3 and 4—the same as 1 and 2 but for the E2 resonance. Curves 1 and 3 have been decreased by 20% and a factor of 4, respectively.

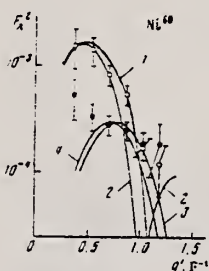


FIG. 2

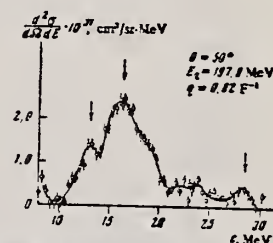


FIG. 3. Energy spectra of electrons scattered by Ni^{60} . The arrows show the locations of the peaks of the E2 (13.0 MeV) and E1 (16.3 MeV) resonances, and also the resonance at excitation energy 28.5 MeV whose nature is unknown. The curve was drawn by eye through the experimental points.

TABLE II. Energy location, half-width, reduced transition probability, radiation width, and enhancement factor of E1 and E2 resonances in Ni^{60} , Zr^{90} , and Pb^{208}

Nucleus	ϵ_1 , MeV	ϵ_2 , MeV	Γ_1 , MeV	Γ_2 , MeV	$B(E1, J_1 \rightarrow J_2)$, $e^2 F^2$	$\Gamma_{\gamma 1}$, keV
Ni^{60}	16.3 ± 0.2	13.0 ± 0.3	4.8 ± 0.3	4.1 ± 0.3	12.0 ± 2.4	13.1 ± 3.6
Zr^{90}	16.65	14.0	4.0	4.8 ± 0.6	17.0 ± 3.0	27.3 ± 3.0
Pb^{208}	14.1	~ 10.7	—	—	64.0 ± 8.0	62.5 ± 7.9

Nucleus	G_1	$B(E2, J_1 \rightarrow J_2)$, $e^2 F^4$	$\Gamma_{\gamma 2}$, eV	G_2	Source of data
Ni^{60}	4.1 ± 0.8	$\begin{cases} 125 \pm 25 \\ 103 \pm 21 \end{cases}$	$\begin{cases} 7.5 \pm 1.5 \\ 6.2 \pm 1.2 \end{cases}$	$\begin{cases} 1.8 \pm 0.4 \\ 1.5 \pm 0.3 \end{cases}$	Present work
Zr^{90}	4.4 ± 1.3	990 ± 300	85.5 ± 25.9	8.3 ± 2.5	[6]
Pb^{208}	9.4 ± 1.2	2600 ± 900	58.7 ± 20.4	7.1 ± 2.5	[7]

Note. The values of $B(E2)$, $\Gamma_{\gamma 2}$, and G_2 given in the upper line were obtained on the basis of the vibrational model, and those in the lower line on the basis of Helm's model.

TABLE I. Form factors of giant dipole and quadrupole resonances of Ni^{60}

θ , deg	ϵ_n , MeV	q' , F^{-1}	$F_{\lambda=1}^2 (\times 10^{-9})$	$F_{\lambda=2}^2 (\times 10^{-9})$
20	199.7	0.366	1.58 ± 0.64	0.53 ± 0.22
30	199.1	0.538	1.44 ± 0.42	0.34 ± 0.10
40	197.6	0.703	0.84 ± 0.19	0.28 ± 0.06
50	197.9	0.866	0.55 ± 0.12	0.25 ± 0.05
60	199.1	1.029	0.17 ± 0.04	0.19 ± 0.05
70	201.0	1.194	0.12 ± 0.04	0.19 ± 0.10

K. Itoh, M. Oyamada, and Y. Torizuka
Phys. Rev. C7, 458 (1973)

Ni

60

28

METHOD

REF. NO.

73 It 1

hmg

REACTION	RESULT	EXCITATION ENERGY	SOURCE		DETECTOR		ANGLE
			TYPE	RANGE	TYPE	RANGE	
E, E/	FMF	0- 7	D	183,250	MAG-D		82

See 09To3.

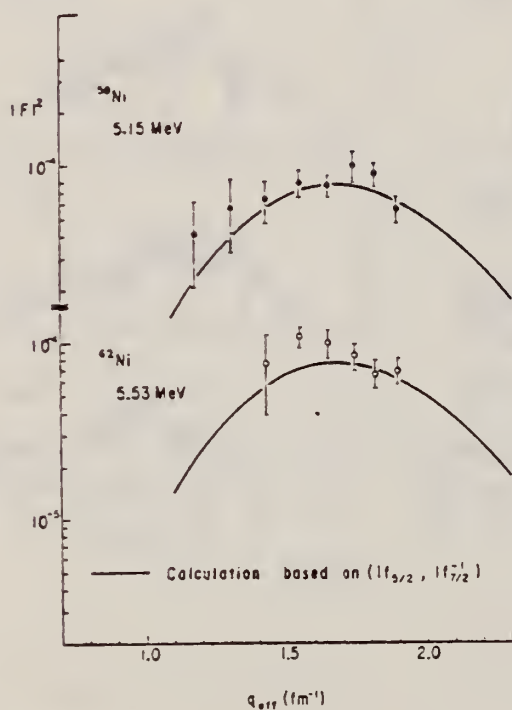
LEVEL AT 5.53 MEV

FIG. 2. The experimental form factors for the 6^+ states compared with the theoretical form factors calculated for the $(1f_{7/2}, 1f_{7/2}^{-1})$ configuration.

REF. H. Miyase, S. Oikawa, A. Suzuki, J. Uegaki, T. Saito,
M. Sugawara, and K. Shoda
PICNS-73, Vol. I, p. 553 Asilomar

ELEM. SYM.	A	Z
Ni	60	28

REF. NO.	hmg
73 M1 7	

REACTION	RESULT	EXCITATION ENERGY	SOURCE		DETECTOR		ANGLE
			TYPE	RANGE	TYPE	RANGE	
E,P	ABX	14- 26	D	0 - 26	MAG-D		DST
						746 744+	

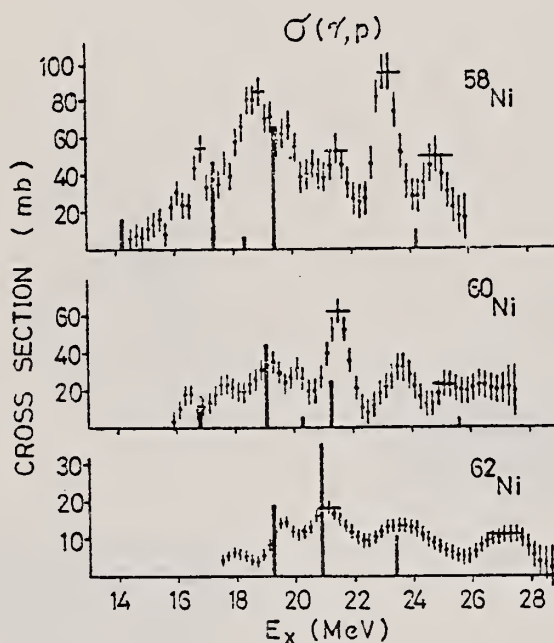


Fig. 1

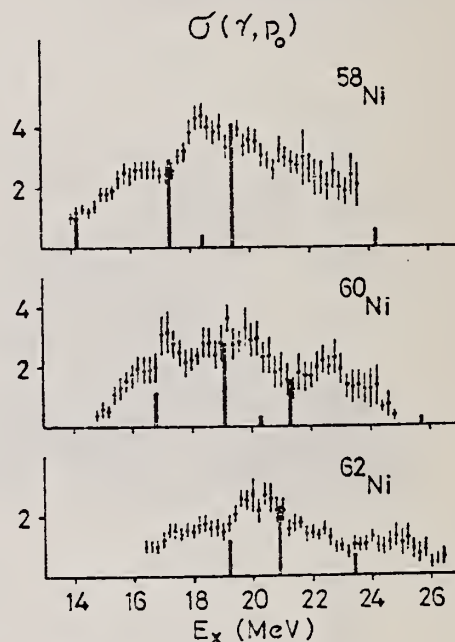


Fig. 2

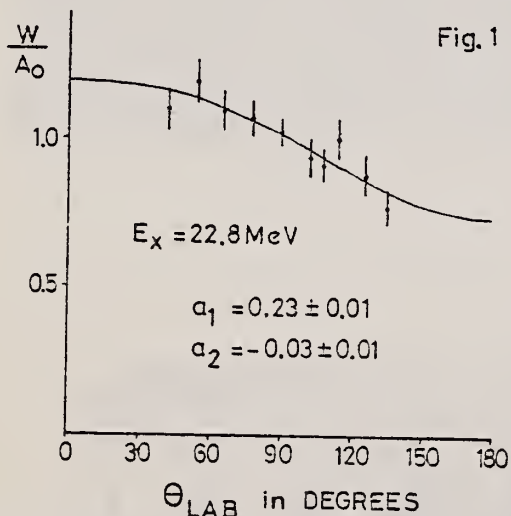


Fig. 3 Angular distribution in $^{60}\text{Ni}(e, e'p_0)$ at $E_x = 22.8$ MeV. The curve is fit obtained with the series $1 + a_1 P_1 + a_2 P_2$. The values of a_1 and a_2 are listed in the figure.

Table 1 Experimental and theoretical results

Nucleus	T_0	$\int \sigma_n^{(3)}$ (mb-MeV)	$\int \sigma_p$ (mb-MeV)	$\int \sigma_n + \int \sigma_p$ (mb-MeV)	$\frac{\int \sigma_p}{\int \sigma_n + \int \sigma_p}$	$\frac{ c_> ^2}{ c_< ^2 + c_> ^2}$
^{58}Ni	1	310 ± 30	480 ± 100	790 ± 130	0.61	0.45
^{60}Ni :	2	620 ± 50	210 ± 80	830 ± 130	0.25	0.27
^{62}Ni	3		110 ± 25			0.17

ELEM. SYM.	A	Z
Ni	60	28
REF. NO.		
73 Ve 3		hmg

METHOD					REF. NO.		
					73 Ve 3	hmg	
REACTION	RESULT	EXCITATION ENERGY	SOURCE		DETECTOR		ANGLE
			TYPE	RANGE	TYPE	RANGE	
G,N	ABX	11- 14	C	12, 13	TOF-D		93
		(11.39-13.27)	(12.02,13.27)				

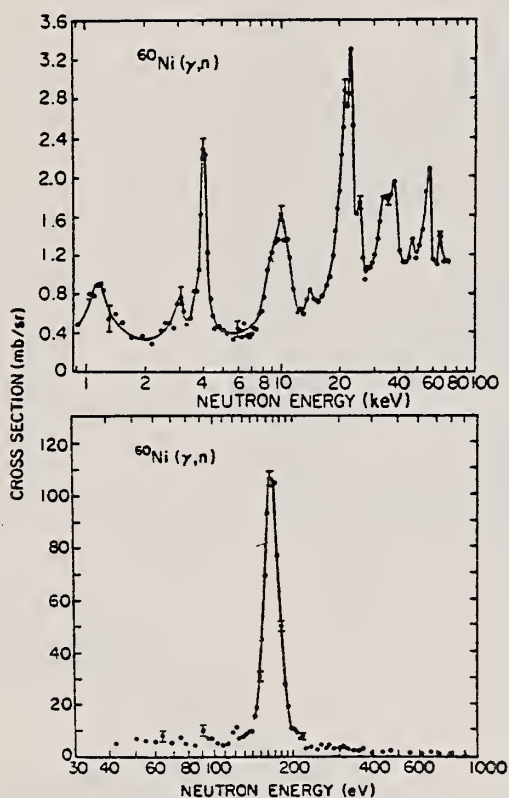


FIG. 2. The 93° differential threshold photoneutron cross section for ^{60}Ni versus the energy of the emitted neutron. Electrons of 13.27-MeV and 3% resolution were incident on the bremsstrahlung converter.

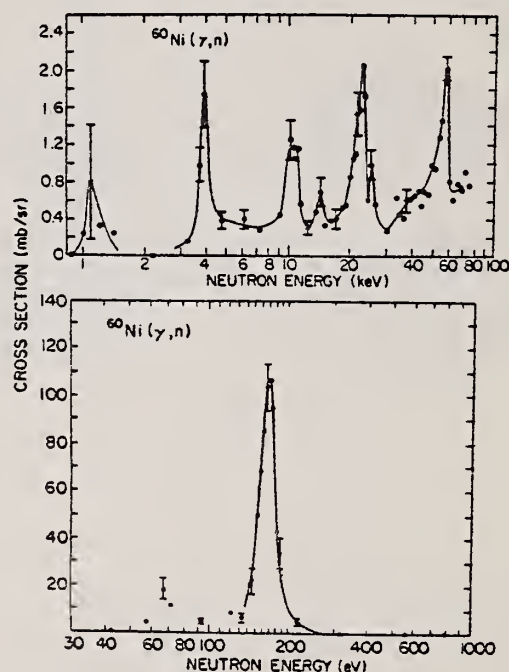


FIG. 3. The 93° differential threshold photoneutron cross section for ^{60}Ni versus the energy of the emitted neutron. Electrons of 12.02-MeV and 1% resolution were incident on the bremsstrahlung converter.

(over)

TABLE I. Resonance parameters from threshold $^{60}\text{Ni}(\gamma, n)$ data.

Neutron energy (keV)	Width at half maximum (keV)	Experimental resolution (keV)	Ratio of peak area for $E_n = 13.27$ MeV to that for $E_n = 12.02$ MeV	Deexcitation to ground state (G) or to excited states (E) of ^{60}Ni	$\Gamma \approx \Gamma_n$ (keV)	$g\Gamma_\gamma\Gamma_n/\Gamma$ (eV)
0.168	0.025	0.0013	0.93	G	0.025	0.65
1.15(?)	0.35(?)	0.017	0.92	?	0.35(?)	0.051(?)
3.0	~0.30	0.065	Very large	E(≈ 0.878 MeV)	~0.29	
4.0	0.36	0.094	1.01	G	0.35	0.20
~9.0	1.7 } 2.9	0.32	Very large	E(≈ 0.878 MeV)		
10.5		0.38		G(?)	1.7	0.26
14.2	~1.2	0.54	1.05	G	~1.1	0.065
21.1	} 3.4	1.0		E(?)		
22.8		1.1	1.5	E(0.340 MeV?)		
25.5	?	1.3		?		
33.7	} 8	2.0	Very large	E(≈ 0.878 MeV)		
38.1		2.5	Very large	E(≈ 0.878 MeV)		
47.5(??)	?	3.4		?		
57	5.4	4.6	0.74	G		
66	?	5.6		?		

REF.

G. S. Foote, D. Branford, R.A.I. Bell, and R.B. Watson
Nucl. Phys. A220, 505 (1974)

ELEM. SYM. A Z

Ni

60

28

METHOD

REF. NO.

74 Fo 2

egf

REACTION	RESULT	EXCITATION ENERGY	SOURCE		DETECTOR		ANGLE
			TYPE	RANGE	TYPE	RANGE	
A,G	ABX	13- 23	D	8- 18	NAI-D		DST
P,G	ABX	16- 17	D	7- 18	NAI-D		90

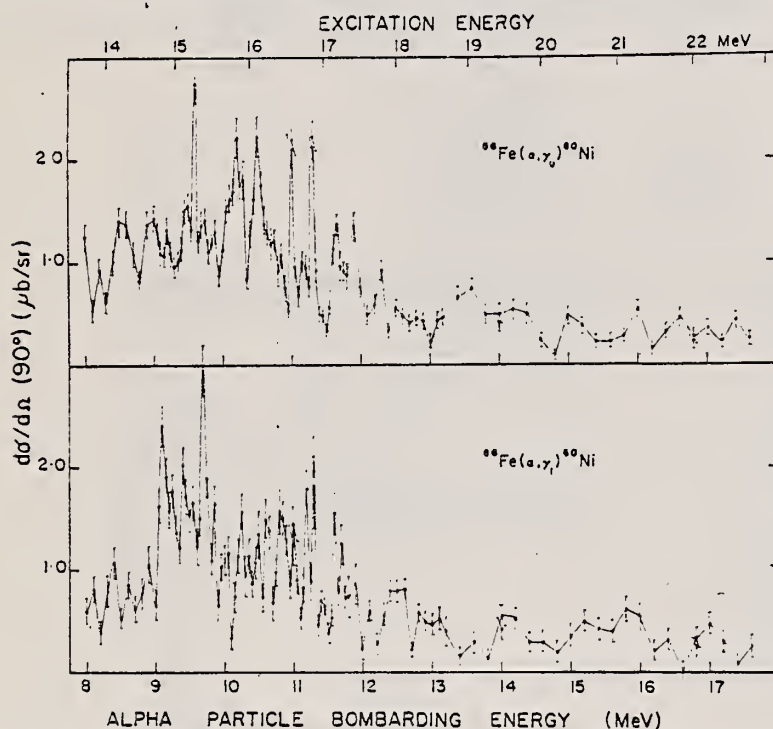


Fig. 2. The absolute differential cross sections for the $^{56}\text{Fe}(\alpha, \gamma)^{60}\text{Ni}$ and $^{56}\text{Fe}(\alpha, \gamma)^{60}\text{Ni}$ reaction at 90° to the beam direction as a function of bombarding energy. The error bars represent statistical errors. The errors in the absolute values are $\pm 25\%$.

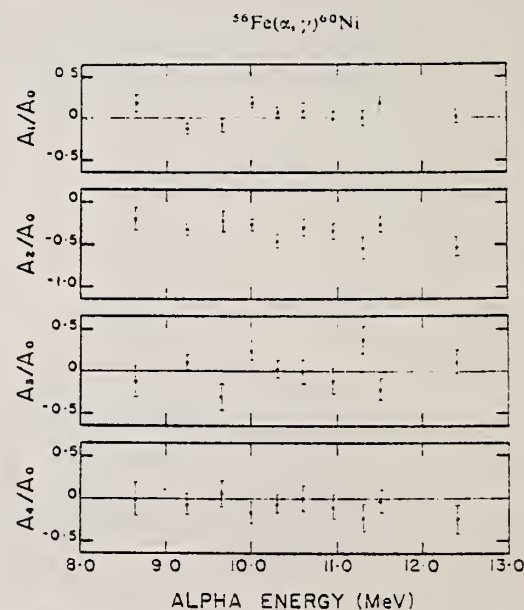


Fig. 7. Normalised Legendre coefficients determined by the method of least squares from the γ_0 angular distributions shown in fig. 5.

(over)

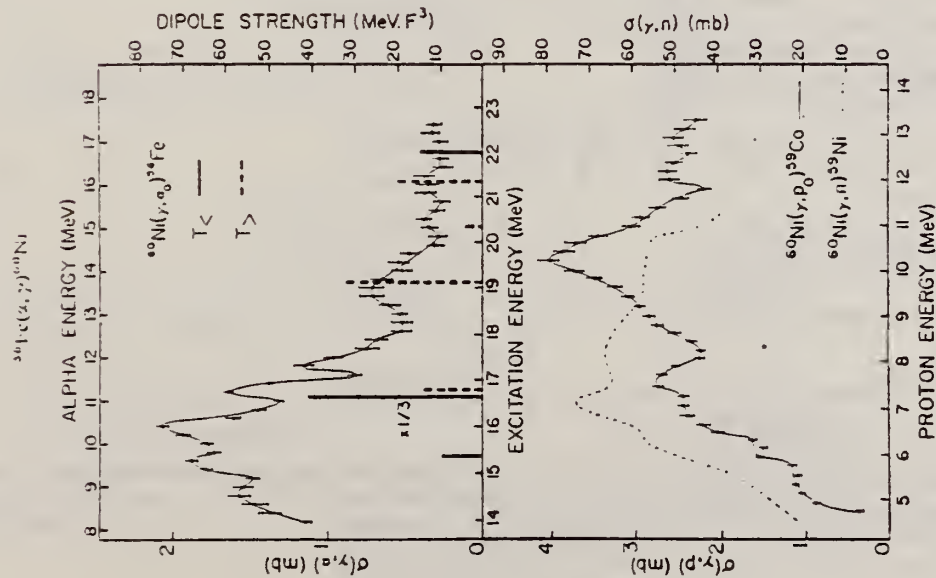


Fig. 10. A comparison of ^{60}Ni photonuclear excitation functions. The (α, γ_0) data were obtained from the results presented here using the principle of detailed balance. The (γ, p_0) and (γ, n) data are from refs. 1) and 14) respectively. The (γ, α_0) and (γ, p_0) data have been averaged over 300 keV intervals. The error bars represent statistical errors. The continuous and dashed vertical line indicate the γ -ray transition strengths associated with levels given by the shell-model calculation of ref. 3).

- 1) E.M. Diener et al., Phys. Rev. C3 (1971) 2303
- 3) O. Ngo-Trong et al., Phys. Lett. 36B (1971) 553
- 14) H.J. Rose et al., Rev. Mod. Phys. 39 (1967) 306

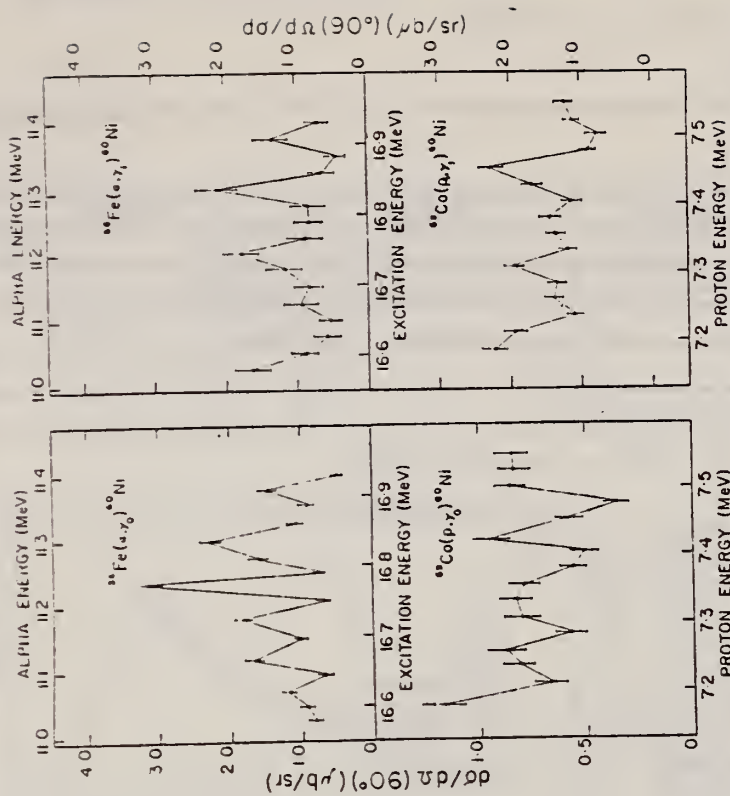


Fig. 3. A comparison of excitation functions for $^{59}\text{Fe}(\alpha, \gamma_0)^{60}\text{Ni}$, $^{59}\text{Fe}(\alpha, \gamma_1)^{60}\text{Ni}$, $^{59}\text{Co}(\alpha, \gamma_0)^{60}\text{Ni}$ and $^{59}\text{Co}(\alpha, \gamma_1)^{60}\text{Ni}$ reactions, which were obtained in 25 keV steps. The error bars represent statistical errors. The errors in the absolute values are $\pm 25\%$.

METHOD

REF. NO.

74 Fo 4

egf

REACTION	RESULT	EXCITATION ENERGY	SOURCE		DETECTOR		ANGLE
			TYPE	RANGE	TYPE	RANGE	
G,A	ABX	14- 22	D	8- 17	NAI-D		90

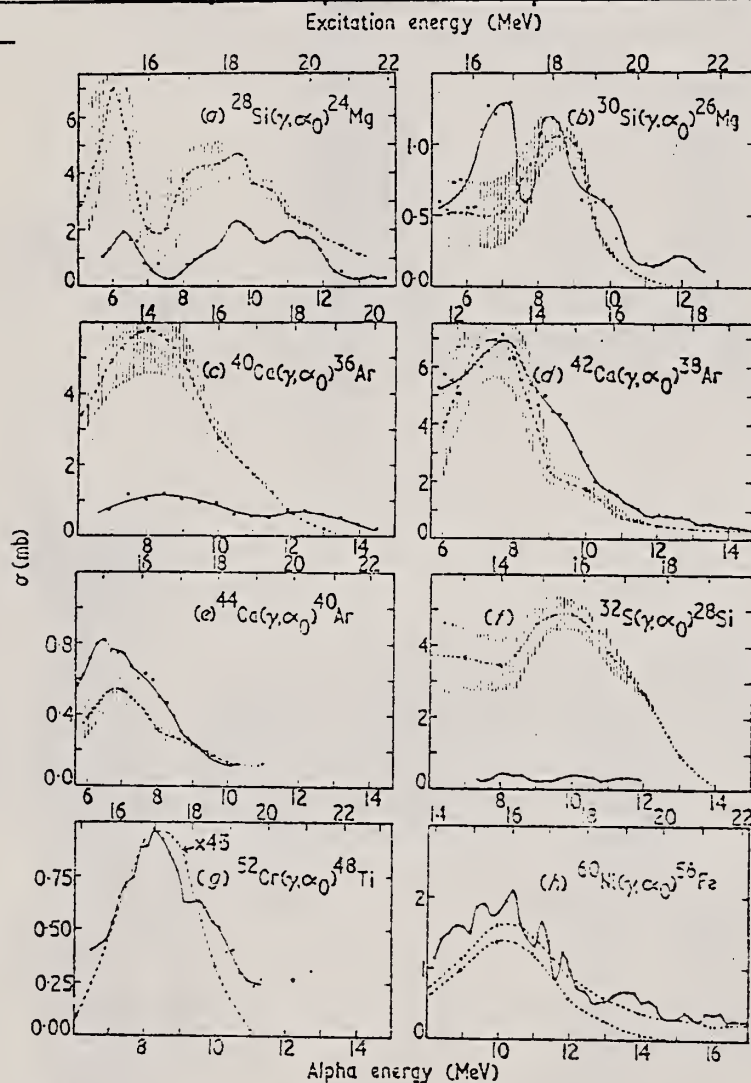


Figure 1. Excitation functions for the (γ, α) reaction obtained from α capture data using the principle of detailed balance. The data shown in (a) and (f) are from Meyer-Shutzmeister *et al* (1968). Those in (b) are from Watson *et al* (1973). The relative experimental errors are approximately $\pm 10\%$. The absolute errors are $\pm 25\%$. The broken curves are the results of calculations (see text). The vertical lines indicate the relative errors due to uncertainties in the total photonuclear cross sections where they are greater than $\pm 10\%$. The crosses indicate the energies at which transmission coefficients were calculated.

REF.

ELEM. SYM.	A	Z
Ni	60	28

METHOD

REF. NO.	
74 Fu 3	hmg

REACTION	RESULT	EXCITATION ENERGY	SOURCE		DETECTOR		ANGLE
			TYPE	RANGE	TYPE	RANGE	
G,N	ABX	11- 34	D	11- 34	BF3-I		4PI
G,2N	ABX	20- 34	D	20- 34	BF3-I		4PI

SEP ISOTOPES

529+

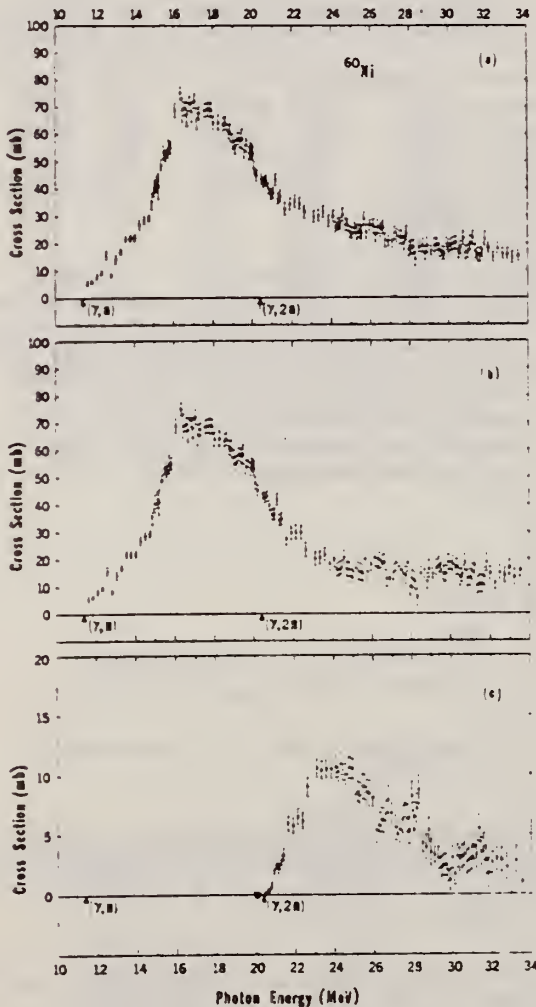


FIG. 3. Measured photoneutron cross sections for ^{60}Ni : (a) $\sigma(\gamma, Sn)$ (see Ref. 17); (b) $\sigma[(\gamma, n) + (\gamma, pn)]$; (c) $\sigma(\gamma, 2n)$.

TABLE II. Integrated photoneutron cross sections and related quantities from the data of the present experiment. The definitions used in this table are

$$\sigma_{\text{int}} \equiv \int_{E_{\text{thr}}}^{E_{\gamma \text{ max}}} \sigma dE_{\gamma}, \quad \sigma_{-2} \equiv \int_{E_{\text{thr}}}^{E_{\gamma \text{ max}}} E_{\gamma}^{-2} \sigma dE_{\gamma},$$

where E_{thr} is the threshold energy (see Table I) and E_{γ} is the photon energy; the quantity (γ, Sn) is defined in Ref. 17. Errors on the integrated cross sections are dominated by the systematic errors as discussed in Sec. III of the text.

	^{58}Ni	^{60}Ni
$E_{\gamma \text{ max}}$	33.5 MeV	33.5 MeV
$\sigma_{\text{int}}(\gamma, Sn)$	286 MeV mb	704 MeV mb
$\sigma_{\text{int}}(\gamma, 2n)$	7.65 MeV mb	72.2 MeV mb
$\sigma_{\text{int}}[(\gamma, n) + (\gamma, pn)]^a$	278 MeV mb	632 MeV mb
$\sigma_{\text{int}}(\gamma, 2n)/\sigma_{\text{int}}(\gamma, Sn)$	0.027	0.103
$\sigma_{-1}(\gamma, Sn)$	13.5 mb	35.6 mb
$\sigma_{-2}(\gamma, Sn)$	0.700 mb MeV $^{-1}$	1.90 mb MeV $^{-1}$
$\sigma_{\text{int}}(\gamma, Sn)/60(NZ/A)$	0.329	0.786

^a This quantity was obtained by subtracting $\sigma_{\text{int}}(\gamma, 2n)$ from $\sigma_{\text{int}}(\gamma, Sn)$; direct integration of the single-photoneutron cross sections gave the same values to within 0.5%.

TABLE IV. Comparison of integrated total photoneutron cross sections $\sigma_{\text{int}}(\gamma, Sn)$ with those from previous experiments.

Reference	$E_{\gamma \text{ max}}$ (MeV)	^{58}Ni (MeV mb)	^{60}Ni (MeV mb)
This experiment	30	256	643
Ref. 6 (Moscow)	30	310	620
This experiment	25	204	537
Ref. 5 (Virginia)	25	185	482

(over)

3/25/75
 REFERENCE

TABLE III. Energies (MeV) at which peaks appear in the (γ, Sn) cross sections of ^{58}Ni and ^{60}Ni . The energies listed are those at which peaks or shoulders exist in the cross section. Actual resonance energies might be slightly different.

Peak No. ^a	^{58}Ni	^{60}Ni
1	12.3	12.6
2	12.8	13.7
3	13.1	14.4
4	13.6	15.1
5	14.2	15.5
6	15.7	16.3
7	16.3	17.0
8	17.3	17.7
9	17.7	18.6
10	18.2	19.6
11	18.6	21.2
12	19.3	22.1
13	22.6	24.5
14	23.8	
15	24.9	
16	25.7	

^a We have included in the tabulations only the more well-defined peaks (or shoulders). In addition there are possible broad peaks at approximately 20.7, 27.8, and 30.9 MeV in ^{58}Ni , and at 23.5, 26.1, 27.5, and 30.3 MeV in ^{60}Ni , but the data are not sufficiently detailed to make a more definitive judgment about these.

TABLE V. Integrated total photon absorption cross sections and related quantities from the combined data of the present experiment and Ref. 7. The (γ, Xp) cross sections of Ref. 7 have been used rather than those of Ref. 8 because the former extend over a wider energy range; in their mutually inclusive energy range (see Figs. 5 and 6) the integrated cross sections from the two (γ, Xp) measurements agree to within 2% for ^{58}Ni and 10% for ^{60}Ni , the values derived from the data of Ref. 8 being the larger in both cases. The total photon absorption cross section $\sigma(\gamma, \text{total})$ is assumed to be equal to $\sigma(\gamma, Sn) + \sigma(\gamma, Xp)$; that is the photon scattering cross section is assumed to be negligible and double counting, owing to the presence of $\sigma(\gamma, pn)$ in both $\sigma(\gamma, Sn)$ and $\sigma(\gamma, Xp)$, is ignored. The latter effect is reasonably compensated for, however (see footnote a).

	^{58}Ni	^{60}Ni
$E_{\gamma \text{ max}}$	33.5 MeV ^a	33.5 MeV ^a
$\sigma_{\text{int}}(\gamma, \text{total})$	850 MeVmb	1025 MeVmb
$\sigma_{-1}(\gamma, \text{total})$	41.3 mb	48.7 mb
$\sigma_{-2}(\gamma, \text{total})$	2.09 mb MeV ⁻¹	2.62 mb MeV ⁻¹
$\sigma_{\text{int}}(\gamma, \text{total}) / (60NZ/A)$	0.98	1.10
$\sigma_{-1}(\gamma, \text{total}) / A^{1/3}$	0.18	0.21
$\sigma_{-2}(\gamma, \text{total}) / A^{5/3}$	0.002 64	0.002 86

^a The (γ, Xp) data extend only to 30.1 MeV for ^{58}Ni and 30.5 MeV for ^{60}Ni ; above these energies we have used the (γ, Sn) cross section only. Since much of the high-energy cross section probably comes from the (γ, pn) process, the error introduced is probably small and might very well compensate for the double counting of the (γ, pn) cross section below 30 MeV.

⁵ K. Min and T.A. White, Phys. Rev. Lett. 21, 1200 (1968).

⁶ B.I. Goryachev, B.S. Ishkhanov, I.M. Kapitonov, I.M. Piskarev, V.G. Shevchenko, and O.P. Shevchenko, Yad. Fiz. 10, 252 (1969); Sov. J. Nucl. Phys. 11, 141 (1970).

⁷ B.S. Ishkhanov, I.M. Kapitonov, I.M. Piskarev, V.G. Shevchenko, and O.P. Shevchenko; Yad. Fiz. 11, 485 (1970); Sov. J. Nucl. Phys. 11, 272 (1970).

⁸ K. Shoda, private communication; see also H. Miyase, S. Oikawa, A. Suzuki, J. Uegaki, T. Saito, M. Sugawara, and K. Shoda, in Proceedings of the International Conference on Photonuclear Reactions and Applications, Asilomar, March, 1973, ed. by B.L. Berman (Lawrence Livermore Laboratory, Livermore, 1973) p.553.

17

In our reaction notation we have essentially adopted the convention used by E.G. Fuller, H.M. Gerstenberg, H. Vander Molen, and T.C. Dunn NBS SP-380, 1973; wherein (γ, Sn) represents the sum of all neutron-producing reactions, (γ, Xp) denotes total proton yield, etc. We use (γ, pn) to represent either the (γ, np) or (γ, pn) reaction, since experimentally the two are indistinguishable.

R. Yen, L. S. Cardman, D. Kalinsky, J. R. Legg,
C. K. Bockelman
Nucl. Phys. A235, 135 (1974)

ELEM. SYM.	A	Z
Ni	60	28
REF. NO.		
74 Ye 1		egf

METHOD				REF. NO.		
				74 Ye 1		egf
REACTION	RESULT	EXCITATION ENERGY	SOURCE		DETECTOR	
			TYPE	RANGE	TYPE	RANGE
E, E/	FMF	1	D	30- 60	MAG-D	

1.332 MEV 2+

TABLE 2
Experimental data for the $^{60}\text{Ni } 2^+$ (1.332 MeV) state

$E_0(\text{MeV})$	$\theta(\text{deg})$	$q(\text{fm}^{-1})$	$ F_{11} ^2$	$10^2 \times R_{10}$	$10^2 \times F_{10} ^2$	$10^2 \times F_{11} ^2_N$	Error(%)	χ^2/n
59.89	110	0.492	0.225	0.675	0.167	0.167	5.2	5/28
42.47	130	0.384	0.465	0.239	0.117	0.110	7.3	12/29
42.45	130	0.384	0.466	0.223	0.109	0.103	8.3	10/28
42.47	110	0.347	0.564	0.154	0.0907	0.0850	6.4	16/28
42.44	110	0.347	0.565	0.130	0.0764	0.0717	7.5	16/28
42.53	90	0.301	0.693	0.0812	0.0564	0.0529	9.0	30/27
42.46	90	0.300	0.696	0.0727	0.0522	0.0488	9.6	28/29
31.67	130	0.285	0.772	0.0640	0.0509	0.0449	11.9	5/18
42.47	70	0.243	0.846	0.0351	0.0303	0.0284	18.3	20/23
42.47	70	0.243	0.846	0.0321	0.0277	0.0260	16.6	16/28

Ground-state charge distributions parameters 21 : $c = 4.15 \pm 0.017$ fm, $t = 2.54 \pm 0.02$ fm.

TABLE 4
Results of the best-fits by allowing both $B(E2^\dagger)$ and $R_{11}^{(2)}$ as free parameters

Assumptions								Results		
Z	$R_{ms}(\text{fm})$	a_{-1}	a_1	a_3	a_4	a_5		$B(E2^\dagger)(e^2 \cdot b^2)$	$R_{11}^{(2)}(\text{fm}^2)$	χ^2/n
^{114}Cd 48	4.624	1.045	0.983	1.056	1.158	1.323		0.553 ± 0.018	38.1 ± 1.0	1.12
^{60}Ni 28	3.862	1.075	0.976	1.078	1.024	1.471		0.102 ± 0.004	31.9 ± 2.0	0.60
^6Li 3	2.540	1.208	0.941	1.189	1.572	2.290		$(0.218 \pm 0.008) \times 10^{-2}$	17.6 ± 1.2	1.05

TABLE 6
Summary of $B(E2^\dagger)$ values for the $^{60}\text{Ni } 2^+$ (1.332 MeV) state

$B(E2^\dagger)(e^2 \cdot b^2)$	Type of experiment	Ref.
0.0873 ± 0.0070	(e, e')	³⁴⁾
0.0938 ± 0.0020	(γ , γ')	³⁶⁾
0.0992 ± 0.0099	(e, e')	³⁷⁾
0.0914 ± 0.0020	CE	³⁸⁾
0.117 ± 0.009	h.p.	³⁹⁾
0.0845 ± 0.0009	(e, e')	⁴⁰⁾
0.097 ± 0.008	CE	⁴¹⁾

(over)

- ²¹V.M. Khvastunov et al., Nucl. Phys. A146, 15 (1970).
- 36) F. R. Metzger, Nucl. Phys. A148 (1970) 362
- 37) Y. Torizuka, Y. Kojima, M. Oyamada, K. Nakahara, K. Sugiyama, T. Terasawa, K. Itoh, A. Yamaguchi and M. Kimura, Phys. Rev. 185 (1969) 1499
- 38) D. Cline, H. S. Gertsman, H. E. Gove, R. M. S. Lesser and J. J. Schwartz, Nucl. Phys. A133 (1969) 445
- 39) R. K. Golby, M. D. Goldberg and A. K. Sengupta, Nucl. Phys. A123 (1969) 54
- 40) M. A. Duguay, C. K. Bockelman, T. H. Curtis and R. A. Eisenstein, Phys. Rev. 171 (1968) 1142
- 41) P. H. Stelson and L. Grodzins, Nuclear Data, sect. A, vol. 1, no. 1 (Academic Press, New York, 1965)
- 54) R. P. Singhal, S. W. Bram, W. A. Gillespie, A. Johnston, E. W. Lees and A. G. Slight, Nucl. Phys. A218 (1974) 189

TABLE 7
Best fits of $R_{tr}^{(2)}$ with $B(E2_{tr})$ fixed

	$R_{tr}^2(\text{fm}^2)$	Statistical error (fm ²)	Systematic error (fm ²)	Total error (fm ²)	χ^2/n	$B(E2_{tr})(e^2 \cdot b^2)$ assumed
¹¹⁴ Cd	35.7	±0.6	±0.3	±0.9	1.19	0.512±0.05
⁶⁰ Ni	27.5	±1.1	±0.8	±1.9	0.66	0.0926±0.15

REF. V.Ya. Kitaev, A.I. Abramov, A.V. Rogov, and M.G. Yutkin
Izv. Akad. Nauk SSSR, Ser. Fiz. 39, 1754 (1975)
Bull. Acad. Sci. USSR Phys. Ser. 39, 159 (1975)

ELEM. SYM.	A	Z
Ni	60	28

METHOD

REF. NO.

75 Ki 12

hmg

REACTION	RESULT	EXCITATION ENERGY	SOURCE		DETECTOR		ANGLE
			TYPE	RANGE	TYPE	RANGE	
G,N	ABX	11- 13	C	11- 13	TOF-D		78

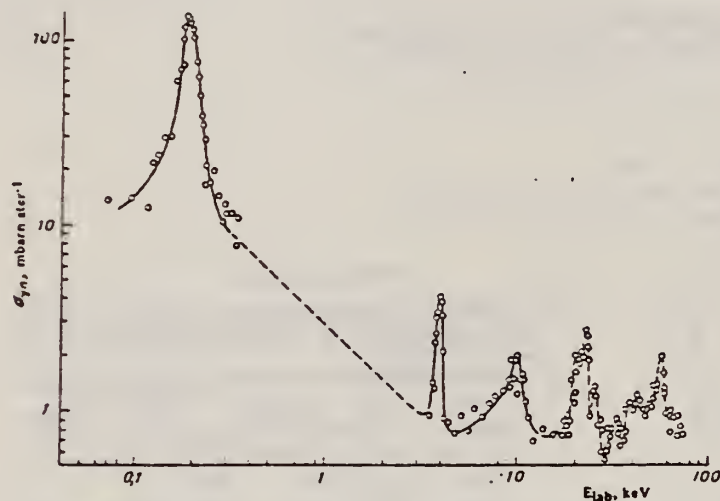


Fig. 1. Measurements of the differential cross sections for the $^{60}\text{Ni}(\gamma n)^{59}\text{Ni}$ reaction at 78° for $E_Y^{\text{max}} = 12.5$ MeV. Solid line - results of an analysis of experimental data based on the Pade approximation of the second kind. Broken line - drawn by "eye."

Table 2
Resonance Parameters of ^{60}Ni Levels

E_{lab}^0 , keV	σ_0 , mbarn-ster ⁻¹	Γ , eV	$\sigma_Y \Gamma_{\gamma_0}$, eV
0.198	129	39.7	1.62
4.113	5.58	160	0.284
10.59	2.0	2100	1.31

Table 1

Energies of the Resonances in the $^{60}\text{Ni}(\gamma n)^{59}\text{Ni}$ Reaction Near the Threshold

E_{lab}^0 , keV	E_{cm} , keV	Final nucleus transition into ground (g) or excited (E) state	E_{lab}^0 , keV	E_{cm} , keV	Final nucleus transition into ground (g) or excited (E) state	E_{lab}^0 , keV	E_{cm} , keV	Final nucleus transition into ground (g) or excited (E) state
0.198	0.193	g						
4.1	4.07	g	23.0	23.1	g	39.6	39.9	E?
10.6	10.6	g	25.9	26.0	E?	43.3	43.7	E?
21.0	21.1	g	33.8	34.1	E?	57	57.6	g

REF.

R.A. Lindgren, W.L. Bendel, E.C. Jones, Jr., L.W. Fagg,
X.K. Maruyama, J.W. Lightbody, Jr., S.P. Fivozinsky
Phys. Rev. C14, 1789 (1976)

ELEM. SYM.

A

Z

Ni

60

28

METHOD

REF. NO.

76 Li 6

hmg

REACTION	RESULT	EXCITATION ENERGY	SOURCE		DETECTOR		ANGLE
			TYPE	RANGE	TYPE	RANGE	
E, E/	ABX	11- 14	D	40- 60	MAG-D		180

Using inelastic electron scattering, several isobaric analog 1^+ states between 9 and 13 MeV excitation in ^{58}Ni and ^{60}Ni have been found. They are identified as components of the $T_0 + 1$ giant M1 state in $^{58,60}\text{Ni}$.

4 M1 STATES

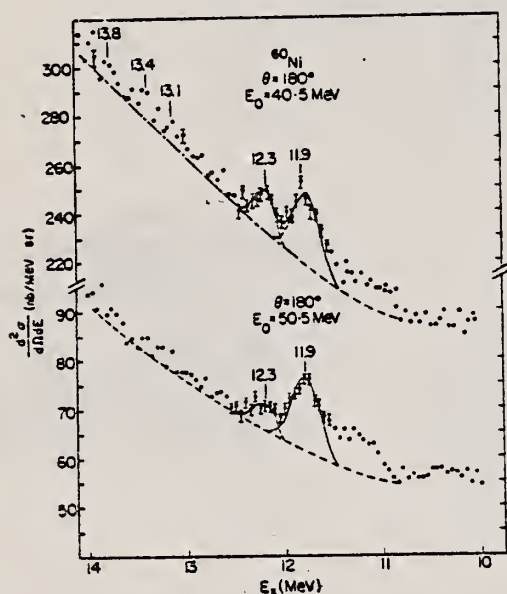


FIG. 5. Portion of spectrum observed at $\theta = 180^\circ$ from 40.5 and 50.5 MeV electrons incident on a ^{60}Ni target.

TABLE II. Measured excitation energies, J^π assignments, and reduced M1 transition probabilities for levels in $^{58,60}\text{Ni}$.

E_x (MeV) Exp ^a	J^π	E_x (MeV) Predicted ^b	Parent	$B(M1)^c$ (μ_N^2)	$\Gamma(M1)^d$ (eV)
^{58}Ni					
9.85	(1^+)	9.87	^{58}Ni	1.05	(0.32) ^c (3.4) ^e
10.19	1^+	10.25	^{58}Ni	1.43	0.59 7.2
10.55	1^+	10.55	^{58}Ni	1.73	0.21 3.0
10.66	1^+	10.68	^{58}Ni	1.86	0.41 5.7
11.03	1^+	11.06	^{58}Ni	2.24	0.36 5.6
^{60}Ni					
11.9	1^+	11.87	^{60}Ni	0.74	0.46 8.9
12.3	1^+	12.34	^{60}Ni	1.21	0.26 5.8
13.1	(1^+)	13.11	^{60}Ni	1.98	≤ 0.06 ≤ 1.5
13.4	(1^+)	13.35	^{60}Ni	2.22	≤ 0.06 ≤ 1.6
13.8	(1^+)	13.84	^{60}Ni	2.71	≤ 0.06 ≤ 1.8

^a Energy uncertainty is ± 0.04 MeV in ^{58}Ni and ± 0.1 MeV in ^{60}Ni .

^b To get predicted energy in ^{58}Ni add 8.82 MeV to excitation energies in ^{58}Co and for ^{60}Ni add 11.13 MeV.

^c M1 strength uncertainty is estimated to be about $\pm 25\%$ for individual levels.

^d $\Gamma(M1) = 0.0115 E_x^3 B(M1)$.

^e Tentative M1 identification (see text).

ELEM. SYM.	A	Z
Ni	60	28
REF. NO.	77 Is 1	egf

REACTION	RESULT	EXCITATION ENERGY	SOURCE		DETECTOR		ANGLE
			TYPE	RANGE	TYPE	RANGE	
G,P	NOX	13 - 28	C	17-28	SCD-D		90

DECAY BRANCHING

TABLE 3
The proton decay probabilities in the various channels

Initial states (MeV)		Final states (MeV)				
		$0(1f_{7/2})$	≈ 1.5	$3.3(1d_{3/2})$	$6.2(2s_{1/2})$	$9.6(1d_{5/2})$
^{58}Ni	11.0-16.0		≈ 100			
	16.8	10	10	80		
	18.4	5	20	75		
	19.1	5	20	25	50	
	21.0		10	20	70	
	23.3			10	30	60
	25.2					x
	26.5					x
	27.3					x
^{60}Ni	11.0-16.0		≈ 100			
	16.4	20	10	70		
	18.6	20	10	70		
	20.4	5	5	40	50	
	23.3	5	5	10	50	30
	25.8, 26.6, 27.5				x	

REF. T.J. Bowles, R.J. Holt, H.E. Jackson, R.M. Laszewski, A.M. Nathan,
J.R. Specht, and R. Starr
Phys. Rev. Lett. 41, 1095 (1978)

ELEM. SYM.	A	Z
Ni	60	28
REF. NO.		
78 Bo 5		rs

METHOD

REACTION	RESULT	EXCITATION ENERGY	SOURCE		DETECTOR		ANGLE
			TYPE	RANGE	TYPE	RANGE	
G,G/	ABX	15- 22	D	15- 22	NAI-D		120°

Monoenergetic photons and a high-resolution NaI spectrometer have been used to measure the absolute 120° scattering cross sections to the ground state and to the first excited state in ⁶⁰Ni for excitations between 15 and 22 MeV. The inelastic scattering to the first excited state was found to be about 15% of the elastic throughout this energy range. Our results do not appear to be in quantitative agreement with the predictions of the dynamic collective model.

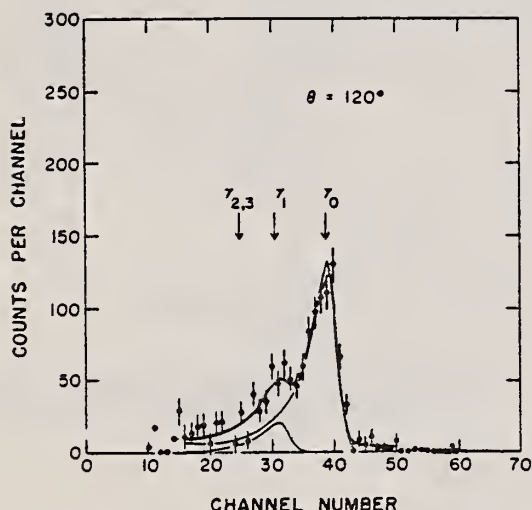


FIG. 2. Scattering spectrum for monoenergetic 19.81-MeV photons incident on ⁶⁰Ni. The fitting procedure by which elastic and inelastic scattering was separated is shown. The shapes of the detector response to monoenergetic photons used in the fit were measured directly by placing the detector in the tagged photon beam.

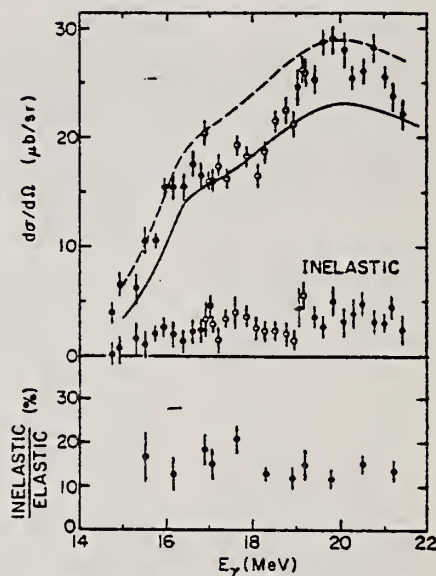


FIG. 3. The cross sections at an angle of 120° for elastic and inelastic scattering to the first excited state in ⁶⁰Ni are shown at the top. The solid curve shows the elastic cross section predicted by dispersion relations using $\sigma(\gamma, n)$ data for the total absorption cross section. The dashed curve indicates an estimate of the contribution that would come from including $\sigma(\gamma, p)$ as well. The ratio of inelastic to elastic scattering is shown below. The open and solid data points represent the three different energy ranges scanned by the monochromator.

ELEM. SYM.	A	Z
Ni	60	28
REF. NO.		
78 F1 1	hmg	

METHOD

REACTION	RESULT	EXCITATION ENERGY	SOURCE		DETECTOR		ANGLE
			TYPE	RANGE	TYPE	RANGE	
E, A	SPC	6-120	D	33-120	MAG-D		DST
							10051
							10052
							10053

Alpha-particle energy and angular distributions have been measured for the reaction $^{60}\text{Ni}(e, \alpha)^{56}\text{X}$ using electrons of energies 33, 60, and 120 MeV. Statistical-model calculations give good quantitative agreement in the region of the peak of the α energy spectra. Higher-energy α particles exhibit a forward-peaked angular distribution and a cross section several orders of magnitude above the statistical-model predictions, indicating the presence of a direct-reaction component.

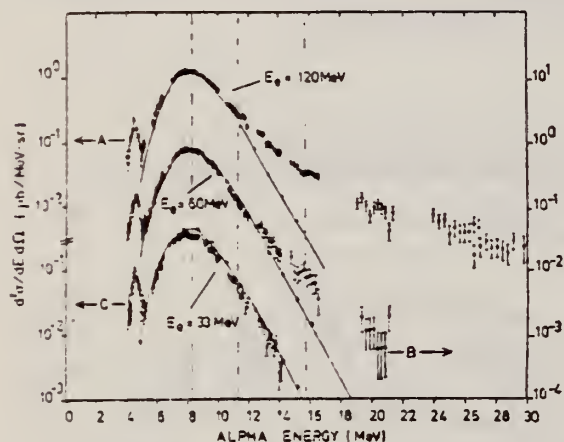


FIG. 1. Alpha-particle energy spectra at $\theta_\alpha = 90^\circ$, for $E_e = 120$ MeV (curve A, upper left-hand scale), $E_e = 60$ MeV (curve B, right-hand scale), and $E_e = 33$ MeV (curve C, lower left-hand scale). Errors shown are absolute. The solid lines are the results of a statistical calculation assuming photon absorption below $E_\gamma = 33$ MeV. The dashed lines mark the mean energies at which angular distributions were taken.

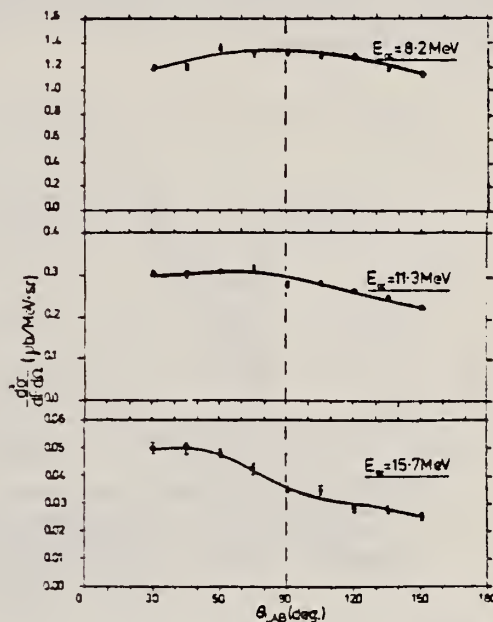


FIG. 2. Alpha-particle angular distributions at $E_e = 120$ MeV averaged over the α energy ranges 7.7–8.7 MeV, 10.6–11.9 MeV, and 14.8–16.4 MeV. Errors shown are relative. The solid lines are merely to guide the eye.

ELEM. SYM.	A	Z
Ni	60	28

METHOD	REF. NO.	
	78 Ma 10	hg

REACTION	RESULT	EXCITATION ENERGY	SOURCE		DETECTOR		ANGLE
			TYPE	RANGE	TYPE	RANGE	
G,PN	ABY	20-68	C.	30-68	ACT - I		4PI

Analysis is made of reactions interfering with photon activation analysis procedures.

The activation yield curves have been presented for a number of photonuclear reactions in the energy range from 30 to 68 MeV, in order to evaluate quantitatively the interferences due to competing reactions in multielement photon activation analysis. The general features of the yields as functions of both target mass number and excitation energy were elucidated from the data obtained, discussion being given on the results in terms of the reaction mechanism.

Simultaneous neutron activation due to appreciable neutron production from the converter and surrounding materials has also been studied, and, finally, the magnitudes of interferences in real multielement analysis were given in the form of their energy dependences.

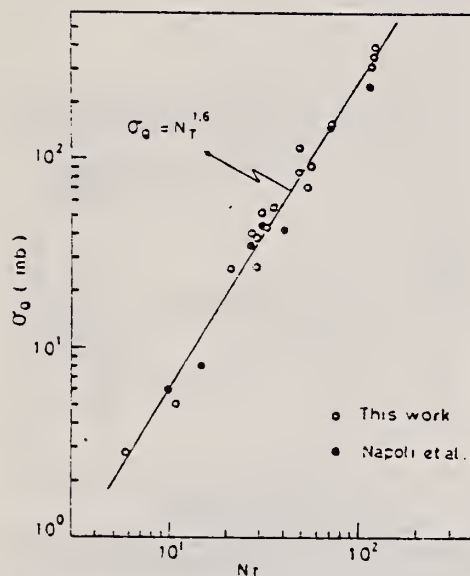


Fig. 2. Yield per equivalent quanta versus target neutron number.

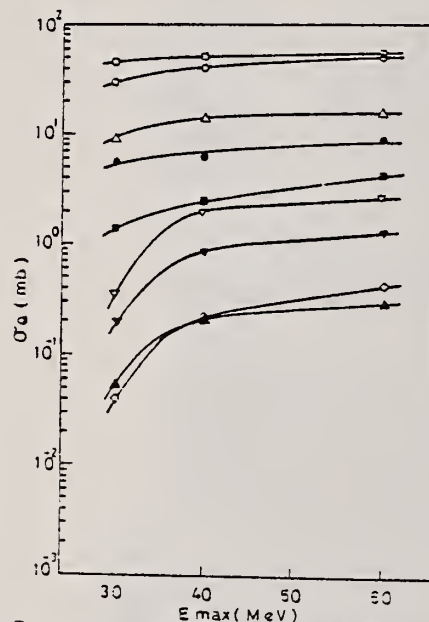


Fig. 6. Activation yield curves for the reactions on Co, Ni and Cu.

○ $^{59}\text{Co}(\gamma, n)^{58}\text{Co}$, ● $^{59}\text{Co}(\gamma, 2n)^{57}\text{Co}$, △ $^{58}\text{Ni}(\gamma, n)^{57}\text{Ni}$,
▽ $^{58}\text{Ni}(\gamma, pn)^{56}\text{Co}$, ▼ $^{58}\text{Ni}(\gamma, pn)^{56}\text{Co}$, ▲ $^{58}\text{Ni}(\gamma, 2n)^{56}\text{Ni}$,
□ $^{63}\text{Cu}(\gamma, n)^{62}\text{Cu}$, ■ $^{63}\text{Cu}(\gamma, 2n)^{61}\text{Cu}$, ◇ $^{63}\text{Cu}(\gamma, zn)^{58}\text{Co}$.

REF. J.D. Turner, C.P. Cameron, N.R. Roberson, H.R. Weller and
D.R. Tilley
Phys. Rev. C 17, 1853 (1978)

ELEM. SYM.	A	Z
Ni	60	28
REF. NO.		hg
78 Tu 2		

REACTION		RESULT	EXCITATION ENERGY	SOURCE		DETECTOR		ANGLE
				TYPE	RANGE	TYPE	RANGE	
\$ P,GO		ABX	10- 25	D	6- 17	NAI-D		DST
					(5.8-16.5)			

Pol Protons

The angular distributions of cross section and of analyzing power for the $^{59}\text{Co}(\beta, \gamma_0) ^{60}\text{Ni}$ reaction have been measured throughout the giant dipole resonance region of ^{60}Ni . In addition, the 90° yield curve has been measured for E_p from 5.8 to 16.5 MeV. The data are analyzed to deduce the amplitudes and phases of the T matrix elements involved. Comparison of the results is made to both the dynamic collective model calculation of Ligensa and Greiner and to a direct-semidirect model calculation. The direct-semidirect calculation indicates that the reaction proceeds predominantly via the radiative capture of $d_{3/2}$ protons. Isospin splitting is also discussed.

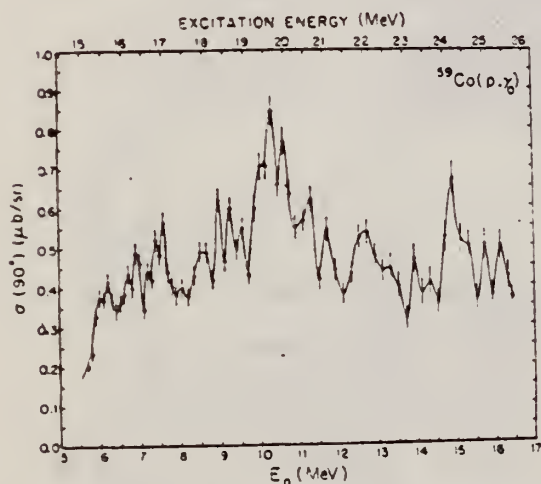


FIG. 2. The 90° yield curve for the $^{59}\text{Co}(p, \gamma_0) ^{60}\text{Ni}$ reaction. The error bars represent the statistical error associated with the data points and the solid curve is a smooth line drawn through the data points.

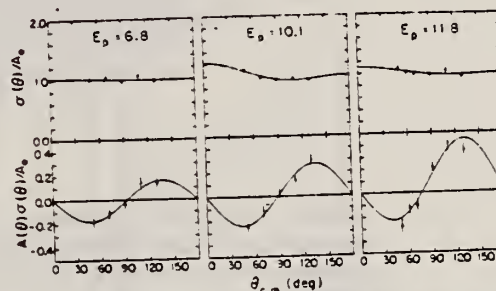


FIG. 3. Typical data at three energies for the quantities $\sigma(\theta)/A_0$ and $A(\theta)\sigma(\theta)/A_0$. The errors bars represent the statistical errors associated with the data points. The solid curves are the result of fitting the data as described in the text.

over

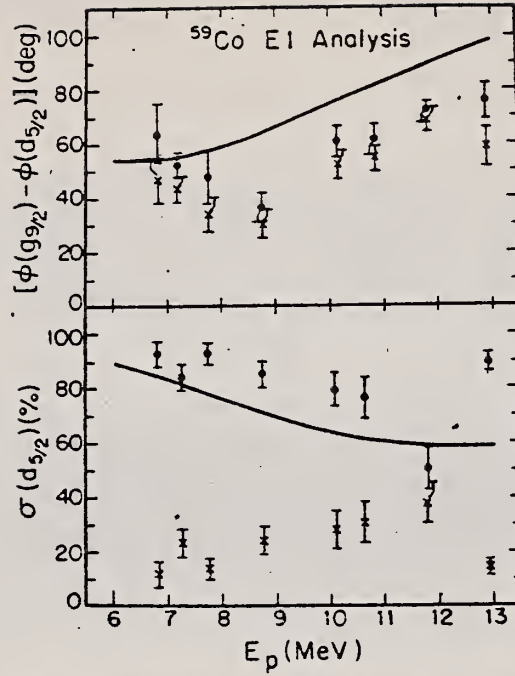


FIG. 5. Comparison of the transition matrix elements extracted from the present data with those from a direct-semidirect reaction model calculation as described in the text. The solid curve shows the results of the calculation. The results are presented as a percentage of the cross section, $\sigma(d_{5/2}) + \sigma(g_{3/2})$, where $\sigma(d_{5/2}) = d_{5/2}^2$, etc. The error bars represent the statistical errors associated with the data.

TABLE I. The a_i and b_i coefficients obtained from least squares fits to the data as described in the text. Also presented are the a_i coefficients from Ref. 1.

E_p (MeV)	a_1	a_2	χ_2	b_1	b_2	b_3	χ_2
6.70 ^a	0.02 ± 0.03	0.03 ± 0.05	1.5				
6.80	0.01 ± 0.05	0.01 ± 0.07	1.8	-0.01 ± 0.03	-0.12 ± 0.02	0.00 ± 0.02	0.5
7.20	0.06 ± 0.03	0.15 ± 0.06	0.4	0.05 ± 0.02	-0.15 ± 0.02	0.04 ± 0.02	1.3
7.55 ^a	0.08 ± 0.05	0.16 ± 0.07	1.5				
7.60 ^a	-0.01 ± 0.02	0.28 ± 0.03	0.6				
7.75	0.02 ± 0.04	0.10 ± 0.08	6.1	0.02 ± 0.03	-0.10 ± 0.02	0.01 ± 0.02	0.1
8.75	0.05 ± 0.03	0.26 ± 0.05	1.5	0.04 ± 0.02	-0.10 ± 0.02	0.00 ± 0.02	0.9
10.00 ^a	0.22 ± 0.03	0.07 ± 0.04	1.5				
10.10	0.11 ± 0.03	0.12 ± 0.06	0.7	0.02 ± 0.02	-0.17 ± 0.02	0.01 ± 0.02	1.1
10.60	0.11 ± 0.04	0.12 ± 0.06	0.4	0.04 ± 0.02	-0.18 ± 0.02	-0.01 ± 0.02	8.1
11.30	0.06 ± 0.04	0.05 ± 0.06	1.2	0.14 ± 0.03	-0.23 ± 0.02	-0.05 ± 0.02	0.8
12.80	0.12 ± 0.03	-0.03 ± 0.06	2.3	0.05 ± 0.02	-0.14 ± 0.02	-0.02 ± 0.02	1.8

^a From Ref. 1.

E.M. Diener, J.F. Amann, P. Paul, and S.L. Blatt,
Phys. Rev. C 3, 2303 (1971)

METHOD

REF. NO.

78 We 4

hmg

REACTION	RESULT	EXCITATION ENERGY	SOURCE		DETECTOR		ANGLE
			TYPE	RANGE	TYPE	RANGE	
S P,G	RLX	16-23	D	6-13	UKN-D		DST

Analysis of data in reference 6.

POLARIZED PROTONS

Measurements of cross sections and analyzing powers are examined for polarized proton capture on ^{14}C , ^{28}Si , ^{54}Fe , ^{56}Fe , ^{58}Fe , ^{59}Co , and ^{88}Sr at energies which cover the giant dipole resonance region. These data are used to extract the relative amplitudes and phases of the contributing $E1$ T -matrix elements. A typical result exhibits two solutions. Calculations using the direct (or a direct-semidirect) capture model appear to provide a means for choosing the physical solution.

NUCLEAR REACTIONS: $^{14}\text{C}(\tilde{p}, \gamma_8)$, $^{28}\text{Si}(\tilde{p}, \gamma_8)$, $^{54}\text{Fe}(\tilde{p}, \gamma_2)$, $^{56}\text{Fe}(\tilde{p}, \gamma_8)$, $^{58}\text{Fe}(\tilde{p}, \gamma_8)$, $^{59}\text{Co}(\tilde{p}, \gamma_8)$, $^{88}\text{Sr}(\tilde{p}, \gamma_0)$; measured $\sigma(\theta)$ and $A(\theta)$ over energy region of the giant dipole resonance. Deduced T -matrix amplitudes and phases. Compare results to direct-semidirect model calculations.

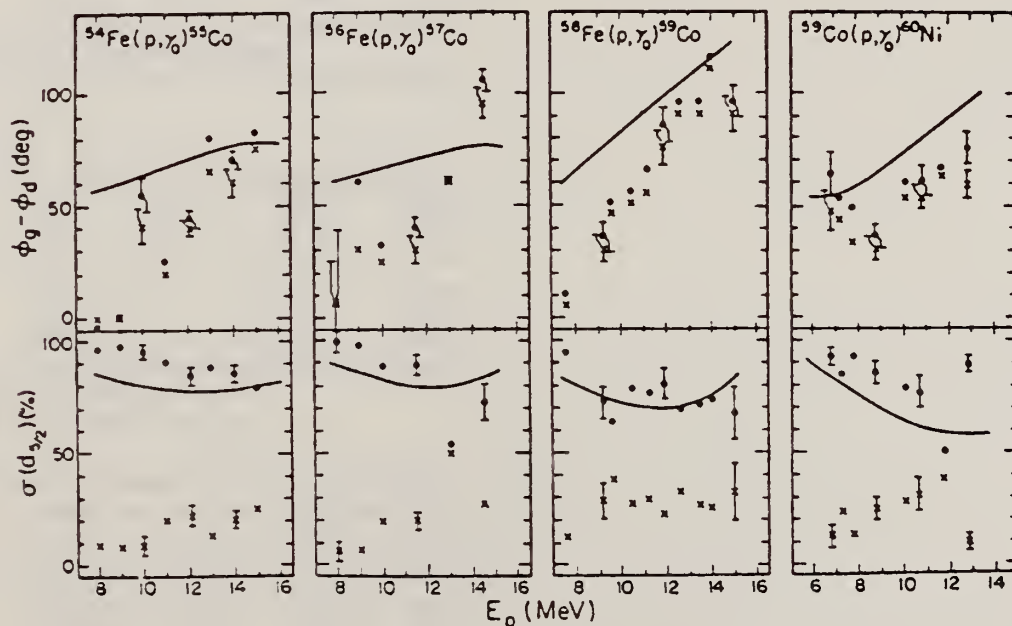


FIG. 2. Same as Fig. 1 for the target nuclei of ^{54}Fe , ^{56}Fe , ^{58}Fe , and ^{59}Co . The remaining cross section is due to the $s_{1/2}$ matrix element.

FIG. 1. The two solutions (dots and x's) resulting from a pure $E1$ analysis of the data are shown along with the results of the calculation for target nuclei of ^{14}C , ^{88}Sr , and ^{30}Si . The remaining cross section in the case of ^{14}C and ^{88}Sr is due to the $s_{1/2}$ matrix element. In the case of ^{30}Si it arises from the $p_{1/2}$ matrix element. The error bars represent typical statistical errors associated with the data points. The amplitudes are presented in terms of the percentage of the total cross section for which they are responsible. The curves represent DSD calculations as described in the text. The dashed curves in the case of ^{88}Sr were obtained using the optical model parameters of Ref. 16 while the solid lines were obtained from the parameters of Ref. 18.

(over)

- ²H. R. Weller, R. A. Blue, N. R. Roberson, D. G. Rickel, S. Maripuu, C. P. Cameron, R. D. Ledford, and D. R. Tilley, Phys. Rev. C 13, 922 (1976). (Note: an error exists in the sign of the phase in this paper. The quantity $\phi_3 - \phi_4$ should be $\phi_4 - \phi_3$ wherever it appears.)
- ³C. P. Cameron, N. R. Roberson, D. G. Rickel, R. D. Ledford, H. R. Weller, R. A. Blue, and D. R. Tilley, Phys. Rev. C 14, 553 (1976).
- ⁴C. P. Cameron, Ph.D. thesis, Duke University, 1976 (unpublished).
- ⁵R. D. Ledford, Ph.D. thesis, Duke University, 1976 (unpublished).
- ⁶J. D. Turner, C. P. Cameron, N. R. Roberson, H. R. Weller, and D. R. Tilley, Phys. Rev. C 17, 1853 (1978).

ELEM. SYM.	A	Z
Ni	60	28
METHOD	REF. NO.	
	79 Wo 3	hg

REACTION	RESULT	EXCITATION ENERGY	SOURCE		DETECTOR		ANGLE
			TYPE	RANGE	TYPE	RANGE	
E,XP	ABX	9-30	D	16-50	MAG-D		4PI
E,XA	ABX	6-30	D	16-50	MAG-D		4PI

The (e,p) and (e,α) cross sections for targets of ^{58}Ni , ^{60}Ni , and ^{62}Ni have been measured in the electron energy range 16-50 MeV. They have been analyzed using the distorted-wave Born-approximation $E1$ and $E2$ virtual-photon spectra. Protons are emitted primarily following $E1$ absorption but α emission results from a combination of $E1$ and $E2$ absorption. The $E2$ isoscalar giant resonance decays predominantly by α emission for these nuclei.

(E,XP) VIRTUAL PHOTON G,XP

(E,XA) VIRTUAL PHOTON G,XA

See also 80 Wo 1

TABLE I. Resonance parameters for $\sigma_{\gamma,p}$.

Nucleus	E_x (MeV)	Γ (MeV) ^a	$\int_0^{30} \sigma dE$ (MeV mb)	SR ^b (%)
^{58}Ni	19.2 ± 0.5	6.5 ± 1.3	738 ± 40	85 ± 5
^{60}Ni	18.5 ± 0.5	9.2 ± 1.3	304 ± 20	34 ± 2
^{62}Ni	21.0 ± 0.5	5.3 ± 1.0	140 ± 10	15 ± 1

^a Γ is the full width at half maximum.

^bSR stands for sum rule; the $E1$ SR equals $60 NZ/A$ MeV mb.

TABLE II. $E1$ components in the (γ,α) reaction.

Nucleus	E_x (MeV)	Γ (MeV) ^a	$\int \sigma dE$ (MeV mb)	SR ^b (%)
^{58}Ni	18.3 ± 0.5	6 ± 1	15.3 ± 1.3	1.3 ± 0.2
^{60}Ni	21.5 ± 1.0	6 ± 1	18.5 ± 1.4	2.1 ± 0.2
^{62}Ni	18.3 ± 1.0	5 ± 1	4.8 ± 0.6	0.5 ± 0.1

^a Γ is the full width at half maximum.

^b $E1$ SR equals $60 NZ/A$ MeV mb.

TABLE III. $E2$ components in the (γ,α) reaction.

Nucleus	E_x (MeV)	Γ (MeV) ^a	$\int \sigma dE$ (MeV mb)	SR ^b (%)
^{58}Ni	16.5 ± 0.5	4.2 ± 1.0	10.4 ± 0.7	56 ± 4
^{60}Ni	16.0 ± 0.5	3.7 ± 0.3	6.9 ± 0.4	52 ± 3
^{62}Ni	16.8 ± 0.5	4.5 ± 1.0	5.1 ± 0.4	28 ± 2

^a Γ is the full width at half maximum.

^b $E2$ SR equals $0.22 Z^2/A^{1/3}$ $\mu\text{b}/\text{MeV}$.

REF.	R. Pitthan, G.M. Bates, J.S. Beachy, E.B. Dally, D.H. Dubois, J.N. Dyer, S.J. Kowalick, F.R. Buskirk Phys. Rev. <u>C21</u> , 147 (1980)			ELEM. SYM.	A	Z	
				Ni	60	28	
METHOD				REF. NO.			
				80 Pi 2		hg	
REACTION	RESULT	EXCITATION ENERGY	SOURCE		DETECTOR		ANGLE
			TYPE	RANGE	TYPE	RANGE	
E, E/	ABX	7-40	D	102	MAG-D		DST
The cross section for electron scattering from the isotopes ⁵⁸ Ni and ⁶⁰ Ni has been measured with electrons 6.483-MeV scattering angles of 45, 60, 75, 90, and 105° between 3 and 50 MeV excitation energy.							

The cross section for electron scattering from the isotopes ^{58}Ni and ^{60}Ni has been measured with electrons of 102 MeV at scattering angles of 45, 60, 75, 90, and 105° between 3 and 50 MeV excitation energy. Resonances or resonancelike structures at approximate excitation energies of (7-8) MeV, 13 MeV, (16-17) MeV, (18-19) MeV, 27 MeV, 32 MeV, and 40 MeV were classified on the basis of their momentum transfer dependence and discussed in the framework of the shell model. Difficulties in the extraction of the cross section and model dependencies of the interpretation are discussed.

BEL

NUCLEAR REACTIONS $^{58}\text{Ni}(e, e')$ and $^{60}\text{Ni}(e, e')$, $E_0=102$ MeV. Measured $d^2\sigma/d\Omega dE_x$, bound and continuum states (giant resonances). Deduced multipolarity, reduced matrix element $B(E\lambda)$, sum rule exhaustion of giant resonances, total width of continuum and clustered states.

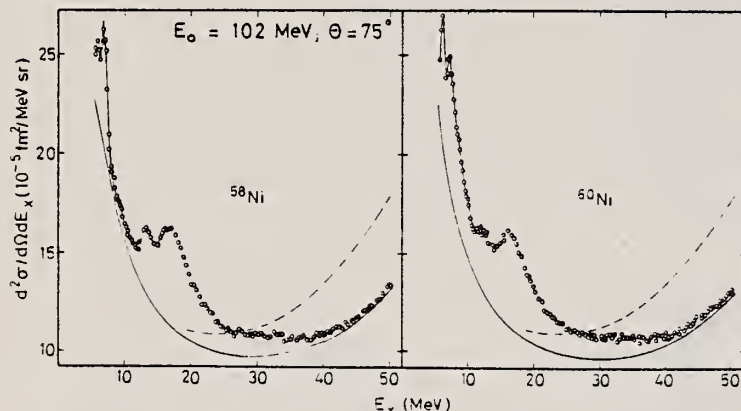


FIG. 4. Comparison of spectra of 102 MeV electrons scattered at 75° from ^{58}Ni and ^{60}Ni . The cross section for ^{60}Ni has been renormalized so that the highest and lowest points in both plots are equal. The spectra were taken with 10 points/MeV but have been reduced for graphical purposes. The broken line is the calculated radiation tail. For demonstration purposes we have subtracted the ghost peak at 3 MeV from the data for ^{58}Ni , but not for ^{60}Ni ; the difference is clearly visible. Note the suppressed zero.

TABLE III. Strength of $E1$ components in the present work. The resonance parameters shown were used to approximate the $E1$ strength distribution for the χ^2 fit. As evident from Fig. 9, where mainly $E1$ contributes, the $E1$ strength function is reasonably well described. The $E1$ strength extracted from the resonances, corresponding to integration to infinity, adds up to approximately 110% of the classical $E1$ sum rule. For ease of comparison, we also give the sum rule strength found by integration from 10 to 30 MeV, 94 ± 10 and $87 \pm 10\%$ for ^{58}Ni and ^{60}Ni , respectively. The table and Fig. 8 also show that the peak strength is shifted to lower excitation energy by going from ^{58}Ni to ^{60}Ni . Although the gross shift is in agreement with the isospin coupling model^{1,37} we do not think it is a sufficient basis for a claim of observed isospin splitting. The average excitation energy, weighted with the $E1$ strength function between 10 and 30 MeV, in contrast, remains virtually unchanged.

^{58}Ni					^{60}Ni				
E_x (MeV)	Γ (MeV)	B (fm ²)	$R\gamma^a$	R_∞^b	E_x (MeV)	Γ (MeV)	B (fm ²)	$R\gamma^a$	R_∞^b
13.1 ± 0.3	1.4 ± 0.5	0.4	2.3	2.5 ± 1	12.65 ± 0.3	1.5 ± 0.4	0.9	4.5	5 ± 1
16.2 ± 0.3	2.5 ± 0.5	1.5	10.5	11 ± 2	16.6 ± 0.4	2.75 ± 0.5	2.5	16.5	18 ± 4
18.3 ± 0.5	4.5 ± 0.5	7.3	54	62 ± 7	19.5 ± 0.5	6.0 ± 1.0	7.4	51	63 ± 3
22.0 ± 1.0	6.0 ± 1.0	3.3	27	34 ± 8	23.5 ± 1.5	6.0 ± 1.5	1.9	15	19 ± 4
			94	110 ± 11				87	105 ± 10

^a $\int_{10}^{30} (dB/dE_x)(dE_x/\text{EWSR } 100)$.

^b $E_x B(E1)/\text{EWSR } 100$.

TABLE VI. Comparative measurements of ^{58}Ni and ^{60}Ni for the $E2$ resonance.

^{58}Ni		^{60}Ni		Ref.	Method
E_x (MeV)	Γ (MeV)	E_x (MeV)	Γ (MeV)		
16.4 ± 0.3	4.9 ± 0.2	16.6 ± 0.3	5.0 ± 0.4	17	(α, α')
16.5 ± 0.5	4.2 ± 1.0	16.0 ± 0.5	3.7 ± 0.8	32	(e, α)
16.2 ± 0.3	4.5 ± 0.4	16.3 ± 0.3	4.5 ± 0.4	Present work	(e, e')

^a $R = E_x B(E2)/\text{EWSR}(E2, \Delta T = 0)$.

(OVER)

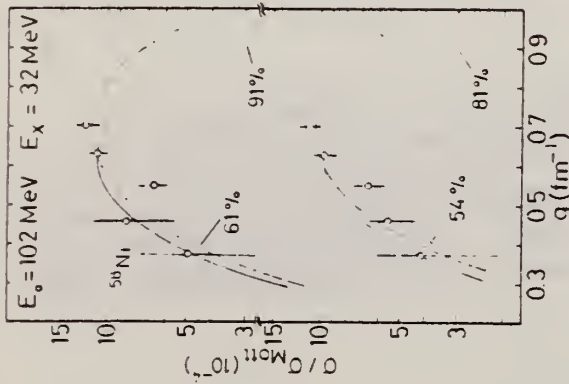


FIG. 14. Comparison between experimental and DWBA cross sections for resonance at 32 MeV. An E2 assignment is preferred, but other multipolarities (not taken into account) could contribute. The Goldhaber-Teller model leads to the higher strength; this strength might be regarded as an upper limit. The Myers-Swiatecki model (broken line) assumed $\alpha = 1$ (see text for definition). Extension of the Myers-Swiatecki model by Kodama to higher multipolarities gives values for α ranging from 0.12 to 0.44. Thus the sum rule values given in the figure for the MS model should be regarded as lower limits. The dependence of the experimental points on the momentum transfer suggest the possibility of more than one multipolarity contributing. This possibility was not investigated due to the accuracy limitations at this high excitation energy.

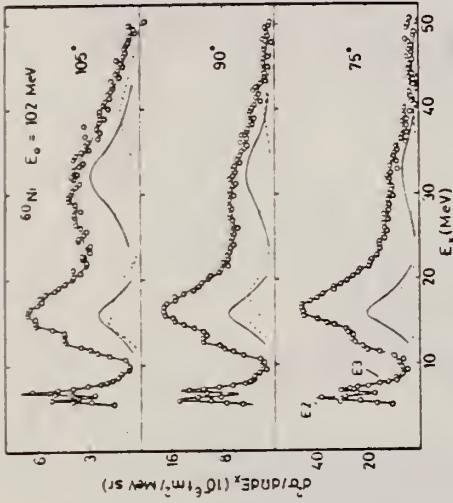


FIG. 6. Similar to Fig. 5, but for ^{60}Ni . The E1 has been omitted and the E4's at 15 and 19 MeV have been added into one line for clarity (but see remark in Sec. IV F).

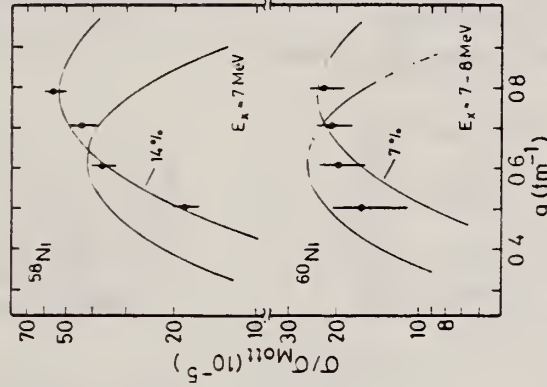


FIG. 11. Comparison of experimental cross sections for a state (group of states?) at 7 MeV in ^{58}Ni and a group of states between 7 and 8 MeV in ^{60}Ni with DWBA calculations. The ^{58}Ni data follow an E3 form factor quite well, but the ^{60}Ni data, which carry only half of the ^{58}Ni strength, may include an E2 or E1 contribution.

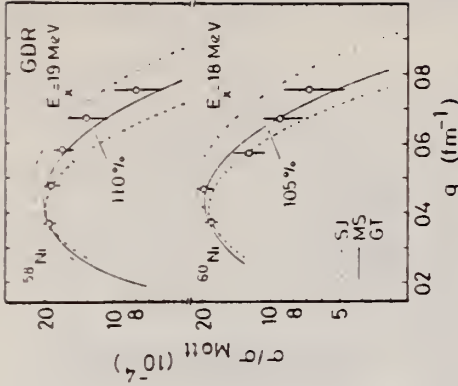


FIG. 9. Comparison between experimental and calculated cross sections for the models of Fig. 8. The curves were normalized to go through the point with the lowest momentum transfer, because this is the one with the least model dependence and the most accurate one. The Myers-Swiatecki model is somewhat favored by this comparison; however, the difficulties with the simultaneous fit of several resonances between 15 and 19 MeV, as discussed in the text, should be noted.

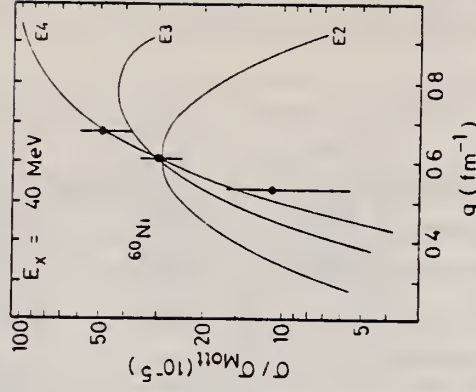


FIG. 16. Comparison of cross section at 40 MeV with DWBA calculations. The experimental points follow an E4 curve. These are two problems connected with this resonance. First, it may be doubted that it is real, that is, it may be produced by our special choice of background, because if we add one parameter to the background function it virtually disappears. Second, it exhausts a rather large fraction of the $4h\omega$ isoscalar strength, namely (150.175)%, compared to the 50% predicted (Ref. 25, Table I).

ELEM. SYM.	A	Z
Ni	60	28
REF. NO.		hg
80 Vo 2		

METHOD

REACTION	RESULT	EXCITATION ENERGY	SOURCE		DETECTOR		ANGLE
			TYPE	RANGE	TYPE	RANGE	
E, P	ABX	9-30	C	12-35	TEL-D		DST
E, A	ABX	6-30	C	12-35	TEL-D		DST

Cross sections have been measured for the reactions $^{58,60}\text{Ni}(e, e'p)$ and $^{58,60}\text{Ni}(e, e'\alpha)$ in the electron-energy range 12-35 MeV. For analysis of the experimental results we used virtual photon spectra calculated in the DWBA. At energies $E_\gamma = 16.0 \pm 1.0$ MeV for ^{58}Ni and $E_\gamma = 15.6 \pm 1.0$ MeV for ^{60}Ni we have observed giant electric-quadrupole resonances which decay mainly by α -particle emission. The integrated cross sections for the reactions $^{58}\text{Ni}(\gamma, \alpha)$ and $^{60}\text{Ni}(\gamma, \alpha)$ due to E2 transitions are respectively 5.4 ± 1.4 and 6.0 ± 3.0 mb-MeV, which amounts to $47 \pm 12\%$ of the total strength of isoscalar E2 transitions for ^{58}Ni and $56 \pm 28\%$ for ^{60}Ni . The integrated cross sections for these same reactions due to E1 transitions are 15.9 ± 2.3 and 16.9 ± 4.8 mb-MeV, which amount to $1.7 \pm 0.3\%$ of the value given by the sum rule for electric-dipole transitions for ^{58}Ni and $1.8 \pm 0.5\%$ for ^{60}Ni . The measured integrated cross sections for the reactions $^{58,60}\text{Ni}(\gamma, p)$ are 539 ± 33 and 300 ± 20 mb-MeV.

VIRT PHOTON ANALYSIS

PACS numbers: 25.30.Cg, 24.30.Cz, 27.40.+z, 27.50.+c

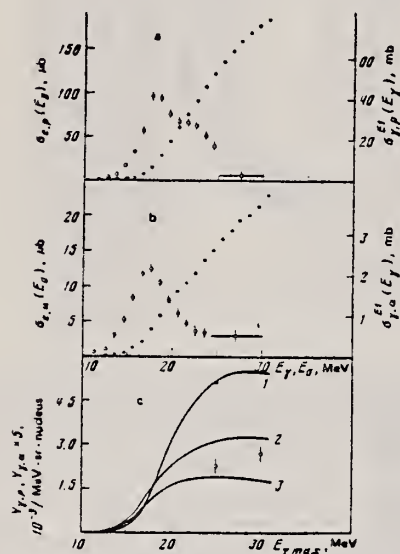


FIG. 3. The same as Fig. 2 but for ^{60}Ni nuclei.

FIG. 2. Cross sections of the reactions $^{58}\text{Ni}(e, e'p)$ (solid points) and $^{58}\text{Ni}(\gamma, p)$, calculated on the assumption that only E1 transitions are excited (hollow points)—a; b—the same but for the reactions $^{58}\text{Ni}(e, e'\alpha)$ and $^{58}\text{Ni}(\gamma, \alpha)$; c—measured yields of protons (solid points) and α particles (hollow points) in the reactions $^{58}\text{Ni}(\gamma, p)$ and $^{58}\text{Ni}(\gamma, \alpha)$. Curves 1 and 2 respectively are the expected yields of protons and α particles obtained on the assumption that only E1 transitions are excited; curve 3 is the same as curve 2 but on the assumption that only E2 transitions are excited. The proton yield has been normalized to curve 1 at an arbitrary point.

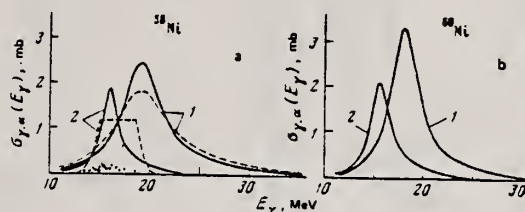


FIG. 5. Resonance curves 1 and 2 (respectively $\sigma_{\gamma, \alpha}^{E1}(E_\gamma)$ and $\sigma_{\gamma, \alpha}^{E2}(E_\gamma)$) of the reaction $^{58}\text{Ni}(\gamma, \alpha)$ obtained as the result of analysis of experimental data. The solid curves are the result of a fit by two Lorentz curves, and the dashed curves are for a fit in which $\sigma_{\gamma, \alpha}^{E2}(E_\gamma)$ has the form of a rectangle; the points show the cross section $\sigma_{\gamma, \alpha}^{E2}(E_\gamma)$ of the reaction $^{58}\text{Ni}(\gamma, \alpha)$ ^{54}Fe from Ref. 2 (a); b—Lorentz curves of $\sigma_{\gamma, \alpha}^{E1}(E_\gamma)$ (1) and $\sigma_{\gamma, \alpha}^{E2}(E_\gamma)$ (2) for the reaction $^{60}\text{Ni}(\gamma, \alpha)$.

TABLE I.

Nucleus	Reaction (γ, p) $\int_0^{20} \sigma(E_\gamma) dE_\gamma$ MeV · mb	(e, γ, α) reaction				
		Multipolarity	E_R , MeV	Γ , MeV	$\sigma_{\text{int}}^{\text{calc}}$ MeV · mb	$\sigma_{\text{int}}^{\text{exp}}$, %
^{58}Ni	539 ± 33 570 ± 60 (1*)	E1	19.1 ± 1.0	4.6 ± 0.4	15.9 ± 2.3	1.7 ± 0.3
		E2	18.0 ± 1.0	2.5 ± 0.5	5.4 ± 1.4	47 ± 12
^{60}Ni	300 ± 20	E1	18.0 ± 1.0	3.3 ± 1.0	16.9 ± 4.8	1.8 ± 0.5
		E2	15.6 ± 1.0	2.4 ± 0.8	6.0 ± 3.0	56 ± 28

ELEM. SYM.	A	Z
NI	60	28
METHOD	REF. NO.	
	80 Wo 1	hg

REACTION	RESULT	EXCITATION ENERGY	SOURCE		DETECTOR		ANGLE
			TYPE	RANGE	TYPE	RANGE	
E,XP	ABX	9-50	D	16-50	MAG-D		DST
E,XA	ABX	6-50	D	16-50	MAG-D		DST

The (e,p) and (e,α) cross sections for targets of ^{58}Ni , ^{60}Ni , and ^{62}Ni have been measured in the electron energy range 16–100 MeV. They have been analyzed using the distorted-wave Born approximation E1 and E2 virtual photon spectra. Protons are emitted primarily following E1 absorption but α-emission results from a combination of E1 and E2 absorption.

NUCLEAR REACTIONS $^{58,60,62}\text{Ni}(e,p)$ and $^{58,60,62}\text{Ni}(e,\alpha)$; measured $\sigma(E_0, E_x, 48^\circ)$, $\sigma(E_0, E_x, 90^\circ)$, $\sigma(E_0, E_x, 132^\circ)$; obtained $\sigma(e,p)$, $\sigma(e,\alpha)$; deduced $\sigma_{T,p}^{E1}(E)$, $\sigma_{T,\alpha}^{E1}(E)$, $\sigma_{T,\alpha}^{E2}(E)$.

(E,XP) VIRTUAL PHOTON G,XP

(E,XA) VIRTUAL PHOTON G,XA

1. Measurement also made at 100 MeV

2. Assumptions:

For photons: $\frac{d\sigma}{dr}(\theta) = \text{constant}$

For alphas:

$$\frac{d\sigma}{dr}(\theta) = \sigma(90^\circ) [A(E_0) + B(E_0) \sin^2 \theta]$$

$A(E_0), B(E_0)$ determined empirically

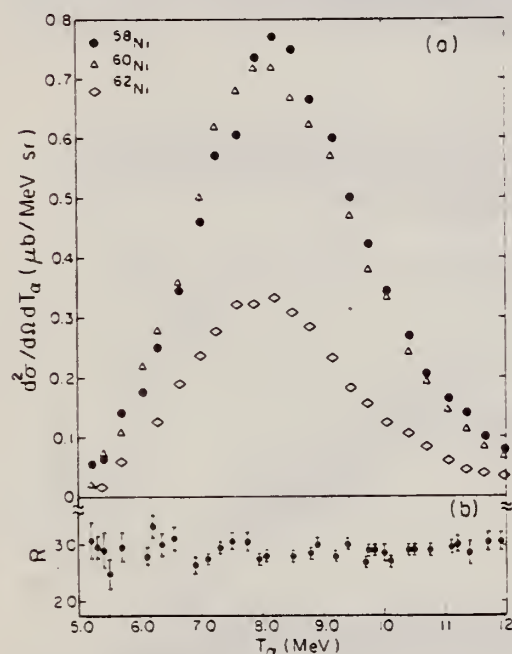


FIG. 2. (a) The α spectra $d^2\sigma/dT_\alpha d\Omega$ measured at 90° when 50 MeV electrons are incident on targets of ^{58}Ni , ^{60}Ni , and ^{62}Ni . (b) The ratio of the number of α particles produced by electro plus photodisintegration in ^{58}Ni to the number produced by electrodisintegration alone. This ratio was obtained by placing a 0.217 g/cm^2 Ta radiator in the beam ahead of the ^{58}Ni target.

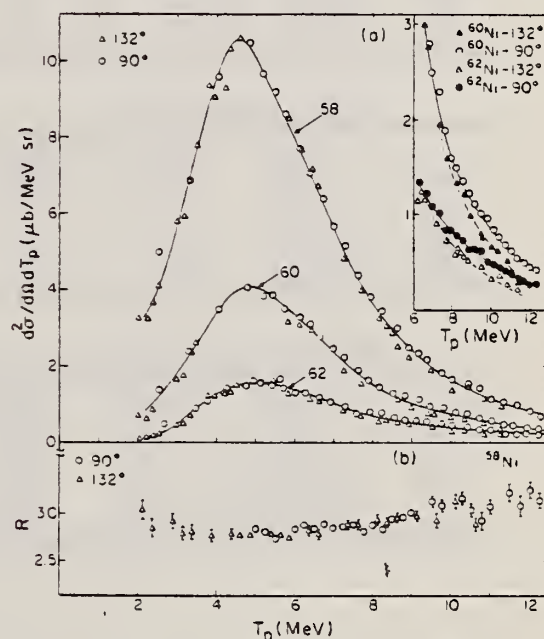


FIG. 3. (a) The proton spectra $d^2\sigma/dT_p d\Omega$ measured at 90° and 132° when 50 MeV electrons are incident on targets of ^{58}Ni , ^{60}Ni , and ^{62}Ni . The insert shows the tails of the energy spectra for ^{60}Ni and ^{62}Ni where the protons are slightly forward peaked. (b) The ratio of the number of protons produced by electro plus photodisintegration in ^{58}Ni to the number produced by electrodisintegration alone. This ratio was determined by placing a 0.217 g/cm^2 Ta radiator in the beam 7.6 cm ahead of the ^{58}Ni target.

(over)

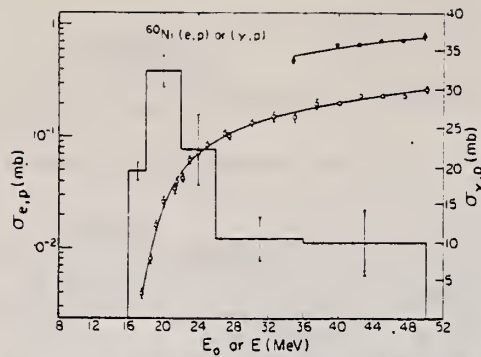


FIG. 7. The cross section (left-hand scale) for the production of protons $\sigma_{e,p}(E_0)$ when electrons of total energy E_0 are incident on a ^{60}Ni target (open circles). The closed circles represent the yield of protons obtained when a 0.217 g/cm^2 Ta foil was interposed in the incident electron beam. The latter have been corrected for the changes in geometry produced by the multiple scattering of the electrons in the radiator. The lines drawn through the points result from folding the histogram, representing the (γ,p) cross section (right-hand scale), with the $E1$ virtual photon spectrum in Eq. (1) and using the Davies-Bethe-Maximon cross section in Eq. (2).

TABLE IV. Percentage of the $E1$ and $E2$ sums in the α channel. $E1$ sum: 60 NZ/A MeV mb . $E2$ sum: $0.22 Z^2 A^{-1/3} \mu\text{b/MeV}$. $E2$ bin: $14\text{--}20 \text{ MeV}$. Upper limits of the integrals = 50 MeV .

Nucleus	$E1$		$E2$	
	Schiff	D-B-M	Schiff	D-B-M
^{58}Ni	4.8 ± 0.5	6.0 ± 0.6	24 ± 3	15 ± 3
^{60}Ni	4.4 ± 0.7	5.4 ± 0.7	24 ± 4	15 ± 4
^{62}Ni	2.4 ± 0.3	2.9 ± 0.3	10 ± 2	6 ± 2

TABLE V. $\sigma_{e,p}$ at 100 MeV .

Nucleus	$\sigma_{e,p}(\text{meas})$ (mb)	$\sigma_{e,p}(\text{calc})$ (mb)	$\sigma_{e,p}(\text{corr})$ (mb)
^{58}Ni	1.15 ± 0.02	1.10	0.98
^{60}Ni	0.50 ± 0.01	0.47	0.42
^{62}Ni	0.24 ± 0.01	0.22	0.19

TABLE VI. $\sigma_{e,\alpha}$ at 100 MeV .

Nucleus	$\sigma_{e,\alpha}(\text{meas})$ (mb)	$\sigma_{e,\alpha}(\text{calc})$ (mb)	$\sigma_{e,\alpha}(\text{corr})$ (mb)
^{58}Ni	0.069 ± 0.002	0.084	0.063
^{60}Ni	0.063 ± 0.002	0.081	0.060
^{62}Ni	0.033 ± 0.001	0.036	0.027

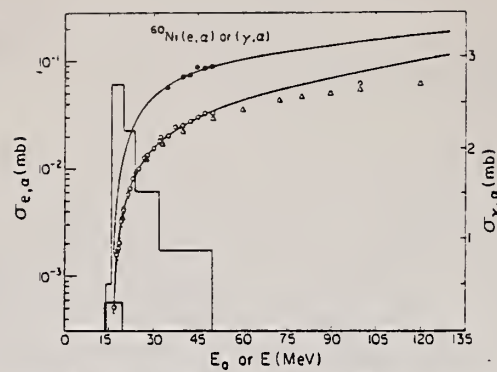


FIG. 12. The measured $\sigma_{e,\alpha}(E_0)$ for ^{60}Ni as a function of total incident electron energy E_0 (open circles). The full circles represent the electro plus photodisintegration yield obtained when the 0.217 g/cm^2 foil was interposed in the incident electron beam and the triangles show the data of Ref. 25. The smooth curves through the points result from combining the histograms, representing the $E1$ and $E2$ (γ,α) cross sections (right-hand scale), in Eqs. (1) and (2) with the $E1$ and $E2$ virtual photon spectra and making use of the Davies-Bethe-Maximon bremsstrahlung cross section. These integrals have been extended to 130 MeV assuming that the (γ,α) cross section is zero above 50 MeV . That the measured cross sections lie below this curve probably stems from the failure of the long wavelength approximation.

REF. T.J. Bowles, R.J. Holt, H.E. Jackson, R.M. Laszewski, R.D. McKeown,
A.M. Nathan, J.R. Specht
Phys. Rev. C24, 1940 (1981)

ELEM. SYM.	A	Z
Ni	60	28
REF. NO.		hg
81 Bo 5		

REACTION	RESULT	EXCITATION ENERGY	SOURCE		DETECTOR		ANGLE
			TYPE	RANGE	TYPE	RANGE	
G,G	ABX	15-23	D	15-23	NAI-D		120

Quasimonochromatic photons have been used to measure elastic and inelastic photon scattering cross sections in the giant dipole resonance region of ^{52}Cr , Fe, ^{60}Ni , ^{92}Mo , and ^{90}Mo in an experiment in which the elastic and inelastic scattering are resolved. The elastic scattering cross sections show clear evidence for isospin splitting of the giant dipole resonance. The inelastic scattering to low-lying vibrational levels, which is a measure of the coupling between the giant dipole resonance and collective surface vibrations, is in qualitative agreement with the predictions of the dynamic collective model. However, when examined in detail, this model does not provide an adequate description of the scattering data.

NUCLEAR REACTIONS ^{52}Cr , Fe, ^{60}Ni , $^{92,96}\text{Mo}$ (γ, γ'), $14 \leq E_\gamma \leq 22$ MeV; measured E_γ , $E_{\gamma'}$, $d\sigma/d\Omega$ for γ_0, γ_1 . Compared to DCM predictions. Tagged photons.

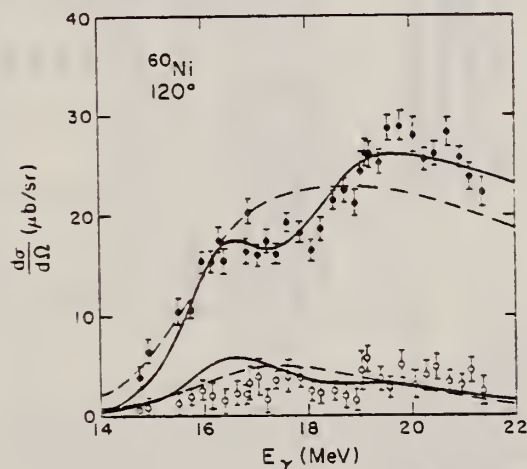


FIG. 6. Elastic (closed circles) and inelastic (open circles) scattering cross sections at $\theta=120^\circ$ for ^{60}Ni . The error bars represent statistical uncertainties only. The solid (dashed) lines are DCM calculations for the elastic and inelastic cross sections including (not including) the effect of isospin splitting.

sorption cross section σ_γ based on application of

ELEM. SYM.	A	Z
NI	60	28
REF. NO.	81 Li 4	
	egf	

REACTION	RESULT	EXCITATION ENERGY	SOURCE		DETECTOR		ANGLE
			TYPE	RANGE	TYPE	RANGE	
E, E/	FMF	7-15	D	1*3	MAG-D		DST

A simple Lane model is used to parametrize the energy systematics of the isospin splitting of high-spin magnetic states in non-self-conjugate nuclei. A strength parameter $V_1 = 106 \pm 10$ MeV is found.

PACS numbers: 25.30.Cg, 21.10.Dr, 21.10.Hw

*DELTA Q 1.5-2.7 FM-1

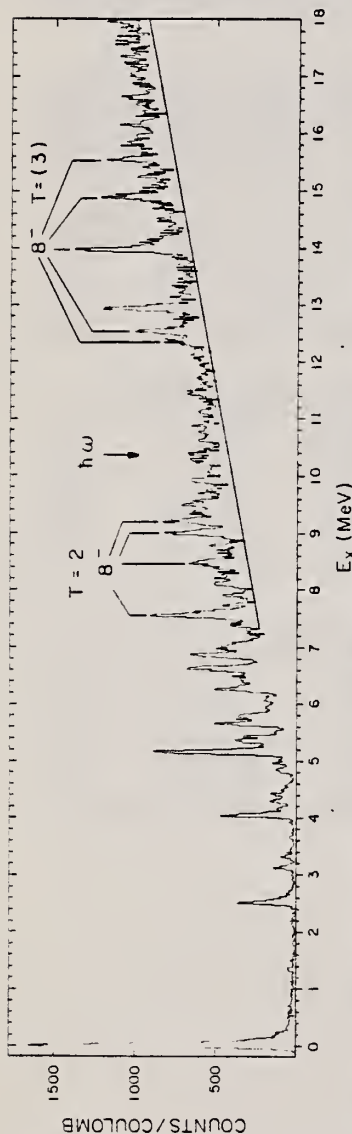


FIG. 1. An energy spectrum of electrons from ^{60}Ni at $\theta = 140^\circ$ and $E_0 = 205.1$ MeV. The base line drawn in the figure is to guide the eye in discerning the peaks of interest from the continuum.

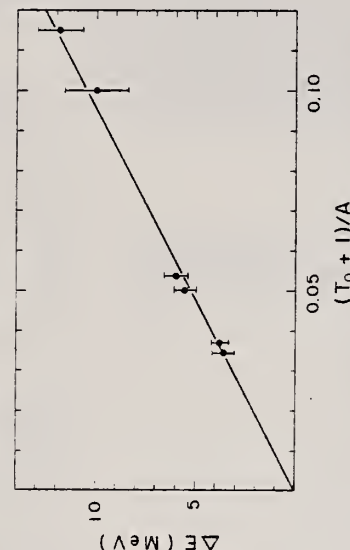


FIG. 2. A plot of the observed isospin splitting ΔE taken from Table II vs $(T_0 + 1)/A$. The straight line is a least-squares fit to the equation $\Delta E = V_1(T_0 + 1)/A$ and the fitting parameter is V_1 which is found to be 106 ± 10 MeV.

TABLE I. A tabulation of excitation energies and extracted $B(M8)$ strengths for $J^\pi = 8^-$ states in ^{60}Ni .

E_x^a	J^π	T	$\text{Exp}^b B(M8)$ ($e^2 \cdot \text{fm}^4 \cdot 10^5$)	$\frac{\text{Exp}^b B(M8)}{\text{Total}^c B(M8)} \times 100\%$
7.522	8^-	2	17.92 ± 0.45	4.82 ± 0.12
8.433	8^-	2	7.56 ± 0.37	2.04 ± 0.10
8.959	8^-	2	10.60 ± 0.35	2.85 ± 0.09
9.172	8^-	2	9.63 ± 0.52	2.59 ± 0.14
12.333	8^-	(3)	6.14 ± 0.30	1.65 ± 0.08
12.505	8^-	(3)	10.69 ± 0.33	2.88 ± 0.09
13.908	8^-	(3)	17.73 ± 0.46	4.77 ± 0.12
14.840	8^-	(3)	11.60 ± 0.50	3.12 ± 0.14
15.499	8^-	(3)	9.23 ± 0.43	2.48 ± 0.12

^a E_x uncertainty is ± 0.010 MeV.

^b Oscillator parameter $b = 1.983$.

^c Calculated under the assumption of a pure $G_{9/2}^{1/2}$ configuration.

TABLE II. A tabulation of centroid energies $E_x(T_0)$ and $E_x(T_0 + 1)$ and isospin splitting energy $\Delta E = E_x(T_0 + 1) - E_x(T_0)$. A calculated ΔE with use of $\Delta E = 100(T_0 + 1)/A$ is also included.

Nucleus	J^π	T_0	M_L	$E_x(T_0)$ (MeV)	$E_x(T_0 + 1)$ (MeV)	ΔE (MeV)	$100(T_0 + 1)/A$
^{13}C	$9/2^+$	1/2	M4	9.50	21.40	11.90	11.15
^{15}N	$9/2^+$	1/2	M4	11.63	21.68	10.05	10.0
$^{54}\text{Fe}^a$	8^-	1	M8	9.48	13.26	3.78	3.70
$^{58}\text{Ni}^a$	8^-	1	M8	9.47	13.14	3.67	3.45
$^{56}\text{Fe}^b$	8^-	2	M8	9.22	15.20	5.98	5.36
^{60}Ni	8^-	2	M8	8.36	13.92	5.56	5.00

^a Additional M8 transitions were found in ^{60}Ni since the publication of Ref. 4.

^b Ref. 13.

REF. T.J. Bowles, R.J. Holt, H.E. Jackson, R.D. McKeown, A.M. Nathan,
J.R. Specht
Phys. Rev. Lett. 48, 986 (1982)

ELEM. SYM.	A	Z
Ni	60	28

METHOD

REF. NO.
82 Bo 11
egf

REACTION	RESULT	EXCITATION ENERGY	SOURCE		DETECTOR		ANGLE
			TYPE	RANGE	TYPE	RANGE	
G,N0	ABX	14-20	C	14-20	TOF-D		90

The most stringent test to date of the concept of isospin splitting of the giant dipole resonance in a medium-weight nucleus has been performed by a study of the (γ, n_0) , (γ, p_0) , and (γ, γ) reaction channels for ^{60}Ni . The ground-state photoneutron cross section for ^{60}Ni was measured and compared with the already known (γ, p_0) reaction cross section in order to demonstrate isospin splitting. The relative strength and separation of the isospin-dependent components of the resonance were estimated from an analysis of photon scattering data.

PACS numbers: 25.20.+y, 24.30.Cz, 27.50.+e

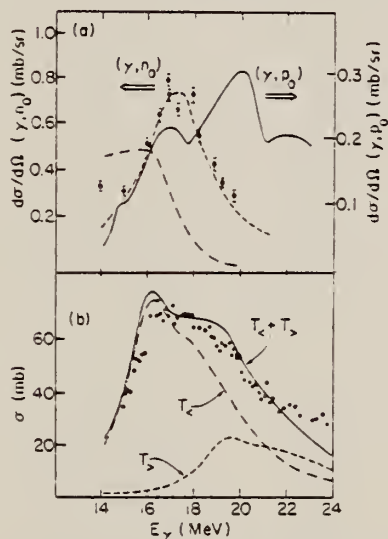


FIG. 1. (a) Ground-state photoneutron (points) and photoproton (solid line) cross sections for ^{60}Ni . The data points are the results of the present measurement. The solid line is from Ref. 5. The dashed curve is a Lorentzian of width 3.4 MeV and peak cross section adjusted to fit the (γ, n_0) data. The dash-dotted curve is a Hauser-Feshbach statistical calculation of the (γ, n_0) cross section. (b) Total photoneutron cross sections for ^{60}Ni from Ref. 7 (circles) and the calculated photoabsorption cross section σ_γ for ^{60}Ni (solid line). The dashed and dash-dotted lines are the calculated T_1 and T_2 components, respectively, of σ_γ . The calculation was performed in the framework of the dynamic collective model with parameters adjusted to fit the elastic photon scattering data.

Ni
A=61

Ni
A=61

Ni
A=61

ELEM. SYM.	A	Z
Ni	61	28
REF. NO.		
71 Ja 1		hmg

REACTION	RESULT	EXCITATION ENERGY	SOURCE		DETECTOR		ANGLE
			TYPE	RANGE	TYPE	RANGE	
G,N	RLX	7-9	C	7-9	TOF-D		DST
		(7.8-8.9)		(7.8-8.9)			

TABLE VI. Energies and parameters for resonances in the reaction $^{61}\text{Ni}(\gamma, n)$. The $\pm 20\%$ error in the quantity $\Gamma_0\Gamma_n/\Gamma$ for all resonances is due mainly to the uncertainty in the absolute normalization of the data. The energies given in column 2 are calculated from those of column 1 by applying a correction for recoil effects. For unassigned levels, column 4 gives $g\Gamma_0\Gamma_n/\Gamma$.

$E_n(n, \gamma)$ Reference 18 (keV)	$E_n(\gamma, n)$ at $\theta = 90^\circ$ Calc. (keV)	Obs. (keV)	$\Gamma_0\Gamma_n/\Gamma$ (eV)
$J = \frac{1}{2}^+$			
12.47	11.64	11.6	0.367
28.64	27.00
43.08	40.86	40.4	0.018
65.13	62.04
86.8	82.77
98.1 ± 0.7	93.62	92.6	0.102
107.8 ± 0.75	103.1	102.9	0.209
156.4	149.3
162.1 ± 1.3	155.0	154.	0.166
186.5	179.1	179.	0.062
198.0 ± 1.8	190.0	192.0	0.557
		Total	1.481
$J = \frac{1}{2}^-$			
...	...	12.6	0.040
47.4 ± 0.22	45.0	45.0	0.166
56.9 ± 0.29	54.1	53.9	0.092
111.3 ± 1.0	106.3	106.0	0.419
136.5 ± 1.4	130.5	129.5	0.256
139.6 ± 1.4	133.5	132.5	0.314
No data		141.6	0.148
No data		159.0	0.216
		Total	1.651
$J = \frac{1}{2}^-$			
23.8 ± 0.1	22.4	22.0	0.020
32.9 ± 0.1	31.1	31.0	0.018
51.5 ± 0.3	48.9	48.8	0.034
under strong s-wave level		62.0	0.189
84.7 ± 0.6	80.7	81.4	0.093
120.6 ± 1.1	115.2	114.8	0.205
...	...	162.0	0.231
...	...	187.0	0.165
		Total	1.067
Unassigned levels			
93.3	89.0	89.0	0.014
...	...	107.9	0.032
No data		175.0	0.067
		Total	0.113

TABLE V. Angular momentum assignments for resonances in the reaction $^{61}\text{Ni}(\gamma, n)$.

$E_n(\gamma, n)$ (keV)	$\frac{d\sigma(90^\circ)/d\Omega}{d\sigma(135^\circ)/d\Omega}$	J^π	$E_n(\gamma, n)$ (keV)	$\frac{d\sigma(90^\circ)/d\Omega}{d\sigma(135^\circ)/d\Omega}$	J^π
11.6	s wave	$\frac{1}{2}^+$	102.9	s wave	$\frac{1}{2}^+$
12.6	1.15 ± 0.15	$\frac{1}{2}^-$	106.0	1.05 ± 0.07	$\frac{1}{2}^-$
22.0	0.59 ± 0.10	$\frac{1}{2}^-$	114.8	0.61 ± 0.05	$\frac{1}{2}^-$
31.0	0.56 ± 0.12	$\frac{1}{2}^-$	129.5	0.95 ± 0.09	$\frac{1}{2}^-$
40.4	s wave	$\frac{1}{2}^+$	132.5	0.91 ± 0.08	$(\frac{1}{2})^-$
45.0	1.13 ± 0.07	$\frac{1}{2}^-$	141.6	1.28 ± 0.19	$\frac{1}{2}^-$
48.8	0.64 ± 0.10	$\frac{1}{2}^-$	154.0	s wave	$\frac{1}{2}^+$
	0.49 ± 0.07		159.0	1.24 ± 0.08	$\frac{1}{2}^-$
53.9	0.97 ± 0.11	$\frac{1}{2}^-$	162.0	0.72 ± 0.06	$\frac{1}{2}^-$
	1.10 ± 0.12		179.0	s wave	$\frac{1}{2}^+$
62.0	0.68 ± 0.04	$\frac{1}{2}^-$	187	0.62 ± 0.05	$\frac{1}{2}^-$
	0.80 ± 0.05		192	s wave	$\frac{1}{2}^+$
81.8	0.61 ± 0.09	$\frac{1}{2}^-$			
92.6	s wave	$\frac{1}{2}^+$			

(over)

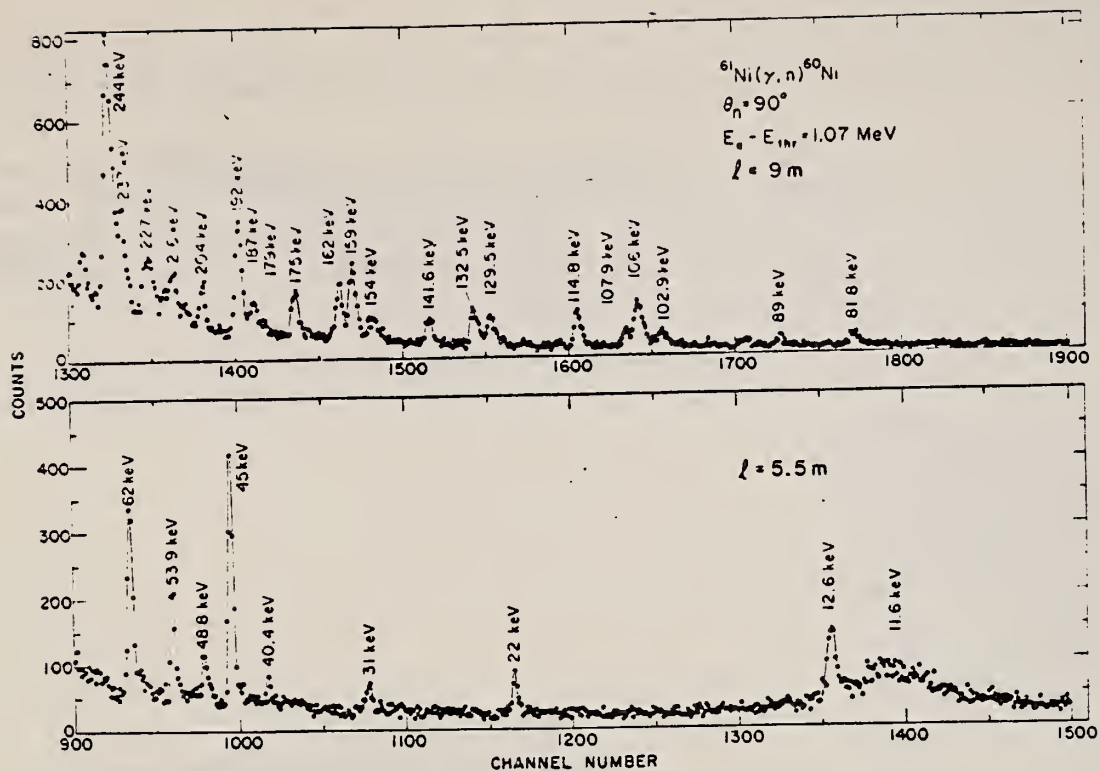


FIG. 7. Photoneutron time-of-flight spectrum for $^{61}\text{Ni}(\gamma, n)$. The upper section was taken with a flight path of 9 m the lower section with a flight path of 5.5 m.

TABLE VII. Integrated yields and reduced widths for electric and magnetic dipole radiation. Integrated yields are given for all resonances observed, but reduced widths for magnetic dipole transitions are calculated only from yields for p -wave levels above 100-keV neutron energy (see discussion in Sec. IV). The number of resonance widths used to obtain each \bar{k} is given by n . The errors given were calculated by assuming that the individual Γ_{γ} 's follow a Porter-Thomas distribution.

Target	J^{π}	$\sum g \Gamma_{\gamma} \Gamma_n / \Gamma$ (eV)	$\sum \Gamma_{\gamma} \Gamma_n / \Gamma$ (eV)	n	$10^3 \times$ reduced width Individual average
^{53}Cr	$\frac{1}{2}^{+}$	0.97	3.88	7	$\bar{k}_{E1} = 1.7^{+0.4}_{-0.3}$
	$\frac{1}{2}^{-}$	1.27	5.06	6	$\bar{k}_{M1} = 41$
	$\frac{3}{2}^{-}$	0.86	1.71	10	$\bar{k}_{M1} = 16$
^{57}Fe	$\frac{1}{2}^{+}$	0.83	1.66	8	$\bar{k}_{E1} = 0.86^{+0.8}_{-0.5}$
	$\frac{1}{2}^{-}$	0.37	0.74	4	$\bar{k}_{M1} = 9$
	$\frac{3}{2}^{-}$	0.84	0.84	3	$\bar{k}_{M1} = 10$
^{61}Ni	$\frac{1}{2}^{+}$	0.37	1.48	11	$\bar{k}_{E1} = 0.96^{+0.42}_{-0.15}$
	$\frac{1}{2}^{-}$	0.41	1.65	5	$\bar{k}_{M1} = 27$
	$\frac{3}{2}^{-}$	0.54	1.07	3	$\bar{k}_{M1} = 12$

Y. Cauchois, H. Ben Abdelaziz, R. Khérouf, C. Schloesing-Möller
 REF. J. Phys. G7, 1539 (1981)

ELEM. SYM.	A	Z
Ni	61	28
REF. NO.		hg
81 Ca 2		

METHOD

REACTION	RESULT	EXCITATION ENERGY	SOURCE		DETECTOR		ANGLE
			TYPE	RANGE	TYPE	RANGE	
G,G	LFT	1	C	0 - 2	SCD-D		
		(1.186)					

1.186 MeV

Abstract. Lifetimes of 49 excited states below 1.65 MeV have been measured in ^{24}Mg , ^{27}Al , ^{48}Ti , ^{58}Ni , ^{59}Co , $^{61,62}\text{Ni}$, $^{63,65}\text{Cu}$, $^{64,66,68}\text{Zn}$, ^{75}As , ^{103}Rh , $^{113,115}\text{In}$, $^{116,118,120}\text{Sn}$ and $^{121,123}\text{Sb}$ by means of nuclear resonance fluorescence experiments. The levels are excited by bremsstrahlung x-ray photons. The self-absorption technique applied to suitable cases provides nuclear absorption cross sections, widths and lifetimes from which the x-ray spectral distributions are also obtained. Scattering experiments are performed for all other cases in order to obtain widths and lifetimes from these x-ray photon curves. The Compton effect in the sample is taken into account. Self-absorption provides $g\Gamma_0$ from which Γ is deduced using adopted J^π and Γ_0/Γ values; scattering provides $u = g(\Gamma_0^2/\Gamma)W(\theta)$ from which Γ is also deduced with J , Γ_0/Γ and mixing ratios taken from the literature. Thanks to simultaneous determination of the x-ray spectra all the lifetimes as given by our programs with their statistical errors form an unusually coherent set of values.

NUCLEAR REACTIONS (γ, γ), bremsstrahlung excitation; natural isotopes: ^{24}Mg , ^{27}Al , ^{48}Ti , ^{58}Ni , ^{59}Co , $^{61,62}\text{Ni}$, $^{63,65}\text{Cu}$, $^{64,66,68}\text{Zn}$, ^{75}As , ^{103}Rh , $^{113,115}\text{In}$, $^{116,118,120}\text{Sn}$ and $^{121,123}\text{Sb}$; $E \approx 0.5-1.65$ MeV; measured $g\Gamma_0$ or $g(\Gamma_0^2/\Gamma)W(\theta)$; deduced $T_{1/2}$.

(OVER)

Tableau 3. Résultats des mesures des niveaux étudiés par diffusion.

Table 3. Results obtained using the diffusion method.

Isotope	Energie (keV)	J^π	J_0^π	Γ_0/Γ	δ	$u = g(\Gamma_0^2/\Gamma)W(\theta)$ (meV)	τ (ps) ce travail	τ_{ref} (ps)	Références†
²⁴ Mg	1368,59(4)	2 ⁺	0 ⁺	1	E2	1,08(13)	1,76(21)	1,98(4)	Endt et van der Leun (1978)
²⁷ Al	1014,45(3)	$\frac{3}{2}^+$	$\frac{1}{2}^+$	0,971	+0,351(12)	0,186(13)	2,20(16)	2,12(8)	Endt et van der Leun (1978)
⁴⁸ Ti	983,512(3)	2 ⁺	0 ⁺	1	E2	0,282(23)	6,74(55)	6,1(13)	Beck (1978)
⁵⁸ Ni	1454,45(15)	2 ⁺	0 ⁺	1	E2	2,11(26)	0,90(11)	0,92(3)	Kocher et Auble (1976)
⁵⁹ Co	1099,224(25)	$\frac{3}{2}^-$	$\frac{1}{2}^-$	1	(E2)	0,069(8)	4,79(55)	3,17(58)	Kim (1976)
⁵⁹ Co	1458,8(3)	$\frac{3}{2}^-$	$\frac{1}{2}^-$	0,91	(E2)	0,68(8)	1,17(14)	1,52(16)	Kim (1976)
⁵⁹ Co	1480,9(3)	$\frac{3}{2}^-$	$\frac{1}{2}^-$	0,8	<0,35 ^a	1,23(15)	0,254(31)	0,31(3)	Kim (1976)
⁶¹ Ni	1185,7(6)	$\frac{3}{2}^-$	$\frac{1}{2}^-$	0,77(8) ⁱ	0,14	1,88(49)	0,21(5)	0,16(3)	Andreiev <i>et al</i> (1974)
⁶² Ni	1172,91(9)	2 ⁺	0 ⁺	1	E2	0,88(17)	2,15(42)	2,09(3)	Halbert (1979a)
⁶³ Cu	1327,00(7)	$\frac{3}{2}^-$	$\frac{1}{2}^-$	0,84	(E2)	1,04(14)	0,84(11)	0,88(4)	Auble (1979b)
⁶³ Cu	1412,05(4)	$\frac{3}{2}^-$	$\frac{1}{2}^-$	0,72	+0,61(-8)	0,260(38)	1,90(28)	1,61(3)	Auble (1979b)
⁶⁴ Zn	991,54(7)	2 ⁺	0 ⁺	1	E2	0,640(54)	2,97(25)	2,60(13)	Halbert (1979b)
⁶⁵ Cu	1481,83(5)	$\frac{3}{2}^-$	$\frac{1}{2}^-$	0,85	(E2)	1,13(19)	0,79(13)	0,49(5)	Auble (1975a)
⁶⁶ Zn	1039,37(6)	2 ⁺	0 ⁺	1	E2	0,70(6)	2,71(23)	2,25(15)	Auble (1975b)
⁶⁸ Zn	1077,38(5)	2 ⁺	0 ⁺	1	E2	0,70(6)	2,71(23)	2,34(23)	Lewis (1975)
⁷⁵ As	572,5(10)	$\frac{3}{2}^-$	$\frac{1}{2}^-$	1 ^d	0,39 ^b	0,236(26)	4,14(46)	3,5(9)	Horen et Lewis (1975)
⁷⁵ As	823,0(10)	$\frac{3}{2}^-$	$\frac{1}{2}^-$	0,86 ^d	(E2)	0,214(22)	4,27(43)	3,5(3)	Robinson <i>et al</i> (1967)
⁷⁵ As	865,5(10)	$\frac{3}{2}^-$	$\frac{1}{2}^-$	0,83 ^d	— ^c	0,78(6)	0,863(68)	0,60(12)	Celliers <i>et al</i> (1977)
⁷⁵ As	1076,0(10)	$\frac{3}{2}^-$	$\frac{1}{2}^-$	0,94 ^d	0,38 ^d	1,97(13)	0,287(19)	0,32(7)	Celliers <i>et al</i> (1977)
⁷⁵ As	1128,5(10)	$\frac{3}{2}^-$	$\frac{1}{2}^-$	1	E1 ^d	0,224(24)	1,47(16)	—	
⁷⁵ As	1349,0(10)	$\frac{3}{2}^-$	$\frac{1}{2}^-$	0,67 ^d	0,20 ^d	1,61(29)	0,180(32)	0,12(3)	Wilson (1970)
⁷⁵ As	1370,0(10)	$\frac{3}{2}^-$	$\frac{1}{2}^-$	0,47 ^d	0,47 ^d	0,64(13)	0,218(44)	—	
¹⁰³ Rh	803,1(2)	$\frac{3}{2}^-$	$\frac{1}{2}^-$	0,70	M1	1,85(16)	0,174(15)	—	Harmatz (1979)
¹⁰³ Rh	1277,0(2)	$\frac{3}{2}^-$	$\frac{1}{2}^-$	0,75	-0,62(30) ^e	0,81(9)	0,87(10)	1,3(9)	Harmatz (1979)
¹¹¹ In	1177(1)	$\frac{3}{2}^-$	$\frac{1}{2}^-$	1	+0,5(2)	9,1(8)	0,086(8)	0,10(6)	Tuttle <i>et al</i> (1976)
¹¹³ In	1510(1)	$\frac{3}{2}^-$	$\frac{1}{2}^-$	0,935	-0,5(-3)	6,4(9)	0,071(10)	0,11(1)	Tuttle <i>et al</i> (1976)
¹¹⁵ In	1077,7(10)	$\frac{3}{2}^-$	$\frac{1}{2}^-$	0,81 ^j	(E2)	0,159(24)	1,61(24)	1,23(7)	Tuttle <i>et al</i> (1976)
¹¹⁵ In	1290,59(3)	$\frac{3}{2}^-$	$\frac{1}{2}^-$	0,98 ^j	(E2)	1,31(11)	0,66(6)	0,55(4)	Tuttle <i>et al</i> (1976)
¹¹⁵ In	1448,78(3)	$\frac{3}{2}^-$	$\frac{1}{2}^-$	0,86	-8 ⁱ	0,90(11)	0,50(6)	0,52(20)	Tuttle <i>et al</i> (1976)
¹¹⁵ In	1486,1(1)	$\frac{3}{2}^-$	$\frac{1}{2}^-$	0,787	-0,8 ^f	0,63(9)	0,63(9)	0,4(3)	Tuttle <i>et al</i> (1976)
¹¹⁵ In	1497,2(4)	$\frac{3}{2}^-$	$\frac{1}{2}^-$	<1	(E2)	1,33(16)	<0,30(4)	—	
¹¹⁵ In	1607,8(15)	$\frac{3}{2}^-$	$\frac{1}{2}^-$	≤1	(E2)	1,54(24)	≤0,26(4)	—	
¹¹⁶ Sn	1293,54(2)	2 ⁺	0 ⁺	1	E2	3,58(37)	0,53(6)	0,522(14)	Carlson <i>et al</i> (1975)
¹¹⁸ Sn	1229,64(4)	2 ⁺	0 ⁺	1	E2	2,75(28)	0,69(7)	0,67(2)	Carlson <i>et al</i> (1976)
¹²⁰ Sn	1171,6(2)	2 ⁺	0 ⁺	1	E2	1,83(16)	1,04(9)	0,91(2)	Kocher (1976)
¹²¹ Sb	1023,5(10)	$\frac{3}{2}^-$	$\frac{1}{2}^-$	1	0,57 ^g	3,69(34)	0,228(21)	0,20(7) ^h	Tamura <i>et al</i> (1979)
¹²¹ Sb	1105,5(10)	$\frac{3}{2}^-$	$\frac{1}{2}^-$	0,4	—	0,47(4)	0,42(4)	—	
¹²¹ Sb	1142,5(10)	$\frac{3}{2}^-$	$\frac{1}{2}^-$	0,6	(E2)	0,85(8)	0,449(40)	0,41(8) ^h	Booth <i>et al</i> (1973)
¹²¹ Sb	1384,0(10)	$\frac{3}{2}^-$	$\frac{1}{2}^-$	1	0,45 ^g	4,7(5)	0,092(10)	0,088(14) ^h	Booth <i>et al</i> (1973)
¹²³ Sb	1029,5(10)	$\frac{3}{2}^-$	$\frac{1}{2}^-$	1	0,57 ^g	2,96(27)	0,272(25)	0,26(4) ^h	Booth <i>et al</i> (1973)
¹²³ Sb	1086,5(10)	$\frac{3}{2}^-$	$\frac{1}{2}^-$	1	δ > 1,26 ^g	1,06(9)	0,67(6)	0,72(15) ^h	Booth <i>et al</i> (1973)

† Références pour les colonnes 3, 4, 5, 6 et 9 de chaque ligne, sauf indication appelée au bas de ce tableau. Pour les autres données se reporter au texte.

Remarque. Pour calculer δ^2 quand nous ne disposons que de $B(E2)$, pour un mélange (E2)+(M1), nous déduisons $g\Gamma_0(E2) \propto B(E2)E_0^5$; en admettant $W(\theta)=1$ et connaissant Γ_0/Γ , notre détermination de u donne une première approximation de $g\Gamma_0$ d'où une valeur de $\delta^2 = (g\Gamma_0(E2))/(g\Gamma_0 - g\Gamma_0(E2))$ qui permet d'améliorer $W(\theta)$ et $g\Gamma_0$ de proche en proche.

^a Swann (1971); ^b Robinson *et al* (1967); ^c $W(\theta)=0,99$ calculé d'après la formule de Celliers *et al* (1977); ^d Abbondanno *et al* (1978); ^e Sayer *et al* (1972); ^f Tuttle *et al* (1976); ^g d'après $B(E2)$ de Barnes *et al* (1966); ^h calculé d'après Booth *et al* (1973); ⁱ Williams *et al* (1975); ^j Dietrich *et al* (1970).

Ni
A=62

Ni
A=62

Ni
A=62

METHOD Synchrotron; proton cross section; radioactivity.

REF. NO.
59 Ca 4 NVB

REACTION	RESULT	EXCITATION ENERGY	SOURCE		DETECTOR		ANGLE
			TYPE	RANGE	TYPE	RANGE	
G, P	ABX	12-32	C	12 - 32	ACT-I		4PI

$$\sigma_{\max} = 0.019 \text{ b}$$

$$\Gamma(1/2 \sigma_{\max}) = 5.2 \text{ MeV}$$

$$\int_0^{32} \sigma(\gamma, p) dE = 0.13 \pm 0.02 \text{ MeV-b}$$

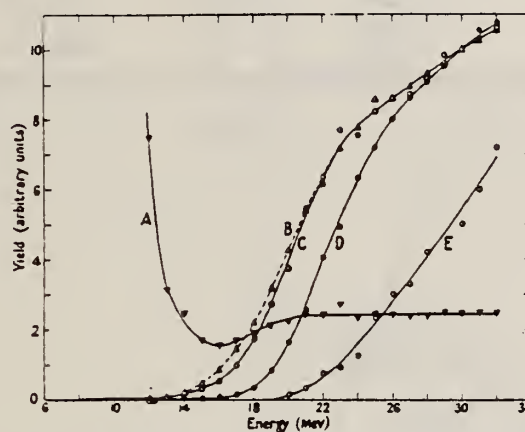


Figure 1. Activation curves for the photodisintegration of nickel: A, $^{58}\text{Ni}(\gamma, p)/^{58}\text{Ni}(\gamma, n)$; B, $^{58}\text{Ni}(\gamma, n)$; C, $^{58}\text{Ni}(\gamma, p)$; D, $^{62}\text{Ni}(\gamma, p)$; E, $^{58}\text{Ni}(\gamma, np + \gamma, 2n)$. The ordinates for curves B, C, D, E are in arbitrary units, while those for curve A give the ratio absolutely.

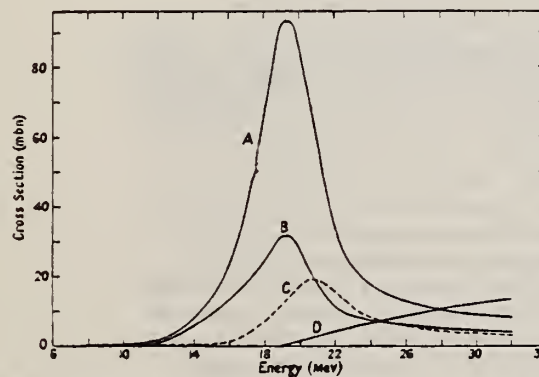


Figure 2. Excitation functions for the photodisintegration of nickel: A, $^{58}\text{Ni}(\gamma, p)$; B, $^{58}\text{Ni}(\gamma, n)$; C, $^{62}\text{Ni}(\gamma, p)$; D, $^{58}\text{Ni}(\gamma, np + \gamma, 2n)$.

REF. M.A. Duguay, C.K. Bockelman, T.H. Curtis, and R.A. Eisenstein Phys. Rev. Letters <u>17</u> , 28 (1966)			ELEM. SYM. Ni	A 62	Z 28
METHOD Linac			REF. NO. 66 Du 1		JDM
REACTION	RESULT	EXCITATION ENERGY	SOURCE		ANGLE
			TYPE	RANGE	
E, E/	FMF	1	D	45-65	DST

Table I. Reduced transition probabilities $B(E2)$ and transition radii R_{tr} for the first excited states of the even Ni isotopes.

Isotope	Level energy (MeV)	J^π	$B(E2, 0^+ \rightarrow 2^+)$ ($e^2 F^4$)		
			Ref. 12	Present work	R_{tr} (F)
Ni ⁵⁸	1.452	2 ⁺	720 ± 10%	620 ± 14%	5.35 ± 10%
Ni ⁶⁰	1.332	2 ⁺	910 ± 9%	776 ± 12%	5.23 ± 12%
Ni ⁶²	1.172	2 ⁺	830 ± 9%	770 ± 12%	5.23 ± 10%

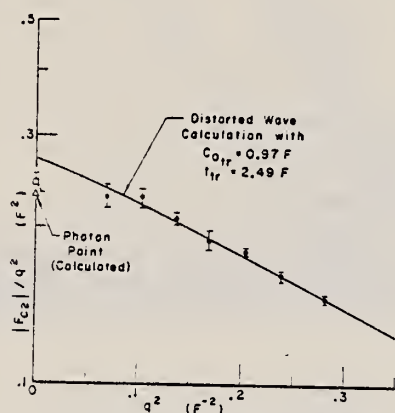


FIG. 1. Form factor for the first excited (2^+) state of Ni⁶², as a function of momentum transfer squared. The solid points represent measured form factors divided by the square of the momentum transfer plotted logarithmically as a function of the square of the momentum transfer. The line is a plot of theoretical results using the computer program of Ref. 9 to calculate form factors corresponding to transition charge densities described by the parameters c_{0tr} and t_{tr} [Eq. (3)]. The open triangle at $q = 0$ represents the photon point, calculated from Eqs. (2) and (4), using the parameters quoted in the figure. The square represents the results of the Coulomb-excitation experiment of Ref. 12.

REF. M. A. Duguay, C. K. Bockelman, T. H. Curtis and R. A. Eisenstein
Phys. Rev. 163, 1259 (1967)

ELEM. SYM. A Z
Ni 62 28

METHOD REF. NO.
67 Du 1 HMG

REACTION	RESULT	EXCITATION ENERGY	SOURCE		DETECTOR		ANGLE
			TYPE	RANGE	TYPE	RANGE	
E.E./	FMF	1-5	D	45-65	MAG-D		DST

TABLE II. Reduced radiative transition probabilities and transition radii.

B(EL), SEP ISOTPS

E2 Transitions ^a					
Excitation energy (MeV)	B(E2, 0 ⁺ → 2 ⁺) (e ² F ⁴)	B(E2, 0 ⁺ → 2 ⁺)	β_2	R_{12} (F)	
Ni ⁶² 1.452	657 ± 11	10	0.177 ± 0.003	5.51	
3.034	83 ± 3	1	0.063 ± 0.002	5.51	
3.26	153 ± 15	2	0.085 ± 0.008	5.51	
Ni ⁶⁰ 1.330	945 ± 9	12	0.197 ± 0.002	5.55	
Ni ⁶⁴ 1.172	877 ± 11	12	0.197 ± 0.001	5.59	
E3 Transitions ^a					
Excitation energy (MeV)	B(E3, 0 ⁺ → 3 ⁻) (e ³ F ⁶)	B(E3, 0 ⁺ → 3 ⁻)	β_3	R_{13} (F)	
Ni ⁶² 4.480	18 600 ± 520	13	0.203 ± 0.005	6.05	
Ni ⁶⁰ 4.038	28 100 ± 640	19	0.241 ± 0.006	6.09	
Ni ⁶⁴ 3.75	20 100 ± 540	13	0.197 ± 0.005	6.11	

^a The errors quoted for B(EL) assume the liquid-drop model for the transition charge density and are purely statistical in nature. The estimate of error from dependence on the parameters of this charge density are ±15% for both B(EL) and $R_{1\ell}$. See text.

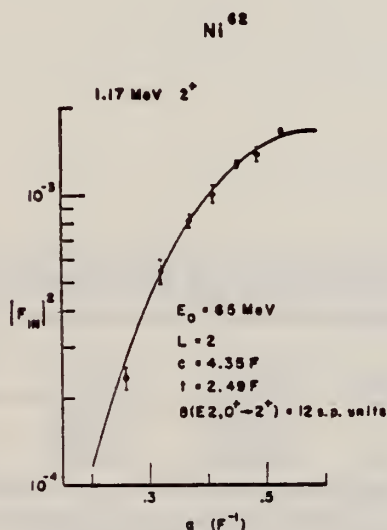


FIG. 25. The theoretical and experimental $|F_{12}|^2$ versus q for the Ni⁶² 1.17-MeV 2⁺ state. The solid curve is the $|F_{12}|^2$ calculated by Code GBROW using the strict hydrodynamic model ($c_{tr}=c$; $t_{tr}=t$). The best fit to the data is obtained by a least-squares analysis.

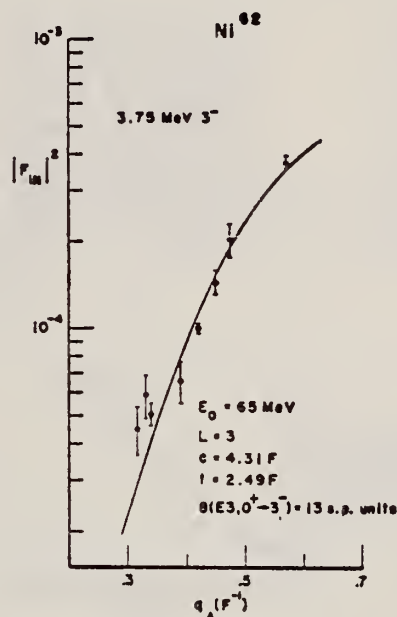


FIG. 26. The theoretical and experimental $|F_{13}|^2$ versus q for the Ni⁶² 3.75-MeV 3⁻ state. The solid curve is the $|F_{13}|^2$ calculated by Code GBROW using the strict hydrodynamic model ($c_{tr}=c$; $t_{tr}=t$). The best fit to the data is obtained by a least-squares analysis.

METHOD

Nuclear resonant scattering

REF. NO.

67 Es 1

JDM

REACTION	RESULT	EXCITATION ENERGY	SOURCE		DETECTOR		ANGLE
			TYPE	RANGE	TYPE	RANGE	
G,G/	ABX	8	D	8	NAI-D		DST

$$\langle (d\sigma/d\Omega)_{1350} \rangle = (16.8 \pm 3.4) \text{ mb/sr.}$$

$$\langle \sigma \rangle = (190 \pm 40) \text{ mb.}$$

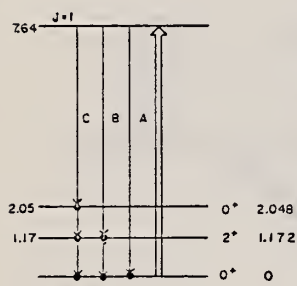


FIG. 5. Energy levels (MeV) and photon transitions observed in this experiment. The energies on the left and the $J=1$ assignment for the 7.64-MeV level were determined in this experiment. For comparison, the energies and the angular momenta determined in other reactions (Ref. 6) are given on the right.

FIG. 6. Angular distribution of the elastically scattered photons. The solid line is the theoretical curve for $J=1$, $W(\theta) = C(1 + \cos^2\theta)$ normalized at 135°.

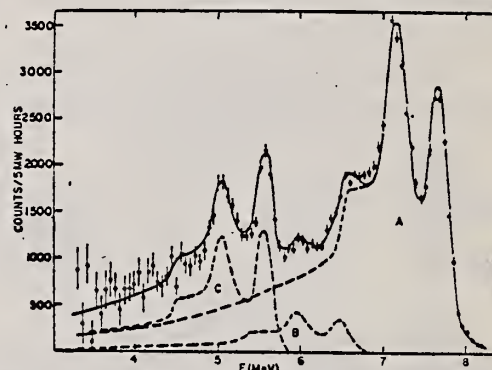
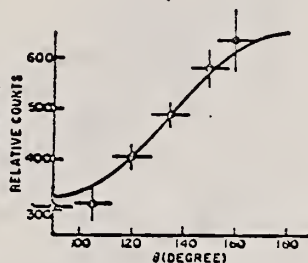


FIG. 2. Decomposition of the scattered-photon spectrum after the background subtraction. The solid line is the sum of the three components A, B, and C.

TABLE I. Energies and relative intensities of the resonantly scattered photon groups. The third column gives the energies of the lower lying levels populated by the scattered photons.

Component	Energy E_i (MeV)	$\epsilon_i = E_A - E_i$ (MeV)	Relative intensity (%)
A	7.64 ± 0.05	0.00 ± 0.07	69 ± 8
B	6.47 ± 0.05	1.17 ± 0.07	8 ± 2
C	5.58 ± 0.05	2.06 ± 0.07	23 ± 8

^a W. F. Miller and William J. Snow, Argonne National Laboratory Report No. ANL-6318, 1961 (unpublished).

REF. S. V. Starobdubtsev, R. B. Begzhanov, A. A. Islamov
Dokl. Akad. Nauk SSSR 174, 332 (1967)
Soviet Phys. Dokl. 12, 472 (1967)

ELEM. SYM.	A	Z
Ni	62	28

METHOD

REF. NO.	
67 St 1	egf

REACTION	RESULT	EXCITATION ENERGY	SOURCE		DETECTOR		ANGLE
			TYPE	RANGE	TYPE	RANGE	
G.G	LFT	7	D	7	NAI-D	4-7	135

7=7.64 MEV

Self-absorption measurement

TABLE 1

Nucleus	Transition energy, MeV	$I_i^{\pi} \rightarrow I_f^{\pi}$	Γ_{γ} , eV	Nucleus	Transition energy, MeV	$I_i^{\pi} \rightarrow I_f^{\pi}$	Γ_{γ} , eV
$^{63}_{24}\text{Ni}$	7.64	$1^{-} \rightarrow 0^{+}$	1.0 ± 0.10	$^{114}_{48}\text{Cd}$	7.64	$1^{-} \rightarrow 0^{+}$	0.20 ± 0.05
	6.47	$1^{-} \rightarrow 2^{+}$	0.33 ± 0.11		7.04	$1^{-} \rightarrow 2^{+}$	0.05 ± 0.01
	5.60	$1^{-} \rightarrow 2^{+}$	1.26 ± 0.38		6.50	$1^{-} \rightarrow 0^{+}$	0.13 ± 0.03
	5.34	$1^{-} \rightarrow 0^{+}$	0.60 ± 0.18		5.80	$1^{-} \rightarrow 2^{+}$	0.18 ± 0.04
	5.0	$1^{-} \rightarrow 2^{+}$	0.36 ± 0.14	$^{208}_{82}\text{Pb}$	7.28	$1^{-} \rightarrow 0^{+}$	0.78 ± 0.03
	4.70	$1^{-} \rightarrow 2^{+}$	2.15 ± 0.64				

REF. R. Moreh and M. Friedman
Phys. Letters 26B, 579 (1968)

ELEM. SYM.	A	Z
Ni	62	28
REF. NO.		EGF
68 Mo 1		

METHOD						REF. NO.		
						68 Mo 1		EGF
REACTION	RESULT	EXCITATION ENERGY	SOURCE		DETECTOR		ANGLE	
			TYPE	RANGE	TYPE	RANGE		
G,G	NOX	7	D	7	NAI-D	5-8	90	

Compton polarimeter.

Table 1

Properties of levels populated by resonance scattering of iron capture γ rays; J_0 and J denote the spins of the ground and resonance levels, respectively.

Scattering isotope	J_0	Resonance level (MeV)	Resonance spin	$N(90, 90)/N(90, 0)$		Transition character
				exp.	calc.	
^{208}Pb	0^+	7.279	1	1.18 ± 0.03	1.18	E1
^{112}Cd	0^+	7.632	1	0.87 ± 0.04	0.855	M1
^{141}Pr	$\frac{1}{2}^+$	7.632	$\frac{1}{2}$	1.03 ± 0.02	1.03	E1
^{62}Ni	0^+	7.646	1	0.88 ± 0.04	0.855	M1
^{203}Tl	$\frac{1}{2}^+$	7.646	$\frac{1}{2}$	1.00 ± 0.01	1.00	-

METHOD				REF. NO.		
				70 Es 1		egf
REACTION	RESULT	EXCITATION ENERGY	SOURCE		DETECTOR	
			TYPE	RANGE	TYPE	RANGE
G ₂ G	NOX	7	D	7	SCD-D	5-8
		(7.64)				

$$7 = 7.64$$

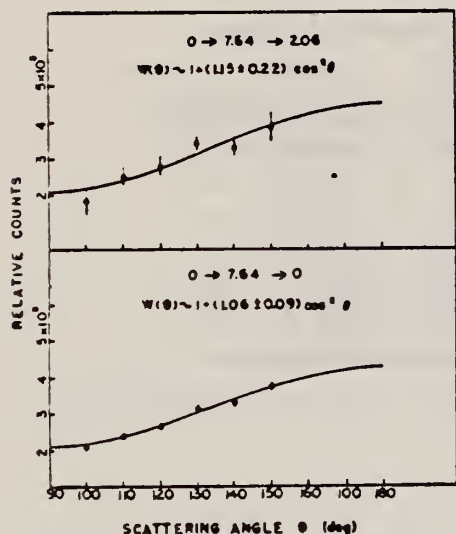


FIG. 9. Angular distributions of resonantly scattered photons in Ni. The solid lines are the least-squares fit through the data points.

TABLE II. Summary of angular distribution measurements in Ni.

E (MeV)	Final state (MeV)	$W(\theta)$ (Experimental)	$W(\theta)$ (Theoretical)	J
7.64	0	$1 + (1.06 \pm 0.09) \cos^2 \theta$	$1 + \cos^2 \theta$ ($0 \rightarrow 1-4$)	1
5.58	2.06	$1 + (1.15 \pm 0.22) \cos^2 \theta$	$1 + \cos^2 \theta$ ($0 \rightarrow 1-4$)	0

ELEM. SYM.	A	Z
Ni	62	28
REF. NO.		hmg
70 Mo 2		

REACTION	RESULT	EXCITATION ENERGY	SOURCE		DETECTOR		ANGLE
			TYPE	RANGE	TYPE	RANGE	
G,G	ABX	8	D	8	SCD-D		DST
		(7.646)		(7.646)			

8 = 7.646, LFT

TABLE III. Summary of the results of spins, parities, and total widths of resonance levels excited by γ rays obtained from neutron capture in iron. Parities in parantheses are uncertain.

Isotope	Energy (MeV)	$\delta = E_r - E_s $ (eV)	J^π_0	J^π_r	Transition	Γ_0/Γ_γ ($\pm 8\%$)	Γ_γ (10^{-3} eV)
⁵⁰ Cr	8.888	18 \pm 1	0 ⁺	1	...	0.90	750 \pm 200
⁶² Ni	7.646	14 \pm 1	0 ⁺	1 ⁻	E1	0.64	480 \pm 50
⁷⁴ Ge	6.018	4.5 \pm 0.5	0 ⁺	1 ⁻	E1	0.19	120 \pm 15
⁷⁵ As	7.646	7.4 \pm 0.3	3/2 ⁻	1/2 ⁽⁺⁾	...	0.11	360 \pm 100
¹⁰⁹ Ag	7.632	9 \pm 1	1/2 ⁻	3/2	...	0.7	2 \pm 1
¹¹² Cd	7.632	4.8 \pm 0.4	0 ⁺	1 ⁻	E1	0.55	86 \pm 15
¹³⁹ La	6.018	8.2 \pm 0.6	7/2 ⁺	7/2 ⁻	E1	0.50	51 ⁺¹⁴ ₋₅
¹⁴¹ Pr	7.632	11.4 ^{+0.3} _{-0.9}	5/2 ⁺	5/2 ⁺	M1	0.46	72 ⁺³ ₋₄
²⁰⁵ Tl	7.646	9.3 \pm 0.3	1/2 ⁺	1/2 ⁽⁻⁾	...	0.58	980 \pm 90
²⁰⁸ Pb	7.279	7.1 \pm 0.3	0 ⁺	1 ⁺	M1	1.00	780 \pm 60

TABLE IV. Effective elastic scattering cross section $\langle\sigma_r\rangle = \sigma_0^r (\Gamma_0/\Gamma_\gamma) \Psi(x_0, t_0)$, where δ , J , Γ_0 , Γ_γ were taken from Table III. The temperature of the scatterer was 300°K, while that of the iron γ source was 640°K.

Target	Resonance energy (MeV)	$\langle\sigma_r\rangle$ (mb)
⁵⁰ Cr	8.888	905
⁶² Ni	7.646	569
⁷⁴ Ge	6.018	61
⁷⁵ As	7.646	4.4
¹⁰⁹ Ag	7.632	3.5
¹¹² Cd	7.632	193
¹³⁹ La	6.018	39
¹⁴¹ Pr	7.632	20
²⁰⁵ Tl	7.646	574
²⁰⁸ Pb	7.279	5560

REF.

A.S. Litvinenko, N.G. Shevchenko, A.Yu. Buki, P.L. Kondrat'ev,
G.A. Savitskii, A.A. Khomich, V.M. Khvastunov, I.I. Chkalov
Ukr. Fiz. Zhur. 17, 1197 (1972)

ELEM. SYM.	A	Z
Ni	62	28
REF. NO.		
72 L1 3		hmg

METHOD

REACTION	RESULT	EXCITATION ENERGY	SOURCE		DETECTOR		ANGLE
			TYPE	RANGE	TYPE	RANGE	
E, E/	FMP	1, 4	D	150, 225	MAG-D		DST

B(EL) L EV 1.17, 3.75

Таблица 1

Параметры фермиевского распределения плотности заряда
(с—радиус полуспада плотности, t —диффузионность ядра)

Ядро	с, ф	t, ф
Fe ⁵⁴	1.012 ± 0.007	2.346 ± 0.011
Fe ⁵⁶	3.971 ± 0.013	2.608 ± 0.020
Fe ⁵⁸	4.027 ± 0.019	2.530 ± 0.031
Ni ⁶²	4.149 ± 0.011	2.506 ± 0.016

¹ Институт ядерных исследований АН СССР.

Таблица 2

Ядро	$E_{\gamma}, \delta E_{\gamma}$	J ^π	Данные настоящей работы	Данные других работ		Литература
			$B(EL) \uparrow, \epsilon \lambda_{\text{пр}} 2\lambda$	$B(EL) \uparrow, \epsilon \lambda_{\text{пр}} 2\lambda$	Тип эксперимента и метод определения	
Fe ⁵⁴	1.4	2 ⁺	531.9 ± 32.4	533	(ee'), борновское приближение	[6]
	4.85	3 ⁻	4563 ± 410	4390		
Fe ⁵⁶	0.85	2 ⁺	678.1 ± 47.5	720	(ee'), борновское приближение	[7]
				1250 ± 270	искаженные волны	
				1240	борновское приближение	
Fe ⁵⁸	0.81	2 ⁺	943.2 ± 79	900 ± 100	кулоновское возбуждение	[8]
	3.86	3 ⁻	13880 ± 1260			
Ni ⁶²	1.17	2 ⁺	618.6 ± 42.1	877 ± 11	(ee'), искаженные волны	[9]
	3.75	3 ⁻	14359 ± 962	20100 ± 540		

REF.

K. Shoda, M. Sugawara, T. Saito, H. Miyase, A. Suzuki, S. Oikawa,
and J. Uegaki
PICNS-72, 321 Sendai

ELEM. SYM.

A

Z

Ni

62

28

METHOD

REF. NO.

72 Sh 10

hvm

REACTION	RESULT	EXCITATION ENERGY	SOURCE		DETECTOR		ANGLE
			TYPE	RANGE	TYPE	RANGE	
G,P	ABX	16- 27	C	16- 27	MAG-D		90

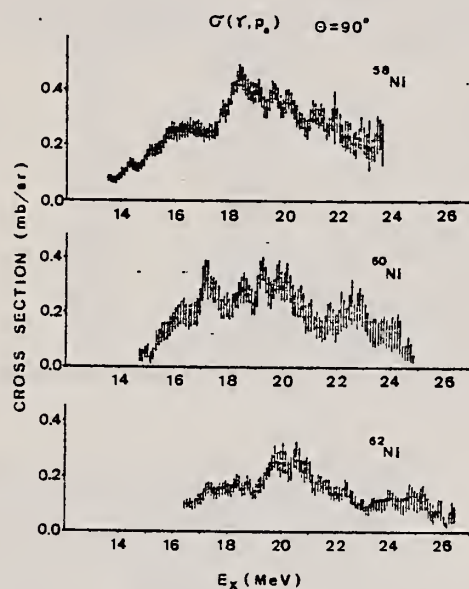
I A STATES

Fig. 10 The (γ, p_0) cross sections of Ni isotopes obtained from proton spectra by the $(e, e'p)$ reaction.

REF.

H. Miyase, S. Oikawa, A. Suzuki, J. Uegaki, T. Saito,
M. Sugawara, and K. Shoda
PICNS-73, Vol. I, p. 553 Asilomar

ELEM. SYM.

A

Z

Ni

62

28

METHOD

REF. NO.

73 M1 7

hmg

REACTION	RESULT	EXCITATION ENERGY	SOURCE		DETECTOR		ANGLE
			TYPE	RANGE	TYPE	RANGE	
E, P	ABX	16- 29	D	0 - 29	MAG-D		DST

745+
747

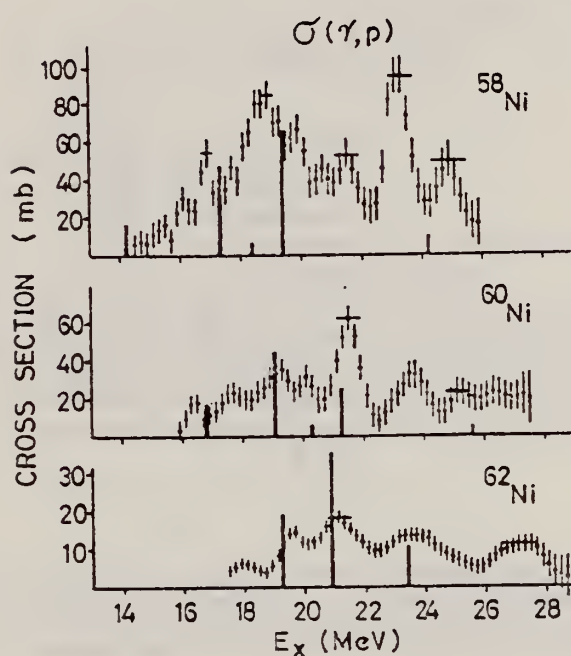


Fig. 1

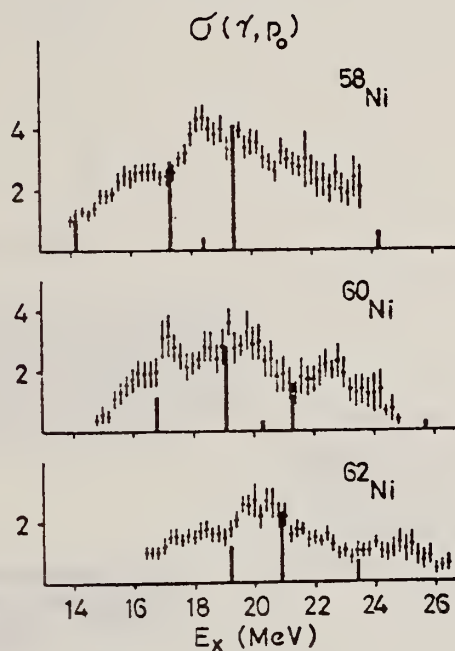


Fig. 2

Table 1 Experimental and theoretical results

Nucleus	T_0	$\int \sigma_n^{(3)}$ (mb-MeV)	$\int \sigma_p$ (mb-MeV)	$\int \sigma_n + \int \sigma_p$ (mb-MeV)	$\frac{\int \sigma_p}{\int \sigma_n + \int \sigma_p}$	$\frac{ c_> ^2}{ c_< ^2 + c_> ^2}$
^{58}Ni	1	310 ± 30	480 ± 100	790 ± 130	0.61	0.45
^{60}Ni	2	620 ± 50	210 ± 80	830 ± 130	0.25	0.27
^{62}Ni	3		110 ± 25			0.17

REACTION	RESULT	EXCITATION ENERGY	SOURCE		DETECTOR		ANGLE
			TYPE	RANGE	TYPE	RANGE	
G,G	LFT	7	D	7	SCD-D		DST

$$\Gamma_Y = 0.48 \pm 0.05 \text{ eV}$$

$$\Gamma_o/\Gamma_\gamma = 0.64$$

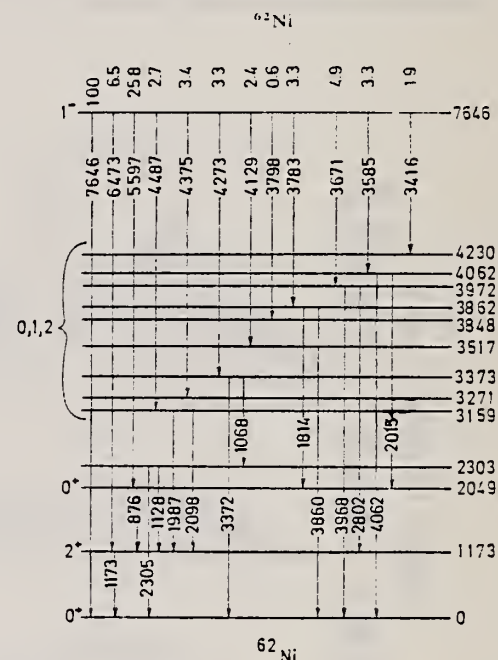
$$T = 7.646 \text{ MEV}$$


Fig. 3. Decay scheme of the 7646 keV level of ^{62}Ni showing level energies and corresponding branching ratios as constructed by assuming that the high-energy γ -lines in the scattered spectrum are emitted in primary transitions. The spin possibilities of the higher excited states are based on the assumption that the resonance level is deexcited by dipole transitions.

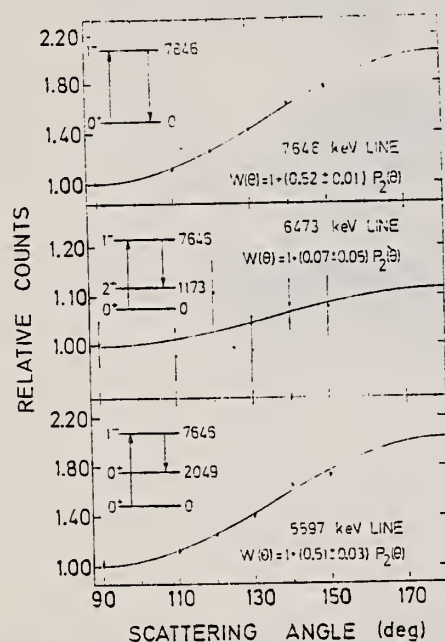


Fig. 4. Angular distribution of the elastic and some inelastic lines in ^{62}Ni as measured using a 30 cm^3 Ge(Li) detector. The solid lines have the form $W(\theta) = 1 + A P_2(\cos \theta)$ and are least squares fits to the experimental distributions. In each case the corresponding $\gamma\text{-}\gamma$ cascade is indicated.

ELEM. SYM.	A	Z
Ni	62	28

METHOD	REF. NO.	
	74 Mo 7	egf

REACTION	RESULT	EXCITATION ENERGY	SOURCE		DETECTOR		ANGLE
			TYPE	RANGE	TYPE	RANGE	
G, G	NOX	7	D	7	NAT-D		135

7=7.646 FUNC TEMP

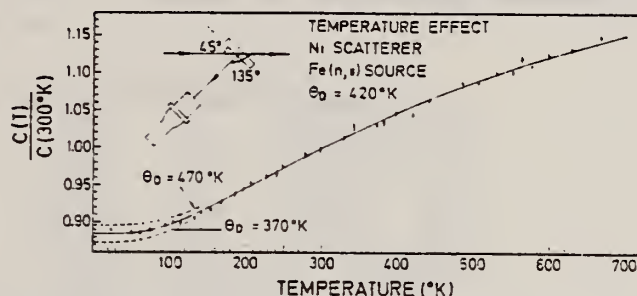


Fig. 4. Relative scattering yield from a Ni scatterer as a function of temperature. The scatterer thickness is 0.9 cm and the geometry is indicated in the figure. The scattering yield is normalised to $T = 300^\circ\text{K}$. The solid curve is the theoretical result obtained using eq. (1) with $\theta_0 = 420^\circ\text{K}$, $\delta = 14.35\text{ eV}$, $I' = 0.48\text{ eV}$, $\Gamma_0/T = 0.63$, while the dotted curves correspond to theoretical results having the same parameters but with $\theta_0 = 470^\circ\text{K}$ and $\theta_0 = 370^\circ\text{K}$. The dotted curves approach the solid curve and nearly coincide with it at higher temperatures; for clarity, this is not shown in the figure.

REF.			B. S. Ratner Yad. Fiz. <u>21</u> , 1147 (1975) Sov. J. Nucl. Phys. <u>21</u> , 590 (1976)			ELEM. SYM.	A	Z
						Ni	62	28
METHOD						REF. NO.		
						75 Ra 2		hmg
REACTION	RESULT	EXCITATION ENERGY	SOURCE		DETECTOR		ANGLE	
			TYPE	RANGE	TYPE	RANGE		
G,P	RLY	11- 16	C	14- 16	ACT-I		4PI	

The yields of (γ , p) reactions on ^{62}Ni , ^{64}Ni , and ^{53}Cr are studied in ranges of $E_{\gamma\text{max}}$ near the respective thresholds. Considerable differences are found between the curve shapes, yields, and observed thresholds for the Ni isotopes and ^{53}Cr .

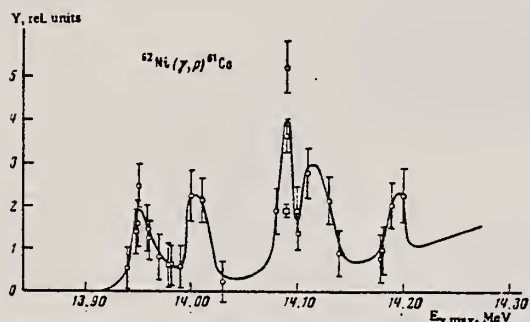


FIG. 4. Measured yields of $^{62}\text{Ni}(\gamma, p)^{61}\text{Co}$ in the region of $E_{\gamma\text{max}} = 13.94\text{--}14.20$ MeV. Statistical errors are indicated; the point with the symbol \square is the rms error.

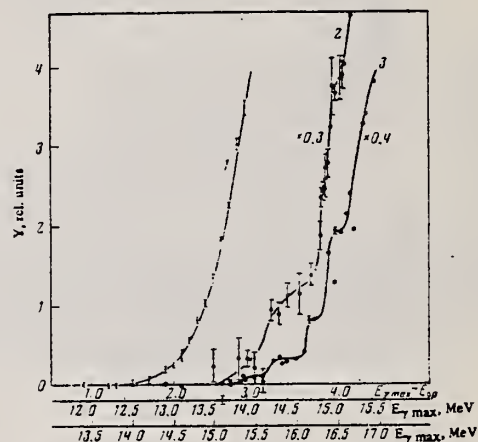


FIG. 3. Yields of the reactions $^{53}\text{Cr}(\gamma, p)^{52}\text{V}$ (curve 1), $^{64}\text{Ni}(\gamma, p)^{63}\text{Co}$ (curve 2), and $^{62}\text{Ni}(\gamma, p)^{61}\text{Co}$ (curve 3) as functions of $E_{\gamma\text{max}}$. Lowest scale for $^{64}\text{Ni}(\gamma, p)$; middle scale for $^{62}\text{Ni}(\gamma, p)$ and $^{53}\text{Cr}(\gamma, p)$.

ELEM. SYM.	A	Z
Ni	62	28
REF. NO.		
79 Wo 3		hg

METHOD					REF. NO.		
					79 Wo 3		hg
REACTION	RESULT	EXCITATION ENERGY	SOURCE		DETECTOR		ANGLE
			TYPE	RANGE	TYPE	RANGE	
E,XP	ABX	11-30	D	16-50	MAG-D		4PI
E,XA	ABX	7-30	D	16-50	MAG-D		4PI

The (e,p) and (e,α) cross sections for targets of ^{58}Ni , ^{60}Ni , and ^{62}Ni have been measured in the electron energy range 16–50 MeV. They have been analyzed using the distorted-wave Born-approximation $E1$ and $E2$ virtual-photon spectra. Protons are emitted primarily following $E1$ absorption but α emission results from a combination of $E1$ and $E2$ absorption. The $E2$ isoscalar giant resonance decays predominantly by α emission for these nuclei.

(E,XP) VIRTUAL PHOTON G,XP

(E,XA) VIRTUAL PHOTON G,XA

See also 80 Wo 1

TABLE I. Resonance parameters for $\sigma_{\gamma,p}$.

Nucleus	E_x (MeV)	Γ (MeV) ^a	$\int_0^{30} \sigma dE$ (MeV mb)	SR ^b (%)
^{58}Ni	19.2 ± 0.5	6.5 ± 1.3	739 ± 40	85 ± 5
^{60}Ni	18.5 ± 0.5	9.2 ± 1.8	304 ± 20	34 ± 2
^{62}Ni	21.0 ± 0.5	5.8 ± 1.0	140 ± 10	15 ± 1

^a Γ is the full width at half maximum.

^bSR stands for sum rule; the $E1$ SR equals $60 NZ/A$ MeV mb.

TABLE II. $E1$ components in the (γ,α) reaction.

Nucleus	E_x (MeV)	Γ (MeV) ^a	$\int \sigma dE$ (MeV mb)	SR ^b (%)
^{58}Ni	18.3 ± 0.5	6 ± 1	15.3 ± 1.3	1.9 ± 0.2
^{60}Ni	21.5 ± 1.0	6 ± 1	18.5 ± 1.4	2.1 ± 0.2
^{62}Ni	18.3 ± 1.0	5 ± 1	4.9 ± 0.6	0.5 ± 0.1

^a Γ is the full width at half maximum.

^b $E1$ SR equals $60 NZ/A$ MeV mb.

TABLE III. $E2$ components in the (γ,α) reaction.

Nucleus	E_x (MeV)	Γ (MeV) ^a	$\int \sigma dE$ (MeV mb)	SR ^b (%)
^{58}Ni	16.5 ± 0.5	4.2 ± 1.0	10.4 ± 0.7	56 ± 4
^{60}Ni	16.0 ± 0.5	3.7 ± 0.8	6.9 ± 0.4	52 ± 3
^{62}Ni	16.8 ± 0.5	4.5 ± 1.0	5.1 ± 0.4	28 ± 2

^a Γ is the full width at half maximum.

^b $E2$ SR equals $0.22 Z^2/A^{1/3} \mu\text{b/MeV}$.

ELEM. SYM.	A	Z
NI	62	28
REF. NO.		
80 Wo 1		hg

METHOD

REACTION	RESULT	EXCITATION ENERGY	SOURCE		DETECTOR		ANGLE
			TYPE	RANGE	TYPE	RANGE	
E, XP	ABX	11-50	D	16-50	MAG-D		DST
E, XA	ABX	7-50	D	16-50	MAG-D		DST

The (e,p) and (e,α) cross sections for targets of ^{58}Ni , ^{60}Ni , and ^{62}Ni have been measured in the electron energy range 16–100 MeV. They have been analyzed using the distorted-wave Born approximation E1 and E2 virtual photon spectra. Protons are emitted primarily following E1 absorption but α-emission results from a combination of E1 and E2 absorption.

NUCLEAR REACTIONS $^{58,60,62}\text{Ni}(e,p)$ and $^{58,60,62}\text{Ni}(e,\alpha)$; measured $\sigma(E_0, E_x, 48^\circ)$, $\sigma(E_0, E_x, 90^\circ)$, $\sigma(E_0, E_x, 132^\circ)$; obtained $\sigma(e,p)$, $\sigma(e,\alpha)$; deduced $\sigma_{7,p}^{E1}(E)$, $\sigma_{7,\alpha}^{E1}(E)$, $\sigma_{7,\alpha}^{E2}(E)$.

(E,XP) VIRTUAL PHOTON G,XP

(E,XA) VIRTUAL PHOTON G,XA

1. Measurement also made at 100 MeV

2. Assumptions:

For photons: $\frac{d\sigma}{dr}(\theta) = \text{constant}$

For alphas:

$\frac{d\sigma}{dr}(\theta) = \sigma(90^\circ)[A(E_0) + B(E_0)\sin^2\theta]$
A(E_0), B(E_0) determined empirically

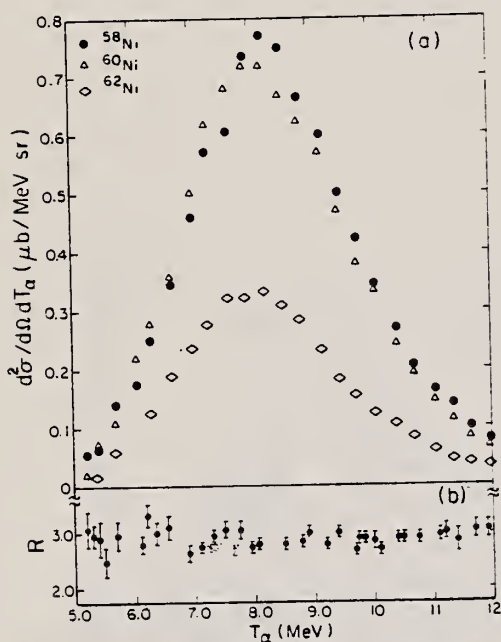


FIG. 2. (a) The α spectra $d^2\sigma/dT_\alpha d\Omega$ measured at 90° when 50 MeV electrons are incident on targets of ^{58}Ni , ^{60}Ni , and ^{62}Ni . (b) The ratio of the number of α particles produced by electro plus photodisintegration in ^{58}Ni to the number produced by electrodisintegration alone. This ratio was obtained by placing a 0.217 g/cm^2 Ta radiator in the beam ahead of the ^{58}Ni target.

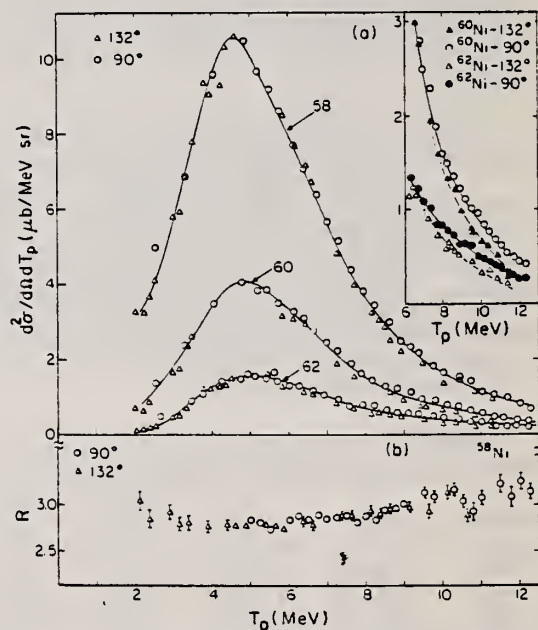


FIG. 3. (a) The proton spectra $d^2\sigma/dT_p d\Omega$ measured at 90° and 132° when 50 MeV electrons are incident on targets of ^{58}Ni , ^{60}Ni , and ^{62}Ni . The insert shows the tails of the energy spectra for ^{60}Ni and ^{62}Ni where the protons are slightly forward peaked. (b) The ratio of the number of protons produced by electro plus photodisintegration in ^{58}Ni to the number produced by electrodisintegration alone. This ratio was determined by placing a 0.217 g/cm^2 Ta radiator in the beam 7.6 cm ahead of the ^{58}Ni target.

(over)

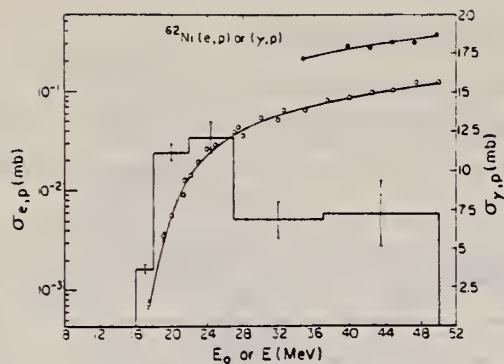


FIG. 9. The $\sigma_{e,p}(E_0)$ and $Y_{\alpha,p}(E_0)$ for ^{62}Ni (left-hand scale) obtained by using the $E1$ virtual photon spectrum in Eq. (1) and the Davies-Bethe-Maximon bremsstrahlung cross section in Eq. (2).

TABLE IV. Percentage of the $E1$ and $E2$ sums in the α channel. $E1$ sum: 60 NZ/A MeV mb . $E2$ sum: $0.22 Z^2 A^{-1/3} \mu\text{b/MeV}$. $E2$ bin: $14\text{--}20 \text{ MeV}$. Upper limits of the integrals = 50 MeV .

Nucleus	$E1$		$E2$	
	Schiff	D-B-M	Schiff	D-B-M
^{58}Ni	4.8 ± 0.5	6.0 ± 0.6	24 ± 3	15 ± 3
^{60}Ni	4.4 ± 0.7	5.4 ± 0.7	24 ± 4	15 ± 4
^{62}Ni	2.4 ± 0.3	2.9 ± 0.3	10 ± 2	6 ± 2

TABLE V. $\sigma_{e,p}$ at 100 MeV .

Nucleus	$\sigma_{e,p}(\text{meas})$ (mb)	$\sigma_{e,p}(\text{calc})$ (mb)	$\sigma_{e,p}(\text{corr})$ (mb)
^{58}Ni	1.15 ± 0.02	1.10	0.98
^{60}Ni	0.50 ± 0.01	0.47	0.42
^{62}Ni	0.24 ± 0.01	0.22	0.19

TABLE VI. $\sigma_{e,\alpha}$ at 100 MeV .

Nucleus	$\sigma_{e,\alpha}(\text{meas})$ (mb)	$\sigma_{e,\alpha}(\text{calc})$ (mb)	$\sigma_{e,\alpha}(\text{corr})$ (mb)
^{58}Ni	0.069 ± 0.002	0.094	0.063
^{60}Ni	0.063 ± 0.002	0.081	0.060
^{62}Ni	0.033 ± 0.001	0.036	0.027

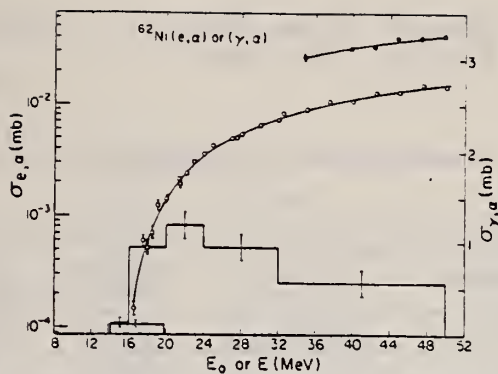


FIG. 13. The measured $\sigma(e,\alpha)$ for ^{62}Ni (open circles) as a function of total incident electron energy E_0 (left-hand scale). The full circles are electro plus photodisintegration yields obtained when the 0.217 g/cm^2 tantalum foil was interposed in the incident electron beam. The smooth curves through the points result from combining the histograms, representing the $E1$ and $E2$ (γ,α) cross sections (right-hand scale), in Eqs. (1) and (2) with the $E1$ and $E2$ virtual photon spectra and making use of the Davies-Bethe-Maximon cross section.

REF. Y. Cauchois, H. Ben Abdelaziz, R. Khérouf, C. Schloesing-Möller
J. Phys. G7, 1539 (1981)

ELEM. SYM.	A	Z
Ni	62	28
REF. NO.		
81 Ca 2		hg

METHOD

REACTION	RESULT	EXCITATION ENERGY	SOURCE		DETECTOR		ANGLE
			TYPE	RANGE	TYPE	RANGE	
G,G	LFT	1	C	0 - 2	SCD-D		
		(1.173)					

1.173 MeV

Abstract. Lifetimes of 49 excited states below 1.65 MeV have been measured in ^{24}Mg , ^{27}Al , ^{48}Ti , ^{58}Ni , ^{59}Co , $^{61,62}\text{Ni}$, $^{63,65}\text{Cu}$, $^{64,66,68}\text{Zn}$, ^{75}As , ^{103}Rh , $^{113,115}\text{In}$, $^{116,118,120}\text{Sn}$ and $^{121,123}\text{Sb}$ by means of nuclear resonance fluorescence experiments. The levels are excited by bremsstrahlung x-ray photons. The self-absorption technique applied to suitable cases provides nuclear absorption cross sections, widths and lifetimes from which the x-ray spectral distributions are also obtained. Scattering experiments are performed for all other cases in order to obtain widths and lifetimes from these x-ray photon curves. The Compton effect in the sample is taken into account. Self-absorption provides $g\Gamma_0$ from which Γ is deduced using adopted J^π and Γ_0/Γ values; scattering provides $u = g(\Gamma_0^2/\Gamma)W(\theta)$ from which Γ is also deduced with J , Γ_0/Γ and mixing ratios taken from the literature. Thanks to simultaneous determination of the x-ray spectra all the lifetimes as given by our programs with their statistical errors form an unusually coherent set of values.

NUCLEAR REACTIONS (γ , γ), bremsstrahlung excitation; natural isotopes: ^{24}Mg , ^{27}Al , ^{48}Ti , ^{58}Ni , ^{59}Co , $^{61,62}\text{Ni}$, $^{63,65}\text{Cu}$, $^{64,66,68}\text{Zn}$, ^{75}As , ^{103}Rh , $^{113,115}\text{In}$, $^{116,118,120}\text{Sn}$ and $^{121,123}\text{Sb}$; $E \approx 0.5\text{--}1.65$ MeV; measured $g\Gamma_0$ or $g(\Gamma_0^2/\Gamma)W(\theta)$; deduced $T_{1/2}$.

(OVER)

Tableau 3. Resultats des mesures des niveaux etudies par diffusion.

Table 3. Results obtained using the diffusion method.

Isotope	Energie (keV)	J^π	J_0^π	Γ_0/Γ	δ	$u = g(\Gamma_0^2/\Gamma)W(\theta)$ (meV)	r (ps) ce travail	r_{ref} (ps)	Références †
²⁴ Mg	1368,59(4)	2 ⁺	0 ⁺	1	E2	1,08(13)	1,76(21)	1,98(4)	Endt et van der Leun (1978)
²⁷ Al	1014,45(3)	$\frac{1}{2}^+$	$\frac{1}{2}^+$	0,971	+ 0,351(12)	0,186(13)	2,20(16)	2,12(8)	Endt et van der Leun (1978)
⁴⁶ Ti	983,512(3)	2 ⁺	0 ⁺	1	E2	0,282(23)	6,74(55)	6,1(13)	Been (1978)
⁵⁸ Ni	1454,45(15)	2 ⁺	0 ⁺	1	E2	2,11(26)	0,90(11)	0,92(3)	Kocher et Auble (1976)
⁵⁹ Co	1099,224(25)	$\frac{3}{2}^-$	$\frac{3}{2}^-$	1	(E2)	0,069(8)	4,79(55)	3,17(58)	Kim (1976)
⁵⁹ Co	1458,8(3)	$\frac{1}{2}^-$	$\frac{1}{2}^-$	0,91	(E2)	0,68(8)	1,17(14)	1,52(16)	Kim (1976)
⁵⁹ Co	1480,9(3)	$\frac{3}{2}^-$	$\frac{3}{2}^-$	0,8	< 0,35 ^a	1,23(15)	0,254(31)	0,31(3)	Kim (1976)
⁶¹ Ni	1185,7(6)	$\frac{1}{2}^-$	$\frac{1}{2}^-$	0,77(8) ⁱ	[0,14]	1,88(49)	0,21(5)	0,16(3)	Andreev et al (1974)
⁶² Ni	1172,91(9)	2 ⁺	0 ⁺	1	E2	0,88(17)	2,15(42)	2,09(3)	Halbert (1979a)
⁶³ Cu	1327,00(7)	$\frac{1}{2}^-$	$\frac{1}{2}^-$	0,84	(E2)	1,04(14)	0,84(11)	0,88(4)	Auble (1979b)
⁶³ Cu	1412,05(4)	$\frac{3}{2}^-$	$\frac{3}{2}^-$	0,72	+ 0,61 $\left\{ \begin{smallmatrix} -2 \\ -8 \end{smallmatrix} \right\}$	0,260(38)	1,90(28)	1,61(3)	Auble (1979b)
⁶⁴ Zn	991,54(7)	2 ⁺	0 ⁺	1	E2	0,640(54)	2,97(25)	2,60(13)	Halbert (1979b)
⁶⁵ Cu	1481,83(5)	$\frac{1}{2}^-$	$\frac{1}{2}^-$	0,85	(E2)	1,13(19)	0,79(13)	0,49(5)	Auble (1975a)
⁶⁶ Zn	1039,37(6)	2 ⁺	0 ⁺	1	E2	0,70(6)	2,71(23)	2,25(15)	Auble (1975b)
⁶⁸ Zn	1077,38(5)	2 ⁺	0 ⁺	1	E2	0,70(6)	2,71(23)	2,34(23)	Lewis (1975)
⁷⁵ As	572,5(10)	$\frac{1}{2}^-$	$\frac{1}{2}^-$	1 ^d	0,39 ^b	0,236(26)	4,14(46)	3,5(9)	Floren et Lewis (1975)
⁷⁵ As	823,0(10)	$\frac{1}{2}^-$	$\frac{1}{2}^-$	0,86 ^d	(E2)	0,214(22)	4,27(43)	3,5(3)	Robinson et al (1967)
⁷⁵ As	865,5(10)	$\frac{1}{2}^-$	$\frac{1}{2}^-$	0,83 ^d	— ^c	0,78(6)	0,863(68)	0,60(12)	Celliers et al (1977)
⁷⁵ As	1076,0(10)	$\frac{1}{2}^-$	$\frac{1}{2}^-$	0,94 ^d	0,38 ^d	1,97(13)	0,287(19)	0,32(7)	Celliers et al (1977)
⁷⁵ As	1128,5(10)	$\frac{1}{2}^-$	$\frac{1}{2}^-$	1	E1 ^d	0,224(24)	1,47(16)	—	
⁷⁵ As	1349,0(10)	$\frac{1}{2}^-$	$\frac{1}{2}^-$	0,67 ^d	0,20 ^d	1,61(29)	0,180(32)	0,12(3)	Wilson (1970)
⁷⁵ As	1370,0(10)	$\frac{1}{2}^-$	$\frac{1}{2}^-$	0,47 ^d	0,47 ^d	0,64(13)	0,218(44)	—	
¹⁰³ Rh	803,1(2)	$\frac{1}{2}^-$	$\frac{1}{2}^-$	0,70	M1	1,85(16)	0,174(15)	—	Harmatz (1979)
¹⁰³ Rh	1277,0(2)	$\frac{1}{2}^-$	$\frac{1}{2}^-$	0,75	— 0,62(30) ^e	0,81(9)	0,87(10)	1,3(9)	Harmatz (1979)
¹¹³ In	1177(1)	$\frac{1}{2}^-$	$\frac{1}{2}^-$	1	+ 0,5(2)	9,1(8)	0,086(8)	0,10(6)	Tuttle et al (1976)
¹¹³ In	1510(1)	$\frac{1}{2}^-$	$\frac{1}{2}^-$	0,935	— 0,5 $\left\{ \begin{smallmatrix} -2 \\ -8 \end{smallmatrix} \right\}$	6,4(9)	0,071(10)	0,11 $\left\{ \begin{smallmatrix} -2 \\ -8 \end{smallmatrix} \right\}$	Tuttle et al (1976)
¹¹³ In	1077,7(10)	$\frac{1}{2}^-$	$\frac{1}{2}^-$	0,81 ⁱ	(E2)	0,159(24)	1,61(24)	1,23(7)	Tuttle et al (1976)
¹¹³ In	1290,59(3)	$\frac{1}{2}^-$	$\frac{1}{2}^-$	0,98 ⁱ	(E2)	1,31(11)	0,66(6)	0,55(4)	Tuttle et al (1976)
¹¹⁵ In	1448,78(3)	$\frac{1}{2}^-$	$\frac{1}{2}^-$	0,86	— 8 ^f	0,90(11)	0,50(6)	0,52(20)	Tuttle et al (1976)
¹¹⁵ In	1486,1(1)	$\frac{1}{2}^-$	$\frac{1}{2}^-$	0,787	— 0,8 ^f	0,63(9)	0,63(9)	0,4(3)	Tuttle et al (1976)
¹¹⁵ In	1497,2(4)	($\frac{1}{2}^-$)	$\frac{1}{2}^-$	< 1	(E2)	1,33(16)	< 0,30(4)	—	
¹¹⁵ In	1607,8(15)	($\frac{1}{2}^-$)	$\frac{1}{2}^-$	≤ 1	(E2)	1,54(24)	≤ 0,26(4)	—	
¹¹⁶ Sn	1293,54(2)	2 ⁺	0 ⁺	1	E2	3,58(37)	0,53(6)	0,522(14)	Carlson et al (1975)
¹¹⁸ Sn	1229,64(4)	2 ⁺	0 ⁺	1	E2	2,75(28)	0,69(7)	0,67(2)	Carlson et al (1976)
¹²⁰ Sn	1171,6(2)	2 ⁺	0 ⁺	1	E2	1,83(16)	1,04(9)	0,91(2)	Kocher (1976)
¹²¹ Sb	1023,5(10)	$\frac{1}{2}^-$	$\frac{1}{2}^-$	1	[0,57] ^g	3,69(34)	0,228(21)	0,20(7) ^h	Tamura et al (1979)
¹²¹ Sb	1105,5(10)	$\frac{1}{2}^-$	$\frac{1}{2}^-$	0,4	—	0,47(4)	0,42(4)	—	
¹²¹ Sb	1142,5(10)	$\frac{1}{2}^-$	$\frac{1}{2}^-$	0,6	(E2)	0,85(8)	0,449(40)	0,41(8) ^h	Booth et al (1973)
¹²¹ Sb	1384,0(10)	$\frac{1}{2}^-$	$\frac{1}{2}^-$	1	[0,45] ^g	4,7(5)	0,092(10)	0,038(14) ^h	Booth et al (1973)
¹²³ Sb	1029,5(10)	$\frac{1}{2}^-$	$\frac{1}{2}^-$	1	[0,57] ^g	2,96(27)	0,272(25)	0,26(4) ^h	Booth et al (1973)
¹²³ Sb	1086,5(10)	$\frac{1}{2}^-$	$\frac{1}{2}^-$	1	[δ] > 1,26 ^g	1,06(9)	0,67(6)	0,72(15) ^h	Booth et al (1973)

† Références pour les colonnes 3, 4, 5, 6 et 9 de chaque ligne, sauf indication appelée au bas de ce tableau. Pour les autres données se reporter au texte.

Remarque. Pour calculer δ^2 quand nous ne disposons que de $B(E2)$, pour un mélange (E2) + (M1), nous déduisons $g\Gamma_0(E2) \propto B(E2)E_x^2$; en admettant $W(\theta) = 1$ et connaissant Γ_0/Γ , notre détermination de u donne une première approximation de $g\Gamma_0$ d'où une valeur de $\delta^2 = (g\Gamma_0(E2))/(g\Gamma_0 - g\Gamma_0(E2))$ qui permet d'améliorer $W(\theta)$ et $g\Gamma_0$ de proche en proche.

^a Swann (1971); ^b Robinson et al (1967); ^c $W(\theta) = 0,99$ calculé d'après la formule de Celliers et al (1977); ^d Abbondanno et al (1978); ^e Sayer et al (1972); ^f Tuttle et al (1976); ^g d'après $B(E2)$ de Barnes et al (1966); ^h calculé d'après Booth et al (1973); ⁱ Williams et al (1975); ^j Dietrich et al (1970).

Ni
A=64

Ni
A=64

Ni
A=64

REF. V. D. Afanas'ev, N. G. Afanas'ev, I. S. Gul'karov, G. A. Savitskii,
V. M. Khvastunov, N. G. Shevchenko and A. A. Khomich
Yad. Fiz. 10, 33 (1969)
Sov. J. Nucl. Phys. 10, 18 (1970)

ELEM. SYM.	A	Z
Ni	64	28
REF. NO.		69 Af 1
		egf

REACTION	RESULT	EXCITATION ENERGY	SOURCE		DETECTOR		ANGLE
			TYPE	RANGE	TYPE	RANGE	
E, E/	FMF	1, 4	D	150, 225	MAG-D		DST

1, 4 = 1.32, 3.55 MEV

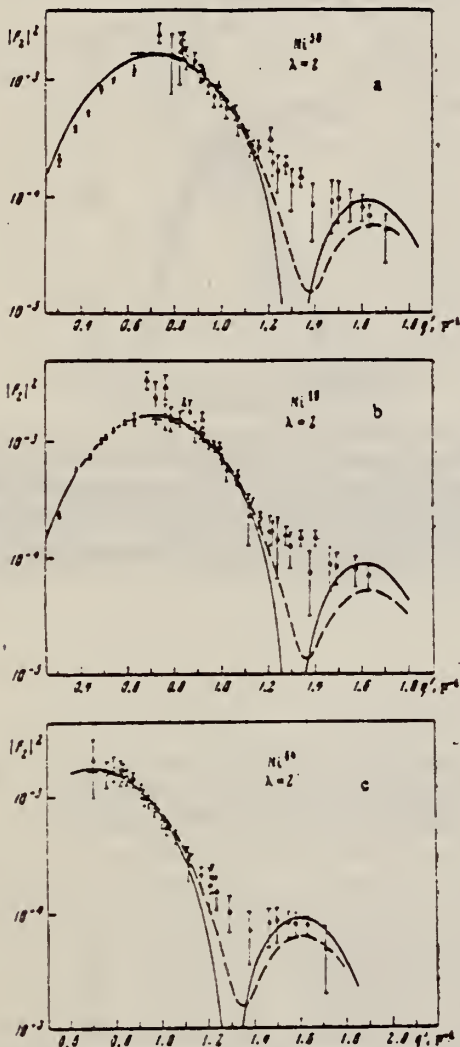


FIG. 2. Form factors for E2 transitions in nickel isotopes: a—Ni⁵⁸, b—Ni⁶⁰, c—Ni⁶⁴. Solid curves—Helm's model, dashed curves—high-energy approximation. Points: ○, ●—our data for 150 and 225 MeV, ▲—Stanford data [9], X—Yale data [10].

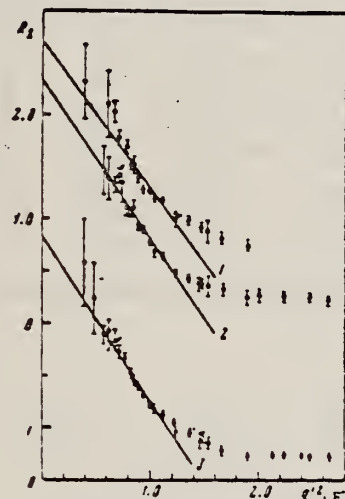


FIG. 3. R_λ as a function of q^2 for E2 transitions. Straight lines: 1—Ni⁵⁸ (the points and straight line are raised by 0.5), 2—Ni⁶⁰, 3—Ni⁶⁴ (the points and straight line are lowered by 1.0). Points: ○—150 MeV, ●—225 MeV.

Table II. Reduced probabilities of quadrupole transitions in the isotopes Ni^{58,60,64}

Isotope	E, MeV	J ^π	B(E2), efm ²				g ₁	Theory		Data of other authors	
			Helm's model	High-energy approximation	Model-independent method	Average		[1]	[2]	B(E2)	Reference
Ni ⁵⁸	1.45	2 ⁺	500 ± 50	544 ± 11	510 ± 62	554	8.4	340	200	800 630 657 600 525 + 750	[1] [2] [3] [4] [5]
Ni ⁶⁰	1.33	2 ⁺	603 ± 55	602 ± 41	606 ± 64	603	8.8	800	400	1100 910 845 1250 790 + 1280	[1] [2] [3] [4] [5]
Ni ⁶⁴	1.32	2 ⁺	650 ± 65	611 ± 53	640 ± 58	650	8.8	1430	690	870	[1]

[over]

Table III. Reduced probabilities of octupole transitions in the isotopes $Ni^{58,60,64}$

Isotope	E_i , MeV	J^π	$B(E3), e^2F^4$			Q_λ	Data of other authors	
			Helm's model	Model-independent method	Average		$B(E3)$	Reference
Ni^{58}	4.45	3^-	13800 ± 1450	13020 ± 780	13400	10	15 800 27 000 14 800	[10] [9] [10]
Ni^{60}	4.04	3^-	13300 ± 1800	13910 ± 830	13600	9	29 100 35 000 19 100	[10] [9] [10]
Ni^{64}	3.55	3^-	16000 ± 1800	17000 ± 1400	16500	9.4		

Table IV. Transition radii and parameters of the vibrational model of the nucleus for E2 and E3 transitions in $Ni^{58,60,64}$

Isotope	$J_i \rightarrow J_f$	R_{trans}		C_λ , MeV	$B\lambda$, MeV-sec \hbar^2	$B\lambda$, ($B\lambda$) _{h.d.}	R_λ^d
		Our result	(\hbar^2)				
Ni^{58}	0 \rightarrow 2	4.85 ± 0.21	5.51	173 ± 19	82 ± 9	20.0 ± 2.2	0.115 ± 0.008
	0 \rightarrow 3	5.13 ± 0.11	6.05	1520 ± 130	77 ± 8	17 ± 2	0.101 ± 0.006
	0 \rightarrow 2	4.92 ± 0.15	5.55	153 ± 17	88 ± 9	20 ± 2.2	0.118 ± 0.008
Ni^{60}	0 \rightarrow 3	5.24 ± 0.10	6.09	1500 ± 130	92 ± 8	18.5 ± 1.8	0.097 ± 0.005
	0 \rightarrow 2	4.99 ± 0.15	—	145 ± 10	83 ± 9	17.8 ± 1.9	0.150 ± 0.009
	0 \rightarrow 3	5.34 ± 0.11	—	1160 ± 130	92 ± 12	17.1 ± 2.2	0.103 ± 0.008

^d($B\lambda$)_{h.d.} is the oscillation parameter of the nucleus, obtained with a hydrodynamical model.

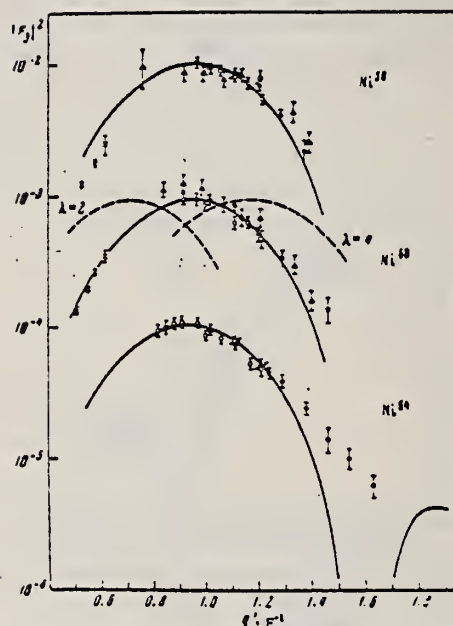


FIG. 4. Form factors for E3 transitions in the isotopes Ni^{58} (the experimental data and curve are multiplied by 10), Ni^{60} , Ni^{64} (the experimental data and curve are divided by 10). The solid curves represent the form factor calculated by Helm's model with $\lambda = 3$, and the dashed curves the form factor calculated by the same model for $\lambda = 2$ and $\lambda = 4$. Points: \circ and \otimes —our data for 150 and 225 MeV, Δ —Stanford data [9], \times —Yale data [10].

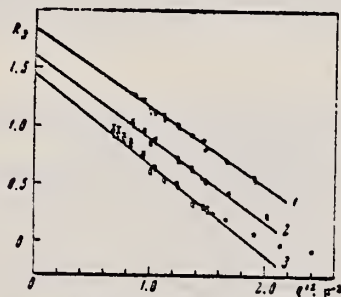


FIG. 5. Analysis of E3 transitions by the model-independent method. Straight lines: 1— Ni^{58} (the data and straight line have been raised by 0.5) 2— Ni^{60} , 3— Ni^{64} (the data and straight line have been lowered by 0.5). Points: \circ —150 MeV, \bullet —225 MeV.

I. S. Gul'karov, N. G. Afanas'ev, V. M. Khvastunov, N. G. Shevchenko, V. D. Afanas'ev, G. A. Savitskii, A. A. Khomich Yad. Fiz. 9, 478 (1969) Sov. J. Nucl. Phys. 9, 274 (1969)			ELEM. SYM.		A	Z
METHOD			Ni		64	28
			REF. NO.		69 Gu 1	
					hmg	
REACTION	RESULT	EXCITATION ENERGY	SOURCE		DETECTOR	
			TYPE	RANGE	TYPE	RANGE
E.E./	ABX	10-30	D	150	MAG-D	55
				(149.7)		

See paper for summary of other data.

FMF 148

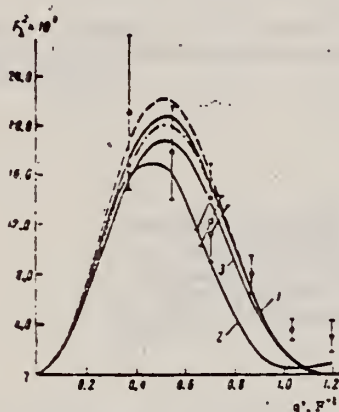


FIG. 2. Giant-resonance form factor as a function of momentum transfer. Points: O—data for Ni⁶⁰, X—for Ni⁶⁴, □—for Ni⁶⁸. The dashed curve, curve 1, and the dot-dash curve were calculated from formula (2) for the nuclei Ni^{60,64,68} respectively, with k = 19 MeV. Curve 3 was calculated from the same formula for Ni⁶⁰ with k = 21 MeV. Curve 2 is a calculation according to the Goldhaber-Teller collective model.

Table I. Absolute differential cross sections for inelastic scattering of electrons with excitation of the giant resonance in nickel isotopes

Nucleus	θ , deg	E_0 , MeV	q , F ⁻¹	q' , F ⁻¹	$d\sigma/d\Omega$, cm ² /sr	F^2 ($\times 10^{-3}$)
Ni ⁶⁰	20	198.7	0.745	0.346	$(2.62 \pm 0.70) \cdot 10^{-28}$	2.10 ± 0.63
	30	191.1	0.767	0.355	$(3.79 \pm 0.81) \cdot 10^{-28}$	1.78 ± 0.38
	50	197.6	0.612	0.703	$(7.50 \pm 1.55) \cdot 10^{-28}$	1.12 ± 0.23
	60	197.9	0.816	0.500	$(2.14 \pm 1.10) \cdot 10^{-28}$	0.80 ± 0.15
	90	199.1	0.970	1.020	$(5.39 \pm 1.03) \cdot 10^{-28}$	0.36 ± 0.08
Ni ⁶⁴	50	201.0	1.125	1.194	$(1.91 \pm 0.81) \cdot 10^{-28}$	0.31 ± 0.13
	90	198.9	0.925	0.706	$(6.98 \pm 1.55) \cdot 10^{-28}$	1.22 ± 0.20
Ni ⁶⁸	55	149.7	0.650	0.702	$(4.44 \pm 0.86) \cdot 10^{-28}$	1.43 ± 0.27

Note. The limits of integration of the spectra are from 10 to 30 MeV.

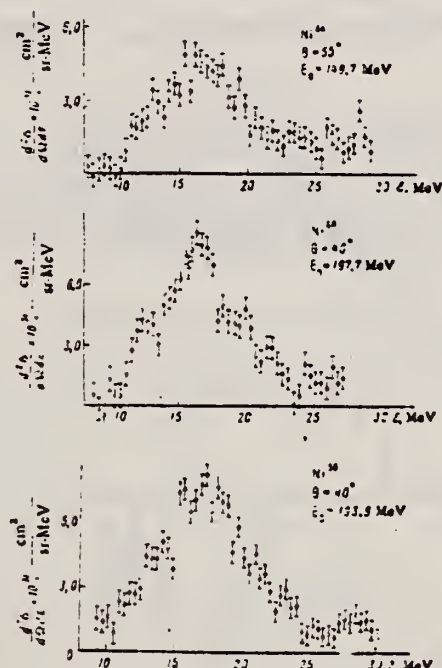


FIG. 3. Energy spectra of electrons inelastically scattered by the isotopes Ni^{60,64,68}. All three spectra were measured at the same value of momentum transfer.

REF.

B. S. Ratner
ZhETF Pis. Red. 13, 628 (1971)
JETP Letters 13, 447 (1971)

ELEM. SYM.

A

Z

Ni

64

28

METHOD

REF. NO.

71 Ra 1

hmg

REACTION	RESULT	EXCITATION ENERGY	SOURCE		DETECTOR		ANGLE
			TYPE	RANGE	TYPE	RANGE	
G,P	RLY	12-17	C	12-17	ACT-I		4PI

$$\sigma = 1 \times 10^{-29} \text{ cm}^2 \text{ at } 16.2 \text{ MeV.}$$

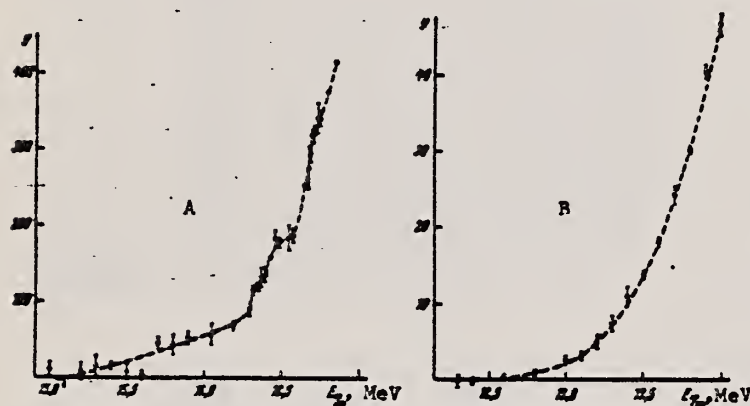


Fig. 1. Yield of reactions $\text{Ni}^{64}(\gamma, p)\text{Co}^{63}$ (A) and $\text{Cr}^{53}(\gamma, p)\text{U}^{52}$ (B) near the threshold, averaged over $E_{\gamma m}$ in the interval 10 - 100 keV

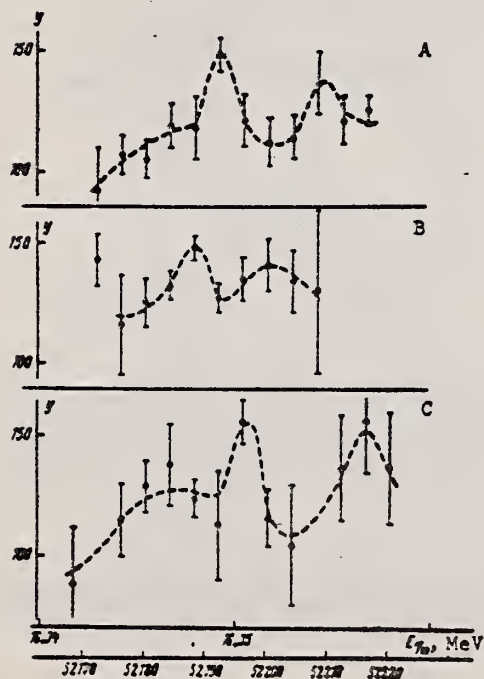


Fig. 2. Yield of reaction $\text{Ni}^{64}(\gamma, p)\text{Co}^{63}$ in the region $E_{\gamma m} = 16.35 \text{ MeV}$.

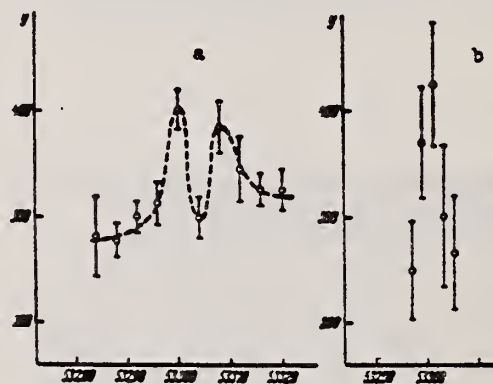


Fig. 3. Yield of reaction $\text{Ni}^{64}(\gamma, p)\text{Co}^{63}$ in the region $E_{\gamma m} = 16.70 \text{ MeV}$: a - summary data obtained during one month; b - results of one cycle of measurements.

REF. B. S. Ratner
Yad. Fiz. 21, 1147 (1975)
Sov. J. Nucl. Phys. 21, 590 (1976)

ELEM. SYM.	A	Z
Ni	64	28

METHOD

REF. NO.

75 Ra 2

hmg

REACTION	RESULT	EXCITATION ENERGY	SOURCE		DETECTOR		ANGLE
			TYPE	RANGE	TYPE	RANGE	
G, P	RLY	12- 17	C	15- 17	ACT-I		4PI

The yields of (γ, p) reactions on ^{62}Ni , ^{64}Ni , and ^{53}Cr are studied in ranges of $E_{\gamma\text{max}}$ near the respective thresholds. Considerable differences are found between the curve shapes, yields, and observed thresholds for the Ni isotopes and ^{53}Cr .

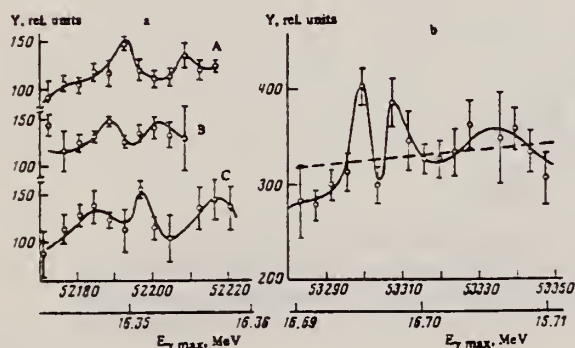


FIG. 5. Yield of $^{64}\text{Ni}(\gamma, p)^{63}\text{Co}$ in the region of $E_{\gamma\text{max}} = 16.35$ MeV (a); yield of $^{64}\text{Ni}(\gamma, p)^{63}\text{Co}$ in the region of $E_{\gamma\text{max}} = 16.70$ MeV (b).

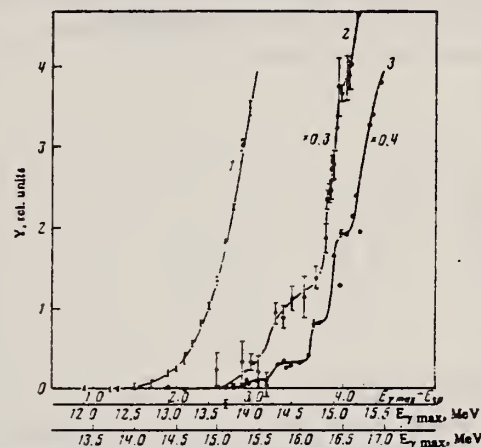


FIG. 3. Yields of the reactions $^{53}\text{Cr}(\gamma, p)^{52}\text{V}$ (curve 1), $^{64}\text{Ni}(\gamma, p)^{63}\text{Co}$ (curve 2), and $^{62}\text{Ni}(\gamma, p)^{61}\text{Co}$ (curve 3) as functions of $E_{\gamma\text{max}}$. Lowest scale for $^{64}\text{Ni}(\gamma, p)$; middle scale for $^{62}\text{Ni}(\gamma, p)$ and $^{53}\text{Cr}(\gamma, p)$.

ELEM. SYM.	A	Z
Ni	64	28
REF. NO.		hg
80 Ar 11		

REACTION	RESULT	EXCITATION ENERGY	SOURCE		DETECTOR		ANGLE
			TYPE	RANGE	TYPE	RANGE	
G,SPL	ABY	THR-999	C	999	ACT-I		4PI

New data are presented on the photodisintegration of the enriched isotopes ^{58}Ni and ^{64}Ni under bombardment by photons with maximum energy 4.5 GeV. The isotope effect in photonuclear reactions with formation of residual nuclei is investigated. The experimental yield values are compared with theoretical calculations by Rudstam's formula. In the results we observe a systematic shift of the experimental disintegration yields in comparison to the calculated values. An exponential dependence is found for the ratios of the yields of the residual nuclei from the ^{58}Ni target to the yields of the same nuclei from ^{64}Ni as a function of the third projection of the isotopic spin of the product nucleus, and an exponential dependence is found for the ratios of the experimental yield values to the theoretical values as a function of the difference of the third projections of the isotopic spins of the target nuclei and the residual nuclei.

999=4.5 GEV

PACS numbers: 25.20. + y, 27.50. + e

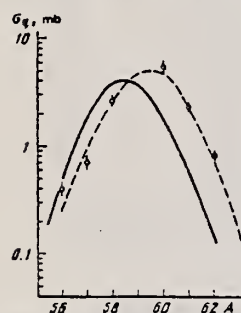


FIG. 1. Distributions of independent yields of Co residual nuclei in mass number. The solid curve is a calculation with Eq. (1), and the dashed curve has been drawn from the experimental points.

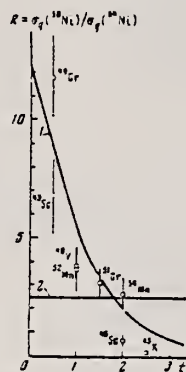


FIG. 3. Ratio of yields of identical residual nuclei from two isotopes of the target nuclei as a function of the third projection of the isotopic spins of the residual nuclei. Curve 1 is the function $15 \exp(-t_3)$, and curve 2 is calculated with Eq. (1).

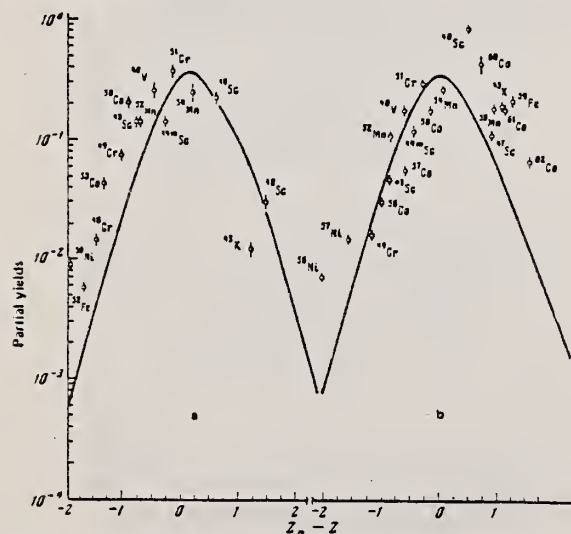


FIG. 2. Charge-dispersion curves of residual nuclei from targets of ^{58}Ni (a) and ^{64}Ni (b).

(OVER)

TABLE II.

Residual nucleus	^{60}Ni target			^{60}Ni target			Type of yield	t_3
	σ_{exp} , mb	σ_{theo} , mb	$\frac{\sigma_{\text{exp}}}{\sigma_{\text{theo}}}$	σ_{exp} , mb	σ_{theo} , mb	$\frac{\sigma_{\text{exp}}}{\sigma_{\text{theo}}}$		
^{60}Zn	0.84 ± 0.04	0.152	5.46				I	4
^{60}Ga	2.31 ± 0.15	0.5622	4.16				C	3.5
^{60}Ge	5.5 ± 1	1.6247	3.38				I	3
^{60}Co	2.6 ± 0.3	3.937	0.65	0.146 ± 0.02			I	2
^{60}Ni	1.0 ± 0.1	1.672	0.604	16.5 ± 1	4.966	9.35	C	1.5
^{60}Cu	0.50 ± 0.04	0.5676	1.25	8.1 ± 1.4	1.2965	0.255	C	1
^{60}Zn	-	0.098	-	1.7 ± 0.1	0.2497	6.81	C	0.5
^{60}Ni	0.27 ± 0.03	0.0971	2.987	17.2 ± 1	0.251	68.1	I	1
^{60}Ni	0.15 ± 0.03	0.01528	9.816	0.5 ± 0.03	0.0358	13.97	I	0
^{60}Fe	1.3 ± 0.2	0.2625	6.85	-	-	-	I	3.5
^{60}Fe	-	0.016788	-	0.133 ± 0.01	0.0383	3.52	I	0
^{60}Mn	1 ± 0.5	0.5075	2.153	-	-	-	C	3
^{60}Mn	1.6 ± 0.2	1.706	0.89	3.8 ± 0.4	5.23	0.7267	I	2
^{60}Mn	0.47 ± 0.04	0.3916	1.71	1.36 ± 0.1	1.042	2.12	C	1
^{60}Mn	0.2 ± 0.03			0.85 ± 0.07				
^{60}Cr	1.1 ± 0.1	0.942	1.1877	3.45 ± 0.3	2.5077	1.33	C	1.5
^{60}Cr	0.063 ± 0.006	0.087	0.721	0.67 ± 0.03	0.211	3.175	C	0.5
^{60}Cr	-	0.0167	-	0.13 ± 0.01	0.037	3.513	C	0
^{60}V	0.45 ± 0.04	0.2953	1.524	1.7 ± 0.15	0.7516	2.28	C	1
^{60}Se	-	0.0233	-	0.07 ± 0.02	0.0524	1.336	I	3
^{60}Se	0.44 ± 0.03	0.078987	1.772	-	0.187	-	C	2.5
^{60}Se	0.91 ± 0.09	0.2004	4.54	0.53 ± 0.05	0.493	1.075	I	2
^{60}Se	0.13 ± 0.02	0.2008	-	0.32 ± 0.03	0.480	-	I	1
^{60}Se	0.053 ± 0.005	0.0631	0.8399	0.32 ± 0.05	0.143	2.24	C	0.5
^{60}K	0.09 ± 0.009	0.0209	4.306	0.011	0.015	0.24	I	2.5

Note. σ_{exp} and σ_{theo} are respectively the experimental and theoretical yield values; t_3 is the third projection of the isospins.

COPPER

Z=29

Copper was probably discovered about 8000 B.C. by Neolithic man during the late stone age. Crude hammers, knives, and other utensils were created from this malleable metal. The early age of copper had its greatest development in Egypt where records show that mining, extracting, and refining of copper was done on the Sinai peninsula. Copper was produced extensively about 3000 B.C. on the island of Cyprus and supplied most of the Roman needs for the metal. The ore was known as *aes cyprium* (ore of cyprus), this was shortened to *cyprium* and later corrupted to *cuprum*. From this comes the English name copper.

Cu

REF.

J. L. Burkhardt
Phys. Rev. 100, 192 (1955)

ELEM. SYM.

A

Z

Cu

29

METHOD

REF. NO.

55 Bu 1

JOC

REACTION	RESULT	EXCITATION ENERGY	SOURCE		DETECTOR		ANGLE
			TYPE	RANGE	TYPE	RANGE	
G.G	RLX	0 - 3	C	3	NAI-D		90

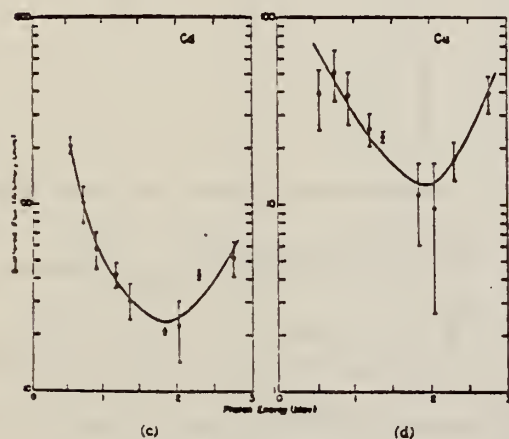
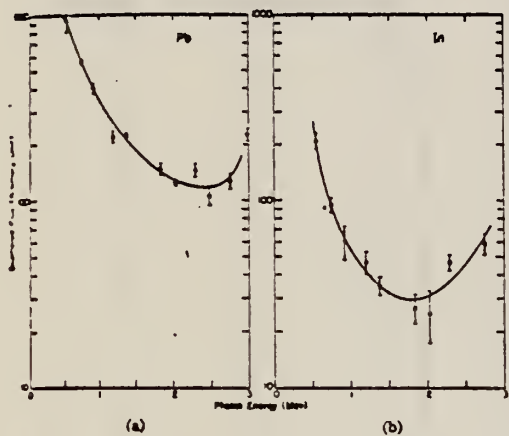


FIG. 3. Scattered photon flux.

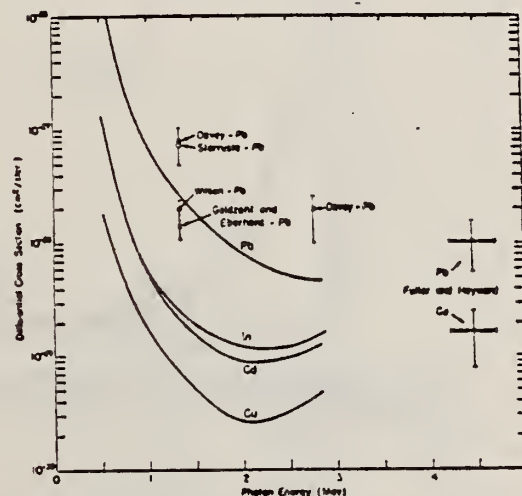


FIG. 4. Differential photon scattering cross sections at 90°. The points shown on the graph are taken from references 3, 5, 7, 8, and 22.

Ref. W.R. Dixon
Can. J. Phys. 33, 785 (1955)

Elem. Sym.	A	Z
Cu		29

Method Synchrotron; neutron spectrum, angular distribution; nuclear emulsion; scintillator; ion chamber

Ref. No.	
55 Di 1	NVB

Reaction	E or ΔE	E_0	Γ	$\int \sigma dE$	$J\pi$	Notes
Cu(γ, xn)	70					Used scintillator for angular distributions. Curves fitted to $a + b \sin^2 \theta$
Cu(γ, xn)		$E_n =$ 0.5-14				Used emulsion for spectra

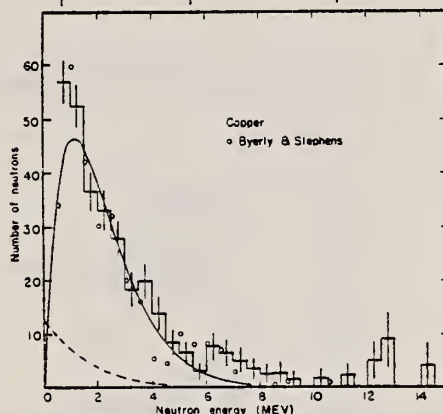


FIG. 4. The energy distribution of photoneutrons from copper. The histogram represents the present results, and the circles the results of Byerly and Stephens. The solid and dashed curves are calculated for the evaporation of first and second neutrons, respectively, their sum being normalized to the histogram.

TABLE II
EXPERIMENTAL VALUES FOR b/a

Target	Correction factor for self-scattering	Corrected b/a
Lead	1.10	-0.08 ± 0.08
Tin	1.08	0.12 ± 0.17
Copper	1.48	0.23 ± 0.15
Iron	1.35	0.09 ± 0.25
Aluminum	1.17	0.36 ± 0.29
Carbon	1.8	1.6 ± 0.8
Beryllium (1)	2.6	
Beryllium (2)	1.35	1.2 ± 0.4

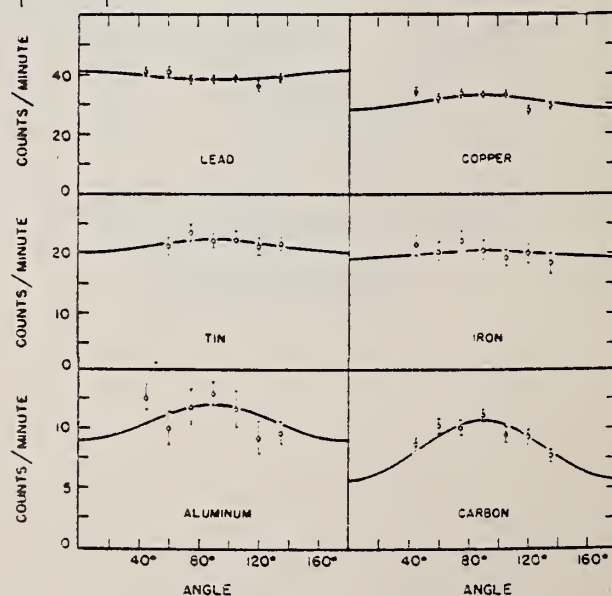


FIG. 2. The angular distributions of photoneutrons as measured with the zinc sulphide lucite detector

Elem. Sym.	A	Z
Cu		29

Method $\text{Li}(p, \gamma)$ source; nuclear emulsions; G-M counter; $\text{Cu}^{63}(\gamma, n)$ reaction; flux calibration.

Ref. No.
55 D2 1
EGF

Reaction	E or ΔE	E_0	Γ	$\int \sigma dE$	$J\pi$	Notes
$\text{Cu}(\gamma, p)$	17.5					<p>Monitor in terms of counts on G-M counter which had been calibrated in terms of $\text{Cu}^{63}(\gamma, n)\text{Cu}^{62}$ (absolute counting and effective $\sigma \text{ Li} = 7.75 \times 10^{-26} \pm 15\% \text{ cm}^2$ given by Shimigu: [Mem. of Un. Kyoto <u>25</u>, 194 (1949)]).</p> <p>Plates used to detect protons $\text{Li } \sigma = (7 \pm 4) 10^{-26} \text{ cm}^2$</p>

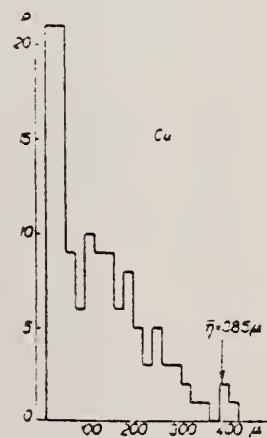


FIG. 3.

Elem. Sym.	A	Z
Cu		29

Method	Ref. No.	
Synchrotron; neutron spectrum; nuclear emulsion	55 Li 1	NVB

Reaction	E or ΔE	E_0	Γ	$\int \sigma dE$	$J\pi$	Notes
Cu(γ , xn)	Bremss. 70					Temperature = 1.2 MeV

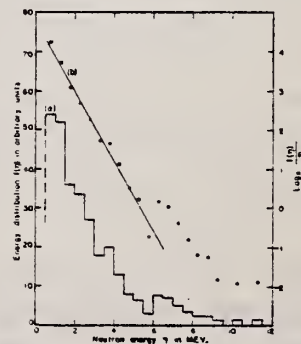


Fig. 1. Energy distribution of photoneutrons emitted from copper exposed to 70 MeV bremsstrahlung. (a) Histogram based on 1000 tracks in nuclear emulsions. (b) Plot of $\log_{10}(N/E^2)$ against neutron energy.

REF.	ELEM. SYM.	A	Z
K. G. McNeill Phil. Mag. <u>46</u> , 321 (1955)	Cu		29
METHOD	REF. NO.		
	55 Mc 1		EGF

REACTION	RESULT	EXCITATION ENERGY	SOURCE		DETECTOR		ANGLE
			TYPE	RANGE	TYPE	RANGE	
G,XN	RLY	THR - 22	C	22	NAI-I		90


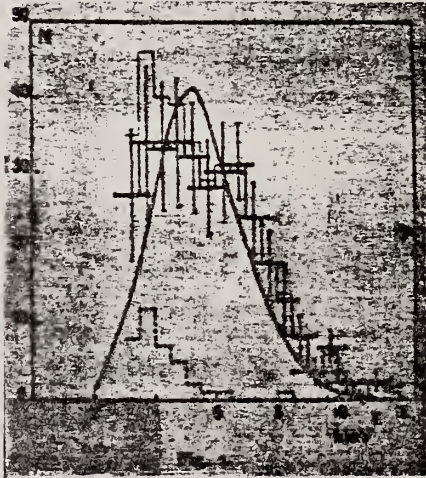
Target element	Counts in 30 minutes per 1000 monitor counts	22 mev yield mol/r relative to copper	Yield, mol/r $\times 10^{-6}$
Cu	288 ± 15	1.0	3.2
Cd	647 ± 28	4.1 ± 0.3	13
Hg	661 ± 26	9.5 ± 0.9	30
Pb	470 ± 17	8.4 ± 0.5	27

Ref. R. Chastel
 Compt. Rend. 242, 1440 (1956); Compt. Rend. 242, 2337 (1956);
 J. Phys. Rad. 17, 518 (1956)

Elem. Sym.	A	Z
Cu		29

Method plates; Li γ 's.

Ref. No.	EGF
56 Ch 1	

Reaction	E or ΔE	E_0	Γ	$\int \sigma dE$	$J\pi$	Notes
Cu(γ ,p)	17.6					
	14.8					
<div style="display: flex; justify-content: space-around; align-items: flex-end;"> <div style="text-align: center;">  <p>Fig. 1. — Spectre des photoprotons de cuivre produits par les rayons γ de 17,6 et 14,8 MeV (rayons γ de : ^{214}Pb, γ); ^{214}Po. Émission de rayons α d'épaisseur. Courbe théorique : $I(\epsilon) d\epsilon = \text{const.} \cdot e^{-\epsilon} \exp\left[-\frac{\epsilon}{\theta(\epsilon_p)}\right] d\epsilon$ avec $\theta = 3 \text{ MeV}$.</p> </div> <div style="text-align: center;">  <p>Fig. 2. — Spectre des photoprotons de cuivre produits par les rayons γ de 17,6 et 14,8 MeV (rayons γ de : ^{214}Pb, γ); ^{214}Po. — Distribution statistique brute des protons sans cuivre. — Fond des neutrons dans la zone sans cuivre. — Distribution statistique des énergies de photoprotons après soustraction du fond. Émission de rayons α d'épaisseur.</p> </div> </div>						

Ref. W.K. Dawson
Can. J. Phys. 34, 1480 (1956)

Elem. Sym.	A	Z
Cu		29
Ref. No.		NVB
56 Da 2		

Method Synchrotron; proton yield, spectrum; angular distribution;
nuclear emulsion; ion chamber

Reaction	E or ΔE	E_0	Γ	$\int \sigma dE$	$J\pi$	Notes
Cu(γ ,xp)	70					Yield = 10.0×10^5 protons (up to 15 MeV)/r-mole $\pm 30\%$ for 70 MeV Bremss.
<div data-bbox="360 1323 736 1764" data-label="Figure"> </div> <div data-bbox="925 1407 1458 1743" data-label="Figure"> </div>						

FIG. 7. The angular distributions of photoprotons of various energies from copper. Standard deviations are shown.

REF.

B. Forkman
Arkiv Fysik 11, 265-75 (1956)

ELEM. SYM.

A

Z

Cu

29

METHOD

Synchrotron; ion chamber

REF. NO.

56 Fo 1

NVB

REACTION	RESULT	EXCITATION ENERGY	SOURCE		DETECTOR		ANGLE
			TYPE	RANGE	TYPE	RANGE	
1) G,D	RLY	THR-30	C	30	EMU-D		90
2) G,P.	RLY	THR-30	C	30	EMU-D		90

$$\frac{Y(\gamma, d)}{Y(\gamma, p)} = 0.16$$

1) YLD REL TO G,P2) YLD REL TO G,D

Elem. Sym.	A	Z
Cu		29
Ref. No.	56 Fu 1	
	NVB	

Method Betatron; photon scattering; NaI spectrometer

Reaction	E or ΔE	E_0	Γ	$\int \sigma dE$	$J\pi$	Notes
Cu(γ, γ)	Bremss. 4-40					<p>Detector at 120°.</p> <p>Cross sections given here are 13% too high due to erroneous $\cos \theta$ factor in denominator of Eq. 5. [See footnote 8 in Phys. Rev. <u>106</u>, 993 (1957)].</p>

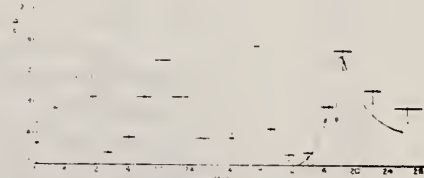


FIG. 5. The elastic scattering cross sections for Ni and Cu. The point at 17.6 Mev is that of Stearns.⁸ The solid curve superimposed on the Cu data is the scattering cross section calculated from the dispersion relation by substituting for $\sigma_e(E)$ in Eq. (7) the γ, γ cross section⁷ multiplied by the ratio of the total particle yield to the neutron yield.⁸ The open circles on the vertical axes indicate the magnitude of the Thomson cross section for Z free protons scattering coherently.

B. I. Gavrilov, L.E. Lazareva
 Zhur. Eksp. i Teoret. Fiz. 30, 855 (1956);
 Soviet Phys. JETP 3, 871 (1957)

Elem. Sym.	A	Z
Cu		29

Method γ -Bremsstrahlung; synchrotron; BF_3 counter

Ref. No.	EGF
56 Ga 1	

Reaction	E or ΔE	E_0	Γ	$\int \sigma dE$	$J\pi$	Notes
----------	-----------------	-------	----------	------------------	--------	-------

570

(γ, xn)	$\sim 18-27$	17.2	4.3	93 MeV-b		
----------------	--------------	------	-----	----------	--	--

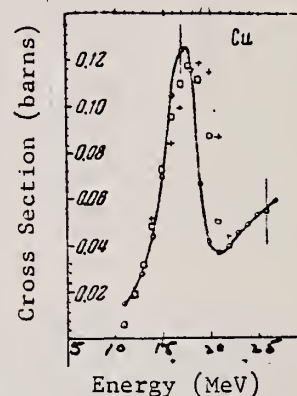


Figure 2: Photoneutron cross section σ_n , computed from the yield curves by the "photon difference method."
 "+" -- cross sections obtained in Ref. 8 [Montalbetti, Katz and Goldemberg, Phys. Rev. 91, 659 (1959)];
 "x" -- cross section of the reaction (γ, n) for copper, obtained by summation of the cross sections of the (γ, n) reaction for Cu^{63} and Cu^{65} (with account taken of isotopic composition) measured in Ref. 6 [Katz and Cameron, Canad. J. Phys. 29, 518 (1951)].

TABLE I. Fundamental characteristics of photoneutron cross sections.

Element	$E_{\sigma_n \text{ max}}$ in mev	$\sigma_n \text{ max}$ in barns	Half width in mev	$\int_{E_0}^{E_{\sigma_n \text{ max}}} \sigma_n(E) dE$ in mev-barns	$\int_{E_0}^{E_{\sigma_n \text{ max}}} \sigma_n(E) dE / \sigma_n \text{ max}$
Copper	17.2	0.128	4.3	0.93	7.4
Zinc	16.3	0.082	4.2	0.86	6.1
Cadmium	16.0	0.270	8.4	2.28	8.4
Iodine	15.5	0.288	6.0	2.35	8.2
Tellurium	14.5	0.452	6.8	3.37	8.6
Gold	14.2	0.571	8.0	4.37	7.6
Thallium	14.6	0.655	5.4	4.90	7.8
Bismuth	13.9	0.537	5.9	3.98	7.4
Thorium	14.5	0.798	5.6	6.33	8.0
Uranium	14.9	1.18	6.8	12.5	10.8

Method Li (p, γ) source, 480 kev protons.

Ref. No.	
56 Ha 1	EGF

Reaction	E or ΔE	E_0	Γ	$\int \sigma dE$	$J\pi$	Notes
(γ, xn)	14.8 17.6					Average Li cross section is <u>64</u> mb; cross section with detector response weighted for low energy neutrons, <u>61</u> mb. Assumed ratio 17.6/14.8 = 1.7. <u>46</u> Calculated cross section at 14.8 and 17.6 MeV assuming cross section curves measured at Pennsylvania and Saskatchewan (refer Table I).

TABLE I. Cross sections for photoneutron emission induced by the lithium gamma rays. The results are compared with previous data.

Element	Present cross-section data		Data of McDaniel et al. ^a	Betatron data					
	Counter Group A	Counter Group B		Pennsylvania		Saskatchewan		$\sigma_{14.8}^b$	$\sigma_{17.6}^b$
				$\sigma_{14.8}^b$	$\sigma_{17.6}^b$	$\sigma_{14.8}^b$	$\sigma_{17.6}^b$		
⁵⁴ Fe	38 mb	33 mb	37 mb	60 ^c mb	0.5	60 ^d mb	0.5	23 mb	47 mb
⁵⁸ Co	49	49	47			95 ^d	0.5	30	60
⁵⁸ Ni	23	25	23			40 ^e	0.7	22	32
⁶³ Cu	64	61	55 ± 12			95 ^d	0.6	45	75
⁶⁶ Zn	48	45	48			90 ^d	0.7	38	54
⁶⁷ Ag	175	170	135			240 ^d	1.0	17 ^f	17 ^f
¹¹⁶ Sn	200	190	180						
¹⁸¹ Ta	355	360	260	350 ^d	1.3	420 ^e	2.3	420 ⁱ	320 ^j
¹⁸⁷ W	365	355	325					550 ^j	240 ^j
¹⁹⁷ Au	330	295		315 ^e	1.7	480 ^d	1.9	460	255
²⁰³ Hg	365	340	290						
²⁰⁸ Pb	310	295	250	320 ^e	1.6	440 ^d	2.5	400 ⁱ	250 ^j
²¹⁴ Bi	305	280	250	270 ^d	2.6	550 ^d	2.4	490	195

^a See reference 3.

^b Average of 14.8- and 17.6-Mev cross sections weighted with relative intensities of the lithium gamma-ray lines.

^c See reference 24.

^d R. Nathans, Ph.D. thesis, University of Pennsylvania, 1954 (unpublished).

^e J. Halpern (private communication).

^f See reference 23.

^g See reference 32.

^h Separate cross sections at 14.8 and 17.6 Mev as obtained from Group A data and 14.8/17.6 betatron cross-section ratios.

ⁱ Obtained using 14.8/17.6 cross-section ratio from Pennsylvania betatron data.

^j Obtained using 14.8/17.6 cross-section ratio from Saskatchewan betatron data.

F. Heinrich and H. Waffler
 Helv. Phys. Acta 29, 232 (1956)

Cu

29

METHOD

REF. NO.

56 He 1

EGF

REACTION	RESULT	EXCITATION ENERGY	SOURCE		DETECTOR		ANGLE
			TYPE	RANGE	TYPE	RANGE	
G,T	RLY	THR-31	C	31	ACT-I		4PI

Yields relative to (G,N) yields.

Tabelle 1.

Experimentelle und theoretische nukleare Ausbeute der (γ, T)-Prozesse.

Element	$\eta_{\text{exp}} \times 10^3$	$\eta_{\text{theor}} \times 10^3$
Al	240 ± 14	200
Co	$6 \pm 1,7$	4
Cu	$4,5 \pm 1,5$	3

Ref. E. Lejkin, R. Osokina, B. Ratner
 Il Nuovo Cimento 2 Suppl. 1, 105 (1956)

Elem. Sym.	A	Z
Cu		29

Method 30.5 MeV Bremss. synchrotron; emulsions; ion chamber monitor

Ref. No.	EGF
56 Le 1	

Reaction	E or ΔE	E_0	Γ	$\int \sigma dE$	$J \pi$	Notes
(γ, p)	Bremss.					Assume Halpern and Mann's [Phys. Rev. <u>83</u> , 370 (1951)] shape for $\sigma(\gamma, p)$ and calculate $\sigma(\gamma, p)$ at peak = $4.0 \times 10^{-26} \text{ cm}^2 \pm 30\%$.
	19.0					
	24.0					
	28.0					
	30.5					

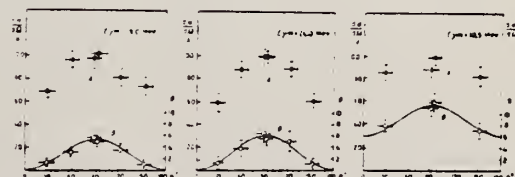


Fig. 4. - Angular distribution of photoprotons from copper. $d\sigma/d\Omega$, relative cross-section: A, for $r_0 \approx 3$ MeV protons; B, for $r_0 \approx 10$ MeV protons. The cross-section for the angle $\theta = 92^\circ$ is taken equal to 100. Smooth curves correspond to a distribution $\sin^2 \theta$ (19.0 and 24.0 MeV) and $\alpha - \beta \sin^2 \theta$ (30.5 MeV).

H. Waffler and F. Heinrich
Physica 22, 1146 (1956)

Cu

29

METHOD

REF. NO.

56 Wa 1

EGF

REACTION	RESULT	EXCITATION ENERGY	SOURCE		DETECTOR		ANGLE
			TYPE	RANGE	TYPE	RANGE	
G,T	RLY	THR - 31	C	31	ACT-I		4PI

Detected activity of tritium. Yields are relative to $^{63}\text{Cu}(\gamma, n)$.

Reaction	Threshold energy MeV	$\eta_{\text{exp}} \times 10^5$	$\eta_{\text{theor}} \times 10^5$
Al	18.2 ± 0.2	34 ± 2	31
Co	16.5 ± 0.3	7 ± 2	5
^{63}Cu	16.2 ± 0.3	6 ± 2	4
^{65}Cu	15.1 ± 0.3		
^{107}Ag	13.9 ± 0.6	6.5 ± 1	0.4
^{109}Ag	13.1 ± 0.6		

The table shows the calculated yield ratios (according to statistical theory) as well as the measured relative yield

$$\eta = \int_0^{31 \text{ MeV}} N(E_\gamma) \sigma^{(x)}(\gamma, t) E_\gamma dE_\gamma / \int_0^{31 \text{ MeV}} N(E_\gamma) \sigma^{(63\text{Cu})}(\gamma, t) E_\gamma dE_\gamma$$

taking the (γ, n) yield on ^{63}Cu as unity. The good agreement between the experimental

J. B. Bellicard, J. Miller and C. Tzara
J. Phys. Radium 18, 201 (1957)

Cu

29

METHOD

REF. NO.

57 Be 1

EGF

REACTION	RESULT	EXCITATION ENERGY	SOURCE		DETECTOR		ANGLE
			TYPE	RANGE	TYPE	RANGE	
G ₂ G	ABX	13 - 21	C	18 - 22	ACT-I		90

Used activity induced in Cu to detect photons scattered by Cu.

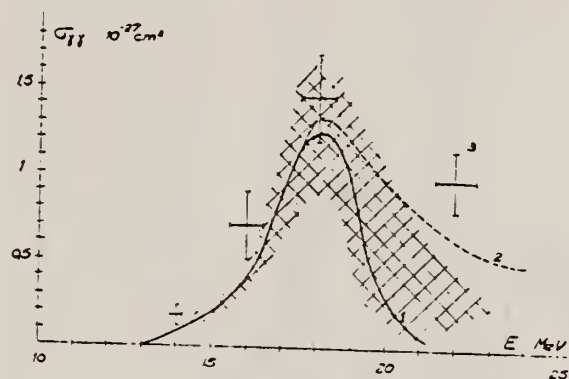


FIG. 3. — Courbe 1 : section efficace.
En grisé : zone d'imprécision.
Courbe 2 : section efficace déduite de la relation de dispersion.
Points 3 : résultats de Fuller et Hayward.

REF.

F. Bobard, G. Boulegue, and P. Chanson
Compt. Rend. 244, 1761 (1957)

ELEM. SYM.

A

Z

Cu

29

METHOD

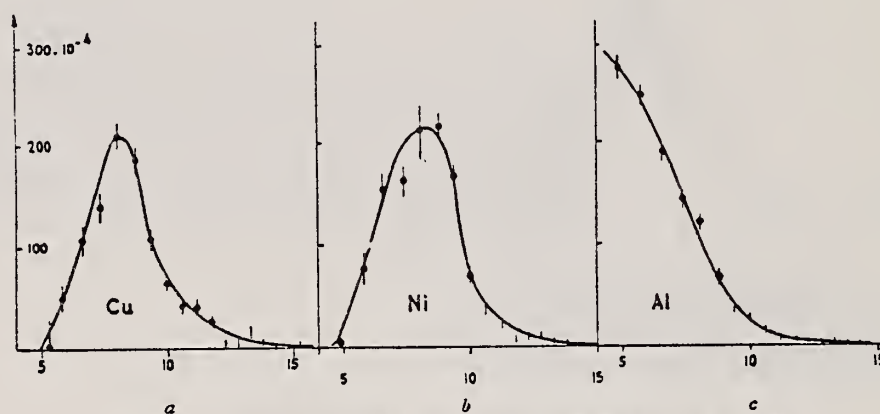
REF. NO.

57 Bo 1

EGF

REACTION	RESULT	EXCITATION ENERGY	SOURCE		DETECTOR		ANGLE
			TYPE	RANGE	TYPE	RANGE	
G,A	SPC	THR - 30	C	31	EMU-D	5-15	DST

Yield per milligram per roentgen Cu 0.86, Ni 0.99, Al 1.15 for 30.5 MeV bremsstrahlung.

Fig. 2. — Nombre de particules n /mg/stéradian/Röntgen/intervalle de : MeV.

Elem. Sym.	A	Z
Cu		29
Ref. No. 57 Fe 1		
EGF		

Method 31 MeV betatron; neutron yield; angular distribution; threshold
detector, Si²⁸(n,p)Al²⁷ reaction.

Reaction	E or ΔE	E ₀	Γ	∫σdE	Jπ	Notes
Cu(γ,n')	Bremss. 15-31					Data not clear but probably normalized at 30 MeV.

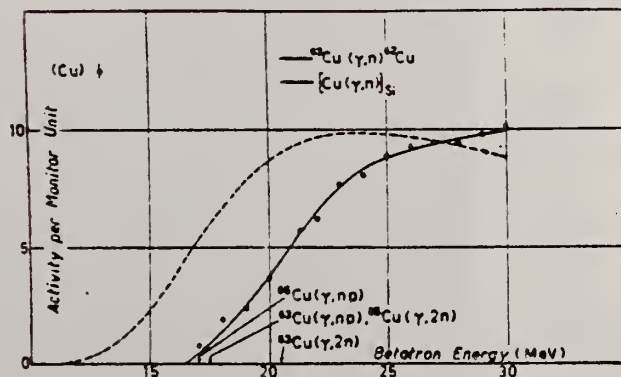


Fig. 5.

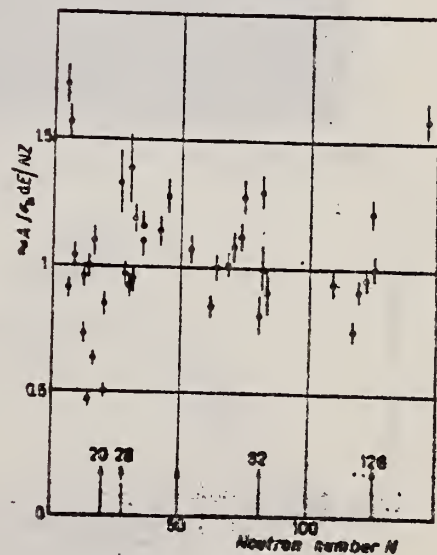


Fig. 9.

Method Betatron; angular distribution; scintillator; ionization chamber

Ref. No.	
58 As 1	EH

Reaction	E or ΔE	E_0	Γ	$\int \sigma dE$	$J\pi$	Notes
Cu(γ, n)	Bremss. 17					Angular distribution is of form, $a + b \sin^2 \theta$ where $b/a = 0.17 \pm 0.06$

Fig. 6. The angular distributions of photoneutrons as measured with Emmerich button type scintillation detector

Energy	Al	Target Cu	nucleus Pb	Be	Detector
Present (17 Mev)	1.6 ± 0.8	0.17 ± 0.06	0.30 ± 0.11	1.29 ± 0.53	Emmerich ^a
Dixon (70 Mev)	0.36 ± 0.29	0.23 ± 0.15	uniform	1.2 ± 0.4	Hornyak ^b
Halpern (70 Mev)				1.26 ± 0.11	Emmerich ^a
Price (22 Mev)		0.33	0.84	uniform	Al n, p ^c
Johanson (65 Mev)	1		0.8	1.5	Hornyak ^b

a) A scintillation detector with a ZnS-paraffin-Lucite light guide
b) A scintillation detector with a ZnS-Lucite
c) A fast neutron detector by measuring the beta activity of $Al^{27} n, p; Mg^{24}$ reaction.

References

- 1) E. D. Courant: Phys. Rev. **82** (1951) 703.
- 2) S. A. E. Johanson: Phys. Rev. **97** (1955) 434.
- 3) W. R. Dixon: Can. J. Phys. **33** (1956) 785.
- 4) G. A. Price: Phys. Rev. **93** (1954) 1269

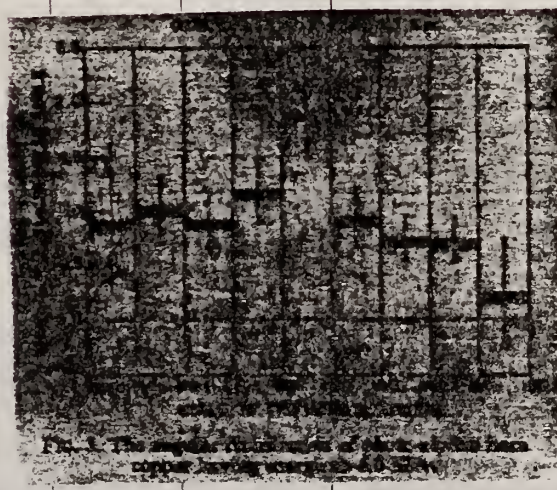
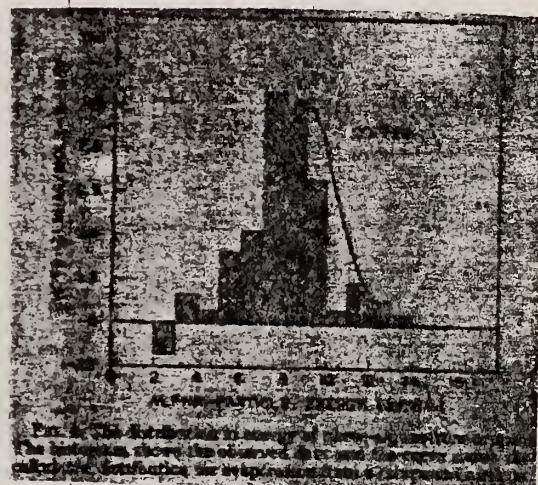
Ref. M.E. Toms, J. McElhinney
Phys. Rev. 111, 561 (1958)

Elem. Sym.	A	Z
Cu		29

Method Betatron; alpha spectrum, angular distribution; nuclear emulsion

Ref. No.	
58 To 2	NVB

Reaction	E or ΔE	E_0	Γ	$\int \sigma dE$	$J\pi$	Notes
Cu(γ, α)	Bremss. 22					Yield = 2.6×10^4 alpha/mole/roentgen

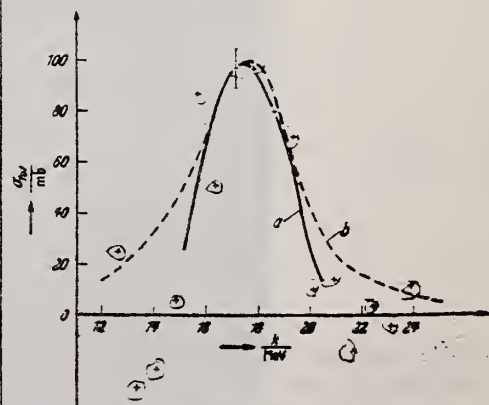


Ref. B. Ziegler
Z. Physik 152, 566 (1958)

Elem. Sym.	A	Z
Cu		29
Ref. No.		
58 Zi 1		EH

Method 32 MeV betatron; pair spectrometer; absorption measurement;
ionization chamber

Reaction	E or ΔE	E_0	Γ	$\int \sigma dE$	$J\pi$	Notes
$\text{Cu}(\mu_e)$	Bremss. 30			$420 \pm 80 \text{ MeV-mb}$		



FORM NBS-418
(8-1-63)
USCOMM-DC 18556-P63

¹⁰ BERMAN, A.I., u. K.L. BROWN: Phys. Rev. 96, 83 (1954).
U.S. DEPARTMENT OF COMMERCE
NATIONAL BUREAU OF STANDARDS

REACTION	RESULT	EXCITATION ENERGY	SOURCE		DETECTOR		ANGLE
			TYPE	RANGE	TYPE	RANGE	
E, N	ABY	THR - 36	D	10 - 36	BF ₃ -I		4PI

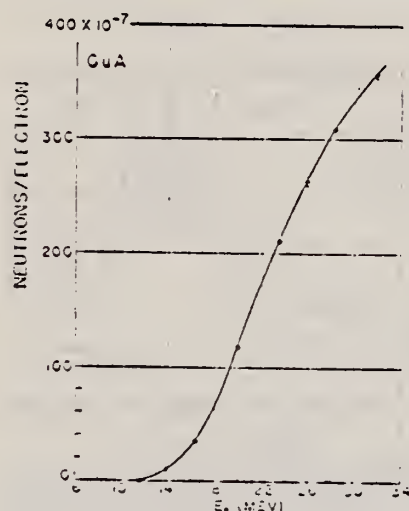


Fig. 4. Neutron yield curve as a function of initial electron energy for a natural Cu target 0.106-radiation-length thick.

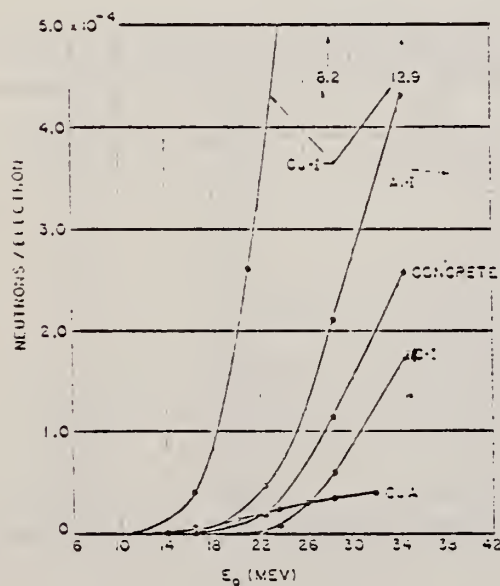


Fig. 5. Yield of neutrons per incident electron as a function of initial electron energy for the low-Z elements. The concrete target is a simple 3:1 sand-cement mixture. The numbers at the top right refer to the Cu-I curve at the indicated energies.

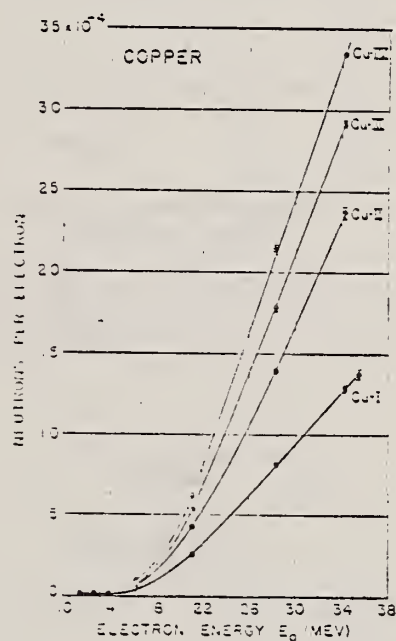


Fig. 6. Yield of neutrons per incident electron as a function of electron energy for natural Cu targets of various thicknesses. The numbers give the target thicknesses to the nearest 1/2 number of radiation lengths.

REACTION	RESULT	EXCITATION ENERGY	SOURCE		DETECTOR		ANGLE
			TYPE	RANGE	TYPE	RANGE	

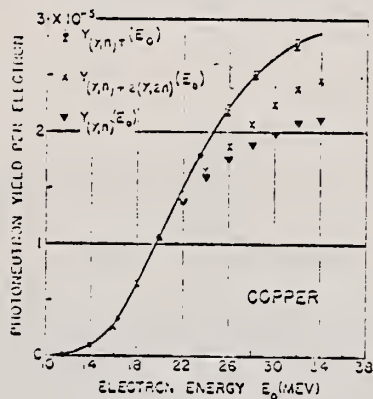


Fig. 12. Yield of neutrons per incident electron as a function of electron energy for the Cu target (0.105 radiation length). The yield shown is due to photodisintegration only. Plotted also are data of Benham and Brown (reference 19) for Cu²⁴.

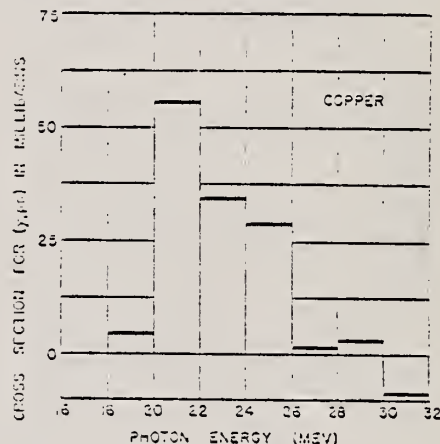


Fig. 13. Gross section for the reaction (γ, pn) as a function of photon energy for Cu.

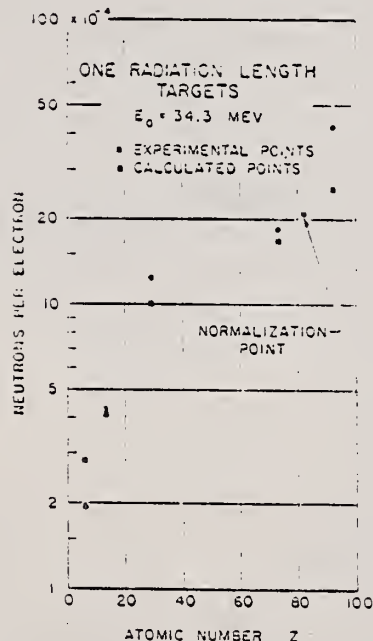


Fig. 14. Experimental and expected yields of neutrons per incident electron for 1-radiation-length targets at 34.3 Mev, as a function of atomic number Z . The experimental yields were obtained by dividing the measured yields from the targets labeled I by the actual target thicknesses listed in Table I. The expected yields were calculated from expression (8).

TABLE I. Thicknesses of the targets used in the experiment, with the exception of heavy water all targets contained isotopes in their naturally-occurring proportions.

Target	Thickness (cm)	Thickness (radiation lengths)
Heavy water	0.095	0.0127
Be	0.559	0.01507
CF	25.01	0.88
Al-I	24.10	1.00
Cu-I	1.072	0.115
Cu-II	13.25	1.04
Cu-III	20.50	1.08
Cu-IV	50.80	3.13
Ta-I	53.13	4.17
Pb-I	0.21	0.008
Pb-II	5.88	1.0
Pb-III	11.72	1.0
Pb-IV	17.30	2.08
Pb-V	22.80	3.04
Pb-VI	34.42	5.93
U-I	6.15	1.14
U-II	12.42	2.30
U-III	18.61	3.40
Concrete	18.5	1.10

ELÉM. SYM.		
Cu		29
REF. NO.	59 Pe 5	JOC

METHOD

REACTION	RESULT	EXCITATION ENERGY	SOURCE		DETECTOR		ANGLE
			TYPE	RANGE	TYPE	RANGE	
G.G	ABX	19 - 61	C	19 - 61	NAI-D		135

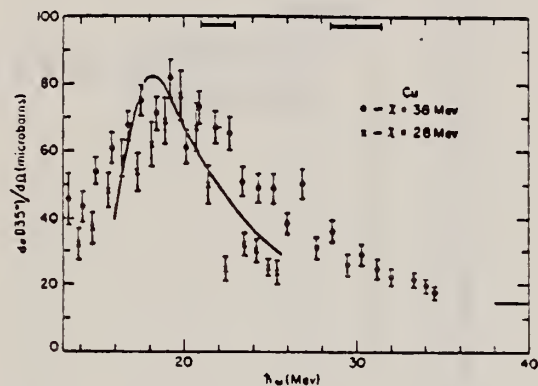


FIG. 4. The scattering cross section for Cu at 135° . The data is for irradiations at bremsstrahlung energies of 28 and 38 Mev. The cross sections are for mixed elastic and inelastic scattering as defined by Eq. (15) in the text. The solid curve is a predicted cross section (see text for details).

Ref. V.P. Chiznov
Zhur. Eksp. i Teoret. Fiz. 38, 809 (1960)
Soviet Phys. JETP 11, 587 (1960)

Elem. Sym.	A	Z
Cu		29
Ref. No.		
60 Ch 1		JHH

Method 90 MeV Bremsstrahlung; scintillator counter telescope.

Reaction	E or ΔE	E_0	Γ	$\int \sigma dE$	$J\pi$	Notes
Cu(γ, p)						Energy Range of particles detected: E_d - 15.5-30 MeV E_p - 15.5-30 MeV E_t - 17-30 MeV Ratios: $\sigma(\gamma, d)/\sigma(\gamma, p)$ at $\theta = 90^\circ$ $\sigma(\gamma, t)/\sigma(\gamma, d)$
Cu(γ, d)						
Cu(γ, t)						

FIG. 3. Ratio of (γ, d) to (γ, p) cross sections for neutrons and deuterons of energies 15.5-30 MeV as function of atomic weight A. The solid curve shows the dependence given by Eq. (2), arbitrarily normalized.

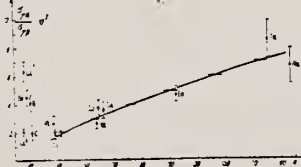


TABLE I

Element	$100N_t/N_d$	Element	$100N_t/N_d$	Element	$100N_t/N_d$	Element	$100N_t/N_d$
Li ⁶	30±3	B	39±8	Ni	10±4	In	5±2.5
Li ⁷	22.5±2.5	Si	10±4	Co	2.5±2	Ta	10±4
Be	13±4.6	S	8±4	Cu	2.5±2	Au	3±3

YIELD DATA TABLE:

It should be noted that the yield of photoprotons of the energy considered rises smoothly with Z for the elements plotted in Fig. 3, and that starting already with Al, no direct proportionality to Z is observed on account of the effect of the Coulomb barrier. For illustration, we give the yields of photoprotons $Y(\gamma, p)$ per proton in the nucleus for several elements in relative units (the error in these measurements was estimated to be $\pm 10\%$):

	Li ⁶	Li ⁷	Be	C	Al	Cu
$Y(\gamma, p) =$	1.49	1.57	1.5	1.31	1.00	0.58

Method Betatron; photon difference; beam passes through one target surrounded by proton (proportional) counters, continues to second target surrounded by B10-lined neutron counters.

Ref. No. 60 Ch 2 JH

Reaction	E or ΔE	E_0	Γ	$\int \sigma dE$	$J\pi$	Notes
(γ, n)	8.3-20.8					
(γ, p)		$\sim 19\text{MeV}$				$\sigma_{\text{max}} = 23\text{mb}$ Order-of-magnitude agreement between measuring $\sigma(\gamma, p)/\sigma(\gamma, n)$ [reciprocal of data in Figure 8] and compound nucleus calculation [Cu_{av} column in Table II].

TABLE II. Calculated ratios of photoproton to photoneutron cross sections.

E_γ (MeV)	Al ²⁷	Cu ⁶³	Cu ⁶⁵	Cu ^{av}
12	...	0.20	...	0.14
13	...	0.16	0.014	0.11
14	0.83	0.16	0.017	0.11
15	0.54	0.16	0.021	0.12
16	0.44	0.18	0.026	0.13
17	0.39	0.19	0.032	0.14
18	0.35	0.22	0.038	0.17
19	0.32	0.24	0.046	0.18
20	0.30	0.26	0.053	0.20
21	0.28	0.29	0.062	0.22
22	0.27	0.29	0.072	0.23

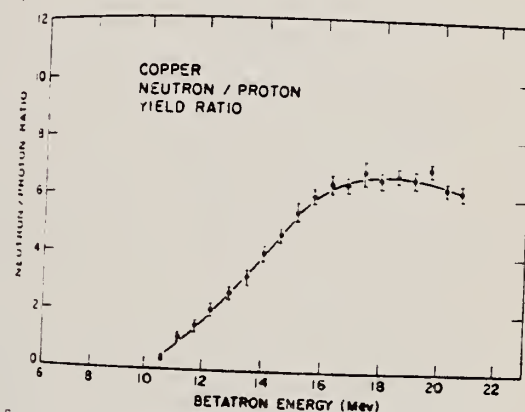


Fig. 8. The photoneutron to photoproton yield ratio for copper as a function of betatron energy.

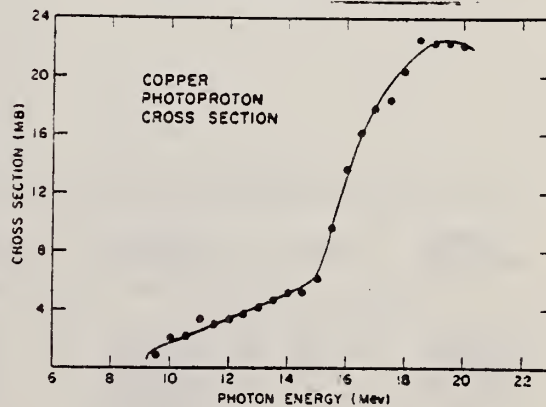


Fig. 10. The photoproton cross section for copper as a function of photon energy.

ELEM. S.M.		
Cu		29
REF. NO.	60 Ko 4	
	NVB	

METHOD

Synchrotron; deuteron spectrum, yield; nuclear emulsion

REACTION	RESULT	EXCITATION ENERGY	SOURCE		DETECTOR		ANGLE
			TYPE	RANGE	TYPE	RANGE	
G, D	RLY	15-35	C	70	EMU-D		DST

Relative yields:

$$4 < E_d < 10 \text{ MeV}, \frac{Y(\gamma, d)}{Y(\gamma, p)} = 0.07 \pm 0.04$$

$$3 < E_d < 10 \text{ MeV}, \frac{Y(\gamma, d)}{Y(\gamma, p)} \geq 0.08 \pm 0.04$$

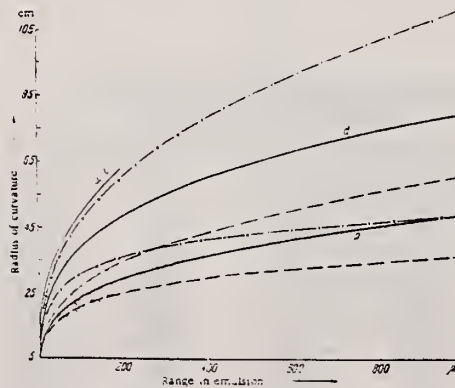


Fig. 2. Radius of curvature versus particle range in emulsion and the "error zones". The points indicate the results of the measurements.

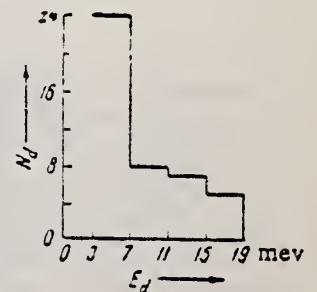


Fig. 3. Photodetector energy distribution.

Elem. Sym.	A	Z
Cu	63	29

Ref. No.	
60 Ku 2	JH

Element	Relative neutron yield	Element	Relative neutron yield
Li	1.00 ± 0.05	Cu	0.37 ± 0.02
Be	1.22 ± 0.09	Cd	0.35 ± 0.02
O	0.74 ± 0.05	I	0.39 ± 0.02
Al	0.49 ± 0.03	Bi	0.41 ± 0.03
Ca	0.33 ± 0.02		

Ref.

K. Reibel, A.K. Mann
Phys. Rev. 118, 701 (1960)

Elem. Sym. A Z

Cu

29

Method

 γ 's from $F^{19}(p,\alpha\gamma)$ reaction; protons from VandeGraaff; NaI

Ref. No.

60 Re 1

JHH

Reaction	E or ΔE	E_0	Γ	$\int \sigma dE$	$J\pi$	Notes
(γ,γ)	$E_p = 2.05$					$\langle \sigma \rangle = 0.57 \pm 0.06$ mb D (average level spacing based on J): 1/2 58 ± 48 kev 3/2 29 ± 24 kev 5/2 19 ± 16 kev $\bar{\Gamma}_{\gamma o} / \bar{\Gamma}_{\gamma} = 0.15 \pm 0.1$ $\bar{\Gamma}_{\gamma} = 2.5 \pm 1.9$ eV $\bar{\Gamma}_{\gamma o} = 0.4 \pm 0.2$ eV $\langle \sigma \rangle = 0.38 \pm 0.06$ mb
	$E_p = 2.40$					
	$E_{\gamma} = 6.9$					$\langle \sigma \rangle = 0.31 \pm 0.07$ mb
	$E_{\gamma} = 7.1$					$\langle \sigma \rangle = 0.63 \pm 0.14$ mb

Elem. Sym.	A	Z
Cu		29

Method	Ref. No.
320 MeV synchrotron; proton telescope; neutron counter	60 St 1

JHH

Reaction	E or ΔE	E ₀	Γ	∫σdE	Jπ	Notes
Cu ⁶⁴ (γ,np)	Bremss. 320					$(\sigma/\sigma_{H^2}) = 6.8 \pm 1.3$ $[\sigma_{H^2} = 63 \mu b]$ Mean photon energy - 262 MeV Proton counter at 76°

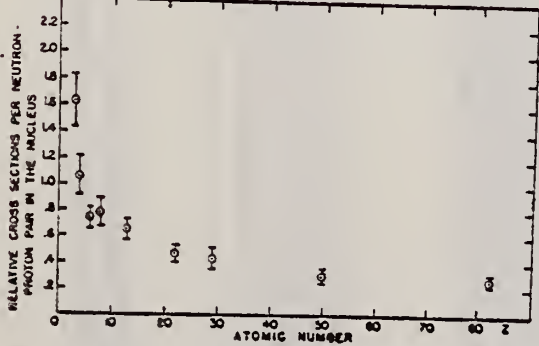


FIG. 2. Relative cross sections per neutron-proton pair in the nucleus versus atomic number. The cross section of the element of interest is divided by the cross section for deuterium and by the factor NZ/A .

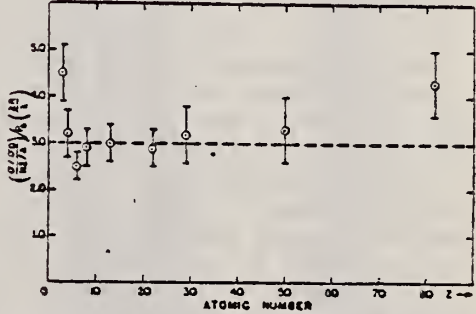


FIG. 3. The relative cross sections per neutron-proton pair corrected for the probability of escape is plotted against atomic number. The probability of escape factor is calculated using $r_0 = 1.30 \times 10^{-13}$ cm and $\lambda = 3.6 \times 10^{-13}$ cm. The probability of escape factor is given in expression (1). The data shown are those of Fig. 2 divided by $P(2R/\lambda)$.

ELEM. SYM.	1	2
Cu		29
REF. NO.	61 Ba 2	NVB

METHOD Betatron; fast neutron yield; angular distribution; Al and Si threshold detectors; ion chamber

REACTION	RESULT	EXCITATION ENERGY	SOURCE		DETECTOR		ANGLE
			TYPE	RANGE	TYPE	RANGE *	
G, XN	ABY	THR-22	C	22	THR-I	3-+	DST
G, XN	ABY	THR-22	C	22	THR-I	5-+	DST

In Tables 2 and 4:

* "3-+" is the detector range of Aluminum and "5-+" of Silicon.

$\bar{\sigma}$ = average cross section of detector weighted with neutron spectrum

ξ = neutrons/100 roentgen/mole

$$W(\theta) = a_0 \sum_{n=1}^{\infty} [1 + A_n P_n(\cos \theta)]$$

TABLE II
Normalized yields for aluminum detectors

Element	Al(π, γ) reaction				Al(π, p) reactions						
	30°	90°	150°	a_0	30°	60°	90°	a_0	a_1	a_2	$(\bar{\sigma}\phi) \times 10^3$
Bismuth	399	567 ± 130	620	541 ± 85	3632	5139 ± 290	3168	4366 ± 185	0.06 ± 0.06	-0.35 ± 0.1	17.76
	478	423 ± 130	641	484 ± 85	2562	5353 ± 290	2955	4144 ± 185	-0.05 ± 0.06	-0.53 ± 0.1	16.87
Lead	426	312 ± 120	725	429 ± 77	3123	5754 ± 260	3154	4591 ± 166	-0.004 ± 0.05	-0.51 ± 0.07	18.63
Tantalum	378	267 ± 100	688	441 ± 122	2757	3024 ± 425	2088	2757 ± 275	0.14 ± 0.14	-0.19 ± 0.17	11.22
Lanthanum	208	222 ± 110	330	243 ± 70	2139	3371 ± 250	1891	2768 ± 160	0.05 ± 0.07	-0.43 ± 0.10	11.27
Arsenic	77	100 ± 50	108	97 ± 32	788	937 ± 115	764	865 ± 74	0.02 ± 0.11	-0.16 ± 0.14	3.52
Copper	13	65 ± 30	70	55 ± 20	710	748 ± 70	569	700 ± 45	0.11 ± 0.08	-0.14 ± 0.11	2.85

* $(\bar{\sigma}\phi) = 4.07 \times 10^4$ millibarn-neutron.

TABLE IV

I Element	II a_0	III a_1	IV a_2	V $(\bar{\sigma}\phi) \times 10^3$	VI $\phi_{total} (22 \text{ Mev}) \times 10^3$	VII ϕ_{fast}/ϕ_{total}
Vanadium	245 (1 ± 0.06)	0.01 ± 0.08	-0.00 ± 0.10	6.05	0.21	0.12
Chromium	164 (1 ± 0.03)	0.04 ± 0.04	-0.05 ± 0.05	4.05	0.17	0.10
Manganese	308 (1 ± 0.02)	0.07 ± 0.03	-0.09 ± 0.04	7.61	0.25	0.12
Iron	200 (1 ± 0.03)	0.05 ± 0.04	-0.17 ± 0.05	4.94	0.18	0.11
Cobalt	390 (1 ± 0.02)	0.08 ± 0.03	-0.22 ± 0.04	9.63	0.26	0.15
Nickel	145 (1 ± 0.05)	0.07 ± 0.07	-0.23 ± 0.09	3.58	0.12	0.12
Copper	347 (1 ± 0.02)	0.05 ± 0.03	-0.29 ± 0.04	8.57	0.30	0.12
Arsenic	482 (1 ± 0.03)	0.11 ± 0.04	-0.24 ± 0.05	11.91	0.33	0.15
Rubidium	638 (1 ± 0.05)	0.13 ± 0.06	-0.14 ± 0.08	15.76		
Strontium	409 (1 ± 0.05)	0.10 ± 0.06	-0.17 ± 0.08	10.10		
Yttrium	290 (1 ± 0.10)	0.08 ± 0.12	-0.12 ± 0.15	7.16		
Silver	590 (1 ± 0.04)	0.10 ± 0.06	-0.22 ± 0.08	14.57	0.87	0.07
Cadmium	905 (1 ± 0.02)	0.02 ± 0.02	-0.26 ± 0.03	22.35		
Iodine	1133 (1 ± 0.03)	0.04 ± 0.04	-0.29 ± 0.05	27.99	1.42	0.08
Barium	1048 (1 ± 0.04)	0.10 ± 0.06	-0.38 ± 0.08	25.89		
Lanthanum	1595 (1 ± 0.02)	0.03 ± 0.03	-0.42 ± 0.04	39.40	1.04	0.15
Cerium	1316 (1 ± 0.05)	0.05 ± 0.06	-0.39 ± 0.08	32.50		
Dysprosium	1652 (1 ± 0.03)	0.04 ± 0.10	-0.34 ± 0.13	40.80		
Tantalum	1558 (1 ± 0.02)	0.04 ± 0.03	-0.22 ± 0.04	38.48	2.50	0.06
Tungsten	1365 (1 ± 0.02)	-0.07 ± 0.03	-0.24 ± 0.04	33.71		
Mercury	1345 (1 ± 0.02)	0.04 ± 0.03	-0.31 ± 0.04	33.22		
Lead	2274 (1 ± 0.01)	0.02 ± 0.02	-0.42 ± 0.03	56.17	2.72	0.08
Bismuth	2162 (1 ± 0.02)	0.05 ± 0.03	-0.45 ± 0.04	53.40	3.36	0.06
Thorium	3031 (1 ± 0.04)	0.06 ± 0.05	-0.32 ± 0.07	74.87		
Uranium	4630 (1 ± 0.02)	0.05 ± 0.03	-0.17 ± 0.04	114.36		

* $(\bar{\sigma}\phi) = 2.47 \times 10^3$ millibarn-neutron. Errors are standard errors due to counting statistics only.

Elem. Sym.	A	Z
Cu		29
Ref. No.		JHH
61 Fo 1		

Method 30 MeV electron synchrotron; emulsions; magnetic analysis

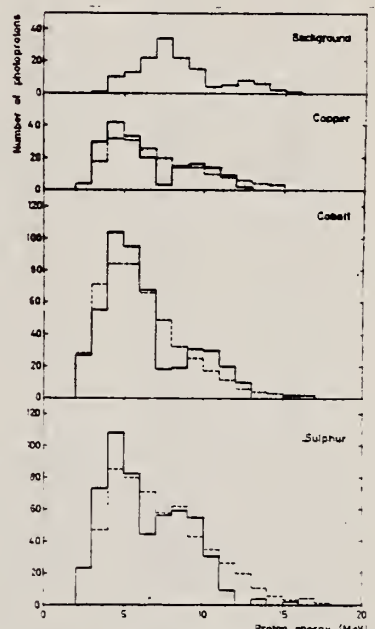
Reaction	E or ΔE	E_0	Γ	$\int \sigma dE$	$J\pi$	Notes
(γ, p) (γ, α)	Bremss. 30			Angle Unknown		<p>No significant (γ, d) yield detected. Ratio of yields:</p> $\frac{(\gamma, \alpha)}{(\gamma, p)} = 0.05$ 

Figure 8: Energy distribution of the photo-proton tracks giving intersection points in the area $-8.4 > x_t > -11.6$ and $-3.0 < x_t < 3.0$.

The lowest section shows the photoprotons from the sulphur exposure. The dashed line is the expected distribution from ref. 19 [Cujec-Dobovisek, Congr. Intern. de Phys. Nucleaire (1958) 634]. The second section shows the photoprotons from the cobalt exposure. The dashed line is the expected distribution from ref. 20 [Toms and Stephens, Phys. Rev. 95, 1209 (1954)]. The third section shows the photoprotons from the copper exposure. The dashed line is the expected distribution from ref. 21 [Lin'kova et al, Soviet JETP 38, 780 (1960)]. The background is subtracted in these 3 sections, but shown in the uppermost section. It originates from the entrance window.

Elem. Sym.	A	Z
Cu		29

Ref. No.	
61 Ho 1	JHH

FORM NBS-418
(8-1-63)
USCOMM-DC 18556-P53

U.S. DEPARTMENT OF COMMERCE
NATIONAL BUREAU OF STANDARDS

REF.

M. Masuda
J. Phys. Soc. 16, 1801 (1961)

ELEM. SYM.	A	Z
Cu		29

METHOD

REF. NO.

Betatron; proton angular distribution; ZnS scintillator

61 Ma 2

REACTION	RESULT	EXCITATION ENERGY	SOURCE		DETECTOR		ANGLE
			TYPE	RANGE	TYPE	RANGE	
G, XP	R ₀ X	6 - 21	C	21	SCI-I	1 - 10	DST

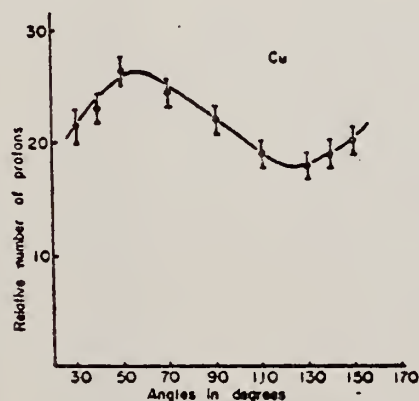


Fig. 8. Angular distribution of photo-protons from copper. The coefficients obtained by the least square fit are listed in Table III, assuming that the form is $\sum_{i=0}^4 C_i P_i(\cos \theta)$.

Table III. Angular distribution coefficients for copper.

Legendre polynomials		Power series	
C_0	21.0494	a_0	21.112
C_1	3.0044	a_1	5.8524
C_2	-1.6930	a_2	8.2572
C_3	-6.0504	a_3	28.449
C_4	-1.0342	a_4	-16.445
		a_5	-55.612

REF.

J. Miller, C. Schuhl, C. Tzara
J. Phys. Radium 22, 529 (1961)

ELEM. SYM.

A

Z

Cu

29

METHOD

Positron annihilation; neutron cross section; BF_3 counter;
ion chamber

REF. NO.

61 Mi 1

NVB

REACTION	RESULT	EXCITATION ENERGY	SOURCE		DETECTOR		ANGLE
			TYPE	RANGE	TYPE	RANGE	
G,XN	ABX	10-20	D	10-20	BF3-I		4PI

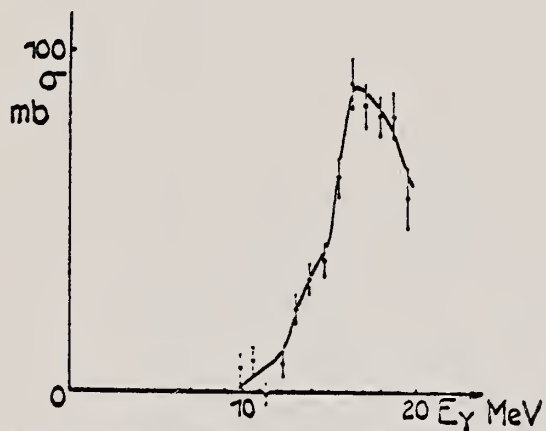


FIG. 5.— Cuivre, $\sigma(\gamma, n) + \sigma(\gamma, np) + 2\sigma(\gamma, 2n) + \dots$

Method 22 MeV betatron; $\text{Si}^{28}(\text{n,p})\text{Al}^{28}$ threshold detector.

Ref. No.	
61 Ta 1	JHH

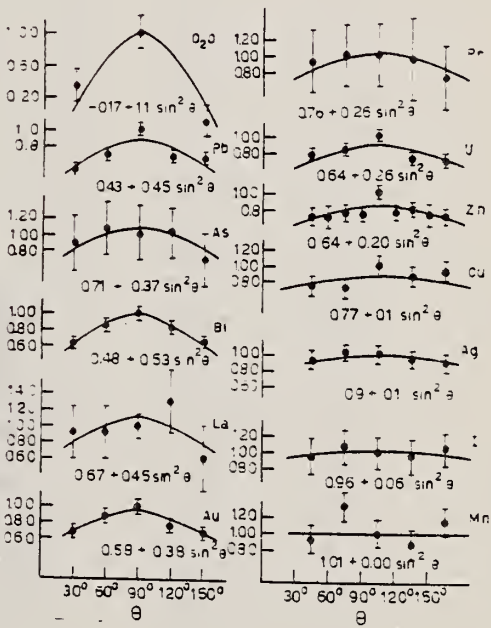
Reaction	E or ΔE	E_0	Γ	$\int \sigma dE$	$J\pi$	Notes
(γ, n)	Bremss. 22					<p>$E_n > 6 \text{ MeV.}$</p> <p>$W(\theta_n) = A + B \sin^2 \theta$ where $B/A = 0.13 \pm 0.31$</p> 

Figure 4: Angular distributions of fast photoneutrons as observed with the $\text{Si}^{28}(\text{n,p})\text{Al}^{28}$ detector. Data normalized at 90° in each case.

Ref. T. Tohei, M. Sugawara, S. Mori, M. Kimura
J. Phys. Soc. Japan 16, 1657 (1961)

Elem. Sym.	A	Z
Cu		29

Method 25 MeV betatron; photon scattering; NaI(Tl) spectrometer;
ion chamber

Ref. No.	NVB
61 To 1	

Reaction	E or ΔE	E_0	Γ	$\int \sigma dE$	$J\pi$	Notes
Cu(γ, γ)	Bremss. 5-12	7.5				Detector at 120° Table II taken from J. Phys. Soc. Japan <u>18</u> , 17-22 (1963)

References

- 1) E. G. Fuller and E. Hayward: Phys. Rev. **101** (1956) 692.
- 2) see E. Segre: *Experimental Nuclear Physics*, vol. 1, p. 346.
- 3) J. S. Levin and D. J. Hughes: Phys. Rev. **101** (1956) 1328.
- 4) K. Reibel and A. K. Mann: Phys. Rev. **118** (1960) 701.

Table II. The correction of the energy scale.

Energy in Ref. 1	should be read
4.0 Mev	3.3 Mev
6.0	5.5
8.0	7.7
10.0	9.9
12.0	12.1
14.0	14.3

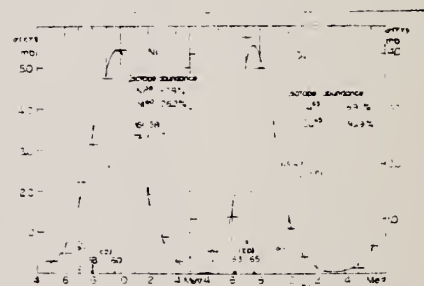


Fig. 7. The elastic scattering cross sections of photons. ---: data from Fuller and Hayward¹. □: data from the experiment using the monochromatic γ -rays.
(a) $\sigma(\gamma, \gamma)$ by Ni. The arrows indicate the positions of the (γ, p) and (γ, n) threshold energies of Ni^{58} and Ni^{60} .
(b) $\sigma(\gamma, \gamma)$ by Cu. The arrows indicate the positions of γ, p and γ, n threshold energies of Cu^{63} and Cu^{65} .

Ref. G. Ben-David (Davis); B. Huebschmann

Elem. Sym.

A

Z

Phys. Letters 3, 87 (1962)

Cu

29

Method

(n, γ) reaction - NaI(Tl)

Ref. No.

62Be2

BG

Reaction	E or ΔE	E_0	Γ	$\int \sigma dE$	$J\pi$	Notes
(γ, γ)	discrete energies in the range 5.44 - 8.997	8.449				σ (total)(mb) γ source 15 Cr

Elem. Sym.	A	Z
Cu		29
Ref. No.		JHH
62 Mi 3		

Method Linac; monoergic photons by e^+ annihilation in flight; NaI

Reaction	E or ΔE	E_0	Γ	$\int \sigma dE$	$J\pi$	Notes
Cu (γ, xn)	10-20	17 ± 0.5		$\int_0^{9.6} = 0.45 \pm 0.015$ MeV-b		

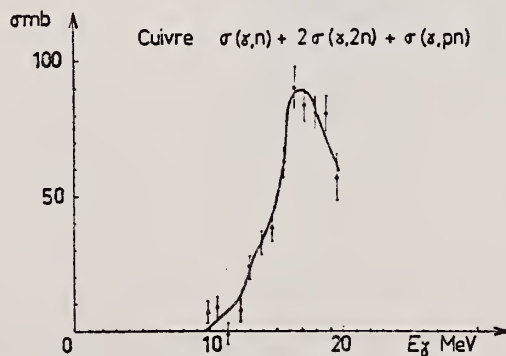


Fig. 6. Section efficace
 $\sigma = \sigma(\gamma, n) + \sigma(\gamma, np) + 2\sigma(\gamma, 2n) + \dots$ pour le cuivre

TABLEAU 5
Resultats experimentaux

Éléments	Fig. No	E_0 (MeV)	σ_{tot} (MeV ⁻¹ b) ^{a)}	σ_{int} 0.06NZ ^{1/2}	Seuils			
					γ, n	γ, p	$\gamma, 2n$	γ, np
Cu	6 17	9.5 ± 0.5	0.45 ± 0.015	0.47 ± 0.015				
La	7 15	6 ± 0.5	1.91 ± 0.03	0.94 ± 0.015	8.30 ⁽¹²⁾		14.25 ⁽¹²⁾	14.90 ⁽¹²⁾
Ce	140 142	15.6 ± 0.5	1.48 ± 0.03	0.92 ± 0.015	19.05 ⁽¹⁴⁾	8.50 ⁽¹⁴⁾	14.1 ⁽¹⁴⁾	
Ta	181	13 ± 0.5	2.97 ± 0.05	1.13 ± 0.02	7.15 ⁽¹⁴⁾	9.50 ⁽¹⁴⁾	14.3 ⁽¹⁴⁾	
Au	197 206	14.2 ± 0.5	3.00 ± 0.05	1.06 ± 0.02	7.90 ⁽¹²⁾		13.71 ⁽¹²⁾	12.94 ⁽¹²⁾
Pb	207 208	13.8 ± 0.5	4.10 ± 0.06	1.38 ± 0.02	10.6 ⁽¹²⁾	7.1 ⁽¹²⁾	14.3 ⁽¹²⁾	14.5 ⁽¹²⁾
Bi	209	14.0 ± 0.5	3.73 ± 0.06	1.24 ± 0.02	7.2 ⁽¹²⁾	8.2 ⁽¹²⁾	15.0 ⁽¹²⁾	14.2 ⁽¹²⁾
					8.9 ⁽¹²⁾	8.4 ⁽¹²⁾	15.0 ⁽¹²⁾	14.2 ⁽¹²⁾
					7.44 ⁽¹⁴⁾	3.76 ⁽¹⁴⁾	10.4 ⁽¹⁴⁾	

^{a)} L'intégrale $\int_0^x \sigma dE$ est prise jusqu'à x égal à 19.6 MeV pour Cu, à 21.2 MeV pour La et Ce et à 22 MeV pour Ta, Au, Pb et Bi. D'autre part, les erreurs indiquées sont les erreurs statistiques.

W. Sebaoun
J. Phys. Radium 23, 989 (1962)

ELEM. SYM.	A	Z
Cu		29

METHOD

Proton cross section; CSI; Cu⁶³(γ ,n) reaction

REF. NO.

62 Se 2

NVB

REACTION	RESULT	EXCITATION ENERGY	SOURCE		DETECTOR		ANGLE
			TYPE	RANGE	TYPE	RANGE	
G,P	ABX	15,18	D	15, 18	SCI-I		
		(14.8, 17.6)		(14.8) (17.6)			

$\sigma = 9.8 \pm 1.4$ mb, assuming $\sigma [\text{Cu}^{63}(\gamma, n)] = 82 \pm 8$ mb.

Ref. Yu.M.Volkov, L.A.Kul'chitskii
 Zhur.Eksptl. i Teoret.Fiz. 42, 108 (1962);
 Soviet Phys.JETP 15, 77 (1962)

Elem. Sym.	A	Z
Cu		29

Method
 scintillation counter telescope

Ref. No.	
62Vol	136

Reaction	E or ΔE	E_0	Γ	$\int \sigma dE$	$J\pi$	Notes
(γ ,p)	$E_{\gamma\max}$					$E_{\gamma\max}$ Particle energy $Y(\gamma,d)$ $Y(\gamma,t)$ interval $Y(\gamma,p)$ $Y(\gamma,p)$
(γ ,t)	34					34 4.5-15 0.007 \pm 0.003 0.005 \pm 0.002
(γ ,d)	90					34 7.5-15 0.007 \pm 0.003 0.005 \pm 0.003 90 7-19 0.021 \pm 0.005 0.013 \pm 0.001 Detector at 90°

REF.

D.K. Kaipov, Yu. K. Shubnyi, Yu. G. Kosyak, R.B. Begzhanov
 Zhur. Eksp. i Teoret. Fiz. 45, 443 (1963); Soviet Phys.
 JETP 18, 305 (1964)

ELEM. SYM.	A	Z
Cu		29
REF. NO.		
63 Ka 3		NVB

METHOD

Radioactive Source

REACTION	RESULT	EXCITATION ENERGY	SOURCE		DETECTOR		ANGLE
			TYPE	RANGE	TYPE	RANGE	
G,G	ABX	1,1	D	1, 1	NAI-D		120
				(1.114, 1.29)			

Average cross section for resonance scattering by Sn^{116} and
 Cu^{65} and attenuation of the resonance effect

Transition	Liquid source			Solid source		
	$\bar{\sigma}, 10^{-27} \text{ cm}^2$	$P_1(E), 10^{-2} \text{ eV}^{-1}$	A	$\bar{\sigma}, 10^{-27} \text{ cm}^2$	$P_2(E), 10^{-2} \text{ eV}^{-1}$	A
$\text{In}^{115} \rightarrow \text{Sn}^{116}$	8.2 ± 1.6	7.0 ± 2.0	0.055	7.4 ± 1.2	6.3 ± 1.7	0.050
$\text{Ni}^{64} \rightarrow \text{Cu}^{65}$	1.58 ± 0.26	3.36 ± 0.26	0.040	0.97 ± 0.18	2.05 ± 0.60	0.024

Ref. M. Kregar, B. Povh
Nuclear Phys. 43, 170 (1963)
Erratum in Nuclear Phys. 47, 528 (1963)

Elem. Sym.	A	Z
Cu		29

Method Betatron; α yields; spectra; solid state detectors; NBS chamber monitor

Ref. No.

63 Kr 1

JHH

Reaction	E or ΔE	E_0	Γ	$\int \sigma dE$	$J\pi$	Notes
Cu(γ, α)	Bremss. 21 30					

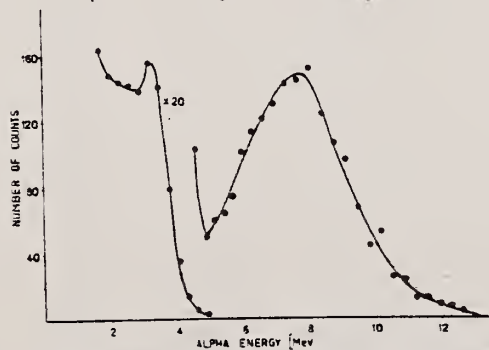


Fig. 5. The x-particle spectrum from Ni taken at 90° and 30 MeV betatron energy by 5000 Ω cm counter.

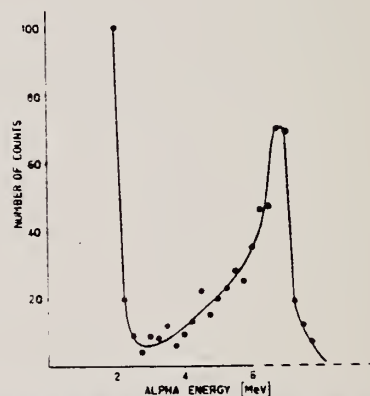


Fig. 6. The x-particle spectrum from Cu taken at 90° and 21 MeV betatron energy by 300 Ω cm counter.

TABLE I
Relative yields

Element	21 MeV		30 MeV	
	Number of alphas	Relative yield at 90°	Number of alphas	Relative yield at 90°
Ni	1209	40	536	13
Cu	1124	13	590	7
Fe	1108	4.5	653	1.7
V	372	1	363	1
Cd	136	0.7		

Elem. Sym.	A	Z
Cu		29
Ref. No.		
63 Mi 5		NVB

Method Betatron; proton yield; angular distribution; scintillator;
ion chamber.

Reaction	E or ΔE	E_0	Γ	$\int \sigma dE$	$J\pi$	Notes
Cu($\gamma, \pi p$)	Bremss. 22					<p>Angular distribution:</p> $Y(\theta) = a + b \cdot \sin^2 \theta (1 + p \cos \theta)^2$ <p>where $a = 46 \pm 6$; $b = 45 \pm 11$; $p = 0.6 \pm 0.2$ and $b/a = 1.0 \pm 0.3$</p> <p>Yield ($E_p > 8$ MeV): $(3.2 \pm 0.2) \cdot 10^5$ protons/mole-r</p> <p>Yield ($3.7 < E_p < 14$): $(19 \pm 2) \cdot 10^5$</p>

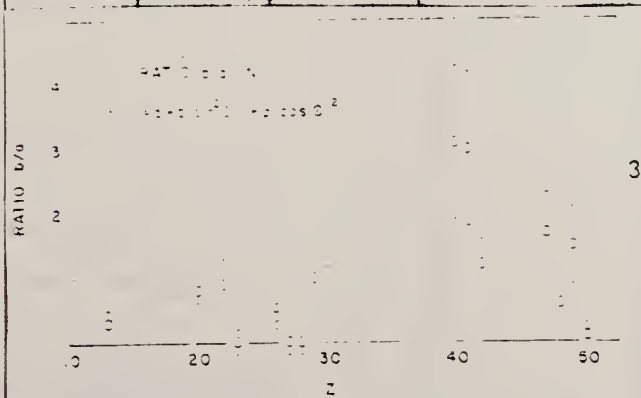
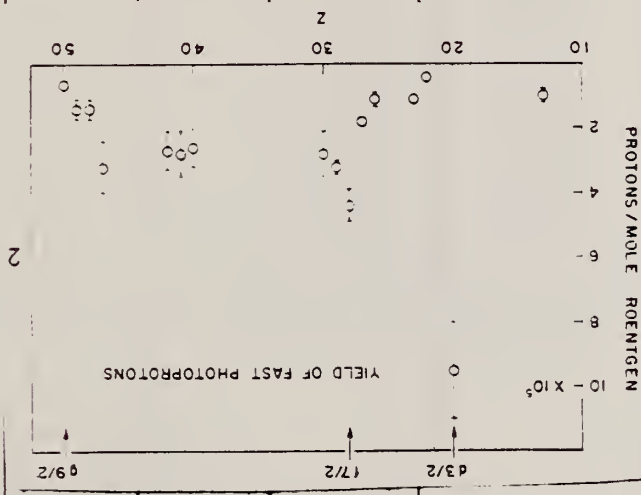


FIG. 2. The yields of fast photoprotons ($E_p > 8$ MeV) obtained from targets of various elements, which are listed with 22-Mev bremsstrahlung. The target thicknesses range from 0.51 to 0.72 g/cm². The error bars are statistical. The σ is calculated from the data.

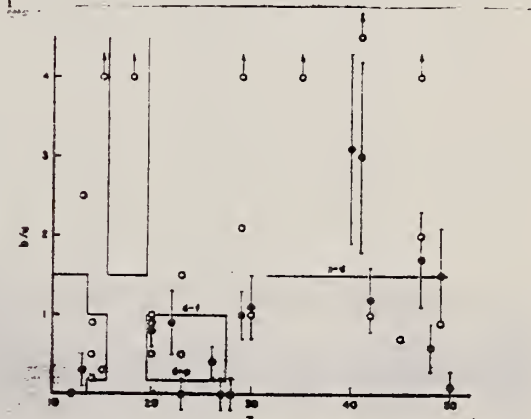


FIG. 4. The values of the fast photoproton anisotropy coefficient b/a found by the present authors (●) and other workers (○) in the region of the periodic table $10 < Z < 50$. Arrows indicate off-scale points. The references to the results of other workers are given in Table II. The demarcations are explained in the text.

Ref. M.Odera, N.Yamamoto

J.Phys.Soc.Japan 18, 325 (1963)

Elem. Sym.

A

Z

Cu

29

Method

Synchrotron; foils; emulsions

Ref. No.

630d1

BG

Reaction	E or ΔE	E_0	Γ	$\int \sigma dE$	$J\pi$	Notes
(γ, p) brems.: 22 MeV $= E_{\gamma \max}$				7.5×10^5 protons/ mole/roentgen		angular distributions: $2 \text{ MeV} \leq E_p \leq 4 \text{ MeV}$ $E_p \geq 7 \text{ MeV}$ total Isotropic

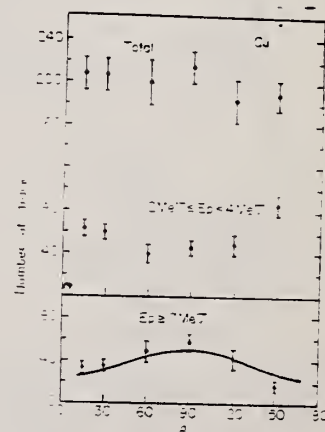


Fig. 3. Angular distribution of photo-protons from Cu. Solid curve drawn for $E_p \geq 7 \text{ MeV}$ is calculated from

$$I(\theta) = 1 - 1.3 \sin^2 \theta$$

Errors are statistical ones.

Ref. M. Yamanouchi
J. Phys. Soc. Japan 18, 638 (1963)

Elem. Sym.	A	Z
Cu		29
Ref. No.		
63 Ya 2 <i>CS</i> NVB		

Method
Betatron; deuteron spectrum; nuclear emulsion

Reaction	E or ΔE	E_0	Γ	$\int \sigma dE$	$J\pi$	Notes
Cu(γ ,d)	Bremss. 25.5					Detectors at 90° and 126°.

Table 1. Ratios of the yield of photoisotopes to that of photoisotopes.

Isotope	Ni	Cu	Sa	Se
Angle of observation	90°	90°	126°	126°
Number of photoisotopes	101	101	177	177
Number of photoisotopes	3	10	7	36
Yield ratio	-0.02	0.08±0.04	0.04±0.02	-0.04
				0.12±0.05

REF.

F.R. Allum, T.W. Quirk, and B.M. Spicer
Nucl. Phys. 53, 545 (1964)

ELEM. SYM. A Z

Cu

29

METHOD

REF. NO.

64 A1 5

JOC

REACTION	RESULT	EXCITATION ENERGY	SOURCE		DETECTOR		ANGLE °
			TYPE	RANGE	TYPE	RANGE	
G,XN	NØX	THR-34	C	34	THR-I	6-	DST

TABLE 1

Summary of present experimental data at 34 MeV bremsstrahlung

Element		$-\frac{a_2}{a_0}$	$\frac{a_1}{a_0}$
⁴ Be		0.43 ± 0.02	0.05 ± 0.01
⁶ C		0.61 ± 0.04	0.09 ± 0.02
¹³ Al		0.39 ± 0.03	0.05 ± 0.01
³³ Ti		0.34 ± 0.02	0.06 ± 0.01
⁵⁴ Cr	34 MeV	0.33 ± 0.02	0.02 ± 0.01
	22 MeV	0.13 ± 0.07	-0.02 ± 0.03
⁶³ Cu		0.36 ± 0.02	0.10 ± 0.01
⁸⁰ Sn		0.38 ± 0.02	0.11 ± 0.01
⁸⁴ Ba		0.39 ± 0.03	0.11 ± 0.02
⁷³ Ta	Before installation of iron shielding	0.26 ± 0.04	0.13 ± 0.02
	After installation of iron shielding	0.27 ± 0.02	0.12 ± 0.01
⁸² Pb	target diameter 3.0 cm	0.39 ± 0.03	0.15 ± 0.02
	target diameter 1.5 cm	0.40 ± 0.03	0.19 ± 0.02
⁸³ Bi		0.42 ± 0.03	0.17 ± 0.02

$$a_0 + a_1 \cos \theta + a_2 \cos^2 \theta$$

ELEM. SYM.	A	Z
Cu		29
REF. NO.	64 Ba 4	
	egf	

METHOD

REACTION	RESULT	EXCITATION ENERGY	SOURCE		DETECTOR		ANGLE
			TYPE	RANGE	TYPE	RANGE	
G,XN	ABX	10-27	C	10-27	BF3-I		4PI

65 BA3 SAME DATA

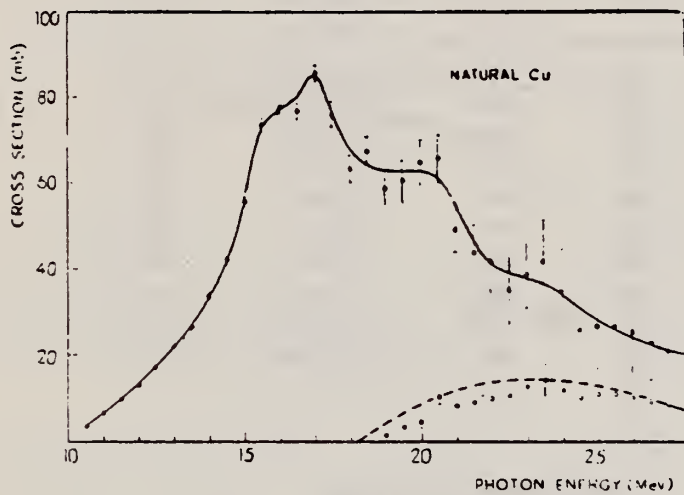


Fig. 3. $\sigma(\gamma, 2n)$ for Cu of natural isotopic abundance. The circles represent the value for $\sigma(\gamma, 2n)$ calculated (for $a = 0.5 \text{ MeV}^{-1}$) in the approximation that $\sigma(\gamma, 2n)$ for natural Cu has the same averaged behaviour as for pure isotopes (see Fultz et al. [18]). The dotted line represents the behaviour of $\sigma(\gamma, 2n)$ measured by Fultz et al.

REF.

K.W. Chen, J.R. Dunning, Jr., J.R. Rees, W. Shlaer, J.K. Walker
and R. Wilson
Phys. Rev. 135, 4B B1030 (1964)

ELEM. SYM.

A

Z

Cu

29

METHOD

REF. NO.

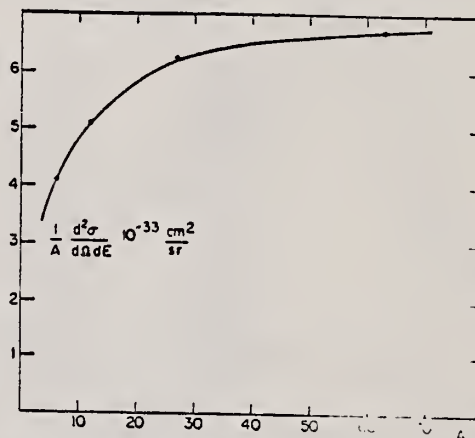
64 Ch 1

JOC

REACTION	RESULT	EXCITATION ENERGY	SOURCE		DETECTOR		ANGLE
			TYPE	RANGE	TYPE	RANGE	
E, P	ABX		D	4 BEV	MAG-D	110-450	DST

TABLE I. Cross sections for production of protons by electron.

Electron target	Energy angle (deg)	4 BeV proton energy (MeV)	$\frac{d^2\sigma}{d\Omega dE}$ $10^{-33} \text{ cm}^2/\text{sr MeV}$
H	59.8	374	3.8*
Li ^a	59.8	448	0.082
Li ^a	59.8	368	0.175
Li ^a	59.8	332	0.280
C	59.8	374	0.425
Al	59.8	374	1.19
H	63.1	291	7.5*
Li ^a	63.1	355	0.146
Li ^a	63.1	319	0.204
Li ^a	63.1	290	0.313
C	63.1	291	1.01
Al	63.1	291	2.42
H	67.1	208	16*
Li ^a	67.1	226	0.6
Li ^a	67.1	206	0.92
C	67.1	209	2.37
Al	67.1	209	6.4
H	72.1	124	46*
Li ^a	72.1	166	1.20
Li ^a	72.1	144	1.53
Li ^a	72.1	124	2.46
Li ^a	72.1	119	2.80
Li ^a	72.1	109	2.90
C	72.1	123	6.6
Al	72.1	124	16.9
Cu	72.1	124	42.3
H	44.8	291	2.9*
Li ^a	44.8	337	0.16
Li ^a	44.8	293	0.29
C	44.8	291	0.76
Al	44.8	291	1.58
H	52.3	208	8.5*
Li ^a	52.3	200	0.91
C	52.3	208	2.13
Al	52.3	208	4.95
H	61.1	124	25*
C	61.1	145	3.95
C	61.1	124	5.75
C	61.1	115	6.43
Al	61.1	145	10.7
Al	61.1	124	16.0

* $d\sigma/d\Omega$ in mb/sr; inside a 5.5% momentum interval.FIG. 4. Cross section, divided by A , as a function of A , for producing protons of 124 MeV from 4-BeV electrons at 72.1°.

75

REF. NO.

Synchrotron; $C^{12}(\gamma, n)$ monitor

64 Co 2

JOC

REACTION	RESULT	EXCITATION ENERGY	SOURCE		DETECTOR		ANGLE
			TYPE	RANGE	TYPE	RANGE	
G.XN	ABY	THR - 80	C	80	BF3-I		4 PI

Table 1

Element	Yield (36) eV cm ² mol MeV	60 NZ/A (mb MeV)	Σ 0	Σ 0	Σ 80 / Σ 0	E_m (MeV)	σ_m (mb)
²⁴ Cr	83 x 10 ⁻⁵	777	1.21	2.1	0.58	18.5	97
²⁵ Mn	108 x 10 ⁻⁵	818	1.52	2.33	0.65	18.5	114
²⁶ Fe	68 x 10 ⁻⁵	832	0.38	1.46	0.60	17.5	75
²⁷ Co	89 x 10 ⁻⁵	878	1.08	1.82	0.59	17.5	92
²⁸ Ni	44 x 10 ⁻⁵	879	0.55	1.07	0.51	18.5	56
²⁹ Cu	95 x 10 ⁻⁵	947	1.06	1.99	0.53	17.5	98
³⁰ Zn	88 x 10 ⁻⁵	975	0.94	1.68	0.56	17.5	86
³¹ Ga	130 x 10 ⁻⁵	1034	1.29	2.13	0.59	17.5	151
³² Ge	139 x 10 ⁻⁵	1064	1.35	2.29	0.59	17.5	158
³³ As	137 x 10 ⁻⁵	1109	1.22	2.13	0.56	17.5	127

$$\Sigma = \int_0^{30} \sigma(\gamma, xn) dE$$

$$0 \quad 60 \text{ NZ/A}$$

Table 2

Element	maximum yield (x 10 ⁻⁵)	$\sigma_{-1}(\text{Th})$	$\sigma_{-1}(\text{Th}) \times \left[\frac{3}{4\pi^2} \frac{hc}{c^2} \left(\frac{A-1}{NZ} \right) A^{-3/2} \right]$
⁶ C	4.0	3.54	2.13
⁸ O	5.2	4.95	1.92
¹¹ Na	10.6	11.60	2.49
¹² Mg	10.0	8.81	1.73
¹³ Al	15.9	13.92	2.30
¹⁴ Si	11.6	9.96	1.55
¹⁵ P	19.3	17.56	2.92
¹⁶ S	9.5	8.55	1.97
¹⁶ Cl	19.5	17.90	1.91
²⁰ Ca	12.1	11.63	1.92
²⁴ Cr	86	61.6	3.56
²⁵ Mn	115	76.1	3.96
²⁶ Fe	71	50.5	2.55
²⁷ Co	94	63.5	2.64
²⁸ Ni	46	34.2	1.59
²⁹ Cu	102	72.3	2.96
³⁰ Zn	93	65.7	2.68
³¹ Ga	140	93.6	3.31
³² Ge	150	101.5	3.36
³³ As	151	99.8	3.12

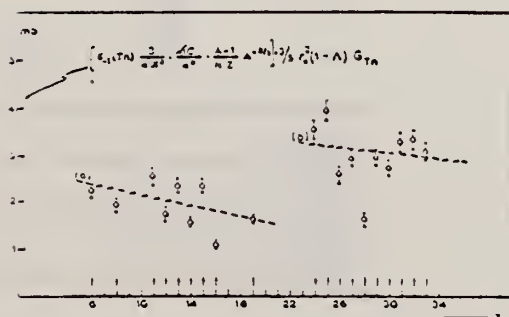


Fig. 2. Bremsstrahlung weighted cross sections, $\sigma_{-1}(\text{Th})$, conveniently normalized, versus Z.

ELEM. SYM.	A	Z
Cu		29
REF. NO.		
64 Fu 1		nvb

METHOD

Positron Annihilation; ion chamber

REACTION	RESULT	EXCITATION ENERGY	SOURCE		DETECTOR		ANGLE
			TYPE	RANGE	TYPE	RANGE	
G,N <u>532+</u>	ABX	9-28	D	9-28	BF3-I		4PI
G,2N <u>534+</u>	ABX	18-28	D	18-28	BF3-I		4PI
							<u>532+</u>

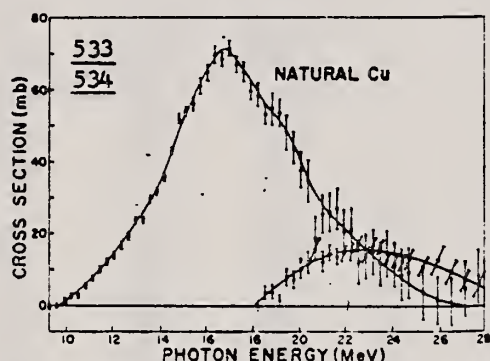


FIG. 2. Measured cross sections for (γ,n) and $(\gamma,2n)$ reactions on natural Cu. The top curve was obtained from single neutron counting data and consists of $\sigma(\gamma,n) + \sigma(\gamma,np)$. The lower curve consists of $\sigma(\gamma,2n)$ and was obtained from double-neutron counting data.

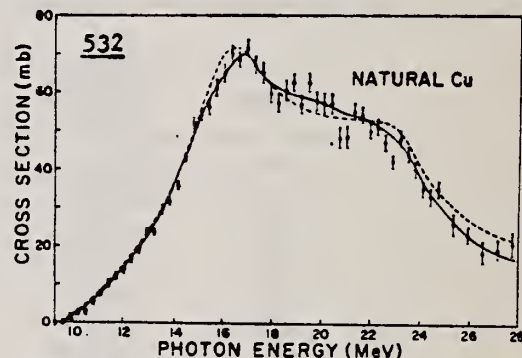


FIG. 1. Solid curve gives the average of data points of the total cross section $[\sigma(\gamma,n) + 2\sigma(\gamma,2n) + \sigma(\gamma,np)]$ for natural Cu. The dashed line represents the total cross section given by the sum of the total cross sections measured for Cu^{63} and Cu^{65} and adjusted for isotopic abundances.

TABLE I. Integrated cross sections up to 28 MeV for copper isotopes.

Element	Reaction	Integrated cross section (MeV-mb)	Fraction of total integrated cross section	Total (MeV-mb)
Natural Cu	$(\gamma,n) + (\gamma,np)$	525 ± 52	0.67	787 ± 113
	$(\gamma,2n)$	110 ± 11	0.14	
	$(\gamma,p)^a$	152 ± 50	0.19	
Cu^{63}	$(\gamma,n) + (\gamma,np) + \text{direct}$	523 ± 52	0.89	764 ± 09
	$(\gamma,2n)$	80 ± 8	0.11	
	$(\gamma,np)^a$	115 ± 20	0.15	
	$(\gamma,p)^a$	161 ± 48	0.21	
	(γ,n)	344 ± 34	0.45	
	direct ^b	64 ± 22	0.08	
Cu^{65}	$(\gamma,n) + (\gamma,np)$	437 ± 43	0.57	766 ± 103
	$(\gamma,2n)$	195 ± 19	0.25	
	$(\gamma,p)^c$	134 ± 40	0.18	

^a Calculated from evaporation theory.
^b Estimated.
^c See Ref. 20.

²⁰ N. V. Lin Kova, R.M. Osokina, B.S. Ratner, R.Sh.Amirov, V.V. Akindinov, Zh.Eksp. Teor. Fiz. 38, 780 (1960); JETP 11, 566 (1960).

TABLE II. Cross section for Li gamma rays.

Natural Cu $\sigma(\gamma,n)$ (mb)	Cu^{63} $\sigma(\gamma,n)$ (mb)	Cu^{65} $\sigma(\gamma,n)$ (mb)	Reference
55 ± 12	120 ± 30		^a
	52 ± 11		^b
85 ± 15	48 ± 8		^c
64 ± 10	80 ± 14		^d
	60 ± 9		^e
	38 ± 6		^f
	64 ± 4		^g
	59 ± 6	70 ± 7	^h
61 ± 6	55 ± 6	66 ± 6	Present work ⁱ

^a H. Waffler and O. Hirzel, Helv. Phys. Acta 25, 491 (1952).
^b See Ref. 9.
^c H. Glättli, O. Seippel, and P. Stoll, Helv. Phys. Acta 25, 491 (1952).
^d See Ref. 11.
^e See Ref. 10.
^f T. Nakamura, K. Takamatsu, K. Fukunaga, M. Yata, and S. Yasumi, J. Phys. Soc. Japan 14, 693 (1959).
^g S. Yasumi, M. Yata, K. Takamatsu, A. Masaike, and Y. Masuda, J. Phys. Soc. Japan 15, 1913 (1960).
^h See Ref. 13.
ⁱ Calculated assuming that the ratio of intensities for the 17.6- to 14.8-MeV Li gamma rays is 2.1.

⁹ B.D. McDaniel, R.L. Walker, and M.B. Stearns, Phys. Rev. 80, 807 (1950).

¹⁰ W.H. Hartley, W.E. Stephens, E.J. Winhold, Phys. Rev. 104, 178 (1956).

¹¹ J.H. Carver and E. Kondaiah, Phil. Mag. 45, 988 (1954).

¹³ G.E. Coote, W.E. Turchinets, I.F. Wright, Nucl. Phys. 23, 468 (1961).

REF. Akira Masaike
J. Phys. Soc. Japan 19, 427 (1964)

ELEM. SYM.	A	Z
Cu		29

METHOD

REF. NO.	
64 Ma 4	egf

REACTION	RESULT	EXCITATION ENERGY	SOURCE		DETECTOR		ANGLE
			TYPE	RANGE	TYPE	RANGE	
G,XXX	ABY	150-720	C	150-720	ACT-I		4PI

XXX=CU62 FINAL

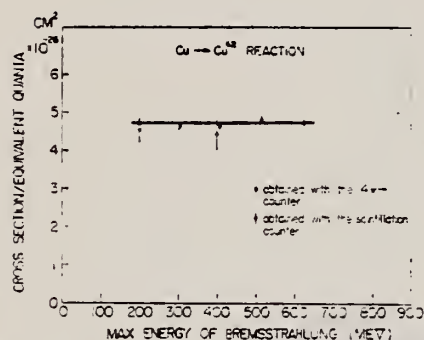
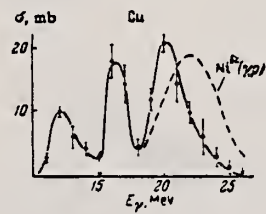


Fig. 8. The yield curve per equivalent quanta for the reaction Cu→Cu⁶².

REACTION	RESULT	EXCITATION ENERGY	SOURCE		DETECTOR		ANGLE °
			TYPE	RANGE	TYPE	RANGE	
G, P	ABX	THR-27	C	30	SCI-I	5-	DST

FIG. 4. Cross section for the emission of photoprotons with energy $\epsilon_p \geq 5$ MeV from copper. Dashed curve—cross section of a $Ni^{62}(\gamma, p)$ reaction obtained in [10].



ELEM. SYM.	A	Z
Cu		29
REF. NO.		
64 Sc 1		JOC

METHOD				REF. NO.	
Betatron				64 Sc 1	
REACTION	RESULT	EXCITATION ENERGY	SOURCE		- ANGLE
			TYPE	RANGE	
G, A	SPC	THR - 33	C	33	90

ABS YIELD

TABELLE 1
Meßdaten und Ergebnisse

	Ti	Ni	Cu	Nb
Targetdicke (mg/cm ²)	2.08	1.52	9.90	8.87
Bestrahlungsdauer (h)	52.5	55.5	18.0	84.5
Registrierte Teilchenanzahl (4 ≤ E _x ≤ 12.6 MeV)	1861	2376	2333	1987
Lage des Maximums E _{max} der Energieverteilung (MeV)	6.4	8.2	8.5	11
Halbwertsbreite des Maximums (MeV)	2.8	2.8	4.0	3.5
Mittlerer Energieverlust im Target bei E _x = E _{max} (MeV)	0.4	0.25	1.7	1.1
Ausbeute in μb/MeV *)	22 ± 3.5	45 ± 7	23 ± 3.5	5.5 ± 0.8

*) Vgl. Bemerkung *) in Tabelle 2.

TABELLE 2
Vergleich der Ergebnisse verschiedener Autoren

E ₀ (MeV)	Ti	Ni	Cu	Nb
<i>Ausbeute</i> (10 ³ × N _x /Mol. r)				
Boulègue 31		58.7	50.8	
Diese Arbeit *) 32.5	48 ± 7	98 ± 15	50 ± 7.5	12 ± 1.8
Toms und McElhinney 21.5		39.4	26	4.6 b)
<i>Relative Ausbeute</i>				
Boulègue 31		1	0.87	
Kregar und Povh 30		1	0.54	
Diese Arbeit 32.5	0.49 ± 0.08	1	0.51 ± 0.08	0.12 ± 0.02
Toms und McElhinney 21.5		1	0.66	0.12 b)

*) Die Fehlerangaben beinhalten auch die Unsicherheit in der Absolut Eichung der Intensität des γ-Strahles.

b) Dieser Wert wurde aus nur 14 beobachteten Ereignissen bestimmt.

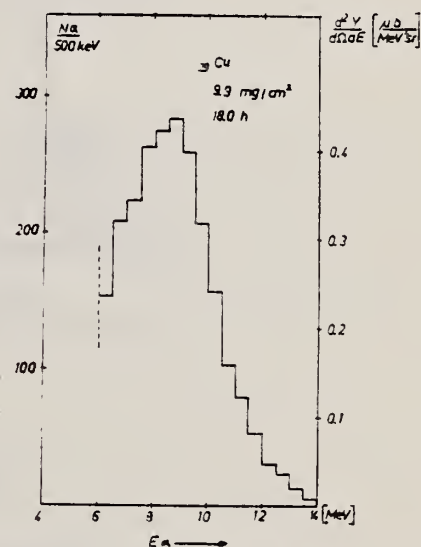


Abb. 1. Die erhaltenen Energie-Spektren der Photoalphateilchen aus Ti, Ni, Cu und Nb.

REF.

J. Shannon, W.E. Stephens, J.S. O'Connell
 Phys. Rev. 134, B113-17 (1964)

ELEM. SYM.

A

Z

Cu

29

METHOD

Linac

REF. NO.

64 Sh 3

NVB

REACTION	RESULT	EXCITATION ENERGY	SOURCE		DETECTOR		ANGLE °
			TYPE	RANGE	TYPE	RANGE	
G,D	RLY	15 - 40	C	24-40	-I		4PI

Measured ratio of HHD^+ to HH^+ currents.MASS SPECTROMETER

TABLE III. Observed deuteron to proton
 ratios for various exposures.

Run	Max. Brem. energy	Observed $Y(\gamma,D)/Y(\gamma,p)$
I	24	<0.0016, no HHD^+ observed
II	30	<0.0003, no HHD^+ observed
III	30	<0.00014, no HHD^+ observed
IV	40	≈ 0.0009

REF.

G. Baciú, G. C. Bonazzola, B. Minetti, C. Molino, L. Pasqualini
and G. Piragino

ELEM. SYM.

A

Z

Cu

29

Nuclear Phys. 67, 178 (1965)

METHOD

NBS Monitor

[Page 1 of 2]

REF. NO.

65 Ba 3

EGF

REACTION	RESULT	EXCITATION ENERGY	SOURCE		DETECTOR		ANGLE
			TYPE	RANGE	TYPE	RANGE	
G,XN	ABX	THR -28	C	10-30	BF3-I		4PI

TABLE 2
Cross sections for Co, Ni, Cu and Ga

	E_m (MeV)	σ_m (mb)	$\int_0^x \sigma(E) dE$ (mb · MeV)	Ref.
Co ⁵⁹	16.9	130	750(24)	^{a)}
	16.75 19	110 103	709(25)	^{a)}
	17.5	68	725 ± 72(28)	^{a)}
	16.5 19	82 80	701 ± 91(29)	¹⁴⁾
	16.5 19	72 74	657 ± 89(28)	this work
			537 ± 34(24)	this work
			445 ± 48(24)	^{a)}
Ni	16.5	50	340(24)	¹¹⁾
	16.5	46 ± 1	313 ± 48(28)	this work
			276 ± 25(24)	this work
Ni ⁵⁸	18.5	60	330(24)	¹²⁾
		30	180(24)	¹³⁾
	20.5	21	160(24)	¹³⁾
	19.0	32	220 ± 30(32)	¹⁴⁾
Ni ⁶⁰	16.5	85	440(± 20 %)(24)	^{b)}
Cu	19.5	120	870(20)	^{a)}
			904(27)	¹⁵⁾
	17.2	126	930(27)	¹⁶⁾
	17	90	450 ± 15(19,6)	¹⁷⁾
	16.75	71 ± 7	745 ± 74(28)	¹⁸⁾
	17.0	86 ± 2	733 ± 105(28)	this work
			451 ± 18(20)	this work
Ga	16.5	115 ± 3	947 ± 98(28)	this work

σ_m is the peak value of the cross section, E_m is the peak energy and $\int_0^x \sigma(E) dE$ is the integrated cross section. The upper limit of the integration is indicated in parentheses.

^{a)} Value obtained subtracting the $(\gamma, 2n)$ reaction contribution from the $\sigma(\gamma, Tn)$.

^{b)} Value obtained by subtracting the $Ni^{58}(\gamma, n)Ni^{57}$ reaction contribution from the $\sigma(\gamma, Tn)$ for natural nickel corrected for the $(\gamma, 2n)$ reaction contribution.

8) R. Montalbetti, L. Katz and J. Goldenberg, Phys. Rev. 91 (1953) 659

9) P. A. Flurnoy, R. S. Ticle and W. D. Whitehead, Phys. Rev. 120 (1960) 1424

10) E. B. Bazhanov, A. P. Komar and A. V. Kulikov, JETP 46 (1964) 1497

11) J. Goldenberg and L. Katz, Can. J. Phys. 32 (1954) 49

12) L. Katz and A. G. W. Cameron, Can. J. Phys. 29 (1951) 518

13) J. P. Roalswing, R. N. H. Haslam and D. J. McKenzie, Can. J. Phys. 37 (1959) 607

14) J. H. Carver, and W. Tuchinetz, Proc. Phys. Soc. 73 (1959) 585

15) L. W. Jones and K. M. Terwillinger, Phys. Rev. 91 (1953) 699

16) B. I. Gavrilov and L. E. Lazareva, JETP (Soviet Physics) 3 (1962) 871

17) J. Miller, C. Schuhl and C. Tzara, Nuclear Physics 32 (1962) 236

18) S. C. Fultz, R. L. Bramblett, J. T. Caldwell and R. R. Harvey, Phys. Rev. 133 (1964) B1149

REACTION	RESULT	EXCITATION ENERGY	SOURCE		DETECTOR		ANGLE
			TYPE	RANGE	TYPE	RANGE	

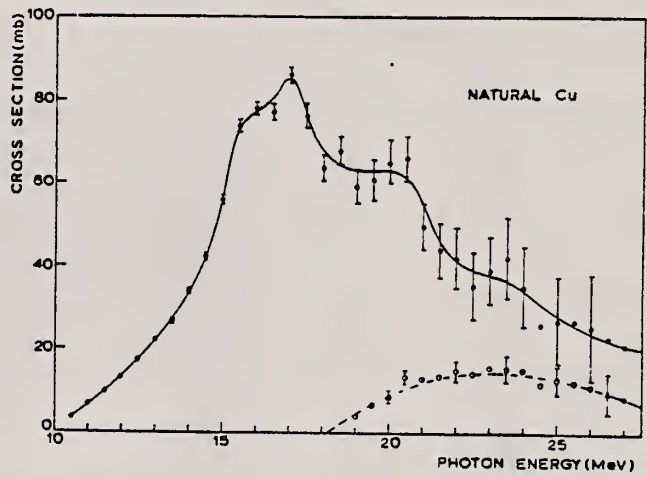


Fig. 3. The $\sigma(\gamma, Tn)$ for natural copper. An average curve is drawn through the experimental points. Open circles represent a calculation of the $\sigma(\gamma, 2n)$ with $a = 6.5 \text{ MeV}^{-1}$ and assuming that $\sigma(\gamma, Tn)$ has the same behaviour for Cu^{63} and Cu^{65} (see ref. ¹⁸). The dashed line gives the $\sigma(\gamma, 2n)$ as measured by Fultz *et al.* ¹⁸).

ELEM. SYM.	A	Z
Cu		29
REF. NO.		EGF
65 Me 2		

METHOD

REACTION	RESULT	EXCITATION ENERGY	SOURCE		DETECTOR		ANGLE
			TYPE	RANGE	TYPE	RANGE	
G, A	SPC	THR - 35	C	35	SCD-D	5- 26	90

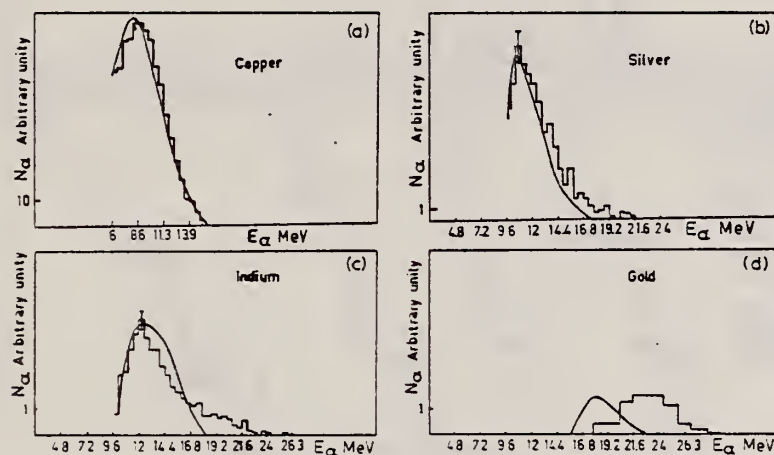


Fig. 2. The histograms show the experimental α -spectra. The solid lines are the calculated evaporative spectra corrected for target self-absorption and normalized to the maximum of the experimental spectra.

TABLE I
 α yields from the 90° data. Yield (per mole R)

Elements	Experimental	Calculated evaporative
Cu	$(1 \pm 0.1)10^3$	$3.1 \cdot 10^4$
Ag	$(2.8 \pm 0.3)10^4$	$3.4 \cdot 10^3$
In	$(1.05 \pm 0.1)10^4$	$3.05 \cdot 10^3$
Au	$(1.7 \pm 0.2)10^3$	8.7

Errors in experimental yields are compounded of statistical errors and errors in the absolute calibration of the beam.

REF.

ELEM. SYM. A Z

J.M. Wyckoff, B. Ziegler, H.W. Koch, and R. Uhlig
Phys. Rev. 137, B576-94 (1965)

Cu

29

METHOD

REF. NO.

65 Wy 1

NVB

Synchrotron; ion chamber monitor

REACTION	RESULT	EXCITATION ENERGY	SOURCE		DETECTOR		ANGLE
			TYPE	RANGE	TYPE	RANGE	
G, MU-T	ABX	10-35	C	90	SCI-D		4 f I

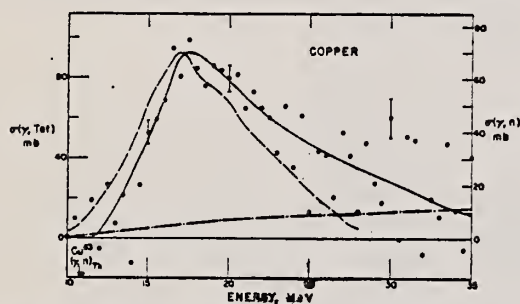


FIG. 27. Copper total photoneuclear cross section. The dashed line represents the $\sigma(\gamma, n)$ cross section of the Livermore group (Ref. 32) used with the right-hand ordinate scale.

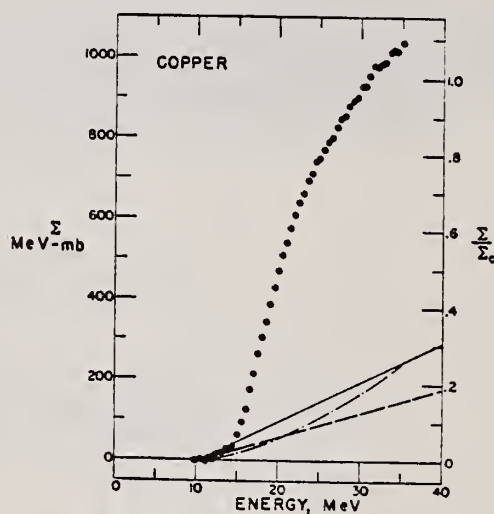


FIG. 28. Copper total photoneuclear cross section integrated over energy.

METHOD

Nuclear Resonance Scattering using N,G reactions.

REF. NO.

66 Be 3

JDM

REACTION	RESULT	EXCITATION ENERGY	SOURCE		DETECTOR		ANGLE
			TYPE	RANGE	TYPE	RANGE	
G,G	RLX	5 - 10	D	5 - 10	NAI-D	5 - 10	135

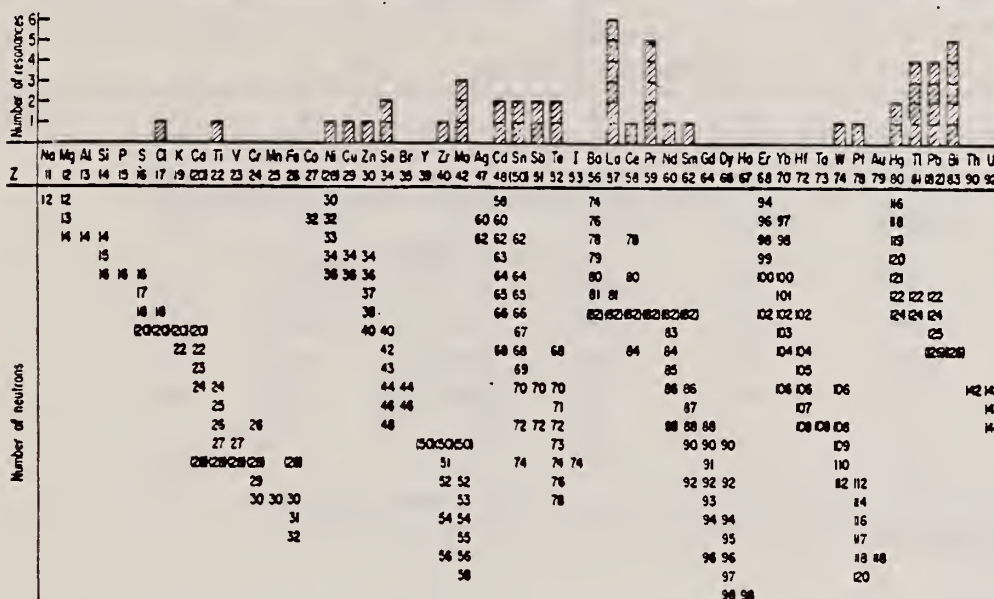


FIG. 3. Histogram of distribution of observed resonances among the different targets. The atomic number is given directly beneath the chemical symbol followed by the neutron numbers of the naturally occurring isotopes. Magic numbers are shown in brackets.

TABLE III. List of effective cross sections.

Scatterer	Energy (MeV)	Gamma source	σ (mb)	Scatterer	Energy (MeV)	Gamma source	σ (mb)
Sm ¹⁴⁴	8.997	Ni	100	Sn	7.01	Cu	110
Pr ¹⁴¹	8.381	Cr	9	Nd	6.867	Co	30
La	8.532	Ni	6	Pr ¹⁴¹	6.867	Co	3
Te	8.532	Ni	3*	Te	6.7	Ni	...
Cu	8.499	Cr	24	La	6.54	Ag	12
Zr	8.496	Se	3050	Cd	6.474	Co	110
Zn	8.119	Ni	13	Mo	6.44	Hg	25*
Se	7.817	Ni	50	La	6.413	Ti	72
Se	7.76	K	90	Mo	6.413	Ti	10
Sb	7.67	V	...	Ti	6.413	Ti	25
Cd	7.64	Fe	40*	W	6.31	Ti	...
Ni	7.64	Fe	7*	Sb	6.31	Hg	6*
Pr ¹⁴¹	7.64	Fe	12*	Ti	6.31	Hg	2*
Ti	7.64	Fe	370*	Sn	6.27	Ag	75
La	7.634	Cu	7	Pb ²⁰⁸	6.15	Gd	...
Mo	7.634	Cu	11	Te	5.8	Ni	...
Bi ²⁰⁹	7.634	Cu	4	La	6.12	Cl	35
Te	7.528	Ni	66*	Pr ¹⁴¹	6.12	Cl	110
Bi ²⁰⁹	7.416	Se	100	Pt	5.99	Hg	40*
Bi ²⁰⁹	7.300	As	30*	Ti	5.99	Hg	5*
Pb ²⁰⁸	7.285	Fe	4100	Pb ²⁰⁸	5.9	Sr	...
Cl	7.285	Fe	34	Ce	5.646	Co	17
Pr ¹⁴¹	7.185	Se	80	Bi ²⁰⁹	5.646	Co	55
Ti	7.16	Cu	120	Pb ²⁰⁸	5.53	Ag	70
La	7.15	Mn	50	Hg	5.44	Hg	75*
Bi ²⁰⁹	7.149	Ti	2000	Hg	4.903	Co	385

- * High-energy component of a complex spectrum.
- * A broad scattered spectrum with no observable peak structure.
- * There are actually two lines of energies 7.647 and 7.633 MeV having equal intensities in the iron capture gamma spectrum. The cross section has therefore been corrected, although there is no possibility at present of deciding which line is responsible for each resonance.
- * Is probably an independent level in the complex spectrum of Ni 7 rays on Te.
- * Rough estimate.
- * May be inelastic component from 7.528 level in Te.
- * The relative line intensities in this case are due to Groshev and co-workers.
- * No line is known for the source at this energy.
- * Difficult to resolve among the many source lines present at this energy.

REF.	H. Hoffmann, B. Prowe and H. Ullrich Nuclear Phys. <u>85</u> , 631 (1966)		ELEM. SYM.	A	Z
			Cu		29
METHOD			REF. NO.		
Betatron			66 Ho 3	JDM	

REACTION	RESULT	EXCITATION ENERGY	SOURCE		DETECTOR		ANGLE °
			TYPE	RANGE	TYPE	RANGE	
G, A	ABY	THR-31	C	31	SCD-D	3-14	130

TABLE 1
Experimental data and results

Element	Mg	Al	S	Ni	Cu	Zn	Error (%)
target thickness (mg/cm ²)	0.81	1.54	0.80	2.50	2.68	3.00	5 ^{a)}
dose (r)	6190	25400	23200	3880	5840	4220	10
yield absolute (10 ⁶ /mole · r) for $E_m > 3.16$ MeV	0.61	0.93	1.46	1.65	0.92	2.42	11 ^{a)}
yield relative to Ni	0.36	0.56	0.88	1	0.55	1.43	5 ^{a)}
$Y_{\gamma, a}/Y_{\gamma, tot}(\%)$	9.6	11.4	12.4	7.0	3.2	^{b)}	
nuclear temp. θ (MeV)	1.43	1.48	1.46	1.04		0.91	10
level density parameter a (MeV ⁻¹)	5.1	4.8	4.9	8.6		10.8	10

^{a)} For S, the error of the target thickness has been 10 %, of the absolute yield 14 % and of the relative yield 10 %.

^{b)} For Zn $\sigma_{\gamma, tot}$ is not known.

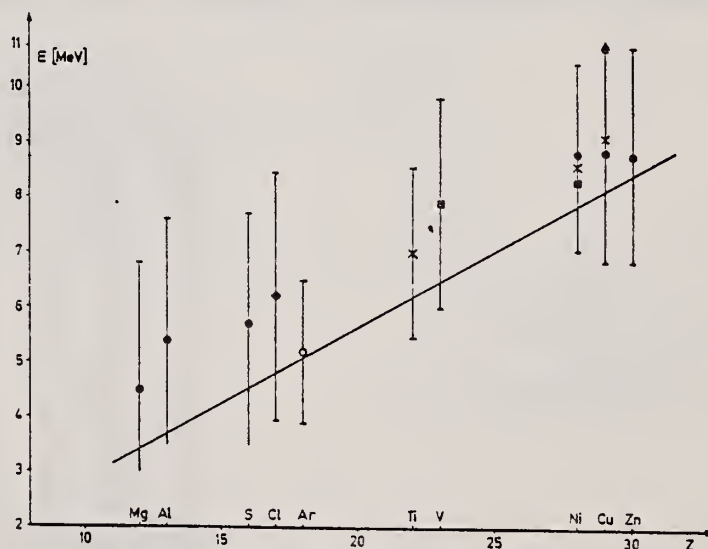


Fig. 4. Position of the peaks in different photoalpha spectra plotted against Z of the target nuclei. \times : Scheer *et al*¹⁰⁾, \blacksquare : Kregar and Povh⁹⁾, \blacktriangle : Meneghetti and Vitale⁶⁾, \blacklozenge : Erdős *et al*¹⁾, \circ : Komar *et al*⁷⁾, \bullet : this work. The signs show the position of the maximum, the bars give the widths at half maximum. The curve shows the height of the Coulomb barrier.

REF.

Yu. M. Volkov, A.P. Komar and V.P. Chizhov
 J. Nucl. Phys. (USSR) 3, 277 (1966)
 Sov. J. Nucl. Phys. 3, 198 (1966)

ELEM. SYM.

A

Z

Cu

29

METHOD

REF. NO.

66 Vo 1

JDM

REACTION	RESULT	EXCITATION ENERGY	SOURCE		DETECTOR		ANGLE
			TYPE	RANGE	TYPE	RANGE	
G,D	RLY	THR - 52	C	23 - 52	TEL-D	3.6 - 6.0	90
G,P	RLY	THR - 52	C	23 - 52	TEL-D	3.6 - 5.2	90

The results of irradiation of Cu are listed in Table II.

Table II

$E_{\gamma m}$, MeV	N	N_p	$(N/N_p) \cdot 10^3$
23	8	606	1.3
26.5	5	593	0.8
28.5	8	502	1.6
33	9	559	1.6
52	2	175	1.1

REF.

H. M. Gerstenberg and E. G. Fuller
NBS Tech. Note 416, June 1967

ELEM. SYM.

A

Z

Cu

29

METHOD

REF. NO.

67 Ge 2

HMG

REACTION	RESULT	EXCITATION ENERGY	SOURCE		DETECTOR		ANGLE
			TYPE	RANGE	TYPE	RANGE	
G,N	ABY	THR-27	C	22,27	BF3-I		4PI

Table 7. Comparison of neutron yields. Yields are given in units of (neutron $\text{cm}^2/\text{MeV nucleus}$) $\times 10^{-30}$. The estimated uncertainties in Y and Y_c are of the order of 6% and 10%, respectively.

Element	E_0	$Y(E_0)$									Ref.
			UCRL	Saclay	Va.	NBS(Old)	UCRL	Saclay	Va.	NBS(Old)	
			Exp	Exp	Exp	Exp	Exp	Exp	Exp	Exp	
			Y_c				Y_c/Y				
Pb	27	103	86				0.83				26,30
	22	111	92	116			0.83	1.05			
Au	27	89	97				1.09				24,30,38
	22	92	98	88		115	1.07	0.96		1.25	
Ta	27	81	82	77			1.01	0.95			27,30,38
	22	85	79	80		113	0.93	0.94		1.33	
Ho	27	67	75				1.12				27,31,39
	22	69	77	82		103	1.12	1.19		1.49	
Ag	27	36									
	22	34.8									
Cu	27	14.4	13.2				0.92				28,30
	22	12.6	11.5	12.4			0.91	0.98			
Co	27	12.7	12.1				0.95				29,34
	22	10.6	9.9		13.5		0.94		1.27		
Cs	27	1.69		1.13	1.01			0.67	0.60		32,35
P	27	2.35			1.76				0.75		36
Al	27	1.92	1.62		1.38		0.84		0.72		25,37
O ¹⁸	27	0.54	0.42	0.48	0.42		0.78	0.89			16,32,37
C	27	0.50	0.35	0.33	0.46		0.70	0.66			25,32,33

[over]

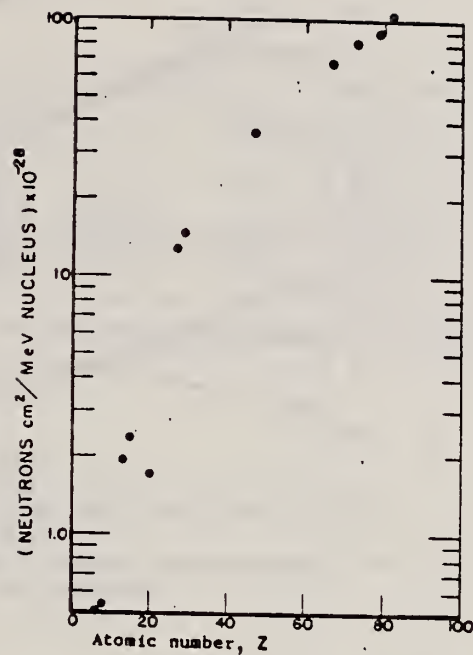


Fig. 31. Absolute neutron yield as a function of atomic number. The neutron yield from calcium ($Z = 20$) is particularly low in comparison with the other elements because its (γ, n) threshold is high compared to the mean energy of the giant resonance.

ELEM. SYM.	A	Z
Cu		29
REF. NO.		
67 Gi 1		egf

METHOD			SOURCE		DETECTOR		ANGLE °
REACTION	RESULT	EXCITATION ENERGY	TYPE	RANGE	TYPE	RANGE	
G,G	LFT	6,8	D	6-8	NAI-D	4-8	DST

Note: Varied Doppler Width

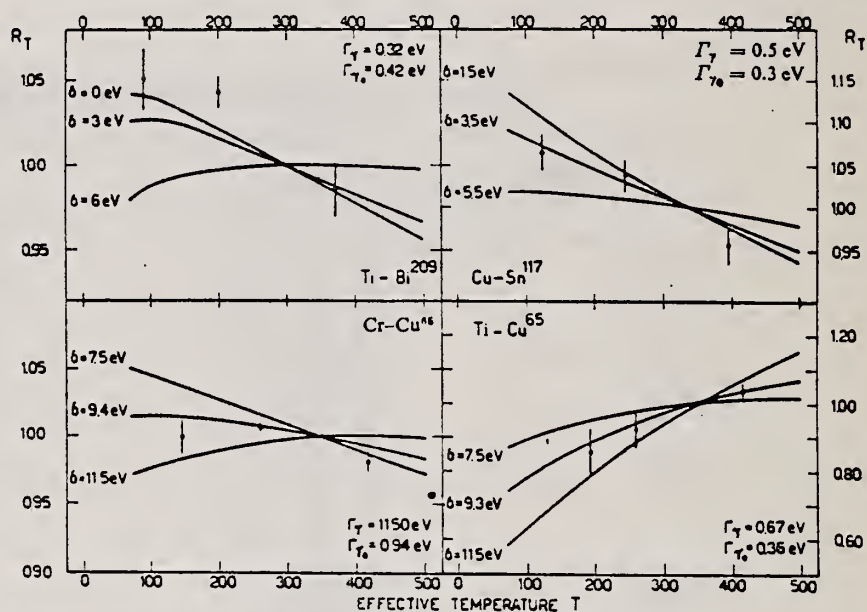


Fig. 7. Calculated variation in resonant scattering cross section as a function of scatterer temperature for different values of δ . Eq. (11) defines R_T .

TABLE 3
Angular distribution results

Resonant isotope	Resonant level energy (MeV)	Ground state spin	Resonant level spin	Statistical factor g	A_1^{exp}	A_1^{th}
Bi	7.15	$\frac{1}{2}$	$\frac{1}{2}$	1.2	0.15 ± 0.04	0.09
			$\frac{3}{2}$	1.0		0.19
			$\frac{5}{2}$	0.8		0.03
Sn	7.01	$\frac{1}{2}$	$\frac{1}{2}$	1.0	0.24 ± 0.04	0
			$\frac{3}{2}$	2.0		0.25
Cu	8.50	$\frac{1}{2}$	$\frac{1}{2}$	0.5	0.00 ± 0.05	0
			$\frac{3}{2}$	1.0		0.16
			$\frac{5}{2}$	1.5		0.14
Cu	6.07	$\frac{3}{2}$	$\frac{1}{2}$	0.5	0.20 ± 0.04	0
			$\frac{3}{2}$	1.0		0.16
			$\frac{5}{2}$	1.5		0.14

[over]

TABLE 4
Experimental results

Source-scatterer	Energy (MeV)	Γ_γ (eV)	$\Gamma'_{\gamma 0}$ (eV)	$\Gamma'_{\gamma 0}/\Gamma_\gamma$	δ (eV)	$\langle\sigma_{\gamma\gamma}\rangle$ (b)	$\bar{\sigma}_{r_s}$ (b)
Ti- ²⁰⁹ Bi	7.15	0.32 ± 0.23	0.42 ± 0.14	> 0.68	< 2	2.6 ± 0.8	3.6 ± 1.2
Cu- ¹¹⁷ Sn	7.01	0.5 ± 1.1	0.3 ± 0.3		3.6 ± 0.7	1.2 ± 0.4	3.4 ± 3.5
Cr- ⁶³ Cu	8.50	11.5 ± 8.0	0.94 ± 0.29	0.08 ± 0.04	9.4 ± 0.7	$(4.2 \pm 1.3) \cdot 10^{-2}$	0.64 ± 0.20
Ti- ⁶³ Cu	6.07	0.67 ± 0.35	0.36 ± 0.07	0.54 ± 0.19	9.3 ± 0.8	0.44 ± 0.13	2.0 ± 0.4
Ti- ⁶³ Cu	6.07	0.32 ± 0.18	0.16 ± 0.03	0.51 ± 0.18	9.2 ± 0.8	0.20 ± 0.06	0.92 ± 0.19

In the last two columns, $\langle\sigma_{\gamma\gamma}\rangle$ and $\bar{\sigma}_{r_s}$ are effective cross sections measured at temperature $T_0 = 300^\circ \text{ K}$.

REF. G. Khr. Tumbev
Compt. Rend. Acad. Bulg. Sci., 20, 541 (1967)

ELEM. SYM.	A	Z
Cu		29
REF. NO.		
67 Tu 4		egf

METHOD

REACTION	RESULT	EXCITATION ENERGY	SOURCE		DETECTOR		ANGLE
			TYPE	RANGE	TYPE	RANGE	
G.G	ABX	6	D	6	NAI-D		
		(6.41)					

NSA 22571

22571 RESONANCE SCATTERING OF GAMMA RAYS BY COPPER. Tumbev, G. Khr. Compt. Rend. Acad. Bulg. Sci., 20: 541-3(1967). (In Russian).

Gamma rays from the capture of thermal neutrons can be used to investigate resonance scattering in the region of 6 to 9 MeV. The advantage of using monochromatic gamma rays for investigating resonance scattering is obvious in this case where excitation of only one level is to be expected. Resonance scattering by copper was observed with the use of TiO_2 having a weight of 1350 g as a source of gamma rays. Source and scatterer were natural isotopic mixtures. Resonance gamma rays having an energy $E_{\gamma} = 6.41$ MeV showed an increased count rate due to nuclear resonance scattering of gamma rays from Ti on Cu. Control experiments were carried out with the source and without it. The cross-section for the gamma ray resonance scattering $\sigma_{\gamma\gamma}$ was determined from the count rates under the 6.41 MeV photopeaks at different reactor power levels for a 4 in. \times 6 in. NaI(Tl) crystal. The value of $\sigma_{\gamma\gamma}$ was found to be 16.6 ± 3.4 mb. Since a natural mixture of copper isotope was used as the scattering agent, it was not possible to determine whether ^{63}Cu or ^{65}Cu scattered the 6.41-MeV gamma rays by resonance. (TTT)

REACTION	RESULT	EXCITATION ENERGY	SOURCE		DETECTOR		ANGLE
			TYPE	RANGE	TYPE	RANGE	
G.N	ABX	50-85	C	55,85	TOF-D	10-85	67
							(67.5)

NEUT ENGY SPEC

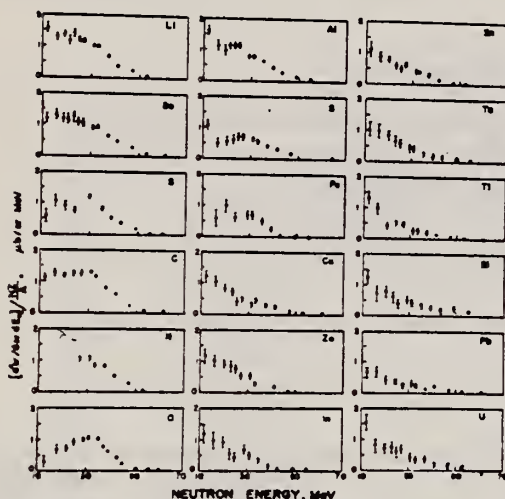


FIG. 6. Observed neutron spectra due to 55-85-MeV difference photon spectra. The effective cross sections have been divided by NZ/A .

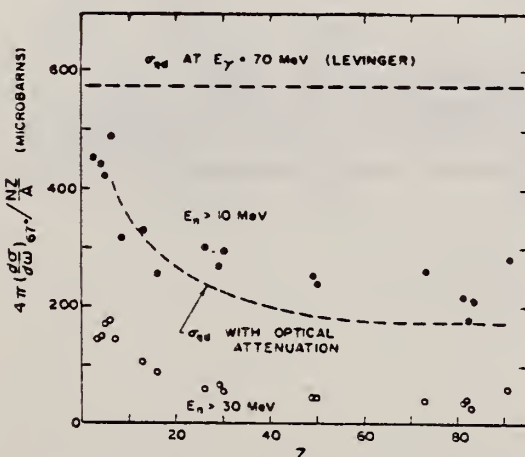


FIG. 7. Effective cross sections for production of fast neutrons with energies greater than 10 MeV (solid circles) and 30 MeV (open circles) by the 55-85-MeV photon difference spectrum. The dashed curves are modified quasideuteron model predictions as discussed in the text.

TABLE I. Comparison of present cross-section values in mb for production of high-energy photoneutrons by 55-85-MeV photons with measured cross sections $\sigma(\gamma, Tn)$, also in mb, for total photoneutron production. The present cross-section values are uncertain by 8 to 10% because of counting statistics and normalization errors; in addition all values depend on an absolute normalization in terms of the deuteron photodisintegration cross section, which is known to about 10% at these energies.

Target	$4\pi(d\sigma/dE)_{\sigma^*}$ ($E_n > 10$ MeV) [Present experiment]	$\sigma(\gamma, Tn)$ Jones and Terwilliger ^a	Costa <i>et al.</i> ^b	Other results
Li	0.75		1.0	
Be	1.0	2.7	2.3	2.3 ^c
B	1.0		1.4	
C	1.5	1.3	1.4	2.4 ^d
O	1.3		1.6	
Al	2.8	5.5	4.6	8 ^d
S	2.1		4.4	6.5 ^d
Fe	4.2	16	12	
Cu	4.3	20	19	
Zn	4.4		15	
In	7.4			
Sn	7.0			
Ta	10.7	95		
Tl	10.7			
Pb	8.3	100		
Bi	13			
U	16	65		

^a Average cross sections between 55 and 85 MeV, as read from Figs. 4 and 5 of Ref. 4.

^b $f_{\sigma} = \int \sigma dE - \int \sigma_{qd} dE/50$, as taken from Fig. 4 of Ref. 5 and Table I of Ref. 6.

^c S. Costa, L. Pasqualini, G. Piragino, and L. Roasio. Nuovo Cimento 42, 306 (1966).

^d G. Bishop, S. Costa, S. Ferroni, R. Malvano, and G. Ricco. Nuovo Cimento 42, 148 (1966).

REF. T. Tomimasu
J. Phys. Soc. Japan 25, 655 (1968)

ELEM. SYM.	A	Z
Cu		29

METHOD

REF. NO.

68 To 1

egf

REACTION	RESULT	EXCITATION ENERGY	SOURCE		DETECTOR		ANGLE
			TYPE	RANGE	TYPE	RANGE	
G, XN	ABX	10-24	C	10-24	BF3-I		4PI

MONITOR CALIBRATIONS

Table II. Parameters of the photoneutron cross sections for natural Cu and Pb. *The contribution of the (γ, p) cross section for Cu was considered.

	K_{α} (MeV)	σ_{α} (mb)	Γ (MeV)	$\sigma_0 = \Sigma$ (MeV-mb)	Σ/Σ_0	$\sigma-2$ (mb/MeV)	$\frac{\sigma-2}{0.00225 A^{2/3}}$
Cu	17.2 ± 0.3	78 ± 8	8.0 ± 0.5	587 ± 90	0.62 ± 0.1	1.81 ± 0.24	0.75 ± 0.11 ($0.95 \pm 0.14^*$)
Pb	14.1 ± 0.3	660 ± 60	5.0 ± 0.2	3910 ± 590	1.32 ± 0.2	18.6 ± 2.4	1.13 ± 0.17

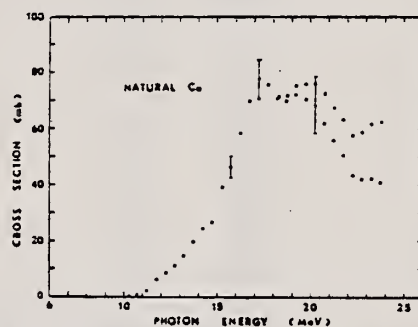


Fig. 10. The photoneutron cross section for natural Cu is represented by the open circles. The photoneutron yield cross section is represented by the closed circles.

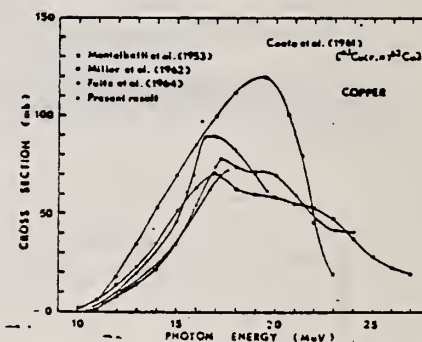


Fig. 12. Comparison of the photoneutron cross sections for natural Cu.

REF.

V. Di Napoli, D. Margadonna & F. Salvetti
Ricerca Scientifica 39, 133 (1969)

ELEM. SYM.

A

Z

Cu

29

METHOD

REF. NO.

69 D1 3

egf

REACTION	RESULT	EXCITATION ENERGY	SOURCE		DETECTOR		ANGLE
			TYPE	RANGE	TYPE	RANGE	
G, SPL	RLY	THR-600	C	600	ACT-I		4PI

TABELLA 1 - Rese relative dei prodotti di spallazione.

REAZIONE CONVENZIONALE (*)	PRODOTTO RADIOATTIVO	RESE RELATIVA (UNITÀ ARBITRARIE)
(γ , 2 p 3 n) (γ , 2 p 5 n)	Co ⁶⁰	8 ± 1
(γ , 2 p 4 n) (γ , 2 p 6 n)	Co ⁵⁹	5 ± 1
(γ , 2 p 5 n) (γ , 2 p 7 n)	Co ⁵⁸	$2,0 \pm 0,4$
(γ , 3 p n) (γ , 3 p 3 n)	Fe ⁵⁶	$0,20 \pm 0,04$
(γ , 4 p 5 n) (γ , 4 p 7 n)	Mn ⁵⁴	$0,11 \pm 0,02$
(γ , 5 p 7 n) (γ , 5 p 9 n)	Cr ⁵¹	$2,0 \pm 0,5$
(γ , 8 p 9 n) (γ , 8 p 11 n)	Sc ⁴⁶	$0,20 \pm 0,05$

(*) Come è stato detto, il metodo usato non permette di stabilire univocamente il numero di nucleoni singoli o di aggregati di nucleoni che fuoriescono dal nucleo; convenzionalmente la reazione è indicata in base al numero di nucleoni singoli che ne permettono il bilancio. Essendo d'altra parte il rame naturale costituito dai due isotopi ⁶³Cu e ⁶⁵Cu con abbondanze relative del 69,1 % e 30,9 % rispettivamente, per ogni prodotto sono indicate due reazioni, la prima per ⁶³Cu e la seconda per ⁶⁵Cu.

REF.

B.S. Ishkhanov, I.M. Kapitonov, E.V. Lazutin, I.M. Piskarev,
V.G. Shevchenko
Ser.III Fiz. Astron. 25, 606 (1970)

ELEM. SYM.

A

Z

Cu

29

METHOD

REF. NO.

70 Is 6

egf

REACTION	RESULT	EXCITATION ENERGY	SOURCE		DETECTOR		ANGLE °
			TYPE	RANGE	TYPE	RANGE	
G,XN	ABX	10-30	C	10-30	BF3-I		4PI

Таблица 2

487

Интегральные сечения фотонейтронных реакций на меди
для образцов, состоящих из естественной смеси
изотопов

$\sigma(\gamma, n) + \sigma(\gamma, np) + \sigma(\gamma, 2n)$ Мэб·мб	$\sigma(\gamma, n)$ Мэб·мб	$\sigma(\gamma, 2n)$ Мэб·мб	Ссылка на публику
870 (23)	—	—	[8]
904 (27)	—	—	[9]
930 (27)	—	—	[10]
—	450 ± 15 (19,6)	—	[11]
—	525 ± 52 (28)	110 ± 11	[12]
733 ± 105 (28)	—	—	[13]
1060 (30)	—	—	[14]
—	480 (23)	—	[15]
610 (24)	—	—	[16]
1200 ± 100 (30)	624 ± 40 (30)	288 ± 30 (30)	настоя- щая статья то же » »
1050 ± 80 (27)	—	—	
710 ± 60 (23)	—	—	

В скобках указан верхний предел интегрирования.

28260 PHOTONEUTRON REACTIONS ON COPPER. Ishkhanov, B. S.; Kapitonov, I. M.; Lazutin, E. V.; Piskarev, I. M.; Shevchenko, V. G. Vestn. Mosk. Univ., Ser. III, Fiz. Astron. 11: 606-13 (Nov-Dec 1970). (In Russian).

The structure of photoneutron differential cross section in copper was studied. The energy dependence of cross sections of photoneutron reactions on copper at excitation from the threshold to 30 MeV was determined. Theoretical and experimental data were compared. (R.V.J.)

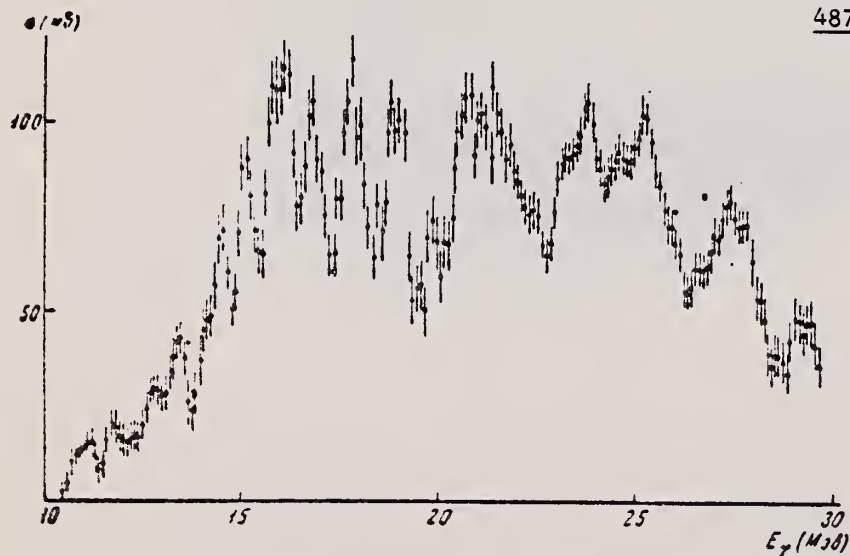


Рис. 2. Дифференциальное сечение реакции Cu (γ, n)

487

Таблица 1

Пороги различных фотонейтронных реакций на изотопах меди

Изотоп	Тип реакции	Порог (Мэв)
Cu ⁶³	(γ, n)	10,81
	(γ, np)	16,72
	(γ, 2n)	19,74
Cu ⁶⁵	(γ, n)	9,91
	(γ, np)	17,11
	(γ, 2n)	17,82
	(γ, 3n)	28,66

REF.

Yu. P. Antuf'ev, V. L. Agranovich, V. B. Ganenko, V. S. Kuz'menko,
I. I. Miroshnichenko, and P. V. Sorokin
Yad. Fiz. 13, 473 (1971); Sov. J. Nucl. Phys. 13, 265 (1971)

ELEM. SYM.	A	Z
Cu		29
71 An 1		hmg

METHOD

REF. NO.

REACTION	RESULT	EXCITATION ENERGY	SOURCE		DETECTOR		ANGLE
			TYPE	RANGE	TYPE	RANGE	
G,P	SPC	37-999	C	700,999	TEL-D	25-400	DST
G,D	SPC	45-999	C	700,999	TEL-D	25-400	DST

999=1.2 GEV, D/P

Table I. Values of the parameter τ , MeV

Target	$E_0 = 700 \text{ MeV}$										$E_0 = 1200 \text{ MeV}$									
	Protons					Deuterons					Protons					Deuterons				
	40°	60°	80°	100°	120°	40°	60°	80°	100°	120°	40°	60°	80°	100°	120°	40°	60°	80°	100°	120°
Li	46	42	34	30	27	28	24	22	21	20		45	28				27	24		
Be	48	43	36	30	27	28	26	24	22	19		45	28				27	24		
C	50	44	38	30	26	34	33	29	23	19	60	48	35	37	34	22				
Si		43			28		27			22		46	35			28	25			
Cu												45	29			27	24			
Ta					28					21		45	34			27	24			
Pb											51		29	36						22

Yield of protons 30-400 MeV, deuterons 30-200 MeV.

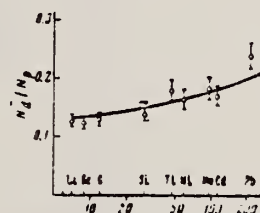


FIG. 4. The ratios N_d/N_p as a function of target-nucleus mass number A at an angle $\theta = 60^\circ$ for $E_0 = 1200 \text{ MeV}$. Solid curve $-A^{0.13}$.

The measured secondary-particle spectra for kinetic energies $T > 80 \text{ MeV}$ are well described by the expression

$$d^2\sigma/d\Omega dTQ = \text{const } T \exp(-T/\tau), \quad (1)$$

which is identical to the formula for the evaporation process.⁽⁴⁾ In Table I we have given the values of the parameter τ for the nuclei studied, at various angles. The accuracy in determination of τ is about 10%.

REF. I.A. Grishaev, A.N. Krinitsyn, N.I. Lapin, V.I. Nikiforov,
G.D. Pugachev, and B.I. Shramenko
Yad. Fiz. 14, 35 (1971)
Sov. J. Nucl. Phys. 14, 20 (1972)

ELEM. SYM.	A	Z
Cu		29
REF. NO.	71 Gr 2	
	hmg	

METHOD

REACTION	RESULT	EXCITATION ENERGY	SOURCE		DETECTOR		ANGLE °
			TYPE	RANGE	TYPE	RANGE	
G, PI+	ABY	150-560	C	560	EMU-D		DST
G, PI-	ABY	150-560	C	560	EMU-D		DST

PI-/PI+ YIELD RATIO

Cross section for photoproduction of π^- and π^+ mesons for
 $E_0 = 560$ MeV

Nucleus	$10^{-28} \text{ cm}^2/\text{sr MeV-equivalent}$							
	$\theta = 60^\circ$			$\theta = 120^\circ$				
	Data of ref. 1, T = 33 MeV			Our data, $T = 40$ MeV				
				Our data, $T = 40$ MeV				
				$T = 40$ MeV		$T = 60$ MeV		
	π^+	π^-	π^0	π^+	π^-	π^+	π^-	
C	21.4 ± 0.5	20.6 ± 1.5	26.2 ± 2	27.6 ± 2.1	36.8 ± 2.5	21.6 ± 2.1	26.8 ± 2.6	
Al	42.4 ± 1.0	38.5 ± 3	47.5 ± 4	57 ± 4	76 ± 5.4	41.2 ± 3.5	52 ± 1.7	
Cu	78.8 ± 1.6	71.6 ± 5.6	96 ± 8.6	109 ± 7.5	152 ± 10.8	81.5 ± 8.6	93.5 ± 10.7	
Pb				206 ± 18.5	369 ± 27	170 ± 19	240 ± 26.5	

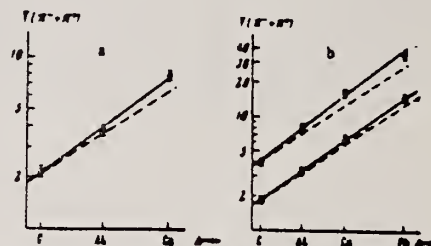


FIG. 1. Total yield of charged mesons as a function of atomic weight. The solid straight line is the experimental dependence, and the dashed straight line is the $A^{2/3}$ law. a— $\theta = 60^\circ$, $T = 40$ MeV; b— $\theta = 120^\circ$. Points: O— $T = 40$ MeV, Δ — $T = 65$ MeV.

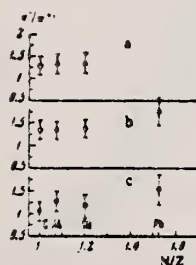


FIG. 3. π^-/π^+ yield ratio as a function of N/Z . a— $\theta = 60^\circ$, $T = 40$ MeV; b— $\theta = 120^\circ$, $T = 40$ MeV; c— $\theta = 120^\circ$, $T = 65$ MeV.

REF. T. Methasiri and S. A. E. Johansson
Nucl. Phys. A167, 97 (1971)

ELEM. SYM.	A	Z
Cu		29
REF. NO.		egf
71 Me 1		

REACTION	RESULT	EXCITATION ENERGY	SOURCE		DETECTOR		ANGLE
			TYPE	RANGE	TYPE	RANGE	
G,F	ABY	THR-900	C	300-900	FRG-1		4PI

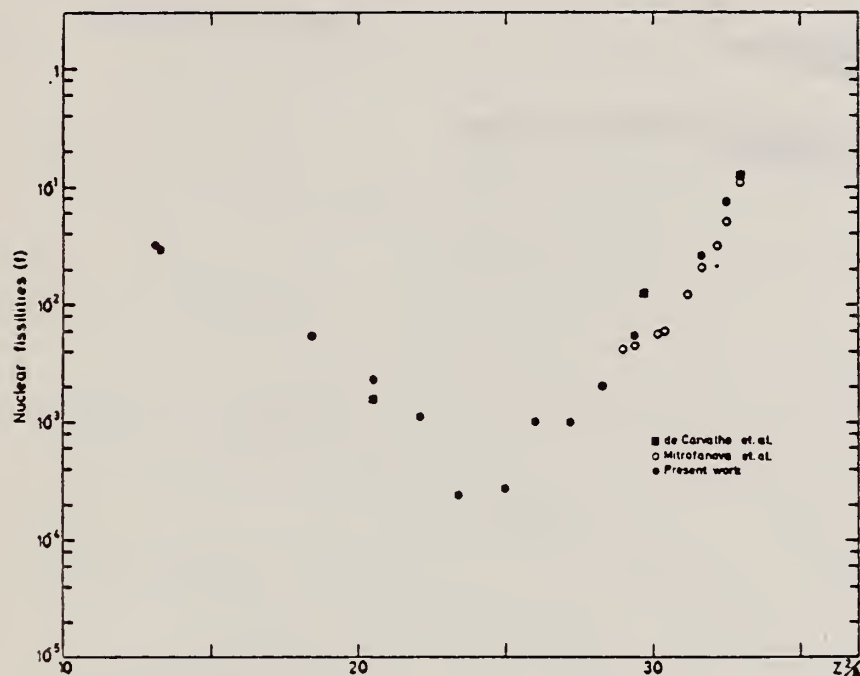


Fig. 2. Nuclear fissionities as a function of Z^2/A .

TABLE 1

The constant fission cross sections above the threshold

Element	σ_f (cm ²)	Element	σ_f (cm ²)
Pb	$(5.0 \pm 0.2) \times 10^{-27}$	La	$(1.1 \pm 0.1) \times 10^{-29}$
Au	$(1.7 \pm 0.1) \times 10^{-27}$	Sn	$(4.3 \pm 1.1) \times 10^{-29}$
Ta	$(3.3 \pm 0.2) \times 10^{-28}$	Ag	$(8.4 \pm 2.0) \times 10^{-29}$
Yb	$(1.2 \pm 0.2) \times 10^{-28}$	Mo	$(1.7 \pm 0.4) \times 10^{-28}$
Ho	$(5.5 \pm 0.3) \times 10^{-29}$	Cu	$(6.6 \pm 1.2) \times 10^{-28}$
Gd	$(5.3 \pm 0.8) \times 10^{-29}$	Ni	$(5.8 \pm 0.1) \times 10^{-28}$
Nd	$(1.3 \pm 0.2) \times 10^{-29}$		

[over]

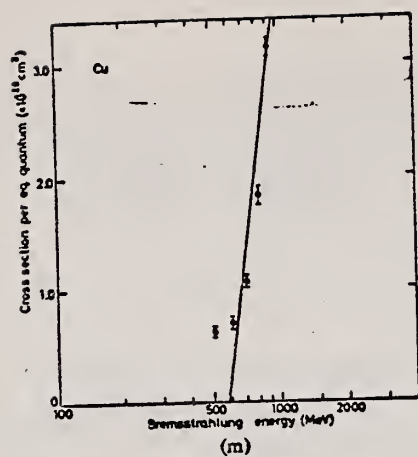


Fig. 1. Cross sections per equivalent quantum $\sigma_e(\hat{E})$ as a function of $\log \hat{E}$ of Pb, Au, Ta, Yb, Ho, Gd, Nd, La, Sn, Ag, Mo, Cu and Ni.

REF.

H. J. Von Eyss, H. Schier, and B. Schoch
 Elba-71, Tagungsbericht Elektronen Beschleuniger Arbeits Gruppen
 (Sept. 1971) Justus Liebig-Universitat Giessen. p.391

ELEM. SYM.

A

Z

Cu

29

METHOD

REF. NO.

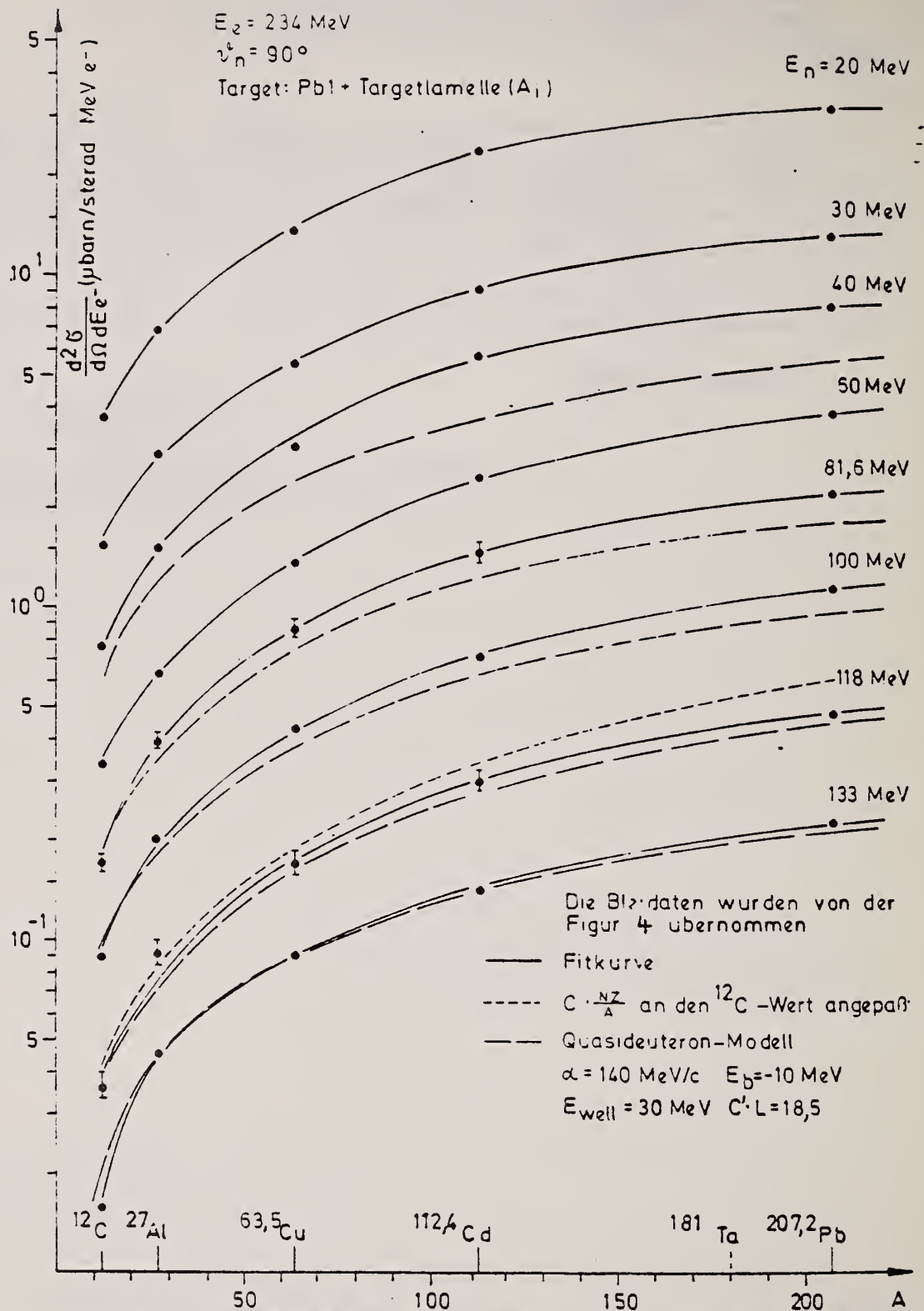
71 Vo 1

hmg

REACTION	RESULT	EXCITATION ENERGY	SOURCE		DETECTOR		ANGLE
			TYPE	RANGE	TYPE	RANGE	
E,N	ABX	THR-266	C	150-266	TOF-D		90

See over for figure.

[over]



Figur 3: Differentieller Neutronenproduktions-Wirkungsquerschnitt als Funktion der Massenzahl A für einige Neutronenenergien

REACTION	RESULT	EXCITATION ENERGY	SOURCE		DETECTOR		ANGLE
			TYPE	RANGE	TYPE	RANGE	
G,A	RLY	5-32	C	5-32	SCD-D		DST

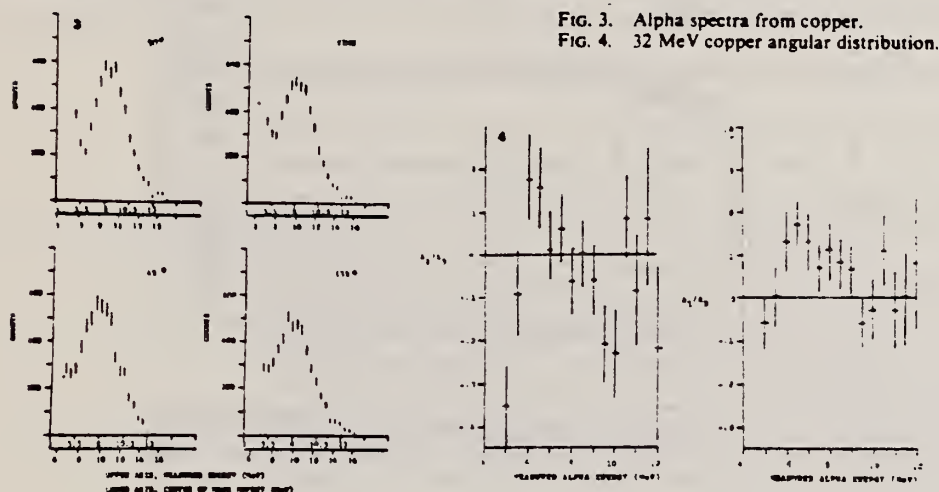


FIG. 3. Alpha spectra from copper.
FIG. 4. 32 MeV copper angular distribution.

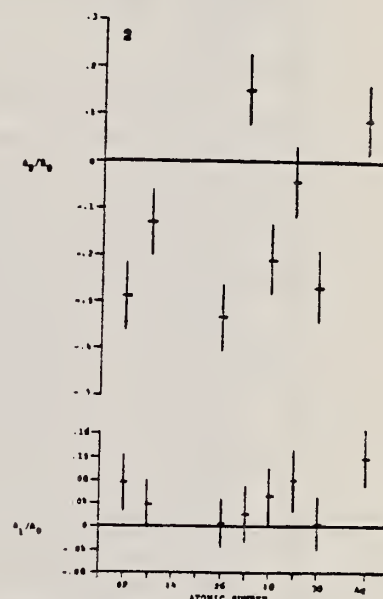


FIG. 2. Angular distributions for 32 MeV electron energy.

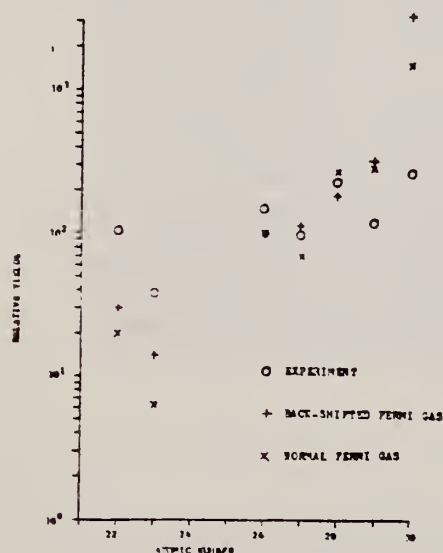


FIG. 13. Experimental and theoretical relative photo-alpha yields for 32 MeV electron beam energy.

TABLE 3. Observed angular distribution parameters for 32 MeV electron energy

Element	A_0	A_1/A_0	A_2/A_0
Ti	7.03 ± 0.15	0.073 ± 0.052	-0.286 ± 0.073
V	2.58 ± 0.06	0.037 ± 0.042	-0.126 ± 0.069
Fe	10.22 ± 0.30	0.006 ± 0.043	-0.333 ± 0.072
Co	6.80 ± 0.20	0.022 ± 0.048	$+0.016 \pm 0.077$
Ni	15.95 ± 0.49	0.051 ± 0.048	-0.213 ± 0.074
Cu	8.37 ± 0.28	0.076 ± 0.056	-0.035 ± 0.081
Zn	17.87 ± 0.61	0.004 ± 0.045	-0.270 ± 0.073
Ag	0.39 ± 0.01	0.115 ± 0.049	$+0.093 \pm 0.074$

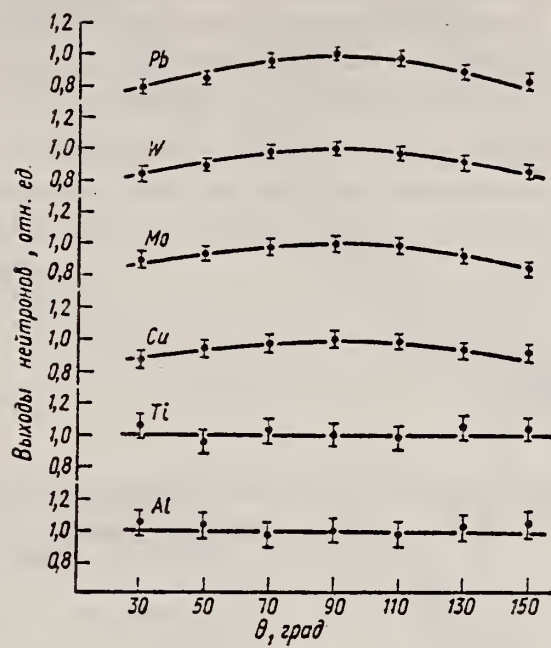
REF. V.P. Kovalev, V.P. Kharits, V.V. Gordeev, V.I. Isaev (USSR)
Atomnaya Energiya 32, 496 (1972)

ELEM. SYM.	A	Z
Cu		29
REF. NO.		hmg -
72 Ko 8		

REACTION	RESULT	EXCITATION ENERGY	SOURCE		DETECTOR		ANGLE
			TYPE	RANGE	TYPE	RANGE	
G,N	NOX	9- 22	C	12- 22	THR-I		DST

Ми- шень	Энер- гия элек- трон- ов, Мэв	Детек- тор	Угол, град							В/А
			30	50	70	90	110	130	150	
Al	22,5	P ³¹ (n, p)	1,05±0,08	1,03±0,08	0,97±0,08	1,0±0,08	0,98±0,08	1,02±0,08	1,04±0,08	Изоотроп- ноо
	22,5	Al ²⁷ (n, p)	0,90±0,15	0,95±0,15	1,02±0,15	1,00±0,14	0,96±0,13	1,07±0,13	1,01±0,13	•
Ti	22,5	P ³¹ (n, p)	1,04±0,07	0,96±0,07	1,03±0,07	1,00±0,07	0,98±0,07	1,05±0,07	1,03±0,07	•
	22,5	Al ²⁷ (n, p)	1,06±0,13	0,94±0,13	1,04±0,12	1,00±0,12	0,95±0,11	0,98±0,11	1,02±0,10	•
Cu	12,8	P ³¹ (n, p)	0,97±0,10	1,04±0,10	1,02±0,10	1,00±0,10	1,01±0,10	0,90±0,10	0,96±0,10	•
	17,0	P ³¹ (n, p)	1,03±0,07	0,97±0,07	1,00±0,07	1,00±0,07	1,06±0,07	0,95±0,07	0,88±0,07	•
	22,5	P ³¹ (n, p)	0,87±0,05	0,94±0,05	0,97±0,05	1,00±0,05	0,99±0,05	0,93±0,05	0,91±0,05	0,18±0,04
	22,5	Al ²⁷ (n, p)	0,75±0,09	0,86±0,07	0,93±0,06	1,00±0,05	1,02±0,05	0,94±0,04	0,90±0,04	0,28±0,06
Mo	22,5	P ³¹ (n, p)	0,90±0,05	0,93±0,05	0,93±0,05	1,00±0,05	0,99±0,05	0,92±0,05	0,84±0,05	0,21±0,04
	22,5	Al ²⁷ (n, p)	0,80±0,08	0,95±0,08	0,95±0,07	1,00±0,06	0,94±0,05	0,83±0,04	0,72±0,04	0,44±0,08
	22,5	Al ²⁷ (n, α)	0,72±0,08	0,84±0,08	0,89±0,08	1,00±0,08	0,95±0,08	0,87±0,08	0,63±0,08	0,78±0,18
W	22,5	P ³¹ (n, p)	0,85±0,04	0,90±0,04	0,98±0,04	1,00±0,04	0,98±0,04	0,92±0,04	0,87±0,04	0,25±0,04
	22,5	Al ²⁷ (n, p)	0,78±0,06	0,84±0,06	0,89±0,05	1,00±0,05	0,97±0,04	0,86±0,04	0,75±0,04	0,54±0,06
Pb	22,5	P ³¹ (n, p)	0,79±0,04	0,85±0,04	0,96±0,04	1,00±0,04	0,98±0,04	0,83±0,04	0,84±0,04	0,36±0,05
	22,5	Al ²⁷ (n, p)	0,70±0,09	0,81±0,08	0,94±0,07	1,00±0,06	0,94±0,06	0,80±0,05	0,69±0,05	0,69±0,12

[over]



Угловые распределения быстрых фотонейтронов из Al, Ti, Cu, Mg, W, Pb, облучаемых электронами с энергией 22,5 Мэв. Детектор ^{121}Si (n, γ) ^{121}Si .

ELEM. SYM.	A	Z
Cu		29
REF. NO.	73 Ba 20	
	egf	

METHOD

REACTION	RESULT	EXCITATION ENERGY	SOURCE		DETECTOR		-ANGLE
			TYPE	RANGE	TYPE	RANGE	
G,N	NOX	THR- 27	C	10- 27	BF3-I		4PI

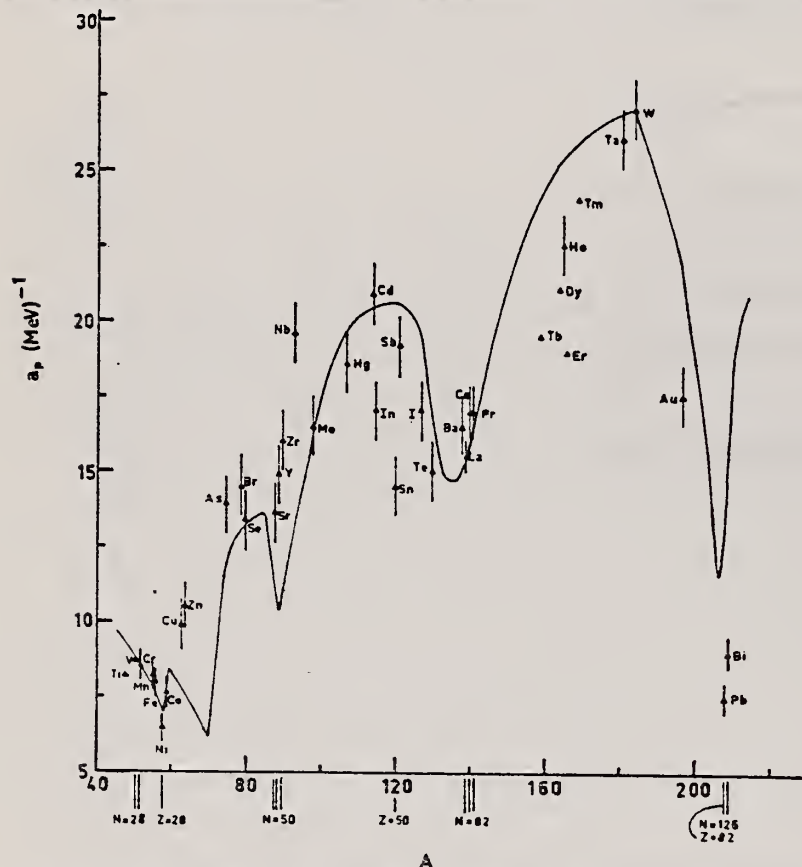


Fig. 12. Experimental values of the level density parameter a_p (Fermi gas formula plus pairing correction) versus atomic number A . The continuous curve is a least-squares fit to the data of a theoretical calculation from Newton ^{1,2}.

- 1 H. Baba and S. Baba, Japan Atomic Energy Research Institute report JAERI-1183 (1969).
- 2 H. Baba, Nucl. Phys. **A159**, 625 (1970).
- 15 T.D. Newton, Can. J. Phys. **34**, 804 (1956).

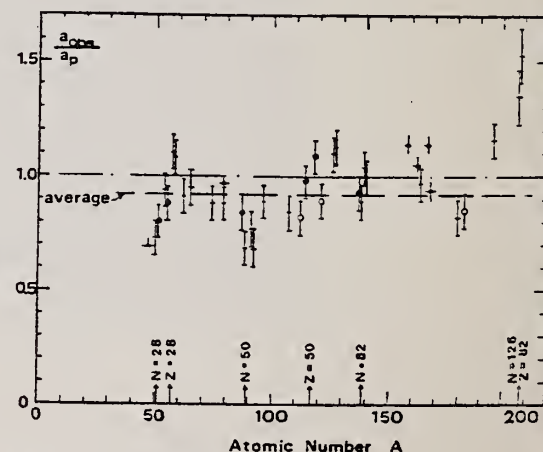


Fig. 15. Ratio a_{obs}/a_p versus atomic number A . Here a_{obs} is the level density parameter taken from the neutron resonance work of refs. ^{1,2}, and a_p is the level density parameter derived from the present (γ, n) work. Filled circles represent points where nuclei in the neutron resonance and in the (γ, n) experiment were the same. Open circles represent points where the respective nuclei were approximately matched. Triangles represent points which are based on measurement of neutron mean energies at two bremsstrahlung energies only.

(over)

TABLE 3

Comparison of experimental and theoretical data on nuclear level densities with Fermi gas formulae, and comparison of nuclear level density parameters from (γ, n) and n-resonance absorption experiments

Target	N (residual nucleus) ^{a)}	Goodness of fit ^{b)} no with p.c. p.c.	$\bar{E}_n(24)$ (MeV) ^{c)}	T (MeV) ^{d)}	a_p (MeV ⁻¹) ^{e)}	a_{obs} (MeV ⁻¹) ^{f)}	a_{obs}/a_p
Ti ^{g)}	23 8%		1.93		8.1- ⁴⁷ Ti	6.41- ⁴⁷ Ti	0.79
	24 8%						
	25 73%						
	26 5%						
	27 5%						
V ^{h)}	27 100%		1.96		8.7- ⁵⁰ V	6.35- ⁵¹ V	0.73
Cr	25 4%	P	1.89		8.6- ⁵¹ Cr	6.9- ⁵¹ Cr	0.80
	27 84%						
	28 10%						
	29 2%						
Mn	29 100%	V.P.	G	2.1	8.2- ⁵⁴ Mn	7.82- ⁵⁶ Mn	0.94
Fe	27 6%	F	G	1.96	8.0- ⁵⁵ Fe	7.06- ⁵⁵ Fe	0.88
	29 92%						
	30 2%						
Co	31 100%	P	F	2.12	7.7- ⁵⁸ Co	8.35- ⁶⁰ Co	1.08
Ni	29 68%	V.P.	P	1.4	6.5- ^{57,7} Ni	7.19- ⁵⁹ Ni	1.10
(Z = 28)	31 26%						
	32 1%						
	33 4%						
	35 1%						
Cu	33 69%	V.P.	P	1.78	9.8- ⁶³ Cu	8.90- ⁶⁴ Cu	0.91
	35 31%						
Zn	33 49%	F	F	1.61	10.5- ^{64,4} Zn	10.0- ⁶⁵ Zn	0.95
	35 28%						
	36 4%						
	37 19%						
As	41 100%	V.P.	F	1.44	14.5- ⁷⁴ As	12.81- ⁷⁶ As	0.88
Se ^{h)}	41 9%						
	42 8%						
	43 24%						
	45 50%						
	47 9%						
Br	43 45%	V.P.	V.P.	1.41	14.5- ⁷⁹ Br	12.69- ⁸⁰ Br	0.88
	45 49%						
Sr	47 10%	F	G	1.31	13.6- ⁸⁷ Sr	11.4- ⁸⁷ Sr	0.84
	48 7%						
	49 83%						

^{a)} Neutron numbers and abundances of respective residual nuclei in (γ, n) experiments.

^{b)} These give an assessment of the goodness of fit of a calculated \bar{E}_n versus E_0 curve to the observed data, using the Fermi gas level density formula both without and with pairing corrections.

^{c)} Bremsstrahlung photon neutron mean energies \bar{E}_n for peak bremsstrahlung energy $E_0 = 24$ MeV.

^{d)} Nuclear temperature from fit with constant-temperature formula.

^{e)} Level density parameter a_p derived from the present (γ, n) experiment, using a Fermi gas formula plus pairing correction, and corresponding residual nucleus (the atomic weight shown is the weighted average of atomic weights of the respective isotopes present).

^{f)} As column 7, but using data on n-resonance absorption from refs. 1, 4).

^{g)} Measurements of $\bar{E}_n(E_0)$ for these nuclei were made only for $E_0 = 21, 23$ and 24 MeV.

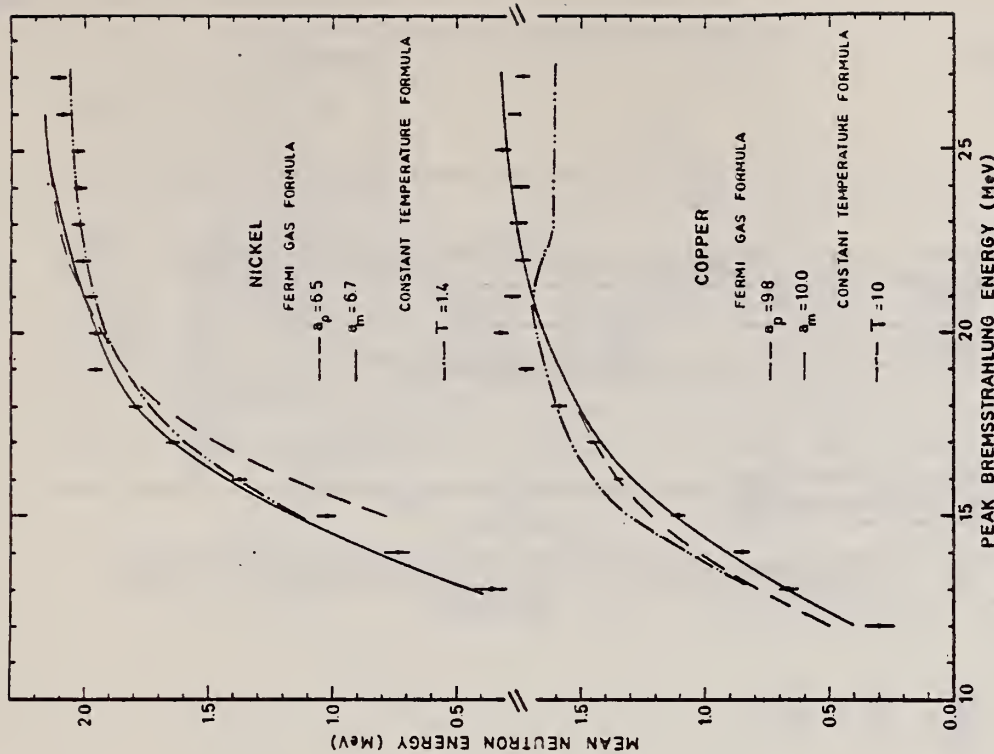


Fig. 6. Same as fig. 5, for nickel and copper.

ELEM. SYM.	A	Z
Cu		29
REF. NO.		egf.
73 Do 9		

METHOD				REF. NO.	
				73 Do 9	
REACTION	RESULT	EXCITATION ENERGY	SOURCE		ANGLE
			TYPE	RANGE	
G,XP	ABY	86-400	C	400	DST

Table 8. Copper. Bremsstrahlung endpoint energy: 400 MeV. Differential cross-sections in microbarns/sterrad · MeV · eq. quantum. Quoted errors: statistical in percent

Energy	Angle							
	30	40	50	60	74	90	110	130
81.9	12.3 2.1				6.17 2.0			
87.3		8.77 2.0	7.65 2.2	6.55 2.0		3.85 2.2	3.02 2.3	2.27 2.9
99.8	10.1 2.5				4.41 2.5			
104.8		6.91 2.5	5.72 2.7	4.95 2.5		2.85 2.7	1.92 3.2	1.48 3.8
106.7	9.17 3.1	7.27 2.8	5.76 2.6	4.93 2.5	3.92 2.6	2.84 2.4	2.16 2.8	
116.8	7.37 2.9				3.36 2.9			
121.3		5.23 2.8	4.17 3.2	3.39 3.0		1.96 3.3	1.28 3.8	0.874 4.9
129.2	6.39 4.0	4.82 3.8	4.02 3.4	3.32 3.2	2.62 3.5	1.88 3.2	1.20 4.0	
150.3	4.08 5.2	3.37 4.6	2.45 4.4	2.14 4.1	1.54 4.6	1.06 4.3	0.710 5.4	
169.7		2.39 3.9	2.00 3.3	1.63 3.3	1.09 2.4	0.660 4.0		
186.7		1.68 4.9	1.39 4.2	1.01 4.5	0.685 3.1	0.368 5.7		
203.6		1.24 5.7	0.949 5.0	0.650 5.5	0.372 4.2	0.180 8.1		
222.3	1.01 3.6	0.844 6.3	0.578 5.7					
225.4				0.340 5.7				
238.7	0.676 4.6	0.528 8.4	0.388 7.3					
241.7				0.221 7.4				
255.1	0.466 5.5	0.334 10.4	0.189 10.3					
258.0				0.109 10.3				

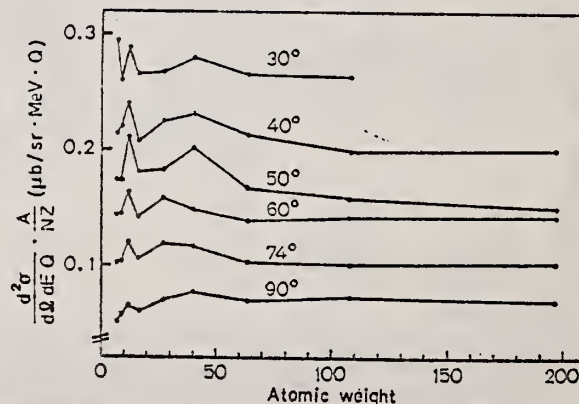


Fig. 8. Experimental cross-sections at various angles for $E_p = 150$ MeV divided by NZ/A plotted as a function of atomic weight

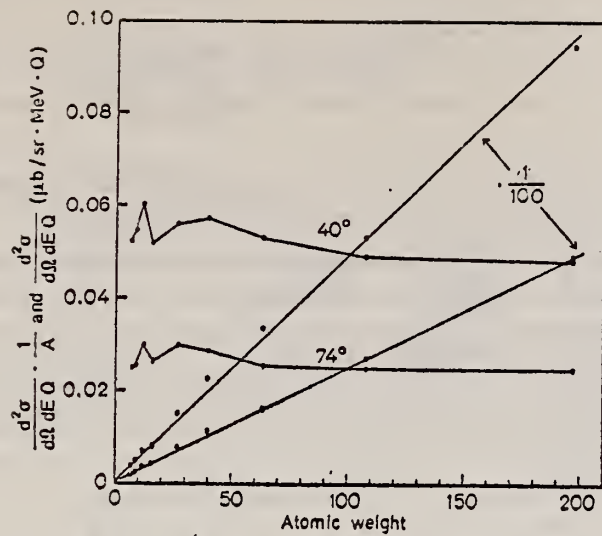


Fig. 9. In this figure, the straight lines show the experimental cross-sections at 40° and 74° for $E_p = 150$ MeV. The other curves are the same cross-sections divided by atomic weight

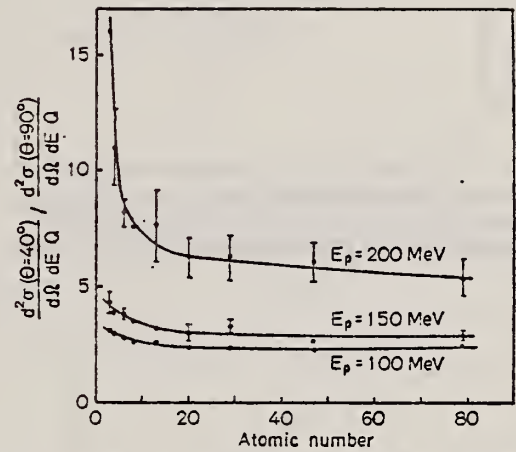


Fig. 6. The ratios of the experimental cross-sections at 40 and 90 degrees for selected proton energies as a function of atomic number

REF.

P. Dougan, T. Kivikas, K. Lugner, V. Ramsay, and W. Stiefler
 Phys. Letters 46B, 359 (1973)

ELEM. SYM.

A

Z

Cu

29

METHOD

REF. NO.

73 Do 11

egf

REACTION	RESULT	EXCITATION ENERGY	SOURCE		DETECTOR		ANGLE
			TYPE	RANGE	TYPE	RANGE	
G, XP	ABY	90-400	C	400	TEL-D		DST

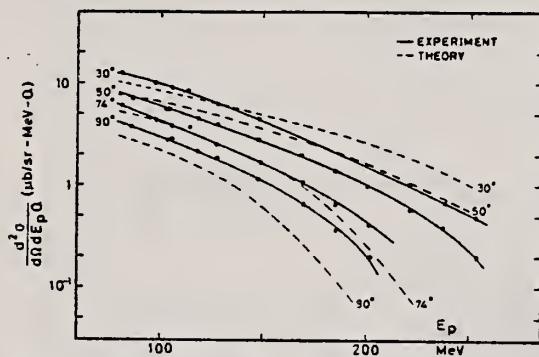


Fig. 2. Comparison of experimental and calculated cross sections for copper. The calculated results have been renormalized at a proton energy of 150 MeV and an angle of 74° by a factor of 0.78.

METHOD

REF. NO.	egf
73 By 3	

REACTION	RESULT	EXCITATION ENERGY	SOURCE		DETECTOR		ANGLE
			TYPE	RANGE	TYPE	RANGE	
G, XN	SPC	THR-234	G	234	TOF-D		90

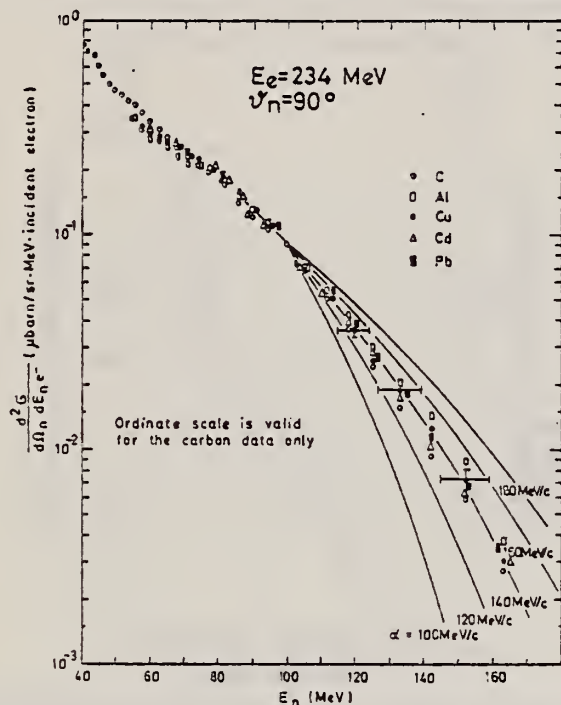


Fig. 8. Comparison of the shape of the high-energy part of the photoneutron spectra from C, Al, Cu, Cd and Pb. These measurements were performed with the same γ -shower spectrum, produced in a 0.3 cm thick lead sheet (see Fig. 2b). All spectra were fitted to the value for carbon at $E_n = 100$ MeV. The values predicted by a quasi-deuteron model (solid lines), which are also fitted at $E_n = 100$ MeV, were calculated with the parameters (defined in the text): $E_b = -10$ MeV, $E_{well} = 30$ MeV and $C'L = 19.0$ for different impulse parameters $\alpha = 100, 120, 140, 160$ and 180 MeV/c

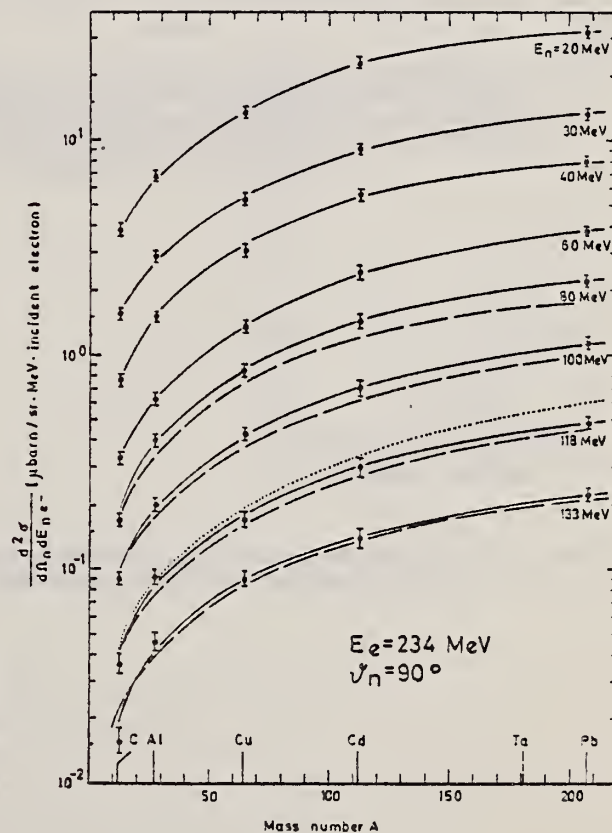


Fig. 9. Dependence of the production cross section on the mass number A with the neutron energy as parameter, measured at $E_e = 234$ MeV. The γ -quanta were produced in a 0.3 cm thick lead sheet (see Fig. 2b) in front of the target of mass number A . The solid lines are fit curves through the measured values. The dashed lines are values calculated using a quasi-deuteron model with the parameters (defined in the text): $E_b = -10$ MeV, $E_{well} = 30$ MeV, $\alpha = 140$ MeV/c and $C'L = 19.0$. The dotted curve represents the dependence NZ/A , fitted at $A = 12$. The error bars correspond to the statistical error

(over)

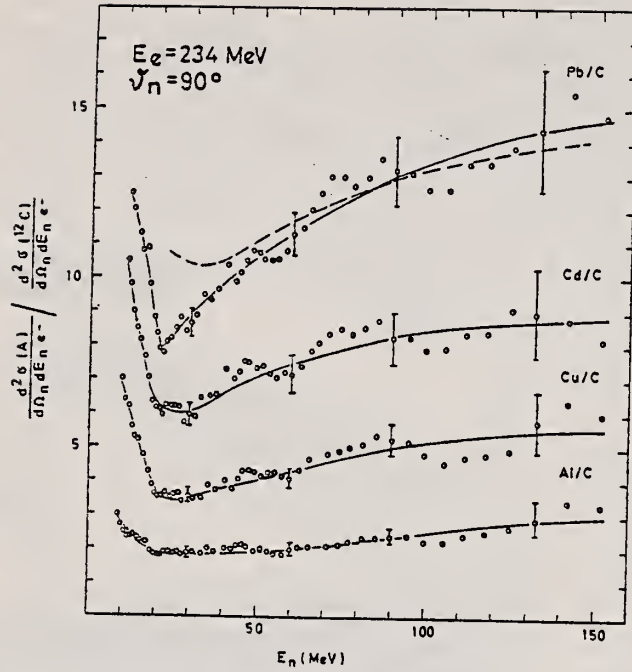


Fig. 10. Neutron yield from targets of mass number A relative to carbon, measured at $E_e = 234$ MeV. The target arrangement is that of Fig. 2b. The solid lines are fit curves through the experimental values. The dashed curve shows the energy dependence of the ratio of the nuclear absorption factors $f_a(\text{Pb})/f_a(\text{C})$, taken from Fig. 6. The error bars correspond to the statistical error.

REF. A. Järund, B. Friberg, and B. Forkman
Z. Physik 262, 15 (1973)

ELEM. SYM.	A	Z
Cu		29
REF. NO.		
73 Ja 3		egf

METHOD

REACTION	RESULT	EXCITATION ENERGY	SOURCE		DETECTOR		ANGLE
			TYPE	RANGE	TYPE	RANGE	
G, NA24	ABY	THR-999	G	100-999	ACT-I		4PI

999=1 GEV

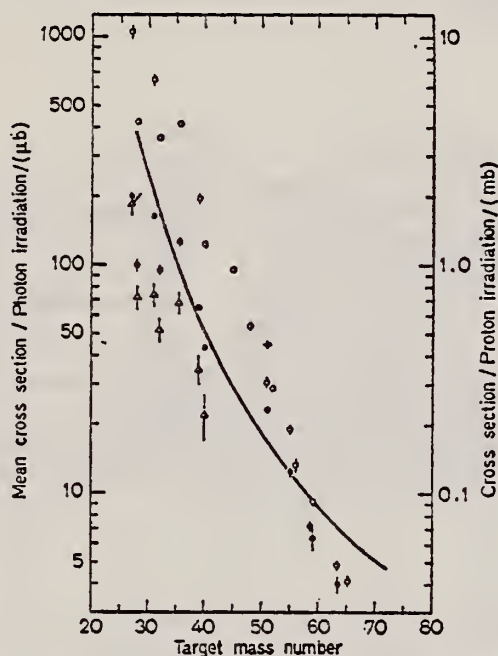


Fig. 7. Mean cross sections for ^{24}Na production as a function of target mass number. Present work filled circles. Noga *et al.* [3] open triangles, Kumbartzki *et al.* [13] cross and Korteling *et al.* [1] 400 MeV protons open circles. The solid line gives the mean cross sections calculated by Jonsson *et al.* [17]

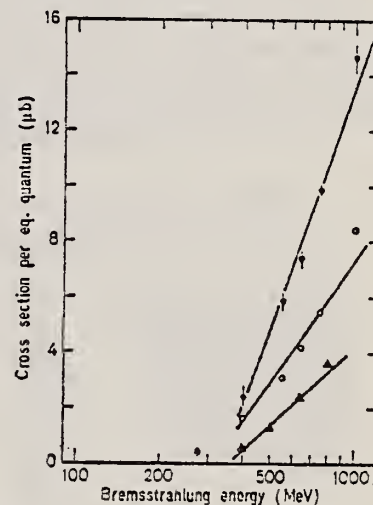


Fig. 6

Fig. 6. The determined yields for the reactions $^{55}\text{Mn} \rightarrow ^{24}\text{Na}$ (filled circles), $^{59}\text{Co} \rightarrow ^{24}\text{Na}$ (open circles) and $^{63,65}\text{Cu} \rightarrow ^{24}\text{Na}$ (filled triangles)

- ¹Korteling, R.G. *et al.*, J. Inorg. Nucl. Chem. 29, 2863 (1967).
- ³Noga, V.I. *et al.*, Sov. J. Nucl. Phys. 9, 637 (1969).
- ¹³Kumbartzki, G. *et al.*, Nucl. Phys. A176, 23 (1971).
- ¹⁷Jonsson, G.G. *et al.*, LUNP7212, Oct. 1972, to be published in Physica Scripta.

REF.

V.I. Noga, Yu.N. Ranyuk, and P.V. Sorokin
Yad. Fiz. 19, 945 (1974)
Sov. J. Nucl. Phys. 19, 484 (1974)

ELEM. SYM.	A	Z
Cu		29
REF. NO.		
74 No 2		hmg

METHOD

REACTION	RESULT	EXCITATION ENERGY	SOURCE		DETECTOR		ANGLE °
			TYPE	RANGE	TYPE	RANGE	
G,C058	RLX	THR-999	C	300*999	ACT-I		4PI
E,C058	RLX	THR-999	C	300*999	ACT-I		4PI

*999=1.2GEV, E/G

The induced-activity method has been used to study the ratio of the cross sections for photo- and electrodisintegration of nuclei for the reactions $^{27}\text{Al} \rightarrow ^{24}\text{Na}$ and $^{63,65}\text{Cu} \rightarrow ^{58}\text{Co}$ in the energy interval 300–1200 MeV. The results of the measurements are compared with calculations with various assumptions regarding the spectra of virtual and real photons.

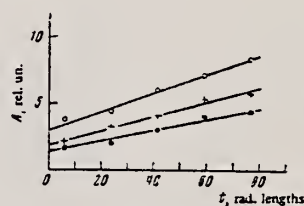


FIG. 1

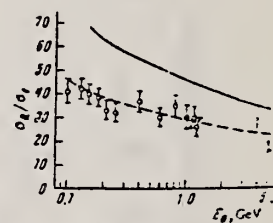
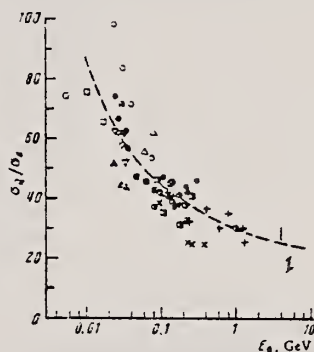


FIG. 2

FIG. 1. Target activity as a function of radiator thickness.
Points: \circ — $E_0 = 800$ MeV, $+$ — 1170 MeV, \bullet — 600 MeV.

FIG. 2. The ratio σ_Q/σ_e as a function of electron energy E_0 .
Points: \circ — $^{27}\text{Al} \rightarrow ^{24}\text{Na}$; \bullet — $^{63,65}\text{Cu} \rightarrow ^{58}\text{Co}$. The thin vertical line shows the data of ref. 4, and the heavy vertical line with end bars shows the data of ref. 5. The curves are theoretical.

FIG. 4. The ratio σ_Q/σ_e as a function of E_0 for various reactions. Points: $+$ — $^{27}\text{Al} \rightarrow ^{24}\text{Na}$; \bullet — $^{63,65}\text{Cu} \rightarrow ^{58}\text{Co}$. These points represent the data of the present work and of ref. 3. The other designations are given in ref. 9.



³V.I. Noga et al., Ukr. Fiz. Zh. 13, 2003 (1968).

⁴F.D.S. Butement, H.M.A. Karim, U.V. Myint, and M.B. Zaman, J. Inorg. Nucl. Chem. 33, 2791 (1971).

⁵C.B. Fulmer, K.S. Toth, I.R. Williams, and G.F. Dell, Phys. Rev. C4, 2123 (1971).

⁹G.G. Jonsson and K. Lindgren, Physica Scripta 7, 49 (1973).

Yu.I. Titov, E.V. Stepula, N.G. Afanas'ev, R.V. Akhmerov,
and N.F. Severin

REF.

Yad. Fiz. 19, 479 (1974)

Sov. J. Nucl. Phys. 19, 240 (1974)

ELEM. SYM.	A	Z
Cu		29
REF. NO.		
74 T1 3		
hmg		

METHOD

REACTION	RESULT	EXCITATION ENERGY	SOURCE		DETECTOR		ANGLE
			TYPE	RANGE	TYPE	RANGE	
E _i E/	ABX	0-600	D	* 1	MAG-D		DST

* 1.2 GEV

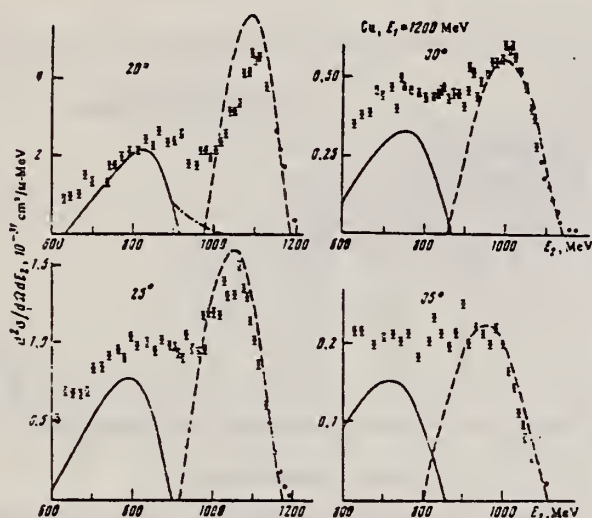


FIG. 2. The same as Fig. 1 but for Cu.

Fig. 2. Spectra of inelastic scattering by Cu for $E_i = 1.2$ GeV. The dashed curve is the quasielastic-scattering cross section, the solid curve is the electroproduction cross section calculated according to ref. 7, and the dot-dash curve is the electro-production cross section at threshold.⁽¹²⁾ A radiation correction has been made to the experimental data.

⁷E.J. Moniz, Phys. Rev. 184, 1154 (1969).

¹²W. Czyz, and J.D. Walecka, Nucl. Phys. 51, 312 (1964).

REF. N. M. Bachschi, P. David, J. Debrus, F. Lubke,
H. Mommsen, R. Schoenmackers, G. G. Jonsson, K. Lindgren
Nucl. Phys. A264, 493 (1976)

ELEM. SYM.	A	Z
Cu		29
REF. NO.		
76 Ba 7		egf

METHOD			SOURCE		DETECTOR		ANGLE
REACTION	RESULT	EXCITATION ENERGY	TYPE	RANGE	TYPE	RANGE	
G, JPKN	ABY	THR* 2	C	* 2	ACT-I		4PI

Abstract: Yields and isomeric yield ratios of nuclei produced in the irradiation of ^{45}Sc and ^{63}Cu with bremsstrahlung of $E_{\gamma}^{\text{max}} = 2 \text{ GeV}$ have been measured by the activation method. The experimental yields are compared to predictions with a Rudstam formula modified to photonuclear reactions.

*GEV, J=1-10, K=1-19

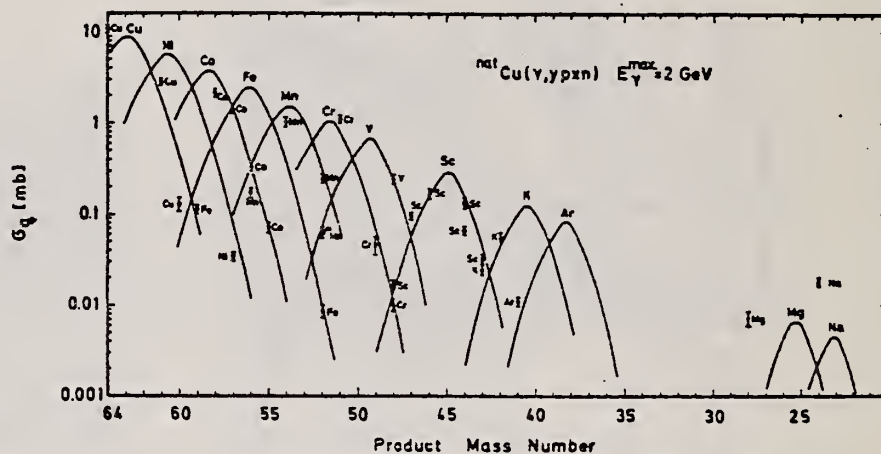


Fig. 2. Yields of nuclei produced in the irradiation of ^{nat}Cu with bremsstrahlung of $E_{\gamma}^{\text{max}} = 2 \text{ GeV}$. The curves are calculated with eq. (1).

TABLE I
Cross section and isomeric ratios

Target	σ_q (ground state)	σ_q (isomer)	$\frac{\sigma_q^{(m)}}{\sigma_q^{(g)}}$
^{45}Sc	$^{44g}\text{Sc}(2^-): 21.4 \pm 1.8 \text{ mb}$	$^{44m}\text{Sc}(6^-): 5.08 \pm 0.50 \text{ mb}$	0.24 ± 0.03
^{nat}Cu	$^{52g}\text{Mn}(6^-): 250 \pm 25 \text{ } \mu\text{b}$	$^{52m}\text{Mn}(2^-): 63 \pm 8 \text{ } \mu\text{b}$	0.25 ± 0.04
^{nat}Cu	$^{44g}\text{Sc}(2^-): 66.5 \pm 6.8 \text{ } \mu\text{b}$	$^{44m}\text{Sc}(6^-): 129 \pm 13 \text{ } \mu\text{b}$	1.9 ± 0.3

REF. A. S. Danagulyan, N. A. Demekhina
Yad. Fiz. 24, 681 (1976)
Sov. J. Nucl. Phys. 24, 355 (1976)

ELEM. SYM.	A	Z
Cu		29

METHOD				REF. NO.	
				76 Da 4	hmg
REACTION	RESULT	EXCITATION ENERGY	SOURCE		ANGLE
			TYPE	RANGE	
G, NA24	ABX	THR* 5	C	2* 5	4PI

*ENERGY, GEV

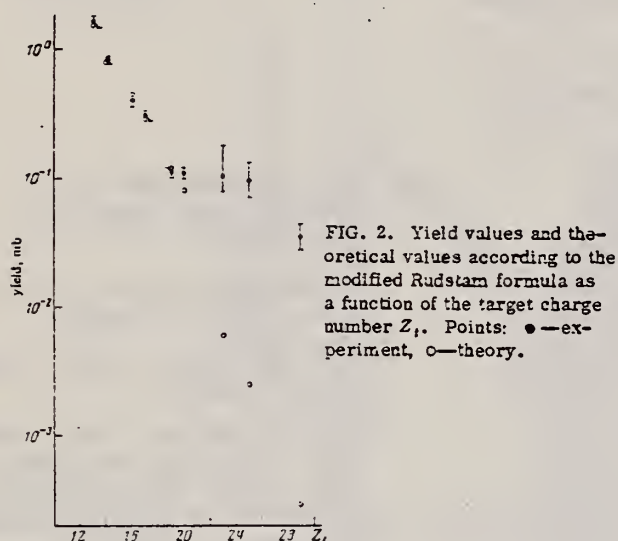


FIG. 2. Yield values and theoretical values according to the modified Rudstam formula as a function of the target charge number Z_t . Points: ●—experiment, ○—theory.

TABLE I. Experimental yields and reaction cross sections obtained in the measurements at the Erevan electron accelerator.

Target nucleus	Reaction yield, mb					Reaction cross section, mb
	E_T max, GeV					
	2	3	4	4.5	5	
^{27}Al	0.81 ± 0.08	0.87		0.57		0.07213 ± 0.0246
^{28}Si	0.27 ± 0.02	0.23		0.29		0.0267 ± 0.013
^{35}S	0.24 ± 0.02	0.22		0.27		0.0323 ± 0.0135
Cl	0.28 ± 0.03	0.30		0.28		—
^{39}K	0.1 ± 0.01	0.125		0.15		0.06 ± 0.0233
^{40}Ca	0.086 ± 0.01	0.58		0.115		0.035 ± 0.0168
^{51}V	0.063 ± 0.02	0.094 ± 0.02	0.098 ± 0.02		0.082 ± 0.025	0.019
^{55}Mn	0.079 ± 0.02	0.075 ± 0.02	0.067 ± 0.017		0.068 ± 0.015	0.01078 ± 0.0053
Cu	0.029 ± 0.008	0.037 ± 0.007	0.036 ± 0.007		0.034 ± 0.007	0.00547 ± 0.0026

Note. The reaction cross sections have been calculated in the $1/E$ approximation of the bremsstrahlung spectrum.

REF.

V. Emma, S. Lo Nigro, C. Milone
Nucl. Phys. **A257**, 438 (1976)

ELEM. SYM.	A	Z
Cu		29
REF. NO.		
76 Em 2		egf-

METHOD

REACTION	RESULT	EXCITATION ENERGY	SOURCE		DETECTOR		ANGLE
			TYPE	RANGE	TYPE	RANGE	
G,F	ABY	THR-999	C	999	TRK-I		4PI

TABLE I

999 = 1 GEVMeasured values of σ_q at $E = 1000$ MeV and deduced values of σ_k assumed constant from E_0 to 1000 MeV

Element	Z^2/A	σ_q (mb)	E_0 (MeV)	σ_k (mb)
Bi	32.96	12.3 ± 0.6	200	7.6 ± 0.6
Pb	32.45	5.4 ± 0.4	220	3.6 ± 0.3
Tl	32.10	4.1 ± 0.3	230	2.8 ± 0.3
Au	31.68	2.0 ± 0.15	240	1.4 ± 0.2
Pt	31.18	1.1 ± 0.08	255	$(8 \pm 0.7) \times 10^{-1}$
Re	30.21	$(3.7 \pm 0.3) \times 10^{-1}$	280	$(2.9 \pm 0.3) \times 10^{-1}$
W	29.78	$(3.5 \pm 0.3) \times 10^{-1}$	290	$(2.8 \pm 0.3) \times 10^{-1}$
Ta	29.45	$(3.3 \pm 0.3) \times 10^{-1}$	300	$(2.7 \pm 0.3) \times 10^{-1}$
Hf	29.04	$(1.7 \pm 0.2) \times 10^{-1}$	310	$(1.4 \pm 0.2) \times 10^{-1}$
Yb	28.31	$(1.3 \pm 0.1) \times 10^{-1}$	330	$(1.2 \pm 0.1) \times 10^{-1}$
Tm	28.18	$(7.5 \pm 0.8) \times 10^{-2}$	335	$(6.8 \pm 0.8) \times 10^{-2}$
Ho	27.21	$(3.6 \pm 0.4) \times 10^{-2}$	355	$(3.5 \pm 0.4) \times 10^{-2}$
Dy	26.80	$(2.6 \pm 0.3) \times 10^{-2}$	360	$(2.5 \pm 0.3) \times 10^{-2}$
Tb	26.58	$(2.5 \pm 0.3) \times 10^{-2}$	370	$(2.5 \pm 0.3) \times 10^{-2}$
Gd	26.04	$(1.6 \pm 0.2) \times 10^{-2}$	380	$(1.7 \pm 0.2) \times 10^{-2}$
Sm	25.56	$(1.3 \pm 0.2) \times 10^{-2}$	390	$(1.4 \pm 0.2) \times 10^{-2}$
Nd	24.96	$(9.2 \pm 0.9) \times 10^{-3}$	405	$(1 \pm 0.1) \times 10^{-2}$
Ce	24.00	$(8 \pm 0.9) \times 10^{-3}$	420	$(9 \pm 1) \times 10^{-3}$
La	23.39	$(8.4 \pm 0.9) \times 10^{-3}$	430	$(1 \pm 0.1) \times 10^{-3}$
Sb	21.36	$(1.2 \pm 0.2) \times 10^{-2}$	460	$(1.5 \pm 0.3) \times 10^{-2}$
Te	21.19	$(8.8 \pm 1) \times 10^{-3}$	465	$(1.2 \pm 0.2) \times 10^{-2}$
Sn	21.06	$(1.3 \pm 0.2) \times 10^{-2}$	465	$(1.7 \pm 0.3) \times 10^{-2}$
Cd	20.49	$(1.7 \pm 0.3) \times 10^{-2}$	470	$(2.2 \pm 0.4) \times 10^{-2}$
Ag	20.47	$(2 \pm 0.3) \times 10^{-2}$	470	$(2.6 \pm 0.4) \times 10^{-2}$
Zn	13.76	$(2 \pm 0.4) \times 10^{-1}$	515	$(3 \pm 0.6) \times 10^{-1}$
Cu	13.44	$(2.4 \pm 0.5) \times 10^{-1}$	515	$(3.6 \pm 0.8) \times 10^{-1}$
Ni	13.35	$(2.4 \pm 0.5) \times 10^{-1}$	510	$(3.6 \pm 0.8) \times 10^{-1}$
Fe	12.10	$(3 \pm 0.6) \times 10^{-1}$	510	$(4.4 \pm 0.9) \times 10^{-1}$

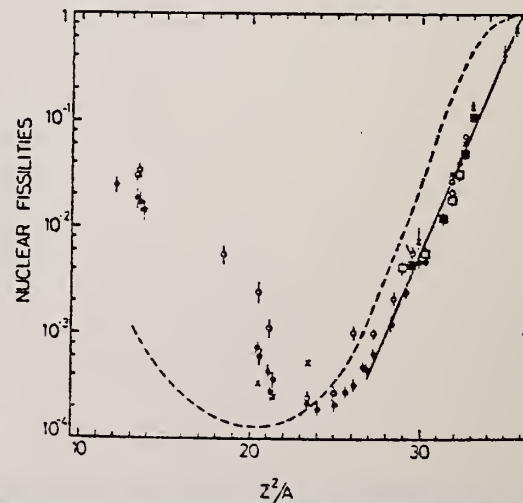
4 A.V. Mitrofanova et al.
Sov. J. Nucl. Phys. **6**,
512 (1968).

7 T. Methasiri et al., Nucl.
Phys. **A167**, 97 (1971).

12 J.R. Nix et al., Nucl. Phys.
81, 61 (1966).

20 N.A. Perfilov et al., JETP
(Sov. Phys.) **14**, 623 (1962);
Proc. Symp. on the physics &
chemistry of fission, Salzburg
1965, vol. 2 (IAEA) Vienna,
1965, p.283.

Fig. 2. Nuclear fissilities as a function of Z^2/A . Experimental points: solid circles represent our data; squares, the data from ref. 4); open circles, the data from ref. 7); and crosses, the data from (p.f) experiments²⁰). The straight line is the best fit calculated from our data for $Z^2/A > 26$. The dashed curve is the curve VI calculated by Nix and Sassi¹²).



REF.

Y. Watase, S. Homma and T. Kitagaki
J. Phys. Soc. Japan 40, 1531 (1976)

ELEM. SYM.

A

Z

Cu

29

METHOD

REF. NO.

76 Wa 3

egf

REACTION	RESULT	EXCITATION ENERGY	SOURCE		DETECTOR		ANGLE
			TYPE	RANGE	TYPE	RANGE	
G,PI+	ABY	140-250	C	250	MAG-D		90
G,PI-	ABY	140-250	C	250	MAG-D		90

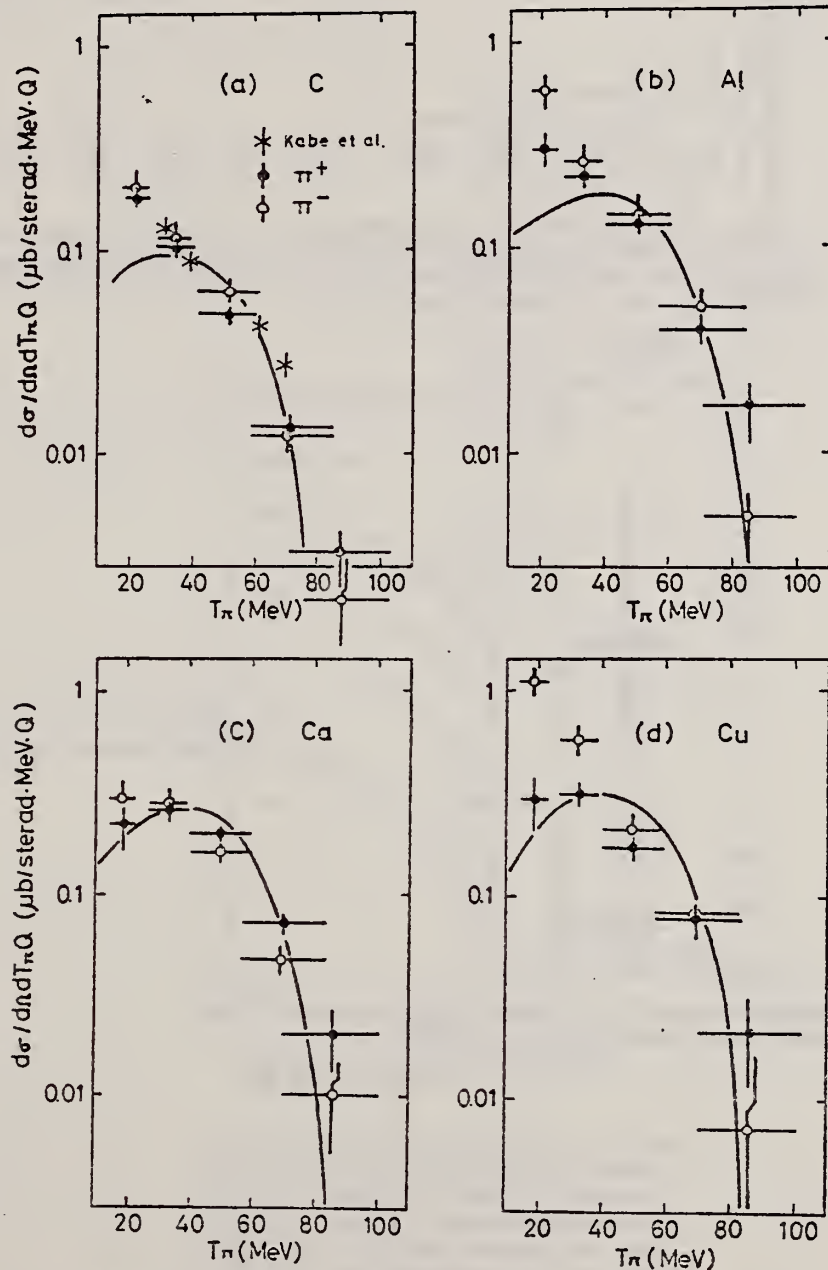


Fig. 2. The energy spectra of photoproduced π^+ from C, Al, Ca, and Cu at 90° in the laboratory system by 250-MeV bremsstrahlung. The data of Ca are normalized to $0.26 \mu\text{b sterad}^{-1} \text{MeV}^{-1} Q^{-1}$ for π^+ at 35 MeV. The solid curves are the calculated spectra of π^+ by a theoretical model.

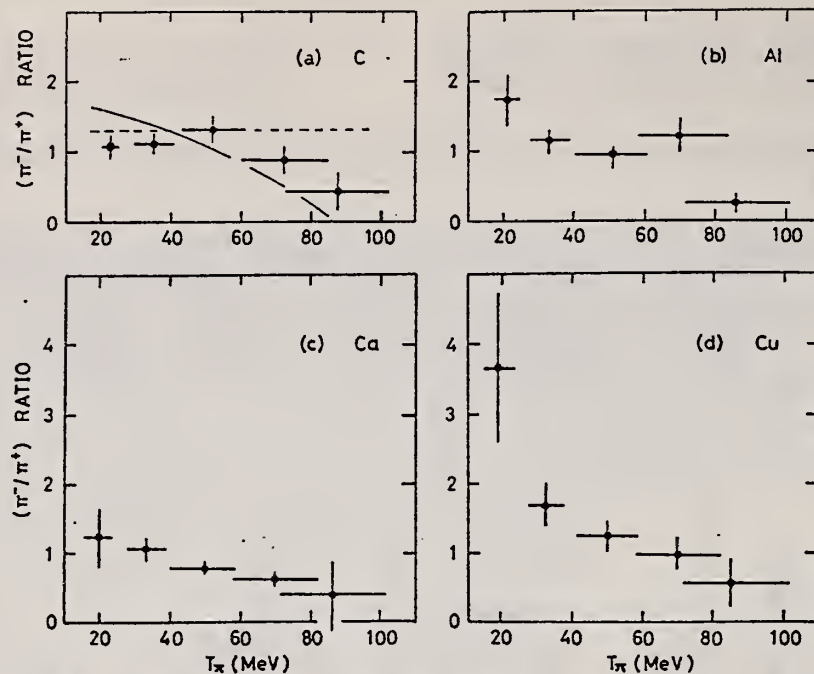


Fig. 3. The π^-/π^+ ratio as a function of the kinetic energy of pions produced from C, Al, Ca, and Cu by 250-MeV bremsstrahlung. The solid curve in (a) is the calculated energy spectrum of π^-/π^+ ratio including the Coulomb potential for C. The dashed curve is the ratio calculated neglecting the Coulomb potential.

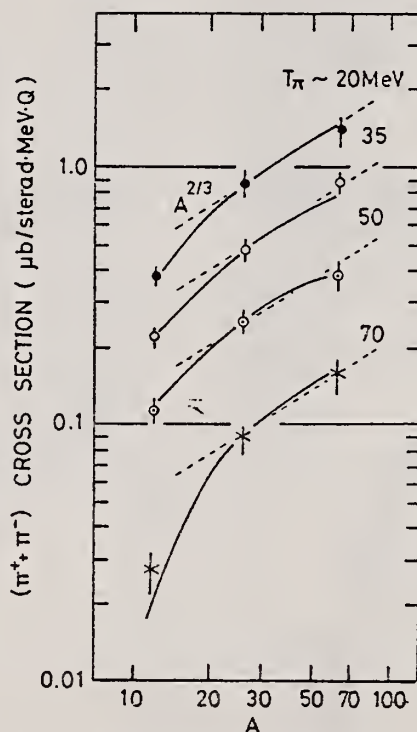


Fig. 4. The A-dependence of the $(\pi^+\pi^-)$ cross sections at the pion kinetic energies of ~ 20 MeV, ~ 35 MeV, ~ 50 MeV and ~ 70 MeV. The solid curves show the relative A-dependence obtained from the theoretical calculation. The dashed lines show $A^{2/3}$ dependence only for guiding eyes.

ELEV. SYM.	A	Z
Cu		29
REF. NO.	77 Da 3	
	egf	

METHOD

REACTION	RESULT	EXCITATION ENERGY	SOURCE		DETECTORS		ANGLE
			TYPE	RANGE	TYPE	RANGE	
G,SPL	ABY	THR * 5	C	2*5	ACT-I		4PI

*ENERGY, GEV

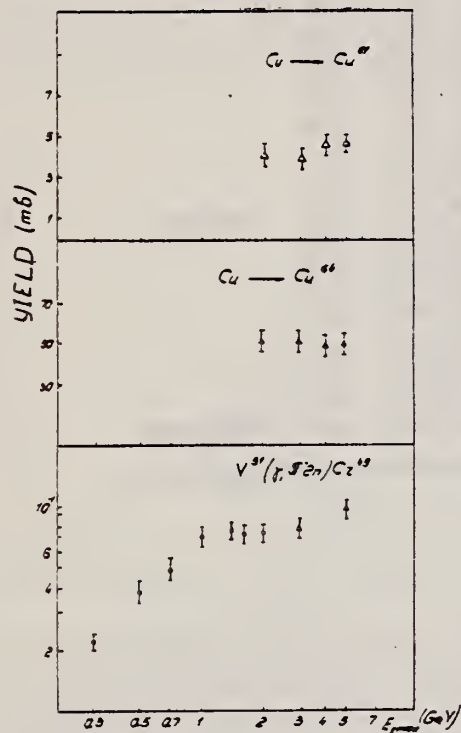
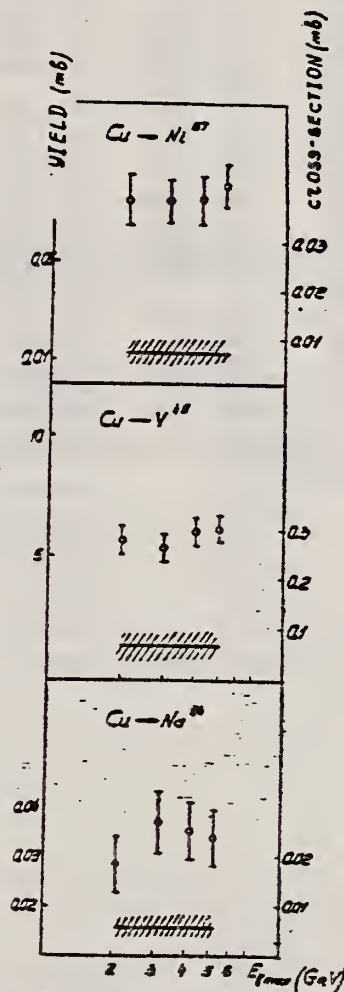


Fig. 1. Characteristic curves of some simple reaction yields.

Fig. 2. Yields of some spallation reactions in ^{51}V , ^{55}Mn and Cu targets. The cross section estimates are obtained in the $1/E$ approximation for bremsstrahlung.

(over)

TABLE 2
Photospallation reaction yields (mb per eq. quantum)

Residual nuclei	Reaction yields (mb)					Reaction cross sections (mb)
	$E_{\text{max}} = 2 \text{ GeV}$ (exp)	3 GeV (exp)	4 GeV (exp)	5 GeV (exp)	5 GeV (cal)	
			<i>Cu target</i>			
⁶² Zn	0.05 ± 0.015	0.07 ± 0.02	0.06 ± 0.02	0.05 ± 0.015		
⁶⁴ Cu	52 ± 5	51 ± 5	49 ± 4.9	50.2 ± 5		
⁶¹ Cu	4.24 ± 0.4	3.98 ± 0.4	4.58 ± 0.46	4.58 ± 0.46	2.4	
⁵⁷ Ni	0.065 ± 0.01	0.064 ± 0.01	0.067 ± 0.011	0.068 ± 0.01	0.12	0.0065 ± 0.003
⁵⁶ Ni	≤ 0.067				0.02	
⁶¹ Co				0.3 ± 0.05	0.54	
⁵⁸ Co	3.67 ± 0.3	3.49 ± 0.3	3.3 ± 0.3	3.5 ± 0.3	4.76	
⁵⁷ Co	2.5 ± 0.25	2.2 ± 0.2	2.47 ± 0.2	2.2 ± 0.2	2.09	
⁵⁶ Co	0.77 ± 0.08	0.7 ± 0.07	0.75 ± 0.07	0.77 ± 0.08	0.606	
⁵⁵ Co	0.16 ± 0.031	0.14 ± 0.025	0.124 ± 0.025	0.16 ± 0.031	0.13	
⁵⁹ Fe	0.34 ± 0.08		0.28 ± 0.07	0.32 ± 0.05	0.274	
⁵⁶ Mn	0.3 ± 0.03	0.27 ± 0.03		0.3 ± 0.03	0.48	
⁵⁴ Mn	1.68 ± 0.17	1.66 ± 0.16	1.65 ± 0.16	1.64 ± 0.16	2.33	
⁵² Mn	0.53 ± 0.05	0.47 ± 0.05	0.525 ± 0.05	0.473 ± 0.05	0.55	
⁵¹ Cr	1.92 ± 0.2	1.92 ± 0.2	1.78 ± 0.18	1.9 ± 0.2	1.36	
⁴⁸ V	0.56 ± 0.06	0.53 ± 0.05	0.6 ± 0.06	0.61 ± 0.06	0.46	0.066 ± 0.03
⁴⁸ Sc	0.07 ± 0.017	0.05 ± 0.012	0.062 ± 0.015	0.061 ± 0.015	0.036	
⁴⁷ Sc	0.13 ± 0.027	0.11 ± 0.022	0.1 ± 0.02	0.122 ± 0.024	0.128	
⁴⁶ Sc	0.41 ± 0.05	0.37 ± 0.074	0.36 ± 0.07	0.35 ± 0.07	0.336	
⁴⁴ Sc		0.13 ± 0.01	0.15 ± 0.015	0.14 ± 0.05		
^{44m} Sc	0.253 ± 0.025	0.27 ± 0.03	0.26 ± 0.026	0.24 ± 0.025	0.35	
⁴³ Sc	0.292 ± 0.03	0.285 ± 0.03	0.265 ± 0.03	0.26 ± 0.02	0.11	
⁴³ K	0.0536 ± 0.005	0.058 ± 0.006		0.051 ± 0.005	0.04	
⁴² K	0.118 ± 0.01	0.097 ± 0.01	0.09 ± 0.01	0.1 ± 0.01	0.117	
²⁴ Na	0.029 ± 0.006	0.037 ± 0.007	0.036 ± 0.007	0.034 ± 0.007	0.012	0.0056 ± 0.0026

Calculated values are obtained using Rudstam's formula. Cross section estimates are made in the $1/E$ approximation.

ELEM. SYM.	A	Z
Cu		29
REF. NO.		
77 Ja 1		
egf		

METHOD			SOURCE		DETECTOR		ANGLE
REACTION	RESULT	EXCITATION ENERGY	TYPE	RANGE	TYPE	RANGE	
G, FRG	NOX	THR - 800	C	800	ACT-I		DST

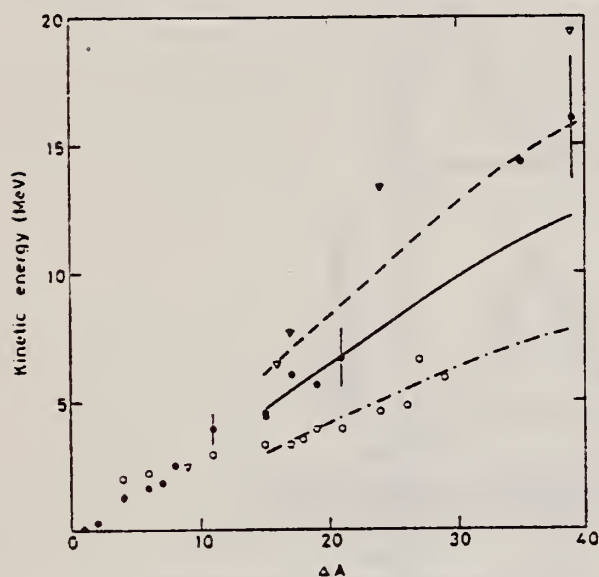


Fig. 1. The kinetic energies of fragments produced in Cu as a function of the mass number difference ΔA between fragments and target: \bullet denotes the measured mean energies, \circ the energies calculated with Monte Carlo program [10], ∇ the energies from fission calculation [11]. ---, — and -.- are the energies calculated from the semiempirical formula of [9] multiplied by factors of 1, 1.56 and 2.02 respectively. The random error is given by bars in some points

MEAN FRAGMENT RANGES

Table 1. Mean ranges and mean kinetic energies in three directions for ^{24}Na produced in different targets

	Range mg/cm ²	Kinetic energy MeV
Cu forward	3.64 ± 0.55	21.0 ± 3.8
Cu backward	2.17 ± 0.33	10.2 ± 1.8
Cu perpendic.	3.09 ± 0.45	16.7 ± 3.0
Ag forward	7.61 ± 1.14	37.1 ± 6.7
Ag backward	6.65 ± 1.00	31.8 ± 5.7
Ag perpendic.	7.20 ± 1.05	35.0 ± 6.3
Au forward	17.4 ± 2.6	69.5 ± 12.5
Au backward	16.0 ± 2.4	64.0 ± 11.5
Au perpendic.*	12.6 ± 3.4	49.2 ± 33.4

* The statistical uncertainty in the yield was specially large

Table 2. Means ranges in three directions, forward to backward ratios and mean kinetic energies of different fragments produced in copper

Fragment	Range mg cm ²				Forward/ Backward	Mean kinetic energy MeV
	Forward	Backward	Perpen- dicular	Random error		
^{64}Cu	0.018	0.009	0.021	± 0.002	2.0	0.043
^{61}Cu	0.10	0.05	0.05	± 0.01	2.0	0.26
^{59}Fe	0.43	0.31	0.28	± 0.05	1.4	1.23
^{57}Ni	0.63	0.20	0.41	± 0.06	3.1	1.6
^{56}Co	0.66	0.24	0.49	± 0.07	2.7	1.8
^{55}Co	0.87	0.32	0.61	± 0.09	2.7	2.5
^{52}Mn	1.07	0.42	1.13	± 0.13	2.5	3.9
^{48}Sc	1.41	0.66	1.08	± 0.16	2.1	4.4
^{48}V	1.41	0.59	0.97	± 0.15	2.4	4.5
^{46}Sc	1.71	0.87	1.24	± 0.19	2.0	6.0
^{44}Sc	1.64	0.67	1.23	± 0.18	2.5	5.6
^{42}Sc	1.91	0.84	1.41	± 0.21	2.3	6.7
^{41}Mg	3.2	1.3	3.4	± 0.4	2.4	14.3
^{40}Ar	7.5	2.0	3.1	± 0.4	1.7	16.0

ELEM. SYM.	A	Z
Cu		29
REF. NO.		egf
77 Ja 2		

REACTION	RESULT	EXCITATION ENERGY	SOURCE		DETECTOR		ANGLE
			TYPE	RANGE	TYPE	RANGE	
G,NA24	ABY	THR-999	C	400-999	ACT-I		4PI

999=1 GEV

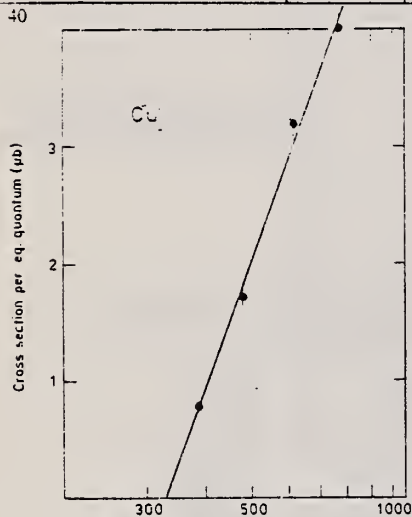


Fig. 1a Bremsstrahlung energy (MeV)

Fig. 1a-j. The measured yield as a function of bremsstrahlung end point energy. The error bars give the statistical errors in the numbers of γ -quanta detected. The solid lines are fitted to the yield points with the least-squares method. The yield from Cu (Fig. 1a) is measured in [1] and has been recalculated using the monitor curve of [5]

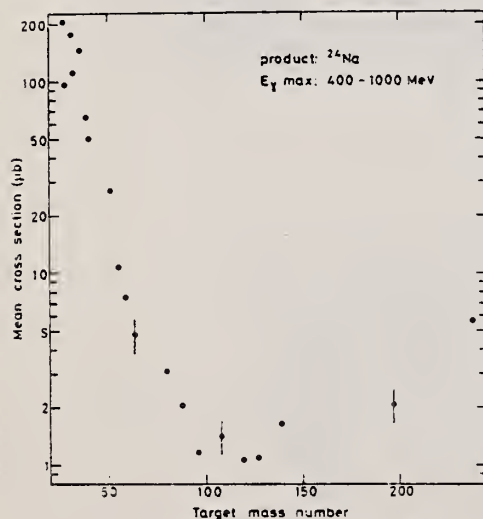


Fig. 2. The mean cross section in the energy range 400 to 1000 MeV calculated from the yields of Figure 1 in this work and of Figures 1 to 10 in [1]. The error bars in some points

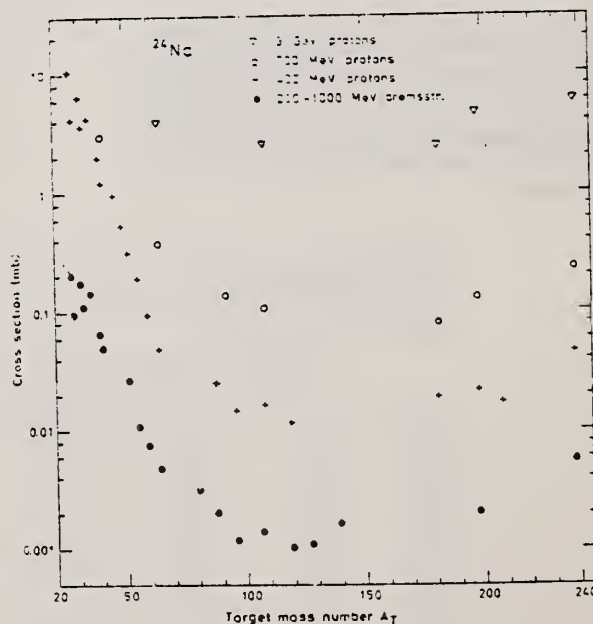


Fig. 4. Mean cross sections of the present work and of [1] (●) compared with the cross sections in proton irradiations: + 400 MeV from [4], ○ 700 MeV from [16] and an extrapolated value from [17], ▽ 3 GeV from [18]

REF.

J.J. Murphy II, H.J. Gehrhardt and D.M. Skopik
Nucl. Phys. A277, 69 (1977)

ELEM. SYM.

A

Z

Cu

29

METHOD

REF. NO.

77 Mu 3

egf

REACTION	RESULT	EXCITATION ENERGY	SOURCE		DETECTOR		ANGLE
			TYPE	RANGE	TYPE	RANGE	
E,A	ABX	12-100	D	100	MAG-D		DST

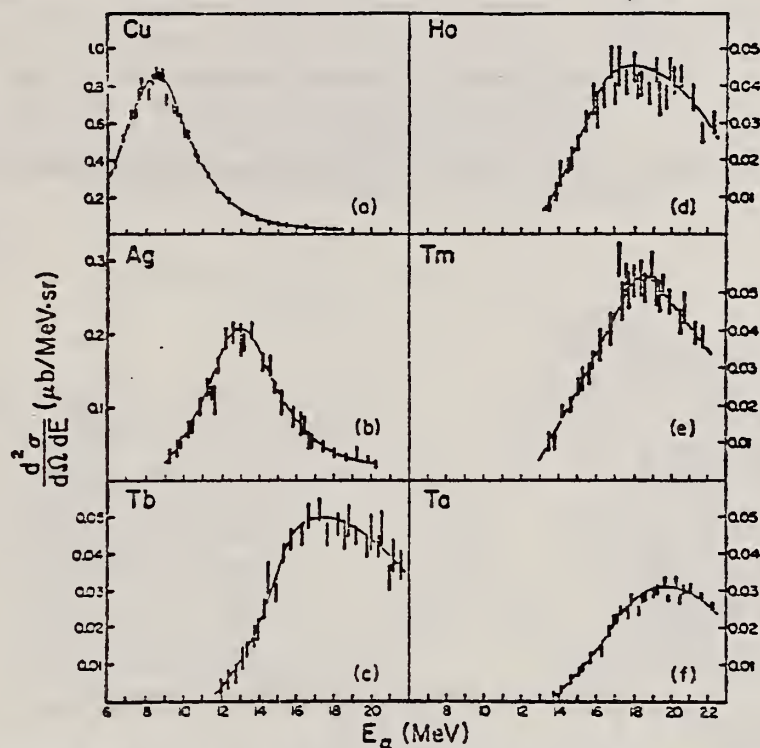


Fig. 1. The α -particle energy spectra at 50° in the lab for the six nuclei studied. Note that as Z increases, the cross section decreases and the energy of the peak increases. Errors are statistical. Curves are to guide the eye.

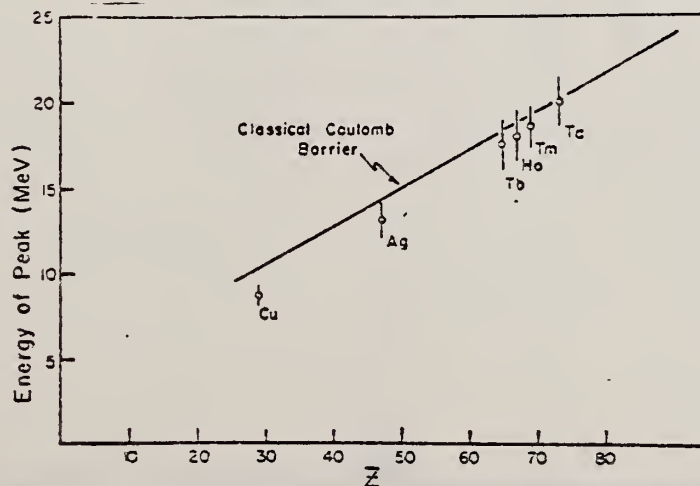


Fig. 2. Energy of the cross section peak as a function of Z . The solid line is the energy of the classical Coulomb barrier.

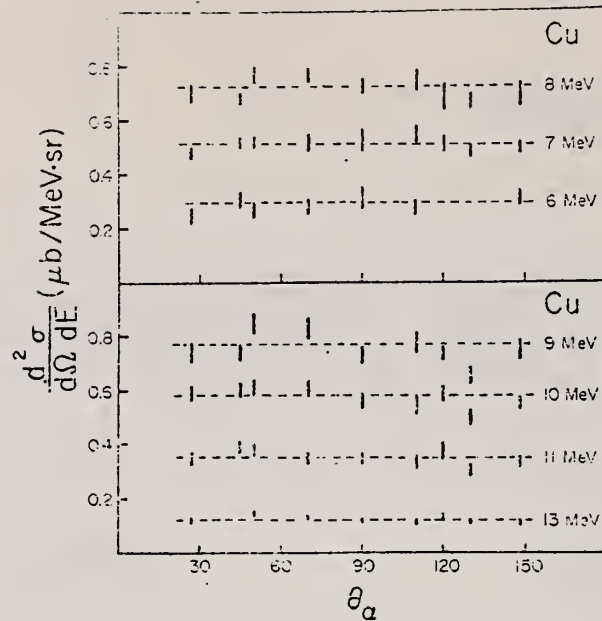


Fig. 3. Angular distributions for copper ($Z = 29$). These isotropic distributions indicate an evaporation process. Errors are statistical. Curves are to guide the eye.

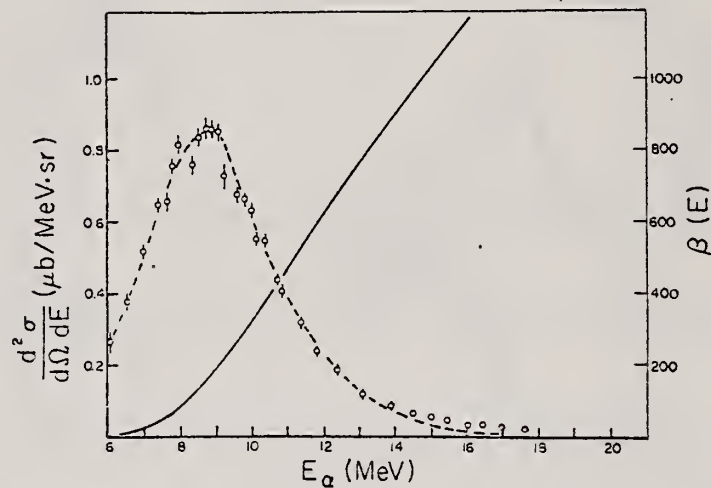


Fig. 4. The α -particle energy spectrum at 50° for copper. The dash curve is the calculated evaporation model cross section. The solid curve (scale to right) gives the penetrabilities used in the calculation.

REF. A.S. Danagulyan, N.A. Demekhina
Yad. Fiz. 27, 877 (1978)
Sov. J. Nucl. Phys. 27, 466 (1978)

ELEM. SYM.	A	Z
Cu		29
METHOD		
REF. NO.		
78 Da 13		
hg		

REACTION	RESULT	EXCITATION ENERGY	SOURCE		DETECTOR		ANGLE
			TYPE	RANGE	TYPE	RANGE	
G,MN52	ABY	THR*5	C	2*5	ACT-D		4PI
G,SC44	ABY	THR*5	C	2*5	ACT-D		4PI

We discuss data concerning the ratios of the yields of different isomeric states in the elements ^{44}Sc and ^{52}Mn . Experimental results are presented for measurement of the yields of ^{44}Sc and ^{52}Mn in disintegration of targets of ^{51}V , ^{55}Mn , and Cu by photons with energies from 2 to 5 GeV; theoretical values of yields for these elements were obtained by means of the five-parameter Rudstam formula. The pattern of formation of high-spin states in photodisintegration reactions is discussed in terms of the cascade-evaporative model.

*GEV, ISOMER YLD

PACS numbers: 25.20. + y, 27.40. + z

TABLE I.

Type of target	Isomeric states	Yield ratio				
		Experiment				Theory
		$E_{\gamma, \text{max}} = 2 \text{ GeV}$	3 GeV	4 GeV	5 GeV	
^{51}V	^{44}Sc	0.47 ± 0.03	0.47 ± 0.03	0.44 ± 0.04	0.46 ± 0.04	1.03
	^{44}Sc	0.55 ± 0.06	0.45 ± 0.06	0.57 ± 0.07	0.56 ± 0.07	
^{55}Mn	^{44}Sc	0.45 ± 0.04	0.47 ± 0.04	0.42 ± 0.06	0.55 ± 0.05	1.3
	^{44}Sc	0.42 ± 0.04	0.42 ± 0.04	0.55 ± 0.1	0.45 ± 0.05	
^{55}Mn	^{52}Mn	0.48 ± 0.05	0.43 ± 0.04	0.6 ± 0.06	0.48 ± 0.05	1.34
	^{52}Mn	0.55	0.55	0.55	0.55	
Cu	^{44}Sc	0.25 ± 0.03	0.27 ± 0.03	0.26 ± 0.028	0.24 ± 0.03	0.35
	^{44}Sc	-	0.13 ± 0.01	0.15 ± 0.02	0.14 ± 0.05	
Cu	^{52}Mn	-	-	0.128 ± 0.01	-	0.55
	^{52}Mn	0.55 ± 0.05	0.47 ± 0.05	0.525 ± 0.05	0.473 ± 0.05	

TABLE II.

Type of target	Photon energy, MeV	Isomeric yield ratio	Remarks
^{51}V	65-300	0.75 ± 0.03	[11] [12] Present work
	100-800	0.88	
	2000-5000	0.87 ± 0.04	
^{54}Fe	250	0.61 ± 0.02	[7] [8]
	250-800	1.03 ± 0.05	
^{55}Mn	225	0.72	[7] [7] [8] Present work
	300	0.64	
	200-800	1.09 ± 0.04	
	2000-5000	1.02 ± 0.02	
^{59}Co	250-800	1.24 ± 0.06	[8] Present work
	2000-5000	1.84 ± 0.16	
^{79}As	250-800	1.9 ± 0.3	[8]
^{54}Fe	70	0.47	[7] [7]
	100-250	0.56	
^{55}Mn	100-300	0.88	[7] Present work
	2000-5000	1.12 ± 0.1	
^{59}Co	150	1.62	[7] Present work
	4000	4.1 ± 0.4	

ELEM. SYM.	A	Z
Cu		29
REF. NO.		79Ba8
		hg

METHOD

REACTION	RESULT	EXCITATION ENERGY	SOURCE		DETECTOR		ANGLE
			TYPE	RANGE	TYPE	RANGE	
G,PI-	SPC	418*718	C	750	MAG-D		DST
G,PI+	SPC	568*668	C	750	MAG-D		DST

Abstract: The photoproduction of charged pions in the sub GeV region has been studied for two nuclear targets, copper and lead, by using a magnetic spectrometer. The photon energies are determined in steps of 50 MeV by a subtraction method for the bremsstrahlung spectrum. The observed pion momentum spectra reveal characteristic features of quasi-free production (QFP) even for such heavy nuclei as copper and lead. The data are compared with results obtained by a PWIA calculation, which give a good fit to the data. The QFP cross sections per relevant nucleon at 44.2° and the average photon energy $\langle k \rangle = 668$ MeV are found to be approximately proportional to $A^{-1/3}$.

*AVG PHOTON ENERGY

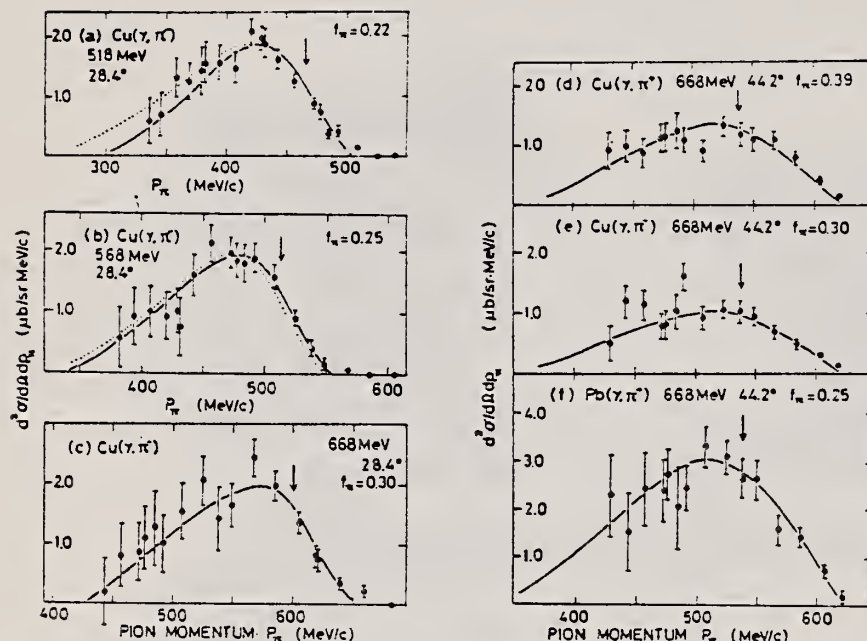


Fig. 1. Typical examples of the measured pion spectra. Errors are statistical only. The solid curves are $f_\pi \times$ (PWIA calculation) with parameter values $p_F = 270$ MeV/c, $\epsilon = 25$ MeV and f_π being shown in the figure. The dotted curves in (a) and (b) correspond to the cases in which $p_F = 300$ MeV/c while ϵ is unchanged, and $\epsilon = 35$ MeV while p_F is unchanged, respectively. Arrows denote the values of the pion momentum, p_{free} , which is calculated from the assumption that the target nucleon is free and at rest.

over

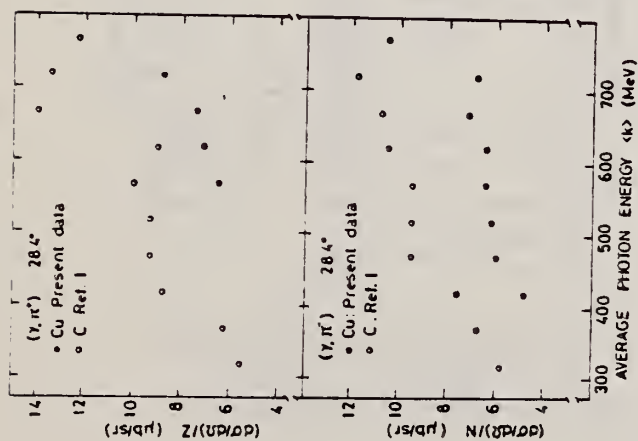


Fig. 3. The QFP cross section at $\theta_p = 28.4^\circ$ for copper as a function of $\langle k \rangle$. Note that the plotted values are those divided by the proton (neutron) number Z (N) for π^+ (π^-), together with the same quantities for carbon taken from I for comparison. Errors of the order of 10% due to fitting uncertainty are not shown.

QFP = QUASI-FREE PRODUCTION

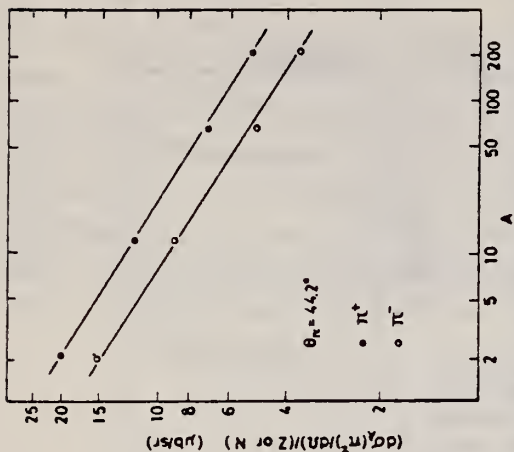


Fig. 4. The QFP cross section at $\theta_p = 44.2^\circ$ and $\langle k \rangle = 668$ MeV as a function of the mass number A . The π^+ (π^-) cross section is divided by Z (N). Errors of the order of 10% due to fitting uncertainty are not shown. Data points at $A = 2$ are taken from ref. 3). The solid lines are:

$$\frac{d\sigma_A(\pi^+)}{d\Omega} \frac{1}{Z} = 24.3A^{-0.3}, \quad \text{and} \quad \frac{d\sigma_A(\pi^-)}{d\Omega} \frac{1}{N} = 18.4A^{-0.3},$$

in units of $\mu\text{b}/\text{sr}$.

QFP = QUASI-FREE PRODUCTION

TABLE 2

Double differential cross section $d^2\sigma/d\Omega_\pi dp_\pi$ for the reactions $\gamma + A \rightarrow \pi^\pm + X$, where A is taken to be copper or lead, as a function of the average photon energy $\langle k \rangle$ and the pion momentum p_π .

$\langle k \rangle$ [MeV]	p_π [MeV/c]	$d^2\sigma/d\Omega_\pi dp_\pi$ [$\mu\text{b}/(\text{sr} \cdot \text{MeV}/c)$]	$\langle k \rangle$ [MeV]	p_π [MeV/c]	$d^2\sigma/d\Omega_\pi dp_\pi$ [$\mu\text{b}/(\text{sr} \cdot \text{MeV}/c)$]
π^- for copper at 28.4°					
431	0.07 \pm 0.07				
420	0.04 \pm 0.04				
407	0.33 \pm 0.11				
394	0.26 \pm 0.11				
382	0.69 \pm 0.19				
379	0.67 \pm 0.17				
369	0.77 \pm 0.15				
357	1.41 \pm 0.23				
346	1.83 \pm 0.28				
336	1.71 \pm 0.35				
324	1.37 \pm 0.38				
316	1.91 \pm 0.34				
306	1.50 \pm 0.39				
296	1.73 \pm 0.43				
287	0.84 \pm 0.43				
281	2.02 \pm 0.69				
274	0.97 \pm 0.51				
266	0.87 \pm 0.57				
257	0.89 \pm 0.59				
250	-0.36 \pm 0.60				
π^- for copper at 28.4°					
485	0.00 \pm 0.02				
472	0.05 \pm 0.02				
457	0.12 \pm 0.04				
443	0.39 \pm 0.90				
429	0.79 \pm 0.13				
431	0.47 \pm 0.15				
420	0.89 \pm 0.13				
407	1.33 \pm 0.20				
394	1.84 \pm 0.23				
382	1.86 \pm 0.31				
379	2.09 \pm 0.34				
369	2.03 \pm 0.25				
357	1.37 \pm 0.32				
346	1.61 \pm 0.38				
336	1.26 \pm 0.41				
325	1.58 \pm 0.55				
317	1.07 \pm 0.46				
306	0.82 \pm 0.49				
297	0.72 \pm 0.53				
288	2.27 \pm 0.55				

ELEM. SYM.	A	Z
Cu		29
REF. NO.		
80 Ad 10		
hg		

METHOD					REF. NO.		hg
					80 Ad 10		
REACTION	RESULT	EXCITATION ENERGY	SOURCE		DETECTOR		ANGLE
			TYPE	RANGE	TYPE	RANGE	
G,P	ABY	THR-500	C	500	TEL-D		DST
G,D	ABY	THR-500	C	500	TEL-D		DST
G,T	ABY	THR-500	C	500	TEL-D		DST
G,HE3	RLY	THR 500	C	500	TEL-D		DST
G,A	ABY	THR-500	C	500	TEL-D		DST

The energy and angular distributions of p , d , t , ^3He and ^4He from the three targets Cu, Ag and Au were measured at five different angles for bremsstrahlung with peak energy 500 MeV. The measurements were made using a telescope consisting of four surface-barrier detectors. The experimental data are compared with cascade-evaporation calculations. For the ^4He -distributions the calculations were extended to include the contribution from knock-out of surface alphas by the cascade nucleons. The comparison shows that the main contribution comes from evaporation but that there is a direct component of the order of 10%.

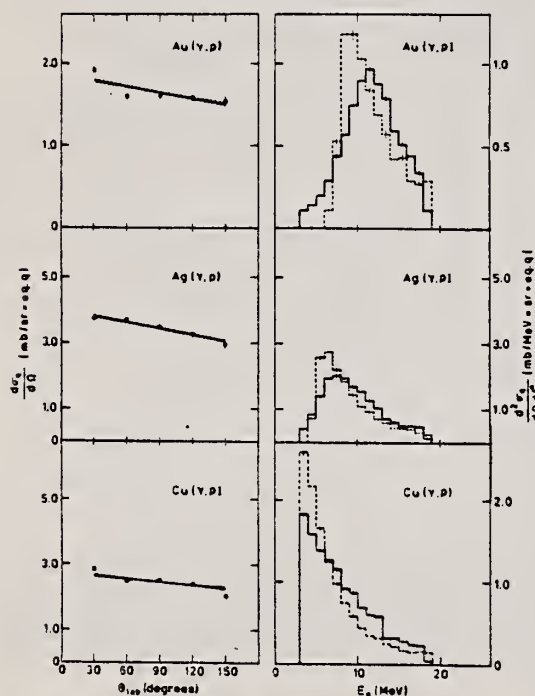


Fig. 2. Experimental proton angular (filled circles) and energy (solid histogram) distributions from the three targets Au, Ag and Cu compared with angular (solid line) and energy (dashed histogram) distributions obtained from cascade-evaporation calculations

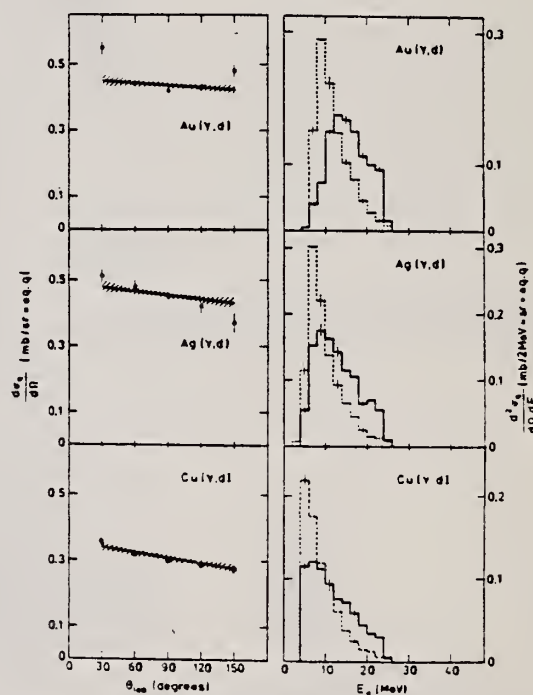


Fig. 3. Deuteron distributions. See caption of Fig. 2

(OVER)

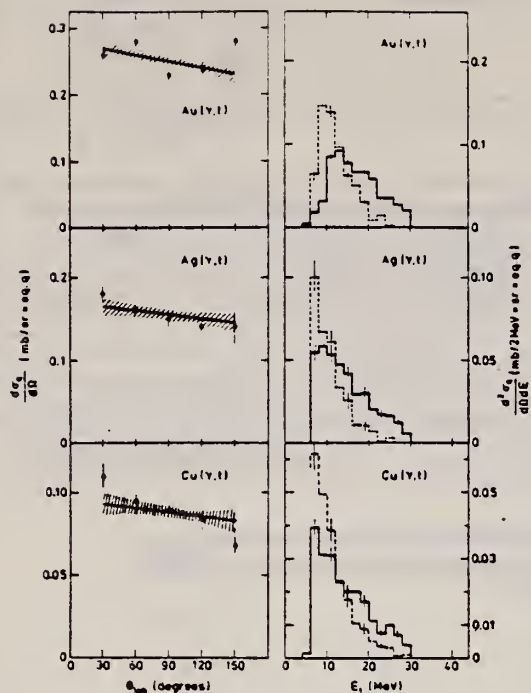


Fig. 4. Triton distributions. See caption of Fig. 2

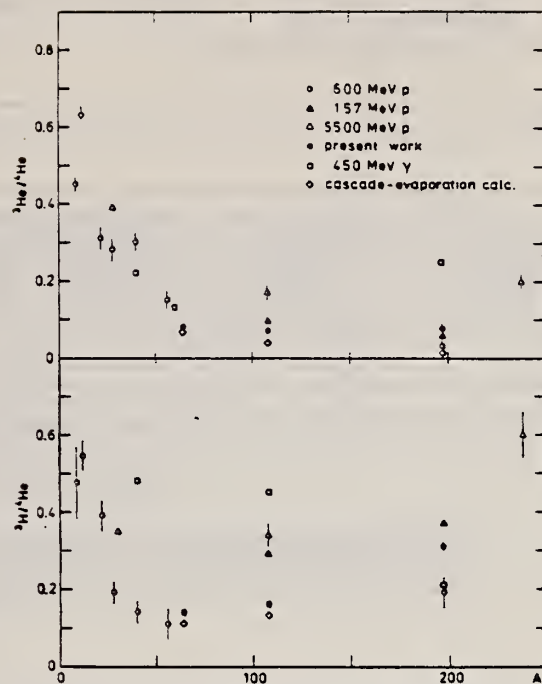


Fig. 6. Comparison between different measurements of the yield ratios ${}^3\text{He}/{}^4\text{He}$ and ${}^3\text{H}/{}^4\text{He}$ as a function of massnumber

Table 2. Integrated yields, normalization factors and calculated direct contributions

Target	Reaction	$Y_{\text{int}}^{\text{exp}}$ (nb eq. q)	Normali- zation factors	Calculated direct con- tribution in percent	GDR-con- tribution in percent
Au	(γ, p)	21	0.42	9	—
	(γ, d)	6	0.34	—	—
	(γ, t)	3	0.48	—	—
	(γ, z)	10	0.66	8	—
Ag	(γ, p)	44	0.86	11	5 (Ref. 21)
	(γ, d)	6	0.86	—	—
	(γ, t)	2	1.52	—	—
	(γ, z)	12	1.32	8	—
Cu	(γ, p)	44	0.54	7	28 (Ref. 22)
	(γ, d)	4	0.96	—	—
	(γ, t)	1	2.10	—	—
	(γ, z)	8	1.22	9	10 (Ref. 23)

REF. J. Arends, J. Eyink, A. Hegerath, K.G. Hilger, B. Mecking,
G. Noldeke, H. Rost
Phys. Lett 98B, 423 (1981)

ELEM. SYM.	A	Z
Cu		29
REF. NO.		hg
81 Ar 1		

METHOD				REF. NO.		hg
REACTION	RESULT	EXCITATION ENERGY	SOURCE		DETECTOR	
			TYPE	RANGE	TYPE	RANGE
G, MU-T	ABX	215-386	D	215-386	TOF-D	4PI

DATA ALSO IN 81AR3

Double differential cross sections for the photo-emission of protons and charged pion production were investigated for a number of target nuclei (He, Be, C, O, Al, Ti, Cu, Sn, Pb) in the photon energy range $k = (215-386)$ MeV. On the basis of these experimental results the total hadronic cross section was determined.

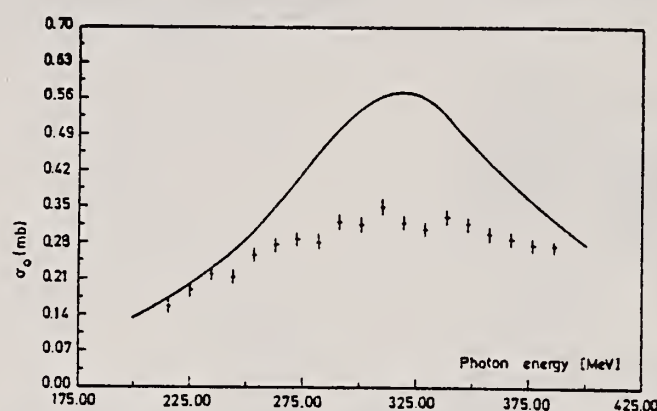


Fig. 7. Parameter σ_0 as a function of photon energy (data points) compared to the mean cross section for a free nucleon (solid line).

The total hadronic cross sections for all measured elements can be parametrized in the form

$$\sigma(k, A) = \sigma_0(k) \cdot A^x,$$

A being the atomic number, with a constant exponent $x = 1.1$. The photon energy dependence of σ_0 is shown in fig. 7. Compared to the mean cross section for a free nucleon (the solid line in fig. 7) the excitation of the Δ -resonance is suppressed. Such a suppression is expected in the Δ -hole model [11].

REF. J. Arends, J. Eyink, A. Hegerath, K.G. Hilger, B. Mecking,
G. Nöldeke, H. Rost
Nucl. Phys. A358, 367c (1981)

ELEM. SYM.	A	Z
Cu		29

METHOD

REF. NO.

81 Ar 3

hg

REACTION	RESULT	EXCITATION ENERGY	SOURCE		DETECTOR		ANGLE
			TYPE	RANGE	TYPE	RANGE	
G,MU-T	ABX	215-386	D	215-386	TOF-D		4PI

Abstract: Double differential cross sections for the photoemission of protons and charged pion photoproduction were investigated for a number of target nuclei (He, Be, C, O, Al, Ti, Cu, Sn, Pb) using the tagged bremsstrahlung beam at the Bonn 500 MeV-Synchrotron in the photon range $k = (215-386)$ MeV. On the basis of these experimental results the total hadronic cross section was determined.

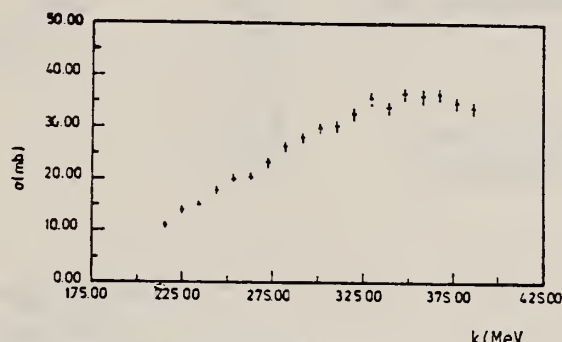


Fig. 2. Cross section for the process: $\gamma + \text{Pb} \rightarrow p + X$. The proton threshold is 58 MeV.

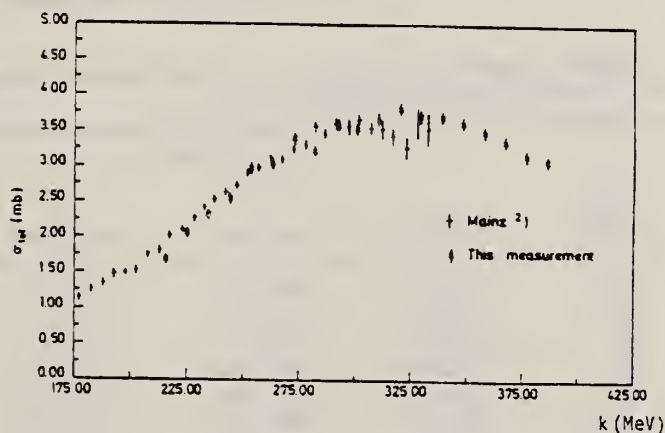


Fig. 3. Total hadronic cross section for Be. The data are compared to the cross section taken from ref.².

The photon energy dependence of the total cross sections for heavier nuclei are similar to the Be results. The complete data set can be parametrized in the form

$$\sigma(k, A) = \sigma_0(k) \cdot A^x.$$

The exponent is constant $x = 1.1$. The photon energy dependence of σ_0 is shown in fig. 4. Compared to the mean cross section for a free nucleon, the excitation of the Δ -resonance is suppressed.

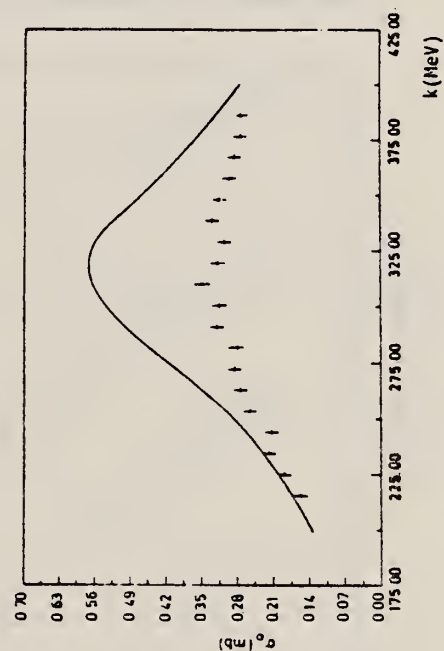


Fig. 4. Parameter σ_0 compared to the cross section for a free nucleon (full line).

REF. R.A. Schumacher, G.S. Adams, D.R. Ingham, J.L. Matthews, W.W. Sapp,
R.S. Turley, R.O. Owens, B.L. Roberts
Phys. Rev. C25, 2269 (1982)

ELEM. SYM.	A	Z
Cu		29
REF. NO.		
82 Sc 3		
egf		

METHOD		SOURCE		DETECTOR		ANGLE
REACTION	RESULT	EXCITATION ENERGY	TYPE RANGE	TYPE RANGE		
G,XP	ABX	150,300	D 150,300	MAG-D		DST

Inclusive photoproton cross sections for the reaction $\text{Cu}(\gamma, p)X$ have been measured for a photon energy of 300 MeV at proton angles 45° , 90° , and 135° , and for 150 MeV at 45° . The data are compared with an intranuclear-cascade calculation and with $\text{Ni}(\pi^\pm, p)$ data. The angular distribution is analyzed to obtain an estimate of the number of nucleons involved in the interaction.

[NUCLEAR REACTIONS $\text{Cu}(\gamma, p)X$, $E = 150$ MeV, $\theta = 45^\circ$, $E = 300$ MeV, $\theta = 45^\circ, 90^\circ, 135^\circ$; measured $\sigma(E_p, \theta)$; intranuclear cascade analysis.]

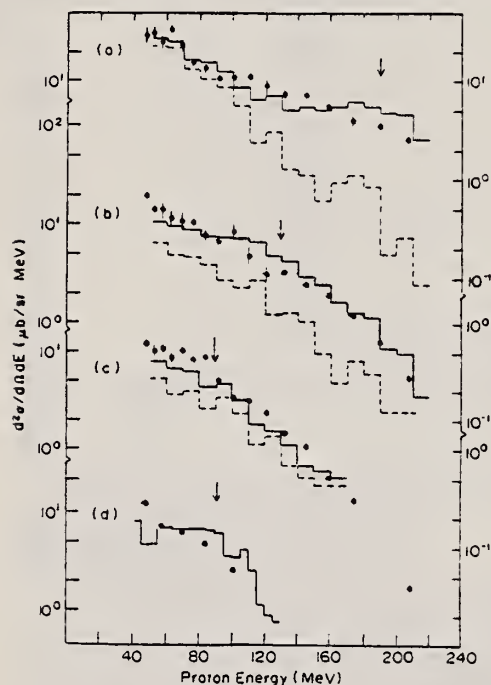


FIG. 2. $\text{Cu}(\gamma, p)X$ cross sections: (a) 300 MeV, 45° ; (b) 300 MeV, 90° ; (c) 300 MeV, 135° ; (d) 150 MeV, 45° . Only statistical errors are shown. Also plotted are the results of a cascade calculation where the solid lines represent the total yield, and the dashed lines the yield due to quasifree pion production only. The arrows indicate the proton energies expected for free deuteron photodisintegration kinematics.

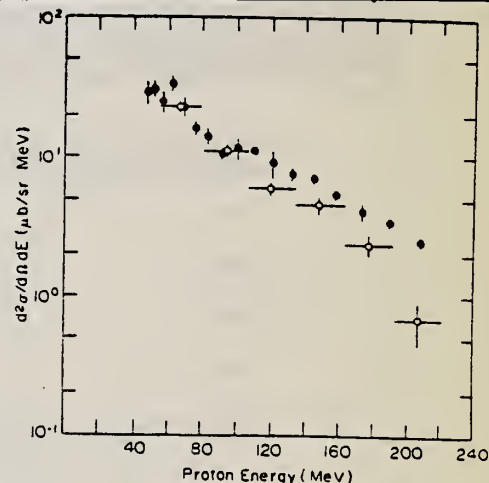


FIG. 3. Comparison of the present data at 300 MeV, 45° (closed circles) with Bonn $\text{Cu}(\gamma, p)X$ data (Ref. 26) for $E_\gamma = 291$ MeV, 44° (open circles).

TABLE I. Inclusive cross sections for the $\text{Cu}(\gamma, p)X$ reaction. Errors given are statistical only. The overall systematic uncertainty is $\pm 7\%$.

θ_p E_p (MeV)	$E_\gamma = 300$ MeV			$E_\gamma = 150$ MeV
	45° ($\mu\text{b/sr MeV}$)	90° ($\mu\text{b/sr MeV}$)	135° ($\mu\text{b/sr MeV}$)	45° ($\mu\text{b/sr MeV}$)
47.0	29.0 ± 6.0	19.8 ± 1.6	11.6 ± 0.9	12.4 ± 1.3
51.7	30.0 ± 4.0	14.0 ± 1.2	9.8 ± 1.4	
56.9	25.0 ± 4.0	14.0 ± 2.7	10.5 ± 1.1	7.2 ± 0.5
62.5	33.0 ± 4.0	11.6 ± 1.8	8.4 ± 0.8	
68.7	23.0 ± 4.0	10.8 ± 2.2	9.9 ± 1.0	6.2 ± 0.4
75.5	15.5 ± 1.6	10.4 ± 0.9	8.0 ± 0.5	
82.9	13.7 ± 1.8	7.7 ± 1.0	8.5 ± 0.5	4.9 ± 0.3
91.0	10.7 ± 1.1	6.8 ± 0.6	5.06 ± 0.26	
99.9	11.2 ± 1.9	8.6 ± 1.8	3.31 ± 0.19	2.5 ± 0.18
109.6	11.0 ± 0.6	4.9 ± 1.1	3.04 ± 0.23	
120.2	8.9 ± 1.9	3.1 ± 0.8	2.28 ± 0.18	
131.8	7.4 ± 0.9	3.3 ± 0.2	1.42 ± 0.07	
144.4	7.1 ± 0.6	2.4 ± 0.2	1.04 ± 0.09	
158.1	5.5 ± 0.3	1.90 ± 0.16	0.51 ± 0.03	
173.0	4.0 ± 0.6	1.19 ± 0.07	0.288 ± 0.018	
189.3	3.4 ± 0.3	0.65 ± 0.04		
206.9	2.5 ± 0.2	0.27 ± 0.02	0.039 ± 0.003	

Cu
A=59

Cu
A=59

Cu
A=59

REF.

K. Beckert, H.W. Hersch, F. Herrmann, P. Kleinvechter,
H. Schobbert, I. Fodor, and I. Szentpetery
Izv. Akad. Nauk SSSR. Ser. Fiz. 38, 2083 (1974)
Bull. Acad. Sci. USSR Phys. Ser. 38, 60 (1974)

ELEM. SYM.	A	Z
Cu	59	29
REF. NO.		74 Be 12
METHOD		hmg

REACTION	RESULT	EXCITATION ENERGY	SOURCE		DETECTOR		ANGLE
			TYPE	RANGE	TYPE	RANGE	
P,G	SPC	8- 9	D	4- 6	SCD-D		DST

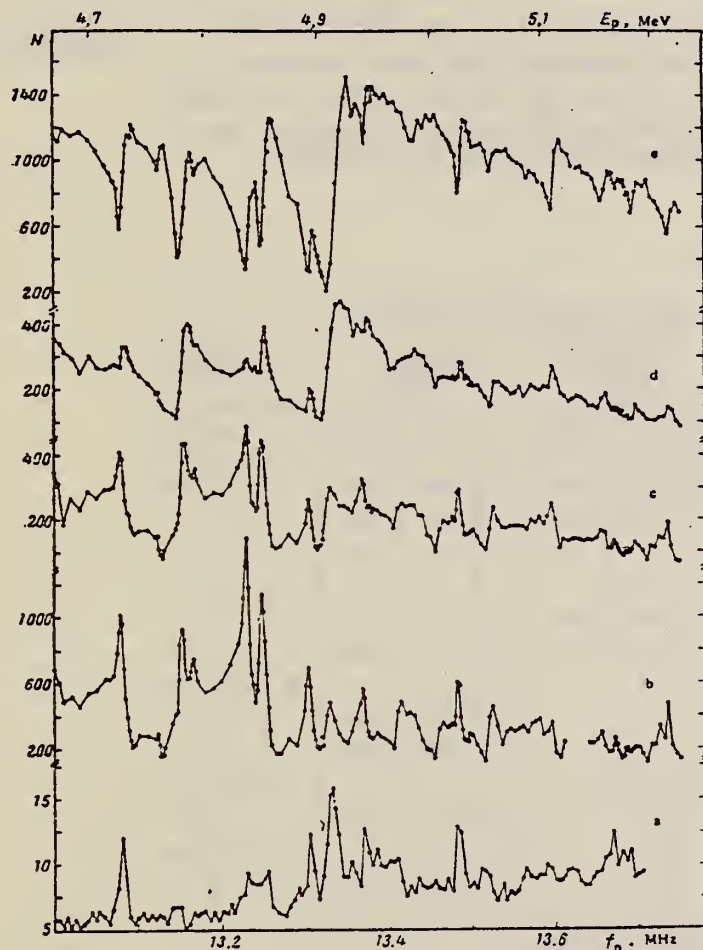


Fig. 1. Excitation functions for: a) $^{58}\text{Ni}(p, \gamma)^{59}\text{Cu}$ at 90° for $E_\gamma > 6.5$ MeV; b-e) $^{58}\text{Ni}(p, p_0)$ for angles of: b) 165° ; c) 145° ; d) 125° ; e) 95° (N is the number of counts per μCi).

TABLE 2

E_p^{lab} , keV	Partial width (eV) for transition to ground state ($5/2^+ \rightarrow 3/2^-$), and intensity Y ($\Delta Y \sim 20\%$)	$\Gamma_{\gamma} \Gamma_{\text{W}} (e^2)$
4740 ± 4	33.2	$3.4 \cdot 10^{-3}$
4900 ± 4	23.6	$6.7 \cdot 10^{-3}$
4850 ± 4	31.2	$8.8 \cdot 10^{-3}$
5040 ± 4	16.6	$4.7 \cdot 10^{-3}$

REF. O.E. Kraft, Yu.V. Naumov, S.S. Parzhitskii, B.F. Petrov, Z. Salekh,
E.V. Sizov
Izv. Akad. Nauk SSSR 41, 82 (1977)
Bull. Acad. Sci. 41, 65 (1977)

ELEM. SYM.	A	Z
Cu	59	29
REF. NO.		egf.
77 Kr 7		

METHOD				REF. NO.	
				77 Kr 7	
REACTION	RESULT	EXCITATION ENERGY	SOURCE		ANGLE
			TYPE	RANGE	
P,G	LFT	4-5	D	1-2	90

A study is reported of the γ -decay of analog resonances in the $^{58}\text{Ni}(p\gamma)^{59}\text{Cu}$ re- 5 STATES, 4.35-5.31
action. The following analogs of the excited states of ^{59}Ni were observed:
0.466, 0.878, and 1303 keV. The quantities μ_γ and the values of $B(M1)$ have been
determined for transitions from the analogs to the ^{59}Cu levels. Analog β and γ -
transitions are compared, and analog-antianalog transitions are analyzed.

Table 1

Intensities of Direct Transitions from ^{59}Cu Resonances

E_p , keV	J_p^p	$E_p = 950 \text{ keV}$ $E^* = 4319 \pm 1 \text{ keV}$ $J^\pi = 1/2^-$			$E_p = 1426 \text{ keV}$ $E^* = 4817 \pm 1 \text{ keV}$ $J^\pi = 1/2^-$			$E_p = 1843 \text{ keV}$ $E^* = 5230 \pm 1 \text{ keV}$ $J^\pi = 1/2^-$			$E_p = 1883 \text{ keV}$ $E^* = 5268 \pm 1 \text{ keV}$ $J^\pi = 1/2^-$			$E_p = 1923 \text{ keV}$ $E^* = 5310 \pm 1 \text{ keV}$		
		I_γ	Γ_γ , eV	$B(M1)$, μ_N^2	I_γ	Γ_γ , eV	$B(M1)$, μ_N^2	I_γ	Γ_γ , eV	$B(M1)$, μ_N^2	I_γ	Γ_γ , eV	$B(M1)$, μ_N^2	I_γ	Γ_γ , eV	$B(M1)$, μ_N^2
0	$3/2^-$	6	0.003	0.003	16	0.08	0.06	91	1.5	0.90	29	0.015	0.01	15	0.03	0.02
491	$1/2^-$	17	0.008	0.01	66	0.32	0.34	5	0.09	0.09	18	0.01	0.08	-	-	-
912	$5/2^-$	-	-	-	3	0.015	0.02	-	-	-	7	0.004	0.01	-	-	-
1087	$5/2^-$	-	-	-	9	0.045	0.17	-	-	-	-	-	-	-	-	-
2265	$3/2^-$	17	0.008	0.08	4	0.02	0.10	4	0.07	0.23	-	-	-	-	-	-
2318	$1/2^-$	25	0.012	0.12	-	-	-	-	-	-	8	0.005	0.015	-	-	-
2324	$3/2^-$	-	-	-	2	0.010	0.08	-	-	-	-	-	-	68	0.13	0.41
2707	$5/2^-$	-	-	-	-	-	-	-	-	-	12	0.007	0.035	-	-	-
2827	$5/2^-$	-	-	-	-	-	-	-	-	-	7	0.004	0.025	-	-	-
3025	$(3/2^-)$	11	0.005	0.18	-	-	-	-	-	-	-	-	-	9	0.018	0.12
3114	$(5/2^-)$	9	0.004	0.18	-	-	-	-	-	-	12	0.007	0.06	-	-	-
3130	$(3/2^-)$	15	0.007	0.33	-	-	-	-	-	-	-	-	-	7	0.017	0.11
3434	$(5/2^-)$	-	-	-	-	-	-	-	-	-	7	0.004	0.05	-	-	-

Note. For the $E_p = 1923 \text{ keV}$ resonance, the spin of which is unknown, we give values of $g\Gamma_\gamma$ and $gB(M1)$, where g is a statistical factor equal to $\frac{2J+1}{(2J_p+1)(2J_0+1)}$. J is the spin of the resonance, J_p is the proton spin, and J_0 is the spin of the target nucleus.

Cu
A=60

Cu
A=60

Cu
A=60

Method Radioactivity

Ref. No.	JOC
61 Ca 1	

Reaction	E or ΔE	E_0	Γ	$\int \sigma dE$	$J\pi$	Notes
$\text{Ni}^{58}(d,\gamma)$	3.5-4.5					At $E_d = 4.5$ MeV, $\sigma(d,\gamma)=61\pm 9 \mu\text{b}$

TABLE I
Reactions at 4.5 MeV deuteron

Target	σ_{total}	σ_{elastic}	$\sigma_{\text{inelastic}}$	$\sigma_{\text{direct capture}}$
Ni^{58}	61 μb 85 mb	48 μb 64 mb		61 μb assuming the measured π to be totally accounted for by this process.
Zn^{64}	80 μb 100 mb	86 μb 175 mb		192 μb
Cu^{63}	295 μb 75 mb	215 μb 29 mb		1280 μb
Cu^{65}	19 μb	74 μb		

* There is a misprint in eq. (5) of ref. 1, the right side of which should be divided by π . Eq. (6) of ref. 1 is correct.

Ref 1: Carver & Jones - Nuclear Phys. 11, 400 (1959)

Fig. 1. Cross-sections for the reactions $\text{Ni}^{58}(d,\gamma)$ - denoted by crosses - and $\text{Ni}^{58}(d,n)$ - denoted by dots - as a function of deuteron energy. The full curves are given by the statistical theory. The scale for $\sigma(\gamma)$ is to the left and for $\sigma(n)$ to the right.

Cu
A=61

...

Cu
A=61

Cu
A=61

REF. O. E. Kraft, Yu. V. Naumov, and I. V. Sizov
Yad. Fiz. 20, 1081 (1974)
Sov. J. Nucl. Phys. 20, 567 (1975)

ELEM. SYM.	A	Z
Cu	61	29

METHOD

REF. NO.	
74 Kr 3	- hmg

REACTION	RESULT	EXCITATION ENERGY	SOURCE		DETECTOR		ANGLE
			TYPE	RANGE	TYPE	RANGE	
P, G	LFT	6- 7	D	1- 2	SCD-D		90
		(6.38-6.41)		(1.588-1.620)			

B (M1)

We measured the γ spectra of the resonance decay in the reaction $^{60}\text{Ni}(p, \gamma)^{61}\text{Cu}$ at proton energies $E_p = 1588, 1599, 1605$, and 1620 keV. These resonances are identified as the components of the fine structure of the analog state $p_{3/2}$. The intensities of the population of the state of ^{61}Cu with excitation energy up to 3 MeV are obtained. The decay scheme of these states is constructed. Comparison with beta decay points to the need for taking into account the l part in the operator of the $M1$ γ transition when assessing the role of the polarization effects in the γ decay of isobar analog resonances. The analog-antianalog transition is slowed down by an approximate factor 10 compared with the single-particle estimate.

E_{lev} , keV	J^π	I_γ , eV				$B(M1) \cdot 10^3$, μ_N^2			
		1588	1599	1605	1620	1588	1599	1605	1620
0	$3/2^-$	3.7	16.8	25.9	25.1	1.2	5.6	8.6	8.2
476.4	$1/2^-$	0.8	11.6	5.4	1.2	0.3	4.9	2.3	0.5
969.9	$3/2^-$	1.5	7.4	2.8	2.7	0.8	4.0	1.5	1.5
1395.1	$3/2^-$	4.0	14.6	10.1	9.8	2.8	10.1	7.0	6.7
1661.8	$3/2^-$	—	0.8	1.5	0.6	—	0.7	1.2	0.5
1904.0	$(1/2^-)$	—	—	2.0	1.3	—	—	1.9	1.2
2089.5	$1/2^-$	1.1	5.8	3.9	6.5	1.1	6.4	4.2	7.0
2203.0	$(1/2^-)$	—	5.0	—	—	—	6.7	—	—
2357.3	$3/2^-$	1.5	—	—	1.0	2.0	—	—	1.3
2473.3	$3/2^-$	1.3	3.0	1.9	—	1.9	4.4	2.7	—
2583.5	$3/2^-$	1.5	4.0	—	—	2.4	6.3	—	—
2687.6	$3/2^-$	1.6	2.8	—	1.9	2.7	4.9	—	3.2
2792.3	$3/2^-$	—	—	2.3	—	—	—	4.3	—
2859.3	$(1/2^- - 1/2^-)$	2.7	2.3	—	5.3	5.5	4.6	—	10.2
2999.5	$(1/2^- - 1/2^-)$	0.4	—	—	2.5	0.8	—	—	5.5
3022.0	$(1/2^- - 1/2^-)$	3.0	1.7	—	2.3	6.9	3.8	—	5.2
3041.6	—	0.8	—	—	—	1.3	—	—	—
3062.4	$(1/2^- - 1/2^-)$	1.9	1.7	—	1.2	4.6	4.0	—	2.9
3094.1	$(1/2^- - 3/2^-)$	0.8	2.8	—	2.5	2.1	6.9	—	6.0

REF.

O.E. Kraft, Yu. V. Naumov, and I.V. Sizov
 Izv. Akad. Nauk SSSR. Ser. Fiz. 39, 70 (1975)
 Bull. Acad. Sci. USSR Phys. Ser. 39, 59 (1975)

ELEM. SYM.

A

Z

Cu

61

29

METHOD

REF. NO.

75 Kr 15

hmg -

REACTION	RESULT	EXCITATION ENERGY	SOURCE		DETECTOR		ANGLE
			TYPE	RANGE	TYPE	RANGE	
P,G	LFT	6- 7	D	1- 2	NAI-D		90
		(6.3-6.6)		(1.6-1.9)			

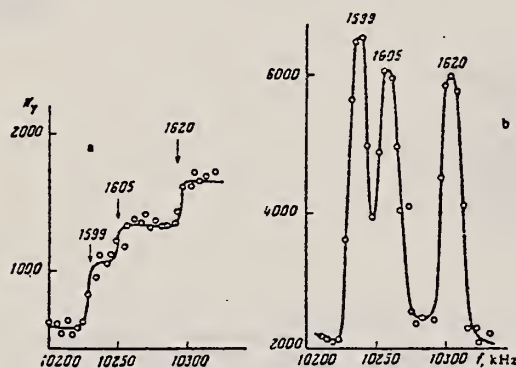


Fig. 1. Excitation function of the $^{60}\text{Ni}(p\gamma)^{61}\text{Cu}$ reaction in the $p_{3/2}$ -IAR region. a) Thick target; b) thin target.

Table 1

Characteristics of the Isobar-Analog Resonances of ^{61}Cu

E^*, keV	E_p, keV	J^π	$\Gamma_{\gamma}, \text{eV}$			$\Gamma_{\text{tot}}, \text{eV}$		
			present paper	[7]	[10]	present paper*	[7]	[10]
6374	1599	$3/2^-$	0.15 ± 0.03	0.1	0.05	0.72	0.6	0.21
6380	1605	$3/2^-$	0.25 ± 0.05	0.4	0.14	0.54	0.5	0.26
6395	1620	$3/2^-$	0.20 ± 0.04	0.3	0.10	0.50	0.4	0.16
6431	1656	$1/2^-$	0.43 ± 0.10	0.4	0.19	0.60	0.5	0.27
6524	1856	$1/2^-$	0.034 ± 0.010	—	—	0.33	—	—
6641	1873	$1/2^-$	0.07 ± 0.02	—	—	0.35	—	—

*The total widths are given without allowance for the angular distribution of γ -rays.

Cu
A=63

Cu
A=63

Cu
A=63

Ref. J.G. Campbell
Australian J. Phys. 8, 445 (1955)

Elem. Sym.	A	Z
Cu	63	29

Method $\text{Li}^7(p,\gamma)$ reaction; 700 keV electrostatic generator; radioactivity

Ref. No.	EGF
55 Ca 1	

Reaction	E or ΔE	E_0	Γ	$\int \sigma dE$	$J\pi$	Notes
$\text{Cu}^{63}(\gamma, n)$	$\sim 350 - 700 \text{ keV}$	$17.5 - \sim 17.85$				

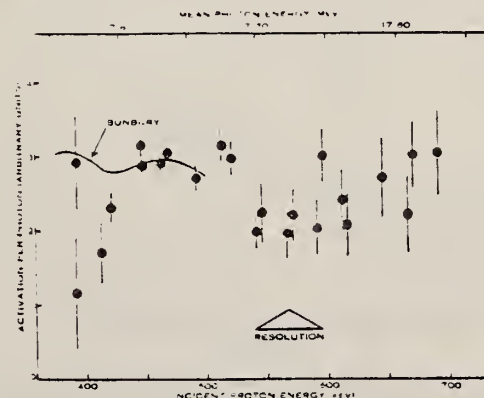


Fig. 2. A set of results for $^{63}\text{Cu}(\gamma, n)^{63}\text{Zn}$. Also shown are results of Bunker et al. (1954).

Method Monoergic electrons from 22 MeV Betatron.

Ref. No.	EGF
55 Sc 1	

Reaction	E or ΔE	E_0	Γ	$\int \sigma dE$	$J\pi$	Notes
(γ, n)	12-20	16.8	4.5	0.41 MeV-mb		$\sigma_{\max} = 80 \text{ mb.}$ Errors estimated to be 25%.

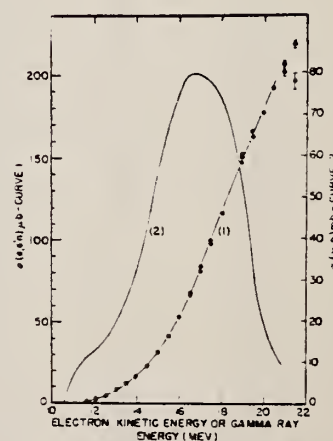


FIG. 5. The electrodisintegration activity as a function of the kinetic energy of the electron, normalized so as to represent the electrodisintegration cross section, is shown as curve 1. The statistical errors are less than the size of the points except where they are shown. The photodisintegration activity is proportional to the product of curve 1 by F as given in Fig. 4. The (γ, n) cross section as obtained from this product by the photon difference method is shown as curve 2.

Method Michigan University synchrotron; Victoreen counter; betatron 10.1 min.

Ref. No.	EGF
57 Hi 1	

Reaction	E or ΔE	E_0	Γ	$\int \sigma dE$	$J\pi$	Notes
(e,e'n)	29.5 46.5 63.5 81.5	16 .				<p>97% electric dipole and 3% electric quadrupole required to fit experimental points.</p> <p>No corrections made for nuclear signs; these would tend to increase fraction of E_2.</p> <p>$\text{Cu}^{63}(\gamma, n) \text{Cu}^{62}$ cross section from Katz and Cameron [Can. J. Phys. <u>29</u>, 518 (1951)].</p>

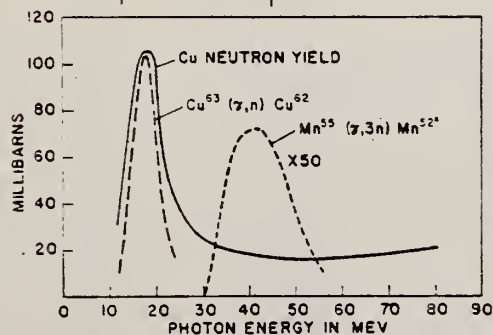


FIG. 1. Photon neutron yield cross section for Cu shown in comparison with $\text{Cu}^{63}(\gamma, n) \text{Cu}^{62}$ and $\text{Mn}^{55}(\gamma, n) \text{Mn}^{52}$ cross sections.

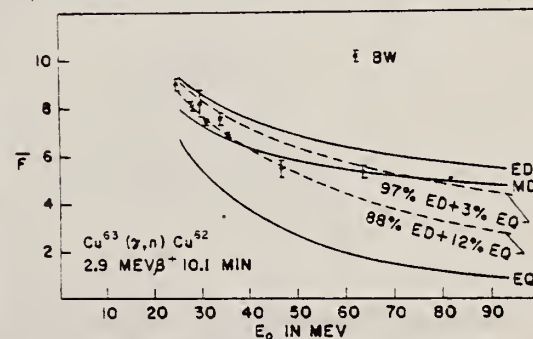


FIG. 3. Experimental and theoretical values of \bar{F} for copper. The dashed lines are computed assuming an effective excitation energy of 14 Mev for the electric quadrupole process.

Elem. Sym.	A	Z
Cu	63	29

Betatron; activation

Ref. No.

58 Be 1

EH

$E_{th} = 10.80 \pm 0.04$ based on thresholds
in F^{19} , N^{14} and C^{12} .

U.S. DEPARTMENT OF COMMERCE
NATIONAL BUREAU OF STANDARDS

Ref. M.E. Toms, J. McElhinney
Phys. Rev. 111, 561 (1958)

Elem. Sym.	A	Z
Cu	63	29

Method Betatron; alpha yield; nuclear emulsion

Ref. No.	NVB
58 To 2	

Reaction	E or ΔE	E_0	Γ	$\int \sigma dE$	$J\pi$	Notes
$\text{Cu}^{63}(\gamma, \alpha)$	Bremss. 22					Yield = 3.6×10^4 alpha/mole/roentgen. Target enriched to 99.5% Cu^{63} .

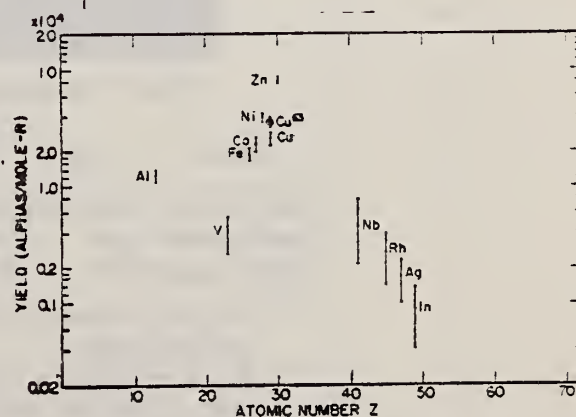


FIG. 8. Photo-alpha yields plotted against atomic numbers for the exposures of the survey.

Method $\text{Li}^7(p, \gamma)$ rays; GH counter; BF_3 ; 4π neutron

Ref. No.	EH
59 Na 1	

Reaction	E or ΔE	E_0	Γ	$\int \sigma dE$	$J\pi$	Notes
$\text{Cu}^{63}(\gamma, n)$	Bremss. 17.6					<p>$\sigma = 42.5 \pm 15\% \text{ mb}$</p> <p>The ratio 1:2 was used as the intensity ratio of 14.8 to 17.6 MeV photons and the results of betatron experiments to make the correction.</p> <p>The incident flux was determined by calculating how many electrons should be ejected per photon from a metal foil placed in front of a geiger counter.</p>

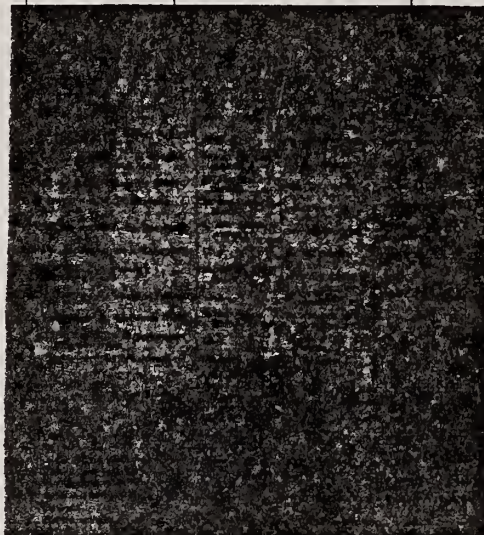


Table I. Results obtained.

Reaction	λ (min^{-1})	$\sigma(\text{Li-p}\gamma)$ (mb)	$\sigma(17.6 \text{ MeV})$ (mb)
$\text{Cu}^{63}(\gamma, n)\text{Cu}^{62}$	$0.0695 \pm 2\%$	$37.7 \pm 15\%$	42.5
$\text{Zn}^{64}(\gamma, n)\text{Zn}^{63}$	0.018	$20.7 \pm 18\%$	23.3
$\text{Ag}^{108}(\gamma, n)\text{Ag}^{107}$	0.295	$54.6 \pm 16\%$	61.5

* The decay constant of Cu^{62} was determined in our measurement.

** For the reduction to 17.6 MeV monochromatic γ -ray, we used the ratio 1:2 as the intensity ratio of 14.8 MeV to 17.6 MeV γ -ray, and the results of bremsstrahlung experiments as the excitation curve for each elements.

- 14) T. Nakamura, K. Fukunaga, K. Takamatsu and S. Yasumi: Mem. Coll. Sci. Kyoto Univ. (to be published).
- 15) S. Yasumi: J. Phys. Soc. Japan **12** (1957) 443.
- 16) P. V. C. Hough: Phys. Rev. **80** (1950) 1069.
- 17) R. W. King: Rev. Mod. Phys. **26** (1954) 327.
- 18) Y. Uemura, M. Sonoda, Y. Saji, S. Yasumi, Y. Ishizaki and Y. Ohno: Bull. Inst. Chem. Res. Kyoto Univ. **29** (1952) 66.
- 19) W. A. Fowler, C. C. Lauritsen and T. Lauritsen: Rev. Mod. Phys. **20** (1948) 235.
- 20) C. A. Barnes, J. H. Carver, G. H. Stafford and D. H. Wilkinson: Phys. Rev. **86** (1952) 359.

γ, n cross sections.

neutron detector	Neutron yield		β -counting calibration	(γ, n) cross section of copper. Author results (mb)	$\sigma_{Cu^{63}}(17.6)^{o)}$ (mb)	relative cross ^{p)} section		
	neutron detector calibration	β -counting				Cu	Zn	Ag
BF ₃ + paraffin	Ra + Be, Po + Be	Al G. M. counter (cylindrical)	cal. $-e-\mu x^{j)}$	$120 \pm 30^{63k)}$	120	100	62 ¹⁾	176 ¹⁰⁹⁾
		G. M. counter (end window)	extrap. S ⁿ⁾ extrap. G	77 ± 13^{63} 17.6	33*			
				$55 \pm 12^{nat^{m)}$ Li-p ⁿ⁾	55	100	86	24.5
		G. M. counter	exper. S ^{l)} exper. G	110 ⁶³ 17.6	110			
		G. M. counter (end window)	RaE	100 ⁶³ 17.6	100	100		190 ¹⁰⁹⁾
		G. M. counter	RaD + E	100 ⁶³ 17.6	100			
		G. M. counter (end window)	extrap. S RaD + E, P ³²⁾	90 ⁶³ 17.6	90			
BF ₃ + paraffin		G. M. counter	exper. S RaD + E	48 ± 8^{63} Li-p	54			
Szillard-Chalmers	D(γ, n) Ra + Be			110 nat 17.6	95	100	95	251
		4 π -scintillation counter	extrap. S	85 ± 15^{nat} Li-p	85			
BF ₃ + paraffin	Ra + Be, Sb + Be			97 ⁶³ 17.6	97			
BF ₃ + paraffin	Ra + Be			75 nat 17.6	65	100	88	270
				120 nat 17.6	104			
		G. M. counter (end window)	extrap. S 4 π . G ^{j)}	38 ± 6^{63} Li-p	43	100	55 ⁴⁾	145 ¹⁰⁹⁾

j) Geometrical factor G was measured by the 4 π -counter.

k) The cross section of Cu⁶³(γ, n).

l) The cross section by 17.6 Mev photons.

m) The cross section of natural copper.

n) The cross section by Li-p γ -ray.

o) The following values were used to reduce the cross section of Cu⁶³(γ, n) by 17.6 Mev photons: the intensity ratio of 17.6 Mev and 14.8 Mev photons in the Li-p γ -ray is 2:1, $\sigma_{17.6 \text{ Mev}}(\text{Cu}) / \sigma_{14.8 \text{ Mev}}(\text{Cu}) = 1.67$ and $\sigma_{17.6 \text{ Mev}}(\text{Cu}^{63}) / \sigma_{17.6 \text{ Mev}}(\text{Cu}^{65}) = 1.5$.

p) Suffix numbers show the mass number of the isotopes.

* See § 4. Discussions or ref. 14.

Elem. Sym.	A	Z
Cu	63	29
Ref. No.		EH
59 Pe 3		

Method 100 MeV Betatron

Ref. No.	
59 Pe 3	EH

Reaction	E or ΔE	E_0	Γ	$\int \sigma dE$	$J\pi$	Notes
(γ, n)						$E_{th} = 10.78 \pm 0.03 \text{ MeV.}$

Ref. E.C. Booth
Nuclear Phys. 19, 426 (1960)

Elem. Sym.	A	Z
Cu	63	29

Method Van de Graaff; electron brems.; Ring scatterer; NaI

Ref. No.	JHH
60 Bo 3	

Reaction	E or ΔE	E_0	Γ	$\int \sigma dE$	$J\pi$	Notes
(γ, γ)	Bremss. 0.5-2.2	0.67 0.96			3/2	Mean lifetime t/g : $= (5.3)10^{-13}$ sec [absorption method] $= (3.1)10^{-13}$ sec [resonance scattering] where $g = (1+2I)/(1+2I_0)$. $= (4.6)10^{-13}$ sec [resonance scattering] Detector at 100°

REF. K. N. Geller, J. Halpern, and E. G. Muirhead
 Phys. Rev. 118, 1302-12 (1960)

ELEM. SYM.	A	Z
Cu	63	29

METHOD	REF. NO.	
Betatron; neutron threshold; ion chamber	60 Ge 3	NVB

REACTION	RESULT	EXCITATION ENERGY	SOURCE		DETECTOR		ANGLE
			TYPE	RANGE	TYPE	RANGE	
G, N	NØX	THR	C	THR	BF3-I		4 PI

THRESHOLD

TABLE I. Summary and comparison of neutron separation energies inferred from present threshold measurements with values predicted from mass data and reaction energies. All energies are expressed in the center-of-mass system in Mev.

Reaction	No. runs	Present results	Other results	Method	Reference
$\text{Cu}^{63}(\gamma, n)\text{Cu}^{62}$	3	10.833 ± 0.017 (calib)	10.826 ± 0.018	mass data	j

i K. S. Quisenberry, T. T. Scolman, and A. O. Nier, Phys. Rev. 104, 461 (1956).

METHOD

Cockcroft-Walton; neutron cross section; radioactivity; Geiger counter; NaI spectrometer

REF. NO.

60 Ya 1

NVB

REACTION	RESULT	EXCITATION ENERGY	SOURCE		DETECTOR		ANGLE
			TYPE	RANGE	TYPE	RANGE	
G,P	ABX	15, 18	D	15, 18	ACT-I		
		(14.8, 17.6)		(14.8, 17.6)			

$$\sigma_{\text{Li}} = 62 \pm 4 \text{ mb (both Li } \gamma\text{'s)}$$

$$\sigma_{17.6} = 76 \pm 5 \text{ mb}$$

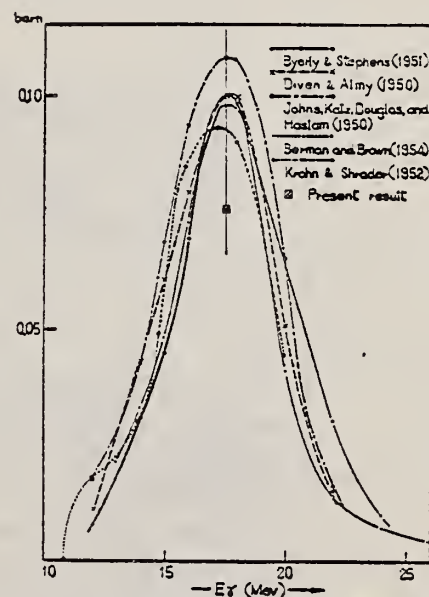


Fig. 10⁸. Excitation curves of the reaction $\text{Cu}^{63}(\gamma, n)\text{Cu}^{62}$ obtained by various authors. A point represents the value for 17.6 Mev γ -ray determined in the present experiment.

Elem. Sym.	A	Z
Cu	63	29

Method Monoergic γ 's from $\text{Li}^7(p,\gamma)$ and $\text{B}^{11}(p,\gamma)$ reactions; activation

Ref. No.
61 Co 2

JHH

Reaction	E or ΔE	E_0	Γ	$\int \sigma dE$	$J\pi$	Notes
(γ, n)	12.2 14.8 16.7 17.6					$\sigma(\gamma, n) =$ 11 ± 2 mb 33 ± 4 mb 63 ± 8 mb 73 ± 8 mb based on 59 ± 6 mb for $\sigma(\gamma, n)$ for total γ spectrum from 440 keV (E_p) resonance in Li^7 . Confirms shape of σ 's previously measured with brems., but absolute values $\sim 25\%$ lower.

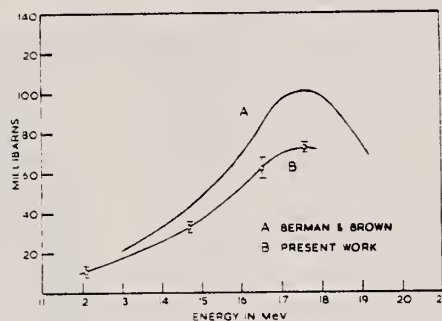


Fig. 2 - Comparison of (γ, n) cross section data for Li^7 . The errors shown do not include the $\pm 25\%$ in the absolute cross section.

TABLE 3
Bremsstrahlung measurements of $\text{Cu}^{63}\gamma/\text{aCu}^{63}$ cross section

Reference	E_{max} (MeV)	E_{min} (MeV)	Half-width (MeV)	E_{res} (MeV)	$\sigma(\gamma)$ (mb)	γ -ray intensity	Measurements of activity
Diven and Almy ⁽¹⁾	17.8	100	5.0	0.0	48	Reactor	β^+ End-window G.M. counter
Katz and Cameron ⁽²⁾	16.1	104	8.1	0.08	48	Reactor	β^+ G.M. counter
Berry and Stephens ⁽³⁾	17.3	100	3.3		60	Reactor	β^+ G.M. counter
Krohn and Shrader ⁽⁴⁾	17.0	94	3.1		70	Pure spectrometer	β^+ End-window G.M. counter
Berman and Brown ⁽⁵⁾	17.3	98	4.0	0.56 ± 0.08	60	Electron current	β^+ Geiger-Müller counter
Scott, Hanson and Kerst ⁽⁶⁾	16.7	98	4.8	0.41	60	Electron current	β^+ Geiger-Müller counter
Rowley et al. ⁽⁷⁾		98			70	Reactor	β^+ Flow proportional counter
Monsubert et al. ⁽⁸⁾	16.8	100	7.1	0.07	94 (Ca) 80 (Cu)	Reactor	BF_3 -paraffin
Lavrov and Lazareva ⁽⁹⁾	17.3	100	4.3	0.08	108 (Ca) 88 (Cu)	Ionization chamber	BF_3 -paraffin

⁽¹⁾ The cross section for the same isotopes of gamma rays as the lithium resonance reactions.
⁽²⁾ Due to the accurate yield as given by Katz and Cameron.

TABLE 4
 $\text{Li}^7(p,\gamma)\text{He}^4$ measurements of $\text{Cu}^{63}\gamma/\text{aCu}^{63}$ cross section

Reference	σ_{Li} (Natural Cu) (mb)	σ_{Cu} (Cu^{63}) (mb)	γ -ray monitoring	Activity measurement	Neutron detection
Wheeler and Hines ⁽¹⁾		130 ± 30	G.M. counter	G.M. counter	
Sheldon ⁽²⁾		29 ± 1	G.M. counter	G.M. counter	
McDaniel, Walker and Stearns ⁽³⁾	58 ± 18	13 ± 1	G.M. counter	G.M. counter	BF_3 -paraffin
Gillett, Seppel and Stoll ⁽⁴⁾		18 ± 1	G.M. counter	G.M. counter	
Hartley, Stephens and Winhold ⁽⁵⁾	64 ± 10	60 ± 9	Small NaI crystal		BF_3 -paraffin
Carver and Kondash ⁽⁶⁾	48 ± 13	40 ± 14	G.M. counter	G.M. counter	Sulfur-Chadwick
Nakamura et al. ⁽⁷⁾		39 ± 4	G.M. counter	G.M. counter	
Yasumi et al. ⁽⁸⁾		43 ± 4	NaI crystal	G.M. counter	
Present work		36 ± 4	NaI crystal	NaI crystal	

⁽¹⁾ As recommended by Nakamura et al.

References

- 1) M. B. Stearns and B. D. McDaniel, *Phys. Rev.* **83** (1951) 488
- 2) V. F. Krohn and E. F. Shrader, *Phys. Rev.* **87** (1953) 686
- 3) A. I. Berman and K. L. Brown, *Phys. Rev.* **96** (1954) 32
- 4) M. B. Scott, A. O. Hanson and D. W. Kerst, *Phys. Rev.* **100** (1952) 209
- 5) R. L. Matter, *J. Appl. Phys.* **28** (1957) 1200
- 6) C. S. Cook, *Nuclear Instruments and Methods* **4** (1959) 103
- 7) J. Kockum and N. Starfelt, *Nuclear Instruments and Methods* **4** (1959) 171
- 8) B. Mainbridge, *Aust. J. Phys.* **13** (1960) 204
- 9) H. E. Gove and E. Paul, *Phys. Rev.* **97** (1955) 104
- 10) H. W. Koch and J. M. Wyckoff, *I.R.E. Trans. Nucl. Sci.* NS-5 (1958) 127
- 11) W. F. Miller, J. Reynolds and W. J. Snow, U.S.A.E.C. Report ANL-5902 (1958)
- 12) S. B. Gerfinkel, private communication from the National Bureau of Standards, Washington (1960)
- 13) L. Katz and A. G. W. Cameron, *Can. J. Phys.* **29** (1951) 518
- 14) Gladys White Grodstein, N.B.S. Circular 583 (1957)
- 15) D. Strominger, J. M. Hollander and G. T. Seaborg, *Revs. Mod. Phys.* **30** (1958) 585
- 16) Nuclear Data Cards, National Research Council (1959)
- 17) B. D. McDaniel, R. L. Walker and M. B. Stearns, *Phys. Rev.* **80** (1950) 807
- 18) W. H. Hartley, W. E. Stephens and E. J. Winhold, *Phys. Rev.* **104** (1956) 178
- 19) S. Yasumi, M. Yata, K. Takamatsu, A. Masaki, and Y. Masuda, *J. Phys. Soc. Japan* **15** (1960) 1913
- 20) J. H. Carver and E. Kondash, *Phil. Mag.* **45** (1954) 985
- 21) J. P. Rossvig, R. N. H. Haslam and D. J. McKenna, *Can. J. Phys.* **37** (1959) 607
- 22) J. P. Rossvig, R. N. H. Haslam and J. L. Berggren, *Can. J. Phys.* **38** (1960) 230
- 23) B. C. Diven and C. M. Almy, *Phys. Rev.* **86** (1950) 497
- 24) E. B. Byerly and W. E. Stephens, *Phys. Rev.* **83** (1951) 54
- 25) E. Monsubert, L. Katz and J. Goldstein, *Phys. Rev.* **91** (1953) 692
- 26) E. I. Gavrilov and L. E. Lazareva, *Soviet Physics JETP* **3** (1957) 871
- 27) E. Wheeler and O. Hines, *Helv. Phys. Acta* **21** (1948) 308
- 28) S. Shimizu, *Mem. Coll. Sci. Kyoto A28* (1949) 193
- 29) Gillett, Seppel and Stoll, *Helv. Phys. Acta* **25** (1953) 491
- 30) Nakamura, Takamatsu, Fukunaga, Yata and Yasumi, *J. Phys. Soc. Japan* **14** (1959) 693
- 31) J. H. Carver and W. Turchinets, *Proc. Phys. Soc. A* **73** (1959) 110
- 32) F. Ferraro, R. Malvano, E. Silva, J. Goldstein and G. Moscati, *Nuclear Physics* **10** (1959)

Elem. Sym.	A	Z
Cu	63	29

Method Resonance scattering; absolute cross section and angular distribution measurement; NaI.

Ref. No.	
61 Ro 1	JHH

Reaction	E or ΔE	E_0	Γ	$\int \sigma dE$	$J\pi$	Notes
(γ, γ)	668 keV				1/2	$W(\theta) = 1 - (0.03 \pm 0.07)P_2(\cos\theta)$; T(mean life) = $(3.1 \pm 0.3) \times 10^{-13}$ sec.
	961 keV				5/2	$W(\theta) = 1 + (0.8 \pm 0.2)P_2(\cos\theta)$; T = $(9 \pm 1.5) \times 10^{-13}$ sec. Gaseous Zn^{63} β source used; gamma line shapes were calculated from β decay scheme of Ricci et al [Nuovo Cimento <u>11</u> , 156 (1959)].

TABLE I
Experimental data and the lifetimes of the 668-keV and 961-keV levels

E_{γ} (keV)	f_{γ}/f_{β}	A_{γ}	σ_{γ} (barns)	$\frac{N(E_{\gamma})}{N}$	τ (sec)
668 ± 10^0	$\frac{1}{2}$	-0.03 ± 0.07	0.68 ± 0.08	2.9×10^{-4}	$(3.1 \pm 0.3) \times 10^{-13}$
961 ± 10^0	$\frac{1}{2}$	0.8 ± 0.2	0.977 ± 0.068	1.69×10^{-4}	$(9 \pm 1.5) \times 10^{-13}$

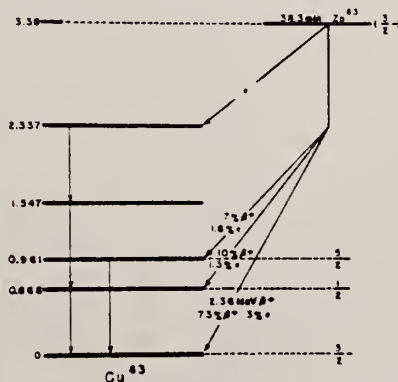


Fig. 3. Partial decay scheme of Zn^{64} . Only those features relevant to the resonance scattering experiment are reproduced.

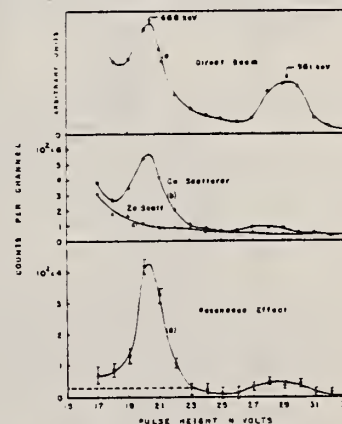


Fig. 3. Pulse height distributions of the direct beam and the scattered radiations. (a) Direct beam from a Zn^{64} source, (b) Cu scatterer, (c) Zn scatterer. (c) resonance effect obtained by the subtraction of curve (a) from (b).

Ref. E.C. Booth, K.A. Wright
Nuclear Phys. 35, 472 (1962)

Elem. Sym.	A	Z
Cu	63	29

Method 4 MeV electron Van de Graaff; brems.; nuclear resonance scattering, ring scatterer; NaI

Ref. No.	
62 Bo 6	JHH

Reaction	E or ΔE	E_0	Γ	$\int \sigma dE$	$J\pi$	Notes
$\text{Cu}^{63} (\gamma, \gamma)$	Brems. 0 - 4					

Table 3
Mean lifetimes of excited states deduced from the resonance scattering of bremsstrahlung

Nucleus	E_x	Energy (MeV)	Spin	Γ	Γ_{rel}	Γ (eV)	$\tau \times 10^{-12}$ (sec)
P^{31}	100	1.46	$1^+ \rightarrow 0^+$	1	0.13	(1)	0.56
N^{14}	100	2.08	$1^+ \rightarrow 0^+$	0	0.1	0.78	> 0.06
		2.20	$1^+ \rightarrow 0^+$	1	0.20	(1)	> 0.06
		2.66	$1^+ \rightarrow 0^+$	1	0.6	(1)	> 0.29
		2.76	$1^+ \rightarrow 0^+$	1	(0.1)	(1)	> 0.002
		2.88	$1^+ \rightarrow 0^+$	1	0.65	(1)	0.09
U^{238}	100	2.72	$1^+ \rightarrow 0^+$	1	0.23	0.02	> 0.20
		2.92	$1^+ \rightarrow 0^+$	1	0.510	1	0.6×10^{-10}
Si^{28}	4.71	1.38	$1^+ \rightarrow 0^+$	0	1	0.85	1.6
		2.40	$1^+ \rightarrow 0^+$	2	(1)	0.20	0.2
P^{32}	100	1.56	$1^+ \rightarrow 0^+$	0	1	0.05	2.5
		1.53	$1^+ \rightarrow 0^+$	0	1	0.70	6.6
		1.13	$1^+ \rightarrow 0^+$	0	(1)	0.05	0.5
		3.20	$1^+ \rightarrow 0^+$	0	1	0.70	> 1.6×10^{-10}
		3.43	$1^+ \rightarrow 0^+$	1	1	(1)	> 1.6×10^{-10}
		3.61	$1^+ \rightarrow 0^+$	0	1	0.05	0.05×10^{-10}
S^{32}	96	2.76	$0^+ \rightarrow 0^+$	1	1	(1)	> 0.4×10^{-10}
S^{34}	6.2	3.137	$0^+ \rightarrow 0^+$	1	1	0.05	> 1.0
C^{12}	75.3	1.33	$1^+ \rightarrow 0^+$	1	1	(1)	4
		1.76	$1^+ \rightarrow 0^+$	1	(1)	(1)	4
		2.7(0.65)	$1^+ \rightarrow 0^+$	1	1	(1)	0.35×10^{-10}
		3.01	$1^+ \rightarrow 0^+$	1	1	(1)	0.37×10^{-10}
O^{16}	78.6	2.1	$1^+ \rightarrow 0^+$	1	1	(1)	> 0.3×10^{-10}
		2.17	$1^+ \rightarrow 0^+$	1	1	(1)	> 0.3×10^{-10}
C^{13}	26.6	0.005	$1^+ \rightarrow 0^+$	1	1	(1)	> 10^{-10}
		1.73	$1^+ \rightarrow 0^+$	1	1	(1)	> 0.3×10^{-10}
O^{18}	98	0.00	$1^+ \rightarrow 0^+$	1	1	(1)	> 0.3×10^{-10}
		2.00	$1^+ \rightarrow 0^+$	1	1	(1)	> 0.3×10^{-10}
		2.09	$1^+ \rightarrow 0^+$	1	1	(1)	> 0.3×10^{-10}
		3.00(0.04)	$1^+ \rightarrow 0^+$	1	1	(1)	> 0.3×10^{-10}
		4.00-4.13	$1^+ \rightarrow 0^+$	1	1	(1)	> 0.3×10^{-10}
S^{32}	96	3.96	$0^+ \rightarrow 0^+$	1	1	0.05	> 0.48
S^{34}	98	1.33	$1^+ \rightarrow 0^+$	1	(1)	0.5	44×10^{-11}

Sci. V.P. Chizh'ov, A.P. Komar, L.A. Kulchitsky, A.V. Kulikov,
E.D. Makhnovsky, Yu.M. Volkov
Nuclear Phys. 24, 562 (1962)

Elem. Sym.	A	Z
Cu	63	29

Method

90 MeV Synchrotron; magnetic spectrometer; emulsions; NaI counter telescope

Ref. No.

62 Ch 2

JHH

Reaction	E or ΔE	E_0	Γ	$\int \sigma dE$	$J\pi$	Notes
	Bremss.					
(γ , d)	34					
(γ , p)	70					
	90					

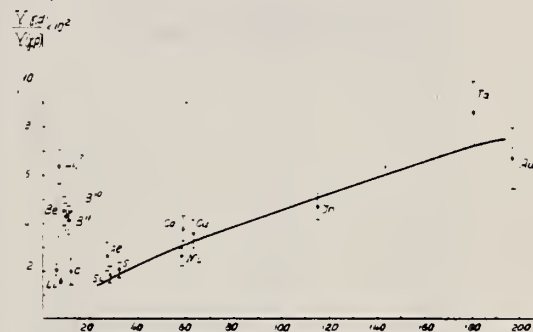


Fig. 4. The ratio of the yields of deuterons and protons with energies 15.5 to 30 MeV depending on the mass number of nuclei A for $E_{\gamma \max} = 90$ MeV. The solid line stands for the normalized dependence (5).

TABLE I
Experimental data

Elements	$E_{\gamma \max}$ MeV	Particle energy interval (MeV)	$\frac{Y(\gamma, d)}{Y(\gamma, p)}$	θ	Method
Li ⁶	30	7.5 to 15	0.003 ± 0.008	90°	I
	43		0.007 ± 0.005		
	90		0.097 ± 0.014		
Li ⁷	25	7.5 to 15	0.020 ± 0.030	90°	I
	43		0.058 ± 0.006		
	90		0.160 ± 0.054		
B ¹¹	40	7.5 to 19	0.006 ± 0.002	90°	I
Al ²⁷	35	2.9 to 10	0.009 ± 0.007	50° - 120°	II
Ca ⁴⁸	35	3.7 to 10	0.036 ± 0.017	50° - 100°	II
Cu ^{63, 65}	34	4.5 to 15	0.007 ± 0.003	90°	I
	34	7.5 to 15	0.007 ± 0.003	90°	I
	70	3 to 10	0.05 ± 0.01	20° - 50°	II
	70	4 to 10	0.04 ± 0.01	20° - 50°	II
	90	7 to 19	0.021 ± 0.005	90°	I

I, scintillation telescope method

II, Method of deflecting charged particles in magnetic field.

Elem. Sym.	A	Z
Cu	63	29
Ref. No.	62 De 1	JHH

Method Electrostatic generator, $H^3(p,\gamma)He^4$ reaction; activation of positron emitter; 2 NaI in coincidence.

Ref. No.	
62 De 1	JHH

Reaction	E or ΔE	E_0	Γ	$\int \sigma dE$	$J\pi$	Notes
(γ, n)	20.48					$\sigma(\gamma, n) = 52.5 \pm 2.1 \text{ mb}$

J. Goldemberg, E.W. Hamburger, A. Szily
An. Acad. Brasil. Cienc. 35, 169 (1963)

ELEM. SYM.	A	Z
Cu	63	29

METHOD

Betatron; deuteron yield; nuclear emulsions

REF. NO.

63 Go 8

NVB

REACTION	RESULT	EXCITATION ENERGY	SOURCE		DETECTOR		ANGLE
			TYPE	RANGE	TYPE	RANGE	
G,D	RLY	14-22	C	22	EMU-I		DST
G,A	RLY	THR-22.	C	22	EMU-I		DST

REL TO PROTONS

$$\frac{Y_{d+He^3}}{Y_p} = 4.5 \pm 2.5\%$$

$$\frac{Y_{\alpha+t}}{Y_p} = 4.5 \pm 2.5\%$$

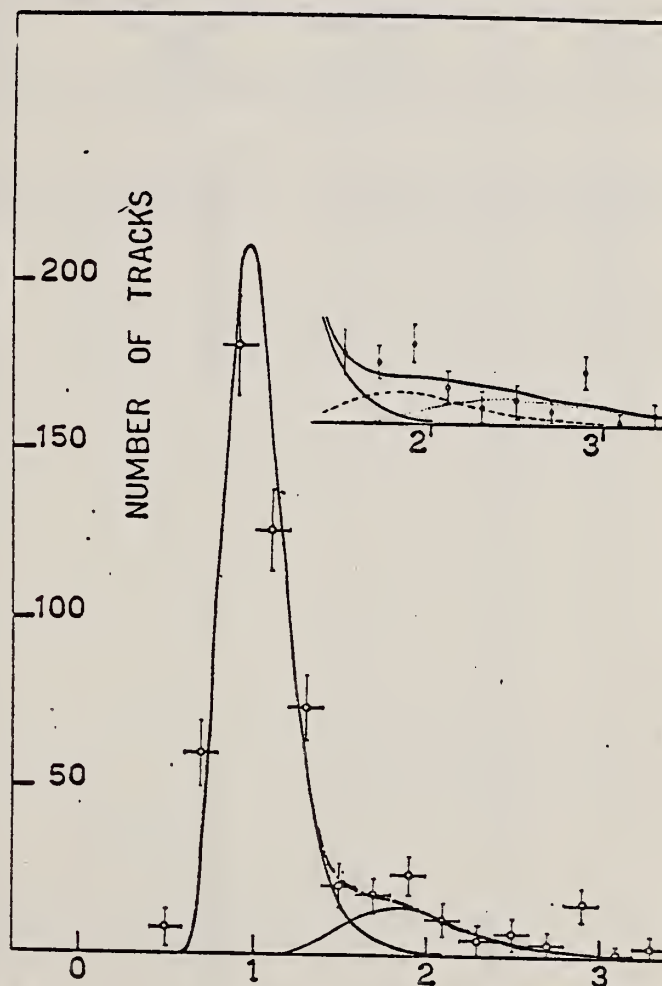


Fig. 6 — Total mass histogram for the plates exposed in positions n°s 1, 2, 8 and 9. The full lines give the calculated shapes of the proton and deuteron peaks, normalized respectively to 460 and 65 tracks; the dot-dashed line is the sum of the two peaks. In the inset the same experimental data is shown, but the deuteron curve is normalized to 42 tracks, while the dotted line corresponds to 44 alpha particles; the dot-dashed line is the sum of the three peaks.

Ref. J.A. McIntyre, G.K. Tandon
Phys. Letters 4, 117 (1963)

Elem. Sym.	A	Z
Cu	63	29

Method Radioactive source; Compton energy-shifter; NaI

Ref. No.	JHH
63 Mc 1	

Reaction	E or ΔE	E_0	Γ	$\int \sigma dE$	$J\pi$	Notes
$\text{Cu}^{63}(\gamma, \gamma)$	0.92-1.0	0.961 ± 0.003				<p>Lifetime of 0.961 MeV level = 6×10^{-13} sec \pm factor of 2.</p> <p>Detector at 90°.</p>

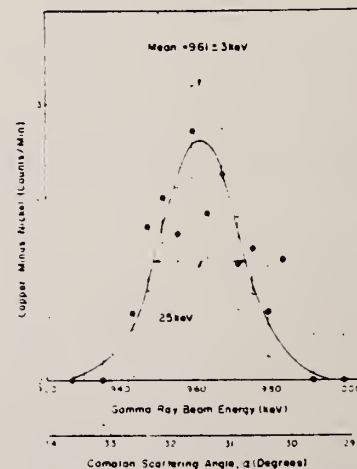


Fig. 2 The difference in counting rate of the NaI(Tl) counter for elastic scattering from the copper and nickel targets is plotted against the Compton scattering angle. The second abscissa scale gives the energy of the γ -rays striking the target corresponding to each angle. Each point represents four hours of counting with the copper target and four hours of counting with the nickel target.

Van de Graaff; resonance fluorescence					REF. NO.
					64 Bo 1 NWB
REACTION	RESULT	EXCITATION ENERGY	SOURCE		ANGLE
			TYPE	RANGE	
G.G	LFT	1-3	C	1 - 3	100
		(0.5 - 3.0)		(0.5 - 3.0)	

ABI

TABLE I
 Cases of observed resonance fluorescence

Nucleus multipol.	State (MeV)	Spin	Γ_0/Γ	$T(gw\Gamma_0^2/\Gamma^2)^{-1}$ (sec).	Mean lifetime T BCW (sec)	Mean lifetime T other (sec)	Ref.	Γ_0/Γ_w BCW
Cu ⁶³	0.00	$\frac{1}{2}^-$						
M1	0.67	$\frac{1}{2}^-$	1	$86 \pm 30 \times 10^{-14}$	$43 \pm 15 \times 10^{-14}$	$31 \pm 3 \times 10^{-14}$	20)	0.25

REF. S. Costa, F. Ferrero, S. Ferroni and R. Malvano Proc. Paris Conference 1034 (1964)				ELEM. SYM.		A	Z
				Cu		63	29
METHOD 100 MeV synchrotron				REF. NO. 64 Co 3		JDM	
REACTION	RESULT	EXCITATION ENERGY	SOURCE		DETECTOR		ANGLE
			TYPE	RANGE	TYPE	RANGE	
G,N	AB I	THR-80	C	10-80	BF3-I		4PI

TABLE

ELEMENT	Yield (36 MeV) $\left(\frac{n. cm^2}{mol. MeV} \times 10^5\right)$	Σ_0^{30}	Σ_0^{80}	$\Sigma_0^{30}/\Sigma_0^{80}$	σ_{-1} (mb)
²⁴ Cr	83	1.21	2.1	0.58	62
²⁵ Mn	108	1.52	2.33	0.65	76
²⁶ Fe	68	0.88	1.46	0.60	50
²⁷ Co	89	1.08	1.82	0.59	64
²⁸ Ni	44	0.55	1.07	0.51	34
²⁹ Cu	95	1.06	1.99	0.53	72
³⁰ Zn	88	0.94	1.68	0.56	66
³¹ Ga	130	1.29	2.18	0.59	94
³² Ge	139	1.35	2.29	0.59	101
³³ As	137	1.22	2.18	0.56	100

$\sum_a^b = \frac{A}{60 NZ} \int_a^b \sigma(E) dE$ is the integrated cross section measured in units of
 the classical dipole $60 NZ/A$ mb. MeV.

METHOD

Positron Annihilation; ion chamber

[Page 1 of 2]

REF. NO.

64 Fu 1

NVB

REACTION	RESULT	EXCITATION ENERGY	SOURCE		DETECTOR		ANGLE
			TYPE	RANGE	TYPE	RANGE	
G,N 18+	ABX	10 - 28	D	10-28	BF3-I		4PI
G,2N 19	ABX	19 - 28	D	10-28	BF3-I		4PI

Sample enriched to 99.35% Cu⁶³.

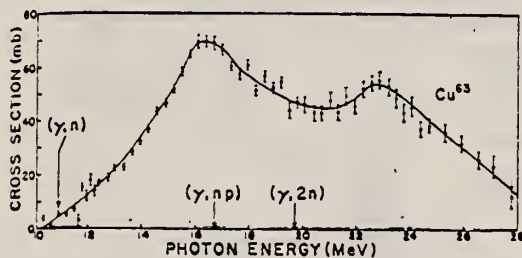


Fig. 3. Total cross section [$\sigma(\gamma,n) + 2\sigma(\gamma,2n) + \sigma(\gamma,np)$] for Cu⁶³ obtained from single-neutron counting data.

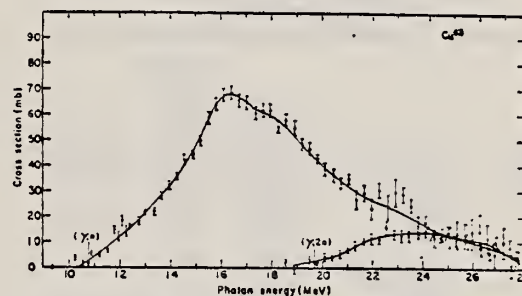


FIG. 4. Partial cross sections measured for Cu⁶³. The top curve consists of $\sigma(\gamma,n) + \sigma(\gamma,np)$ plus contributions from direct interactions and was obtained from single-neutron counting data. The lower curve consists of $\sigma(\gamma,2n)$ and was obtained from double-neutron counting data.

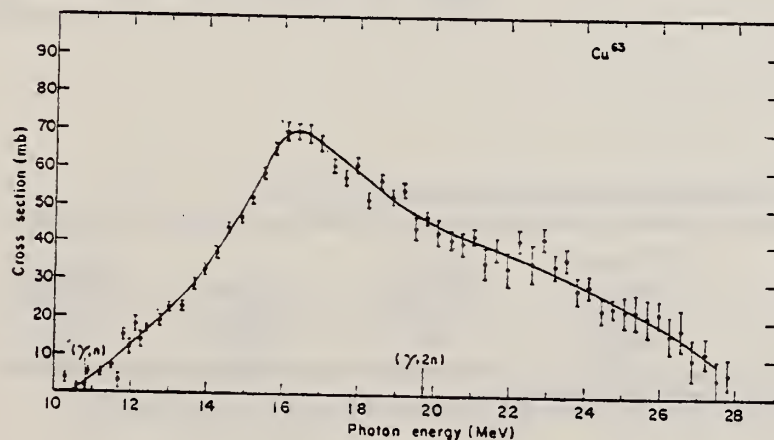


FIG. 5. The formation cross section of Cu⁶³, $\sigma(\gamma,n) + \sigma(\gamma,np) + \sigma(\gamma,2n) + \sigma_{\text{direct}}$. Contributions from $\sigma(\gamma,p)$ are not included here.

Cu

63

29

METHOD

Positron Annihilation; ion chamber

[Page 2 of 2]

REF. NO.

64 Fu 1

NVB

REACTION	RESULT	EXCITATION ENERGY	SOURCE		DETECTOR		ANGLE
			TYPE	RANGE	TYPE	RANGE	

TABLE I. Integrated cross sections up to 28 MeV for copper isotopes.

Element	Reaction	Integrated cross section (MeV-mb)	Fraction of total integrated cross section	Total (MeV-mb)
Natural Cu	$(\gamma, n) + (\gamma, np)$	525 ± 52	0.67	787 ± 113
	$(\gamma, 2n)$	110 ± 11	0.14	
	$(\gamma, p)^a$	152 ± 50	0.19	
	—	—	—	
Cu ⁶³	$(\gamma, n) + (\gamma, np)$	523 ± 52	0.89	764 ± 9
	+ direct	—	—	
	$(\gamma, 2n)$	80 ± 8	0.11	
	$(\gamma, np)^a$	115 ± 20	0.15	
	$(\gamma, p)^a$	161 ± 48	0.21	
	(γ, n)	344 ± 34	0.45	
Cu ⁶⁵	direct ^b	64 ± 22	0.08	766 ± 103
	$(\gamma, n) + (\gamma, np)$	437 ± 43	0.57	
	$(\gamma, 2n)$	195 ± 19	0.25	
	$(\gamma, p)^c$	134 ± 40	0.18	

^a Calculated from evaporation theory.^b Estimated.^c See Ref. 20.

TABLE II. Cross section for Li gamma rays.

Natural Cu $\sigma(\gamma, n)$ (mb)	Cu ⁶³ $\sigma(\gamma, n)$ (mb)	Cu ⁶⁵ $\sigma(\gamma, n)$ (mb)	Reference
55 ± 12	120 ± 30	—	a
	52 ± 11	—	b
	48 ± 8	—	c
	80 ± 14	—	d
85 ± 15	60 ± 9	—	e
	38 ± 6	—	f
	64 ± 4	—	g
	59 ± 6	70 ± 7	h
64 ± 10	55 ± 6	66 ± 6	Present work ⁱ

TABLE III. Quadrupole moments and Lorentz line parameters.

Nuclear shape	Isotope	E_n (MeV)	σ_n (mb)	Γ_n (MeV)	E_n (MeV)	σ_n (mb)	Γ_n (MeV)	Q_n (b)
Prolate Spheroid	Cu ⁶³	16.00	48.5	3.5	19.0	44.5	7.5	1.1 ± 0.4
	Cu ⁶⁵	16.00	54.7	4.2	19.25	62.0	7.5	1.2 ± 0.4
Oblate Spheroid	Cu ⁶³	16.50	62.5	5.0	21.25	22.0	7.1	-1.4 ± 0.4
	Cu ⁶⁵	16.75	37.5	5.0	20.5	36.4	6.0	-1.1 ± 0.4

TABLE IV. Integrated nuclear formation cross sections and σ_{-2} values.

Isotope	$\int_0^{28} \sigma dE$ (MeV-mb) ^a	$\int_0^{28} \sigma dE + W$ (MeV-mb) ^b	$0.06VZ/4$ (MeV-mb)	σ_{-2} (mb/MeV)	$0.00225 A^{5/3}$ (mb/MeV)
Cu ⁶³	764 ± 109	913 ± 121	939	2.1 ± 0.3	2.4
Cu ⁶⁵	766 ± 103	960 ± 124	964	2.6 ± 0.3	2.4

^a The integrated cross sections include estimated contributions from (γ, p) reactions.^b The correction "W" is the sum of the high- and low-energy wing corrections to the area under the resonance curves for the oblate case.

REF.

M. Masuda, M. Kondo, S. Takeda, M. Okumura, and J. Ookuma
 J. Phys. Soc. Japan 19, 2339 (1964)

ELEM. SYM.	A	Z
Cu	63	29

METHOD

REF. NO.

64 Ma 2

EGF

REACTION	RESULT	EXCITATION ENERGY	SOURCE		DETECTOR		ANGLE
			TYPE	RANGE	TYPE	RANGE	
G, XP	SPC	THR - 17	C	17	SCD-D	3 - 9	

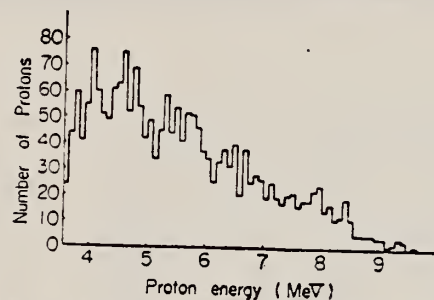


Fig. 3. Energy spectrum of emitted protons from copper foil irradiated by 17 MeV bremsstrahlung.

REF. I.A. Grishaev, D.I. Sikora, V.A. Shkoda-Ul'yanov, B.I. Shramenko
Atomnaya Energiya 18, 28 (1965)
Soviet Atomic Energy 18, 29 (1965)

ELEM. SYM.	A	Z
Cu	63	29
REF. NO.		EGF
65 Gr 1		

METHOD

REACTION	RESULT	EXCITATION ENERGY	SOURCE		DETECTOR		ANGLE
			TYPE	RANGE	TYPE	RANGE	
G,N	ABX	THR-44	C	10-66	ACT-I		4PI

Measure yields from electrons bombarding thick targets. Cross section derived from shower theory.

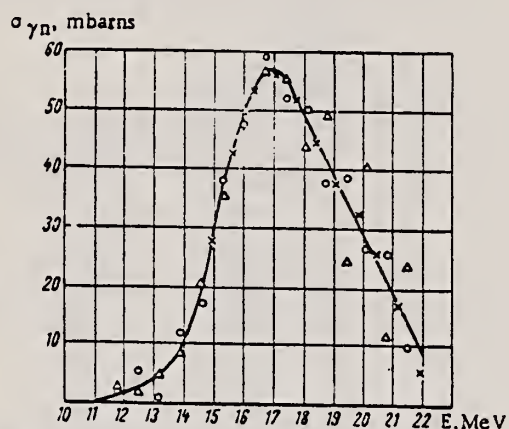


Fig. 8. Excitation function of the (γ, n) reaction in Cu^{63} , calculated by means of the Belen'kii-Tamm equilibrium photon spectrum and the experimental yields of the present study: x) Method using first and second derivatives [1, 15]; O) abbreviated photon difference method for thick specimens, proposed by D. I. Sikora; Δ) photon-difference method for thick specimens.

REF.

D. F. Herring, I. C. Nascimento, R. B. Walton, and R. E. Sund
 Phys. Rev. 139, B562 (1965)

ELEM. SYM.	A	Z
Cu	63	29
REF. NO.		
65 He 1		EGF

METHOD

REACTION	RESULT	EXCITATION ENERGY	SOURCE		DETECTOR		ANGLE
			TYPE	RANGE	TYPE	RANGE	
E,N	RLY	THR-32	D	14-32	ACT-I		4PI
E+,N	RLY	THR-32	D	14-32	ACT-I		4PI

Ratio of positron to electron induced activity determined.

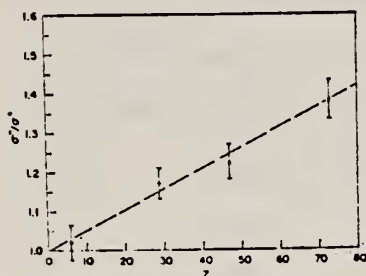


FIG. 4. The ratio σ^-/σ^+ as a function of atomic number at 27-MeV (total) bombarding energy. The straight line is for comparison purposes.

REF.

K. Abe, N. Kawamura, H. Nihei, H. Tsubota and N. Mutsuro
J. Phys. Soc. Japan 25, 1723 (1968)

ELEM. SYM.

A

Z

Cu

63

29

METHOD

REF. NO.

68 Ab 2

egf

REACTION	RESULT	EXCITATION ENERGY	SOURCE		DETECTOR		ANGLE
			TYPE	RANGE	TYPE	RANGE	
G, XP	SPC	THR-27	C	27	SCD-D	2-16	90
		(26.6)					

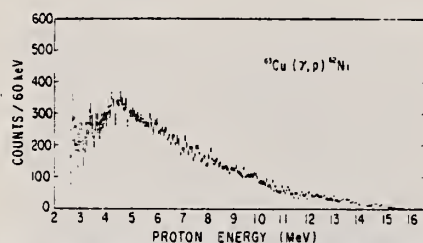


Fig. 1. Energy spectrum of photoprotons from ^{63}Cu at 90° , with bremsstrahlung end-point energy 26.6 MeV.

REF. W. J. Alston III, H. H. Wilson and E. C. Booth
Nucl. Phys. A116, 281 (1968)

ELEM. SYM.	A	Z
Cu	63	29

METHOD

REF. NO.	
68 Al 1	egf

REACTION	RESULT	EXCITATION ENERGY	SOURCE		DETECTOR		ANGLE
			TYPE	RANGE	TYPE	RANGE	
G, G	LFT	0 - 2	C	4	SCD-D	0-3	130
		(1.55)					

Angle greater than 90° for all measurements.

SELF-ABSORPTION

TABLE 1
Direct and absorption measurements of resonance fluorescence

Nucleus	E_r (MeV)	J_r	Γ_a/Γ	$gW\Gamma_a\Gamma_0/\Gamma$ (meV)	Error (%)	This work Γ_0 (meV)	Other work Γ_0
⁵⁵ Mn	0.000	$\frac{1}{2}^-$					
	1.527	$(\frac{1}{2}^-)$	0.9	5.2	25	8-12	
				abs ^{a)}	40	8.0	
	1.884	?	0.82 ^{b)}	41	25	50/gW	
				abs ^{a)}	10	55/g	
	2.197	?	(0.8) ^{c)}	17	25	21/gW	
				abs	20	17/g	
	2.252	?	(0.9) ^{c)}	17	25	19/gW	
				abs	20	13/g	
	2.365	?	?	3.5	36	(2-6) Γ/Γ_0	
⁵⁹ Co	2.564	?	(1.0)	50	25	50/gW	
				abs ^{a)}	20	61/g	
	2.751	?	?	6.7	42	6.7(Γ/Γ_0)/gW	
	0.000	$\frac{7}{2}^-$					
	1.187	$(\frac{7}{2}^-)$	(1.0)	6.8	25	7.5	0.33(E2) ^{d)}
				abs	25 ^{a)}	12	
		$(\frac{3}{2}^-)$	(1.0)	6.8	25	(5.4-6.5)	0.27(E2)
				abs	25 ^{a)}	9.6	
	⁶³ Cu	$\frac{3}{2}^-$?	1.6	30	(1.1-1.7) Γ/Γ_0	
	1.414	$\frac{3}{2}^-$?	1.7	37	(1.7-2.5) Γ/Γ_0	0.1(E2) ^{e)}
⁶⁷ Ga	0.000	$\frac{3}{2}^-$					
	0.872	$(\frac{1}{2}^-)$	0.95	1.1	35	0.8/W	
	1.107	$(\frac{1}{2}^-)$	0.95	8.0	20	8.4/W	
⁷⁵ As	0.000	$\frac{3}{2}^-$					
	0.86	?	?	1.7	20	1.7 $\Gamma/gW\Gamma_0$	
	1.07	?	?	2.6	30	2.6 $\Gamma/gW\Gamma_0$	
⁸⁷ Y	1.35	?	?	3.6	20	3.6 $\Gamma/gW\Gamma_0$	
	0.000	$\frac{1}{2}^-$					
	1.51	$\frac{1}{2}^-$	(1.0)	52 ^{a)}	30	28	0.37(E2) ^{f)}
				abs ^{a)}	15	22	

^{a)} Measured with NaI.

^{b)} Ref. ¹⁴⁾.

^{c)} Measured with a Ge(Li) detector to $\pm 10\%$.

^{d)} Ref. ¹³⁾. ^{e)} Ref. ¹⁴⁾. ^{f)} Ref. ¹⁵⁾.

¹³ D.G. Alkhazov, K.I. Erokhina and I.K. Lemberg, Izv.Akad.Nauk.SSSR (ser.fiz.) 28 (1964) 1667.

²³ G.A. Peterson and J. Alster, Phys. Rev. 166 (1968) 136.

²⁴ N. Nath, M.A. Rothman, D.M. Van Patter and C.E. Mandeville, Nucl. Phys. 13 (1959) 74.

[over]

TABLE 3
Information on the 1.414, 1.551 and 1.862 MeV states in ⁶³Cu

Energy (MeV)	J, π ^{a)}	Experimental $B(E2 \downarrow)$ (e ² fm ⁴)	$\Gamma_0(E2)$		$\Gamma_0(M1 + E2)$ present work (meV)
			expt.	calc.	
			(meV)		
1.414	$\frac{3}{2}^-$	< 4 ^{b)}	< 0.019	0.20 ^{c)}	1.1(Γ/Γ_0) ^{d)}
1.551	$\frac{3}{2}^-$	13 ± 6 ^{e)}	0.10 ± 0.05		(1.7-2.5)(Γ/Γ_0)
1.862	$\frac{7}{2}^-$	< 8 ^{b)}	< 0.016		< 0.7(Γ/Γ_0)

^{a)} Ref. ¹⁴⁾.

^{b)} Ref. ¹⁷⁾; the upper limits quoted here were not published later by Gove.

^{c)} Based upon the value $B(E2 \downarrow)(1.17)$ for ⁶³Ni of 1.7×10^{-28} e²cm⁴; see ref. ¹⁸⁾.

^{d)} A pure M1 transition is assumed; see discussion in text.

^{e)} Ref. ¹⁴⁾.

¹⁴⁾ B.G. Harvey, J.R. Meriwether and A. Bussiere, Nucl. Phys. 70 (1965) 305.

¹⁷⁾ H.E. Gove, Nucl. Instr. 28 (1964) 180.

¹⁸⁾ Nuclear Data A1 (1966) no. 1; B1 (1966) no. 6.

²⁵⁾ D. Bachner et al., Nucl. Phys. A99 (1967) 487.

REF. Y. Oka, T. Kato, K. Nomura, T. Saito and H. T. Tsai
Bull. Chem. Soc. Japan 41, 2660 (1968)

ELEM. SYM.	A	Z
Cu	63	29
REF. NO.		egf
68 Ok 1		

REACTION	RESULT	EXCITATION ENERGY	SOURCE		DETECTOR		ANGLE
			TYPE	RANGE	TYPE	RANGE	
G, A	ABY	THR-20	C	20	ACT-I		4PI

TABLE 1. SUMMARY OF DATA ON (γ, α) REACTIONS WITH 20 MeV BREMSSTRAHLUNG

Nuclide		E_{th} (-Q, MeV)	Observed gamma-ray			Results obtained	
Parent (Natural abundance, %)	Product (Half-life)		Energy (MeV)	Branching ratio (%)	Type of multipole transition	$\mu\text{Ci/mg}^a$	Yield ($\text{mol}^{-1}\cdot\text{R}^{-1}$)
^{51}V (99.75)	^{47}Sc (3.4 d)	10.27	0.160	100	$M1 + E2$	1.99×10^{-3}	2.8×10^3
^{63}Cu (30.9)	^{61}Co (99 min)	6.75	0.068	99	$M1 + E2$	7.23×10^{-3}	9.7×10^3
^{71}Ga (39.6)	^{67}Cu (61 hr)	5.15	0.184	41	$M1$	2.70×10^{-3}	9.6×10^3
^{73}Ge (7.67)	^{69}Zn (14 hr)	5.89	0.435	100	$M4$	1.11×10^{-3}	5.0×10^3
^{81}Br (49.48)	^{77}As (39 hr)	6.46	0.246	2.81	$M1 + E2$	1.97×10^{-4}	4.3×10^2
^{109}Ag (48.65)	^{105}Rh (36 hr)	3.28	$0.319 + 0.306$	24.8	$M1 + E2$	8.29×10^{-4}	3.7×10^1
^{115}In (95.77)	^{111}Ag (7.6 d)	3.78	0.340	6	$M1 + E2$	5.70×10^{-5}	4.3×10^1

a) The value corrected at the end of 1 hr irradiation ($9.4 \times 10^9 \text{ R/min}$).

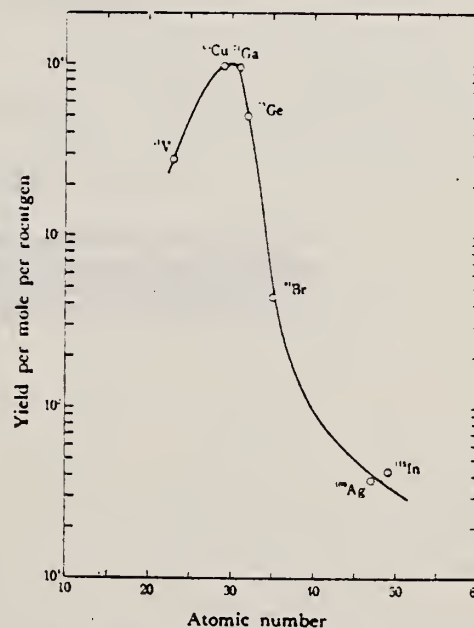


Fig. 1. The yield curve for (γ, α) reaction with 20 MeV bremsstrahlung.

REF. D. G. Owen, E. G. Muirhead and B. M. Spicer
Nucl. Phys. A122, 177 (1968)

ELEM. SYM.	A	Z
Cu	63	29

METHOD

REF. NO.	
68 Ow 1	egf

REACTION	RESULT	EXCITATION ENERGY	SOURCE		DETECTOR		ANGLE
			TYPE	RANGE	TYPE	RANGE	
G,N	RLX	12-24	C	10-24	ACT-I		4PI

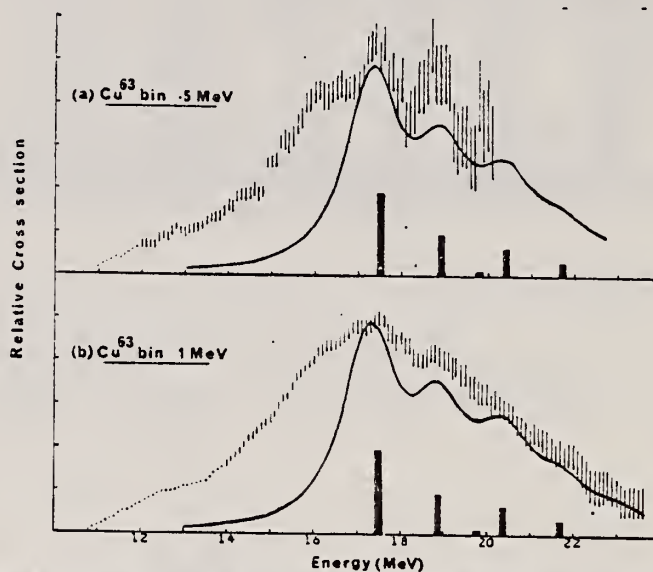


Fig. 2. The $^{63}\text{Cu}(\gamma, n)^{62}\text{Cu}$ cross section analysed in (a) 0.5 and (b) 1 MeV bins. The errors shown represent the total experimental uncertainty for each point. The continuous curve is the shape of the ^{62}Ni photo-absorption cross section predicted by Huber ⁴⁾ using the parameters in table 1 displaced by 1.5 MeV to a lower energy. The vertical bars represent the relative strengths of the individual shifted theoretical levels.

REF. J. C. Ritter, R. E. Larson and J. I. Hoover
Nucl. Phys. A110, 463 (1968)

ELEM. SYM.	A	Z
Cu	63	29

METHOD

REF. NO.	
68 Ri 3	egf

REACTION	RESULT	EXCITATION ENERGY	SOURCE		DETECTOR		ANGLE
			TYPE	RANGE	TYPE	RANGE	
G,AN	RLY	THR-50	C	30-50	ACT-I		4PI
G,A2N	RLY	THR-50	C	30-50	ACT-I		4PI

RLY G,2N

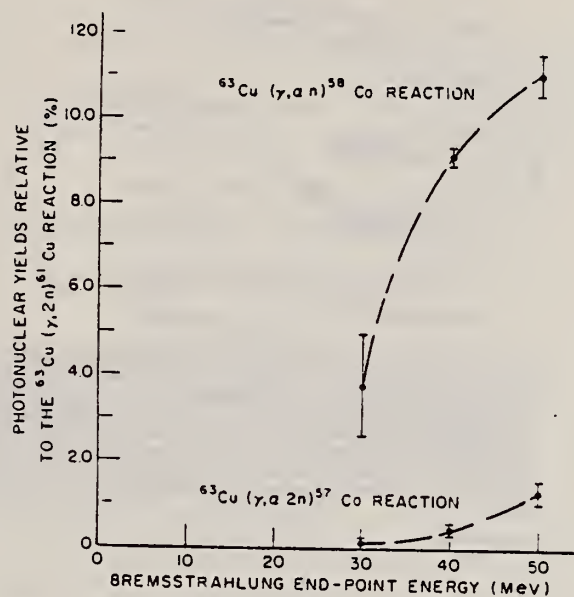


Fig. 1. Yields of the $(\gamma, \alpha n)$ and $(\gamma, \alpha 2n)$ reactions relative to the $(\gamma, 2n)$ reaction on ^{63}Cu .

ELEM. SYM.	A	Z
Cu	63	29
REF. NO.		
68 Su 1		HMG

METHOD			REF. NO.			
			68 Su 1			HMG
REACTION	RESULT	EXCITATION ENERGY	SOURCE		DETECTOR	
			TYPE	RANGE	TYPE	RANGE
G,N 420	ABX	THR-25	D	10-25	ACT-I	
G,2N 421+	ABX	THR-26	D	10-26	ACT-I	
		(25.7)				

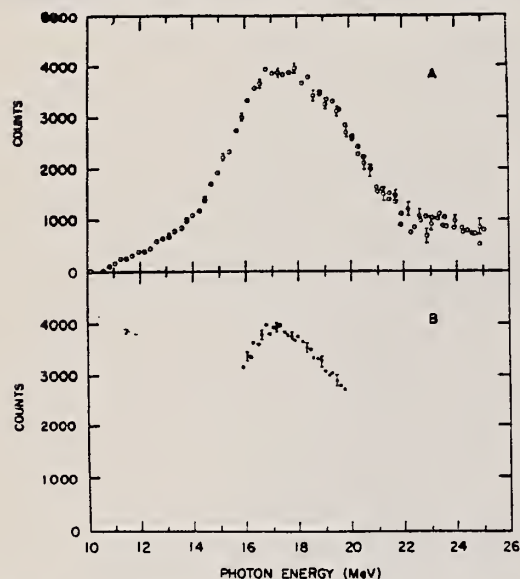


FIG. 8. (A) The $^{63}\text{Cu}(\gamma, n)$ yield versus annihilation γ -ray energy for 2% γ -ray resolution. This yield is the difference between the positron and electron data shown in Fig. 7. (B) The $^{63}\text{Cu}(\gamma, n)$ yield versus annihilation γ -ray energy for 1.5% γ -ray resolution. These data were approximately normalized to the data in Fig. 8(A).

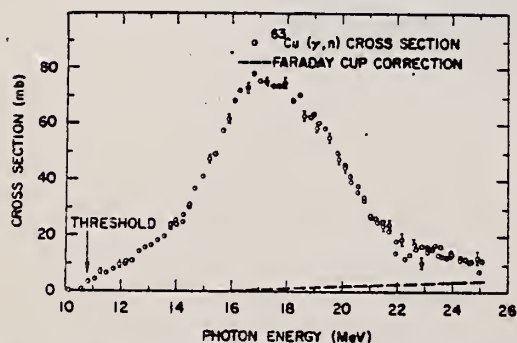


FIG. 9. The $^{63}\text{Cu}(\gamma, n)$ cross section versus photon energy for 2% γ -ray resolution. The data shown were corrected for the emission of secondary electrons from the Faraday cup, and the magnitude of this correction is also shown. See text for discussion of errors.

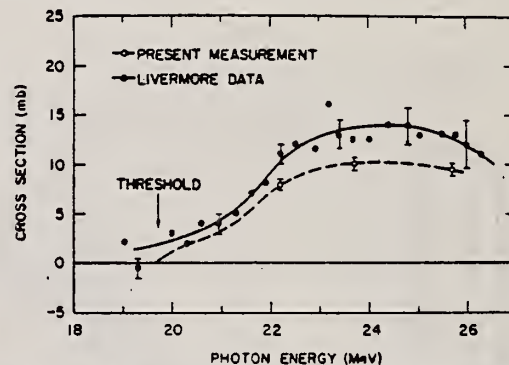


FIG. 12. The $^{63}\text{Cu}(\gamma, 2n)$ cross section from the present measurement and from the measurement by Fultz *et al.* at Livermore (Ref. 5). The latter data were shifted upward in energy by 2.7% as explained in the caption of Fig. 11. The error bars include only the statistical uncertainties in the yield measurements. See text for a discussion of the errors. The dashed curve through the present data was used in the integration and is drawn on the basis of the data points, the threshold energy, and the shape of the Livermore data.

TABLE I. $^{63}\text{Cu}(\gamma, 2n)$ cross sections. See text for a discussion of errors.

γ -ray energy (MeV)	Cross section (mb)
22.2	8.0 ± 0.5
23.7	10.0 ± 0.5
25.7	9.3 ± 0.5

TABLE II. Integrated photoreaction cross sections of ^{63}Cu up to 25 MeV.

Experiment	Reaction	Integrated cross section (MeV mb)	Total (MeV mb)
Present	(γ, n)	490 ± 40	586 ± 67
	$(\gamma, 2n)$	36 ± 12^a	
	(γ, pn)	60 ± 15^b	
Fultz <i>et al.</i>	$(\gamma, n) + (\gamma, pn)$	515 ± 52^c	563 ± 57
	$(\gamma, 2n)$	48 ± 5^d	

^a Based on the dashed curve in Fig. 12.

^b Derived from (γ, n) data of present work and $[(\gamma, n) + (\gamma, pn)]$ data of Fultz *et al.* (Ref. 5).

^c Energy scale of these data (Ref. 5) shifted by the factor 1.027. Without the shift the result is 511 ± 51 .

^d Energy scale of these data (Ref. 5) shifted by the factor 1.027. Without the shift the result is 56 ± 6 .

REF.

G. K. Tandon and J. A. McIntyre
Nucl. Instr. and Meth. 59, 131 (1968)

ELEM. SYM.	A	Z
Cu	63	29

METHOD

REF. NO.

68 Ta 2

egf

REACTION	RESULT	EXCITATION ENERGY	SOURCE		DETECTOR		ANGLE
			TYPE	RANGE	TYPE	RANGE	
G, G	LFT	.1	D	1	NAI-D	1	90
		(963 keV)		(963 keV)			

COMPTON SCTD SOURCE

TABLE I
Lifetime measurements.

Line	Mean life (10^{-14} sec)	Investigator
963-keV level in ^{63}Cu		
1	91 ± 6	Avg. of ref. 18-20)
2	110 ± 16	This measurement
963-keV level in ^{152}Sm		
3	4.3 ± 0.3	Avg. of ref. 23,24)
4	7.1 ± 2.1	This measurement
Ratio $\tau(\text{Cu})/\tau(\text{Sm})$		
5	21 ± 2	From 1 and 3
6	16 ± 5	This measurement

¹⁸⁾ J. B. Cumming, A. Schwarzschild, A. W. Sunyar and N. Porile, Phys. Rev. **120** (1960) 2128.

¹⁹⁾ T. Rothem, F. R. Metzger and C. P. Swann, Nucl. Physics **22** (1961) 505.

²⁰⁾ M. A. Eswaran, H. E. Gove, A. E. Litherland and C. Brown, Phys. Letters **8** (1964) 52.

²¹⁾ I. Marklund, Nucl. Physics **9** (1958) 83.

²²⁾ L. Grodzins, Phys. Rev. **109** (1958) 1014.

²³⁾ G. G. Shute and B. S. Sood, Proc. Roy. Soc. (London) **A25** (1960) 52.

²⁴⁾ F. R. Metzger, Phys. Rev. **137** (1965) B1415.

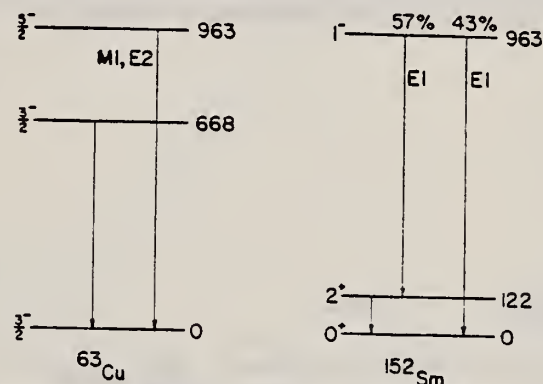


Fig. 11. Level schemes of ^{63}Cu and ^{152}Sm below 1000 keV. All energies are in keV.

Cu	63	29
REF. NO.		69 An 6
		egf

METHOD					REF. NO.	
					69 An 6	egf
REACTION	RESULT	EXCITATION ENERGY	SOURCE		DETECTOR	
			TYPE	RANGE	TYPE	RANGE
G,P	ABY	103-999	C	700,999	TEL-D	97-230
G,D	ABY	112-999	C	700,999	TEL-D	97-205

999 = 1.2 GEV

Summary

The cross-sections of the (γ, p) (γ, d) reactions were investigated. Li^7 , Be^9 , C^{12} , Si^{28} , Cu^{63} , Mo^{98} and Ta^{181} targets were irradiated with the bremsstrahlung of 700 and 1200 MeV maximum energy from the Kharkov PhTI Ac. Sci. UkrSSR linear accelerator. The photo-protons and deuterons were detected by the scintillation telescope at 30° , 60° , and 120° with the beam. Possible mechanisms of the proton and deuteron photoproduction are discussed. The qualitative agreement of A dependence of the cross-sections is observed with a suggestion on the meson mechanism for these reactions.

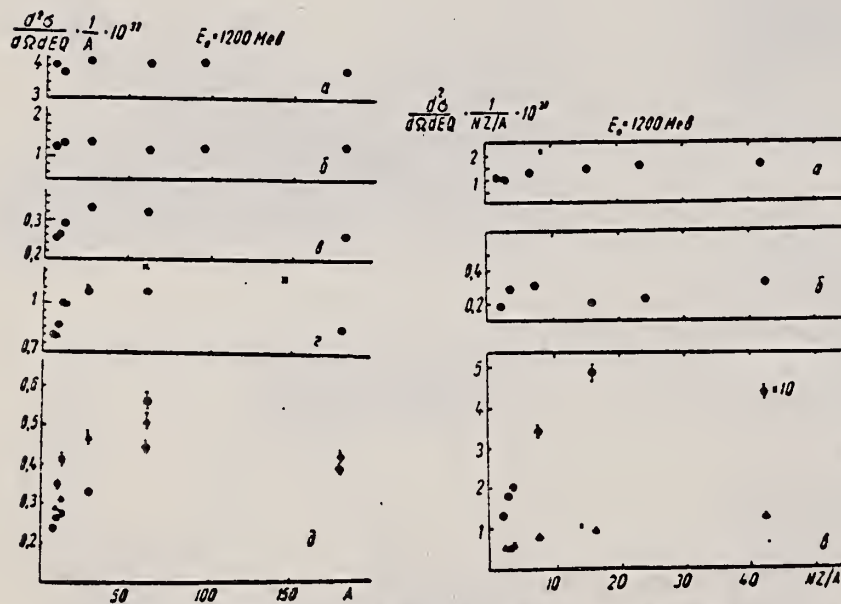


Рис. 1. Залежність перерізу (γ, p) -реакції від A : а — $\phi = 30^\circ$, $E_\gamma = 97$ Мев; б — $E_\gamma = 205$ Мев; в — $\phi = 60^\circ$, $E_\gamma = 230$ Мев; г — $E_\gamma = 157$ Мев (\times — дані [3]); д — $\phi = 120^\circ$, \bigcirc — $E_\gamma = 120$ Мев, Δ — $E_\gamma = 157$ Мев, \blacksquare — $E_\gamma = 230$ Мев. Абсолютне значення перерізу наведено при енергії протонів $E_p = 120$ Мев. Інші дані нормовані до перерізу для Li^7 при $E_p = 120$ Мев.

Рис. 2. Залежність перерізу (γ, d) -реакції від NZ/A : а — $\phi = 30^\circ$, $E_d = 97$ Мев; б — $\phi = 30^\circ$, $E_d = 205$ Мев; в: Δ — $\phi = 60^\circ$, $E_d = 97$ Мев, \bigcirc — $\phi = 120^\circ$, $E_d = 97$ Мев (перерізи наведені в одиницях 10^{-32} см²/стер. Мев \cdot Q).

METHOD					REF. NO.	
					69 Be 7	hmg
REACTION	RESULT	EXCITATION ENERGY	SOURCE		DETECTOR	
			TYPE	RANGE	TYPE	RANGE
G,G	LFT	6,8	D	6,8	D	
						(90,135)

Self-Absorption.

6.07, 8.50 MEV

Results of determination of the resonance-level parameters

Source-scatterer	E_{γ} , MeV	$\langle\sigma_{pp}\rangle$, mb	$\Gamma_{\gamma 0}$, eV	D , keV	Reference
Pb \rightarrow Zn ⁶⁴	7.38	33 \pm 4.5	0.58 \pm 0.12	53.70 \pm 0.13	This work
Ti \rightarrow Mo ⁹⁶	6.413	11.2 \pm 1.4	0.11 \pm 0.02	8.68 \pm 1.57	"
Ti \rightarrow La ¹³⁹	6.413	16.04 \pm 2.10	0.23 \pm 0.05	8.03 \pm 1.42	"
Ti \rightarrow Bi ²⁰⁹	7.15	1200 \pm 230	0.32 \pm 0.07	1.84 \pm 0.40	"
	6.996	1550	-	-	[1]
	7.15	2600 \pm 800	0.42 \pm 0.14	-	[5]
Ti \rightarrow Cu ⁶⁵	6.07	423 \pm 103	0.34 \pm 0.06	99.1 \pm 17.4	This work
	6.07	440 \pm 130	0.36 \pm 0.07	-	[5]
Ti \rightarrow Cu ⁶³	6.07	215 \pm 71	0.13 \pm 0.04	57.14 \pm 12.70	This work
	6.07	200 \pm 50	0.16 \pm 0.03	-	[6]
	8.50	22 \pm 7	0.26 \pm 0.08	130 \pm 40	This work
Cr \rightarrow Cu ⁶³	8.499	35	75	-	[1]
	8.50	19 \pm 6	0.23 \pm 0.09	-	[5]
	8.50	36 \pm 9	0.47 \pm 0.10	21.36 \pm 4.54	This work
Cr \rightarrow Cu ⁶⁵	8.499	80	10.5	-	[1]
	8.50	42 \pm 13	0.94 \pm 0.29	-	[6]
Cu \rightarrow Sn ¹¹⁷	7.01	1150 \pm 240	0.15 \pm 0.04	0.44 \pm 0.12	This work
	7.01	1000	-	-	[1]
	7.01	1200 \pm 400	0.3 \pm 0.3	-	[5]
Hg \rightarrow Mo ⁹⁶	6.44	201 \pm 37	0.12 \pm 0.04	0.23 \pm 3.07	This work

METHOD

REF. NO.

72 Dr 2

egf

REACTION	RESULT	EXCITATION ENERGY	SOURCE		DETECTOR		ANGLE
			TYPE	RANGE	TYPE	RANGE	
G,N	ABX	11-26	C	11-26	ACT-I		4PI

446

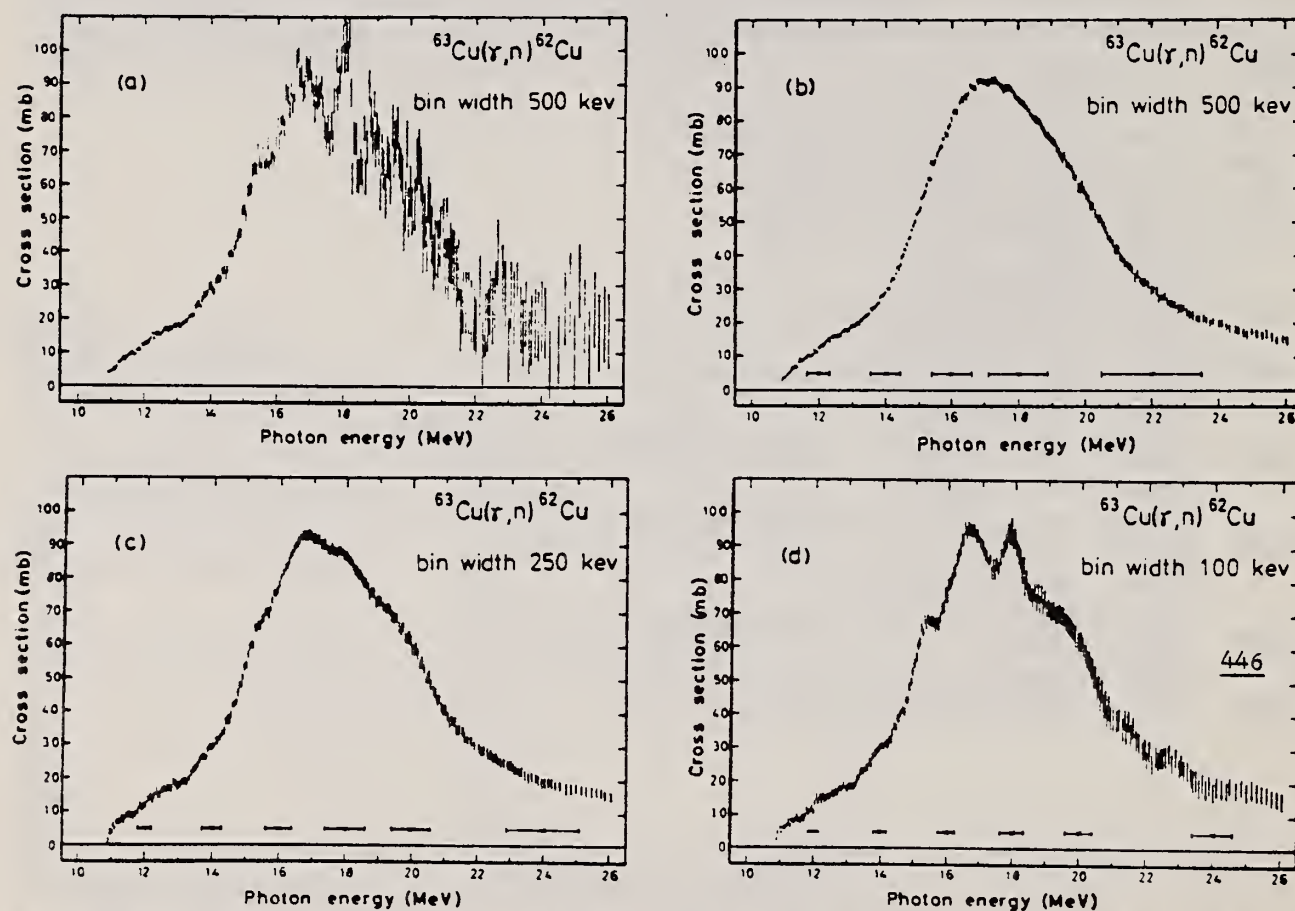


Fig. 2. Cross section for $^{63}\text{Cu}(\gamma, n)^{62}\text{Cu}$ from threshold energy to 26 MeV. (a) shows the cross-section curve obtained with an analysis bin width of 0.5 MeV using the LP method. (b), (c) and (d) show the same cross section calculated from yield data with the analysis bin widths of 500 keV, 250 keV and 100 keV using the CLS method. The horizontal bars represent the FWHM of experimental resolution and not the uncertainty in energy.

REF. A.A.C. Klaasse, P.F.A. Goudsmit, P.K.A. de Witt Huberts
PICNS-72, 425 (1972) Sendai

ELEM. SYM.	A	Z
Cu	63	29

METHOD

REF. NO.

72 K1 7

hvm

REACTION	RESULT	EXCITATION ENERGY	SOURCE		DETECTOR		ANGLE
			TYPE	RANGE	TYPE	RANGE	
E,E/	FMF	1	D	25- 85	MAG-D		DST

1=0.96 MEV

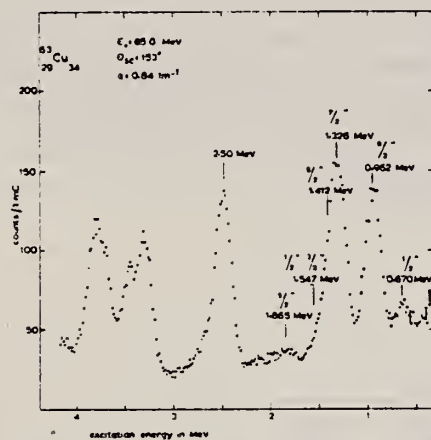


Fig. 12. Spectrum of electrons inelastically scattered by ^{63}Cu .

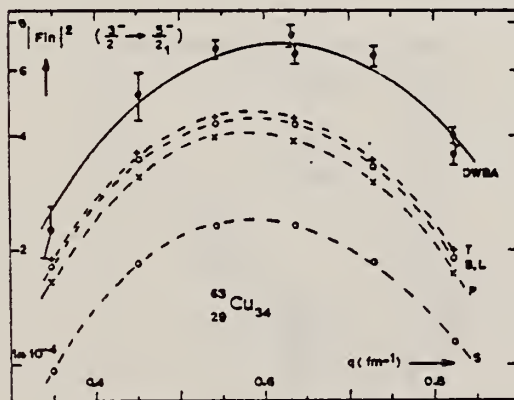


Fig. 13. Experimental and theoretical form factors of the 0.96 MeV excitation in ^{63}Cu .

REF.

G. Kuhl and U. Kneissl
Nucl. Phys. A195, 559 (1972)

ELEM. SYM.	A	Z
Cu	63	29

METHOD

REF. NO.

72 Ku 6

egf

REACTION	RESULT	EXCITATION ENERGY	SOURCE		DETECTOR		ANGLE
			TYPE	RANGE	TYPE	RANGE	
E,N	ABX	11-30	D	20-30	ACT-I		4PI

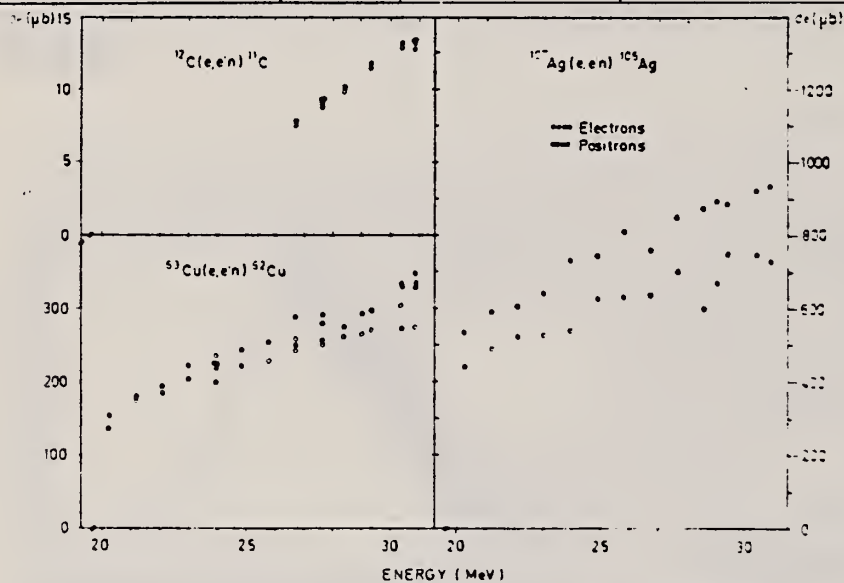
E+/E- YIELD RATIO

Fig. 3. Absolute cross sections of the three reactions investigated. The error of the absolute scale is estimated to be $\pm 8\%$.

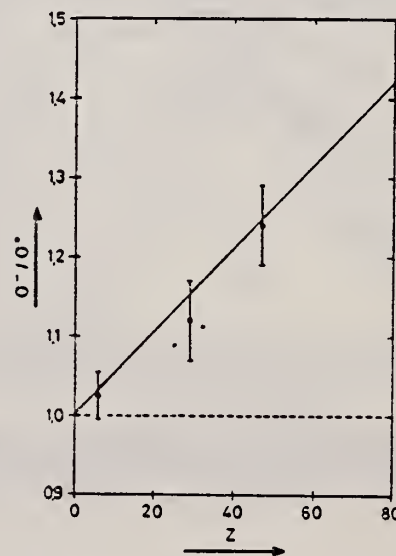


Fig. 4. The measured ratios of σ^-/σ^+ at an energy of 27 MeV compared with the straight line given by Herring *et al.* ⁶.

REF.

J.F. Wimpey, G.E. Mitchell, and E.G. Bilpuch
Nucl. Phys. A233, 9 (1974)

ELEM. SYM.

A

Z

Cu

63

29

METHOD

REF. NO.

74 Wi 8

egf

REACTION	RESULT	EXCITATION ENERGY	SOURCE		DETECTOR		ANGLE
			TYPE	RANGE	TYPE	RANGE	
P,G	LFT	9	D	2- 3	SCD-D		55
			(2.6123-2.6704)				

14 LEVELS 2.612-2.670 MEV

Abstract: The $^{62}\text{Ni}(p,p)$, $(p,p'\gamma)$ and (p,γ) reactions were studied in the vicinity of the $\frac{1}{2}^-$ fragmented analogue of the first-excited state of ^{63}Ni . The overall proton energy resolution was about 300 eV. The γ -rays were detected with both NaI(Tl) and Ge(Li) detectors. Elastic and inelastic proton widths and partial and total γ -ray widths were measured for each of the fourteen fine structure states of the analogue. Statistically significant correlations were observed between the elastic proton widths, the inelastic proton widths and the total γ -ray widths.

E

NUCLEAR REACTION $^{62}\text{Ni}(p,p)$, $(p,p'\gamma)$, (p,γ) ; $E = 2.3\text{--}2.7$ MeV, measured $\sigma(E)$, ^{63}Cu isobaric analogue resonance, J , π , Γ , Γ_p , $\Gamma_{p'}$, Γ_{γ} for fine structure resonances.

TABLE 3
Partial γ -ray widths for the $\frac{1}{2}^-$ analogue state in ^{63}Cu

E_p (MeV)	Γ_p^b (eV)	E_r (keV)	Γ_{γ}^c (meV)	M1 d (W.u.)	E2 d (W.u.)
2.6123	20	0	83.0	0.609E-02	0.142E-00
		670	15.3	0.143E-02	0.393E-01
		2011	30.4	0.491E-02	0.194E-00
2.6193	15	0	17.3	0.127E-02	0.295E-01
		670	13.9	0.130E-02	0.357E-01
		1411	6.9	0.859E-03	0.286E-01
2.6376	10	0	172.3	0.126E-01	0.291E-00
		962	13.4	0.138E-02	0.405E-01
2.6335	5	0	11.2	0.814E-03	0.189E-01
		962	15.0	0.155E-02	0.455E-01
2.6390	5	0	18.1	0.132E-02	0.306E-01
		962	17.1	0.183E-02	0.537E-01
		1547	26.2	0.343E-02	0.118E-00
		1863	20.1		0.113E-00
		2081	12.1		
2.6466 ^e	15	2092	31.7		
		0	156.4	0.114E-01	0.263E-00
		670	43.5	0.401E-02	0.109E-00
		1411	19.2	0.237E-02	0.782E-01
		2062	15.6		
		2081	26.1		

[over]

TABLE 3 (continued)

E_p (MeV)	Γ_p ^{b)} (eV)	E_r (keV)	Γ_γ ^{c)} (meV)	M1 ^{d)} (W.u.)	E2 ^{d)} (W.u.)
2.6508	10	0	8.6	0.622E-03	0.144E-01
		962	105.5	0.109E-01	0.317E-00
		1411	33.1	0.408E-02	0.134E-00
2.6536 ^{a)}	5	0	23.4	0.170E-02	0.392E-01
		670	14.3	0.132E-02	0.357E-01
		962	62.5	0.643E-02	0.188E-00
		1547	56.3	0.731E-02	0.250E-00
2.6584	10	0	12.4	0.895E-03	0.207E-01
		670	12.1	0.112E-02	0.303E-01
		962	31.8	0.326E-02	0.951E-01
		2011	16.9	0.267E-02	0.104E-00
		2062	19.8		
2.6617	40	0	132.1	0.954E-02	0.220E-00
		962	72.1	0.739E-02	0.215E-00
		1411	101.9	0.125E-01	0.410E-00
		1547	30.5	0.395E-02	0.135E-00
2.6631	125	0	97.1	0.702E-02	0.162E-00
		670	62.8	0.576E-02	0.156E-00
		962	120.0	0.123E-01	0.359E-00
		1411	42.2	0.517E-02	0.169E-00
		1547	53.8	0.697E-02	0.238E-00
2.6664	5	0	11.3	0.819E-03	0.189E-01
		670	10.6	0.973E-03	0.263E-01
		962	17.8	0.182E-02	0.531E-01
2.6675	20	0	13.3	0.961E-03	0.222E-01
		670	21.2	0.195E-02	0.528E-01
		962	51.3	0.525E-02	0.153E-00
2.6704	5	0	77.2	0.557E-02	0.123E-00
		670	9.3	0.848E-03	0.229E-01
		962	7.9	0.811E-03	0.236E-01
		1547	19.7	0.254E-02	0.864E-01

^{a)} Resonant energy for resonances which are very close to another resonance observed in the capture excitation function.

^{b)} The j -value assignment is tentative for resonances with elastic widths ≤ 10 eV.

^{c)} The estimated uncertainty in the γ -ray widths is 30 % for widths greater than 50 meV, 50 % for widths between 10 and 50 meV, and 100 % for widths less than 10 meV. The limit of observability for the γ -ray widths is about 5 meV.

^{d)} These strengths are calculated assuming that the transition is either pure M1 or E2. If the spin and parity of the final state is unknown, then no entry is shown.

REF. M. Boivin, Y. Cauchois, Y. Heno, C. Schloesing-Moller,
V. Zecevic
C.R. Acad. Sc. Paris 281B, 201 (1975)

ELEM. SYM.	A	Z
Cu	63	29
REF. NO.		
75 Bo 11		egf

METHOD

REACTION	RESULT	EXCITATION ENERGY	SOURCE		DETECTOR		ANGLE
			TYPE	RANGE	TYPE	RANGE	
G,G	LFT	670*962	C	2	UKN		UKN

*KEV

TABLEAU

Niveau....	⁶³ Cu 670	⁶³ Cu 771	⁶³ Cu 962	⁶³ Cu 1115	¹¹³ In 1133	⁵⁹ Co 1190
τ(ps).....	0,28 ± 8 %	0,15 ± 12,5 %	0,76 ± 15 %	0,38 ± 14 %	0,094 ± 4,5 %	0,074 ± 3 %

REF.

O.E. Kraft, Yu.V. Naumov, S.S. Parzhitskii, I.V. Sizov
 Izv. Akad. Nauk SSSR Ser. Fiz. 39, 1268 (1975)
 Bull. Acad. Sci. USSR Phys. Ser. 39, 150 (1975)

ELEM. SYM.	A	Z
Cu	63	29

METHOD

REF. NO.

75 Kr 14

hmg

REACTION	RESULT	EXCITATION ENERGY	SOURCE		DETECTOR		ANGLE
			TYPE	RANGE	TYPE	RANGE	
P,G	SPC	8- 9	D	2- 3	SCD-D		UKN

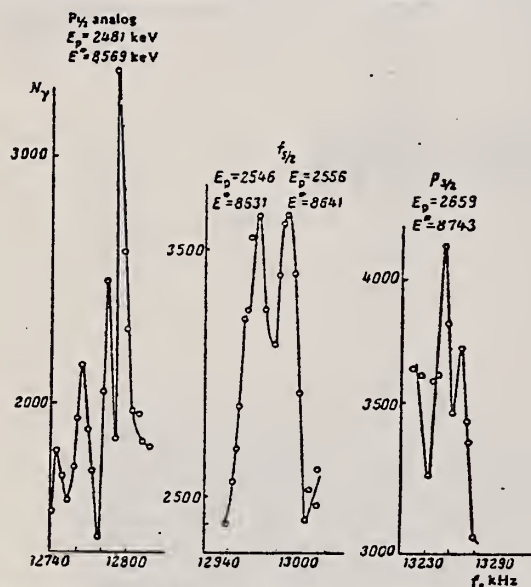


Fig. 1. Excitation function near the $p_{1/2}$, $f_{5/2}$, and $p_{3/2}$ analog states in ^{63}Cu .

Table 1

E_{ke}	I^{π}	$p_{1/2}$ analog		$f_{5/2}$ analog				$p_{3/2}$ analog	
		$E_{\text{p}} = 2481 \text{ keV}$	$E_{\text{res}} = 2481.1 \pm 1.5 \text{ keV}$	$E_{\text{p}} = 2546 \text{ keV}$	$E_{\text{res}} = 2551.7 \pm 2.0 \text{ keV}$	$E_{\text{p}} = 2556 \text{ keV}$	$E_{\text{res}} = 2559.6 \pm 1.5 \text{ keV}$	$E_{\text{p}} = 2659 \text{ keV}$	$E_{\text{res}} = 2659.7 \pm 1.5 \text{ keV}$
		$\Gamma_{\gamma} \cdot 10^4, \text{eV}$	$B(M1) \times 10^4, \text{eV}$	$\Gamma_{\gamma} \cdot 10^4, \text{eV}$	$B(M1) \times 10^4, \text{eV}$	$\Gamma_{\gamma} \cdot 10^4, \text{eV}$	$B(M1) \times 10^4, \text{eV}$	$\Gamma_{\gamma} \cdot 10^4, \text{eV}$	$B(M1) \times 10^4, \text{eV}$
0	$3/2^-$	22	3.0	1.8	0.24	4.6	0.61	6.0	0.77
868.3 ± 0.5	$1/2^-$	11	1.9	0.25	0.2	1.0	0.52	5.0	0.82
961.6 ± 0.5	$3/2^-$	2.6	0.2	2.0	0.38	2.8	0.56	7.9	1.45
1325.6 ± 0.5	$1/2^-$	—	—	1.1	0.24	1.4	0.31	1.1	0.2
1410.4 ± 0.5	$3/2^-$	5.5	0.2	1.1	0.25	2.9	0.66	4.6	1.0
1546.5 ± 0.5	$1/2^-$	17	4.3	2.3	0.55	2.6	0.63	1.8	0.41
1860.0 ± 1.0	$3/2^-, 1/2^-$	—	—	1.0	0.28	—	—	—	—
2012.2 ± 1.0	$1/2^- (1/2^-)$	3.7	1.1	1.4	0.41	0.8	0.24	1.6	0.45
2080.0 ± 1.0	$1/2^- (1/2^-)$	7.7	2.4	—	—	1.1	0.2	0.8	0.23
2080.0 ± 1.5	$1/2^- (1/2^-)$	—	—	—	—	1.1	0.33	1.3	0.38
2333.6 ± 1.5	$3/2^-, 1/2^- (1/2^-)$	—	—	—	—	0.87	0.30	1.6	0.52
2405 ± 3	$1/2^-$	1.9	0.69	—	—	—	—	—	—
2497.3 ± 1.5	$1/2^-$	10	3.9	—	—	1.5	0.56	0.4	0.13
2533.7 ± 2.0	$3/2^- (1/2^-)$	0.7	0.27	—	—	2.2	0.83	0.9	0.32
2677.9 ± 1.8	$1/2^-, 3/2^-, 1/2^-$	9.9	4.2	—	—	0.8	0.32	1.7	0.66
2697 ± 2	$1/2^-, 3/2^-, 1/2^-$	5.1	2.2	—	—	—	—	—	—
2778 ± 2	$1/2^-, 3/2^-, 1/2^-$	—	—	1.0	0.39	1.2	0.51	—	—
2831 ± 2.5	$1/2^-, 3/2^-, 1/2^-$	—	—	—	—	—	—	2.4	1.0
2860 ± 2	$1/2^-, 3/2^-, 1/2^-$	3.3	1.6	—	—	0.7	0.32	0.8	0.30
2886 ± 2	$1/2^-, 3/2^-, 1/2^-$	3.3	1.6	—	—	—	—	1.1	0.49
2956 ± 1	—	2.6	1.3	—	—	—	—	0.9	0.40
2978.6 ± 1.6	$1/2^-, 3/2^-, 1/2^-$	—	—	—	—	—	—	—	—
3042 ± 3	$1/2^-, 3/2^-, 1/2^-$	3.5	1.8	—	—	1.6	0.78	0.4	0.43
3100 ± 3	$1/2^-, 3/2^-, 1/2^-$	4.4	2.3	—	—	0.9	0.46	—	—
3127 ± 3	—	—	—	—	—	0.9	0.46	—	—
3224 ± 3	—	4.8	2.7	—	—	0.9	0.49	1.6	0.82
3264 ± 3	—	1.6	0.90	—	—	1.3	0.72	—	—
3292 ± 4	—	5.7	3.0	—	—	1.1	0.62	2.4	1.3
3309 ± 4	—	7.5	4.5	0.7	0.40	2.5	1.42	3.8	2.0
3406 ± 3	—	3.5	2.2	—	—	—	—	—	—
3429 ± 2	—	4.8	3.0	—	—	—	—	—	—
3461 ± 4	—	3.7	2.4	—	—	—	—	4.2	2.4
3476 ± 4	—	—	—	—	—	—	—	1.8	1.1
3535 ± 3	—	—	—	—	—	—	—	1.6	0.78
3657 ± 4	—	4.4	3.2	—	—	—	—	—	—
3774 ± 4	—	2.6	2.0	—	—	—	—	—	—
3802 ± 3	—	—	—	—	—	—	—	2.0	1.5
3860 ± 3	—	—	—	—	—	—	—	1.8	1.4
4058 ± 5	—	—	—	—	—	—	—	2.2	1.8
4119 ± 5	—	—	—	—	—	—	—	4.6	4.0

Note. The values of the resonant forces $(2I+1) \Gamma_D \Gamma_{\gamma} / T$ are determined within 20% for the case of a 90° angle between the directions of the γ rays and the incident beam. The Γ_{γ} values given do not incorporate the angular distribution.

REF. O.E. Kraft, Yu. V. Naumov, and I.V. Sizov
Izv. Akad. Nauk SSSR. Ser. Fiz. 39, 70 (1975)
Bull. Acad. Sci. USSR Phys. Ser. 39, 59 (1975)

ELEM. SYM.	A	Z
Cu	63	29

METHOD

REF. NO.

75 Kr 15

hmg

REACTION	RESULT	EXCITATION ENERGY	SOURCE		DETECTOR		ANGLE
			TYPE	RANGE	TYPE	RANGE	
P, G	LFT	8- 9	D	2- 3	NAI-D		90
		(8.6-8.7)		(2.5-2.7)			

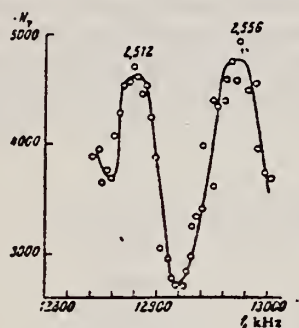


Fig. 2. Excitation function of the $^{82}\text{Ni}(p\gamma)^{63}\text{Cu}$ reaction. The target "thickness" was 15 keV for $E_p = 2.5$ MeV.

Table 2
Characteristics of the Resonances of ^{63}Cu

E^*, keV	E_{γ}, keV	J^{π}	$(2J+1)P_{\gamma}^2 \Gamma^2, \text{eV}$
8567	2481	$1/2^-$	0.44 ± 0.08
8597	2512		0.32 ± 0.10
8631	2546	$(3/2^-)$	0.11 ± 0.03
8641	2556	$(1/2^-)$	0.28 ± 0.10
8743	2659	$3/2^-$	0.24 ± 0.10

*The values of the forces are given without allowance for the angular distribution of the γ -rays.

REF.

C. O. Wene
Z. Phys. **A272**, 77 (1975)

ELEM. SYM.	A	Z
Cu	63	29

METHOD

REF. NO.

75 We 4

egf

REACTION	RESULT	EXCITATION ENERGY	SOURCE		DETECTOR		ANGLE
			TYPE	RANGE	TYPE	RANGE	
G,P	ABX	18	D	18	SCD-D		90

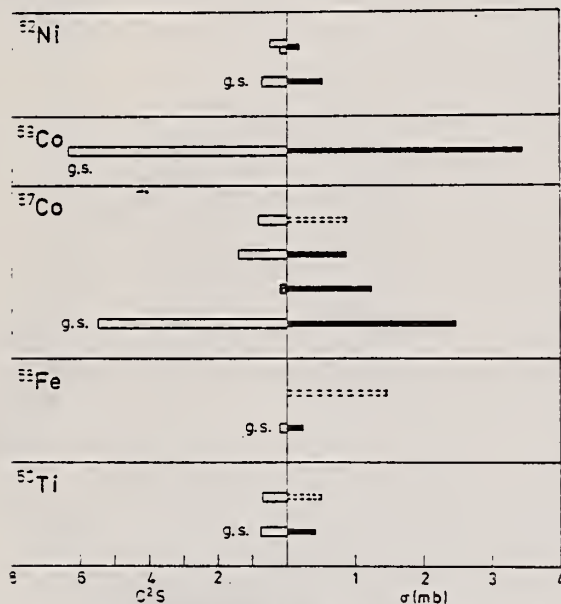
 $18 = 17.6 \text{ MEV}$ 

Fig. 5. Correlation between the spectroscopic factors and the cross-sections measured in this work. Open staples indicate $\ell_p = 3$ pick-up and cross hatched staples $\ell_p = 1$ pick-up. Dashed staples indicate that the cross section is uncertain due to the subtraction of a large back-ground

Table 2

Daughter nucleus	Level		σ^a (mb)
	(MeV)	J^π	
^{44}Ca	0	0^+	0.2 ± 0.2^b
	1.16	2^+	0.5^b
^{50}Ti	0	0^+	0.41 ± 0.05
	2.68	4^+	$(0.5)^c$
^{55}Fe	0	0^+	0.23 ± 0.08
	3.24 ^d	$0^+?$	$(1.5)^c$
^{57}Co	0	$7/2^-$	2.5 ± 0.2^d
	1.76	$3/2^-$	1.2 ± 0.3
	1.90	$7/2^-$	0.9 ± 0.2
	2.31	$7/2^-$	$(0.9)^c$
^{59}Co	0	$7/2^-$	3.5 ± 0.8
^{52}Ni	0	0^+	0.51 ± 0.09
	1.18	2^+	0.2 ± 0.1

^a The quoted errors are only those due to counting statistics.^b Confidence level 95%.

Uncertain because of large background.

^c $\sigma = 2.4 \text{ mb}$ from [43].

43. Miyase, H., Oikawa, S., Suzuki, A., Uegaki, J., Saito, T., Sugawara, M., Shoda, K.: The photoproton reactions of Ni-isotopes. In: Proc. Int. Conf. Photoneuclear Reactions and Applications, Vol. I, p. 553. Livermore, USA 1973 (see Ref. 13)

REF.

C.P. Swann
Phys. Rev. C13, 1104 (1976)

ELEM. SYM.	A	Z
Cu	63	29

METHOD

REF. NO.

76 Sw 7

hmg

REACTION	RESULT	EXCITATION ENERGY	SOURCE		DETECTOR		ANGLE
			TYPE	RANGE	TYPE	RANGE	
G,G	LFT	1- 5	C	1- 5	SCD-D		DST

The properties of levels in ^{63}Cu and ^{65}Cu have been investigated using the resonance fluorescence technique with bremsstrahlung serving as the source of exciting radiation. The energies and scattering cross sections for 24 levels in ^{63}Cu and 30 levels in ^{65}Cu up to about 4.5 MeV were measured. A few levels known to exist in the region of 2 MeV for both nuclei were not observed. For a number of the lower lying levels, spin and parity assignments have been made through angular distribution measurements and limits on J^π set by others. Mixing ratios for a few of these are also given. Where J^π and the ground state branching ratios are known the partial widths for decays to the ground state are presented. Comparisons are made with the predictions of the latest theoretical calculations.

24 LEV 1.32-4.51 MEV

TABLE L. Properties of levels in ^{63}Cu .

E_γ^a (keV)	J^π^b	$g\Gamma_0^2/\Gamma$ (meV)	Γ_0/Γ^c	Γ_0 (meV)
1327.0(5)	$\frac{1}{2}^-$	1.28(13)	0.84	0.76(3)
1412.0(10)	$\frac{3}{2}^-$	0.31(6)	0.72	0.29(6)
1547.0(5)	$\frac{3}{2}^- \dagger$	2.53(25)	0.80	3.16(32)
1861.0(10)	$\frac{1}{2}^- (\frac{3}{2}^-)$	0.42(3)	0.57	0.37(7) (for $\frac{1}{2}^-$)
2011.1(5)	$\frac{3}{2}^- \dagger$	2.90(28)	0.56	5.0(5)
2062.2(3)*	$\frac{1}{2}^- (\frac{3}{2}^-)$	<0.16	0.20	<1.6 (for $\frac{1}{2}^-$)
2082.4(10)	$\frac{3}{2}^- \dagger$	0.76(17)	0.39	1.3(3)
2092.7(5)*	$\frac{1}{2}^- (\frac{5}{2}^-)$	<0.17	0.10	<0.3 (for $\frac{1}{2}^-$)
2337.0(10)	$\frac{5}{2}^-$	0.23(5)	0.60	0.26(6)
2497.5(10)	$\frac{3}{2}^-$	3.0(6)	0.83	3.6(4)
2513.2(10)		2.3(3)	1.00	
2536.0(10)	$\frac{5}{2}^-$	0.5(1)	0.28	1.2(6)
2697.0(10)	$\frac{1}{2}^+, \frac{3}{2}^+, \frac{5}{2}^-$	0.71(35)	0.34	
2780.1(10)	$\frac{1}{2}^+, \frac{3}{2}^+, \frac{5}{2}^-$	4.5(5)	0.58	
2858.5(10)	$\frac{1}{2}^+, \frac{3}{2}^+, \frac{5}{2}^-$	3.7(6)	0.36	
2977.3(10)	$(\frac{1}{2}^+, \frac{3}{2}^+, \frac{5}{2}^-)^\dagger$	18(2)	≤ 0.78	
3045.4(10)		2.5(4)	1.00	
3100.9(10)		0.5(3)	0.55	
3405.1(10)		32(4)		
3430.7(10)		14(2)		
3458.6(10)		12(2)		
4038(2)		22(4)		
4117(2)		18(5)		
4294(2)		44(6)		
4358(2)		66(7)		
4513(2)		97(10)		

^a The energies indicated with an asterisk were taken from Ref. 9.^b The values for J indicated with a dagger are from this study; the others were taken from Refs. 8 and 13.^c The values for Γ_0/Γ were taken from Ref. 10 except for the limit given for 2977 keV level. The observed branch is to the 670 keV $\frac{1}{2}^-$ level.

over

TABLE III. Experimental A_2 values and resultant mixing ratios.

Nuclei	E_γ (keV)	J^π	A_2	δ
^{63}Cu	1547	$\frac{3}{2}^-$	0.58(9)	0.27(5), (1.7(2))
	2011	$\frac{3}{2}^-$	0.75(16)	0.41(14), 1.4(3)
	2977	$\frac{1}{2}^-, \frac{3}{2}^-, \frac{5}{2}^-$	-0.04(18)	
^{65}Cu	1725	$\frac{3}{2}^-$	0.39(7)	0.15(5), 1.8(8)
	2329	$\frac{3}{2}^-$	0.38(8)	0.15(6), 1.9(5)
	2862	$\frac{3}{2}^-$	0.09(28)	
	2875		0.43(24)	
	3166		-0.18(16)	
	3326	$\frac{3}{2}^-, \frac{5}{2}^-$	0.89(17)	0.9(5) if $\frac{3}{2}$

- ⁸ R.L. Auble, Nucl. Data Sheets 14, 119 (1975).
¹⁰ A. Hartas et al., private communication.
¹³ H. Verheul, Nucl. Data B2 (#3), 31 (1967).

REF. K.V. Alanakyan, M.Dzh. Amaryan, R.A. Demirchyan, K.Sh. Egiyan,
M.S. Ogandzhanyan, & Yu.G. Sharabyan
Yad. Fiz. 25, 545 (March 1977)
Sov. J. Nucl. Phys. 25, 292 (March 1977).

ELEM. SYM.	A	Z
63	Cu	29

REF. NO.	
77 A1 9	hmg

REACTION	RESULT	EXCITATION ENERGY	SOURCE		DETECTOR		ANGLE
			TYPE	RANGE	TYPE	RANGE	
G,P	ABX	70-999	C	2 *5 (4-5)	TEL-D	---	DST

COMMENTS:

$$f \sim \exp(-Bp^2)$$

$$B = \frac{E}{p^4(d^2\sigma/d\Omega dpQ)}$$

*E, GEV, 999=4.5 GEV

The A^n -dependence and momentum spectra of photoprotons in the nuclei ^{12}C , ^{27}Al , ^{63}Cu , ^{118}Sn , and ^{208}Pb have been studied experimentally for maximum bremsstrahlung energies of 2.0, 3.0, and 4.5 GeV. The A -dependence shows that the proton photoproduction mechanism for $E_\gamma > 400$ MeV is identical for the entire kinetic-energy region 65–280 MeV and the angle region 45° – 150° for the secondary protons studied. The dependence of the exponent n on the transverse momentum p_t is in good agreement with the same dependence for protons produced in nuclei by primary protons. In the momentum spectra of the invariant cross section $f = (E/p^2)(d^2\sigma/d\Omega dpQ) \sim \exp(-Bp^2)$ it is observed that the parameter B does not depend on the incident-photon energy and on the target nucleus, but depends on the proton-detection angle.

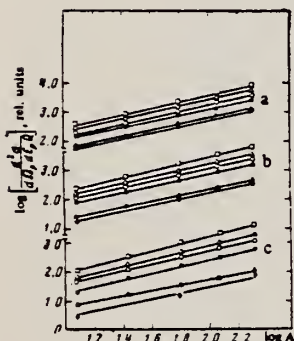


FIG. 1. Differential cross section for proton photoproduction as a function of atomic number A of the nucleus at $E_0 = 2$ GeV. The lines a correspond to $\vartheta_p = 60^\circ$, b to 90° , and c to 150° . Points: \circ — $E_p = 64$, Δ —80, \square —101, \blacksquare —137, \blacktriangle —209, and \bullet —280 MeV.

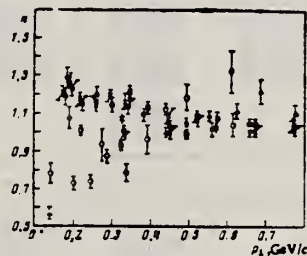


FIG. 3. The same as Fig. 2. Experimental points: \blacktriangle — $E_0 = 0.13$, \triangle —0.25, Δ —0.4, \square —1.2, \square —2.0, \times —3.0, and \bullet —4.5 GeV.

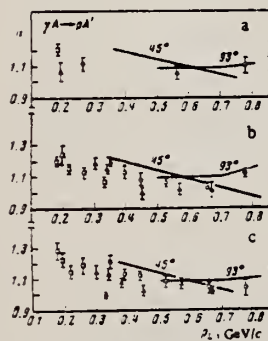


FIG. 2. Dependence of the exponent n in the A^n dependence of the cross section for the reaction $\gamma A \rightarrow pA'$ as a function of proton transverse momentum: a — $E_0 = 2.0$ GeV, b — $E_0 = 3.0$ GeV, c — $E_0 = 4.5$ GeV. The points for a and b : Δ — $\vartheta_p = 60^\circ$, \circ — 90° , \square — 150° ; for c : Δ — $\vartheta_p = 46^\circ$, \circ — 86° , \square — 136° . The curves show the dependence of n on p_t for the reaction $A(p, p')A'$ taken from Ref. 9.

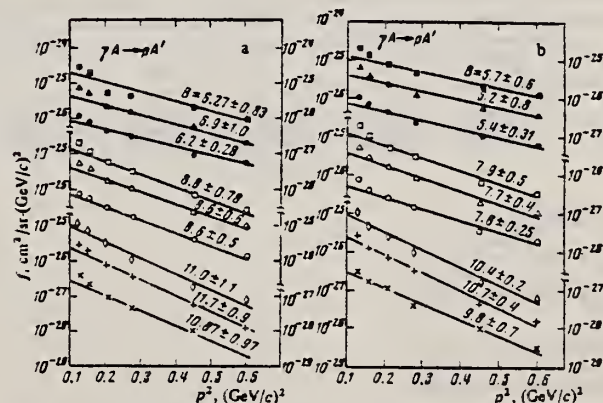


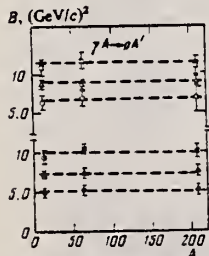
FIG. 4. Invariant cross section f as a function of p^2 . a —for $E_0 = 2.0$ GeV, b —for $E_0 = 3.0$ GeV. Experimental points: \bullet , Δ , \blacksquare —for $\vartheta_p = 60^\circ$ for the respective nuclei ^{12}C , ^{63}Cu , and ^{208}Pb ; \circ , Δ , \square —the same for $\vartheta_p = 90^\circ$; \times , $+$, \diamond —the same for $\vartheta_p = 150^\circ$.

TABLE I. Differential cross section $d^2\sigma/d\Omega dTQ$ of the reaction $\gamma A \rightarrow pA'$ in $\mu\text{b}/\text{MeV}\cdot\text{sr}$.

A	E_γ , GeV	θ_p , deg	E_p , MeV					
			64	80	101	137	209	279
^{12}C	2	60	3.720 ± 0.056	2.630 ± 0.052	1.907 ± 0.057	1.425 ± 0.038	0.725 ± 0.220	0.429 ± 0.018
		90	2.274 ± 0.045	1.587 ± 0.047	1.130 ± 0.039	0.763 ± 0.022	0.256 ± 0.008	0.117 ± 0.007
		150	1.152 ± 0.032	0.690 ± 0.014	0.505 ± 0.026	0.218 ± 0.007	0.071 ± 0.005	0.021 ± 0.002
	3	60	4.240 ± 0.100	3.424 ± 0.063	1.960 ± 0.043	1.829 ± 0.048	0.653 ± 0.024	0.452 ± 0.019
		90	2.440 ± 0.056	2.031 ± 0.040	1.145 ± 0.029	0.807 ± 0.028	0.243 ± 0.009	0.068 ± 0.005
		150	1.360 ± 0.042	0.877 ± 0.029	0.428 ± 0.018	0.300 ± 0.010	0.057 ± 0.003	—
^{27}Al	2	60	8.460 ± 0.127	8.014 ± 0.120	4.083 ± 0.109	3.253 ± 0.097	1.513 ± 0.046	—
		90	5.920 ± 0.107	3.750 ± 0.088	2.502 ± 0.084	1.718 ± 0.052	0.803 ± 0.018	—
		150	3.127 ± 0.078	1.797 ± 0.035	1.189 ± 0.060	0.644 ± 0.019	0.184 ± 0.011	—
	3	60	9.960 ± 0.239	7.492 ± 0.131	4.160 ± 0.092	3.527 ± 0.100	1.568 ± 0.058	0.925 ± 0.037
		90	6.090 ± 0.130	4.845 ± 0.107	2.688 ± 0.078	1.995 ± 0.065	0.596 ± 0.021	0.239 ± 0.013
		150	3.750 ± 0.103	2.943 ± 0.081	1.234 ± 0.042	0.747 ± 0.023	0.136 ± 0.006	—
^{63}Cu	2	60	23.500 ± 0.329	15.170 ± 0.299	10.931 ± 0.289	8.163 ± 0.240	3.939 ± 0.110	2.115 ± 0.064
		90	16.721 ± 0.288	9.757 ± 0.231	6.856 ± 0.082	4.411 ± 0.134	1.424 ± 0.042	0.743 ± 0.037
		150	10.592 ± 0.212	5.217 ± 0.103	3.362 ± 0.165	1.697 ± 0.050	0.342 ± 0.021	0.115 ± 0.011
	3	60	26.180 ± 0.590	20.580 ± 0.340	10.200 ± 0.191	8.594 ± 0.248	3.869 ± 0.140	1.661 ± 0.064
		90	17.800 ± 0.320	13.801 ± 0.280	7.518 ± 0.118	5.243 ± 0.172	1.403 ± 0.046	0.676 ± 0.032
		150	11.640 ± 0.271	7.834 ± 0.205	3.388 ± 0.107	2.237 ± 0.075	0.368 ± 0.017	0.097 ± 0.008
^{118}Sn	2	60	43.601 ± 0.538	30.050 ± 0.593	19.970 ± 0.587	13.102 ± 0.380	7.137 ± 0.210	—
		90	32.550 ± 0.553	18.890 ± 0.466	13.840 ± 0.428	8.297 ± 0.320	2.588 ± 0.078	—
		150	19.571 ± 0.391	10.289 ± 0.203	6.548 ± 0.321	3.032 ± 0.090	0.585 ± 0.041	—
	4.5	48	—	9.510 ± 0.250	—	—	—	1.320 ± 0.720
		86	—	8.200 ± 0.095	—	—	—	0.248 ± 0.020
		136	—	3.380 ± 0.050	—	—	—	—
^{208}Pb	2	60	80.000 ± 1.280	56.850 ± 1.120	35.200 ± 1.030	23.930 ± 0.720	13.440 ± 0.400	7.745 ± 0.310
		90	60.990 ± 0.970	34.080 ± 0.800	23.690 ± 0.720	14.220 ± 0.480	4.522 ± 0.135	2.453 ± 0.120
		150	38.890 ± 0.730	18.980 ± 0.370	10.638 ± 0.520	5.794 ± 0.168	1.102 ± 0.077	0.531 ± 0.035
	3	60	100.740 ± 2.130	76.030 ± 1.300	28.00 ± 0.970	28.000 ± 0.820	12.810 ± 0.450	7.092 ± 0.250
		90	71.350 ± 1.270	48.320 ± 0.900	24.794 ± 0.650	16.420 ± 0.520	4.580 ± 0.170	2.244 ± 0.120
		150	42.090 ± 0.970	27.240 ± 0.680	12.150 ± 0.42	7.294 ± 0.250	1.220 ± 0.054	0.589 ± 0.039
^{208}Pb	4.5	48	—	85.000 ± 0.350	—	—	—	11.600 ± 0.540
		86	—	58.780 ± 0.920	—	—	—	3.050 ± 0.214
		136	—	29.600 ± 0.430	—	—	—	0.465 ± 0.084
	4.5	48	—	5.210 ± 0.260	3.670 ± 0.088	2.530 ± 0.064	1.190 ± 0.048	0.785 ± 0.042
		86	—	2.440 ± 0.080	1.350 ± 0.052	0.845 ± 0.037	0.363 ± 0.019	0.105 ± 0.007
		136	—	1.330 ± 0.029	0.427 ± 0.029	0.196 ± 0.015	0.045 ± 0.015	0.018 ± 0.002

 TABLE II. Values of the parameter B in $(\text{GeV}/c)^{-2}$ in the relation $E_p/p_p^2 (d^2\sigma/d\Omega_p dp_p Q) = f \sim \exp(-Bp^2)$.

Target	$E_\gamma = 2.0 \text{ GeV}$			3.0 GeV			4.0 GeV		
	$\theta_p = 60^\circ$	90°	150°	60°	90°	150°	60°	90°	136°
^{12}C	4.874 ± 0.512	7.278 ± 0.482	9.481 ± 0.303	6.238 ± 0.806	8.823 ± 0.497	10.873 ± 0.977	8.047 ± 0.173	8.066 ± 0.49	11.262 ± 0.481
^{63}Cu	5.300 ± 0.627	7.337 ± 0.627	10.473 ± 0.609	8.972 ± 0.939	8.559 ± 0.622	11.697 ± 0.944	—	—	—
^{208}Pb	5.204 ± 0.753	7.605 ± 0.721	10.068 ± 0.96	8.870 ± 1.514	8.858 ± 0.783	10.983 ± 1.188	—	—	—


 FIG. 6. Dependence of the parameter B from the relation $f \sim \exp(-Bp^2)$ on the atomic number of the target nucleus. The solid points refer to $E_\gamma = 2.0 \text{ GeV}$, and the hollow points to $E_\gamma = 3.0 \text{ GeV}$; the points \circ and \triangle are for $\theta_p = 60^\circ$, \triangle and \square are for 90° , and \blacksquare and \square are for 150° .

REF. U. Kneissl, G. Kuhl, and K.H. Leister
Z. Physik A281, 35 (1977)

ELEM. SYM.	A	Z
Cu	63	29

METHOD	REF. NO. 77 Kn 2	egf
--------	---------------------	-----

REACTION	RESULT	EXCITATION ENERGY	SOURCE		DETECTOR		ANGLE
			TYPE	RANGE	TYPE	RANGE	
E-,N	ABX	11-32	D	20-32	ACT-I		4PI
E+,N	ABX	11-32	D	20-32	ACT-I		4PI

See figure on other side

over

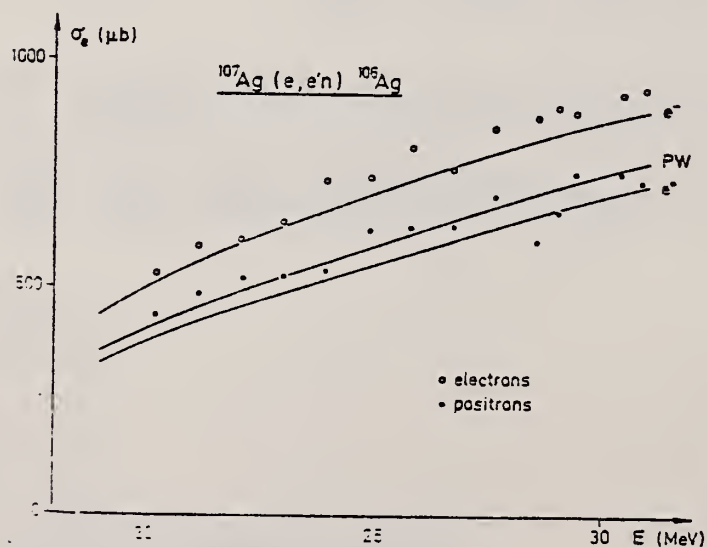
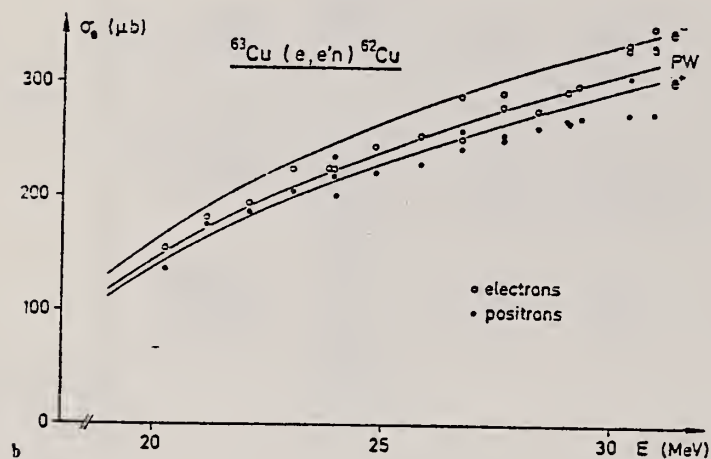
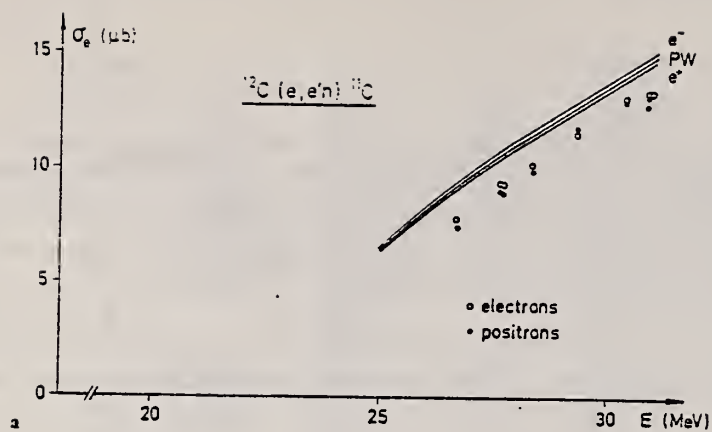


Fig. 1. a Experimental absolute $(e, e'n)$ cross section for ^{12}C together with the results of DWBA and PW calculations. b Experimental absolute $(e, e'n)$ cross section for ^{63}Cu together with the results of DWBA and PW calculations. c Experimental absolute $(e, e'n)$ cross section for ^{107}Ag together with the results of DWBA and PW calculations

METHOD					REF. NO.	
					77 Kr 6	egf
REACTION	RESULT	EXCITATION ENERGY	SOURCE		DETECTOR	
			TYPE	RANGE	TYPE	RANGE
P,G	NOX	8-9	D	2-3	SCD-D	

Measurements are reported of the angular distributions of γ -rays due to transitions from the analog resonances corresponding to the ground and the first and second excited states of ^{63}Ni to the levels of ^{63}Cu . The spins of the following resonances have been determined: 8743 keV (3/2) and 8640 keV (5/2).

8.57, 8.74,
8.64 MEV

$E_{\text{res}} \rightarrow E_f$ keV	a_2	a_4	a_6	δ
1	2	3	4	5
8569 \rightarrow 0.0	-0.01 ± 0.09	-0.07 ± 0.11	-0.05 ± 0.06	—
8569 \rightarrow 0.68	-0.23 ± 0.22	-0.42 ± 0.25	-0.40 ± 0.24	—
8569 \rightarrow 962	$+0.11 \pm 0.05$	-0.13 ± 0.06	$+0.05 \pm 0.07$	—
8569 \rightarrow 1326	-0.21 ± 0.35	$+0.15 \pm 0.43$	-0.14 ± 0.21	—
8569 \rightarrow 1410	$+0.03 \pm 0.03$	-0.21 ± 0.03	-0.06 ± 0.11	—
8569 \rightarrow 1547	-0.14 ± 0.13	$+0.06 \pm 0.16$	-0.11 ± 0.08	—
8569 \rightarrow 2060	-0.20 ± 0.25	-0.07 ± 0.31	-0.23 ± 0.15	—
8569 \rightarrow 2080	$+0.75 \pm 0.07$	-0.09 ± 0.03	$+0.72 \pm 0.07$	—
8569 \rightarrow 2407	-0.13 ± 0.13	$+0.42 \pm 0.17$	$+0.04 \pm 0.21$	—
8569 \rightarrow 2512	$+1.3 \pm 0.8$	$+0.15 \pm 0.77$	$+1.3 \pm 0.6$	—
8569 \rightarrow 2534	$+0.07 \pm 0.21$	-0.12 ± 0.26	$+0.02 \pm 0.15$	—
8569 \rightarrow 2673	-0.11 ± 0.22	-0.18 ± 0.26	-0.19 ± 0.16	—
8569 \rightarrow 2856	$+0.04 \pm 0.11$	$+0.01 \pm 0.14$	$+0.01 \pm 0.07$	—
8569 \rightarrow 2956	-0.50 ± 0.15	$+0.16 \pm 0.19$	-0.42 ± 0.11	—
8569 \rightarrow 2978	-0.74 ± 0.21	$+0.40 \pm 0.27$	-0.50 ± 0.23	—
8569 \rightarrow 3160	-0.10 ± 0.42	-0.36 ± 0.49	-0.05 ± 0.32	—
8569 \rightarrow 3127	-0.27 ± 0.17	$+0.03 \pm 0.21$	-0.25 ± 0.10	—
8569 \rightarrow 3300	-0.24 ± 0.12	$+0.23 \pm 0.16$	-0.14 ± 0.13	—
8569 \rightarrow 3406	-0.43 ± 0.33	$+0.10 \pm 0.48$	-0.43 ± 0.21	—
8569 \rightarrow 3420	-0.32 ± 0.10	$+0.77 \pm 0.14$	-0.18 ± 0.32	—
8569 \rightarrow 3561	-0.11 ± 0.15	-0.39 ± 0.18	-0.05 ± 0.22	—
8743 \rightarrow 0.0	-0.01 ± 0.06	$+0.05 \pm 0.07$	$+0.03 \pm 0.04$	$+0.23 \pm 0.02$ or $40^\circ < \delta < -60^\circ$
8743 \rightarrow 568	-0.17 ± 0.04	-0.10 ± 0.05	-0.22 ± 0.06	-0.15 ± 0.06 or $+2.8 \pm 0.5$
8743 \rightarrow 962	$+0.09 \pm 0.02$	-0.03 ± 0.03	$+0.07 \pm 0.02$	$+0.14 \pm 0.12$ or $+2.8 \pm 0.3$ -0.07
8743 \rightarrow 1410	-0.10 ± 0.01	-0.03 ± 0.01	-0.11 ± 0.02	-0.02 ± 0.08 or 4.8 ± 3.9 -1.3
8743 \rightarrow 1547	-0.21 ± 0.03	-0.07 ± 0.10	$+0.13 \pm 0.06$	$+0.15 \pm 0.10$ or $+7^\circ < \delta < -10^\circ$
8640 \rightarrow 0.0	$+0.20 \pm 0.01$	-0.10 ± 0.01	$+0.16 \pm 0.05$	-0.20 ± 0.01
8640 \rightarrow 568	-0.20 ± 0.15	$+0.02 \pm 0.02$	$+0.21 \pm 0.10$	—
8640 \rightarrow 962	$+0.58 \pm 0.41$	$+0.35 \pm 0.50$	$+0.63 \pm 0.33$	$-0.3 < \delta < -0.1$
8640 \rightarrow 1326	$+0.03 \pm 0.15$	-0.26 ± 0.18	-0.03 ± 0.16	-0.09 ± 0.11
8640 \rightarrow 1410	$+0.67 \pm 0.40$	$+0.12 \pm 0.46$	$+0.70 \pm 0.28$	$-0.3 < \delta < -0.1$
8640 \rightarrow 1547	$+0.24 \pm 0.08$	$+0.23 \pm 0.10$	$+0.32 \pm 0.13$	-0.38 ± 0.09 -0.02

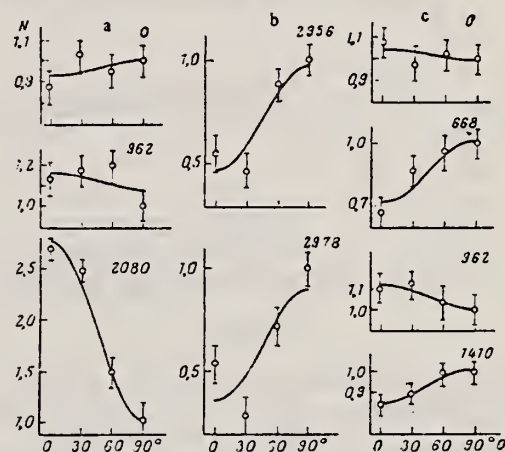


Fig. 1. Angular distributions of γ -rays due to transitions from the analog resonances at 8569 (a, b) and 8743 (c) keV to the levels of ^{63}Cu . Numbers indicated against curves are the energies of these levels in keV.

REF. E.A. Anakelvan, G.L. Bayatyan, G.S. Vartanyan, N.K. Griqoryan,
S.G. Knyazyan, A.T. Margaryan, S.S. Stepanyan, P.K. Kir'yanov,
V.A. Maisheev & A.M. Frolov
Phys. Lett. 79B, 143 (November 1978)

ELEM. SYM.	A	Z
Cu	63	29

METHOD

REF. NO.

78 Ar 9

hmg

REACTION	RESULT	EXCITATION ENERGY	SOURCE		DETECTOR		ANGLE
			TYPE	RANGE	TYPE	RANGE	
G,MU-T	ABX	THR-30		12*30	NAI-D	---	4PI

The total cross section of hadron photoproduction on C, Cu and Pb nuclei is measured for six energy values in the range 12-30 GeV. The obtained cross-section values for C and Cu nuclei have a weak energy dependence at high energies (above 20 GeV). The cross section for the Pb nucleus is somewhat higher in comparison with that expected, and energy dependence is not observed. The A-dependence of the effective number of hadrons agrees with VDM predictions.

*Energy in GeV

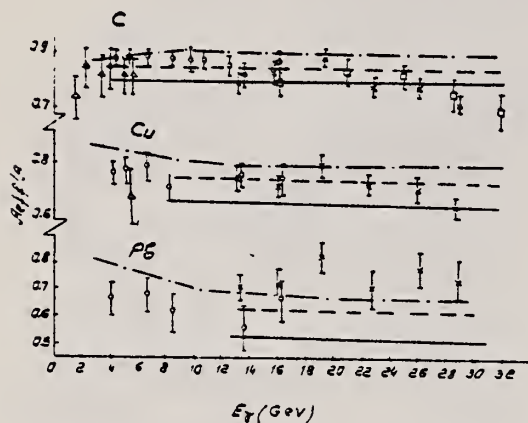


Fig. 3. Energy dependence of A_{eff}/A for C, Cu, Pb nuclei. For comparison the data of DESY and SLAC-UCSB, and also the theoretical curves, corresponding to VDM and to the case when the photon is ~20% of the time in a "pure" state, without shadowing. Δ , DESY; \circ , SLAC-UCSB; \times , Serpukhov; \square , Serpukhov [4]; — VDM; --- 0.8 VDM + 0.2 pomflike interaction; -.- general VDM.

Table 2

Value of A_{eff} for nuclei C, Cu, Pb for different energies of γ -quanta. Only statistical errors are given.

γ -quanta energy (GeV)	^{12}C	^{64}Cu	^{207}Pb
12.6-15.0	0.79 ± 0.04	0.77 ± 0.04	0.73 ± 0.05
15.0-17.7	0.81 ± 0.04	0.72 ± 0.05	0.75 ± 0.06
17.7-21.0	0.87 ± 0.4	0.80 ± 0.05	0.85 ± 0.7
21.0-24.6	0.80 ± 0.05	0.74 ± 0.07	0.72 ± 0.08
24.6-27.9	0.79 ± 0.05	0.69 ± 0.05	0.79 ± 0.09
27.9-30.0	0.71 ± 0.05	0.68 ± 0.07	0.75 ± 0.13

$$\frac{A_{eff}}{A} = \frac{\sigma_t(\gamma, A)}{Z\sigma_t(\gamma, p) + (A-Z)\sigma_t(\gamma, n)},$$

where

$$\sigma_t(\gamma, p) = (98.7 \pm 3.6) + (65 \pm 10)E^{-1/2} \mu\text{b},$$

$$\sigma_t(\gamma, n) = \sigma_t(\gamma, p) - (18.3 \pm 6.1)E^{-1/2} \mu\text{b}.$$

Table 1

Hadron photoproduction cross sections (in μb) for C, Cu, Pb nuclei for different energies of γ -quanta. Only statistical errors are given.

γ -quanta energy (GeV)	^{12}C	^{64}Cu	^{207}Pb
12.6-15.0	1084 ± 48	5600 ± 240	17140 ± 1170
15.0-17.7	1100 ± 43	5200 ± 310	17480 ± 1140
17.7-21.0	1175 ± 34	5740 ± 340	19680 ± 1720
21.0-24.6	1058 ± 53	5220 ± 460	16400 ± 1720
24.6-27.9	1047 ± 55	4870 ± 350	17920 ± 1920
27.9-30.0	930 ± 66	4730 ± 510	16840 ± 2810

ELEM. SYM.	A	Z
Cu	63	29

METHOD	REF. NO.	
	78 Ma 10	hg

REACTION	RESULT	EXCITATION ENERGY	SOURCE		DETECTOR		ANGLE
			TYPE	RANGE	TYPE	RANGE	
G,2N	ABY	20-68	C	30-68	ACT - \bar{I}		4PI
G,AN	ABY	16-68	C	30-68	ACT - \bar{I}		4PI

Analysis is made of reactions interfering with photon activation analysis procedures.

The activation yield curves have been presented for a number of photonuclear reactions in the energy range from 30 to 68 MeV, in order to evaluate quantitatively the interferences due to competing reactions in multielement photon activation analysis. The general features of the yields as functions of both target mass number and excitation energy were elucidated from the data obtained, discussion being given on the results in terms of the reaction mechanism.

Simultaneous neutron activation due to appreciable neutron production from the converter and surrounding materials has also been studied, and, finally, the magnitudes of interferences in real multielement analysis were given in the form of their energy dependences.

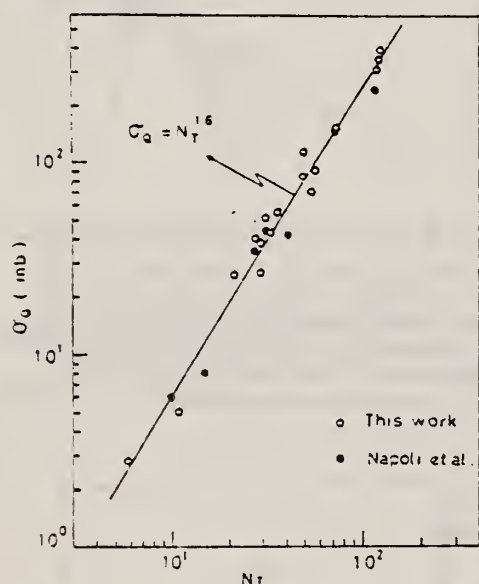


Fig. 2. Yield per equivalent quanta versus target neutron number.

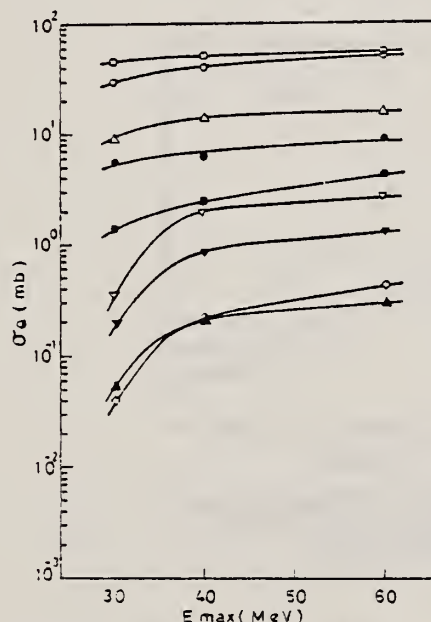


Fig. 6. Activation yield curves for the reactions on Co, Ni and Cu.
 \square $^{59}\text{Co}(\gamma, n)^{58}\text{Co}$, \bullet $^{59}\text{Co}(\gamma, 2n)^{57}\text{Co}$, \triangle $^{58}\text{Ni}(\gamma, n)^{57}\text{Ni}$,
 ∇ $^{58}\text{Ni}(\gamma, pn)^{56}\text{Co}$, \blacktriangledown $^{59}\text{Ni}(\gamma, pn)^{58}\text{Co}$, \blacktriangle $^{59}\text{Ni}(\gamma, 2n)^{56}\text{Ni}$,
 \square $^{63}\text{Cu}(\gamma, n)^{62}\text{Cu}$, \blacksquare $^{63}\text{Cu}(\gamma, 2n)^{61}\text{Cu}$, \diamond $^{61}\text{Cu}(\gamma, xn)^{58}\text{Co}$.

REF.

J.J. Murphy, II, D.M. Skopik, J. Asai, and J. Uegaki
Phys. Rev. C 18, 736 (1978)

ELEM. SYM.

A

Z

Cu

63

29

METHOD

REF. NO.

78 Mu 9

hg

REACTION	RESULT	EXCITATION ENERGY	SOURCE		DETECTOR		ANGLE
			TYPE	RANGE	TYPE	RANGE	
E,A	ABX	5-100	D	100	MAG-D		DST

α particles from the electrodisintegration of seven nuclei with Z between 29 and 79 have been observed. Energy spectra at 50° in the laboratory for six nuclei and angular distributions for five nuclei are reported. The cross sections exhibit a broad peak whose magnitude decreases with increasing Z ; the energy of the peak increases as Z increases. Angular distributions at the highest energies measured become increasingly forward peaked suggesting a direct-reaction process.

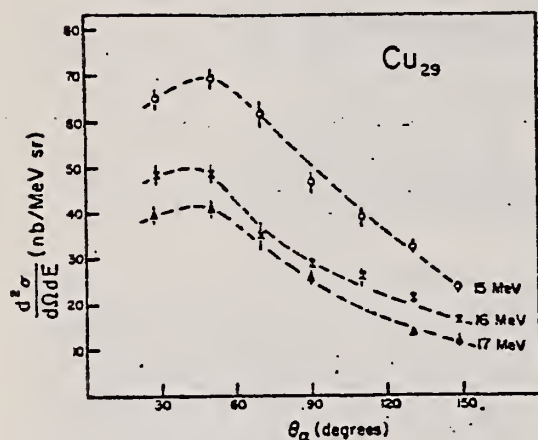


FIG. 1. High energy angular distributions for copper ($Z=29$). The expected forward peaking due to the importance of the direct process is seen.

¹J.J. Murphy, II, H.J. Gehrhardt, and D.M. Skopik, Nucl. Phys. A277, 69 (1977).

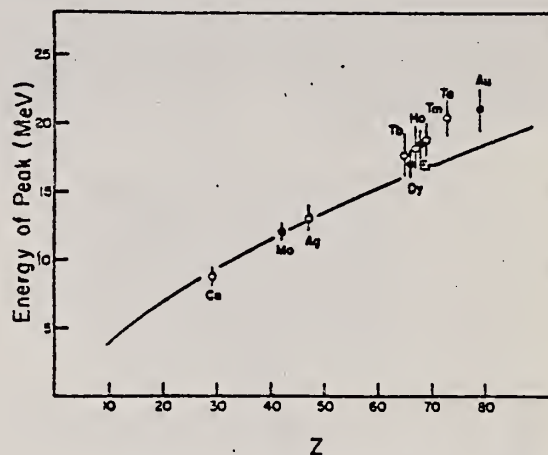


FIG. 3. Energy of the cross section peak as a function of Z . The solid line is the energy of the classical Coulomb barrier. The closed circles are the current work; the open circles are from Ref. 1.

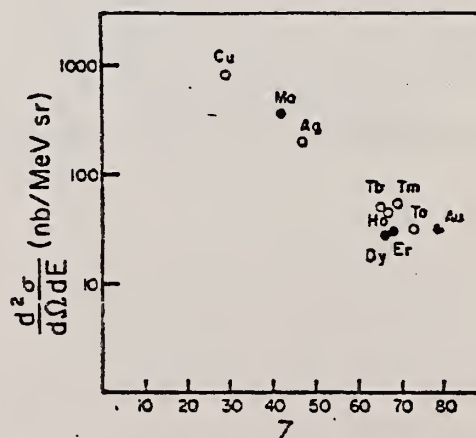


FIG. 4. Magnitude of cross section peak as a function of Z . The closed circles are the current work; the open circles are from Ref. 1.

REF. L.Z. Dzhilavyan, N.P. Kucher
Yad. Fiz. 30, 294 (1979)
Sov. J. Nucl. Phys. 30, 151 (1979)

ELEM. SYM.	A	Z
Cu	63	29
REF. NO.		
79 Dz 2		hg

METHOD

REACTION	RESULT	EXCITATION ENERGY	SOURCE		DETECTOR		ANGLE
			TYPE	RANGE	TYPE	RANGE	
G,N	ABX	12-25	D	12-25	ACT-D		4PI

A beam of quasimonochromatic photons at energy 12-25 MeV has been utilized to measure the cross section for the $^{63}\text{Cu}(\gamma, n)$ reaction by detecting the induced beta activity with a two-crystal scintillation gamma spectrometer. The results are in good agreement with Ref. 12 and differ appreciably from other data obtained in bremsstrahlung beams.

PACS numbers: 25.20. + y

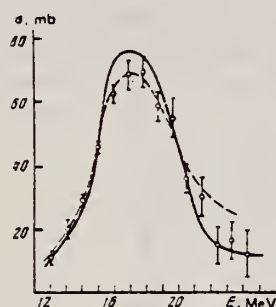


FIG. 5. Cross section for the reaction $^{63}\text{Cu}(\gamma, n)$. Solid curve—data of Ref. 12, dashed curve—data of Ref. 11, points—our data (the errors are statistical).

REF. K. Sh. Egiyan
Yad. Fiz. 30, 890 (1979)
Sov. J. Nucl. Phys. 30, 461 (1979)

ELEM. SYM.	A	Z
Cu	63	29

REF. NO.		
79 Eg 3		hg

METHOD					REF. NO.		
					79 Eg 3	hg	
REACTION	RESULT	EXCITATION ENERGY	SOURCE		DETECTOR		ANGLE
			TYPE	RANGE	TYPE	RANGE	
G,XP	RLY	6-250	C	130,250	MAG-D		DST

Experimental data are presented on the inclusive photoproduction of protons in the nuclei ^{12}C , ^{24}Mg , ^{63}Cu , ^{118}Sn , and ^{208}Pb irradiated by bremsstrahlung with maximum energies 0.13 and 0.25 GeV. The regions of angles $30-90^\circ$ and of photoproton momenta 0.24-0.48 GeV/c were studied.

PACS numbers: 25.20. + y

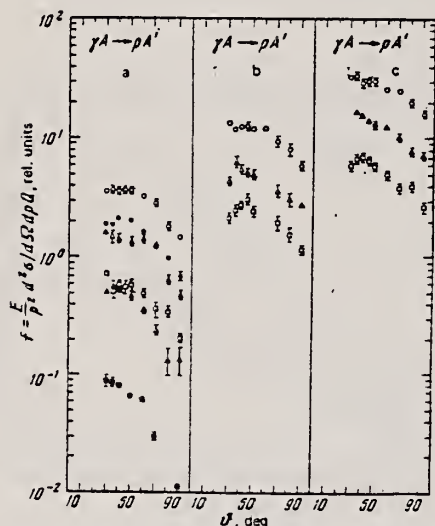


FIG. 2. Relative yields of photoprotons as a function of emission angle; experimental points: O, ●—for $p_p = 0.29$ GeV/c; Δ , \blacktriangle —0.34 GeV/c; \square , \blacksquare —0.40 GeV/c. The hollow points are for $E_{\gamma\text{max}} = 0.25$ GeV and the solid points for $E_{\gamma\text{max}} = 0.13$ GeV: a—for ^{12}C , b—for ^{63}Cu , c—for ^{208}Pb .

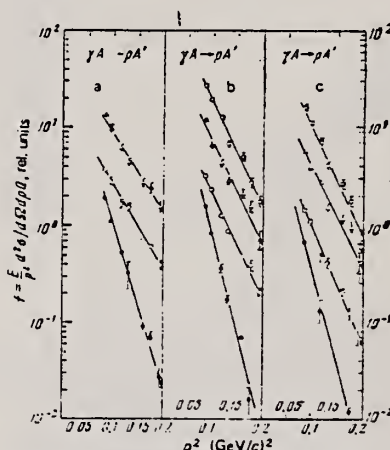


FIG. 3. Momentum spectra of protons. The experimental points are as follows: O and ●—for ^{12}C , Δ —for ^{63}Cu , \square —for ^{208}Pb . The hollow points are for $E_{\gamma\text{max}} = 0.25$ GeV and the solid points are for $E_{\gamma\text{max}} = 0.13$ GeV; a—for $\theta_p = 30^\circ$, b—for $\theta_p = 60^\circ$, c—for $\theta_p = 90^\circ$. The lines have been drawn through the experimental points by the method of least squares.

TABLE II. Values of the exponent n in the A^n dependence of the proton yield in reactions (2) and (3).

θ_p , deg	$E_\gamma = 0.25$ GeV			$E_\gamma = 0.13$ GeV	
	p_p , GeV/c			p_p , GeV/c	
	0.29	0.34	0.40	0.29	0.34
30	1.15 ± 0.04	1.17 ± 0.04	1.20 ± 0.05	0.59 ± 0.18	0.62 ± 0.06
60	—	1.17 ± 0.02	1.22 ± 0.03	—	—
90	1.02 ± 0.03	1.11 ± 0.03	1.24 ± 0.05	—	—

(over)

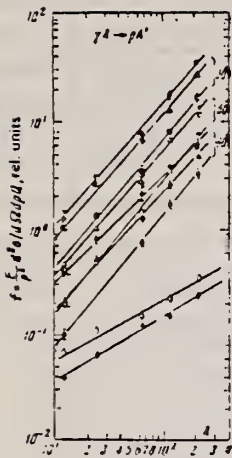


FIG. 5. A-dependence of the photoproton yield in reactions (2) and (3). Experimental points for $E_{\gamma \max} = 0.25$ GeV: circles— $p_p = 0.29$ GeV/c; triangles— $p_p = 0.34$ GeV/c, squares— $p_p = 0.40$ GeV/c; half-open symbols—for $\theta_p = 30^\circ$, open symbols— $\theta_p = 60^\circ$, solid symbols— $\theta_p = 90^\circ$, for $E_{\gamma \max} = 0.13$ GeV: \diamond — $p_p = 0.29$ GeV/c, $\theta_p = 30^\circ$; \circ — $p_p = 0.34$ GeV/c, $\theta_p = 30^\circ$. The lines have been drawn through the experimental points by the method of least squares.

REF.

A.V. Gann, V.I. Noga, Yu.N. Ranyuk, Yu.N. Telegin, G.G. Jonsson
 Sov. J. Nucl. Phys. 32, 599 (1980)
 Yad. Fiz. 32, 1161 (1980)

ELEM. SYM.

A

Z

Cu

63

29

METHOD

REF. NO.

80 Ga 8

hg

REACTION	RESULT	EXCITATION ENERGY	SOURCE		DETECTOR		ANGLE
			TYPE	RANGE	TYPE	RANGE	
E,N	ABY	10-999	D	320-999	ACT-I		4PI
G,N	ABY	10-999	D	320-999	ACT-I		4PI

999=1.2 GEV

The reactions $^{12}\text{C} \rightarrow ^{11}\text{C}$ and $^{63}\text{Cu} \rightarrow ^{62}\text{Cu}$ have been studied by the induced-activity method at electron and photon energies from 0.32 to 1.2 GeV. Activation of the targets was carried out directly by an electron beam. The use of targets in the form of stacks permitted cross sections to be obtained for photodisintegration and electrodisintegration of the nuclei. Comparison of the experiment with theoretical calculations in the plane-wave approximation indicates a dominant role of E1 transitions of photons in these reactions.

PACS numbers: 25.20. + y, 25.30.Cg, 27.20. + n, 27.50. + e

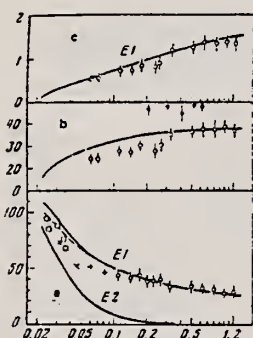


FIG. 2. The same as Fig. 1 but for the reactions $^{63}\text{C}(\gamma, n)^{62}\text{C}$.
 Points: ○—Results of the present work and Ref. 3, ●—Ref. 7,
 □—Ref. 9, ×—Ref. 10, +—Ref. 5.

REF. K.V. Alanakyan, M.Dzh. Amaryan, R.A. Demirchyan, K.Sh. Egijan,
M.S. Ogandzhanyan, Yu.G. Sharabyan
Nucl. Phys. A367, 429 (1981)

ELEM. SYM.	A	Z
Cu	63	29
REF. NO.		
81 A1 8		hg

METHOD

REACTION	RESULT	EXCITATION ENERGY	SOURCE		DETECTOR		ANGLE
			TYPE	RANGE	TYPE	RANGE	
G,P	ABY	6-999	C	999	TEL-D		DST

Abstract: The angular dependences of proton photoproduction from the nuclei ^{12}C , ^{63}Cu and ^{208}Pb irradiated by bremsstrahlung γ -quanta with maximum energy 4.5 GeV, both in the cumulative region (i.e. in the kinematical region in which the production of protons in the collision of γ -quanta of the given energy with the quasi-free nuclear nucleon is forbidden) and in the non-cumulative region, are investigated. The experimental data obtained are compared with the results of theoretical calculations of cumulative proton photoproduction according to the following models: the "quasi-two-body" scaling model, the low-nucleon correlation model, the flucton model and the cluster model.

999=4.5 GEV

E

NUCLEAR REACTIONS ^{12}C , ^{63}Cu , $^{208}\text{Pb}(\gamma, p)$, $E = 4.5$ GeV bremsstrahlung; measured $\sigma(E_p, \theta_p)$; deduced reaction mechanism. Natural target.

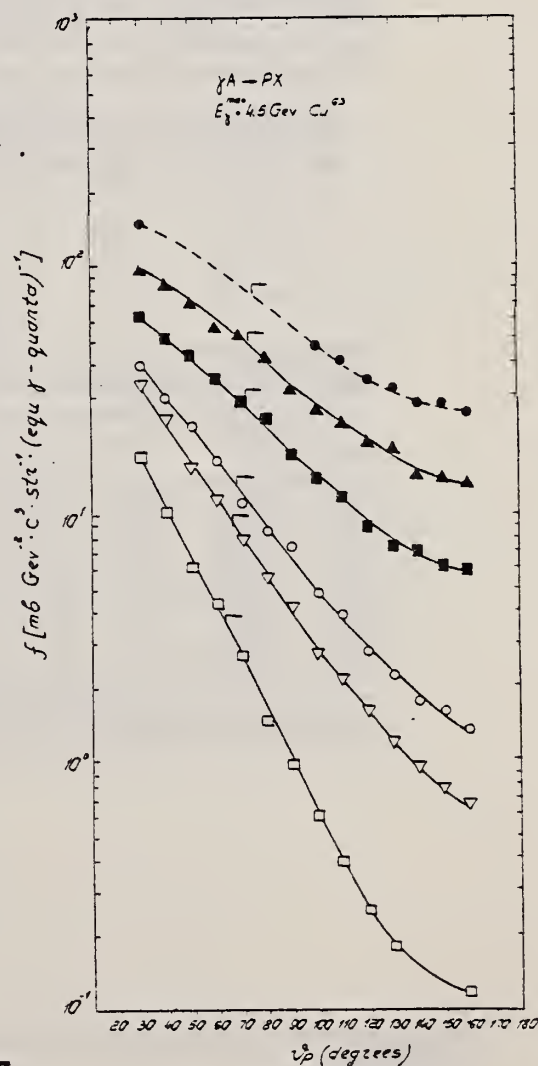


Fig. 4. The same as in fig. 3 for ^{63}Cu .

ELEM. SYM.	A	Z
Cu	63	29
REF. NO.		hg
81 Ca 2		

METHOD

REACTION	RESULT	EXCITATION ENERGY	SOURCE		DETECTOR		ANGLE
			TYPE	RANGE	TYPE	RANGE	
G,G	LFT	1,1	C	0 - 2	SCD-D		
		(1.327, 1.412)					

1.327,1.412 MEV

Abstract. Lifetimes of 49 excited states below 1.65 MeV have been measured in ^{24}Mg , ^{27}Al , ^{48}Ti , ^{58}Ni , ^{59}Co , $^{61,62}\text{Ni}$, $^{63,65}\text{Cu}$, $^{64,66,68}\text{Zn}$, ^{75}As , ^{103}Rh , $^{113,115}\text{In}$, $^{116,118,120}\text{Sn}$ and $^{121,123}\text{Sb}$ by means of nuclear resonance fluorescence experiments. The levels are excited by bremsstrahlung x-ray photons. The self-absorption technique applied to suitable cases provides nuclear absorption cross sections, widths and lifetimes from which the x-ray spectral distributions are also obtained. Scattering experiments are performed for all other cases in order to obtain widths and lifetimes from these x-ray photon curves. The Compton effect in the sample is taken into account. Self-absorption provides $g\Gamma_0$ from which Γ is deduced using adopted J^π and Γ_0/Γ values; scattering provides $u = g(\Gamma_0^2/\Gamma)W(\theta)$ from which Γ is also deduced with J , Γ_0/Γ and mixing ratios taken from the literature. Thanks to simultaneous determination of the x-ray spectra all the lifetimes as given by our programs with their statistical errors form an unusually coherent set of values.

NUCLEAR REACTIONS (γ , γ), bremsstrahlung excitation; natural isotopes: ^{24}Mg , ^{27}Al , ^{48}Ti , ^{58}Ni , ^{59}Co , $^{61,62}\text{Ni}$, $^{63,65}\text{Cu}$, $^{64,66,68}\text{Zn}$, ^{75}As , ^{103}Rh , $^{113,115}\text{In}$, $^{116,118,120}\text{Sn}$ and $^{121,123}\text{Sb}$; $E \approx 0.5\text{--}1.65$ MeV; measured $g\Gamma_0$ or $g(\Gamma_0^2/\Gamma)W(\theta)$; deduced $T_{1/2}$.

Tableau 2. Résultats des mesures des niveaux étudiés par self-absorption.

Table 2. Results obtained using the self-absorption method.

Isotope	Energie (keV)	J^π	J_0^π	Γ_0/Γ	$g\Gamma_0$ (meV) ce travail	τ (ps) ce travail	τ_{ref} (ps)	Références †
^{59}Co	1190.0(3)	2^-	2^-	1	11.3(5)	0.0729(32)	0.080(4)	Kim (1976)
^{63}Cu	669.62(5)	1^-	1^-	1	1.19(4)	0.277(10)	0.297(9)	Auble (1979b)
^{63}Cu	962.06(4)	1^-	1^-	1	1.25(6)	0.792(38)	0.851(43)	Auble (1979b)
^{63}Cu	1547.02(6)	3^-	3^-	0.803	2.6(1,7)	0.20(13)	0.160(16)	Auble (1979b)
^{65}Cu	770.6(2)	1^-	1^-	1	2.18(13)	0.151(9)	0.13(4)	Auble (1975a)
^{65}Cu	1115.54(4)	1^-	1^-	1	2.47(28)	0.400(45)	0.38(2)	Auble (1975a)
^{115}In	1132.57(3)	1^-	1^-	1	8.59(48)	0.0920(51)	0.092(5)	Cauchois <i>et al</i> (1977)
^{115}In	1463.5(12)	2^-	2^-	0.942	5.22(66)	0.095(12)	0.095(12)	Cauchois <i>et al</i> (1979)

† Références pour les colonnes 3, 4, 5 et 8 de ce tableau.

over

Tableau 3. Resultats des mesures des niveaux étudiés par diffusion.

Table 3. Results obtained using the diffusion method.

Isotope	Energie (keV)	J^π	J_0^π	Γ_0/Γ	δ	$u = g(\Gamma_0^2/\Gamma)W(\theta)$ (meV)	τ (ps) ce travail	τ_{ref} (ps)	Références†
²⁴ Mg	1368,59(4)	2 ⁺	0 ⁺	1	E2	1,08(13)	1,76(21)	1,98(4)	Endt et van der Leun (1978)
²⁷ Al	1014,45(3)	$\frac{3}{2}^+$	$\frac{1}{2}^+$	0,971	+0,351(12)	0,186(13)	2,20(16)	2,12(8)	Endt et van der Leun (1978)
⁴⁶ Ti	983,512(3)	2 ⁺	0 ⁺	1	E2	0,282(23)	6,74(55)	6,1(13)	Been (1978)
⁵⁸ Ni	1454,45(15)	2 ⁺	0 ⁺	1	E2	2,11(26)	0,90(11)	0,92(3)	Kocher et Auble (1976)
⁵⁹ Co	1099,224(25)	$\frac{1}{2}^-$	$\frac{1}{2}^-$	1	(E2)	0,069(8)	4,79(55)	3,17(58)	Kim (1976)
⁵⁹ Co	1458,8(3)	$\frac{1}{2}^-$	$\frac{1}{2}^-$	0,91	(E2)	0,68(8)	1,17(14)	1,52(16)	Kim (1976)
⁵⁹ Co	1480,9(3)	$\frac{1}{2}^-$	$\frac{1}{2}^-$	0,8	<0,35 ^a	1,23(15)	0,254(31)	0,31(3)	Kim (1976)
⁶¹ Ni	1185,7(6)	$\frac{1}{2}^-$	$\frac{1}{2}^-$	0,77(8) ⁱ	0,14	1,88(49)	0,21(5)	0,16(3)	Andreev <i>et al</i> (1974)
⁶² Ni	1172,91(9)	2 ⁺	0 ⁺	1	E2	0,88(17)	2,15(42)	2,09(3)	Halbert (1979a)
⁶³ Cu	1327,00(7)	$\frac{1}{2}^-$	$\frac{1}{2}^-$	0,84	(E2)	1,04(14)	0,84(11)	0,88(4)	Auble (1979b)
⁶³ Cu	1412,05(4)	$\frac{1}{2}^-$	$\frac{1}{2}^-$	0,72	+0,61($\pm 0,3$)	0,260(38)	1,90(28) ⁱ	1,61(3)	Auble (1979b)
⁶⁴ Zn	991,54(7)	2 ⁺	0 ⁺	1	E2	0,640(54)	2,97(25)	2,60(13)	Halbert (1979b)
⁶⁵ Cu	1431,83(5)	$\frac{1}{2}^-$	$\frac{1}{2}^-$	0,85	(E2)	1,13(19)	0,79(13)	0,49(5)	Auble (1975a)
⁶⁶ Zn	1039,37(6)	2 ⁺	0 ⁺	1	E2	0,70(6)	2,71(23)	2,25(15)	Auble (1975b)
⁶⁸ Zn	1077,38(5)	2 ⁺	0 ⁺	1	E2	0,70(6)	2,71(23)	2,34(23)	Lewis (1975)
⁷⁵ As	572,5(10)	$\frac{1}{2}^-$	$\frac{1}{2}^-$	1 ^d	0,39 ^b	0,23(26)	4,14(46)	3,5(9)	Horen et Lewis (1975)
⁷⁵ As	823,0(10)	$\frac{1}{2}^-$	$\frac{1}{2}^-$	0,86 ^d	(E2)	0,214(22)	4,27(43)	3,5(3)	Robinson <i>et al</i> (1967)
⁷⁵ As	865,5(10)	$\frac{1}{2}^-$	$\frac{1}{2}^-$	0,83 ^d	— ^c	0,78(6)	0,863(68)	0,60(12)	Celliers <i>et al</i> (1977)
⁷⁵ As	1076,0(10)	$\frac{1}{2}^-$	$\frac{1}{2}^-$	0,94 ^d	0,38 ^d	1,97(13)	0,287(19)	0,32(7)	Celliers <i>et al</i> (1977)
⁷⁵ As	1128,5(10)	$\frac{1}{2}^-$	$\frac{1}{2}^-$	1	E1 ^d	0,224(24)	1,47(16)	—	
⁷⁵ As	1349,0(10)	$\frac{1}{2}^-$	$\frac{1}{2}^-$	0,67 ^d	0,20 ^d	1,61(29)	0,180(32)	0,12(3)	Wilson (1970)
⁷⁵ As	1370,0(10)	$\frac{1}{2}^-$	$\frac{1}{2}^-$	0,47 ^d	0,47 ^d	0,64(13)	0,218(44)	—	
¹⁰³ Rh	803,1(2)	$\frac{1}{2}^-$	$\frac{1}{2}^-$	0,70	M1	1,85(16)	0,174(15)	—	Harmatz (1979)
¹⁰³ Rh	1277,0(2)	$\frac{1}{2}^-$	$\frac{1}{2}^-$	0,75	-0,62(30) ^f	0,81(9)	0,37(10)	1,3(9)	Harmatz (1979)
¹¹³ In	1177(1)	$\frac{1}{2}^-$	$\frac{1}{2}^-$	1	+0,5(2)	9,1(8)	0,086(8)	0,10(6)	Tuttle <i>et al</i> (1976)
¹¹³ In	1510(1)	$\frac{1}{2}^-$	$\frac{1}{2}^-$	0,935	-0,5($\pm 0,2$)	6,4(9)	0,071(10)	0,11($\pm 0,4$)	Tuttle <i>et al</i> (1976)
¹¹⁵ In	1077,7(10)	$\frac{1}{2}^-$	$\frac{1}{2}^-$	0,81 ^j	(E2)	0,159(24)	1,61(24)	1,23(7)	Tuttle <i>et al</i> (1976)
¹¹⁵ In	1290,59(3)	$\frac{1}{2}^-$	$\frac{1}{2}^-$	0,98 ^j	(E2)	1,31(11)	0,66(6)	0,55(4)	Tuttle <i>et al</i> (1976)
¹¹⁵ In	1448,78(3)	$\frac{1}{2}^-$	$\frac{1}{2}^-$	0,86	-8 ^f	0,90(11)	0,50(6)	0,52(20)	Tuttle <i>et al</i> (1976)
¹¹⁵ In	1486,1(1)	$\frac{1}{2}^-$	$\frac{1}{2}^-$	0,787	-0,8 ^f	0,63(9)	0,63(9)	0,4(3)	Tuttle <i>et al</i> (1976)
¹¹⁵ In	1497,2(4)	($\frac{1}{2}^-$)	$\frac{1}{2}^-$	<1	(E2)	1,33(16)	<0,30(4)	—	
¹¹⁵ In	1607,8(15)	($\frac{1}{2}^-$)	$\frac{1}{2}^-$	≠1	(E2)	1,54(24)	≦0,26(4)	—	
¹¹⁶ Sn	1293,54(2)	2 ⁺	0 ⁺	1	E2	3,58(37)	0,53(6)	0,522(14)	Carlson <i>et al</i> (1975)
¹¹⁸ Sn	1229,64(4)	2 ⁺	0 ⁺	1	E2	2,75(28)	0,69(7)	0,67(2)	Carlson <i>et al</i> (1976)
¹²⁰ Sn	1171,6(2)	2 ⁺	0 ⁺	1	E2	1,83(16)	1,04(9)	0,91(2)	Kocher (1976)
¹²¹ Sb	1023,5(10)	$\frac{1}{2}^-$	$\frac{1}{2}^-$	1	0,57 ^g	3,69(34)	0,228(21)	0,20(7) ^h	Tamura <i>et al</i> (1979)
¹²¹ Sb	1105,5(10)	$\frac{1}{2}^-$	$\frac{1}{2}^-$	0,4	—	0,47(4)	0,42(4)	—	
¹²¹ Sb	1142,5(10)	$\frac{1}{2}^-$	$\frac{1}{2}^-$	0,6	(E2)	0,85(8)	0,449(40)	0,41(8) ^h	Booth <i>et al</i> (1973)
¹²¹ Sb	1384,0(10)	$\frac{1}{2}^-$	$\frac{1}{2}^-$	1	0,45 ^g	4,7(5)	0,092(10)	0,088(14) ^h	Booth <i>et al</i> (1973)
¹²³ Sb	1029,5(10)	$\frac{1}{2}^-$	$\frac{1}{2}^-$	1	0,57 ^g	2,96(27)	0,272(25)	0,26(4) ^h	Booth <i>et al</i> (1973)
¹²³ Sb	1086,5(10)	$\frac{1}{2}^-$	$\frac{1}{2}^-$	1	δ > 1,26 ^d	1,06(9)	0,67(6)	0,72(15) ^h	Booth <i>et al</i> (1973)

† Références pour les colonnes 3, 4, 5, 6 et 9 de chaque ligne, sauf indication appelée au bas de ce tableau. Pour les autres données se reporter au texte.

Remarque. Pour calculer δ^2 quand nous ne disposons que de $B(E2)$, pour un mélange (E2) + (M1), nous déduisons $g\Gamma_0(E2) \propto B(E2)E_p^2$; en admettant $W(\theta) = 1$ et connaissant Γ_0/Γ , notre détermination de u donne une première approximation de $g\Gamma_0$ d'où une valeur de $\delta^2 = (g\Gamma_0(E2))/(g\Gamma_0 - g\Gamma_0(E2))$ qui permet d'améliorer $W(\theta)$ et $g\Gamma_0$ de proche en proche.

^a Swann (1971); ^b Robinson *et al* (1967); ^c $W(\theta) = 0,99$ calculé d'après la formule de Celliers *et al* (1977); ^d Abbondanno *et al* (1978); ^e Sayer *et al* (1972); ^f Tuttle *et al* (1976); ^g d'après $B(E2)$ de Barnes *et al* (1966); ^h calculé d'après Booth *et al* (1973); ⁱ Williams *et al* (1975); ^j Dietrich *et al* (1970).

ELEM. SYM.	A	Z
Cu	63	29
REF. NO.		82 Ma 3
METHOD		egf

REACTION	RESULT	EXCITATION ENERGY	SOURCE		DETECTOR		ANGLE
			TYPE	RANGE	TYPE	RANGE	
E, α	ABX	6-34	D	14-34	ACT-I		4PI
E, 2N	ABX	20-34	D	14-34	ACT-I		4PI

The (e, α) cross section for ^{63}Cu has been measured in the electron energy range 14–34 MeV. The results have been analyzed using the distorted-wave Born approximation $E1$ and $E2$ virtual photon spectra and the $E1$ and $E2$ components of the corresponding (γ, α) cross section were obtained. To assess the accuracy of the virtual photon analysis, the $(e, 2n)$ cross section for ^{63}Cu was also measured and the obtained $(\gamma, 2n)$ cross section is compared with direct measurement of this cross section performed with annihilation gamma rays.

NUCLEAR REACTIONS $^{63}\text{Cu}(e, \alpha)$ and $^{63}\text{Cu}(e, 2n)$. Measured $\sigma_{e, \alpha}(E_0)$ and $\sigma_{e, 2n}(E_0)$. Deduced $\sigma_{\gamma, \alpha}^{E1}(E)$, $\sigma_{\gamma, \alpha}^{E2}(E)$, and $\sigma_{\gamma, 2n}^{E1}(E)$.

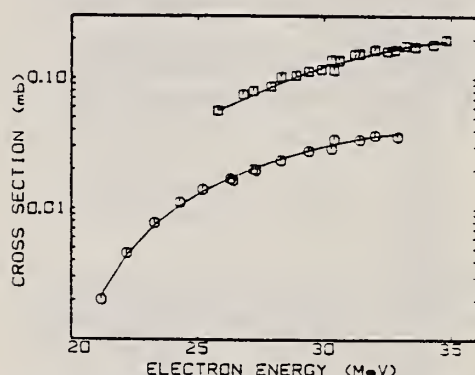


FIG. 3. $\sigma_{e, 2n}(E_0)$ for ^{63}Cu (circles) and the yield of electrodisintegration plus photodisintegration (squares). The smooth curves are the best fit to the data and were obtained by combining the histogram shown in Fig. 5 with the $E1$ virtual photon spectrum and the Davies-Bethe-Maximom (DBM) bremsstrahlung cross section in Eqs. (1) and (2).

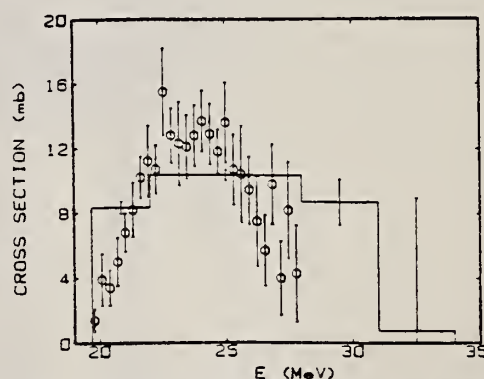


FIG. 5. $^{63}\text{Cu}(\gamma, 2n)$ cross section. The histogram is the result derived from this work and the points show the measurement of Fultz *et al.*¹

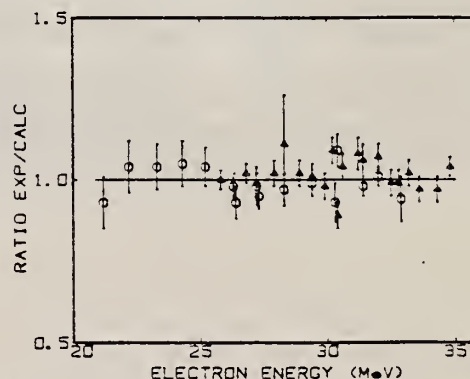


FIG. 6. Ratio of measured to calculated $(e, 2n)$ cross section (circles) and measured to calculated yield of electrodisintegration plus photodisintegration (triangles).

Cu
A=65

Cu
A=65

Cu
A=65

Ref. P. Erdos, P. Scherrer, P. Stoll
Helva. Phys. Acta 30, 639 (1957)

Elem. Sym.	A	Z
Cu	65	29

Method Betatron; α yield; radioactivity; $\text{Cu}^{65}(\gamma, n)$ reaction

Ref. No.	NVB
57 Er 1	

Reaction	E or ΔE	E_0	Γ	$\int \sigma dE$	$J\pi$	Notes
$\text{Cu}^{65}(\gamma, \alpha)$	Bremss. 32			10 ± 2 MeV-mb		Based on yield measurement.

Elem. Sym.	A	Z
Cu	65	29
Ref. No. 58 Be 1		EH

Method	Activation
1. <u>Preparation of the sample</u>	
2. <u>Preparation of the solution</u>	
3. <u>Preparation of the reagent</u>	
4. <u>Preparation of the standard</u>	
5. <u>Preparation of the blank</u>	
6. <u>Preparation of the control</u>	
7. <u>Preparation of the sample</u>	
8. <u>Preparation of the solution</u>	
9. <u>Preparation of the reagent</u>	
10. <u>Preparation of the standard</u>	
11. <u>Preparation of the blank</u>	
12. <u>Preparation of the control</u>	
13. <u>Preparation of the sample</u>	
14. <u>Preparation of the solution</u>	
15. <u>Preparation of the reagent</u>	
16. <u>Preparation of the standard</u>	
17. <u>Preparation of the blank</u>	
18. <u>Preparation of the control</u>	
19. <u>Preparation of the sample</u>	
20. <u>Preparation of the solution</u>	
21. <u>Preparation of the reagent</u>	
22. <u>Preparation of the standard</u>	
23. <u>Preparation of the blank</u>	
24. <u>Preparation of the control</u>	
25. <u>Preparation of the sample</u>	
26. <u>Preparation of the solution</u>	
27. <u>Preparation of the reagent</u>	
28. <u>Preparation of the standard</u>	
29. <u>Preparation of the blank</u>	
30. <u>Preparation of the control</u>	
31. <u>Preparation of the sample</u>	
32. <u>Preparation of the solution</u>	
33. <u>Preparation of the reagent</u>	
34. <u>Preparation of the standard</u>	
35. <u>Preparation of the blank</u>	
36. <u>Preparation of the control</u>	
37. <u>Preparation of the sample</u>	
38. <u>Preparation of the solution</u>	
39. <u>Preparation of the reagent</u>	
40. <u>Preparation of the standard</u>	
41. <u>Preparation of the blank</u>	
42. <u>Preparation of the control</u>	
43. <u>Preparation of the sample</u>	
44. <u>Preparation of the solution</u>	
45. <u>Preparation of the reagent</u>	
46. <u>Preparation of the standard</u>	
47. <u>Preparation of the blank</u>	
48. <u>Preparation of the control</u>	
49. <u>Preparation of the sample</u>	
50. <u>Preparation of the solution</u>	
51. <u>Preparation of the reagent</u>	
52. <u>Preparation of the standard</u>	
53. <u>Preparation of the blank</u>	
54. <u>Preparation of the control</u>	
55. <u>Preparation of the sample</u>	
56. <u>Preparation of the solution</u>	
57. <u>Preparation of the reagent</u>	
58. <u>Preparation of the standard</u>	
59. <u>Preparation of the blank</u>	
60. <u>Preparation of the control</u>	
61. <u>Preparation of the sample</u>	
62. <u>Preparation of the solution</u>	
63. <u>Preparation of the reagent</u>	
64. <u>Preparation of the standard</u>	
65. <u>Preparation of the blank</u>	
66. <u>Preparation of the control</u>	
67. <u>Preparation of the sample</u>	
68. <u>Preparation of the solution</u>	
69. <u>Preparation of the reagent</u>	
70. <u>Preparation of the standard</u>	
71. <u>Preparation of the blank</u>	
72. <u>Preparation of the control</u>	
73. <u>Preparation of the sample</u>	
74. <u>Preparation of the solution</u>	
75. <u>Preparation of the reagent</u>	
76. <u>Preparation of the standard</u>	
77. <u>Preparation of the blank</u>	
78. <u>Preparation of the control</u>	
79. <u>Preparation of the sample</u>	
80. <u>Preparation of the solution</u>	
81. <u>Preparation of the reagent</u>	
82. <u>Preparation of the standard</u>	
83. <u>Preparation of the blank</u>	
84. <u>Preparation of the control</u>	
85. <u>Preparation of the sample</u>	
86. <u>Preparation of the solution</u>	
87. <u>Preparation of the reagent</u>	
88. <u>Preparation of the standard</u>	
89. <u>Preparation of the blank</u>	
90. <u>Preparation of the control</u>	
91. <u>Preparation of the sample</u>	
92. <u>Preparation of the solution</u>	
93. <u>Preparation of the reagent</u>	
94. <u>Preparation of the standard</u>	
95. <u>Preparation of the blank</u>	
96. <u>Preparation of the control</u>	
97. <u>Preparation of the sample</u>	
98. <u>Preparation of the solution</u>	
99. <u>Preparation of the reagent</u>	
100. <u>Preparation of the standard</u>	
101. <u>Preparation of the blank</u>	
102. <u>Preparation of the control</u>	
103. <u>Preparation of the sample</u>	
104. <u>Preparation of the solution</u>	
105. <u>Preparation of the reagent</u>	
106. <u>Preparation of the standard</u>	
107. <u>Preparation of the blank</u>	
108. <u>Preparation of the control</u>	
109. <u>Preparation of the sample</u>	
110. <u>Preparation of the solution</u>	
111. <u>Preparation of the reagent</u>	
112. <u>Preparation of the standard</u>	
113. <u>Preparation of the blank</u>	
114. <u>Preparation of the control</u>	
115. <u>Preparation of the sample</u>	
116. <u>Preparation of the solution</u>	
117. <u>Preparation of the reagent</u>	
118. <u>Preparation of the standard</u>	
119. <u>Preparation of the blank</u>	
120. <u>Preparation of the control</u>	
121. <u>Preparation of the sample</u>	
122. <u>Preparation of the solution</u>	
123. <u>Preparation of the reagent</u>	
124. <u>Preparation of the standard</u>	
125. <u>Preparation of the blank</u>	
126. <u>Preparation of the control</u>	
127. <u>Preparation of the sample</u>	
128. <u>Preparation of the solution</u>	
129. <u>Preparation of the reagent</u>	
130. <u>Preparation of the standard</u>	

Ref. No.	
58 Be 1	EH

Reaction	E or ΔE	E_0	Γ	$\int \sigma dE$	$J\pi$	Notes
(γ, n)						$E_{th} = 9.89 \pm 0.11$ based on (γ, n) thresholds in F^{19} , N^{14} and C^{12} .

Method

Bremss.; activation

Ref. No.

60 Ai 1

JHL

Reaction	E or ΔE	E_0	Γ	$\int \sigma dE$	$J\pi$	Notes
$(\gamma, 3n)$	Bremss.; $E_{\gamma\max} = 28.8-110\text{MeV}$	$33 \pm 2 \text{ MeV}$		$0.037 \pm 0.004 \int_0^{110} \text{MeV-barn}$		Determined ratio of Cu^{62} produced by $\text{Cu}^{63}(\gamma, n)$ and $\text{Cu}^{65}(\gamma, 3n)$ in normal copper as function of bremsstrahlung energy. See Table II.

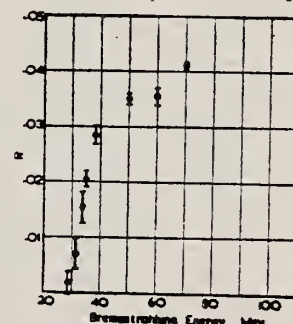


FIG. 1. $\text{Cu}^{63}(\gamma, 3n)\text{Cu}^{62}$ yield curve: R is the ratio of Cu^{62} activity induced in equal weights of Cu^{63} and Cu^{65} .

TABLE I. The ratio of Cu^{62} activities produced in Cu^{63} and Cu^{65} by bremsstrahlung beams.

Bremsstrahlung energy Mev	Ratio of activity in copper and Cu^{63} $\text{Cu}^{62}/\text{Cu}^{65}$
110	0.0444 ± 0.0007
70	0.0411 ± 0.0007
60	0.0356 ± 0.0017
50	0.0350 ± 0.0010
38.2	0.0285 ± 0.0017
35	0.0205 ± 0.0014
33.8	0.0070 ± 0.0028
28.8	0.0017 ± 0.0021

TABLE II. Error introduced into absolute intensity calibration of bremsstrahlung beams by the $\text{Cu}^{63}(\gamma, 3n)\text{Cu}^{62}$ reaction when $\text{Cu}^{65}(\gamma, 3n)$ is not allowed for.

Bremsstrahlung energy Mev	Error %
40	0.9 ± 0.2
50	1.1 ± 0.2
70	1.3 ± 0.2
110	1.4 ± 0.2

Ref. E.C. Booth
Nuclear Phys. 19, 426 (1960)

Elem. Sym.	A	Z
Cu	65	29

Method Van de Graaff; electron brems.; Ring scatterer; NaI

Ref. No.	JHH
60 Bo 3	

Reaction	E or ΔE	E_0	Γ	$\int \sigma dE$	$J\pi$	Notes
(γ, γ)	Bremss. 0.5-2.2	0.77			3/2	Mean lifetime τ/g : $= (3.3)10^{-13} \text{ sec}$ [resonance scattering] where $g = (1+2I)/(1+2I_0)$. Detector at 100° .

Cu	65	29
----	----	----

METHOD	REF. NO.
Betatron; neutron threshold; ion chamber	60 Ge 3 NVB

REACTION	RESULT	EXCITATION ENERGY	SOURCE		DETECTOR		ANGLE
			TYPE	RANGE	TYPE	RANGE	
G,N	NØX	THR	C	THR	BF3-I		4 PI

THRESHOLD

TABLE I. Summary and comparison of neutron separation energies inferred from present threshold measurements with values predicted from mass data and reaction energies. All energies are expressed in the center-of-mass system in Mev.

Reaction	No. runs	Present results	Other results	Method	Reference
Cu ⁶⁶ (γ,n)Cu ⁶⁶	2	9.896 \pm 0.028	9.913 \pm 0.006 9.89 \pm 0.11	mass data threshold	1 1

1 K. S. Quisenberry, T. T. Scolman, and A. O. Nier, Phys. Rev. 104, 461 (1956).
 2 See reference 2.
 3 See reference 3.

Ref. N.V. Lin'kova, R.M. Osokina, B.S. Ratner, R.Sh. Amirov
V.V. Akindinov
Zhur. Eksp. i Teoret. Fiz. 38, 780 (1960)
Soviet Phys. JETP 11, 566 (1960)

Elem. Sym.	A	Z
Cu	65	29
Ref. No.		
60 Li 1		
JHH		

Method
Bremss.; emulsions

Reaction	E or ΔE	E_0	Γ	$\int \sigma dE$	$J\pi$	Notes
(γ, p)	12-28			190 MeV-mb		<p>Integrated cross section based on (γ, p) of 27 mb at peak (See Figures 4 and 5).</p> <p>Angular distribution fitted to $I(\theta) = a + b \sin^2\theta + c \sin^2\theta \cos\theta$.</p>

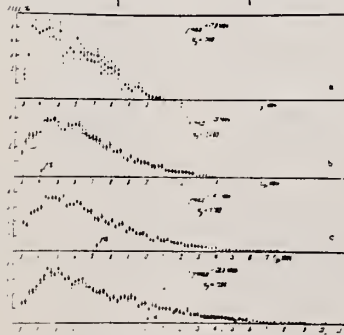


FIG. 2. Energy distributions of photoelectrons from Cu for different values of E_γ . Statistical errors are indicated.

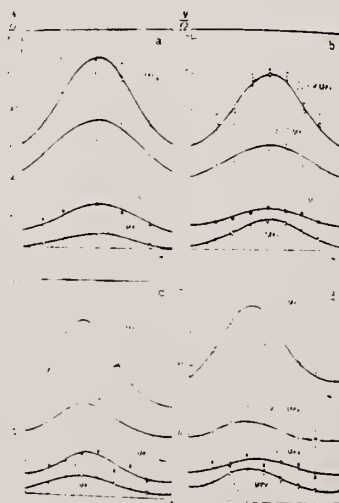


FIG. 3. Angular distributions of photoelectrons from Cu for different values of E_γ . (a) 17.9 MeV, (b) 20.3 MeV, (c) 24.5 MeV, (d) 28.5 MeV. The number of protons with energies E_p is taken as 100. Statistical errors are indicated.

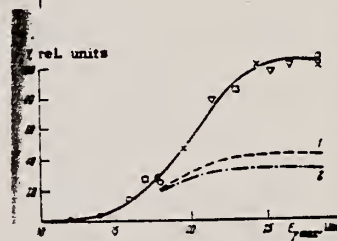


FIG. 4. Cu photo-proton yield as a function of $E_{\gamma \max}$. Different symbols represent different sets of data. The broken lines were calculated from the statistical model: curve 1 for $a = 16 \text{ MeV}^{-1.18}$, curve 2 for $a = 8 \text{ MeV}^{-1.16}$.

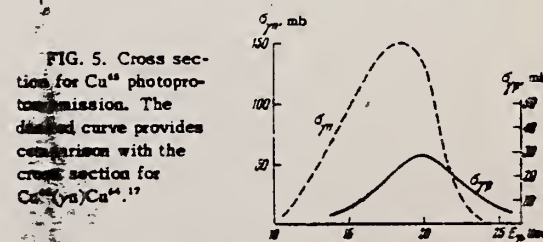


FIG. 5. Cross section for Cu photo-proton emission. The dashed curve provides comparison with the cross section for $\text{Cu}^{64}(\gamma)\text{Cu}^{64}$.¹⁷

Parameters in the Angular Distribution of Protons.

E_p , Mev	$E_{\gamma \max} = 17.9$ Mev	20.9 Mev	24.5 Mev	28.5 Mev		
	b/a	b/a	b/a	c/b	b/a	c/b
> 4	0.81	0.68	0.76	0.79	0.52	0.86
4-7	0.50	0.87	0.40	0.83	0.44	0.19
7-9	1.60	0.75	1.00	0.89	0.47	0.52
> 9	83	10.0	1.90	0.87	1.23	0.91

Ref. G.E. Coote, W.E. Turchinetz, I.F. Wright
Nuclear Phys. 23, 468 (1961)

Elem. Sym.	A	Z
Cu	65	29

Method

$\text{Li}^7(p,\gamma)$ source; activation; NaI

Ref. No.

61 Co 2

JHH

Reaction	E or ΔE	E_0	Γ	$\int \sigma dE$	$J\pi$	Notes
(γ, n)						$\sigma = 70 \pm 7$ mb relative to 59 ± 6 mb for $\text{Cu}^{63}(\gamma, n)$, measured for 440 kev (E_p resonance radiation from Li^7).

Ref. V.P. Chizhov, A.P. Komar, L.A. Kulchitsky, A.V. Kulikov,
E.D. Makhnovsky, Yu.M. Volkov
Nuclear Phys. 5, 562 (1962)

Elem. Sym.	A	Z
Cu	65	29

Method	Ref. No.
90 MeV Synchrotron; magnetic spectrometer; emulsions; NaI counter telescope	62 Ch 2 JHH

Reaction	E or ΔE	E_0	Γ	$\int \sigma dE$	$J\pi$	Notes
	Bremss.					
(γ, d)	34					
(γ, p)	70					
	90					

TABLE I
Experimental data

Elements	$E_{\gamma, max}$ (MeV)	Particle energy interval (MeV)	$Y(\gamma, d)$ $Y(\gamma, p)$	θ	Method
$Li^{6,7}$	30	7.5 to 15	0.008 ± 0.008	90°	I
	43		0.007 ± 0.006		
	90		0.097 ± 0.014		
Li^7	25		0.030 ± 0.030	90°	I
	43	7.5 to 15	0.056 ± 0.006		
	90		0.160 ± 0.054		
Be^9	40	7.5 to 19	0.006 ± 0.008	90°	I
Al^{27}	36	3.9 to 10	0.008 ± 0.007	$50^\circ + 130^\circ$	II
Ca^{40}	36	2.7 to 10	0.036 ± 0.017	$30^\circ + 160^\circ$	II
	34	4.5 to 15	0.097 ± 0.008	90°	I
	34	7.5 to 15	0.007 ± 0.008	90°	I
$Cu^{63,65}$	70	3 to 10	0.08 ± 0.01	$30^\circ + 80^\circ$	II
	70	4 to 10	0.04 ± 0.01	$30^\circ + 80^\circ$	II
	90	7 to 19	0.021 ± 0.006	90°	I

I: Scintillation telescope method.
II: Method of deflecting charged particles in magnetic field.

Ref. D.K. Kaipov, R.B. Begzhanov, A.V. Kuz'minov, Yu.K. Shubnyi
Zhur. Eksp. i Teoret. Fiz. 44, 1811 (1963)
Soviet Phys. JETP 17, 1217 (1963)

Elem. Sym.	A	Z
Cu	65	29
Ref. No. 63 Ka 1		JHH

Method Gaseous radioactive source; resonance scattering; NaI

Reaction	E or ΔE	E_0	Γ	$\int \sigma dE$	$J\pi$	Notes
Cu ⁶⁵ (γ, γ)	1.114	1.114	$\Gamma_\gamma =$ 1.01×10^{-3} eV		$(\frac{5}{2})^-$	Mean resonance scattering cross section: $\bar{\sigma}(1.114 \text{ MeV}) = (1.42 \pm 0.14) 10^{-26} \text{ cm}^2$ The measured Γ_γ infers a lifetime: $\tau_\gamma = (6.5 \pm 1.6) 10^{-13} \text{ sec.}$ for 1.114 MeV state. Detector at $\sim 108^\circ$

REF.

G.B. Beard
Phys. Rev. **135**, B577-80 (1964)

ELEM. SYM.	A	Z
Cu	65	29

METHOD	REF. NO.	
Radioactive source Ni ⁶⁵ ; self-absorption	64 Be 6	NVB

REACTION	RESULT	EXCITATION ENERGY	SOURCE		DETECTOR		ANGLE
			TYPE	RANGE	TYPE	RANGE	
G, G	LFT	1	D	1	NAI-D		DST
		(1.114)		(1.114)			

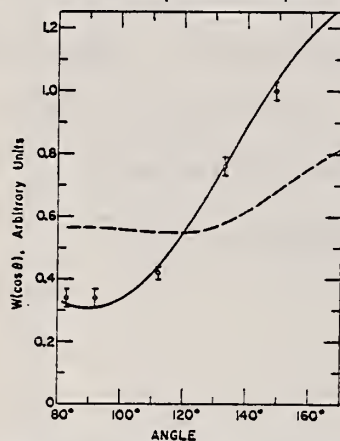


FIG. 2. Angular-correlation data. The solid curve represents the fit of the data for $A_2 = 1.02$ and $A_4 = 0.07$. The dashed curve shows the theoretical angular distribution, corrected for the finite angular resolution, for the assumption of pure $E2$ transitions for a spin sequence of $\frac{3}{2} - \frac{1}{2} - \frac{3}{2}$. The two curves are normalized at 120° .

MIXING RATIO

TABLE II. Measured values of the total lifetime τ .

τ (10^{-13} sec)	Method	Reference
$5.3_{-0.04}^{+0.08}$	Doppler shift	Eswaran <i>et al.</i> (Ref. 8)
4.4 ± 1.1	Resonance fluorescence	This work
6.5 ± 1.6	Resonance fluorescence	Kaipov <i>et al.</i> (Ref. 9)

$$W(\cos \theta) = 1 + A_2^2 P_2(\cos \theta) + A_4^2 P_4(\cos \theta)$$

TABLE III. Summary of properties of the 1.114-MeV state. Rows 7 and 8 give the ratio of the observed transition probabilities to the Weisskopf estimate* for the $E2$ and $M1$ transitions, respectively. ($R = 1.2A^{1/3} \times 10^{-13}$ cm.)

$$\begin{aligned}
 B(E2) \downarrow &= (0.019 \pm 0.001) e^2 \times 10^{-48} \text{ cm}^4 \\
 \tau(E2) &= (2.60 \pm 0.14) \times 10^{-12} \text{ sec} \\
 B(M1) \downarrow &= (0.065 \pm 0.008) (eh/2Mc)^2 \\
 \tau(M1) &= (6.7 \pm 0.8) \times 10^{-12} \text{ sec} \\
 \tau &= 5.3_{-0.4}^{+0.6} \times 10^{-12} \text{ sec} \\
 \Gamma &= 1.25_{-0.10}^{+0.08} \times 10^{-3} \text{ eV} \\
 T(E2)/T(E2)_w &= 12 \\
 T(M1)/T(M1)_w &= 0.034 \\
 \delta &= -0.51 \pm 0.03
 \end{aligned}$$

* D. H. Wilkinson in *Nuclear Spectroscopy*, edited by F. Ajzenberg-Selove (Academic Press Inc., New York, 1960), p. 858.

Van de Graaff; resonance fluorescence
 REF. NO. 64 Bo 1 NW3

REACTION	RESULT	EXCITATION ENERGY	SOURCE		DETECTOR		ANGLE
			TYPE	RANGE	TYPE	RANGE	
G.G	LFT	1-3	C	1 - 3	NAI-D		100
		(0.5 - 3.0)		(0.5 - 3.0)			

ABI

TABLE I
 Cases of observed resonance fluorescence

Nucleus multipol.	State (MeV)	Spin	Γ_0/Γ	$T(gw\Gamma_0^2/\Gamma^2)^{-1}$ (sec.)	Mean lifetime T ECW (sec)	Mean lifetime T other (sec)	Ref.	Γ_0/Γ_W ECW
Cu⁶⁵								
M1	0.96	$\frac{1}{2}^-$	1	$67 \pm 20 \times 10^{-14}$	$93 \pm 30 \times 10^{-14}$	$90 \pm 15 \times 10^{-14}$	20)	4.2×10^{-2}
[M1]	1.55	$[\frac{1}{2}^-]$?	$31 \pm 12 \times 10^{-14}$				$0.05\Gamma/\Gamma_0$

REF.

S.C. Fultz, R.L. Bramblett, J.T. Caldwell, R.R. Harvey
Phys. Rev. 133, B1149-54 (1964)

ELEM. SYM.

A

Z

Cu

65

29

METHOD

Positron Annihilation; ion chamber

[Page 1 of 2]

REF. NO.

64 Fu 1

NVB

REACTION	RESULT	EXCITATION ENERGY	SOURCE		DETECTOR		ANGLE
			TYPE	RANGE	TYPE	RANGE	
G,N 61+	ABX	10 - 28	D	10-28	EF3-I		4PI
G,2N 63+	ABX	16 - 28	D	10-28	BF3-I		4PI

Sample enriched to 99.7% Cu⁶⁵.

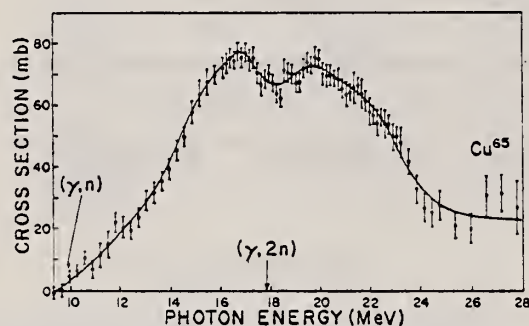


FIG. 6. Total cross section $[\sigma(\gamma, n) + 2\sigma(\gamma, 2n) + \sigma(\gamma, np)]$ for Cu⁶⁵ obtained from single-neutron counting data.

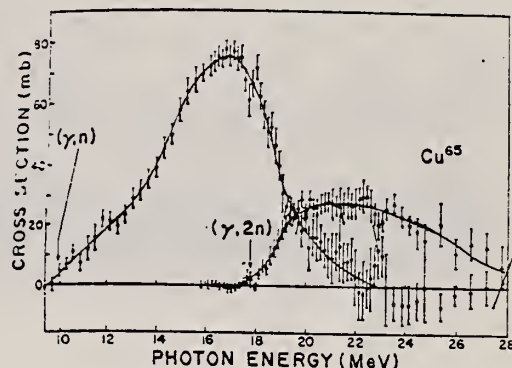


FIG. 7. Partial cross sections for Cu⁶⁵. The top curve consists of $\sigma(\gamma, n) + \sigma(\gamma, np)$. The lower curve consists of $\sigma(\gamma, 2n)$ and was obtained from double-neutron counting data.

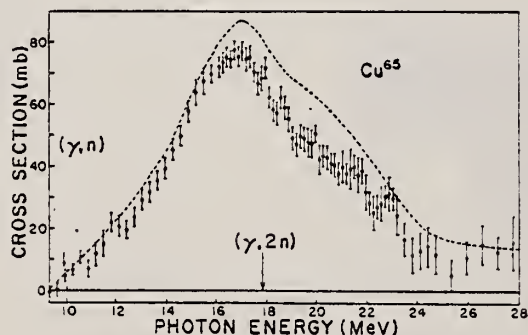


FIG. 8. The data points represent the sum $\sigma(\gamma, n) + \sigma(\gamma, np) + \sigma(\gamma, 2n)$. The dashed line represents the nuclear formation cross section $\sigma(\gamma, n) + \sigma(\gamma, 2n) + \sigma(\gamma, np) + \sigma(\gamma, p)$ for which the $\sigma(\gamma, p)$ data was obtained from Ref. 20.

REACTION	RESULT	EXCITATION ENERGY	SOURCE		DETECTOR		ANGLE
			TYPE	RANGE	TYPE	RANGE	

TABLE I. Integrated cross sections up to 28 MeV for copper isotopes.

Element	Reaction	Integrated cross section (MeV-mb)	Fraction of total integrated cross section	Total (MeV-mb)
Natural Cu	$(\gamma, n) + (\gamma, np)$	525 ± 52	0.67	787 ± 113
	$(\gamma, 2n)$	110 ± 11	0.14	
	$(\gamma, p)^a$	152 ± 50	0.19	
Cu ⁶³	$(\gamma, n) + (\gamma, np)$ + direct	523 ± 52	0.89	764 ± 09
	$(\gamma, 2n)$	80 ± 8	0.11	
	$(\gamma, np)^a$	115 ± 20	0.15	
	$(\gamma, p)^a$	161 ± 48	0.21	
	(γ, n)	344 ± 34	0.45	
	direct ^b	64 ± 22	0.08	
Cu ⁶⁵	$(\gamma, n) + (\gamma, np)$	437 ± 43	0.57	766 ± 103
	$(\gamma, 2n)$	195 ± 19	0.25	
	$(\gamma, p)^c$	134 ± 40	0.18	

^a Calculated from evaporation theory.
^b Estimated.
^c See Ref. 20.

TABLE II. Cross section for Li gamma rays.

Natural Cu $\sigma(\gamma, n)$ (mb)	Cu ⁶³ $\sigma(\gamma, n)$ (mb)	Cu ⁶⁵ $\sigma(\gamma, n)$ (mb)	Reference
55 ± 12	120 ± 30		a
	52 ± 11		b
	48 ± 8		c
85 ± 15	80 ± 14		d
64 ± 10	60 ± 9		e
	38 ± 6		f
	64 ± 4		g
	59 ± 6	70 ± 7	h
61 ± 6	55 ± 6	66 ± 6	Present work ⁱ

TABLE III. Quadrupole moments and Lorentz line parameters.

Nuclear shape	Isotope	E_α (MeV)	σ_α (mb)	Γ_α (MeV)	E_β (MeV)	σ_β (mb)	Γ_β (MeV)	Q_β (b)
Prolate	Cu ⁶³	16.00	48.5	3.5	19.0	44.5	7.5	1.1 ± 0.4
Spheroid	Cu ⁶⁵	16.00	54.7	4.2	19.25	62.0	7.5	1.2 ± 0.4
Oblate	Cu ⁶³	16.50	62.5	5.0	21.25	22.0	7.1	-1.4 ± 0.4
Spheroid	Cu ⁶⁵	16.75	87.5	5.0	20.5	36.4	6.0	-1.1 ± 0.4

TABLE IV. Integrated nuclear formation cross sections and σ_{-2} values.

Isotope	$\int_0^{28} \sigma dE$ (MeV-mb) ^a	$\int_0^{28} \sigma dE + W$ (MeV-mb) ^b	$0.06NZ/A$ (MeV-mb)	σ_{-2} (mb/MeV)	$0.00225 A^{5/3}$ (mb/MeV)
Cu ⁶³	764 ± 109	913 ± 121	939	2.1 ± 0.3	2.4
Cu ⁶⁵	766 ± 103	960 ± 124	964	2.6 ± 0.3	2.4

^a The integrated cross sections include estimated contributions from (γ, p) reactions.
^b The correction "W" is the sum of the high- and low-energy wing corrections to the area under the resonance curves for the oblate case.

REF. F. P. Denisov, A. Duisebaev, and P. A. Cerenkov
ZhETF Pis'ma 5, 249 (1967)
JETP Letters 5, 200 (1967)

ELEM. SYM.	A	Z
Cu	65	29

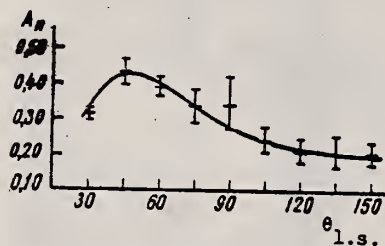
METHOD

REF. NO.

67 De 4

hmg

REACTION	RESULT	EXCITATION ENERGY	SOURCE		DETECTOR		ANGLE
			TYPE	RANGE	TYPE	RANGE	
G,N	NOX	THR-260	C	260	TRK-I		DST



Angular distributions of Cu^{64} recoil nuclei in the reaction
 $\text{Cu}^{65}(\gamma, n)\text{Cu}^{64}$

REF.

K. Abe, N. Kawamura, H. Nihei, H. Tsubota and N. Mutsuro
J. Phys. Soc. Japan 25, 1723 (1968)

ELEM. SYM.	A	Z
Cu	65	29

METHOD	REF. NO.	
	68 Ab 2	egf

REACTION	RESULT	EXCITATION ENERGY	SOURCE		DETECTOR		ANGLE
			TYPE	RANGE	TYPE	RANGE	
G, XP	SPC	THR-27 (26.6)	C	27	SCD-D	2-16	90

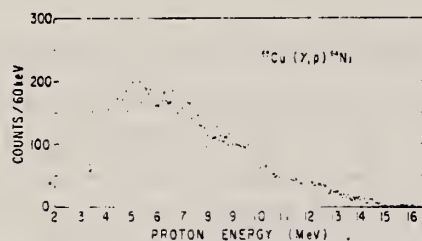


Fig. 2. Energy spectrum of photoprotons from ^{65}Cu at 90° , with bremsstrahlung end-point energy 26.6 MeV.

F. R. Metzger
Phys. Rev. 171, 1257 (1968)

ELEM. SYM.	A	Z
Cu	65	29
REF. NO.		
68 Me 3		egf

METHOD

REACTION	RESULT	EXCITATION ENERGY	SOURCE		DETECTOR		ANGLE
			TYPE	RANGE	TYPE	RANGE	
G,G	LFT	1	D	1	NAI-D		DST

Angular distribution gives E2/M1
 $\delta = -0.437 \pm 0.015$

 $1 = 1.116 \text{ MEV}$

TABLE II. Results of the self-absorption experiment.

Path length in Cu absorber (cm)	Resonant attenuation	Radiative width Γ^* (eV)
1.26	0.913 ± 0.006	$(1.62 \pm 0.13) \times 10^{-3}$
2.56	0.809 ± 0.014	$(1.89 \pm 0.15) \times 10^{-3}$

REF.

R. B. Begzhanov and S. M. Akhrarov
ZhETF Pis. Red. 10, 39 (1969)
JETP Letters 10, 26 (1969)

ELEM. SYM.	A	Z
Cu	65	29

METHOD

REF. NO.

69 Be 7

hmg

REACTION	RESULT	EXCITATION ENERGY	SOURCE		DETECTOR		ANGLE
			TYPE	RANGE	TYPE	RANGE	
G,G	LFT	6,8	D	6,8	D		DST
							(90,135)

Self-Absorption.

6.07, 8.50 MEV

Results of determination of the resonance-level parameters

Source-scatterer	E_{γ} , MeV	$\langle \sigma_{pp} \rangle$, mb	Γ_{γ_0} , eV	D, keV	Reference
Pb \rightarrow Zn ⁶⁴	7.38	33 \pm 4.5	0.58 \pm 0.12	53.70 \pm 0.13	This work
Ti \rightarrow Mo ⁹⁶	6.413	11.2 \pm 1.4	0.11 \pm 0.02	8.68 \pm 1.57	"
Ti \rightarrow La ¹³⁹	6.413	16.04 \pm 2.10	0.28 \pm 0.05	8.03 \pm 1.42	"
Ti \rightarrow Bi ²⁰⁹	7.15	1200 \pm 230	0.32 \pm 0.07	1.84 \pm 0.40	"
	6.996	1560	-	-	[1]
	7.15	2600 \pm 800	0.42 \pm 0.14	-	[5]
Ti \rightarrow Cu ⁶⁵	6.07	423 \pm 108	0.34 \pm 0.06	99.1 \pm 17.4	This work
	6.07	440 \pm 130	0.36 \pm 0.07	-	[5]
Ti \rightarrow Cu ⁶³	6.07	215 \pm 71	0.18 \pm 0.04	57.14 \pm 12.70	This work
	6.07	200 \pm 50	0.16 \pm 0.03	-	[6]
	8.50	22 \pm 7	0.25 \pm 0.08	130 \pm 40	This work
Cr \rightarrow Cu ⁶³	8.499	35	75	-	[1]
	8.50	19 \pm 6	0.28 \pm 0.09	-	[6]
	8.50	36 \pm 9	0.47 \pm 0.10	21.36 \pm 4.54	This work
Cr \rightarrow Cu ⁶⁵	8.499	80	10.5	-	[1]
	8.50	42 \pm 13	0.94 \pm 0.29	-	[6]
	7.01	1150 \pm 240	0.15 \pm 0.04	0.44 \pm 0.12	This work
Cu \rightarrow Sn ¹¹⁷	7.01	1000	-	-	[1]
	7.01	1200 \pm 400	0.3 \pm 0.3	-	[5]
Hg \rightarrow Mo ⁹⁶	6.44	201 \pm 37	0.12 \pm 0.04	0.23 \pm 3.07	This work

REF. I. Blomqvist, G. Nydahl and B. Forkman
Nucl. Phys. A162, 193 (1971)

ELEM. SYM.	A	Z
Cu	65	29
REF. NO.		
71 Bl 1		egf

METHOD

REACTION	RESULT	EXCITATION ENERGY	SOURCE		DETECTOR		ANGLE
			TYPE	RANGE	TYPE	RANGE	
G ₂ PI+	ABY	150-700	C	150-700	ACT-I		4PI

SEE 68 NY 1

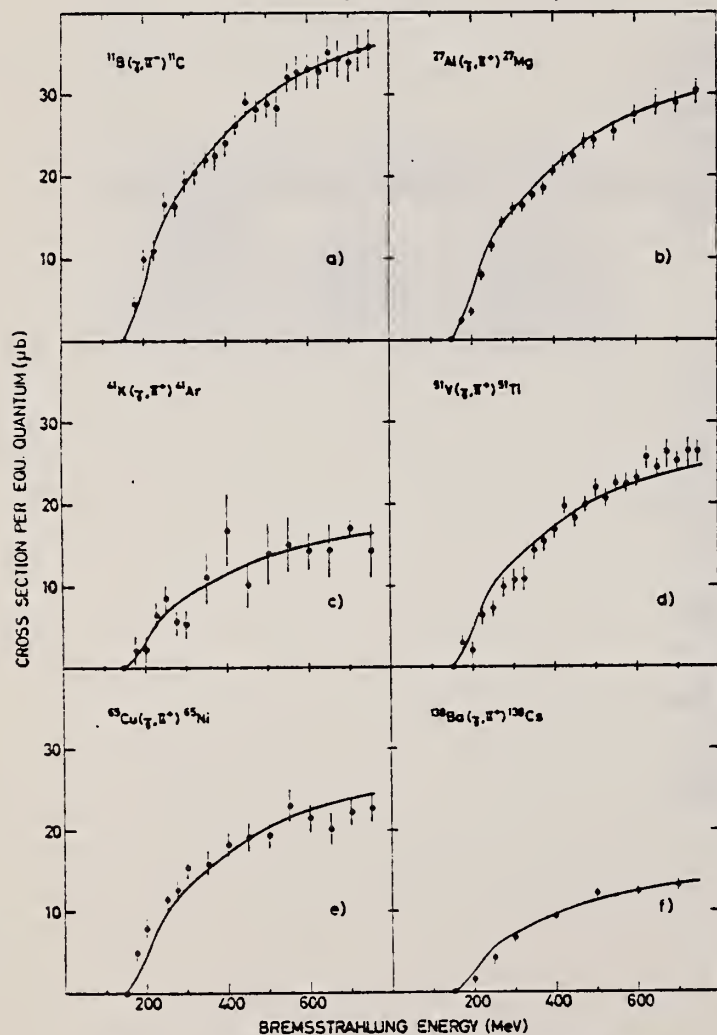


Fig. 2. Absolute yields for all but one of the measured reactions.

REF.

P. R. Oliva
Nuovo Cimento Lett. 1, 77 (1971)

ELEM. SYM.	A	Z
Cu	65	29

METHOD	REF. NO.	
	71 01 1	egf

REACTION	RESULT	EXCITATION ENERGY	SOURCE		DETECTOR		ANGLE
			TYPE	RANGE	TYPE	RANGE	
γ G,G	NOX	8	D	8	SCD-D		DST

 $\delta = 8.484 \text{ MEV}$

The results of the angular distribution measurement of the elastically scattered radiation in the $^{65}\text{Cu}(\gamma, \gamma)$ reaction ($E = 8484 \text{ keV}$) are shown in Fig. 2. A parametric plot of A_{22} and A_{44} vs. $\delta' = \delta/(1+|\delta|)$ is also reported. Two values for δ are consistent with these measurements. They are $\delta = -0.14 \pm 0.02$ and $\delta = 0.61 \pm 0.01$. The experimental asymmetry ratio is $K = 1.10 \pm 0.02$, which is only consistent with the value $K = 1.07$ calculated for $\delta = 0.61$ and for the resonant level spin value $j^\pi = 5/2^-$. Thus, the decay from this level to the $3/2^-$ ground state is an M1-E2 mixture, with mixing ratio $\delta^2 = 0.37 \pm 0.01$.

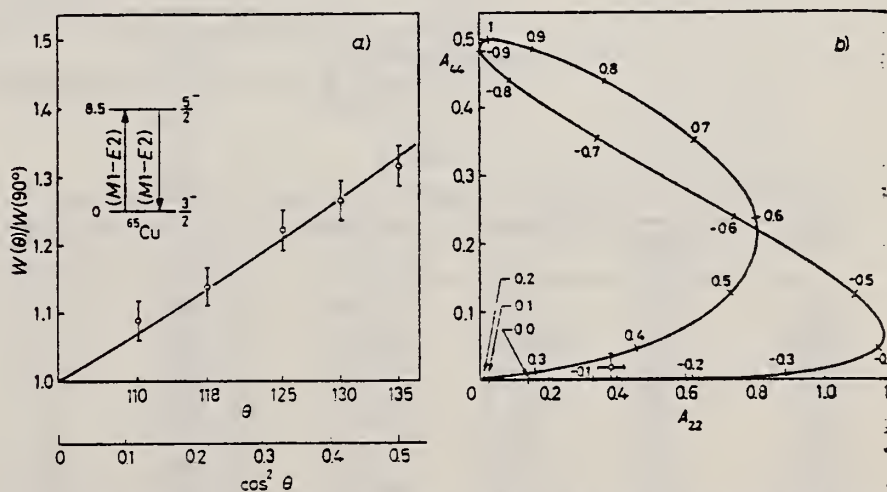


Fig. 2. - a) Angular distribution of resonantly scattered photons in ^{65}Cu . The solid line is the least-square fit through the data points. $\delta^2 = 0.37 \pm 0.01$, $W(\theta) = 1 + a \cos^2 \theta + b \cos^4 \theta$, $a = 0.56 \pm 0.04$, $b = 0.21$. b) Parametric plot of A_{22} and A_{44} vs. $\delta' = \delta/(1+|\delta|)$. The experimental values $A_{22} = 0.38 \pm 0.04$ and $A_{44} = 0.04$ are also shown.

REF.

A. Wolf, R. Moreh, and O. Shahal
Nucl. Phys. A227, 373 (1974)

ELEM. SYM.	A	Z
Cu	65	29

METHOD

REF. NO.

74 Wo 2

egf

REACTION	RESULT	EXCITATION ENERGY	SOURCE		DETECTOR		ANGLE
			TYPE	RANGE	TYPE	RANGE	
\$ G,G	LFT	6- 8	D	6- 8	SCD-D		DST

6. 556

 δ = Doppler width

TABLE 4

Upper limit of I'_0/I' , the temperature variation ratio R_T , and the self-absorption ratio R

Scatterer (γ -source)	E_0 (MeV)	I'_0/I' ($\pm 15\%$)	$R_T^{a)}$	$R(\%)^{b)}$
$^{65}\text{Cu}(\text{Ti})$	6.556	0.80	0.94 ± 0.02	1.1 ± 0.5
$^{69}\text{Ga}(\text{Cu})$	7.306	0.52	1.035 ± 0.004	3.5 ± 0.5
$^{100}\text{Mo}(\text{Cu})$	7.637	0.28	1.043 ± 0.007	0.8 ± 0.3
$^{100}\text{Mo}(\text{Ti})$	6.418	0.85	1.032 ± 0.003	0.6 ± 0.3
$^{118}\text{Sn}(\text{Cu})$	6.988	0.84	1.020 ± 0.009	5.7 ± 0.2
$^{126}\text{Te}(\text{Cu})$	7.915	0.4 ± 0.1	0.95 ± 0.05	6 ± 5
$^{130}\text{Te}(\text{Cu})$	7.637	0.45 ± 0.10	0.84 ± 0.05	0.9 ± 1.5
$^{139}\text{La}(\text{Cu})$	7.637	0.55	0.95 ± 0.01	2.2 ± 0.3
$^{139}\text{La}(\text{Ti})$	6.418	0.78	0.968 ± 0.008	6.4 ± 0.8
$^{141}\text{Pr}(\text{Cu})$	7.915	0.25	1.02 ± 0.01	0.9 ± 0.9
$^{141}\text{Pr}(\text{Cu})$	7.252	0.51	1.005 ± 0.003	5.9 ± 0.4
$^{144}\text{Nd}(\text{Cu})$	7.915	0.27	0.89 ± 0.05	< 0.5
$^{186}\text{W}(\text{Ti})$	6.418	0.31	1.030 ± 0.004	< 0.5
$^{203}\text{Tl}(\text{Ti})$	6.418	0.28	1.03 ± 0.01	1.6 ± 0.3
$^{205}\text{Tl}(\text{Cu})$	7.252	0.58	1.02 ± 0.01	1.6 ± 0.7
$^{209}\text{Bi}(\text{Cu})$	7.637	1.00	1.00 ± 0.02	2 ± 1
$^{209}\text{Bi}(\text{Ti})$	7.168	1.00	0.971 ± 0.005	28.0 ± 0.6

a) The values of R_T are given for 10 g/cm² thick scatterers placed at an angle of 60° and a detector angle of 135°.

b) The values of R are given for the same scatterer-detector geometry as that of R_T and a 20 g/cm² thick absorber.

TABLE 7

Summary of Γ , Γ_0 and δ of resonance levels measured in the present work and in earlier works ^{3, 16, 17)}

Isotope	Energy (MeV)	Γ (meV)	Γ_0 (meV)	δ (eV)	Ground state transition
^{65}Cu	6.556	70^{+60}_{-30}	28^{+15}_{-5}	11.2 ± 0.8	
$^{69}\text{Ga}^a)$	7.306	105 ± 40	48 ± 7	6.2 ± 0.5	E1
$^{100}\text{Mo}^c)$	7.637	140 ± 40	40 ± 5	4.5 ± 0.5	E1
$^{100}\text{Mo}^c)$	6.418	50 ± 35	25 ± 8	4.25 ± 0.25	E1
^{118}Sn	6.988	152 ± 5	128 ± 3	5.5 ± 0.5	E1
^{126}Te	7.915	12 ± 6	5 ± 2	11 ± 2	M1
^{130}Te	7.637	60 ± 30	30 ± 10	15 ± 2	E1
$^{139}\text{La}^b)$	7.637	170 ± 40	47 ± 6	10.5 ± 0.5	E1
$^{139}\text{La}^b)$	6.418	85^{+13}_{-7}	67 ± 8	9.5 ± 0.5	E1
$^{141}\text{Pr}^b)$	7.915	7 ± 3	2 ± 1	6.6 ± 1.0	M1
$^{141}\text{Pr}^b)$	7.252	290 ± 30	110 ± 10	6.4 ± 0.5	E1
$^{144}\text{Nd}^b)$	7.915	30 ± 10	8 ± 3	14.0 ± 0.5	M1
^{186}W	6.418	46 ± 35	6 ± 3	1 ± 1	E1
$^{203}\text{Tl}^b)$	6.418	350 ± 60	32 ± 15	0.5 ± 0.5	
$^{205}\text{Tl}^b)$	7.252	50 ± 30	25 ± 6	5.2 ± 1.5	M1
^{209}Bi	7.637	> 500	> 30		
$^{209}\text{Bi}^b)$	7.168	820 ± 40	820 ± 40	5.8 ± 0.8	E1

a) Ref. 16).

b) Ref. 8).

c) Ref. 17).

[over]

TABLE 6
Values of A_2 , N_{\parallel}/N_{\perp} , spins, and mixing amplitudes x

Scatterer (γ -source)	E_0 (MeV)	A_2	N_{\parallel}/N_{\perp}	J_0^{π}	J^{π}	J_f^{π}	x
$^{65}\text{Cu}(\text{Ti})$	6.556	0		$\frac{3}{2}^-$	$\frac{1}{2}^+$	$\frac{3}{2}^-$	0
$^{69}\text{Ga}(\text{Cu})$	7.306	0.14 ± 0.01	1.046 ± 0.022	$\frac{3}{2}^-$	$\frac{1}{2}^+$	$\frac{3}{2}^-$	0
$^{100}\text{Mo}(\text{Cu})$	7.637	0.49 ± 0.05	1.17 ± 0.05	0^+	1^-	0^+	0
$^{100}\text{Mo}(\text{Cu})$	7.102 ^{a)}	0.013 ± 0.016		0^+	1^-	2^+	-0.06 ± 0.02 ^{b)}
$^{100}\text{Mo}(\text{Ti})$	6.418	0.52 ± 0.02	1.15 ± 0.03	0^+	1^-	0^+	0
$^{100}\text{Mo}(\text{Ti})$	5.355 ^{a)}	0.19 ± 0.08		0^+	1^-	2^+	0.21 ± 0.12 ^{b)}
$^{118}\text{Sn}(\text{Cu})$	6.988	0.48 ± 0.02	1.12 ± 0.05	0^+	1^-	0^+	0
$^{126}\text{Te}(\text{Cu})$	7.915	0.46 ± 0.11	0.86 ± 0.10	0^+	1^+	0^+	0
$^{130}\text{Te}(\text{Cu})$	7.637	0.48 ± 0.04	1.12 ± 0.04	0^+	1^-	0^+	0
$^{139}\text{La}(\text{Cu})$	7.637	0.16 ± 0.02	1.024 ± 0.015	$\frac{3}{2}^+$	$\frac{3}{2}^-$	$\frac{3}{2}^-$	0
$^{139}\text{La}(\text{Ti})$	6.418	0.093 ± 0.004	1.018 ± 0.006	$\frac{3}{2}^+$	$\frac{3}{2}^-$	$\frac{3}{2}^+$	0
$^{141}\text{Pr}(\text{Cu})$	7.915	0.41 ± 0.06	0.94 ± 0.03	$\frac{3}{2}^+$	$\frac{3}{2}^-$	$\frac{3}{2}^+$	0.26 ± 0.13 -0.08
$^{141}\text{Pr}(\text{Cu})$	7.252	0.23 ± 0.06	1.03 ± 0.02	$\frac{3}{2}^+$	$\frac{3}{2}^-$	$\frac{3}{2}^-$	0
$^{144}\text{Nd}(\text{Cu})$	7.915	0.50 ± 0.03	0.92 ± 0.09	0^+	1^+	0^+	0
$^{186}\text{W}(\text{Ti})$	6.418	0.49 ± 0.05	1.15 ± 0.06	0^+	1^-	0^+	0
$^{186}\text{W}(\text{Ti})$	6.296 ^{a)}	-0.011 ± 0.014		0^+	1^-	2^+	-0.10 ± 0.03 ^{c)}
$^{203}\text{Tl}(\text{Ti})$	6.418	0	1.01 ± 0.01	$\frac{1}{2}^+$	$\frac{1}{2}^-$	$\frac{1}{2}^-$	0
$^{203}\text{Tl}(\text{Cu})$	7.252	0.71 ± 0.08	0.90 ± 0.02	$\frac{1}{2}^+$	$\frac{3}{2}^+$	$\frac{1}{2}^+$	-0.25 ± 0.05
$^{205}\text{Tl}(\text{Cu})$	7.047 ^{a)}	-0.69 ± 0.03		$\frac{1}{2}^+$	$\frac{3}{2}^+$	$\frac{1}{2}^+$	0.33 ± 0.04
$^{209}\text{Bi}(\text{Cu})$	7.637	0.24 ± 0.04		$\frac{3}{2}^-$	$(\frac{3}{2})$	$\frac{3}{2}^-$	
$^{209}\text{Bi}(\text{Ti})$	7.168	0.20 ± 0.02	1.040 ± 0.015	$\frac{3}{2}^-$	$\frac{3}{2}^+$	$\frac{1}{2}^-$	

Errors refer to one standard deviation.

^{a)} Inelastic transitions.

^{b)} Ref. ¹⁷⁾.

^{c)} Ref. ¹⁵⁾.

TABLE 8
Values of Γ_i , D , k_{E1} and k_{M1}

E1 transitions					M1 transitions				
scatterer (γ -source)	$E_0 \rightarrow E_f$ (MeV)	Γ_i (meV)	D (eV)	k_{E1} (10^{-9} MeV^{-1})	scatterer (γ -source)	$E_0 \rightarrow E_f$ (MeV)	Γ_i (meV)	D (eV)	k_{M1} (10^{-9} MeV^{-1})
$^{62}\text{Ni}(\text{Fe})$ ^{a)}	7.646		12300		$^{126}\text{Te}(\text{Cu})$	7.915		260	
	$\rightarrow 1.172$	24		0.5		$\rightarrow 0.666$	2.5		
$^{69}\text{Ga}(\text{Cu})$	7.306		660		$^{141}\text{Pr}(\text{Cu})$	$\rightarrow 1.421$	1.7		
	$\rightarrow 0.572$	3.2		1.0		7.915		90	
	$\rightarrow 0.872$	2.7		0.9		$\rightarrow 1.298$	1.3		
$^{100}\text{Mo}(\text{Cu})$	7.637		670		$^{141}\text{Pr}(\text{Fe})$ ^{c)}	$\rightarrow 1.437$	0.8		
	$\rightarrow 0.535$	40		7.7		$\rightarrow 1.580$	1.4		
	$\rightarrow 1.063$	5.7		1.4		$\rightarrow 1.655$	1.0		
	$\rightarrow 1.461$	1.4		0.4		7.632		170	
$^{112}\text{Cd}(\text{Fe})$ ^{b)}	7.632		350		$^{144}\text{Nd}(\text{Cu})$	$\rightarrow 0.145$	5.6		
	$\rightarrow 0.617$	11		4		$\rightarrow 1.130$	6.4		
	$\rightarrow 1.223$	7.3		3.4		$\rightarrow 1.293$	0.4		
	$\rightarrow 1.429$	2		1		$\rightarrow 1.437$	5.6		
	$\rightarrow 1.468$	1.7		0.9		$\rightarrow 1.451$	6.3		
$^{130}\text{Te}(\text{Cu})$	7.637		360		$^{205}\text{Tl}(\text{Cu})$	$\rightarrow 1.582$	1.1		
	$\rightarrow 0.837$	16		5.5		7.915		380	
	$\rightarrow 1.589$	18		8.8		$\rightarrow 0.697$	13		
$^{139}\text{La}(\text{Cu})$	7.637		190		$^{209}\text{Bi}(\text{Cu})$	$\rightarrow 1.041$	2.7		
	$\rightarrow 1.384$	3		2.5		$\rightarrow 1.564$	6.2		
	$\rightarrow 1.538$	3		2.7		7.252		1200	
$^{141}\text{Pr}(\text{Cu})$	7.252		220			$\rightarrow 0.205$	4		
	$\rightarrow 0.146$	82		38					
	$\rightarrow 1.120$	8.6		6.5					
$^{186}\text{W}(\text{Cu})$	6.418		110						
	$\rightarrow 0.122$	12		14					

The values of D refer to an excitation energy E_0 .

^{a)} Ref. ¹⁾.

^{b)} Ref. ²⁹⁾.

^{c)} Ref. ³⁰⁾.

- 1) R. Moreh et al., Phys. Rev. C2 (1970) 1144
- 8) A. Wolf, et al., Phys. Rev. C6 (1972) 2276
- 15) R. Moreh et al., Phys. Lett. 33B (1971) 71
- 16) R. Moreh et al., Phys. Rev. C7 (1973) 1885
- 17) R. Moreh et al., Nucl. Phys. A217 (1973) 477
- 29) R. Moreh et al., Phys. Rev. C4 (1971) 2265
- 30) R. Moreh et al., Phys. Rev. 173 (1969) 1961

REF. M. Boivin, Y. Cauchois, Y. Heno, C. Schloesing-Moller,
V. Zecevic
C.R. Acad. Sc. Paris 281B, 201 (1975)

ELEM. SYM.	A	Z
Cu	65	29

METHOD

REF. NO.
75 Bo 11
egf

REACTION	RESULT	EXCITATION ENERGY	SOURCE		DETECTOR		ANGLE
			TYPE	RANGE	TYPE	RANGE	
G,G	LFT	0- 1	C	2	UKN		UKN

771 and 1115 KEV

TABLEAU

Niveau....	⁶³ Cu 670	⁶³ Cu 771	⁶³ Cu 962	⁶³ Cu 1115	¹¹⁵ In 1133	⁵⁹ Co 1190
τ (ps).....	0,28 ± 8 %	0,15 ± 12,5 %	0,76 ± 15 %	0,38 ± 14 %	0,094 ± 4,5 %	0,074 ± 3 %

REF. E. Wolyneć, G. Moscati, J. R. Moreira, O. D. Goncalves,
M. N. Martins
Phys. Rev. C11, 1083 (1975)

ELEM. SYM.	A	Z
Cu	65	29

METHOD

REF. NO.

75 Wo 2

hmg

REACTION	RESULT	EXCITATION ENERGY	SOURCE		DETECTOR		ANGLE
			TYPE	RANGE	TYPE	RANGE	
G, N *	RLY	20- 40	C	20- 40	ACT-I		4PI
G, 2N *	RLY	21- 38	C	21- 38	ACT-I		4PI

*RATIO (G,N)/(E,N)
**RATIO (G,2N)/(E,2N)

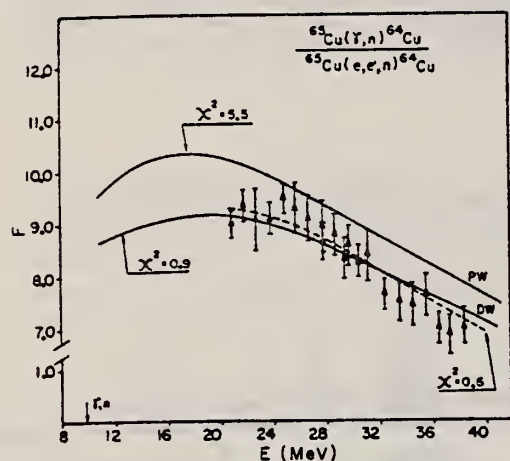


FIG. 4. Measured F for $^{65}\text{Cu}(\gamma, n)$. Dashed curve is a polynomial fit to the points. Full curves are F_{pw} and F_{dw} predictions.

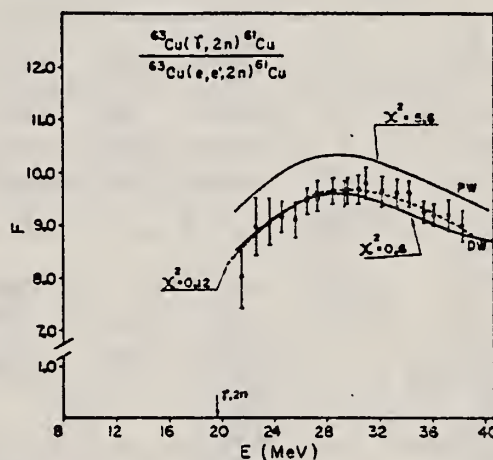


FIG. 5. Measured F for $^{63}\text{Cu}(\gamma, 2n)$. Dashed curve is a polynomial fit to the points. Full curves are F_{pw} and F_{dw} predictions.

$$F_{pw}^{(E)} = (N_r / Z_r^2 r_e^2 N_r)$$

$$\times \frac{\int_0^{E_1 - m_e} \sigma_\gamma(\omega) \phi(E_1, \omega, Z_r) (d\omega/\omega)}{\int_0^{E_1 - m_e} \sigma_\gamma(\omega) N_{pw}^{E_1}(E_1, \omega) (d\omega/\omega)}, \quad (10)$$

$$F_{dw}^{(E)} = (N_r / Z_r^2 r_e^2 N_r)$$

$$\times \frac{\int_0^{E_1 - m_e} \sigma_\gamma(\omega) \phi(E_1, \omega, Z_r) (d\omega/\omega)}{\int_0^{E_1 - m_e} \sigma_\gamma(\omega) N_{dw}^{E_1}(E_1, \omega, Z_r) (d\omega/\omega)}, \quad (11)$$

ELEM. SYM.	A	Z
Cu	65	29
REF. NO.		
76 Sw 7		hmg

REACTION	RESULT	EXCITATION ENERGY	SOURCE		DETECTOR		ANGLE
			TYPE	RANGE	TYPE	RANGE	
G, G	LFT	1- 5	C	1- 5	SCD-D		DST

The properties of levels in ^{63}Cu and ^{65}Cu have been investigated using the resonance fluorescence technique with bremsstrahlung serving as the source of exciting radiation. The energies and scattering cross sections for 24 levels in ^{63}Cu and 30 levels in ^{65}Cu up to about 4.5 MeV were measured. A few levels known to exist in the region of 2 MeV for both nuclei were not observed. For a number of the lower lying levels, spin and parity assignments have been made through angular distribution measurements and limits on J^π set by others. Mixing ratios for a few of these are also given. Where J^π and the ground state branching ratios are known the partial widths for decays to the ground state are presented. Comparisons are made with the predictions of the latest theoretical calculations.

30 LEV 1.48-4.53 MEV

TABLE II. Properties of levels in ^{65}Cu .

E_γ^a (keV)	J^π^b	$g\Gamma_0^2/\Gamma$ (meV)	Γ_0/Γ	Γ_0 (meV)
1481.7 ± 0.5	$\frac{1}{2}^-$	1.95(2)	0.85 ^c	1.15(12)
1624 ± 1	$\frac{3}{2}^-$	0.24(5)	0.57 ^d	0.28(6)
1724.9 ± 0.5	$\frac{3}{2}^- \dagger$	2.92(30)	0.74 ^d	3.95(40)
2090(6)*	$\frac{5}{2}^-, \frac{1}{2}^-$	<0.24		
2208(6)*	$\frac{1}{2}^-, \frac{3}{2}^-$	<0.24		
2276(6)*	$\frac{3}{2}^-, \frac{1}{2}^-$	<0.24		
2328.6 ± 1.0	$\frac{3}{2}^- \dagger$	6.5(7)	≤0.73 ^e	
2862.1 ± 1.0		11.8(12)		
2875.1 ± 1.0		13.5(14)		
2898 ± 2		3.0(9)		
3086 ± 2		3.2(9)		
3166.5 ± 1.0		20.7(21)		
3265 ± 2		3.6(12)		
3326.0 ± 1.0	$(\frac{3}{2}^-, \frac{5}{2}^-) \dagger$	20.6(21)		
3356 ± 2		2.3(8)		
3504 ± 2		6.8(14)		
3631 ± 2		7.1(12)		
3753 ± 2		6.4(22)		
3925 ± 2		6.3(16)		
3995 ± 2		12.2(20)		
3926 ± 2		19.2(19)		
3958 ± 2		30.3(30)		
4006 ± 2		9.9(34)		
4056 ± 2		48.3(48)		
4099 ± 2		18.2(24)		
4126 ± 2		37.8(38)		
4141 ± 2		42.4(42)		
4271 ± 2		29.7(44)		
4356 ± 2		20.8(34)		
4376 ± 2		15.3(34)		
4397 ± 2		67.6(77)		
4525 ± 2		84(16)		
4533 ± 2		43(10)		

TABLE III. Experimental A_2 values and resultant mixing ratios.

Nuclei	E_γ (keV)	J^π	A_2	δ
^{63}Cu	1547	$\frac{3}{2}^-$	0.58(9)	0.27(5), (1.7(2))
	2011	$\frac{3}{2}^-$	0.75(16)	0.41(14), 1.4(3)
	2977	$\frac{1}{2}^-, \frac{1}{2}^-, \frac{5}{2}^-$	-0.04(18)	
^{65}Cu	1725	$\frac{3}{2}^-$	0.39(7)	0.15(5), 1.8(8)
	2329	$\frac{3}{2}^-$	0.38(8)	0.15(6), 1.9(9)
	2862		0.09(28)	
	2875		0.43(24)	
	3166		-0.18(16)	
	3326	$\frac{3}{2}^-, \frac{5}{2}^-$	0.89(17)	0.9(5) if $\frac{3}{2}$

- ⁹S.C. Pancholi et al., Nucl. Data B2 (#6), 1 (1967).
¹¹T. Paradellis et al., Can. J. Phys. 50, 2728 (1972).
¹²R.L. Robinson et al., Nucl. Phys. A191, 225 (1972).

^a The energies indicated with an asterisk were taken from Ref. 9.

^b The values for J^π indicated with a dagger are from this study; the others were taken from Ref. 9.

^c This value for Γ_0/Γ was taken from Ref. 12.

^d These values for Γ_0/Γ were taken from Ref. 11.

^e This limit was obtained in this study where a branch is observed to the 771 keV $\frac{1}{2}^-$ level.

REF. V.N. Polishchuk, N.G. Shevchenko, N.G. Afanas'ev, A.A. Khomich,
I.I. Chkalov, & A.S. Litvinenko
Yad. Fiz. 26, 20 (July 1977)
Sov. J. Nucl. Phys. 26, 9 (July 1977)

ELEM. SYM.	A	Z
Cu	65	29

METHOD

REF. NO.

77 Po 3

hmg
11/18/80

REACTION	RESULT	EXCITATION ENERGY	SOURCE		DETECTOR		ANGLE
			TYPE	RANGE	TYPE	RANGE	
E, E/	FMF	0-5 (0.77-4.26)	D	120	MAG-D	---	DST

We report the results of an experimental study of low-lying states in ^{65}Cu by the method of inelastic scattering of electrons with energy $E_0 = 120$ MeV in the region of momentum transfer to the nucleus $q' = 0.78-1.15 \text{ F}^{-1}$. Values are obtained for the reduced transition probability $B(E\lambda)^\dagger$ from the ground state of the nucleus to excited states with $\omega = 0.77, 1.11, 1.48, 2.62, 3.16, 3.52, 3.85$, and 4.26 MeV.

8 STATES .77-4.26 MeV

TABLE I. Value of reduced probability $B(E\lambda)^\dagger$ for transition of the nucleus from the ground state to an excited state.

Nucleus	E, MeV	λ	I^π	$B(E\lambda)^\dagger, e^2 \text{ fm}^2 \lambda$		
				Our data (vibrational mode)	Data of Ref. 2	Data of Ref. 4
^{65}Cu	0.77	2	$1/2^-$	115 ± 15	117	100
	1.11	2	$3/2^-$	210 ± 25	351	280
	1.48	2	$5/2^-$	218 ± 25	364	340
	2.62	3	$(3/2^+)$	7482 ± 226	1815	
	3.16	3	$(3/2^+)_1$	4211 ± 463	891	
	3.52	3	$(1/2^+)$	4846 ± 533	1320	
	3.85	3	$(3/2^+)$	3665 ± 454	594	
	4.26	3	$(3/2^+)_2$	2260 ± 310	792	
^{66}Ni	1.32	2	2^+	661 ± 58 [16]		
	3.55	3	3^-	16800 ± 1200 [17]		
Sum of $B_2(E2)^\dagger$ $J = 1/2^-, 3/2^-, 5/2^-$				543 ± 37	832	720
Sum of $B_2(E3)^\dagger$ $J = (3/2^+), (3/2^+)_1, (1/2^+), (3/2^+)$				20200 ± 1110	4620	
Sum of $B_2(E3)^\dagger$ $J = (3/2^+), (3/2^+)_1, (1/2^+), (3/2^+)$				18420 ± 1090	4521	

Note. The values of $B(E\lambda)^\dagger$ from Ref. 2 were recalculated from the relation

$$R = \frac{B(E\lambda, J = 1, 2, 3, 4, 5, 6)}{B(E\lambda, J = 0, 1, 2, 3, 4, 5, 6)}$$

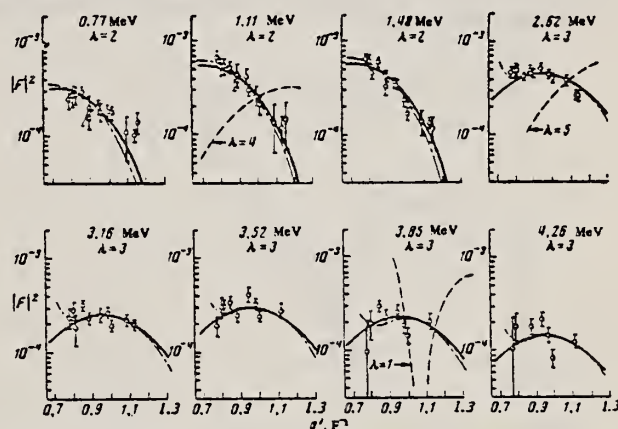


FIG. 2. Inelastic form factors as functions of the momentum transfer to the nucleus.

METHOD

REF. NO.

78 Ma 10

hg

REACTION	RESULT	EXCITATION ENERGY	SOURCE		DETECTOR		ANGLE
			TYPE	RANGE	TYPE	RANGE	
G,N	ABY	10-68	C	30-68	ACT -I		4PI

Analysis is made of reactions interfering with photon activation analysis procedures.

The activation yield curves have been presented for a number of photonuclear reactions in the energy range from 30 to 68 MeV, in order to evaluate quantitatively the interferences due to competing reactions in multielement photon activation analysis. The general features of the yields as functions of both target mass number and excitation energy were elucidated from the data obtained, discussion being given on the results in terms of the reaction mechanism.

Simultaneous neutron activation due to appreciable neutron production from the converter and surrounding materials has also been studied, and, finally, the magnitudes of interferences in real multielement analysis were given in the form of their energy dependences.

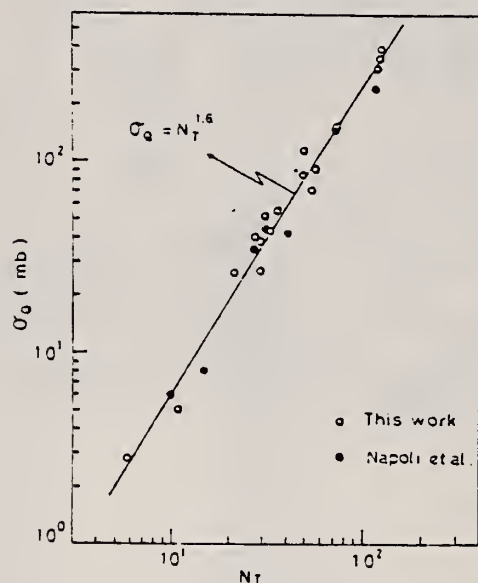


Fig. 2. Yield per equivalent quanta versus target neutron number.

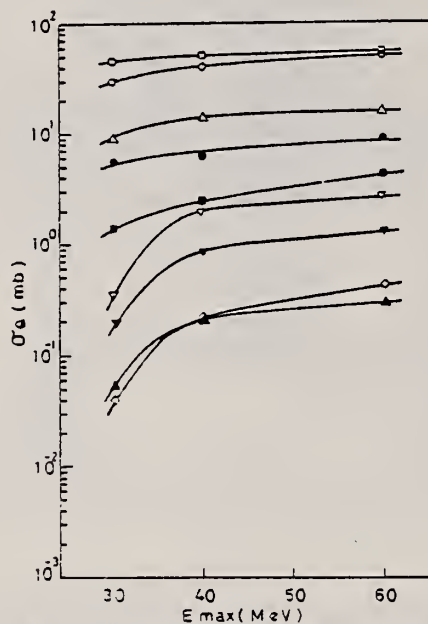


Fig. 6. Activation yield curves for the reactions on Co, Ni and Cu.

○ $^{59}\text{Co}(\gamma, n)^{58}\text{Co}$, ● $^{59}\text{Co}(\gamma, 2n)^{57}\text{Co}$, △ $^{58}\text{Ni}(\gamma, n)^{57}\text{Ni}$,
 ▽ $^{58}\text{Ni}(\gamma, pn)^{50}\text{Co}$, ▴ $^{58}\text{Ni}(\gamma, 2n)^{56}\text{Ni}$,
 □ $^{63}\text{Cu}(\gamma, n)^{62}\text{Cu}$, ▤ $^{63}\text{Cu}(\gamma, 2n)^{61}\text{Cu}$, ◇ $^{63}\text{Cu}(\gamma, xn)^{58}\text{Co}$.

[over]

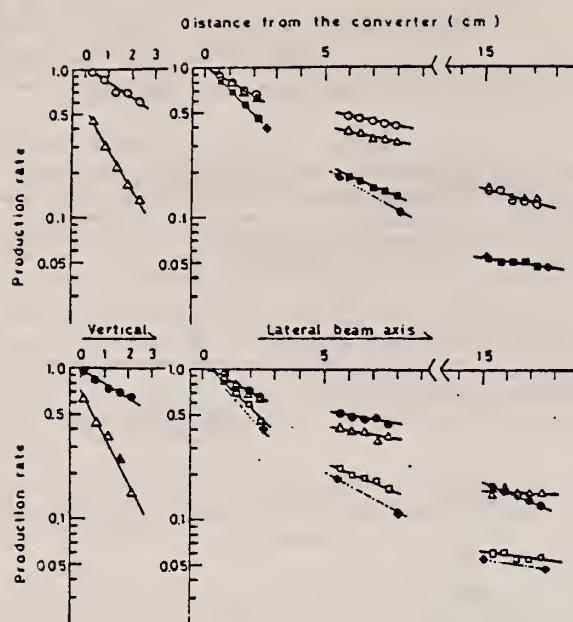


Fig. 13. Production rates of the neutron reactions and the photonuclear reactions as a function of distance from the converter in vertical and lateral directions
 \circ $^{55}\text{Mn}(n, \gamma)^{55}\text{Mn}$, \bullet $^{23}\text{Na}(n, \gamma)^{24}\text{Na}$, Δ $^{27}\text{Al}(n, \alpha)^{24}\text{Na}$,
 \blacksquare $^{55}\text{Mn}(\gamma, n)^{54}\text{Mn}$, \square $^{23}\text{Na}(\gamma, n)^{22}\text{Na}$, \blacklozenge $^{65}\text{Cu}(\gamma, n)^{64}\text{Cu}$.

R.O. Avakyan, A.É. Avetisyan, N.Z. Akopov, S.S. Danagulyan,
I.Kh. Kosakov, A.A. Oganesyan, Zh.V. Petrosyan, S.P. Taroyan,
G.M. Elbakyan
Sov. J. Nucl. Phys. 33, 192 (1981)
Yad. Fiz. 33, 362 (1981)

ELEM. SYM.	A	Z
Cu	65	29

METHOD

REF. NO.

81 Av 10

hg

REACTION	RESULT	EXCITATION ENERGY	SOURCE		DETECTOR		ANGLE
			TYPE	RANGE	TYPE	RANGE	
γ G, XP	RLX	0*2	D.	0*2	TEL-D		100

We report the results of a study of the reaction $\gamma A \rightarrow pX$ at an angle $\theta_{pp} = 100^\circ$ lab in a beam of quasimonochromatic polarized photons. The measurements were made for three values of photon energy ($E_\gamma = 0.69, 1.40$, and 1.95 GeV) in the nuclei ^{12}C , ^{64}Cu , and ^{207}Pb . The range of kinetic energies of the protons was ≈ 100 –230 MeV. It is shown that the slope parameter B for the invariant cross section $f = C \exp(-Bp^2)$ is a weak function of A and does not depend on E_γ , but the parameter $C_\gamma = C/A\bar{\sigma}$ increases with increase of E_γ , the slope of the lines $C_\gamma(E_\gamma)$ being greater for larger A .

COH-BRMS .69*1.95 GEV

PACS numbers: 25.20. + y, 13.60.Rj

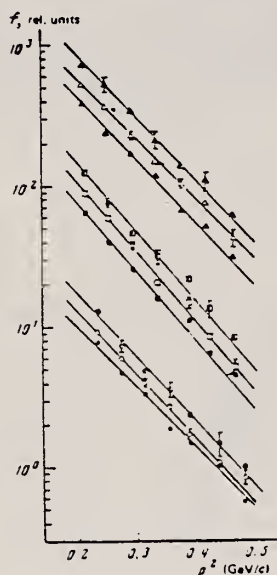


FIG. 2. Invariant cross sections f for photoproduction of cumulative protons as a function of their momentum squared for three target nuclei (^{12}C —lower family of points, ^{64}Cu —middle family of points, ^{207}Pb —upper family of points). The solid, hollow, and combined points correspond respectively to the values $E_\gamma = 0.69, 1.40$ and 1.95 GeV. The curves are described in the text.

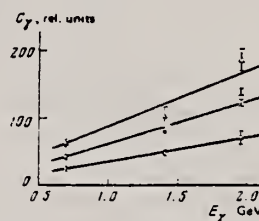


FIG. 3. The dependence of the parameter C_γ on E_γ . Points: \circ — ^{12}C , \square — ^{64}Cu , \triangle — ^{207}Pb .

TABLE II.

E_γ , GeV	Parameter	Nucleus		
		^{12}C	^{64}Cu	^{207}Pb
0.69	B	9.80 ± 0.51	11.01 ± 0.32	10.19 ± 0.36
	C	71.9 ± 11.9	663 ± 61	3252 ± 302
1.40	B	10.45 ± 0.31	11.21 ± 0.22	9.63 ± 0.45
	C	105.4 ± 9.9	973 ± 51	3858 ± 305
1.95	B	10.36 ± 0.49	11.14 ± 0.37	10.07 ± 0.31
	C	136.0 ± 29.6	1317 ± 140	6201 ± 430

Note. The parameter B is given in units of $(\text{GeV}/c)^{-2}$, while C is given in relative units.

TABLE I. Invariant cross section f (in relative units)

Nucleus	E_γ , GeV	T_p , MeV						
		116	125	133	173	199	210	230
^{12}C	0.69	7.35 ± 0.13	4.50 ± 0.10	3.40 ± 0.08	1.39 ± 0.05	1.55 ± 0.05	1.05 ± 0.04	0.75 ± 0.06
	1.40	9.15 ± 0.31	6.04 ± 0.30	4.04 ± 0.24	2.00 ± 0.19	1.64 ± 0.16	1.07 ± 0.12	0.85 ± 0.09
	1.95	13.12 ± 1.00	7.24 ± 0.71	4.91 ± 0.53	3.02 ± 0.46	2.31 ± 0.38	1.48 ± 0.29	1.00 ± 0.22
^{64}Cu	0.69	64.75 ± 0.89	39.86 ± 0.66	26.10 ± 0.55	15.97 ± 0.43	11.54 ± 0.33	6.49 ± 0.25	4.59 ± 0.20
	1.40	89.74 ± 2.32	54.13 ± 2.14	37.70 ± 1.73	21.15 ± 1.11	14.58 ± 1.05	8.57 ± 0.80	5.21 ± 0.61
	1.95	125.0 ± 6.63	77.7 ± 5.53	46.32 ± 4.11	31.61 ± 3.30	21.82 ± 2.44	13.42 ± 1.37	8.37 ± 1.42
^{207}Pb	0.69	392.7 ± 8.3	242.1 ± 5.4	172.5 ± 4.6	118.2 ± 3.7	66.8 ± 2.6	51.4 ± 2.2	31.2 ± 1.2
	1.40	529.3 ± 23.2	365.8 ± 17.3	229.2 ± 13.2	147.2 ± 9.9	108.2 ± 8.7	76.8 ± 7.0	42.8 ± 5.5
	1.95	734.0 ± 68.0	525.0 ± 50.6	338.6 ± 36.7	213.4 ± 29.3	137.4 ± 21.1	108.5 ± 16.9	62.4 ± 12.5

REF. R.O. Avakyan, A.É. Avetisyan, N.Z. Akopov, S.S. Danagulyan,
I.Kh. Kosakov, A.A. Oganessian, Zh.V. Petrosyan, S.P. Taroyan,
G.M. Elbakyan
Sov. J. Nucl. Phys. 33, 448 (1981)
Yad. Fiz. 33, 858 (1981)

ELEM. SYM.	A	Z
Cu	65	29
REF. NO.		
81 Av 13		hg

REACTION	RESULT	EXCITATION ENERGY	SOURCE		DETECTOR		ANGLE
			TYPE	RANGE	TYPE	RANGE	
\$ G,XP	ASM	0*2	C	0*2	UKN		100

COH-BRMS .69*1.95 GEV

At the present time it is rather well established that the experimental values of the invariant cross section $f = (E/p^2)(d^2\sigma/d\Omega dp)$ of the reaction

$$aA \rightarrow bX \quad (1)$$

in the cumulative region^{1,2} are described by an exponential dependence of the form $f = C \exp(-Bp^2)$. Most of the experiments in which reaction (1) induced by various particles (π , p , γ , ...), has been studied were designed to study the energy, angular, and A dependence of the parameters B and C .³⁻⁹ As a result of the investigations it is has been established that the parameter B does not depend on the mass number A of the target nucleus, on the type of incident particle, or on its energy, beginning with $E_a \approx 1$ GeV, while the parameter C , $C = C/\sigma_{\text{tot}}$ (σ_{tot} is the total cross section for the aA interaction) does not depend on the type of particle a . In addition to the established properties of the quantities B and C it would be interesting to check the dependence of the parameters B and C on the direction of polarization of the initial particle. For this purpose it is necessary to measure the asymmetry Σ of the cross section for reaction (1) as a function of the direction of the initial-particle polarization vector.

In the present work we report the results of a study of the photoproduction of cumulative protons at an angle $\theta_{\gamma p} = 100^\circ$ in the laboratory system in the nuclei ^{12}C , ^{64}Cu , and ^{207}Pb for three photon energy values ($E_\gamma = 0.69, 1.40$, and 1.95 GeV). The possibility of measurement at a definite photon energy was based on the use of the method of subtraction of the coherent peak^{10,11} in the spectrum of quasimonochromatic polarized photons emitted by electrons in passing through a diamond crystal.¹² The existence of a significant degree of polarization of the photons in the coherent

peak has enabled us to measure the value of the cross-section asymmetry Σ of the reaction $\gamma A \rightarrow pX$. The asymmetry was calculated from the relation

$$\Sigma = \frac{1}{\bar{P}} \frac{y^+ - y^-}{y^+ + y^- - 2y^*},$$

where y^+ , y^- are the reaction yields in the case of perpendicular and parallel orientation of the photon polarization vector with respect to the reaction plane in the coherent bremsstrahlung spectrum; y^* is the reaction yield for an ordinary bremsstrahlung spectrum; \bar{P} is the average value of photon polarization in the subtracted coherent peak.

Measurements of Σ were made in the nuclei ^{12}C , ^{64}Cu , and ^{207}Pb for protons with kinetic energy respectively $T_p = 173, 164$, and 163 MeV. The energy bin was $\Delta T = 60$ MeV.

The experimental apparatus and measurement technique have been described in detail elsewhere.¹³

Numerical values of Σ with their standard deviations $\sigma(\Sigma)$ are given in the table.

The values of $\sigma(\Sigma)$ contain both the statistical error and the error in determination of the quantity \bar{P} .¹³

From the figure, where we have shown Σ as a function of E_γ for the three nuclei it can be seen that the absolute values of the asymmetry in the region investigated are insignificant and depend weakly on E_γ . We note that Σ for carbon is close to zero for all E_γ , and the maximum value 0.29 ± 0.16 is achieved in the case of lead for $E_\gamma = 1.95$ GeV. The data show that within experimental error the asymmetry is almost indepen-

TABLE I.

E_γ , GeV	Nucleus					
	^{12}C		^{64}Cu		^{207}Pb	
	Σ	$\sigma(\Sigma)$	Σ	$\sigma(\Sigma)$	Σ	$\sigma(\Sigma)$
0.69	-0.0784	± 0.0233	-0.1539	± 0.0351	-0.1192	± 0.0323
1.40	0.0402	± 0.0386	0.0831	± 0.0369	-0.0796	± 0.0350
1.95	0.0530	± 0.0936	0.1858	± 0.1031	0.2931	± 0.1633

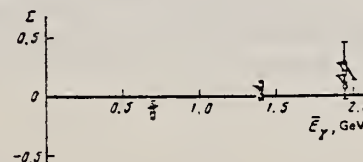


FIG. 1. Asymmetry Σ of the cross section for photoproduction of cumulative protons as a function of the photon energy E_γ for target nuclei ^{12}C (\circ), ^{64}Cu (\square), and ^{207}Pb (\triangle).

REF. Y. Cauchois, H. Ben Abdelaziz, R. Khérouf, C. Schloesing-Möller
J. Phys. G7, 1539 (1981)

ELEM. SYM.	A	Z
Cu	65	29
REF. NO.		
81 Ca 2		hg

METHOD

REACTION	RESULT	EXCITATION ENERGY	SOURCE		DETECTOR		ANGLE
			TYPE	RANGE	TYPE	RANGE	
G,G	LFT	1	C	0 - 2	SCD-D		
		(1.482)					

1.482 MeV

Abstract. Lifetimes of 49 excited states below 1.65 MeV have been measured in ^{24}Mg , ^{27}Al , ^{48}Ti , ^{58}Ni , ^{59}Co , $^{61,62}\text{Ni}$, $^{63,65}\text{Cu}$, $^{64,66,68}\text{Zn}$, ^{75}As , ^{103}Rh , $^{113,115}\text{In}$, $^{116,118,120}\text{Sn}$ and $^{121,123}\text{Sb}$ by means of nuclear resonance fluorescence experiments. The levels are excited by bremsstrahlung x-ray photons. The self-absorption technique applied to suitable cases provides nuclear absorption cross sections, widths and lifetimes from which the x-ray spectral distributions are also obtained. Scattering experiments are performed for all other cases in order to obtain widths and lifetimes from these x-ray photon curves. The Compton effect in the sample is taken into account. Self-absorption provides $g\Gamma_0$ from which Γ is deduced using adopted J^π and Γ_0/Γ values; scattering provides $u = g(\Gamma_0^2/\Gamma)W(\theta)$ from which Γ is also deduced with J , Γ_0/Γ and mixing ratios taken from the literature. Thanks to simultaneous determination of the x-ray spectra all the lifetimes as given by our programs with their statistical errors form an unusually coherent set of values.

NUCLEAR REACTIONS (γ , γ), bremsstrahlung excitation; natural isotopes: ^{24}Mg , ^{27}Al , ^{48}Ti , ^{58}Ni , ^{59}Co , $^{61,62}\text{Ni}$, $^{63,65}\text{Cu}$, $^{64,66,68}\text{Zn}$, ^{75}As , ^{103}Rh , $^{113,115}\text{In}$, $^{116,118,120}\text{Sn}$ and $^{121,123}\text{Sb}$; $E \approx 0.5\text{--}1.65$ MeV; measured $g\Gamma_0$ or $g(\Gamma_0^2/\Gamma)W(\theta)$; deduced $T_{1/2}$.

Tableau 2. Résultats des mesures des niveaux étudiés par self-absorption.

Table 2. Results obtained using the self-absorption method.

Isotope	Energie (keV)	J^π	J_0^π	Γ_0/Γ	$g\Gamma_0$ (meV) ce travail	τ (ps) ce travail	τ_{ref} (ps)	Références†
^{59}Co	1190.0(3)	0^-	0^-	1	11.3(5)	0.0729(32)	0.080(4)	Kim (1976)
^{63}Cu	669.62(5)	1^-	1^-	1	1.19(4)	0.277(10)	0.297(9)	Auble (1979b)
^{63}Cu	962.06(4)	1^-	1^-	1	1.25(6)	0.792(38)	0.851(43)	Auble (1979b)
^{63}Cu	1547.02(6)	1^-	1^-	0.803	2.6(1.7)	0.20(13)	0.160(16)	Auble (1979b)
^{63}Cu	770.6(2)	1^-	1^-	1	2.18(13)	0.151(9)	0.13(4)	Auble (1975a)
^{65}Cu	1115.54(4)	1^-	1^-	1	2.47(28)	0.400(45)	0.38(2)	Auble (1975a)
^{115}In	1132.57(3)	1^-	1^-	1	8.59(48)	0.0920(51)	0.092(5)	Cauchois <i>et al</i> (1977)
^{115}In	1463.5(12)	1^-	1^-	0.942	5.22(66)	0.095(12)	0.095(12)	Cauchois <i>et al</i> (1979)

† Références pour les colonnes 3, 4, 5 et 8 de ce tableau.

[over]

Tableau 3. Résultats des mesures des niveaux étudiés par diffusion.

Table 3. Results obtained using the diffusion method.

Isotope	Energie (keV)	J^π	J_0^π	Γ_0/Γ	δ	$u = g\Gamma_0^2/\Gamma W(\theta)$ (meV)	τ (ps) ce travail	τ_{ref} (ps)	Références †
²⁴ Mg	1368,59(4)	2 ⁺	0 ⁺	1	E2	1,08(13)	1,76(21)	1,98(4)	Endt et van der Leun (1978)
²⁷ Al	1014,45(3)	$\frac{1}{2}^+$	$\frac{1}{2}^+$	0,971	+ 0,351(12)	0,186(13)	2,20(16)	2,12(8)	Endt et van der Leun (1978)
⁴⁸ Ti	983,512(3)	2 ⁺	0 ⁺	1	E2	0,282(23)	6,74(55)	6,1(13)	Been (1978)
⁵⁸ Ni	1454,45(15)	2 ⁺	0 ⁺	1	E2	2,11(26)	0,90(11)	0,92(3)	Kocher et Auble (1976)
⁵⁹ Co	1099,224(25)	$\frac{1}{2}^-$	$\frac{1}{2}^-$	1	(E2)	0,069(8)	4,79(55)	3,17(58)	Kim (1976)
⁵⁹ Co	1453,8(3)	$\frac{1}{2}^-$	$\frac{1}{2}^-$	0,91	(E2)	0,68(8)	1,17(14)	1,52(16)	Kim (1976)
⁵⁹ Co	1480,9(3)	$\frac{1}{2}^-$	$\frac{1}{2}^-$	0,8	< 0,35 ^a	1,23(15)	0,254(31)	0,31(3)	Kim (1976)
⁶¹ Ni	1185,7(6)	$\frac{1}{2}^-$	$\frac{1}{2}^-$	0,77(8) ⁱ	[0,14]	1,88(49)	0,21(5)	0,16(3)	Andreev <i>et al</i> (1974)
⁶² Ni	1172,91(9)	2 ⁺	0 ⁺	1	E2	0,88(17)	2,15(42)	2,09(3)	Halbert (1979a)
⁶³ Cu	1327,00(7)	$\frac{1}{2}^-$	$\frac{1}{2}^-$	0,84	(E2)	1,04(14)	0,84(11)	0,88(4)	Auble (1979b)
⁶³ Cu	1412,05(4)	$\frac{1}{2}^-$	$\frac{1}{2}^-$	0,72	+ 0,61($\pm \frac{2}{3}$)	0,260(38)	1,90(28)	1,61(3)	Auble (1979b)
⁶⁴ Zn	991,54(7)	2 ⁺	0 ⁺	1	E2	0,640(54)	2,97(25)	2,60(13)	Halbert (1979b)
⁶⁵ Cu	1481,83(5)	$\frac{1}{2}^-$	$\frac{1}{2}^-$	0,85	(E2)	1,13(19)	0,79(13)	0,49(5)	Auble (1975a)
⁶⁶ Zn	1039,37(6)	2 ⁺	0 ⁺	1	E2	0,70(6)	2,71(23)	2,25(15)	Auble (1975b)
⁶⁸ Zn	1077,38(5)	2 ⁺	0 ⁺	1	E2	0,70(6)	2,71(23)	2,34(23)	Lewis (1975)
⁷⁵ As	572,5(10)	$\frac{1}{2}^-$	$\frac{1}{2}^-$	1 ^d	0,39 ^b	0,236(26)	4,14(46)	3,5(9)	Horen et Lewis (1975)
⁷⁵ As	823,0(10)	$\frac{1}{2}^-$	$\frac{1}{2}^-$	0,86 ^d	(E2)	0,214(22)	4,27(43)	3,5(3)	Robinson <i>et al</i> (1967)
⁷⁵ As	865,5(10)	$\frac{1}{2}^-$	$\frac{1}{2}^-$	0,83 ^d	— ^c	0,78(6)	0,863(68)	0,60(12)	Celliers <i>et al</i> (1977)
⁷⁵ As	1076,0(10)	$\frac{1}{2}^-$	$\frac{1}{2}^-$	0,94 ^d	0,38 ^d	1,97(13)	0,287(19)	0,32(7)	Celliers <i>et al</i> (1977)
⁷⁵ As	1128,5(10)	$\frac{1}{2}^-$	$\frac{1}{2}^-$	1	E1 ^d	0,224(24)	1,47(16)	—	
⁷⁵ As	1349,0(10)	$\frac{1}{2}^-$	$\frac{1}{2}^-$	0,67 ^d	0,20 ^d	1,61(29)	0,180(32)	0,12(3)	Wilson (1970)
⁷⁵ As	1370,0(10)	$\frac{1}{2}^-$	$\frac{1}{2}^-$	0,47 ^d	0,47 ^d	0,64(13)	0,218(44)	—	
¹⁰³ Rh	803,1(2)	$\frac{1}{2}^-$	$\frac{1}{2}^-$	0,70	M1	1,85(16)	0,174(15)	—	Harmatz (1979)
¹⁰³ Rh	1277,0(2)	$\frac{1}{2}^-$	$\frac{1}{2}^-$	0,75	- 0,62(30) ^e	0,81(9)	0,87(10)	1,3(9)	Harmatz (1979)
¹¹³ In	1177(1)	$\frac{1}{2}^-$	$\frac{1}{2}^-$	1	+ 0,5(2)	9,1(8)	0,086(8)	0,10(6)	Tuttle <i>et al</i> (1976)
¹¹³ In	1510(1)	$\frac{1}{2}^-$	$\frac{1}{2}^-$	0,935	- 0,5($\pm \frac{2}{3}$)	6,4(9)	0,071(10)	0,11($\pm \frac{2}{3}$)	Tuttle <i>et al</i> (1976)
¹¹⁵ In	1077,7(10)	$\frac{1}{2}^-$	$\frac{1}{2}^-$	0,81 ⁱ	(E2)	0,159(24)	1,61(24)	1,23(7)	Tuttle <i>et al</i> (1976)
¹¹⁵ In	1290,59(3)	$\frac{1}{2}^-$	$\frac{1}{2}^-$	0,98 ^j	(E2)	1,31(11)	0,66(6)	0,55(4)	Tuttle <i>et al</i> (1976)
¹¹⁵ In	1448,78(3)	$\frac{1}{2}^-$	$\frac{1}{2}^-$	0,86	- 8 ^f	0,90(11)	0,50(6)	0,52(20)	Tuttle <i>et al</i> (1976)
¹¹⁵ In	1486,1(1)	$\frac{1}{2}^-$	$\frac{1}{2}^-$	0,787	- 0,8 ^f	0,63(9)	0,63(9)	0,4(3)	Tuttle <i>et al</i> (1976)
¹¹⁵ In	1497,2(4)	($\frac{1}{2}^-$)	($\frac{1}{2}^-$)	< 1	(E2)	1,33(16)	< 0,30(4)	—	
¹¹⁵ In	1607,8(15)	($\frac{1}{2}^-$)	($\frac{1}{2}^-$)	< 1	(E2)	1,54(24)	≤ 0,26(4)	—	
¹¹⁶ Sn	1293,54(2)	2 ⁺	0 ⁺	1	E2	3,58(37)	0,53(6)	0,522(14)	Carlson <i>et al</i> (1975)
¹¹⁸ Sn	1229,64(4)	2 ⁺	0 ⁺	1	E2	2,75(28)	0,69(7)	0,67(2)	Carlson <i>et al</i> (1976)
¹²⁰ Sn	1171,6(2)	2 ⁺	0 ⁺	1	E2	1,83(16)	1,04(9)	0,91(2)	Kocher (1976)
¹²¹ Sb	1023,5(10)	$\frac{1}{2}^-$	$\frac{1}{2}^-$	1	[0,57] ^g	3,69(34)	0,228(21)	0,20(7) ^h	Tamura <i>et al</i> (1979)
¹²¹ Sb	1105,5(10)	$\frac{1}{2}^-$	$\frac{1}{2}^-$	0,4	—	0,47(4)	0,42(4)	—	
¹²¹ Sb	1142,5(10)	$\frac{1}{2}^-$	$\frac{1}{2}^-$	0,6	(E2)	0,85(8)	0,449(40)	0,41(8) ^h	Booth <i>et al</i> (1973)
¹²¹ Sb	1384,0(10)	$\frac{1}{2}^-$	$\frac{1}{2}^-$	1	0,451 ^g	4,7(5)	0,392(10)	0,088(14) ^h	Booth <i>et al</i> (1973)
¹²³ Sb	1029,5(10)	$\frac{1}{2}^-$	$\frac{1}{2}^-$	1	0,571 ^g	2,96(27)	0,272(25)	0,26(4) ^h	Booth <i>et al</i> (1973)
¹²³ Sb	1086,5(10)	$\frac{1}{2}^-$	$\frac{1}{2}^-$	1	$\delta > 1,26^g$	1,06(9)	0,67(6)	0,72(15) ^h	Booth <i>et al</i> (1973)

† Références pour les colonnes 3, 4, 5, 6 et 9 de chaque ligne, sauf indication appelée au bas de ce tableau. Pour les autres données se reporter au texte.

Remarque. Pour calculer ρ^2 quand nous ne disposons que de $B(E2)$, pour un mélange (E2) + (M1), nous déduisons $g\Gamma_0(E2) \propto B(E2)E_2^5$ en admettant $W(\theta) = 1$ et connaissant Γ_0/Γ , notre détermination de u donne une première approximation de $g\Gamma_0$ d'où une valeur de $\delta^2 = (g\Gamma_0(E2))/(g\Gamma_0 - g\Gamma_0(E2))$ qui permet d'améliorer $W(\theta)$ et $g\Gamma_0$ de proche en proche.

^a Swann (1971); ^b Robinson *et al* (1967); ^c $W(\theta) = 0,99$ calculé d'après la formule de Celliers *et al* (1977); ^d Abbondanno *et al* (1978); ^e Sayer *et al* (1972); ^f Tuttle *et al* (1976); ^g d'après $B(E2)$ de Barnes *et al* (1966); ^h calculé d'après Booth *et al* (1973); ⁱ Williams *et al* (1975); ^j Dietrich *et al* (1970).

METHOD

REF. NO.

82 Ma 3

egf

REACTION	RESULT	EXCITATION ENERGY	SOURCE		DETECTOR		ANGLE
			TYPE	RANGE	TYPE	RANGE	
E, α	ABX	7-34	D	14-34	ACT-I		4PI

The (e, α) cross section for ^{65}Cu has been measured in the electron energy range 14–34 MeV. The results have been analyzed using the distorted-wave Born approximation $E1$ and $E2$ virtual photon spectra and the $E1$ and $E2$ components of the corresponding (γ, α) cross section were obtained. To assess the accuracy of the virtual photon analysis, the $(e, 2n)$ cross section for ^{63}Cu was also measured and the obtained $(\gamma, 2n)$ cross section is compared with direct measurement of this cross section performed with annihilation gamma rays.

NUCLEAR REACTIONS $^{65}\text{Cu}(e, \alpha)$ and $^{63}\text{Cu}(e, 2n)$. Measured $\sigma_{e, \alpha}(E_0)$ and $\sigma_{e, 2n}(E_0)$. Deduced $\sigma_{\gamma, \alpha}^{E1}(E)$, $\sigma_{\gamma, \alpha}^{E2}(E)$, and $\sigma_{\gamma, 2n}^{E1}(E)$.

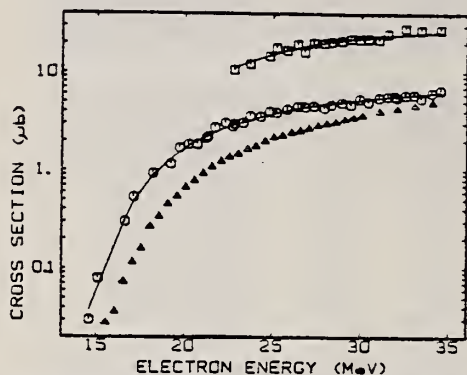


FIG. 4. $\sigma_{e, \alpha}(E_0)$ for ^{65}Cu (circles) and the yield of electrodisintegration plus photodisintegration (squares). The smooth curves are the best fit to the data and were obtained by combining the $E1$ and $E2$ histograms of Fig. 7 with the virtual photon spectra and the DBM bremsstrahlung cross section in Eqs. (1) and (2). The triangles show the (e, α) cross section from Ref. 6.

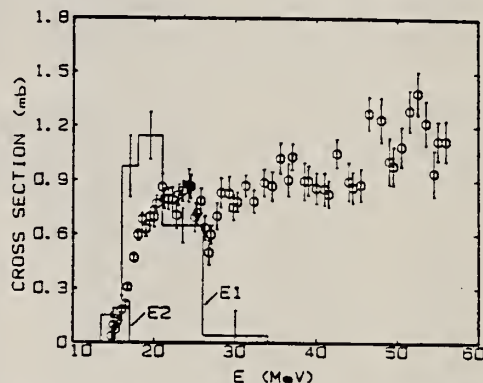


FIG. 7. $^{65}\text{Cu}(\gamma, \alpha)$ cross sections. The $E1$ and $E2$ histograms are the results from this work. The points show the (γ, α) cross section from Ref. 6.

TABLE III. (γ, α) strength for nuclei in the $A = 60$ region. $E1$ sum: $60 NZ/A$ MeV mb; $E2$ sum: $0.22Z^2 A^{-1/3}$ $\mu\text{b}/\text{MeV}$.

Nucleus	$\int_0^{30} \sigma_{\gamma, \alpha}(E) dE$ (MeV mb)	Fraction of $E1$ sum	Fraction of $E2$ sum	Ref.
^{56}Fe	21 ± 3	2.1 ± 0.3	7 ± 1	2
^{58}Ni	43 ± 4	3.9 ± 0.4	21 ± 3	1
^{59}Co	17 ± 2	1.7 ± 0.2	5 ± 1	2
^{60}Ni	41 ± 4	3.5 ± 0.4	21 ± 5	1
^{62}Ni	17 ± 2	1.5 ± 0.2	8 ± 2	1
^{64}Zn	78 ± 16	6.9 ± 1.5	25 ± 3	2
^{65}Cu	10 ± 1	1.0 ± 0.1	3 ± 1	This work

ZINC
Z=30

Zinc, in combination with copper, was known in Roman times as the alloy brass; the individual metal was not isolated until much later. The first smelting and extraction of the impure metal was carried out in China and India about 1000 A.D. Paracelsus (1490-1541) refers to zinc as a bastard form of copper. This is the earliest authenticated use of the word "zinc" to describe the metal.

Elem. Sym.	A	Z
Zn		30

Method $\text{Li}(p,\gamma)$ source; nuclear emulsions; G-M counters; $\text{Cu}^{63}(\gamma,n)$ reaction; flux calibration.

Ref. No.	
55 Dł 1	EGF

Reaction	E or ΔE	E_0	Γ	$\int \sigma dE$	$J\pi$	Notes
Zn (γ, p)	17.6					$\sigma = (4 \pm 2) 10^{-26} \text{ cm}^2$ Monitor in terms of counts on G-M counter which had been calibrated in terms of $\text{Cu}^{63}(\gamma,n)\text{Cu}^{62}$ (absolute counting and effective $\sigma \text{ Li} = 7.75 \times 10^{-26} \pm 15\% \text{ cm}^2$ given by Shimigu: [Mem. of Un. Kyoto <u>25</u> , 194 (1949)]

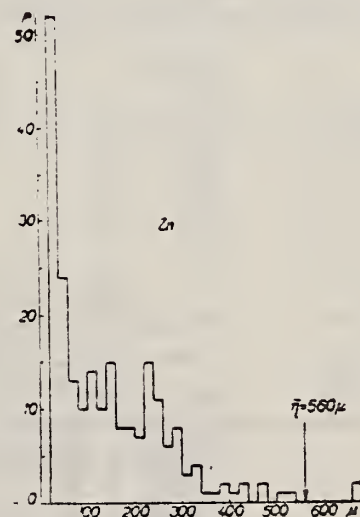


Рис. 4.

Ref. B.I. Gavrilov, L.E. Lazareva
 Zhur. eksp. i Teoret. Fiz. 30, 855 (1956);
 Soviet Phys. JETP 3, 871 (1957)

Elem. Sym.	A	Z
Zn		30
Ref. No.		EGF
56 Ga 1		

Method γ -Bremsstrahlung; synchrotron; BF₃ counter

Reaction	E or ΔE	E ₀	Γ	$\int \sigma dE$	$J\pi$	Notes <u>569</u>
(γ, xn)	$\sim 9-27$	16.3	6.3	0.66 MeV-b		

TABLE I. Fundamental characteristics of photoneutron cross sections.

Element	$E_{\gamma} \text{ max}$ in mev	$\sigma_{\gamma} \text{ max}$ in barns	Half width in mev	$\int_{E_{\gamma}}^{\infty} \sigma_{\gamma}(E) dE$ in mev-barns	$\int_{E_{\gamma}}^{\infty} \sigma_{\gamma}(E) dE / \sigma_{\gamma} \text{ max}$
Copper	17.2	0.126	4.3	0.33	7.4
Zinc	16.3	0.082	6.3	0.66	8.1
Cadmium	16.0	0.270	6.4	2.28	8.4
Iodine	15.5	0.288	6.0	2.33	8.2
Tantalum	14.5	0.452	6.8	3.37	8.6
Gold	14.2	0.571	6.0	4.37	7.3
Thallium	14.6	0.655	5.4	4.90	7.6
Bismuth	13.9	0.537	5.9	3.96	7.4
Thorium	14.5	0.796	5.6	6.33	8.0
Uranium	14.9	1.18	6.8	12.5	10.6

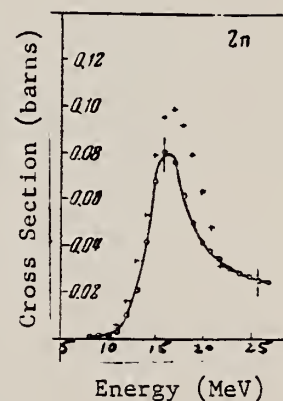


Figure 2: Photoneutron cross section σ_n , computed from the yield curves by the "photon difference method."
 "+" -- cross sections obtained in Ref. 8 [Montalbetti, Katz, and Goldemberg, Phys. Rev. 91, 659 (1959)].

Elem. Sym.	A	Z
Zn		30
Ref. No.		
56 Ha 1		EGF

Method Li (p,γ) source, 480 kev protons; BF₃ counters.

Reaction	E or ΔE	E ₀	Γ	∫ σ dE	J π	Notes
(γ, xn)						Average Li cross section is <u>48</u> mb; cross section with detector response weighted for low energy neutrons, <u>75</u> mb. Assumed ratio 17.6/14.8 = 1.7. Calculated cross section at 14.8 and 17.6 MeV assuming cross section curves measured at Pennsylvania and Saskatchewan (refer Table I).

TABLE I. Cross sections for photoneutron emission induced by the lithium gamma rays. The results are compared with previous data.

Element	Present cross-section data		Data of McDaniel et al. ^a	Betatron data					
	Counter Group A	Counter Group B		Pennsylvania		Saskatchewan		$\sigma_{14.8}^b$	$\sigma_{17.6}^b$
				$\sigma_{14.8}^c$	$\sigma_{17.6}^c$	$\sigma_{14.8}^d$	$\sigma_{17.6}^d$		
⁶ Fe	38 mb	33 mb	37 mb			60 ^f mb	0.5	23 mb	47 mb
⁷ Co	49	49	47	60 ^e mb	0.5	95 ^f	0.5	30	60
¹² Ni	28	25	23			40 ^e	0.7	22	32
¹³ Ni						95 ^f	0.6	45	75
¹³ Cu	64	61	55±12			90 ^f	0.7	38	54
¹⁶ Zn	48	45	48			240 ^f	1.0	175	175
¹⁷ Ag	175	170	135						
¹⁸ Sn	200	190	180						
⁷³ Ta	355	360	260	350 ^d	1.3	420 ^e	2.3	420 ^f	320 ^f
⁷⁴ W	365	355	325			550 ^f		550 ^f	240 ^f
⁷⁹ Au	330	295		315 ^e	1.7	480 ^f	1.9	460	255
⁸⁰ Hg	365	340	290						
⁸² Pb	310	295	250	320 ^e	1.6	440 ^f	2.5	400 ^f	250 ^f
⁸³ Bi	305	280	250	270 ^d	2.6	550 ^f	2.4	500 ^f	200 ^f
								490	195

- ^a See reference 3.
^b Average of 14.8- and 17.6-Mev cross sections weighted with relative intensities of the lithium gamma-ray lines.
^c See reference 24.
^d R. Nathans, Ph.D. thesis, University of Pennsylvania, 1954 (unpublished).
^e J. Halpern (private communication).
^f See reference 23.
^g See reference 32.
^h Separate cross sections at 14.8 and 17.6 Mev as obtained from Group A data and 14.8/17.6 betatron cross-section ratios.
ⁱ Obtained using 14.8/17.6 cross-section ratio from Pennsylvania betatron data.
^j Obtained using 14.8/17.6 cross-section ratio from Saskatchewan betatron data.

REF.

R. M. Osokina and B. S. Ratner
 Zhur. Eksp. i Teoret. Fiz. 32, 20 (1957)
 Soviet Phys. JETP 5, 1 (1957)

ELEM. SYM.

A

Z

Zn

30

METHOD

REF. NO.

[Page 1 of 2]

57 Os 1

EGF

REACTION	RESULT	EXCITATION ENERGY	SOURCE		DETECTOR		ANGLE
			TYPE	RANGE	TYPE	RANGE	
G,P	ABX	THR-31	C	20-31	EMU-D	4-18	DST

Note: Fast photoproton mean $E_p \geq 9$ MeV.

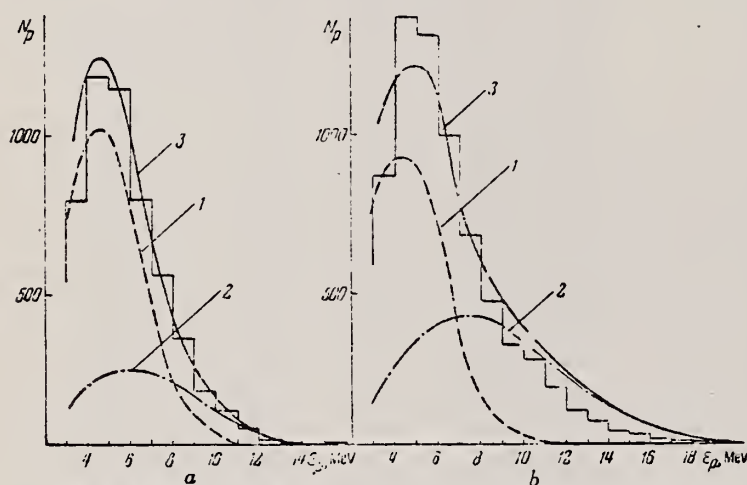


FIG. 2. Energy distributions of photoprotons from zinc obtained at energies $E_{\gamma m}$: a - 20.8 mev and b - 28.6 mev. 1 - spectra calculated according to evaporation theory; 2 - spectra calculated according to the direct photoeffect model¹⁴ taking shells into account; 3 - the sum of curves 1 and 2.

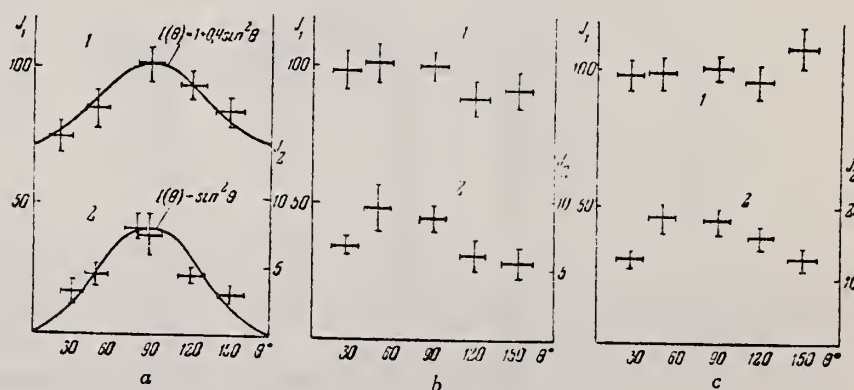


FIG. 4. Angular distributions of photoprotons from zinc obtained at energy values $E_{\gamma m}$: a - 20.8, b - 21.3 and c - 28.6 mev. I_1 and I_2 are the relative numbers of protons per unit solid angle for protons: 1 - with energies $\epsilon_p \geq 3$ mev, 2 - with energies $\epsilon_p \geq 9$ mev.

REF. R. M. Osokina and B. S. Ratner
Zhur. Eksp. i Teoret. Fiz. 32, 20 (1957)
Soviet Phys. JETP 5, 1 (1957)

ELEM. SYM.	A	Z
Zn		30

METHOD

[Page 2 of 2]

REF. NO.

57 Os 1

EGF

REACTION	RESULT	EXCITATION ENERGY	SOURCE		DETECTOR		ANGLE
			TYPE	RANGE	TYPE	RANGE	

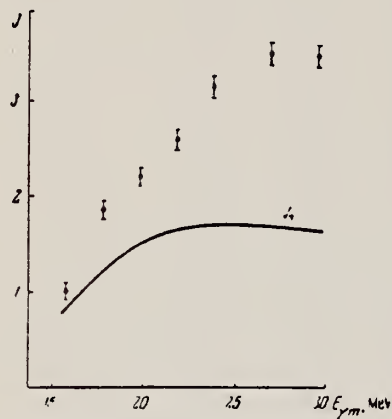


FIG. 5. Dependence on E_{γ_m} of the yield of photo-protons with energies $\epsilon_p \geq 3$ mev from zinc. I_T is the curve calculated according to evaporation theory and normalized according to the data on angular distribution on the assumption that at $E_{\gamma_m} = 20.8$ mev the isotropic part of the yield (75%) is determined by evaporation. I is the yield in relative units reduced to the same ionization in a thick-walled ionization chamber.

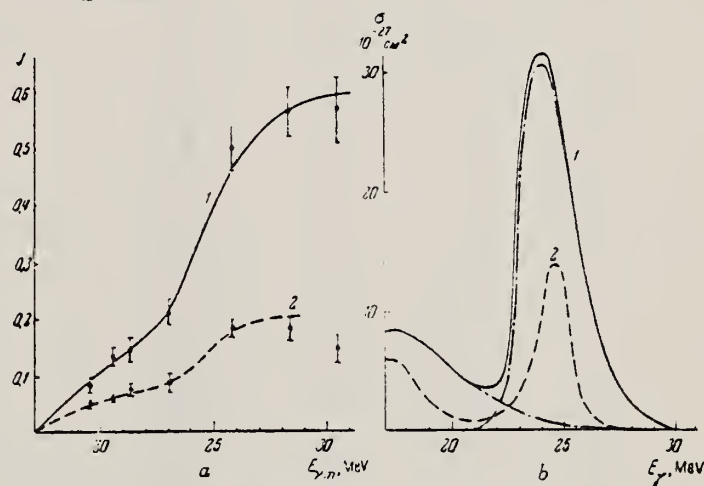


FIG. 6. a - dependence on E_{γ_m} of the yield of fast photoprotons from zinc; b - cross-section for the emission of fast protons from zinc. 1 - $\epsilon_p \geq 9$, 2 - $8 \leq \epsilon_p \leq 10$ mev.

Ref. M.E. Toms, J. McElhinney
Phys. Rev. 111, 561 (1958)

Elem. Sym.	A	Z
Zn		30

Method
Betatron; alpha yield; nuclear emulsion

Ref. No.	
58 To 2	NVB

Reaction	E or ΔE	E_0	Γ	$\int \sigma dE$	$J\pi$	Notes
$Zn(\gamma, \alpha)$	Bremss. 22					Yield = 8.2×10^4 alpha/mole/roentgen

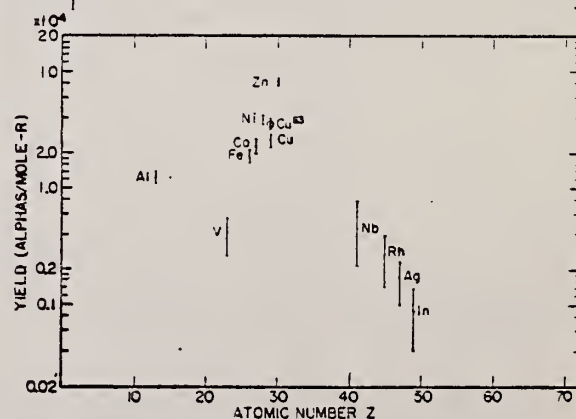


FIG. 8. Photo-alpha yields plotted against atomic numbers for the exposures of the survey.

Ref. K. Reibel, A.K. Mann
Phys. Rev. 118, 701 (1960)

Elem. Sym.	A	Z
Zn		30

Method γ 's from $F^{19}(p, \alpha\gamma)$ reaction; protons from Van de Graaff; NaI

Ref. No.	
60 Re 1	JHH

Reaction	E or ΔE	E_0	Γ	$\int \sigma dE$	$J\pi$	Notes
Zn (γ, γ)	$E_\gamma = \sim 7$					Detector at 90° $\langle \bar{\sigma} \rangle (E_p = 2.05 \text{ MeV}) = 0.86 \pm 0.13 \text{ mb}$

Rev. F. Tagliabue, J. Goldemberg
Nuclear Phys. 25, 144 (1961)

Elem. Sym.	A	Z
Zn		30

Method 22 MeV betatron; Si²⁸(n,p)Al²⁸ threshold detector.

Ref. No.	JHH
61 Ta 1	

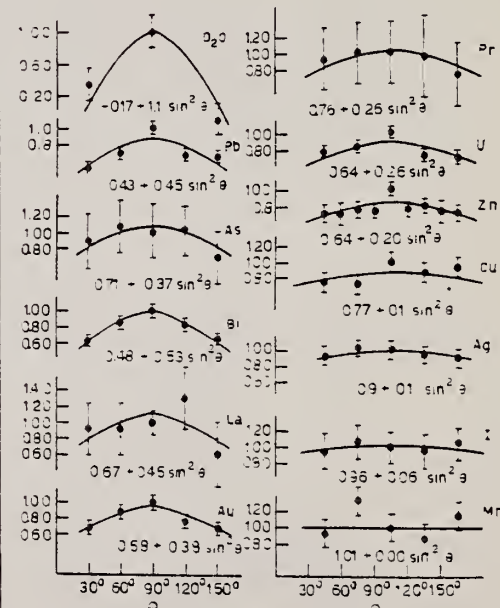
Reaction	E or ΔE	E ₀	Γ	∫σdE	Jπ	Notes
(γ, n)	Bremss. 22					<p>$E_n > 6$ MeV.</p> <p>$W(\theta_n) = A + B \sin^2 \theta$ where $B/A = 0.31 \pm 0.17$</p> 

Figure 4: Angular distributions of fast photoneutrons as observed with the Si²⁸(n,p)Al²⁸ detector. Data normalized at 90° in each case.

Method Betatron; proton yield; angular distribution; scintillator;
ion chamber.

Ref. No.	
63 Mi 5	NVB

Reaction	E or ΔE	E_0	Γ	$\int \sigma dE$	$J\pi$	Notes
$Zn(\gamma, xp)$	Bremss. 22					<p>Angular distribution: $Y(\theta) = a + b \sin^2 \theta (1 + p \cos \theta)^2$ <p>where $a = 47 \pm 10$; $b = 53 \pm 16$; $p = 0.5 \pm 0.2$ and $b/a = 1.1 \pm 0.4$.</p> <p>Yield ($E_p > 8$ MeV): $(2.8 \pm 0.7) \cdot 10^5$ protons/mole-r.</p> <p>Yield ($3.7 < E_p < 14$): $(22 \pm 2) \cdot 10^5$</p> </p>

2

3

FIG. 4. The values of the fast photoproton anisotropy coefficient b/a found by the present authors (●) and other workers (○) in the region of the periodic table $10 \leq Z \leq 50$. Arrows indicate off-scale points. The references to the results of other workers are given in Table II. The demarcations are explained in the text.

Ref. M. Sugawara, S. Mori, A. Ono, A. Hotta, M. Kimura
J. Phys. Soc. Japan 18, 17 (1963)

Elem. Sym.	A	Z
Zn		30

Method 25 MeV betatron; photon scattering; NaI spectrometer; NBS chamber

Ref. No.	NVB
63 Su 1	

Reaction	E or ΔE	E_0	Γ	$\int \sigma dE$	$J\pi$	Notes
Zn(γ, γ)	Bremss. 4- 14					<p>Detector at 120°.</p> <p>$\sigma_{\max} = 1.3$ mb.</p> <p>[Corrects results in J. Phys. Soc. Japan <u>16</u>, 1657 (1961)]</p>

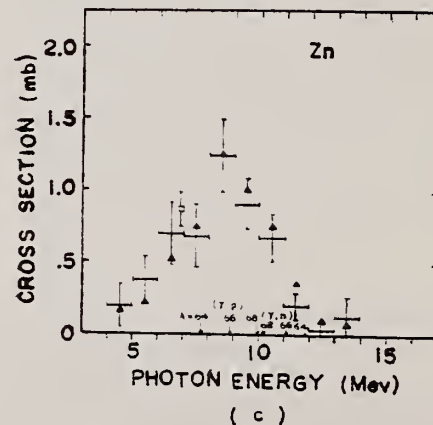


Fig. 1. The elastic scattering cross sections for Mn, Fe, Co, Ni, Cu, Zn and Br. The indicated spread in energies is the width of the sum-up channels, and the vertical lines are the statistical errors including background counts. The arrows represent the positions of the threshold energies of the γ or γ, n reaction taken from Ref. 10. The open squares at 7 Mev are Reibel and Mann's data. In Fig. 2, the cross section values, which are analyzed by displacing the sum-up channels by five channels to lower energy side than the positions generally used, are indicated by the closed triangles.

- 9 K. Reibel and A. K. Mann, Phys. Rev. 118, 1047 (1960).
- 10 J. S. Pruthi and S. R. Isichen, NBS Monograph 10, U.S. Government Printing Office, Washington, D.C., 1962.
- 11 E. G. Fuller and J. H. Ewing, Phys. Rev. 118, 1047 (1960).

					REF. NO.	
Synchrotron; $C^{12}(\gamma, n)$ monitor					64 Co 2	JOC
REACTION	RESULT	EXCITATION ENERGY	SOURCE		DETECTOR	
			TYPE	RANGE	TYPE	RANGE
G.XN	ABY	THR - 80	C	80	BF3-I	4 PI

Table 1

Element	Yield (30) eV cm ² mol MeV	60 NZ/A (mb MeV)	30 Σ 0	80 Σ 0	$30 \text{ } 30$ Σ / Σ 0 0	E_m (MeV)	σ_m (mb)
^{24}Cr	83×10^{-5}	777	1.21	2.1	0.53	18.5	97
^{25}Mn	106×10^{-5}	813	1.52	2.23	0.65	18.5	114
^{26}Fe	68×10^{-5}	832	0.88	1.46	0.60	17.5	75
^{27}Co	89×10^{-5}	878	1.03	1.32	0.59	17.5	92
^{28}Ni	44×10^{-5}	879	0.55	1.07	0.51	18.5	56
^{29}Cu	95×10^{-5}	947	1.06	1.99	0.53	17.5	93
^{30}Zn	88×10^{-5}	975	0.94	1.63	0.56	17.5	86
^{31}Ga	130×10^{-5}	1034	1.29	2.13	0.59	17.5	131
^{32}Ge	139×10^{-5}	1034	1.35	2.29	0.59	17.5	133
^{33}As	137×10^{-5}	1109	1.22	2.13	0.56	17.5	127

$$\frac{30}{\Sigma} = \frac{\int_0^{30} \sigma(\gamma, xn) dE}{60 \text{ NZ/A}}$$

Table 2

Element	maximum yield ($\times 10^{-5}$)	$\sigma_{-1}(\text{Fe})$	$\sigma_{-1}(\text{Fe}) \times \frac{3}{2} \frac{A}{A-1} \left(\frac{A-1}{NZ} \right)^{1-\frac{1}{2}}$
^{12}C	4.0	3.54	2.13
^{16}O	5.2	4.05	1.92
^{23}Na	10.6	11.30	2.45
^{27}Al	10.0	8.31	1.73
^{29}Si	15.9	10.92	2.30
^{32}S	11.6	9.06	1.55
^{35}P	19.3	17.56	2.62
^{36}S	9.5	8.55	1.37
^{39}K	19.6	17.90	2.61
^{40}Ca	12.1	11.63	1.92
^{52}Cr	83	61.6	3.56
^{55}Mn	115	70.1	3.96
^{56}Fe	71	50.5	2.55
^{59}Co	64	60.5	2.64
^{58}Ni	45	34.2	1.53
^{63}Cu	102	72.3	2.80
^{66}Zn	93	65.7	2.63
^{71}Ga	140	93.6	3.61
^{76}Ge	150	101.5	3.33
^{75}As	131	65.3	2.12

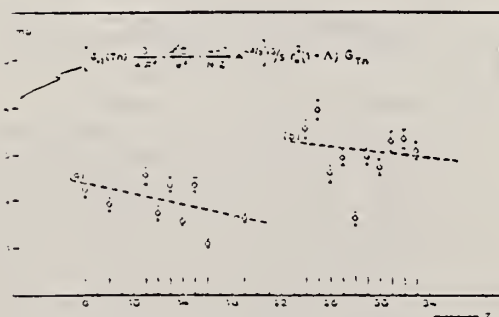


Fig. 2. Bremsstrahlung-weighted cross sections, $\sigma_{-1}(\text{Fe})$, conveniently normalized, versus Z .

REF.

J. R. Van Hise, R. A. Meyer, and J. P. Hummel
Phys. Rev. 139, B554 (1965)

ELEM. SYM.	A	Z
Zn		30

METHOD

Betatron; NBS chamber monitor

REF. NO.

65 Va 3

NVB

REACTION	RESULT	EXCITATION ENERGY	SOURCE		DETECTOR		ANGLE
			TYPE	RANGE	TYPE	RANGE	
G,XXX	ABI	50 - 300	C	50 - 300	ACT-I		4PI

XXX=CU64

TABLE 1. Integrated cross sections for the $S^{32}(\gamma, np)P^{30}$, $Ca^{40}(\gamma, np)K^{38}$, and $Zn^{66}(\gamma, np)Cu^{64}$ reactions.

E_{max} (MeV)	$\int_0^{E_{max}} \sigma dE$ (MeV mb)		
	$S^{32}(\gamma, np)P^{30}$	$Ca^{40}(\gamma, np)K^{38}$	$Zn^{66}(\gamma, np)Cu^{64}$
50	64 ± 2	31 ± 1	128 ± 3
100	79 ± 5	35 ± 5	160 ± 7
140	81 ± 6	35 ± 7	160 ± 20
200	107 ± 8	43 ± 9	270 ± 30
250	150 ± 10	72 ± 11	370 ± 45
300	190 ± 12	88 ± 14	400 ± 60

METHOD

REF. NO.

66 Ac 1

egf

REACTION	RESULT	EXCITATION ENERGY	SOURCE		DETECTOR		ANGLE
			TYPE	RANGE	TYPE	RANGE	
G,D	YLD	16-22	C	22	MAG-D		4PI

YIELD UPPER LIMIT

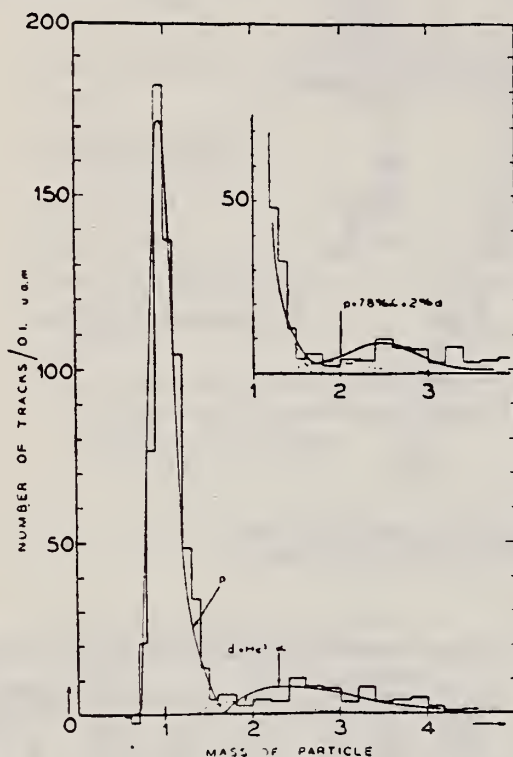


Fig. 2 "Mass" histogram for the 1917 tracks measured in four plates irradiated at -165° , -15° , $+45^\circ$ and $+105^\circ$ to the incident beam, respectively (positions n° 1, 5, 8 e 10). Only tracks with ranges less than 140μ were included. The dashed curves calculated shapes of the proton, deuteron and alpha particles peaks for a standard error of 2.3% in σ , normalised respectively to 616 protons, 28 deuterons and 110 alpha particles. In the lower part, the full curve gives the sum of the alpha and proton curves (i.e. with 0% of deuterons). In the upper part the full curve represents the sum of the three particles curves (i.e. with 2% of deuterons and 7.8% of alpha particles).

METHOD

Nuclear Resonance Scattering using N,G reactions.

REF. NO.

66 Be 3

JDM

REACTION	RESULT	EXCITATION ENERGY	SOURCE		DETECTOR		ANGLE
			TYPE	RANGE	TYPE	RANGE	
G,G	RLX	5 - 10	D	5 - 10	NAI-D	5 - 10	135

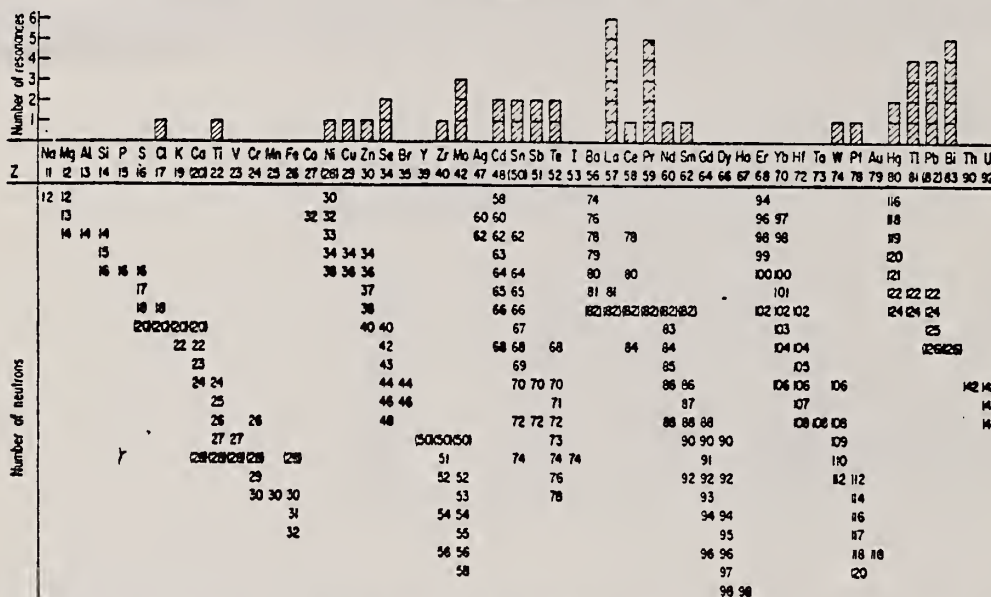


FIG. 3. Histogram of distribution of observed resonances among the different targets. The atomic number is given directly beneath the chemical symbol followed by the neutron numbers of the naturally occurring isotopes. Magic numbers are shown in brackets.

TABLE III. List of effective cross sections.

Scatterer	Energy (MeV)	Gamma source	δ (mb)	Scatterer	Energy (MeV)	Gamma source	δ (mb)
Sm ¹⁴⁴	8.997	Ni	100	Sn	7.01	Cu	110
Pr ¹⁴³	8.881	Cr	9	Nd	6.867	Co	30
La	8.532	Ni	6	Pr ¹⁴¹	6.867	Co	3
Te	8.532	Ni	3*	Te	6.7	Ni	...
Cu	8.499	Cr	24	La	6.54	Ag	12
Zr	8.496	Se	3050	Cd	6.474	Co	110
Zn	8.119	Ni	13	Mo	6.44	Hg	25*
Se	7.817	Ni	50	La	6.413	Ti	10
Se	7.76	K	90	Mo	6.413	Ti	25
Sb	7.67	V	...	Ti	6.413	Ti	...
Cd	7.64	Fe	40*	W	6.3	Ti	...
Ni	7.64	Fe	7*	Sb	6.31	Hg	6*
Pr ¹⁴¹	7.64	Fe	12*	Ti	6.31	Hg	2*
Ti	7.64	Fe	370*	Sn	6.27	Ag	75
La	7.634	Cu	7	Pb ²⁰⁸	6.15	Gd	...
Mo	7.634	Cu	11	Te	5.8	Ni	...
Ri ²⁶⁰	7.634	Cu	4	La	6.12	Cl	35
Te	7.528	Ni	664	Pr ¹⁴¹	6.12	Cl	110
Bi ²⁰⁹	7.416	Se	100	Pt	5.99	Hg	40*
Bi ²⁰⁹	7.300	As	80*	Ti	5.99	Hg	5*
Pb ²⁰⁸	7.285	Fe	4100	Pb ²⁰⁸	5.9	Sr	...
Cl	7.285	Fe	34	Ce	5.646	Co	17
Pr ¹⁴¹	7.185	Se	80	Bi ²⁰⁹	5.646	Co	55
Ti	7.16	Cu	120	Pb ²⁰⁸	5.53	Ag	70
La	7.15	Mn	50	Hg	5.44	Hg	75*
Bi ²⁰⁹	7.149	Ti	2000	Hg	4.903	Co	385

- * High-energy component of a complex spectrum.
- * A broad scattered spectrum with no observable peak structure.
- * There are actually two lines of energies 7.647 and 7.633 MeV having equal intensities in the iron capture gamma spectrum. The cross section has therefore been corrected, although there is no possibility at present of deciding which line is responsible for each resonance.
- * Is probably an independent level in the complex spectrum of Ni γ rays on Te.
- * Rough estimate.
- * May be inelastic component from 7.528 level in Te.
- * The relative line intensities in this case are due to Groshev and co-workers.
- * No line is known for the source at this energy.
- * Difficult to resolve among the many source lines present at this energy.

REF. H. Hoffmann, B. Prowe and H. Ullrich
Nuclear Phys. 85, 631 (1966)

ELEM. SYM. A Z
Zn 30

METHOD

Betatron

REF. NO.

66 Ho 3

JDM

REACTION	RESULT	EXCITATION ENERGY	SOURCE		DETECTOR		ANGLE
			TYPE	RANGE	TYPE	RANGE	
G, A	SPC	THR-31	C	31	SCD-D	3-14	130

TABLE 1
Experimental data and results

Element	Mg	Al	S	Ni	Cu	Zn	Error (%)
target thickness (mg/cm ²)	0.81	1.54	0.80	2.50	2.68	3.00	.5 *
dose (r)	6190	25400	23200	3880	5840	4220	10
yield absolute (10 ⁵ /mole · r) for $E_m > 3.16$ MeV	0.61	0.93	1.46	1.65	0.92	2.42	11 *
yield relative to Ni	0.36	0.56	0.88	1	0.55	1.43	5 *
$Y_{\gamma, \alpha}/Y_{\gamma, \text{tot}}(\%)$	9.6	11.4	12.4	7.0	3.2	b)	
nuclear temp. θ (MeV)	1.43	1.48	1.46	1.04		0.91	10
level density parameter a (MeV ⁻¹)	5.1	4.8	4.9	8.6		10.8	10

*) For S, the error of the target thickness has been 10 %, of the absolute yield 14 % and of the relative yield 10 %.

b) For Zn $\sigma_{\gamma, \text{tot}}$ is not known.

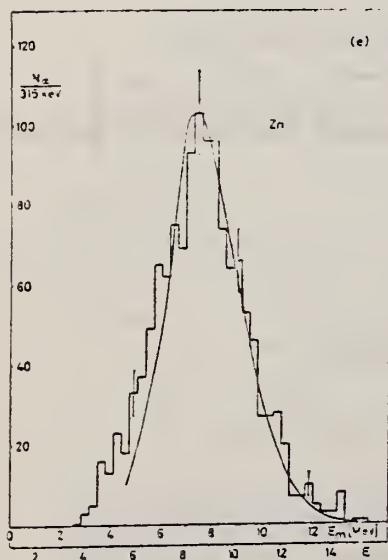


Fig. 3d-e. Photoalpha spectra of Ni and Zn. Notations as in fig. 3a-c.

Fig. 3f. Statistical plot of the measured spectra. The straight lines are drawn to give the best fit.

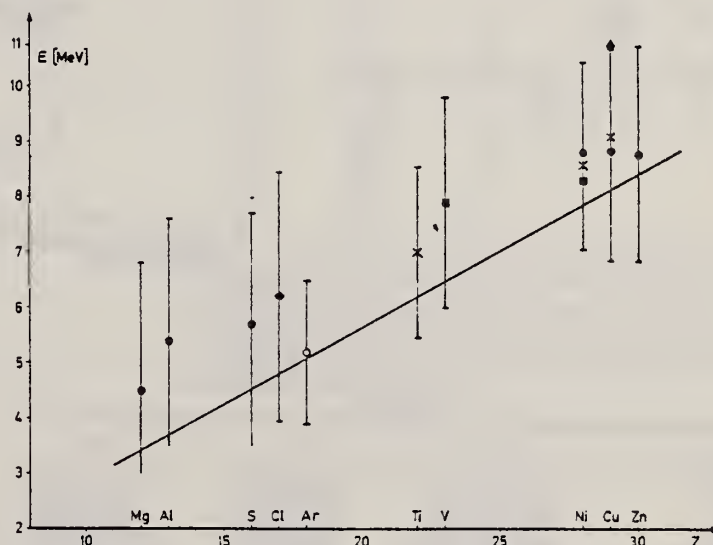
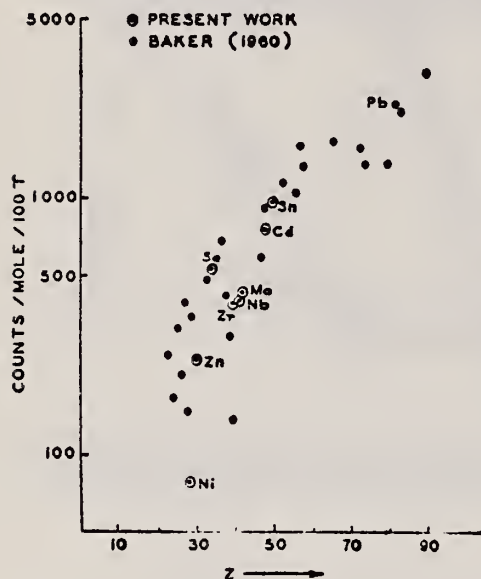


Fig. 4. Position of the peaks in different photoalpha spectra plotted against Z of the target nuclei. x : Scheer *et al*¹⁰), ■ : Kregar and Povh⁹), ▲ : Meneghetti and Vitale⁵), ◆ : Erdős *et al*¹), ○ : Komar *et al*⁷), ● : this work. The signs show the position of the maximum, the bars give the widths at half maximum. The curve shows the height of the Coulomb barrier.

REF.			ELEM. SYM.			A		Z	
S. M. Hussain and K. G. McNeill Can. J. Phys. <u>45</u> , 2851 (1967)			Zn					30	
METHOD						REF. NO.			
						67 Hu 2		EGF	
REACTION	RESULT	EXCITATION ENERGY	SOURCE		DETECTOR		ANGLE		
			TYPE	RANGE	TYPE	RANGE			
G,N	ABY	THR-22	C	22	THR	4-	DST		

FIG. 3. The yields of fast photoneutrons from various elements as measured in the present work and by Baker. The present results have been normalized to Baker's measurements for lead.

YIELD AT $E_0 = 22 \text{ MeV}$
 $^{28}\text{Si}(n,p)$ ACTIVATION BY PHOTONEUTRONS



ANISOTROPY COEFFICIENT $-a_2$

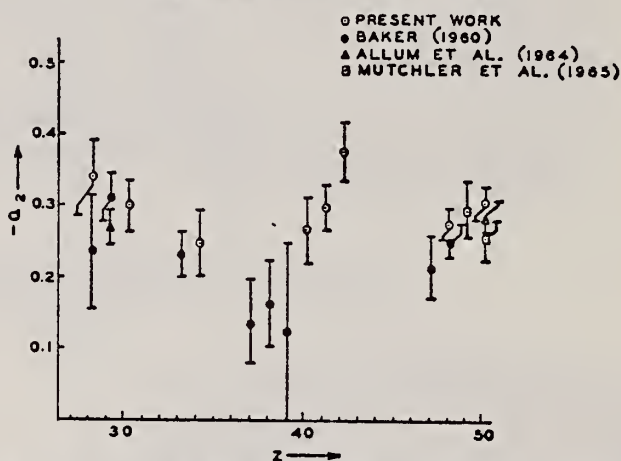


FIG. 2. The anisotropy coefficients a_2 , in the formula $W(\theta) = a_0(1 + a_1P_1 + a_2P_2)$, obtained in the present work, and those obtained by other workers in the same part of the Periodic Table.

TABLE I

Element	a_0^*	a_1	a_2
Nickel	77 (1.0±0.05)	0.14±0.04	-0.34±0.06
Zinc	236 (1.0±0.04)	0.06±0.03	-0.30±0.04
Selenium	525 (1.0±0.05)	0.10±0.04	-0.25±0.05
Zirconium	380 (1.0±0.05)	0.03±0.04	-0.27±0.05
Niobium	392 (1.0±0.03)	0.04±0.02	-0.30±0.03
Molybdenum	410 (1.0±0.03)	0.05±0.03	-0.41±0.04
Cadmium	755 (1.0±0.02)	0.05±0.01	-0.28±0.02
Tin	955 (1.0±0.02)	0.08±0.02	-0.30±0.02
Lead	2274 (1.0±0.02)	0.06±0.02	-0.48±0.02

*For comparison purposes the experimental value of a_0 for Pb has been normalized to coincide with that obtained by Baker and McNeill (1961) and is the yield per mole per 100 roentgen. All other values of a_0 have also been quoted with the same normalization.

ELEM. SYM.	A	Z
Zn		30
REF. NO.		
68 Ka 1		
HMG		

REACTION	RESULT	EXCITATION ENERGY	SOURCE		DETECTOR		ANGLE
			TYPE	RANGE	TYPE	RANGE	
G,N	ABX	50-85	C	55,85	TOF-D	10-85	67
							(67.5)

NEUT ENGY SPEC

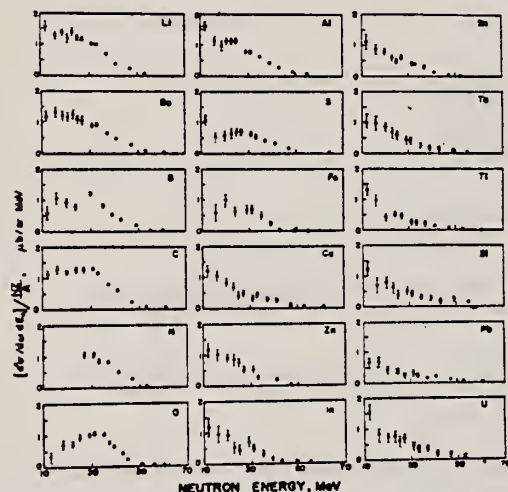


FIG. 6. Observed neutron spectra due to 55-85-MeV difference photon spectra. The effective cross sections have been divided by NZ/A .

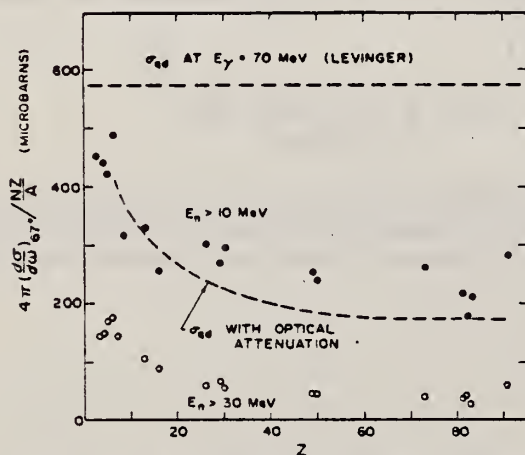


FIG. 7. Effective cross sections for production of fast neutrons with energies greater than 10 MeV (solid circles) and 30 MeV (open circles) by the 55-85-MeV photon difference spectrum. The dashed curves are modified quasideuteron model predictions as discussed in the text.

TABLE I. Comparison of present cross-section values in mb for production of high-energy photoneutrons by 55-85-MeV photons with measured cross sections $\sigma(\gamma, Tn)$, also in mb, for total photoneutron production. The present cross-section values are uncertain by 8 to 10% because of counting statistics and normalization errors; in addition all values depend on an absolute normalization in terms of the deuteron photodisintegration cross section, which is known to about 10% at these energies.

Target	$4\pi(d\sigma/d\Omega)_0^a$ ($E_n > 10$ MeV) [Present experiment]	$\sigma(\gamma, Tn)$ Jones and Terwilliger ^c	Costa <i>et al.</i> ^b	Other results
Li	0.75		1.0	
Be	1.0	2.7	2.3	2.3 ^a
B	1.0		1.4	
C	1.5	1.3	1.4	2.4 ^d
O	1.3		1.6	
Al	2.8	5.5	4.6	8 ^d
S	2.1		4.4	6.5 ^d
Fe	4.2	16	12	
Cu	4.3	20	19	
Zn	4.4		15	
In	7.4			
Sn	7.0			
Ta	10.7	95		
Tl	10.7			
Pb	8.3	100		
Bi	13			
U	16	65		

^a Average cross sections between 55 and 85 MeV, as read from Figs. 4 and 5 of Ref. 4.

^b $\int_0^\infty \sigma dE - \int_0^\infty \sigma dE/50$, as taken from Fig. 4 of Ref. 5 and Table I of Ref. 6.

^c S. Costa, L. Pasqualini, G. Piragino, and L. Roasio, Nuovo Cimento **42**, 306 (1966).

^d G. Bishop, S. Costa, S. Ferroni, R. Malvano, and G. Ricco, Nuovo Cimento **42**, 148 (1966).

REF. L. A. Currie and R. H. Rodriguez-Pasques
Nucl. Phys. A157, 49 (1970)

ELEM. SYM.	A	Z
Zn		30
REF. NO.		egf
70 Cu 1		

REACTION	RESULT	EXCITATION ENERGY	SOURCE		DETECTOR		ANGLE
			TYPE	RANGE	TYPE	RANGE	
G,T	ABY	THR-90	C	90	ACT- I		4PI

TABLE 4
Bremsstrahlung-weighted and integrated (p,t) and s sections (90 MeV)

	²⁷ Al	Zn	Sn	²⁰⁹ Bi
$\sigma_{-1}(\text{mb})$	0.072	0.0074	0.065	0.0072
$\sigma_0(\text{MeV} \cdot \text{mb})$	4.0	0.42	3.8	0.41

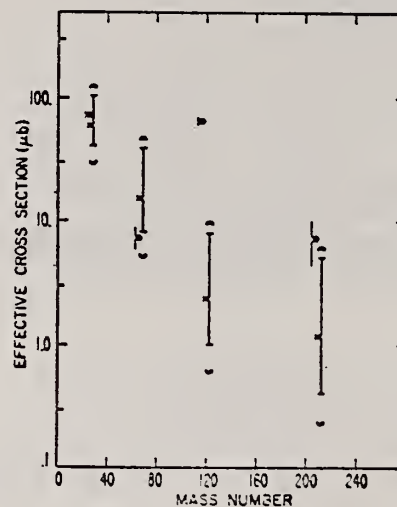


Fig. 3. Experimental (o) and statistical model (x) absolute phototriton yields (90 MeV). Yields, expressed in terms of "effective cross sections" (μb), are plotted versus mass number. Limits for the experimental yields represent \pm one standard deviation; those for the calculated yields correspond to limiting values for the level density parameter (—) and for the photon absorption cross section (\ominus).

ELEM. SYM.		
Zn		30
REF. NO.	71 Co 2	egf

METHOD

REACTION	RESULT	EXCITATION ENERGY	SOURCE		DETECTOR		ANGLE
			TYPE	RANGE	TYPE	RANGE	
G,XN	ABI	36-64	C	10-64	BF3-I		4PI

FAST N YIELD

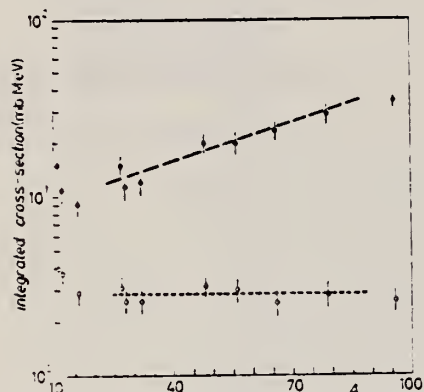


Fig. 2.

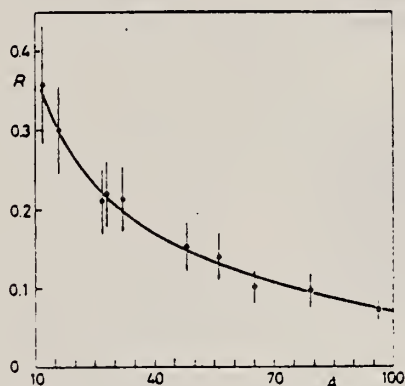


Fig. 3.

Fig. 2. - Experimental photoneutron cross-sections integrated over photon energy between 36 and 64 MeV and divided by NZ/A are plotted as a function of the mass number. Black dots are total cross-sections not corrected for neutron multiplicity; open circles represent fast neutron cross-sections (see text). The dashed lines are drawn only to guide the eye.

Fig. 3. - The ratio between «fast» and total photoneutron integrated cross-sections as a function of the mass number A . The solid line represents a fit of the ratios calculated for some nuclei by taking into account the theoretical neutron energy spectra given by GABRIEL and ALSMILLER (*) and the efficiencies of our detector (see Fig. 1).

METHOD

REF. NO.

72 Ke 4

hmg

REACTION	RESULT	EXCITATION ENERGY	SOURCE		DETECTOR		ANGLE
			TYPE	RANGE	TYPE	RANGE	
G,A	ABX	4-32	C	16-32	SCD-D		DST

TABLE 3. Observed angular distribution parameters for
32 MeV electron energy

Element	A_0	A_1/A_0	A_2/A_0
Ti	7.03 ± 0.15	0.073 ± 0.052	-0.286 ± 0.073
V	2.58 ± 0.06	0.037 ± 0.042	-0.126 ± 0.069
Fe	10.22 ± 0.30	0.006 ± 0.043	-0.333 ± 0.072
Co	6.80 ± 0.20	0.022 ± 0.048	$+0.016 \pm 0.077$
Ni	15.95 ± 0.49	0.051 ± 0.048	-0.213 ± 0.074
Cu	8.37 ± 0.28	0.076 ± 0.056	-0.035 ± 0.081
Zn	17.87 ± 0.61	0.004 ± 0.045	-0.270 ± 0.073
Ag	0.39 ± 0.01	0.115 ± 0.049	$+0.093 \pm 0.074$

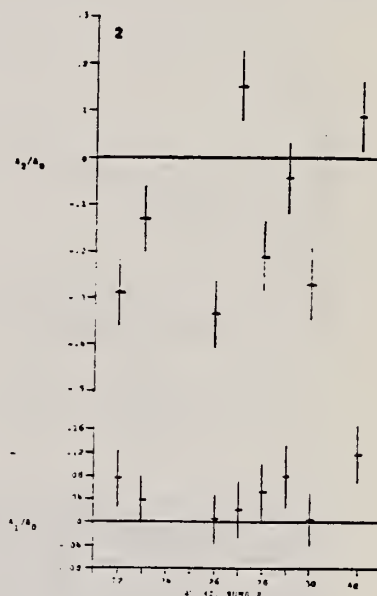


FIG. 2. Angular distributions for 32 MeV electron energy.

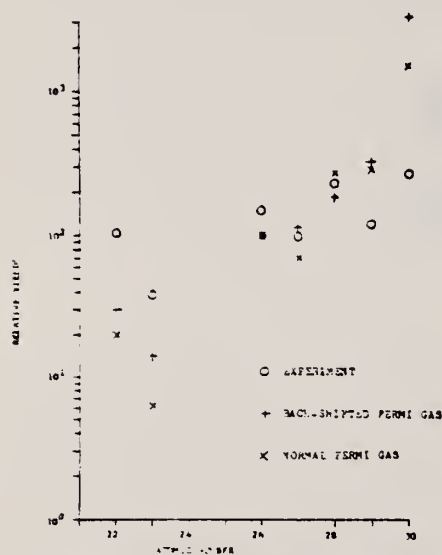


FIG. 13. Experimental and theoretical relative photo-alpha yields for 32 MeV electron beam energy.

TABLE 4. Zinc end points

Electron energy (MeV)	Effective end point (MeV)	A_1/A_0	A_2/A_0
16	14.4	-0.010 ± 0.050	-0.747 ± 0.096
18	16.9	-0.078 ± 0.044	-0.562 ± 0.075
20	19.0	-0.020 ± 0.038	-0.463 ± 0.064
22	21.2	-0.012 ± 0.033	-0.430 ± 0.060
24	23.5	-0.003 ± 0.033	-0.400 ± 0.061
26	25.5	-0.028 ± 0.035	-0.361 ± 0.060
28	27.6	-0.007 ± 0.037	-0.313 ± 0.063
30	29.5	-0.002 ± 0.035	-0.313 ± 0.062

(over)

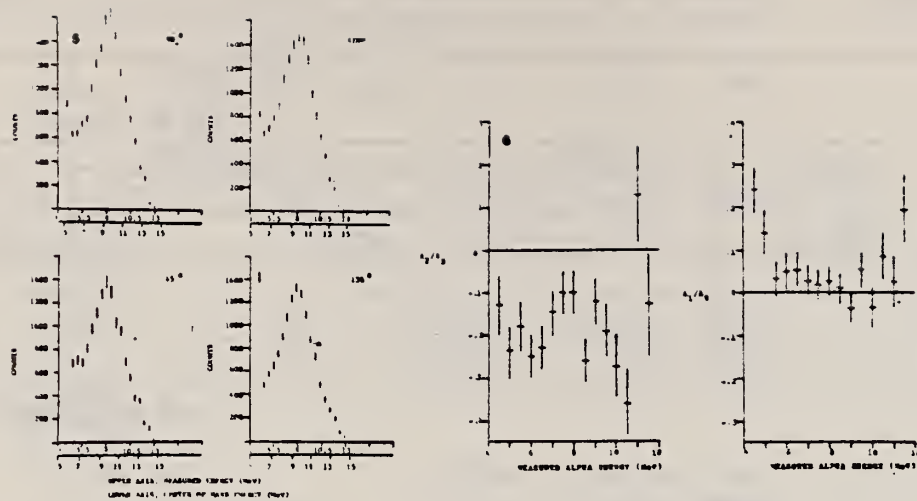


FIG. 5. Alpha spectra from zinc.

FIG. 6. 32 MeV zinc angular distribution.

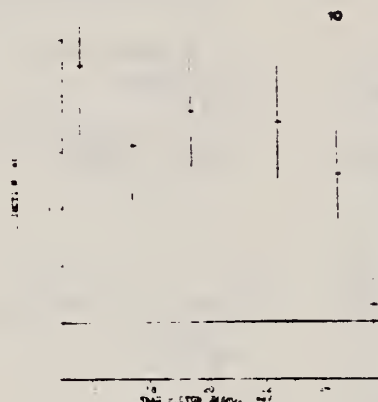


FIG. 7. Zinc photoalpha cross section.

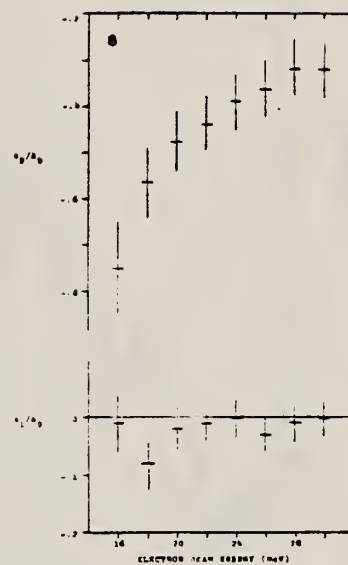


FIG. 8. Zinc angular distributions for electron energies from 16-30 MeV.

ELEM. SYM.	A	Z
Zn		30
REF. NO.		
73 Ba 20		egf

METHOD

REACTION	RESULT	EXCITATION ENERGY	SOURCE		DETECTOR		ANGLE
			TYPE	RANGE	TYPE	RANGE	
G ₂ N	NOX	THR- 27	C	10- 27	BF3-I		4PI

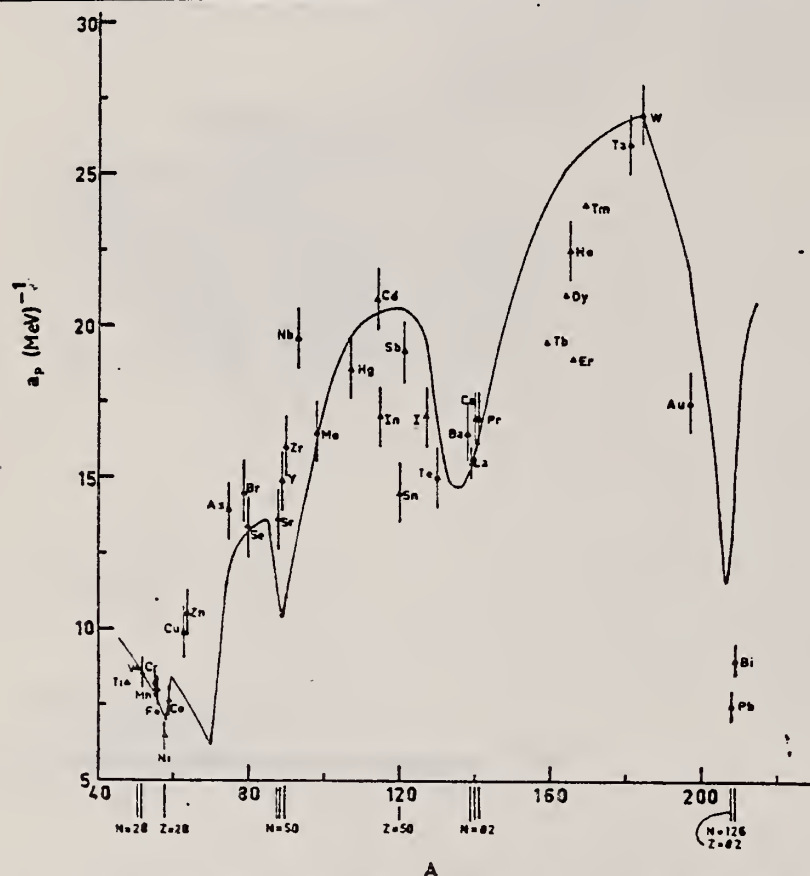


Fig. 12. Experimental values of the level density parameter a_p (Fermi gas formula plus pairing correction) versus atomic number A . The continuous curve is a least-squares fit to the data of a theoretical calculation from Newton ¹⁵).

- 1 H. Baba and S. Baba, Japan Atomic Energy Research Institute report JAERI-1183 (1969).
- 2 H. Baba, Nucl. Phys. A159, 625 (1970).
- 5 T.D. Newton, Can. J. Phys. 34, 804 (1956).

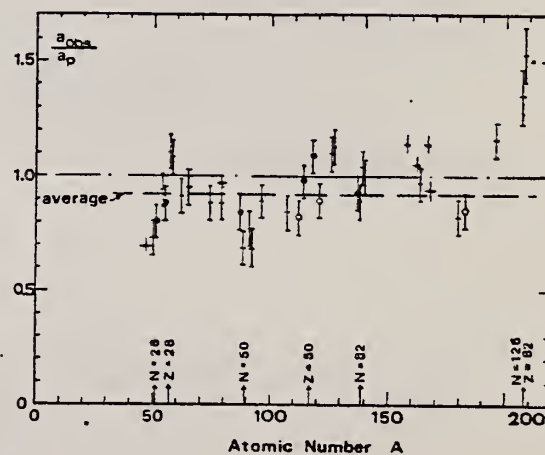


Fig. 15. Ratio a_{obs}/a_p versus atomic number A . Here a_{obs} is the level density parameter taken from the neutron resonance work of refs. ^{1,2}, and a_p is the level density parameter derived from the present (γ, n) work. Filled circles represent points where nuclei in the neutron resonance and in the (γ, n) experiment were the same. Open circles represent points where the respective nuclei were approximately matched. Triangles represent points which are based on measurement of neutron mean energies at two bremsstrahlung energies only.

(over)

TABLE 3

Comparison of experimental and theoretical data on nuclear level densities with Fermi gas formulae, and comparison of nuclear level density parameters from (γ , n) and n-resonance absorption experiments

Target	N (residual nucleus) ^{a)}		Goodness of fit ^{b)}		$\bar{E}_o(24)$ (MeV) ^{c)}	T (MeV) ^{d)}	a_p (MeV ⁻¹) ^{e)}	a_{obs} (MeV ⁻¹) ^{f)}	a_{obs}/a_p
			no p.c.	with p.c.					
Ti ^{g)}	23	8%			1.93		8.1- ⁴⁷ Ti	6.41- ⁴⁷ Ti	0.79
	24	8%							
	25	73%							
	26	5%							
	27	5%							
V ^{g)}	27	100%			1.96		8.7- ⁵⁰ V	6.35- ⁵¹ V	0.73
Cr	25	4%	P	G	1.89		8.6- ⁵¹ Cr	6.9 - ⁵¹ Cr	<u>0.80</u>
	27	84%							
	28	10%							
	29	2%							
Mn	29	100%	V.P.	G	2.1		8.2- ⁵⁴ Mn	7.82- ⁵⁶ Mn	0.94
Fe	27	6%	F	G	1.96		8.0- ⁵⁵ Fe	7.06- ⁵⁵ Fe	<u>0.88</u>
	29	92%							
	30	2%							
Co	31	100%	P	F	2.12		7.7- ⁵⁸ Co	8.35- ⁶⁰ Co	1.08
Ni (Z = 28)	29	68%	V.P.	P	2.04	1.4	6.5- ^{57,7} Ni	7.19- ⁵⁹ Ni-	1.10
	31	26%							
	32	1%							
	33	4%							
	35	1%							
Cu	33	69%	V.P.	P	1.78	1.0	9.8- ⁶² Cu	8.90- ⁶⁴ Cu	0.91
	35	31%							
Zn	33	49%	F	F	1.61		10.5- ^{64,4} Zn	10.0- ⁶⁵ Zn	0.95
	35	28%							
	36	4%							
	37	19%							
As	41	100%	V.P.	F	1.44		14.5- ⁷⁴ As	12.81- ⁷⁶ As	0.88
Se ^{g)}	41	9%			1.39		13.3- ⁷⁸ Se	12.8 - ⁷⁸ Se	<u>0.97</u>
	42	8%							
	43	24%							
	45	50%							
	47	9%							
Br	43	45%	V.P.	V.P.	1.41		14.5- ⁷⁹ Br	12.69- ⁸⁰ Br	0.88
	45	49%							
Sr	47	10%	F	G	1.31		13.6- ⁸⁷ Sr	11.4 - ⁸⁷ Sr	<u>0.84</u>
	48	7%							
	49	83%							

^{a)} Neutron numbers and abundances of respective residual nuclei in (γ , n) experiments.

^{b)} These give an assessment of the goodness of fit of a calculated \bar{E}_n versus E_0 curve to the observed data, using the Fermi gas level density formula both without and with pairing corrections.

^{c)} Bremsstrahlung photoneutron mean energies \bar{E}_n for peak bremsstrahlung energy $E_0 = 24$ MeV.

^{d)} Nuclear temperature from fit with constant-temperature formula.

^{e)} Level density parameter a_0 derived from the present (γ , n) experiment, using a Fermi gas formula plus pairing correction, and corresponding residual nucleus (the atomic weight shown is the weighted average of atomic weights of the respective isotopes present).

^{f)} As column 7, but using data on n-resonance absorption from refs. ^{1, 2}).

^{g)} Measurements of $\bar{E}_n(E_0)$ for these nuclei were made only for $E_0 = 21, 23$ and 24 MeV.

REF.

V. Emma, S. Lo Nigro, C. Milone
Nucl. Phys. A257, 438 (1976)

ELEM. SYM.	A	Z
Zn		30
REF. NO.		
76 Em 2		egf

REACTION	RESULT	EXCITATION ENERGY	SOURCE		DETECTOR		ANGLE
			TYPE	RANGE	TYPE	RANGE	
G, F	ABY	THR-999	C	999	TRK-I		4PI

TABLE I

999 = 1 GEVMeasured values of σ_q at $E=1000$ MeV and deduced values of σ_k assumed constant from E_0 to 1000 MeV

Element	Z^2/A	σ_q (mb)	E_0 (MeV)	σ_k (mb)
Bi	32.96	12.3 ± 0.6	200	7.6 ± 0.6
Pb	32.45	5.4 ± 0.4	220	3.6 ± 0.3
Tl	32.10	4.1 ± 0.3	230	2.8 ± 0.3
Au	31.68	2.0 ± 0.15	240	1.4 ± 0.2
Pt	31.18	1.1 ± 0.08	255	$(8 \pm 0.7) \times 10^{-1}$
Re	30.21	$(3.7 \pm 0.3) \times 10^{-1}$	280	$(2.9 \pm 0.3) \times 10^{-1}$
W	29.78	$(3.5 \pm 0.3) \times 10^{-1}$	290	$(2.8 \pm 0.3) \times 10^{-1}$
Ta	29.45	$(3.3 \pm 0.3) \times 10^{-1}$	300	$(2.7 \pm 0.3) \times 10^{-1}$
Hf	29.04	$(1.7 \pm 0.2) \times 10^{-1}$	310	$(1.4 \pm 0.2) \times 10^{-1}$
Yb	28.31	$(1.3 \pm 0.1) \times 10^{-1}$	330	$(1.2 \pm 0.1) \times 10^{-1}$
Tm	28.18	$(7.5 \pm 0.8) \times 10^{-2}$	335	$(6.8 \pm 0.8) \times 10^{-2}$
Ho	27.21	$(3.6 \pm 0.4) \times 10^{-2}$	355	$(3.5 \pm 0.4) \times 10^{-2}$
Dy	26.80	$(2.6 \pm 0.3) \times 10^{-2}$	360	$(2.5 \pm 0.3) \times 10^{-2}$
Tb	26.58	$(2.5 \pm 0.3) \times 10^{-2}$	370	$(2.5 \pm 0.3) \times 10^{-2}$
Gd	26.04	$(1.6 \pm 0.2) \times 10^{-2}$	380	$(1.7 \pm 0.2) \times 10^{-2}$
Sm	25.56	$(1.3 \pm 0.2) \times 10^{-2}$	390	$(1.4 \pm 0.2) \times 10^{-2}$
Nd	24.96	$(9.2 \pm 0.9) \times 10^{-3}$	405	$(1 \pm 0.1) \times 10^{-2}$
Ce	24.00	$(8 \pm 0.9) \times 10^{-3}$	420	$(9 \pm 1) \times 10^{-3}$
La	23.39	$(8.4 \pm 0.9) \times 10^{-3}$	430	$(1 \pm 0.1) \times 10^{-3}$
Sb	21.36	$(1.2 \pm 0.2) \times 10^{-2}$	460	$(1.5 \pm 0.3) \times 10^{-2}$
Te	21.19	$(8.8 \pm 1) \times 10^{-3}$	465	$(1.2 \pm 0.2) \times 10^{-2}$
Sn	21.06	$(1.3 \pm 0.2) \times 10^{-2}$	465	$(1.7 \pm 0.3) \times 10^{-2}$
Cd	20.49	$(1.7 \pm 0.3) \times 10^{-2}$	470	$(2.2 \pm 0.4) \times 10^{-2}$
Ag	20.47	$(2 \pm 0.3) \times 10^{-2}$	470	$(2.6 \pm 0.4) \times 10^{-2}$
Zn	13.76	$(2 \pm 0.4) \times 10^{-1}$	515	$(3 \pm 0.6) \times 10^{-1}$
Cu	13.44	$(2.4 \pm 0.5) \times 10^{-1}$	515	$(3.6 \pm 0.8) \times 10^{-1}$
Ni	13.35	$(2.4 \pm 0.5) \times 10^{-1}$	510	$(3.6 \pm 0.8) \times 10^{-1}$
Fe	12.10	$(3 \pm 0.6) \times 10^{-1}$	510	$(4.4 \pm 0.9) \times 10^{-1}$

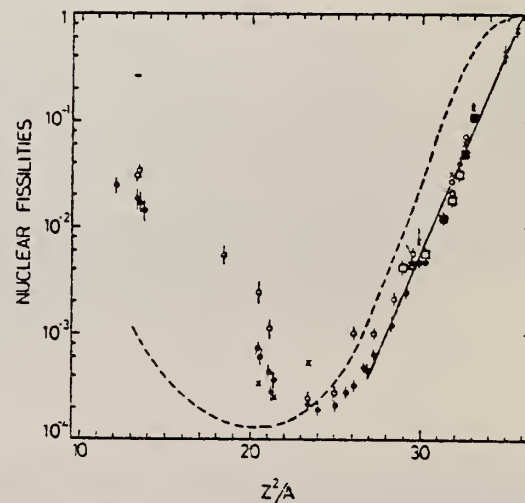
⁴ A.V. Mitrofanova et al.
Sov. J. Nucl. Phys. 6,
512 (1968).

⁷ T. Methasiri et al., Nucl.
Phys. A167, 97 (1971).

¹² J.R. Nix et al., Nucl. Phys.
81, 61 (1966).

²⁰ N.A. Perfilov et al., JETP
(Sov. Phys.) 14, 623 (1962);
Proc. Symp. on the physics &
chemistry of fission, Salzburg
1965, vol. 2 (IAEA) Vienna,
1965, p.283.

Fig. 2. Nuclear fissilities as a function of Z^2/A . Experimental points: solid circles represent our data; squares, the data from ref. ⁴); open circles, the data from ref. ⁷); and crosses, the data from (p,f) experiments²⁰). The straight line is the best fit calculated from our data for $Z^2/A > 26$. The dashed curve is the curve VI calculated by Nix and Sassi¹²).



Z_N
 $A=64$

Z_N
 $A=64$

Z_N
 $A=64$

M.D. DeSouza Santos, J. Goldemberg, R.R. Pieroni, E. Silva,
O.A. Borello, S.S. Villaca, J.L. Lopes
Int. Conf. Peaceful Uses of Atomic Energy II (UN, NY), 1969 (1955)

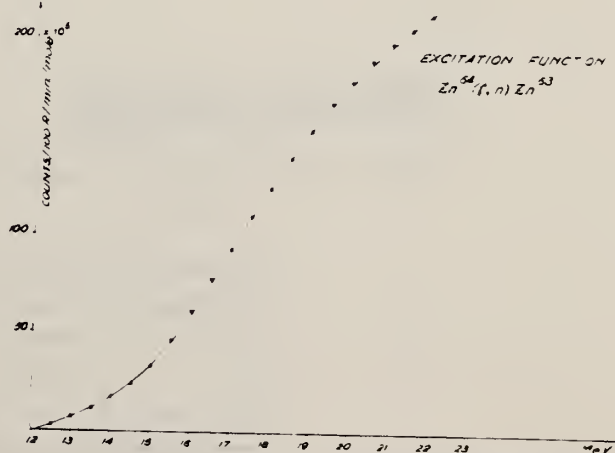
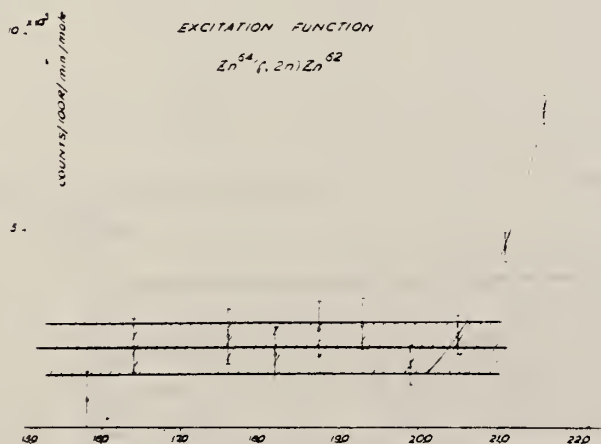
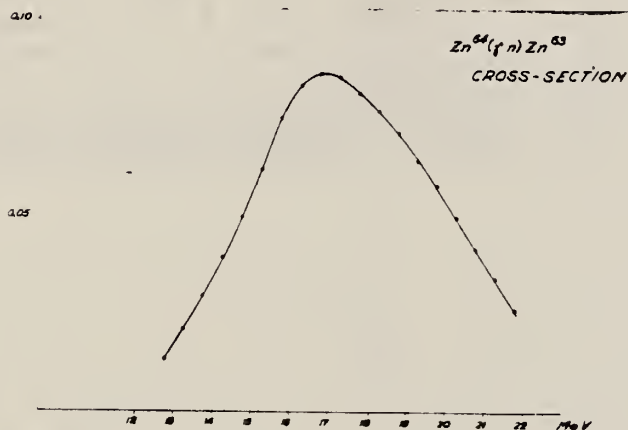
ELEM. SYM.	A	Z
Zn	64	30
REF. NO.		EGF
55 De 1		EGF

METHOD Beta; neutron yield; radioactivity; r-chamber

REACTION	RESULT	EXCITATION ENERGY	SOURCE		DETECTOR		ANGLE
			TYPE	RANGE	TYPE	RANGE	
G,N	ABX	12-23	C	12-23	ACT-I		4PI
G,2N	ABY	20-23	C	20-23	ACT-I		4PI

threshold ($\gamma, 2n$) = 20.35 ± 0.35 MeV

THRESHOLD 2N



REF. S.S. Villaca, J. Goldemberg
An. Acad. Brasil. Cienc. 27, 427 (1955)

ELEM. SYM.	A	Z
Zn	64	30

METHOD Betatron; ion chamber monitor

REF. NO.	
55 Vi 1	NVB

REACTION	RESULT	EXCITATION ENERGY	SOURCE		DETECTOR		ANGLE
			TYPE	RANGE	TYPE	RANGE	
G, N	ABX	12-22	C	12-22	ACT-I		4PI
G, 2N	ABY	15-22	C	12-22	ACT-I		4PI

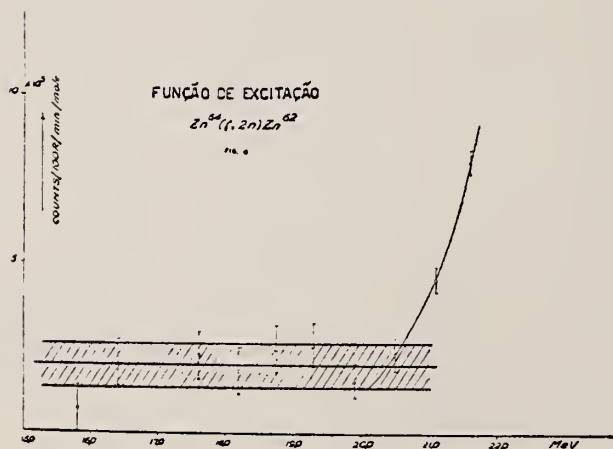


Fig. 8

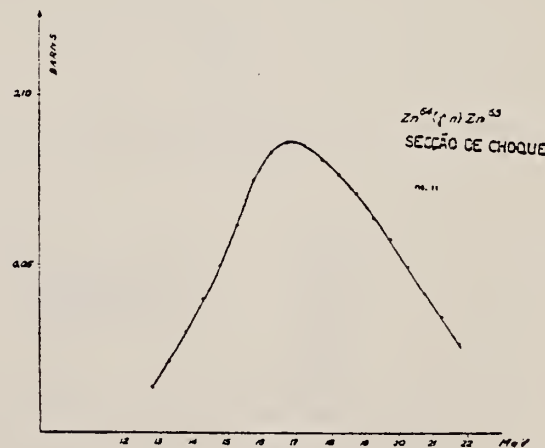


Fig. 11

Elemento	Limiar	$E_{max.}$	$\sigma_{max.}$	Δ	$\Gamma(larg.)$	$\int \sigma. dt$
$Zn^{64}(\gamma, n)$	11,62 Mev.	17 Mev.	0,087 barns	2,9 Mev.	6,2 Mev.	2,03 Mev \times barn

REF. A. El Sioufi, P. Erdos, and P. Stoll
Helv. Phys. Acta 30, 265 (1957)

ELEM. SYM.	A	Z
Zn	64	30
REF. NO.		
57 El 1		egf

METHOD					REF. NO.		
					57 E1 1	egf	
REACTION	RESULT	EXCITATION ENERGY	SOURCE		DETECTOR		ANGLE
			TYPE	RANGE	TYPE	RANGE	
G, 2N	ABI	THR- 30	C	32	ACT-I		4PI

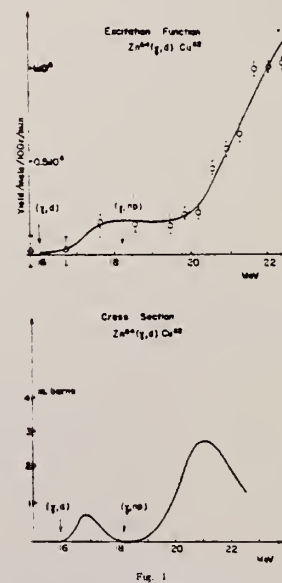
Tabelle 1.
Zusammenstellung der gem. W. Q.

Reaktion	Q-Wert MeV	MeV barn	Verhältnis der Querschnitte
Zn ⁶⁴ (γ , np)Cu ⁶⁴ *	18,65	0,02	$\frac{\sigma_{\text{Zn}^{64}(\gamma, p)}}{\sigma_{\text{Zn}^{64}(\gamma, np)}} = 3,6 \pm 0,5$
Zn ⁶⁶ (γ , p)Cu ⁶⁷ **)	10,01	0,08	
Zn ⁶⁴ (γ , 2n)Zn ⁶²	20,82	0,08	$\frac{\sigma_{\text{Zn}^{64}(\gamma, np)}}{\sigma_{\text{Zn}^{64}(\gamma, 2n)}} = 0,25$
Mo ⁹² (γ , np)Nb ⁹⁰	19,5	0,02	
Mo ⁹⁸ (γ , p)Nb ⁹⁷		0,09	$\frac{\sigma_{\text{Mo}^{98}(\gamma, p)}}{\sigma_{\text{Mo}^{92}(\gamma, np)}} = 4,5$
<p>*) σ_{max}: 5,3 mb bei $E_{\gamma} = 27 \pm 0,5$ MeV $\Gamma = 3,7$ MeV.</p> <p>**) σ_{max}: 11,5 mb bei $E_{\gamma} = 22 \pm 0,5$ MeV $\Gamma = 6,4$ MeV.</p>			

Method
Activation; 22 MeV Betatron

Ref. No.	EH
58 Go 3	

Reaction	E or ΔE	E_0	Γ	$\int \sigma dE$	$J\pi$	Notes
$(\gamma, d)^+$	16-22	~ 17				$\sigma_{\max} = \sim 1 \text{ mb.}$
(γ, np)		~ 21				$\sigma_{\max} = \sim 3 \text{ mb.}$



REF.

A. Hofmann, P. Stoll
 Helv. Phys. Acta 31, 591 (1958)

ELEM. SYM.	A	Z
Zn	64	30

METHOD

REF. NO.

58 Ho 1

egf

REACTION	RESULT	EXCITATION ENERGY	SOURCE		DETECTOR		ANGLE
			TYPE	RANGE	TYPE	RANGE	
G,NP	ABI	18- 32	C	32	ACT-I		4PI

(γ ,np) yields include (γ ,d).

Tabelle I

Reaktion	Q-Wert MeV	I.W.Q. $\bar{\sigma}$ MeV barn	σ_{\max} mb	E_{\max} MeV	Γ MeV
Ca ⁴⁰ (γ , pn) K ³⁹	- 24,3	0,005	2,4	30 \pm 1	2,1
Zn ⁶⁴ (γ , pn) Cu ⁶³	- 18,36	0,03			
Zn ⁶⁶ (γ , pn) Cu ⁶⁴	- 18,65	0,031	7,2	28 \pm 1	4
Zn ⁶⁸ (γ , p) Cu ⁶⁷	- 10,01	0,19	11,4	22,7 \pm 1	6
Se ⁸⁰ (γ , pn) As ⁷⁸	- 20,43	0,02			
Zn ⁶⁴ (γ , 2n) Zn ⁶²	- 20,82	0,08			
Mo ⁹² (γ , pn) Nb ⁹⁰	- 19,5	0,02			
Sb ¹²³ (γ , pn) Sn ¹²¹	- 18,2	0,0006			

Ref. T. Nakamura, K. Takamatsu, K. Fukunaga, N. Yata, S. Yasumi
J. Phys. Soc. Japan 14, 693 (1959)

Elem. Sym.	A	Z
Zn	64	30

Method $\text{Li}^7(p, \gamma)$ rays; GH counter; BF_3 ; 4π neutron

Ref. No.	
59 Na 1	EH

Reaction	E or ΔE	E_0	Γ	$\int \sigma dE$	$J\pi$	Notes
$\text{Zn}^{64}(\gamma, n)$	Bremss. 17.6					<p>$\sigma = 23.3 \pm 18\%$ mb.</p> <p>The ratio 1:2 was used as the intensity ratio of 14.8 to 17.6 MeV photons and the results of betatron experiments to make the correction.</p> <p>The incident flux was determined by calculating how many electrons should be ejected per photon from a metal foil placed in front of a geiger counter.</p>

Reference	Reaction	Method	Notes
H. Waples and G. Krieger (1956)	$\text{Li}^7(p, \gamma)$	Geiger counter	ad. F. L. L.
S. Hoshino (1957)	$\text{Li}^7(p, \gamma)$	Geiger counter	ad. H. Waples
R. D. Macfarlane, R. L. Walker and M. A. Szwed (1958)	$\text{Li}^7(p, \gamma)$	Geiger counter	ad. H. Waples
R. E. John, I. Katz, R. A. Douglas and R. E. H. Nelson (1958)	$\text{Li}^7(p, \gamma)$	Geiger counter	ad. F. L. L.
R. C. Dixon and G. M. Allen (1958)	$\text{Li}^7(p, \gamma)$	Geiger counter	ad. F. L. L.
P. E. Smith and W. E. Stephens (1958)	$\text{Li}^7(p, \gamma)$	Geiger counter	ad. F. L. L.
V. F. Krizan and E. F. Strickland (1958)	$\text{Li}^7(p, \gamma)$	Geiger counter	ad. F. L. L.
H. Ghent, O. Schepfer and P. Schell (1958)	$\text{Li}^7(p, \gamma)$	Geiger counter	ad. F. L. L.
R. Muehlebach, L. Kato and J. Goldberger (1958)	$\text{Li}^7(p, \gamma)$	Geiger counter	ad. F. L. L.
J. E. Carver and E. Koshikawa (1958)	$\text{Li}^7(p, \gamma)$	Geiger counter	ad. F. L. L.
A. I. Barnea and H. L. Brown (1958)	$\text{Li}^7(p, \gamma)$	Geiger counter	ad. F. L. L.
W. H. Hartley, W. E. Stephens and E. J. Winkler (1958)	$\text{Li}^7(p, \gamma)$	Geiger counter	ad. F. L. L.
R. J. Carver and L. E. Lohrman (1958)	$\text{Li}^7(p, \gamma)$	Geiger counter	ad. F. L. L.
F. Waples (1958)	$\text{Li}^7(p, \gamma)$	Geiger counter	ad. F. L. L.



- T. Nakamura, K. Takamatsu, K. Fukunaga, N. Yata, S. Yasumi: *Mem. Coll. Sci. Kyoto Univ.* (to be published).
- 13) S. Yasumi: J. Phys. Soc. Japan 12 (1957) 443.
- 14) P. V. C. Hough: Phys. Rev. 80 (1950) 1060.
- 15) R. W. King: Rev. Mod. Phys. 26 (1954) 327.
- 16) Y. Uemura, M. Sonoda, Y. Saji, S. Yasumi, Y. Ishizaki and Y. Ohno: Bull. Inst. Chem. Res. Kyoto Univ. 29 (1952) 66.
- 17) W. A. Fowler, C. C. Lauritsen and T. Lauritsen: Rev. Mod. Phys. 20 (1948) 238.
- 18) C. A. Barnes, J. H. Carver, G. H. Stafford and D. H. Wilkinson: Phys. Rev. 86 (1952) 352.

METHOD Betatron; neutron cross section; radioactivity; $\text{Cu}^{63}(\gamma, n)$ monitor

REF. NO.	NVB
60 Ro 4	

REACTION	RESULT	EXCITATION ENERGY	SOURCE		DETECTOR		ANGLE
			TYPE	RANGE	TYPE	RANGE	
G, N	ABX	12-23	C	12-23	ACT-I		4PI

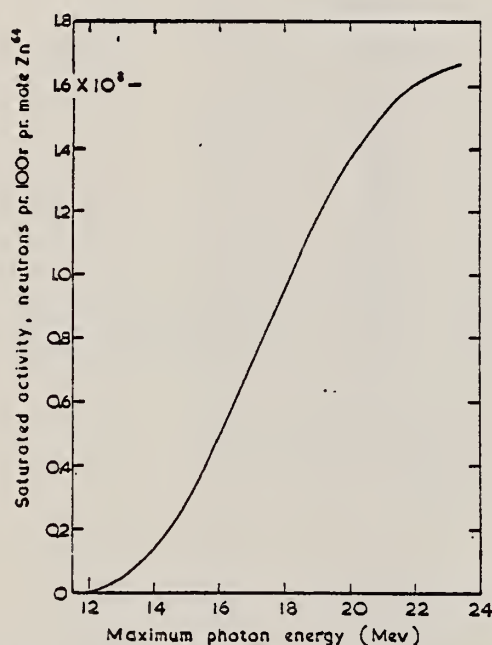


FIG. 1. Activation curve for the reaction $\text{Zn}^{64}(\gamma, n)\text{Zn}^{63}$ (corrected for K -capture).

TABLE I

References	Yield, n/mole 100 r	σ_{max} , mb	E_{max} , Mev	$\Gamma_{1/2}$, Mev	$\int_0^{E_1} \sigma(\gamma, n) dE$, Mev-barn	(E_1, Mev)	Ratio $\{\sigma \text{ for } \text{Cu}^{63}(\gamma, n)\} / \{\sigma \text{ for } \text{Zn}^{64}(\gamma, n)\} \text{ at } 17.6 \text{ Mev}$
Price and Kerst (1950)	2.35×10^8 at 22 Mev†						
Katz <i>et al.</i> (1951)	2.82×10^8 at 22 Mev	120	18.5	7.1	0.83	(24)	
Katz and Cameron (1951)*		124	18.7	7.9	0.99	(24)	
Strauch (1951)	(0.83 rel. to Cu^{63} at 322 Mev)				(~.56)	(322)†	
Marshall (1951)	(1.05 rel. to Cu^{63} at 50 Mev)				0.77	(50)	
Sagane (1952)					(~.56)	(67)†	
Montalbetti <i>et al.</i> (1953)	2.9×10^8 at 22 Mev						
Bunbury (1954)							1.3
Gavrilov and Lazareva (1956)		82	16.3	6.3	0.66	(27)	
Present work	1.60×10^8 at 22 Mev (.71 rel. to Cu^{63} at 22 Mev)	48	17.2	7.0	0.33	(23)	1.9

*Recalculation of values of Katz *et al.* (1951) using photon difference method.

†For natural element.

‡These values are calculated from a relative integrated cross section of 0.89 compared to the reaction $\text{Cu}^{63}(\gamma, n)\text{Cu}^{63}$, assuming the cross section to be small above the giant dipole resonance.

Ref. G.E. Coote, W.E. Turchinets, I.F. Wright
Nuclear Phys. 23, 468 (1961)

Elem. Sym.	A	Z
Zn	64	30
Ref. No.		
61 Co 2		JHH

Method
Li⁷(p,γ) source; activation; NaI

Reaction	E or ΔE	E ₀	Γ	$\int \sigma dE$	J π	Notes
(γ,n)						$\sigma = 40 \pm 4$ mb relative to 59 ± 6 mb for Cu ⁶³ (γ,n), measured for 440 keV (E _p) resonance radiation from Li ⁷ .

Elem. Sym.	A	Z
Zn	64	30

Ref. No.	
62- DA-1	JHH

Reaction	E or ΔE	E_0	Γ	$\int \sigma dE$	$J\pi$	Notes
(γ, n)	20.48					$\sigma(\gamma, n) = 35.7 \pm 1.7 \text{ mb}$

REF. S. Costa, F. Ferrero, S. Ferroni and R. Malvano
Proc. Paris Conference 1034 (1964)

ELEM. SYM.	A	Z
Zn	64	30

METHOD

100 MeV synchrotron

REF. NO.

64 Co 3

JDM

REACTION	RESULT	EXCITATION ENERGY	SOURCE		DETECTOR		ANGLE
			TYPE	RANGE	TYPE	RANGE	
G,N	AB I	THR-80	C	10-80	BF3-I		4PI

TABLE

ELEMENT	Yield (36 MeV) $\left(\frac{\text{n. cm}^2}{\text{mol. MeV}}\right) \times 10^5$	Σ_0^{30}	Σ_0^{80}	$\Sigma_0^{30}/\Sigma_0^{80}$	σ_{-1} (mb)
²⁴ Cr	83	1.21	2.1	0.58	62
²⁵ Mn	108	1.52	2.33	0.65	76
²⁶ Fe	68	0.88	1.46	0.60	50
²⁷ Co	89	1.08	1.82	0.59	64
²⁸ Ni	44	0.55	1.07	0.51	34
²⁹ Cu	95	1.06	1.99	0.53	72
³⁰ Zn	88	0.94	1.68	0.56	66
³¹ Ga	130	1.29	2.18	0.59	94
³² Ge	139	1.35	2.29	0.59	101
³³ As	137	1.22	2.18	0.56	100

$\sum_a^b = \frac{A}{60 NZ} \int_a^b \sigma(E) dE$ is the integrated cross section measured in units of the classical dipole $60 NZ/A$ mb. MeV.

METHOD

Betatron

REF. NO.

66 Ho 3

JDM

REACTION	RESULT	EXCITATION ENERGY	SOURCE		DETECTOR		ANGLE
			TYPE	RANGE	TYPE	RANGE	
G, A	SPC	THR-31	C	31	SCD-D	3-14	130

TABLE I
Experimental data and results

Element	Mg	Al	S	Ni	Cu	Zn	Error (%)
target thickness (mg/cm ²)	0.31	1.54	0.80	2.50	2.68	3.00	5 ^{a)}
dose (r)	6190	25400	23200	3880	5840	4220	10
yield absolute (10 ⁴ /mole · r) for $E_m > 3.16$ MeV	0.61	0.93	1.46	1.65	0.92	2.42	11 ^{a)}
yield relative to Ni	0.36	0.56	0.88	1	0.55	1.43	5 ^{a)}
$Y_{7,a}/Y_{7,tot}$ (%)	9.6	11.4	12.4	7.0	3.2	^{b)}	
nuclear temp. θ (McV)	1.43	1.48	1.46	1.04		0.91	10
level density parameter a (McV ⁻¹)	5.1	4.8	4.9	8.6		10.8	10

^{a)} For S, the error of the target thickness has been 10 %, of the absolute yield 14 % and of the relative yield 10 %.
^{b)} For Zn $\sigma_{7,tot}$ is not known.

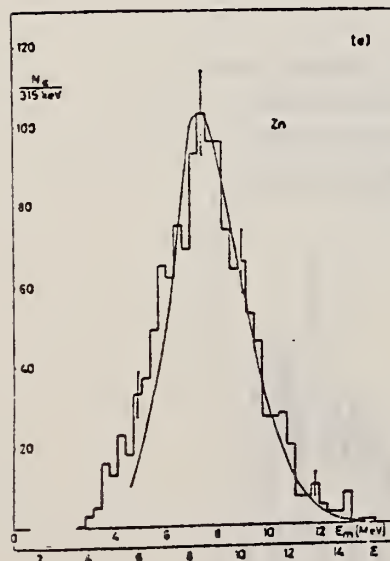


Fig. 3d-e. Photoalpha spectra of Ni and Zn. Notations as in fig. 3a-c.

Fig. 3f. Statistical plot of the measured spectra. The straight lines are drawn to give the best fit.

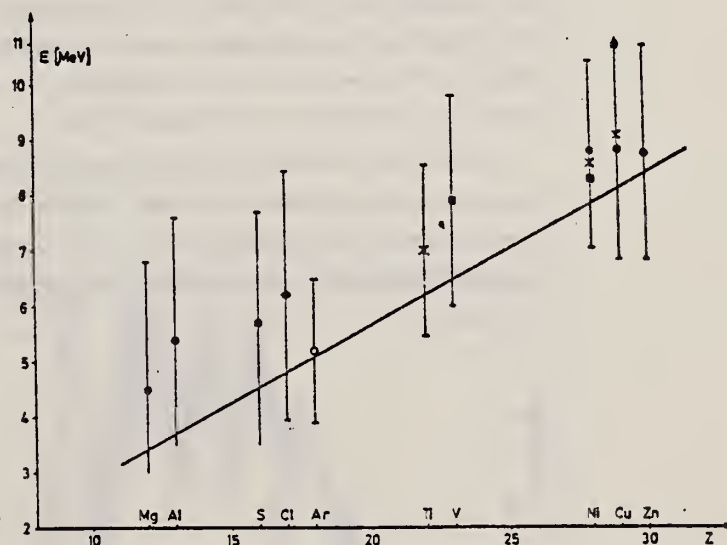


Fig. 4. Position of the peaks in different photoalpha spectra plotted against Z of the target nuclei. \times : Scheer *et al.*¹⁹⁾, \blacksquare : Kregar and Povh⁹⁾, \blacktriangle : Meneghetti and Vitale⁴⁾, \blacklozenge : Erdős *et al.*¹⁾, \circ : Komar *et al.*¹⁾, \bullet : this work. The signs show the position of the maximum, the bars give the widths at half maximum. The curve shows the height of the Coulomb barrier.

ELEM. SYM.	A	Z
Zn	64	30
REF. NO.	67 Ca 1	EGF

METHOD

REACTION	RESULT	EXCITATION ENERGY	SOURCE		DETECTOR		ANGLE
			TYPE	RANGE	TYPE	RANGE	
G,N	RLX	12-22	C	12-22	ACT-I		4PI

Experimental Measurements of Vibrational Splitting of the Giant Dipole Resonance*

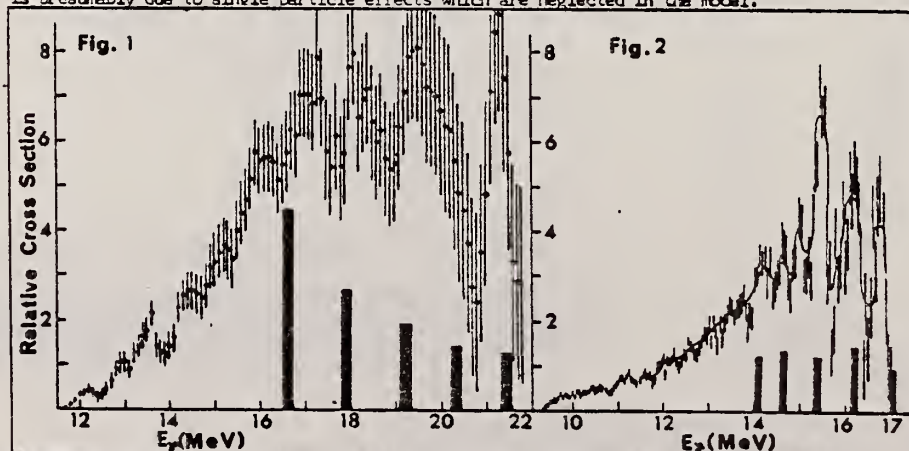
P. H. Cannington, D. G. Owen, R.J.J. Stewart, E. G. Muirhead and B. M. Spicer
 University of Melbourne, Australia

The yield curve for the reaction $Zn^{64}(\gamma,n)$ has been measured in 0.1 MeV steps from threshold to 23 MeV, and that for $Pr^{141}(\gamma,n)$ has been measured in 0.05 MeV steps from threshold to 17.5 MeV. In both cases, the positron activity of the residual nucleus was detected by counting annihilation radiation. The cross sections were obtained from the yield curve by the Leiss-Penfold method.

The cross section for the $Zn^{64}(\gamma,n)$ reaction is shown in Fig. 1. Also shown are the predictions of Greiner¹⁾, whose model considers the Goldhaber-Teller type dipole vibration, the low energy surface vibrations of spherical nuclei, and the coupling of these two vibrations. The predictions show only the energy, and integrated absorption cross section for the several transitions.

The $Pr^{141}(\gamma,n)$ cross section is shown in Fig. 2, and the calculations of Huber²⁾ are shown in blocked form; their detail is the same as above. In this case, the surface vibration phonon energy was not so easily fixed as in the case of even-A Zn^{64} . There were, in the case of Pr^{141} , two possible choices indicated by the low energy spectra of neighbouring nuclei. The more suitable one is indicated in Fig. 2.

In both cases, the amount of structure found experimentally exceeds that predicted by the dipole-surface vibration-interference model. However, by worsening the experimental resolution, the agreement can be readily improved. The surplus structure in both cross sections is presumably due to single particle effects which are neglected in the model.



*Supported in part by the U.S. Army Research Office and the Australian Research Grants Committee.

- References: 1) W. Greiner, private communication (1965).
 2) M. Huber, private communication (1966).

REF.

S. Costa, F. Ferrero, C. Manfredotti, L. Pasqualini and G. Piragino
and H. Arenhovel
Nuovo Cimento 48B, 461 (1967)

ELEM. SYM.	A	Z
Zn	64	30

METHOD

Betatron; NBS ionization chamber

REF. NO.

67 Co 1

JDM

REACTION	RESULT	EXCITATION ENERGY	SOURCE		DETECTOR		ANGLE
			TYPE	RANGE	TYPE	RANGE	
G, XN	ABX	12-24	C	24	BF3-I		4PI

433

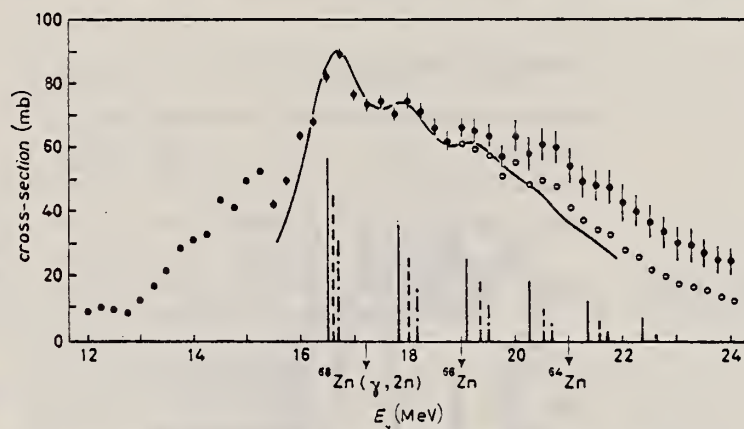


Fig. 2. $\sigma(\gamma, 2n)$ cross-section for ^{68}Zn . The vertical bars represent the dipole strengths calculated for ^{68}Zn (—), ^{68}Zn (---) and ^{64}Zn (-.-.-). Open circles give the $(\gamma, 2n)$ cross-section corrected for neutron multiplicity. The level density parameter used has been taken from ref. (*).

ELEM. SYM.	A	Z
Zn	64	30

METHOD	REF. NO.	
	68 Ow 1	egf

REACTION	RESULT	EXCITATION ENERGY	SOURCE		DETECTOR		ANGLE
			TYPE	RANGE	TYPE	RANGE	
G,N	RLX	12-24	C	10-24	ACT-I		4PI

109

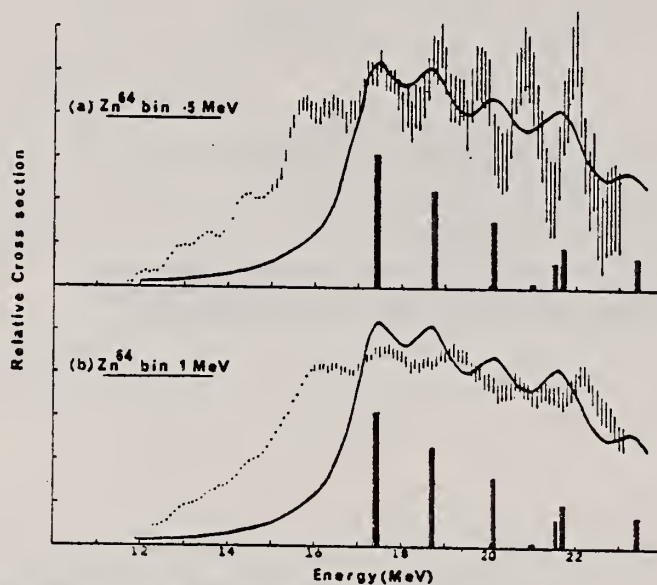


Fig. 1. The $^{64}\text{Zn}(\gamma, n)^{64}\text{Zn}$ cross section analysed in (a) 0.5 and (b) 1 MeV bins. The errors shown represent the total experimental uncertainty in each point. The continuous curve is the shape of the ^{64}Zn photo-absorption cross section predicted by Huber ⁴⁾ using the parameters in table 1. The vertical bars represent the relative strengths of the individual theoretical levels.

R. B. Begzhanov and S. M. Akhrarov
ZhETF Pis. Red. 10, 39 (1969)
JETP Letters 10, 26 (1969)

ELEM. SYM.	A	Z
Zn	64	30
REF. NO.		
69 Be 7		hmg

METHOD

REACTION	RESULT	EXCITATION ENERGY	SOURCE		DETECTOR		ANGLE
			TYPE	RANGE	TYPE	RANGE	
G, G	LFT	7.0	D	7.0	D		DST
		(7.38)		(7.38)			(90, 135)

Self-Absorption.

7.38 MEV

Results of determination of the resonance-level parameters

Source-scatterer	E_γ , MeV	$\langle\sigma_{pp}\rangle$, mb	Γ_{γ_0} , eV	D, keV	Reference
Pb \rightarrow Zn ⁶⁴	7.38	33 \pm 4.5	0.58 \pm 0.12	53.70 \pm 0.13	This work
Ti \rightarrow Mo ⁹⁶	6.413	11.2 \pm 1.4	0.11 \pm 0.02	8.68 \pm 1.57	"
Ti \rightarrow La ¹³⁹	6.413	16.04 \pm 2.10	0.23 \pm 0.05	8.93 \pm 1.42	"
Ti \rightarrow Bi ²⁰⁹	7.15	1200 \pm 230	0.32 \pm 0.07	1.84 \pm 0.40	"
	6.996	1560	-	-	[1]
	7.15	2600 \pm 800	0.42 \pm 0.14	-	[5]
Ti \rightarrow Cu ⁶⁵	6.07	423 \pm 108	0.34 \pm 0.06	99.1 \pm 17.4	This work
	6.07	440 \pm 130	0.36 \pm 0.07	-	[5]
Ti \rightarrow Ca ⁶³	6.07	215 \pm 71	0.18 \pm 0.04	57.14 \pm 12.70	This work
	6.07	200 \pm 50	0.16 \pm 0.03	-	[6]
Cr \rightarrow Cu ⁶³	8.50	22 \pm 7	0.25 \pm 0.08	130 \pm 40	This work
	8.499	35	75	-	[1]
	8.50	19 \pm 6	0.28 \pm 0.09	-	[6]
Cr \rightarrow Ca ⁶⁵	8.50	36 \pm 9	0.47 \pm 0.10	21.36 \pm 4.54	This work
	8.499	80	10.5	-	[1]
	8.50	42 \pm 13	0.94 \pm 0.29	-	[6]
Ca \rightarrow Se ¹¹⁷	7.01	1150 \pm 240	0.15 \pm 0.04	0.44 \pm 0.12	This work
	7.01	1000	-	-	[1]
	7.01	1200 \pm 400	0.3 \pm 0.3	-	[5]
Hg \rightarrow Mo ⁹⁶	6.44	201 \pm 37	0.12 \pm 0.04	0.23 \pm 3.07	This work

REF. V.D. Afanas'ev, N.G. Afanas'ev, A. Yu. Buki, G.A. Savitskii,
V.M. Khvastunov, N.G. Shevchenko
Yad. Fiz. 12, 885 (1970)
Sov. J. Nucl. Phys. 12, 480 (1971)

ELEM. SYM.	A	Z
Zn	64	30

METHOD

REF. NO.	
70 Af 1	hmg

REACTION	RESULT	EXCITATION ENERGY	SOURCE		DETECTOR		ANGLE
			TYPE	RANGE	TYPE	RANGE	
E _γ /E _γ	FME	0-3	D	150,225	MAG-D		DST

.99,3.0 MEV, B(EL)

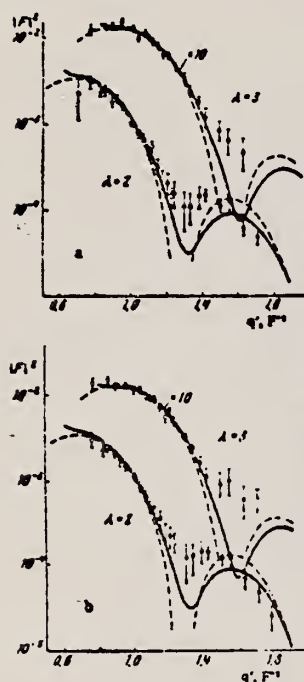


FIG. 2. Form factors of E₂ and E₃ transitions in Zn⁶⁴ (a) and Zn⁶⁶ (b). The solid curves pertain to the vibrational model with calculations in the high-energy approximation; the dashed curves pertain to Helm's model with calculations in the Born approximation. The experimental values and curves for E₃ transitions are enlarged 10-fold. Points: O—E₂, ●—E₃, = 150 MeV, ●—E₃, = 225 MeV.

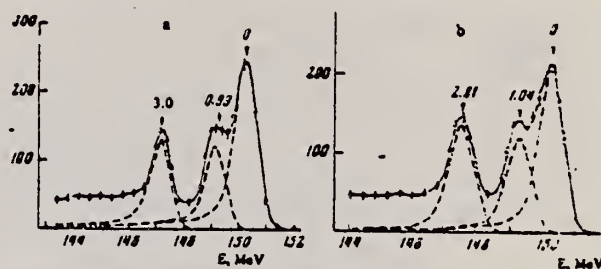


FIG. 1. Spectra of electrons scattered by (a) Zn⁶⁴ and (b) Zn⁶⁶ at 75° (E₀ = 150 MeV). Ordinates are given in arbitrary units.

Table I. Reduced probabilities and fitting parameters N_λ and B_λ of E2 and E3 transitions in Zn isotopes

Isotope	E, MeV	J ^π	Vibrational model		Helm's model		Other results	
			N _λ · 10	B (Aλ) †	N _λ · 10	B (Aλ) †	B(E2) (experiment)	B(E2) (theory)
Zn ⁶⁴	1.04	2 ⁺	0.141 ± 0.008	1720 ± 140	0.546 ± 0.018	1'00 ± 70	1100 [1], 1700 ± 160 [1]	1400 [11], 1540 [12]
	3.3	3 ⁻	0.070 ± 0.003	32300 ± 2300	0.489 ± 0.011	29100 ± 1500		
	0.99	2 ⁺	0.144 ± 0.008	1800 ± 150	0.567 ± 0.017	1650 ± 74	1100 [1], 1450 ± 150 [1]	2000 [11]
Zn ⁶⁶	2.81	3 ⁻	0.870 ± 0.003	33700 ± 2400	0.498 ± 0.013	29700 ± 1700		

Note. B(Eλ) is given in units of e² · F^{2λ}.

Table II. Parameters of the charge distribution in Zn isotopes for the Fermi model and the Gaussian uniform model

Isotope	Fermi model		Gaussian uniform model	
	a, F	t, F	R, F	g, F
Zn ⁶⁴	4.265 ± 0.016	2.754 ± 0.017	4.500 ± 0.017	0.721 ± 0.015
Zn ⁶⁶	4.271 ± 0.022	2.803 ± 0.027	4.508 ± 0.025	0.877 ± 0.014

REF. B.C. Cook, R.C. Morrison, and F.H. Schamber
Phys. Rev. Letters 25, 685 (1970)

ELEM. SYM.	A	Z
Zn	64	30

METHOD

REF. NO.	
70 Co 1	hmg

REACTION	RESULT	EXCITATION ENERGY	SOURCE		DETECTOR		ANGLE
			TYPE	RANGE	TYPE	RANGE	
G,N	RLX	12-40 (11.9-40)	C	10-40	ACT-I		4PI.
G,2N	RLX	21-40	C	10-40	ACT-I		4PI
G,NP	RLX	19-40 (18.6-40)	C	10-40	ACT-I		4PI

Abstract: The (γ, np) reaction is discussed as a probable channel for observation of the $T = T_0 + 1$ component of the giant dipole resonance, and experimental evidence is presented in support of this conjecture in the case of ^{64}Zn .

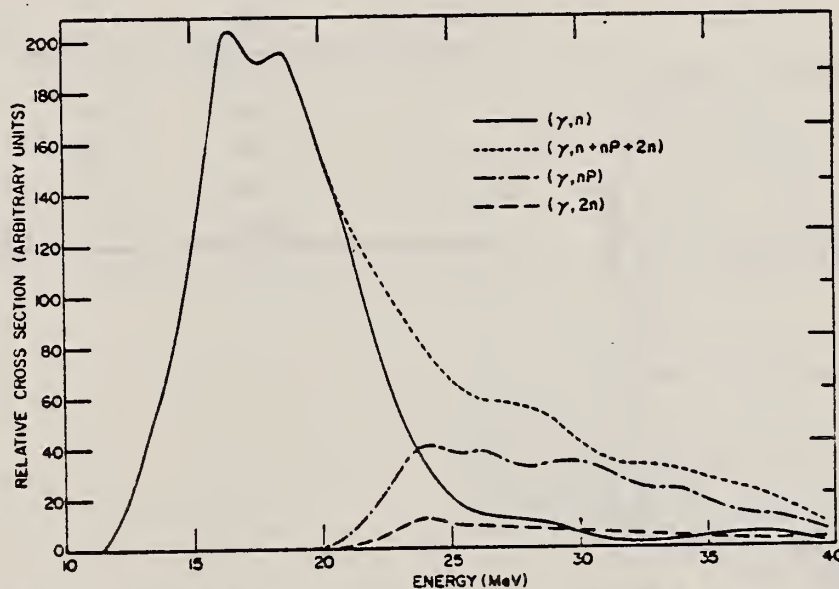


FIG. 2. The relative cross sections for $^{64}\text{Zn}(\gamma, n)$, (γ, np) , and $(\gamma, 2n)$, along with the sum cross section for all three reactions.

[over]

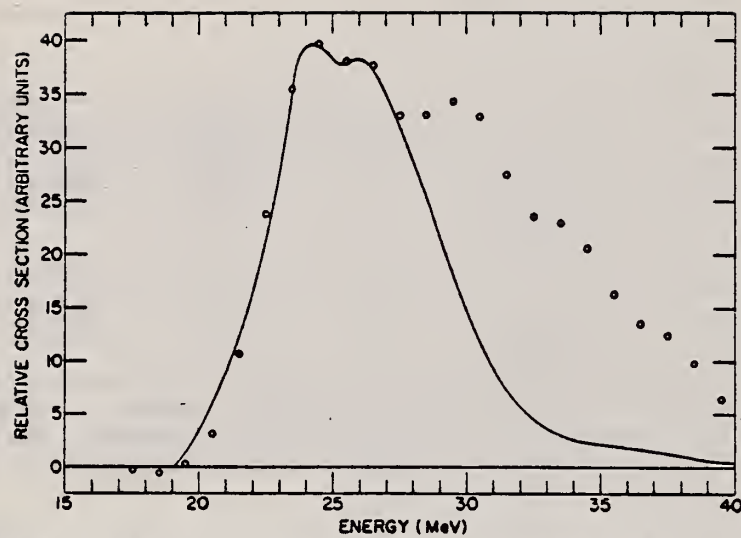


FIG. 3. The measured cross section for $^{64}\text{Zn}(\gamma, np)^{62}\text{Cu}$ (points). The solid curve is the measured (γ, n) cross section shifted up in energy by 7.7 MeV and multiplied by 0.196.

ELEM. SYM.	A	Z
Zn	64	30
REF. NO.		
71 Pa 3		hmg

METHOD			SOURCE		DETECTOR		ANGLE
REACTION	RESULT	EXCITATION ENERGY	TYPE	RANGE	TYPE	RANGE	
P,G	ABX	10-26	D	2-18	NAI-D		90

TABLE I. Separation energies $\Delta E = E_p - E_n$ of the $T+1$ and T components of the GDR observed from proton capture into various nuclei with ground-state isospin T . \bar{V} is obtained from Eq. (2) in the text.

Nucleus	ΔE (MeV)	T	\bar{V} (MeV)	Ref.
^{42}Ca	3.0 ± 0.2	1	63 ± 4	13
^{49}Sc	4.8 ± 0.2	$7/2$	52 ± 2	Present
^{60}Ni	3.0 ± 0.2	2	60 ± 4	5
^{64}Zn	3.2 ± 0.3	2	68 ± 6	Present
$^{64}\text{Zn}^a$	2.9 ± 0.3	2	62 ± 6	Present
^{88}Sr	3.7 ± 0.5	6	47 ± 6	1
^{89}Y	3.9 ± 0.5	$11/2$	54 ± 7	2
$^{89}\text{Y}^a$	3.8 ± 0.4	$11/2$	52 ± 6	2
^{90}Zr	3.9 ± 0.5	5	58 ± 7	1
^{91}Nb	3.6 ± 0.7	$9/2$	59 ± 10	2

^aFirst excited state.

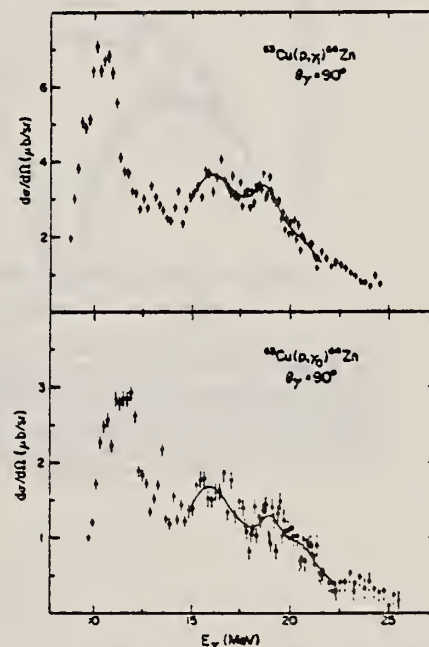


FIG. 2. Proton-capture yield curves for the ground-state (γ_0) and first-excited-state (γ_1) transitions in ^{64}Zn plotted as a function of γ -ray energy.

REF.

J. W. Lightbody Jr.
Phys. Letters 38B, 475 (1972)

ELEM. SYM.	A	Z
Zn	64	30
REF. NO.		
72 Li 1		egf

METHOD

REACTION	RESULT	EXCITATION ENERGY	SOURCE		DETECTOR		ANGLE
			TYPE	RANGE	TYPE	RANGE	
E, E/	FMF	0-2	D	60-120	MAG-D		DST

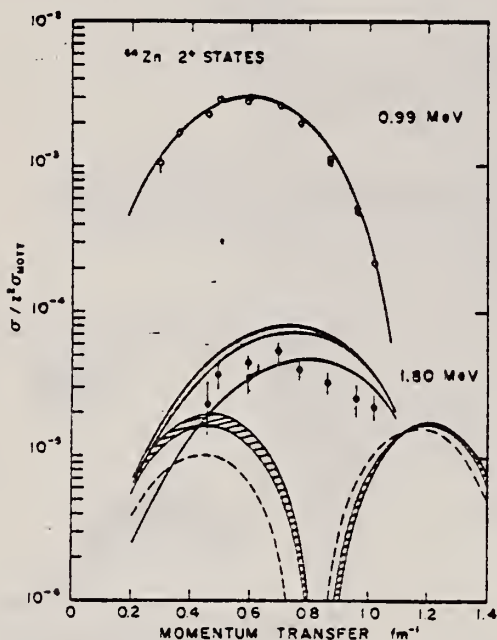
.99, 1.80 MEV

Fig. 3. Electron scattering form factors for the lowest two 2^+ states in ^{64}Zn . Solid lines were calculated using a best fit admixture and phase. The dashed line represents the harmonic two-phonon form factor. The shaded and cross-hatched regions were determined by using admixtures which fit the measured BR for $\Phi = \pi$ and 0, respectively.

F. R. Metzger
Nucl. Phys. A189, 409 (1972)

Zn

64

30

METHOD

REF. NO.

72 Me 3

egf

REACTION	RESULT	EXCITATION ENERGY	SOURCE		DETECTOR		ANGLE
			TYPE	RANGE	TYPE	RANGE	
G _g G	LFT	3-5	C	5	SCD-D		DST

J-PI

TABLE I

Properties of the Zn levels observed in the bremsstrahlung experiments

Energy (keV)	Isotope	Spin	Parity	Γ_0/Γ'	Γ_0 (meV)	Γ_0^{*+} (meV)
3346	(68)	1		(0.70) ^{a)}	42 \pm 7	9.9 $\times 10^{-4}$ (E1) (0.061 (M1)
3366	64	1 ^{b)}	+ ^{b)}	0.54 ^{c)}	8.2 \pm 1.3	0.012
3381	66	1	(+) ^{d)}	0.69 ^{a)}	16 \pm 3	0.022
3425	64	1 ^{b)}	+ ^{b)}	0.72 ^{c)}	6.9 \pm 1.6	0.009
3433	(66)	(1) ^{d,e)}	(-) ^{a)}	0.51 ^{a)}	8 \pm 3	1.7 $\times 10^{-4}$
3704	64	1	(-)	(1.0) ^{f)}	18 \pm 3	3.2 $\times 10^{-4}$
3717	(68)	(1)		(1.0) ^{f)}	8.5 \pm 2.2	1.5 $\times 10^{-4}$ (E1) (0.009 (M1)
3739	66	1	(-)	(1.0) ^{f)}	24 \pm 3	4.1 $\times 10^{-4}$
4159	64	1	(-)	(0.54) ^{a)}	32 \pm 9	4.0 $\times 10^{-4}$
4295	66	1 ^{b)}	(+) ^{b)}	0.60 ^{a)}	67 \pm 20	0.046
4339	(68)	(1)		(1.0) ^{f)}	38 \pm 10	4.2 $\times 10^{-4}$ (E1) (0.025 (M1)
4426	66	1	(-)	(1.0) ^{f)}	65 \pm 10	6.8 $\times 10^{-4}$
4455	64	1 ^{b)}	- ^{b)}	(1.0) ^{f,g)}	51 \pm 9	0.031
4462	66	1 ^{d)}	(+) ^{d,h)}	0.29 ^{a)}	28 \pm 21	0.017
4466	(68)	1		(1.0) ^{f)}	65 \pm 19	6.5 $\times 10^{-4}$ (E1) (0.040 (M1)
4503	(68)	(1)		(1.0) ^{f)}	38 \pm 13	3.6 $\times 10^{-4}$ (E1) (0.023 (M1)
4609	(66)	(1)		(1.0) ^{f)}	54 \pm 15	5.0 $\times 10^{-4}$ (E1) (0.030 (M1)
4664	(64)	(1)		(1.0) ^{f)}	11 \pm 4	1.0 $\times 10^{-4}$ (E1) (0.006 (M1)
4685	(66)	(1)		(1.0) ^{f)}	64 \pm 16	5.6 $\times 10^{-4}$ (E1) (0.034 (M1)
4806	(66)	1 ^{a)}	+ ^{a)}	0.81 ^{a)}	100 \pm 25	0.049

^{a)} Based on ref. ⁹⁾, see text.^{b)} Ref. ¹⁾.^{c)} Ref. ¹²⁾.^{d)} Ref. ²⁾.^{e)} Ref. ¹⁰⁾.^{f)} Assumed in the absence of evidence for branching.^{g)} Assuming that the branch to the 2_1^+ state, seen in the bremsstrahlung experiment, is the only branch to an excited state.^{h)} Refs. ^{11,12)} contradict each other with respect to this branching.ⁱ⁾ Ref. ¹⁰⁾ favors a (-) assignment. See text.

(over)

- 1) H. Verheul, Nucl. Data B2-3 (1967) 65
- 2) M. J. Martin and M. N. Rao, Nucl. Data B2-6 (1968) 43
- 3) F. R. Metzger, Annual progress report for 1967, AEC contract AT(30-1)-3525, Nucl. Sci. Abstr. 22-7661, 1968
- 4) F. R. Metzger, Annual progress report for 1968, AEC contract AT(30-1)-3525, Nucl. Sci. Abstr. 23-15431, 1969
- 5) F. R. Metzger, Phys. Rev. Lett. 18 (1967) 434; Phys. Rev. 171 (1968) 1257;
M. Berman and G. B. Beard, Phys. Rev. C2 (1970) 1506;
M. Schumacher, J. Weiss and H. Langhoff, Phys. Lett. 31B (1969) 61;
H. Langhoff, Phys. Rev. A3 (1971) 1
- 6) F. R. Metzger, Phys. Rev. 187 (1969) 1680, 1700; Nucl. Phys. A182 (1972) 213
- 7) F. R. Metzger, Nucl. Phys. A158 (1970) 88
- 8) R. P. Singh and M. L. Rustgi, Phys. Rev. C3 (1971) 1172
- 9) H. Ottmar, N. M. Ahmed, U. Fanger, D. Heck, W. Michaelis and H. Schmidt, Nucl. Phys. A164 (1971) 69
- 10) D. C. Camp and G. L. Meredith, Nucl. Phys. A166 (1971) 349
- 11) J. Konijn, R. van Lieshout, J. P. Deutsch and L. Grenacs, Nucl. Phys. A91 (1967) 439
- 12) L. G. Mann, K. G. Tirsell and S. D. Bloom, Nucl. Phys. A97 (1967) 425

ELEM. SYM.	A	Z
Zn	64	30
REF. NO.		egf
73 Cl 6		

REACTION	RESULT	EXCITATION ENERGY	SOURCE		DETECTOR		ANGLE
			TYPE	RANGE	TYPE	RANGE	
G,XP	ABX	8- 26	C	15- 26	SCD-D		DST

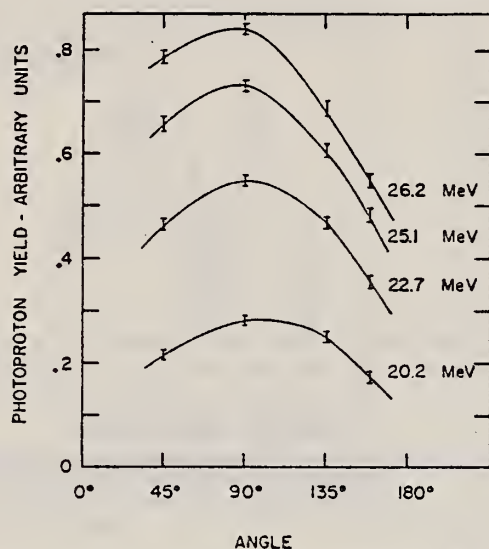


Fig. 3. Angular distributions of protons with energies greater than 8 MeV, for several bremsstrahlung end-point energies.

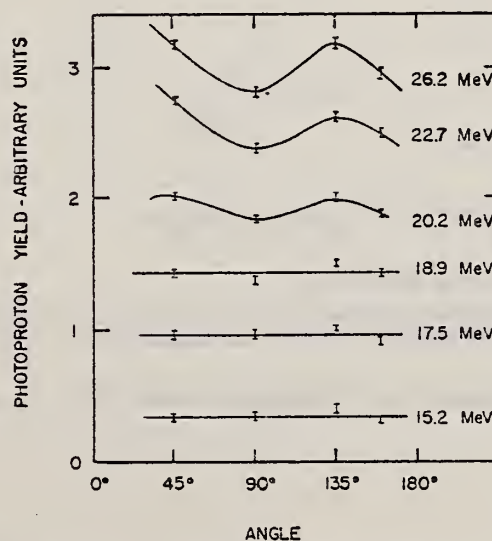


Fig. 4. Angular distributions of protons with energies between 4 and 8 MeV, for several bremsstrahlung end-point energies.

(over)

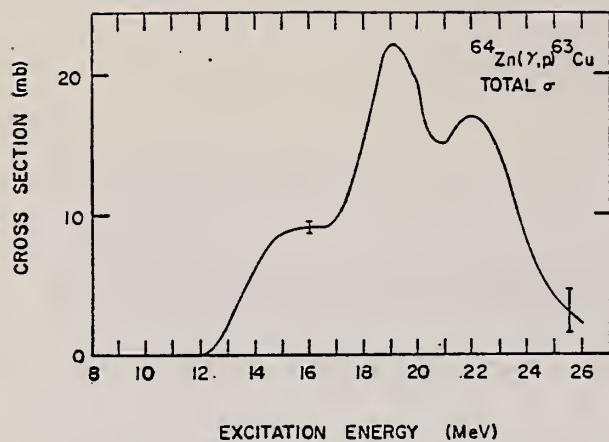


Fig. 6. Total cross section for production of photoprotons with energies above 4 MeV.

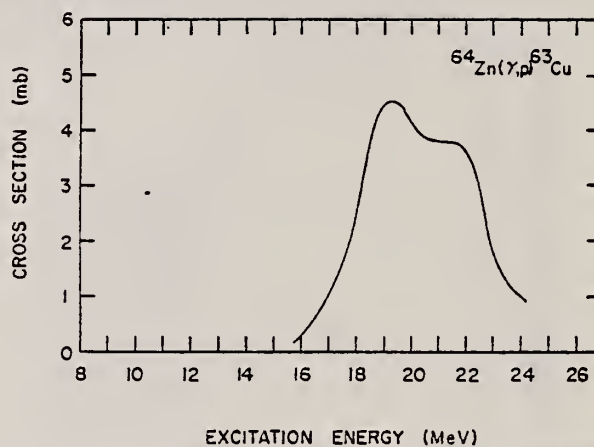


Fig. 7. Total cross section for production of photoprotons with energies above 8 MeV.

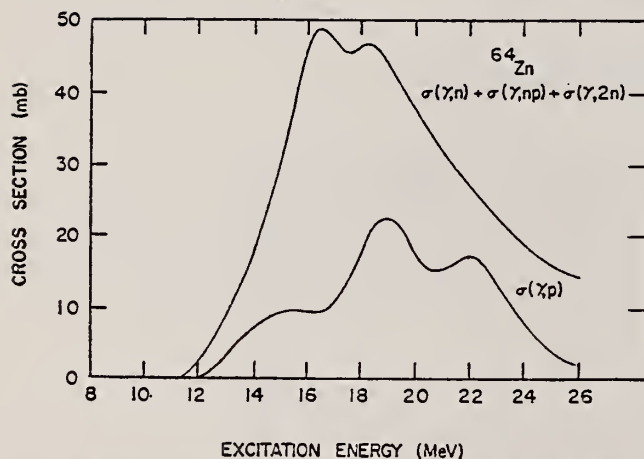


Fig. 8. The ^{64}Zn photoproton cross section of this work, and the sum of the (γ, n) , (γ, p) , $(\gamma, 2n)$ and (γ, np) cross sections obtained by Schamber and co-workers^{8,9}.

⁹B. G. Cook, R. G. Morrison, F. H. Schamber, Phys. Rev. Lett. 25, 685 (1970).

REF. W. Del Bianco, S. Kundu, and P. Boucher
Can. J. Phys. 51, 1302 (1973)

ELEM. SYM.	A	Z
Zn	64	30
REF. NO.		
73 De 3		hmg

METHOD			SOURCE		DETECTOR		ANGLE
REACTION	RESULT	EXCITATION ENERGY	TYPE	RANGE	TYPE	RANGE	
G,N	RLX	20- 22 (20.43-21.94)	D	20- 22	ACT-I		90

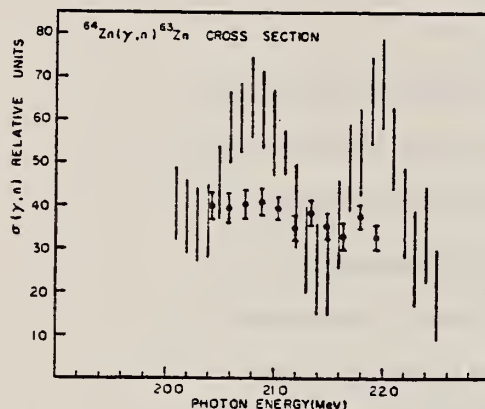


FIG. 1. Relative cross section of the $^{64}\text{Zn}(\gamma,n)^{63}\text{Zn}$ reaction. The dots represent the results of this experiment and the vertical lines the results of Owen *et al.* (1968) analyzed in 0.5 MeV bins.

Owen *et al.*, Nucl. Phys. A122, 177 (1968).

ELEM. SYM.	A	Z
Zn	64	30
REF. NO.		
73 De 8		hmg

METHOD

REACTION	RESULT	EXCITATION ENERGY	SOURCE		DETECTOR		ANGLE
			TYPE	RANGE	TYPE	RANGE	
G,N	ABX	20- 22	D	20- 22	ACT-I		4PI

The measurement of (γ, n) cross sections in spherical medium weight nuclei is of great interest for determining the coupling of low energy surface vibrations and high energy dipole oscillations. The coupling has been theoretically investigated by Huber et al.¹⁾ and found to result in a considerable splitting of the photonuclear resonance. Experimentally bremsstrahlung measurements have indicated a pronounced structure in (γ, n) cross sections^{2, 3)} which is not present in measurements with γ -rays from positron annihilation in flight^{4, 5)}. In this experiment a photoactivation method and monochromatic γ -rays from the ${}^3\text{H}(p, \gamma){}^4\text{He}$ reaction were employed to measure the (γ, n) cross section for ${}^{50}\text{Cr}$ and ${}^{64}\text{Zn}$. The γ -rays were monitored by a NaI(Tl) crystal enclosed in a lead and paraffin shield to reduce background radiation. The positron activity was determined by a coincidence detector consisting of two NaI(Tl) crystals set on the annihilation radiation photopeaks. The γ -ray energy was varied in steps of 150 keV from 20.43 to ≈ 22.2 MeV and the energy resolution was less than 110 keV over the entire energy range. The experimental cross sections of the two reactions were found to vary smoothly as a function of energy. The results for the ${}^{64}\text{Zn}(\gamma, n)$ process do not agree with those of Owen et al.²⁾, who observed two resonances ≈ 0.5 to 1 MeV wide in the same energy range. The shape of the ${}^{50}\text{Cr}(\gamma, n)$ cross section is in fair agreement with the calculation of Huber et al.¹⁾ for widths of the dipole states of the order of 3 MeV.

(over)

- 1) M.G. Huber, M. Danos, H. Weber and W. Greiner, Phys. Rev. 155, 1073(1967).
- 2) D.G. Owen, E.G. Muirhead and B.M. Spicer, Nucl. Phys. A122, 177(1968).
- 3) P.H. Cannington, R.J. Stewart and B.M. Spicer, Nucl. Phys. A102, 385(1968).
- 4) R.L. Bramblett, J.T. Caldwell, B.L. Berman, R.R. Harvey and S.C. Fultz,
Phys. Rev. 148, 1198 (1966).
- 5) R.E. Sund, V.V. Verbinski, H. Weber and L.A. Kull, Phys. Rev. C2, 1129 (1970).

METHOD

REF. NO.

73 Ne 4

hmg

REACTION	RESULT	EXCITATION ENERGY	SOURCE		DETECTOR		ANGLE
			TYPE	RANGE	TYPE	RANGE	
E, E/	FMF	0- 3	D	150,275	MAG-D		DST

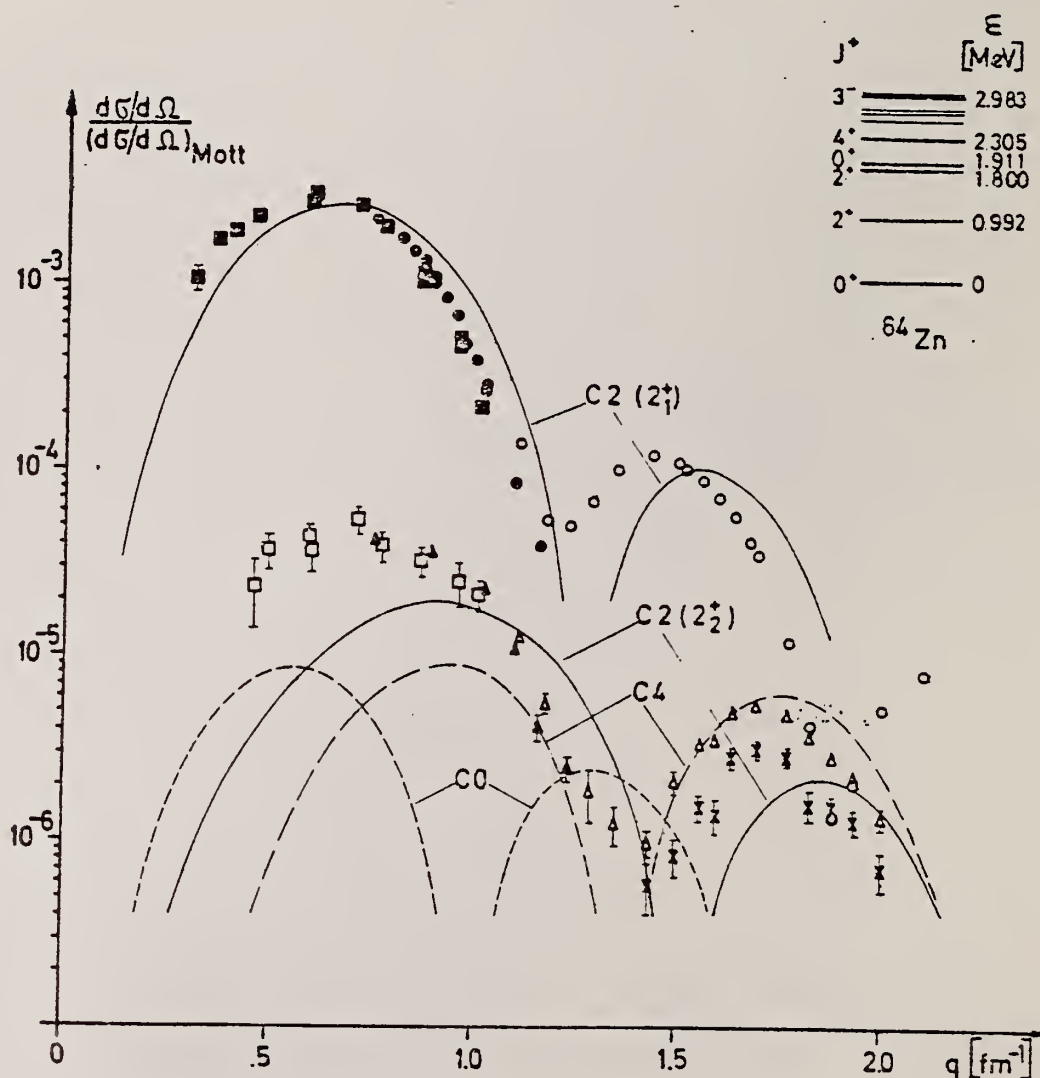


Fig. 1: Form factors for the transitions to the $2^+_{1,2}$ and $4^+_{2,3}$ states in ^{64}Zn .
 C2 transition to the 0.992 MeV 2^+_1 state: \blacksquare NBS, $E_0 = 40-110$ MeV; \bullet MAINZ, $E_0 = 150$ MeV; \circ MAINZ, $E_0 = 275$ MeV. C2 transition to the 1.800 MeV 2^+_2 state: (over)
 \blacksquare NBS, $E_0 = 40-110$ MeV; \blacktriangle MAINZ, $E = 150$ MeV; \triangle MAINZ, $E_0 = 275$ MeV. C4 transition to the 2.305 MeV 4^+_2 state: \times MAINZ, $E_0 = 275$ MeV.

References:

- 1) H. Ehrenberg, et. al.; Nucl. Instr. and Meth. 105 (1972) 253
- 2) R. Neuhausen, S.P. Fivozinsky, J. W. Lightbody, Jr. and S. Penner;
Bull. Am. Phys. Soc. 15 (1970) 501
- 3) S. Penner, et. al.; Proc. of the Int. Conf. on Nucl. Structure; Sendai
1972
- 4) H. Herminghaus and H. Kaiser; to be published
- 5) E. Borie, D. Drechsel, and K. Lezuog; Contribution to the Int. Conf.
on Photonuclear Reactions and Applications; Asilomar; 1973

REF. Chiri Yamaguchi
J. Phys. Soc. Japan 34, 1123 (1973)

ELEM. SYM.	A	Z
Zn	64	30

METHOD

REF. NO.	
73 Ya 1	egf

REACTION	RESULT	EXCITATION ENERGY	SOURCE		DETECTOR		ANGLE
			TYPE	RANGE	TYPE	RANGE	
G,N	RLX	11- 30	C	12- 30	ACT-I		4PI
G,NP	RLX	19- 30	C	19- 30	ACT-I		4PI

$$\text{Ratio } \frac{\sigma_o(30)(\gamma, np)}{\sigma_o(30)(\gamma, n)} = 0.23$$

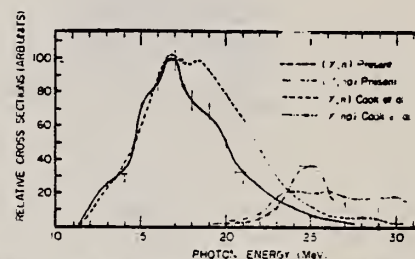


Fig. 2. The relative cross section curves for the $^{64}\text{Zn}(\gamma, n)$ and (γ, np) along with the corresponding results of ref. 17.

¹⁷ B.C. Cook et al., Phys. Rev. Letters 25, 685 (1970).

REF.			B. S. Ishkhanov, I. M. Kapitonov, E. V. Lazutin, I. M. Piskarev, O. P. Shevchenko Yad. Fiz. <u>20</u> , 433 (1974) Sov. J. Nucl. Phys. <u>20</u> , 233 (1975)		ELEM. SYM.	A	Z
					Zn	64	30
METHOD					REF. NO.		
					74 Is 3		hmg
REACTION	RESULT	EXCITATION ENERGY	SOURCE		DETECTOR		ANGLE
			TYPE	RANGE	TYPE	RANGE	
G,XN	ABX	11- 27	C	11- 27	BF3-I		4PI

SEP ISOTOPES

Total photoneutron cross sections have been obtained for ⁶⁴Zn and ⁶⁸Zn. The measurements were carried out from threshold to 27 MeV in 50-keV steps. A distinct structure is observed in the cross sections. The half-width of the curves is about 10 MeV. The integrated cross sections for ⁶⁴Zn and ⁶⁸Zn without taking into account multiple processes are 800±80 and 1630±160 MeV mb. The experimental data are compared with the predictions of the dynamic collective model and with the concept of isospin splitting of the giant resonance.

Target	Percentage content of various isotopes					Weight of target, g	Thresholds of photoneutron reactions (MeV) for the principal isotope of the target (¹⁴)		
	⁶⁴ Zn	⁶⁶ Zn	⁶⁷ Zn	⁶⁸ Zn	⁷⁰ Zn		(γ, n)	(γ, 2n)	(γ, np)
⁶⁴ Zn	91.6	4.8	1.2	1.8	0.6	78	11.855	21.020	18.548
⁶⁸ ZnO	3.3	7.9	1.6	86.3	0.4	67	10.203	17.255	19.099

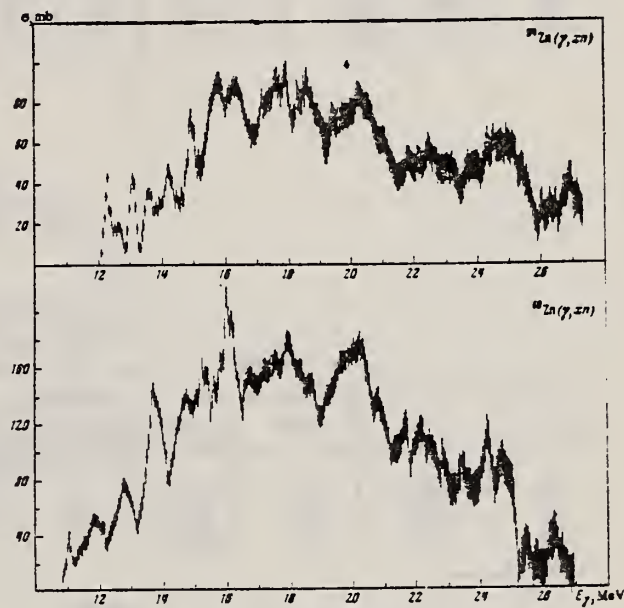


FIG. 1. Total photoneutron cross sections $\sigma(\gamma, xn)$ for ⁶⁴Zn (upper figure) and ⁶⁸Zn (lower figure).

¹⁴J.H.E. Mattauch et al., Nucl. Phys. 67, 54 (1965)

REF.

A.M. Goryachev, G.N. Zalesnyi, and B.A. Tulupov

Izv. Akad. Nauk SSSR. Ser. Fiz. 39, 134 (1975)Bull. Acad. Sci. USSR Phys. Ser. 39, 116 (1975)

ELEM. SYM.

A

Z

Zn

64

30

METHOD

REF. NO.

75 Go 1

hmg

REACTION	RESULT	EXCITATION ENERGY	SOURCE		DETECTOR		ANGLE
			TYPE	RANGE	TYPE	RANGE	
G, XN	ABX	12- 25	C	9- 25	BF3-I		4PI

$\sigma(G, SN)$. Statistical theory used to obtain SN cross section from XN cross section.

Table 2

Nuclide	β_0	E_2 , MeV	E_1 , MeV	Nuclide	β_0	E_2 , MeV	E_1 , MeV
^{64}Zn	0.25	0.99	18	^{76}Ge	0.25	0.562	18
^{66}Zn	0.23	1.04	18	^{78}Se	0.33	0.559	18
^{68}Zn	0.2	1.08	18	^{80}Se	0.3	0.616	18
^{70}Ge	0.23	1.04	18	^{82}Se	0.25	0.654	18
^{72}Ge	0.25	0.835	18	^{84}Se	0.2	0.653	18
^{74}Ge	0.3	0.6	18				

Table 3

Nuclide	σ , mb	Nuclide	σ , mb	Nuclide	σ , mb
^{64}Zn	397 ± 19	^{76}Ge	760 ± 37	^{78}Se	1021 ± 52
^{66}Zn	570 ± 27	^{78}Se	872 ± 41	^{80}Se	1020 ± 50
^{68}Zn	718 ± 35	^{80}Se	911 ± 43	^{82}Se	1087 ± 53
^{70}Ge	733 ± 37	^{82}Se	930 ± 50		

* Mean - square errors

Values given are for σ_0 (24.2 MeV).

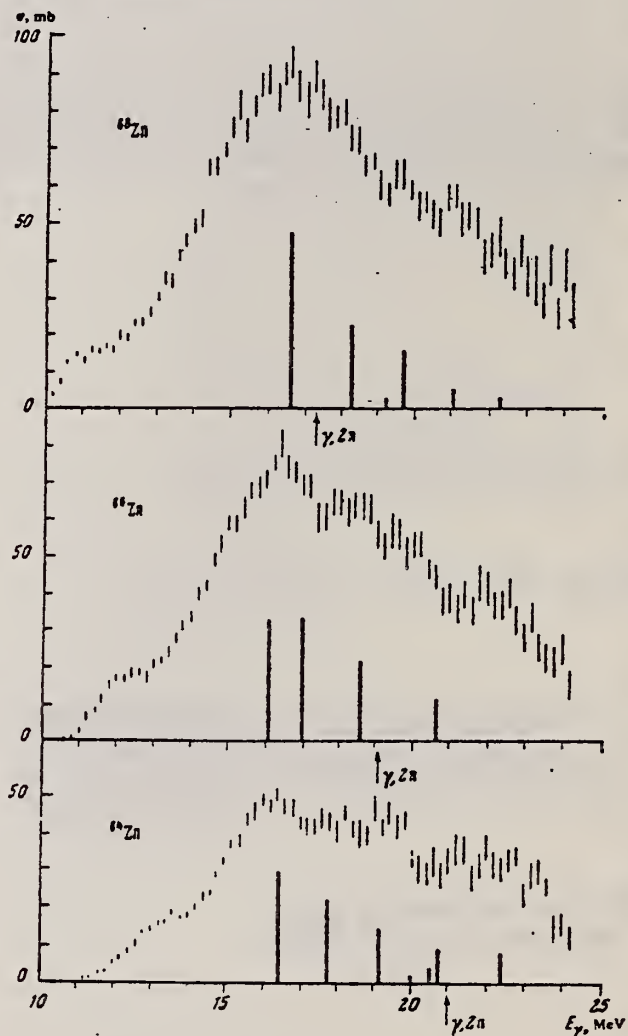


Fig. 1. Cross sections of photoneutron reactions on $^{64}, ^{66}, ^{68}\text{Zn}$. The dipole photoabsorption forces are taken from [6,7] (the solid black columns).

⁶ M.G. Huber et al., Phys. Rev. 155, 1073 (1967)

⁷ M.G. Huber et al., Z. Phys. 192, 223 (1966).

REF. P. Carlos, H. Beil, R. Bergere, J. Fagot, A. Lepretre,
A. Veyssiere, G. V. Solodukhov
Nucl. Phys. A258, 365 (1976)

ELEM. SYM.	A	Z
Zn	64	30

METHOD

REF. NO.

76 Ca 1

egf

REACTION	RESULT	EXCITATION ENERGY	SOURCE		DETECTOR		ANGLE
			TYPE	RANGE	TYPE	RANGE	
G,N	ABX	12- 30	D	12- 30	MOD-I		4PI
G,2N	ABX	15- 30	D	12- 30	MOD-I		4PI

969+

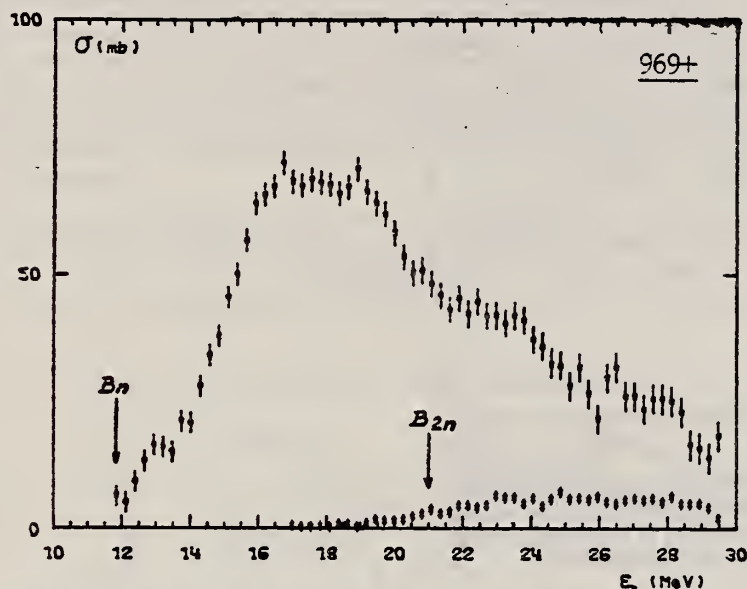


Fig. 1. Partial photoneutron cross sections $[\sigma(\gamma, n) + \sigma(\gamma, pn)]$ and $\sigma(\gamma, 2n)$ for ^{64}Zn . Arrows B_n and B_{2n} indicate theoretical threshold values for (γ, n) and $(\gamma, 2n)$ reactions respectively. Data were corrected for oxygen but not for impurities.

TABLE 3

Integrated photoneutron cross sections and comparison with sum rules

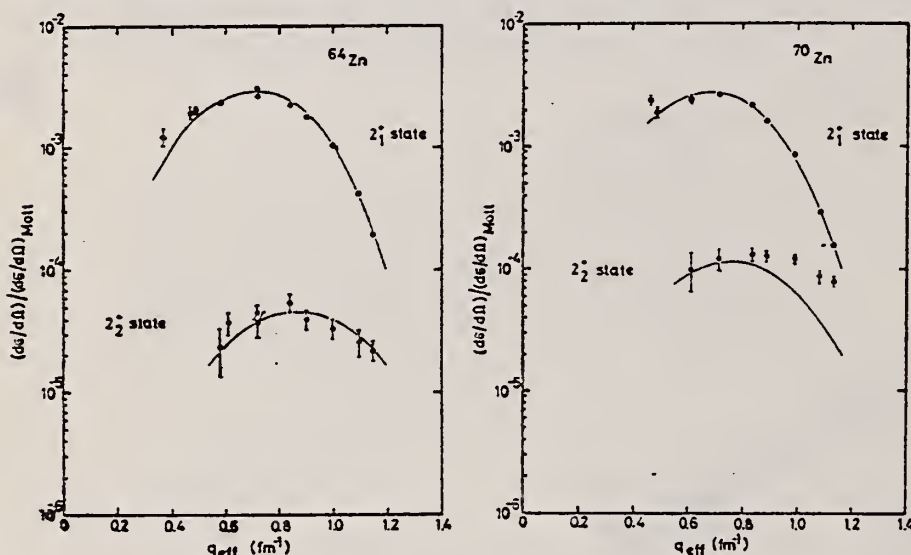
Nucleus,	^{64}Zn	$\begin{pmatrix} 69\text{Ga} \\ 71\text{Ga} \end{pmatrix}$	^{70}Ge	^{72}Ge	^{74}Ge	^{76}Ge	^{75}As	^{76}Se	^{78}Se	^{80}Se	^{82}Se
E_M (MeV)	29	26.5	26.5	26.5	26.5	26.5	26.5	26.5	26.5	26.5	26.5
σ_{0n} (MeV · b)	0.75	0.91	0.78	0.94	1.02	1.12	1.09	1.01	1.06	1.11	1.13
$\frac{\sigma_{0n} A}{0.06 NZ}$	0.78	0.87	0.75	0.88	0.94	1	0.98	0.90	0.92	0.94	0.95
$B_n - B_p$ (MeV)	4.2	$\begin{pmatrix} 3.7 \\ 1.4 \end{pmatrix}$	3	1	-0.8	-2.6	3.3	1.7	0.1	-1.5	-3
σ_{-1n} (mb)	38	52	44	54	59	64	63	58	62	65	67
$\sigma_{-1n} A^{-1}$ (mb)	0.15	0.18	0.15	0.18	0.19	0.20	0.20	0.18	0.19	0.19	0.19
σ_{-2n} (mb · MeV $^{-1}$)	2.0	3.1	2.5	3.2	3.6	3.9	3.7	3.4	3.8	3.9	4.2
$\sigma_{-2n} A^{-1}$ (mb · MeV $^{-1}$)	1.9	2.6	2.1	2.6	2.8	2.9	2.8	2.5	2.7	2.6	2.7

The notation used is defined in the text. The average experimental errors $\Delta\sigma_{0n}/\sigma_{0n}$, $\Delta\sigma_{-1n}/\sigma_{-1n}$ and $\Delta\sigma_{-2n}/\sigma_{-2n}$ are approximately 8%.

ELEM. SYM.	A	Z
Zn	64	30
REF. NO.		
76 Ne 1		egf

REACTION	RESULT	EXCITATION ENERGY	SOURCE		DETECTOR		ANGLE
			TYPE	RANGE	TYPE	RANGE	
E, E/	ABX	1- 3	D	40-112	MAG-D		DST

States: .992(2+), 1.800(2+), and 2.98(3-) MeV.



2+, 2+, 3- STATES

Fig. 2. Cross sections divided by the Mott cross section for the excitation of the first and second 2^+ states in ^{64}Zn and ^{70}Zn , respectively, versus the effective momentum transfer. The cross sections measured at different values of the incident energy E were transformed to the common energy $E_0 = 120$ MeV. The curves are the best fit of the anharmonic vibrator model.

TABLE 6
Reduced transition probabilities in single particle units, deformation parameters and deformation lengths ($R = 1.2 \text{ fm} \times A^{1/3}$)

	$B_{\uparrow}(E2)/B_{\uparrow}^{s.p.}(E2)$	β_2	$\beta_2 R$ (fm)	$B_{\uparrow}(E3)/B_{\uparrow}^{s.p.}(E3)$	β_3	$\beta_3 R$ (fm)
^{64}Zn	20.4 ± 1.2	0.230 ± 0.007	1.10 ± 0.03	23.5 ± 4.0	0.224 ± 0.019	1.08 ± 0.09
^{66}Zn	17.3 ± 1.3	0.212 ± 0.008	1.03 ± 0.04	23.4 ± 4.9	0.224 ± 0.023	1.09 ± 0.11
^{68}Zn	13.5 ± 1.0	0.187 ± 0.007	0.92 ± 0.04	19.3 ± 4.3	0.206 ± 0.022	1.01 ± 0.11
^{70}Zn	24.0 ± 2.2	0.249 ± 0.011	1.23 ± 0.06			

TABLE 7
The 2_1^+ and 2_2^+ state AVM fitting parameters for ^{64}Zn and ^{70}Zn

	$(\hbar/2\sqrt{BC})^{1/2}$	c_{1r} (fm)	z_{1r} (fm)	a	$Q(2_1^+)$ (AVM) (b)	BR(AVM)	BR(our)	$B(E2; 0_1^+ \rightarrow 2_1^+)$
^{64}Zn	0.109 ± 0.004	4.47 ± 0.08	0.53 ± 0.06	0.165 ± 0.005	-0.124 ± 0.012	456 ± 70	159 ± 12	8 ± 2
^{70}Zn	0.122 ± 0.006	4.29 ± 0.08	0.71 ± 0.05	0.25 ± 0.02	-0.233 ± 0.022	$72(\pm 16)$		50 ± 13

Derived 2_1^+ state static quadrupole moments, 2_2^+ state branching ratios, and $B(E2; 0_1^+ \rightarrow 2_2^+)$ are given.

^{a)} Ref. ¹⁹⁾.

ELEM. SYM.	A	Z
Zn	64	30

REF. NO.	
77 Ne 3	hg

REACTION	RESULT	EXCITATION ENERGY	SOURCE		DETECTOR		ANGLE
			TYPE	RANGE	TYPE	RANGE	
E, E/	FMF	1-3	D	100-275	MAG-D		DST

Abstract: The inelastic electron scattering cross sections for the quadrupole transitions to the 2_1^+ and 2_2^+ states in the even Zn isotopes ^{64}Zn , ^{66}Zn and ^{68}Zn and for the hexadecapole transition to the 4_1^+ state in ^{64}Zn have been measured in a momentum transfer range up to $q = 2.2 \text{ fm}^{-1}$. In the framework of the vibrational model these states are considered as one- and two-quadrupole-phonon states. The measurements are characterized by high statistical accuracy and by an overall resolution of $\delta E/E_0 = 10^{-3}$ which permitted separation of almost all members of the two-phonon triplet. The measured cross sections are analyzed with phenomenological models as well as with a Fourier-Bessel expansion of the transition charge density. The latter analysis yields realistic error bands for the transition charge densities and model-independent values for the reduced transition probabilities and transition radii.

LEV. .992, 1.800, 2.305

NUCLEAR REACTIONS $^{64,66,68}\text{Zn}(e, e')$, $E = 100\text{--}275 \text{ MeV}$; measured $d\sigma/d\Omega(E, \theta)$.
 $^{64,66,68}\text{Zn}$ levels deduced transition charge density, $B_1(E_2)$ and transition charge radii R_{tr} .
 Enriched targets.

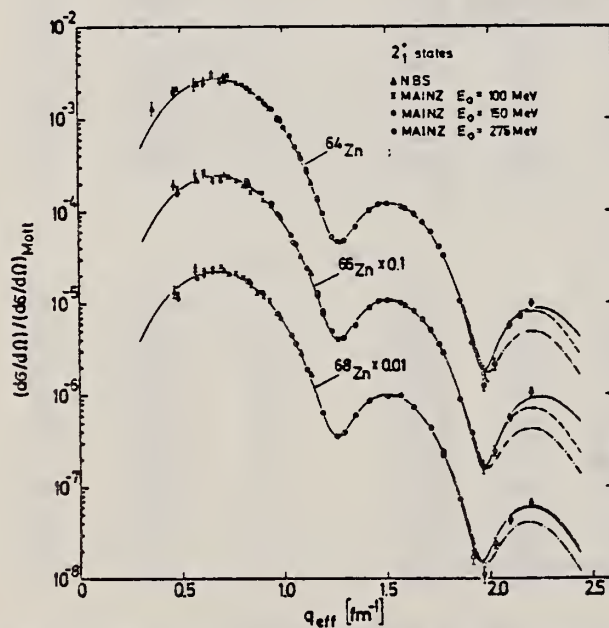


Fig. 3. Cross sections divided by the Mott cross section for the allowed transitions to the 2_1^+ state in ^{64}Zn , ^{66}Zn and ^{68}Zn versus the effective momentum transfer. The measured cross sections are transformed to a common incident energy $E_0 = 275 \text{ MeV}$. The curves represent best fit DWBA calculations with the Fourier-Bessel expansion of the transition charge density (solid line), the modified Tassie model (dashed line) and the Gaussian model (dashed-dotted line).

TABLE 3
Fitted parameters of the Gaussian model for the first 2_1^+ states in ^{64}Zn , ^{66}Zn and ^{68}Zn

	^{64}Zn $\epsilon = 0.992 \text{ MeV}$	^{66}Zn $\epsilon = 1.039 \text{ MeV}$	^{68}Zn $\epsilon = 1.077 \text{ MeV}$
$a \text{ (fm)}$	4.148 ± 0.004	4.154 ± 0.005	4.192 ± 0.005
$b \text{ (fm)}$	1.470 ± 0.005	1.478 ± 0.005	1.469 ± 0.006
$B_1(E_2) \text{ (fm}^4\text{)}$	1470 ± 15	1340 ± 15	1200 ± 15
χ^2/ν	3.95	5.43	3.12

TABLE 5

Reduced transition probabilities $B_1(E2)$ and transition radii R_{1r} for the 2_1^+ states in ^{64}Zn , ^{66}Zn and ^{68}Zn

	^{64}Zn $\epsilon = 0.992 \text{ MeV}$	^{66}Zn $\epsilon = 1.039 \text{ MeV}$	^{68}Zn $\epsilon = 1.077 \text{ MeV}$
$B_1(E2) (\text{fm}^4)$			
(e, e') ^{a)}	1620 ± 90	1410 ± 80	1320 ± 70
CE ^{b)}	1700 ± 150	1450 ± 130	1250 ± 110
$R_{1r} (\text{fm})$	5.44 ± 0.09	5.39 ± 0.09	5.47 ± 0.09
R_{1r}/R_m	1.38 ± 0.03	1.37 ± 0.03	1.38 ± 0.03

^{a)} Model independent analysis, this work.^{b)} Ref. 16).

TABLE 8

Reduced transition probabilities $B_1(E\lambda)$ and transition radii R_{1r} for the forbidden transition to the 2_2^+ states in ^{64}Zn , ^{66}Zn and ^{68}Zn and to the 4_1^+ state in ^{64}Zn

	^{64}Zn $\epsilon = 1.800 \text{ MeV}$ $\lambda = 2$	^{66}Zn $\epsilon = 1.873 \text{ MeV}$ $\lambda = 2$	^{68}Zn $\epsilon = 1.883 \text{ MeV}$ $\lambda = 2$	^{64}Zn $\epsilon = 2.305 \text{ MeV}$ $\lambda = 4$
$B_1(E\lambda) (\text{fm}^{2\lambda})$	17.0 ± 1.2	4.5 ± 0.7	46 ± 7	$(3.4 \pm 1.0) \times 10^4$
$R_{1r} (\text{fm})$	4.6 ± 0.1	4.5 ± 0.1	5.9 ± 0.1	6.7 ± 0.3
R_{1r}/R_m	1.17 ± 0.03	1.14 ± 0.03	1.49 ± 0.03	1.70 ± 0.08
$R_{1r}^2(2_2^+)/R_{1r}^2(2_1^+)$	0.71 ± 0.03	0.69 ± 0.04	1.17 ± 0.06	

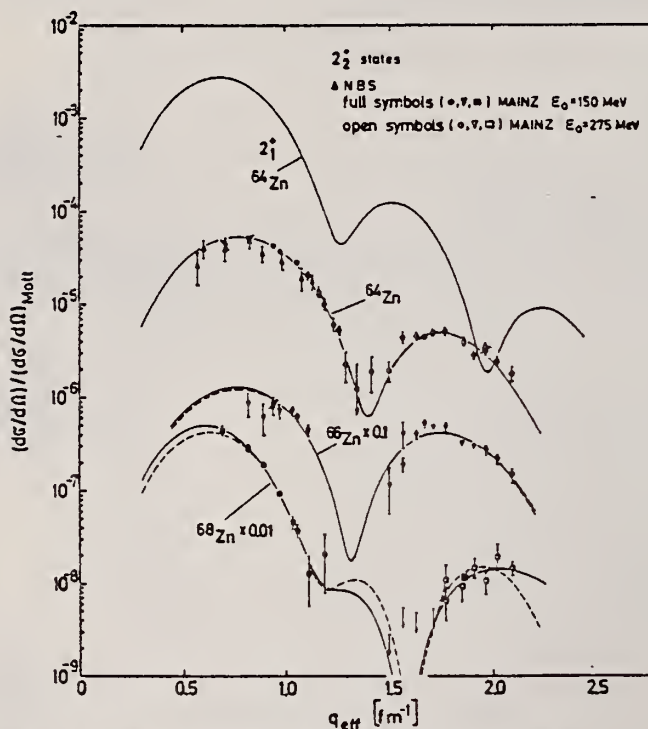


Fig. 8. Same as fig. 3, but for the forbidden transitions to the 2_2^+ states in ^{64}Zn , ^{66}Zn and ^{68}Zn , respectively. The curves represent best-fit DWBA calculations with the Fourier-Bessel expansion of the transition charge density (solid line) and the phenomenological model given in eq. (22) (dashed line). For comparison, the shape of the cross section for the allowed transition to the 2_1^+ state in ^{68}Zn is shown (uppermost curve).

ELEM. SYM.	A	Z
Zn	64	30
REF. NO.		
77 Ne 3		hg

METHOD

TABLE I

Compilation of the measured inelastic cross sections. The cross sections are multiplied by 10^4 , where the power x is given in cols. 4 and 8, respectively

DETECTOR		ANGLE
TYPE	RANGE	
MAG-D		DST

E_0 (MeV)	θ (deg)	$10^4(d\sigma/d\Omega)$ (cm ² /sr)	x	E_0 (MeV)	θ (deg)	$10^4(d\sigma/d\Omega)$ (cm ² /sr)	x
⁶⁴ Zn: $\epsilon = 0.992$ MeV 2_1^+							
100.1	60.0	1.30 ± 0.16	29	149.9	100.0	9.78 ± 0.39	33
100.1	65.0	9.94 ± 0.99	30	149.8	100.0	9.64 ± 0.30	33
100.1	70.0	8.91 ± 0.65	30	275.2	47.0	2.83 ± 0.08	31
100.1	75.0	5.64 ± 0.39	30	275.2	50.0	8.25 ± 0.26	32
100.1	80.0	4.93 ± 0.24	30	275.2	52.5	6.19 ± 0.18	32
100.1	85.0	3.08 ± 0.14	30	275.3	55.0	7.24 ± 0.27	32
100.1	90.0	2.29 ± 0.09	30	275.2	58.0	8.61 ± 0.20	32
100.0	95.0	1.53 ± 0.06	30	275.1	60.0	8.74 ± 0.20	32
100.0	100.0	9.92 ± 0.33	31	275.2	62.0	7.70 ± 0.18	32
100.0	105.0	7.24 ± 0.22	31	275.3	65.0	5.82 ± 0.15	32
100.0	110.0	4.87 ± 0.15	31	275.1	65.0	5.99 ± 0.14	32
149.9	60.0	5.55 ± 0.14	30	275.1	66.0	5.20 ± 0.18	32
150.1	65.0	3.10 ± 0.11	30	275.2	68.0	3.99 ± 0.10	32
150.0	67.5	2.23 ± 0.07	30	275.1	70.0	2.89 ± 0.09	32
150.1	70.0	1.69 ± 0.05	30	275.1	70.0	2.94 ± 0.07	32
149.8	70.0	1.70 ± 0.04	30	275.2	72.0	1.99 ± 0.05	32
150.0	72.5	1.13 ± 0.03	30	275.1	74.0	1.23 ± 0.04	32
150.0	72.5	1.19 ± 0.04	30	275.3	75.0	9.17 ± 0.30	33
150.1	75.0	7.92 ± 0.23	31	275.2	79.0	2.32 ± 0.09	33
150.1	77.5	5.47 ± 0.16	31	274.9	82.0	7.10 ± 0.49	34
149.8	80.0	3.71 ± 0.09	31	275.3	85.0	2.71 ± 0.55	34
150.1	82.5	2.34 ± 0.08	31	275.1	85.0	2.00 ± 0.31	34
150.0	85.0	1.43 ± 0.04	31	275.2	88.0	2.89 ± 0.37	34
150.1	85.0	1.52 ± 0.06	31	275.1	92.0	6.36 ± 0.47	34
149.8	90.0	5.46 ± 0.14	32	275.1	95.0	6.92 ± 0.52	34
150.2	92.5	3.02 ± 0.10	32	275.1	98.0	7.93 ± 0.57	34

⁶⁴Zn: $\epsilon = 1.800$ MeV 2_1^+

149.9	60.0	1.30 ± 0.05	31	275.2	58.0	1.6 ± 0.7	33
149.8	70.0	5.57 ± 0.16	32	275.2	62.0	1.25 ± 0.29	33
150.0	72.5	4.15 ± 0.17	32	275.1	65.0	2.35 ± 0.29	33
149.8	80.0	2.03 ± 0.06	32	275.2	68.0	1.99 ± 0.16	33
150.0	85.0	1.16 ± 0.11	32	275.1	70.0	1.72 ± 0.12	33
149.8	90.0	5.56 ± 0.23	33	275.2	72.0	1.67 ± 0.09	33
150.2	92.5	3.86 ± 0.46	33	275.3	75.0	1.43 ± 0.09	33
149.9	100.0	1.33 ± 0.21	33	275.2	79.0	8.77 ± 0.58	34
149.8	100.0	1.43 ± 0.14	33	274.9	82.0	5.43 ± 0.45	34
275.2	47.0	2.73 ± 0.38	32	275.3	85.0	5.50 ± 0.64	34
275.2	50.0	9.7 ± 1.3	33	275.1	85.0	5.01 ± 0.42	34
275.2	52.5	2.9 ± 1.1	33	275.2	88.0	3.26 ± 0.34	34
275.3	55.0	1.3 ± 1.3	33	275.1	92.0	1.99 ± 0.33	34

⁶⁴Zn: $\epsilon = 2.305$ MeV 4_1^+

149.9	60.0	1.69 ± 0.37	32	275.2	72.0	7.4 ± 0.8	34
149.8	70.0	8.05 ± 0.62	33	275.3	75.0	7.8 ± 0.9	34
149.8	80.0	3.55 ± 0.32	33	275.2	79.0	5.36 ± 0.52	34
149.8	90.0	1.30 ± 0.15	33	274.9	82.0	3.77 ± 0.42	34
149.8	100.0	3.5 ± 1.4	34	275.3	85.0	3.58 ± 0.58	34
275.2	62.0	3.7 ± 1.2	34	275.1	85.0	2.72 ± 0.43	34
275.1	65.0	9.1 ± 2.3	34	275.2	88.0	1.83 ± 0.30	34
275.2	68.0	8.8 ± 1.3	34	275.1	92.0	1.17 ± 0.32	34
275.1	70.0	8.6 ± 1.4	34				

REF. A.A. Nemashkalo, N.G. Afanas'ev, Yu.V. Vladimirov, V.P. Likhachev,
G.A. Savitskii, & V.M. Khvastunov
Pis'ma Zh. Eksp. Teor. Fiz. 26, No. 7, 569 (1977)
JETP Lett. 26, No. 7, 422 (Oct. 1977)

ELEM. SYM.	A	Z
Zn	64	30

METHOD	REF. NO.	hmg
	77 Ne 4	11/18/80

REACTION	RESULT	EXCITATION ENERGY	SOURCE		DETECTOR		ANGLE
			TYPE	RANGE	TYPE	RANGE	
E, E/	FMF	10-35	C	UKN	MAG-D	---	UKN

Results are presented of the investigation of giant multiple resonances in the nuclei ^{64}Zn and ^{124}Sn with the aid of inelastic scattering of electrons, performed in Khar'kov with the LUÉ-300 linear electron accelerator.

B(EL)

TABLE II.

^{64}Zn

EL	E_x, MeV	Γ_x, MeV	$B(EL), e^2 \text{F}^{-2L}$	ΔT	Lim. of EWSR, %		E_x, MeV	
					total	$\Delta T = 0.1$	our data	others
E1	17.7 ± 0.6	4.3 ± 0.8	35 ± 2.1	1	-	63 ± 16	71 ± 3	78-82
	24.4 ± 0.6	3.5 ± 0.8	4.5 ± 1.2	-	-	40 ± 11	85 ± 3	-
	0-11	-	1380 ± 90	0	-	10 ± 1	-	-
					4.7 ± 0.5	-	-	-
E2	15.0 ± 0.2	6.0 ± 0.4	600 ± 70	0	-	49 ± 6	50 ± 1	58-65
	25.1 ± 0.7	3.7 ± 1.6	90 ± 50	-	23 ± 3	-	-	-
	25.1 ± 0.7	3.7 ± 1.6	90 ± 50	1	-	11 ± 6	100 ± 4	-
	30.4 ± 0.8	5.0 ± 1.7	110 ± 50	-	6 ± 3	-	-	-
				1	-	16 ± 7	121 ± 3	111-140
				-	9 ± 4	-	-	-
	0-11	-	44100 ± 1200	0	-	19 ± 2	-	-
E3	16.6 ± 0.4	4.2 ± 1.4	2500 ± 1300	-	8.6 ± 0.8	-	64 ± 2	70-82
	21.4 ± 2.6	6.5 ± 3.1	6500 ± 2200	-	5.5 ± 1.2	-	86 ± 10	403-453
				-	5.4 ± 2.0	-	-	-
	0-11	-	$(11.3 \pm 0.2) \text{MeV}^6$	-	4.0 ± 0.2	-	-	-
E4	17.9 ± 0.5	3.2 ± 1.1	$(2.3 \pm 1.2) \text{MeV}^5$	-	2.0 ± 1.2	-	52 ± 2	-
	25.4 ± 0.8	2.5 ± 1.4	$(4.4 \pm 2.5) \text{MeV}^4$	-	0.7 ± 0.3	-	102 ± 4	-
E5	0-35	-	$(1.0 \pm 0.5) \text{MeV}^7$	-	2.0 ± 1.0	-	-	-

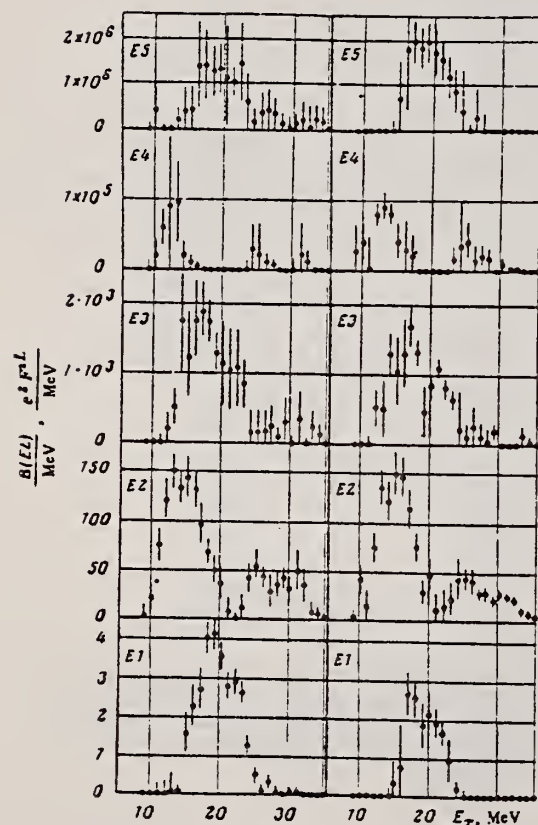


FIG. 1. ^{64}Zn . Dependence of the relative probabilities of transitions with multiplicities $L=1-5$ on the excitation energies. Left—Helm's model, right—high-energy approximation.

ELEM. SYM.	A	Z
Zn	64	30
REF. NO.		hg
78 Ve 6		

METHOD			SOURCE		DETECTOR		ANGLE
REACTION	RESULT	EXCITATION ENERGY	TYPE	RANGE	TYPE	RANGE	
G,XN	ABX	16-26	C	12-27	SCI-D		4PI
				(11.9-26.3)			

The cross section of the reaction $^{64}\text{Zn}(\gamma, n)^{63}\text{Zn}$ was investigated for the high-energy component of the neutron spectrum ($\epsilon_n \geq 3.7$ MeV). An analysis of the results indicates that the interpretation of the structure observed in the cross section of the $^{64}\text{Zn}(\gamma, n)^{63}\text{Zn}$ as a manifestation of isospin splitting is in error.

NEUTS ABOVE 3.7 MEV

PACS numbers: 25.20.+y, 24.30.Cz

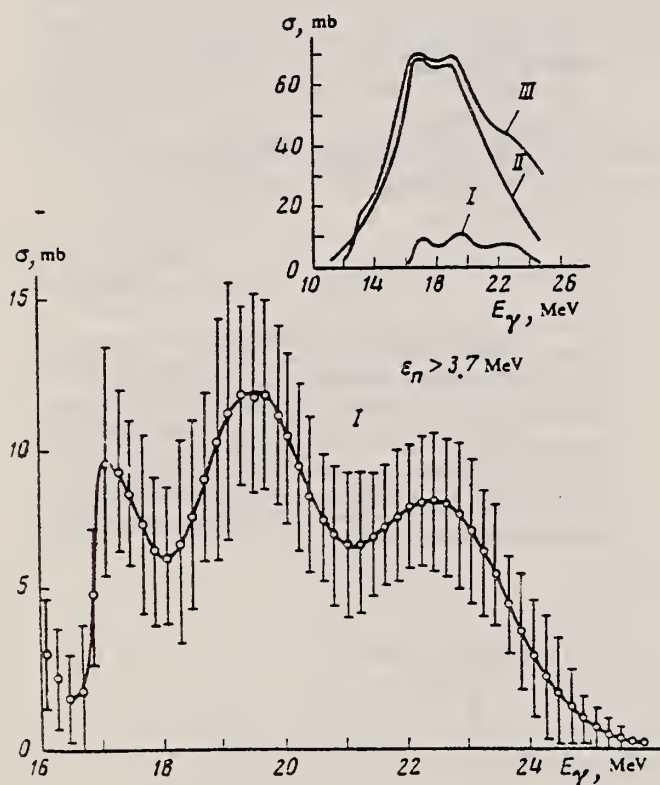


FIG. 1. Curve I) Cross section of the reaction $^{64}\text{Zn}(\gamma, n)^{63}\text{Zn}$ for neutrons with energy $\epsilon_n > 3.7$ MeV, obtained in the present study. Curve II) Cross section of the reaction $^{64}\text{Zn}(\gamma, n)^{63}\text{Zn}$ from [1]. Curve III) Total cross section of the reactions $^{64}\text{Zn}(\gamma, n)^{63}\text{Zn}$ and $^{64}\text{Zn}(\gamma, np)^{63}\text{Cu}$ from [1].

ELEM. SYM.	A	Z
Zn	64	30

METHOD

REF. NO.

78 Ve 7

hg

REACTION	RESULT	EXCITATION ENERGY	SOURCE		DETECTOR		ANGLE
			TYPE	RANGE	TYPE	RANGE	
G,XN	SPC	16-26	C	15-27	SCI-D		4PI

The yield curve of the reaction $^{64}\text{Zn}(\gamma, n)^{63}\text{Zn}$ was measured for neutrons with $\epsilon_n > 3.7$ MeV; the energy spectra of the photoneutrons were also measured at various values of the bremsstrahlung maximum energy $E_{\gamma m}$. It is concluded from analysis of the obtained data and from comparison with the results of analogous studies made for iron isotopes that the probability of decay of doorway states into more complex configurations increases with increasing distance from the region of nuclei with filled shells.

NEUTS ABOVE 3 MEV

See also 78 Ve 6

PACS numbers: 25.20. + y, 24.30.Cz, 27.50. + e

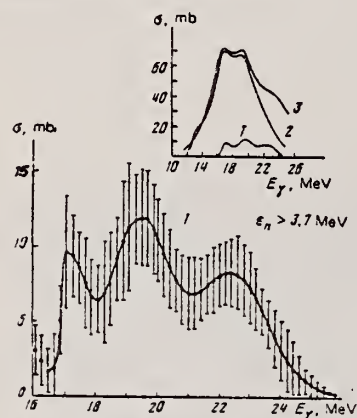


FIG. 2. Cross section of the reaction $^{64}\text{Zn}(\gamma, n)^{63}\text{Zn}$ for $\epsilon_n > 3.7$ MeV (curve 1). Comparison of the data for the high-energy neutrons with results obtained for neutrons of all energies in Refs. 12 (curve 2) and 14 (curve 3).

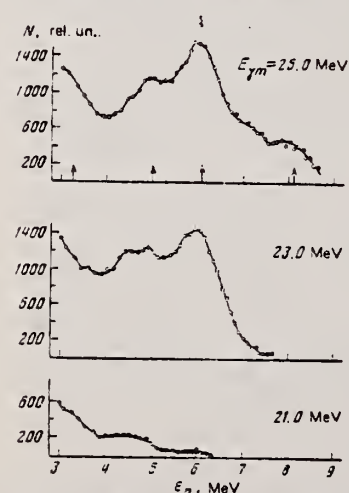


FIG. 4. Energy spectra of the neutrons from the reaction $^{16}\text{O}(\gamma, n)^{15}\text{O}$. The arrows indicate the positions of the main peaks in the spectrum, measured by the time-of-flight procedure.¹⁸

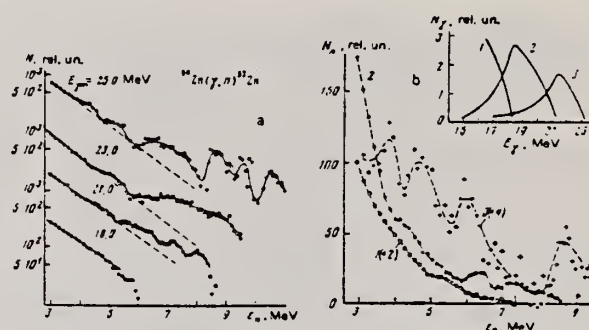


FIG. 3. a) Energy spectra of neutrons from the reaction $^{64}\text{Zn}(\gamma, n)^{63}\text{Zn}$ obtained at different values of $E_{\gamma m}$. b) Difference energy spectra of neutrons from the reaction $^{64}\text{Zn}(\gamma, n)^{63}\text{Zn}$ obtained by subtracting the spectrum at $E_{\gamma m} = 18.0$ MeV from the spectrum at $E_{\gamma m} = 21.0$ MeV (curve 2) and subtracting the spectrum at $E_{\gamma m} = 21.0$ MeV from the spectrum at $E_{\gamma m} = 23.0$ MeV (curve 3) (the spectra are reduced to the same irradiation dose), compares with the spectrum at $E_{\gamma m} = 18.0$ MeV (curve 1). The insert shows the spectra of the bremsstrahlung that produced the neutron spectra.

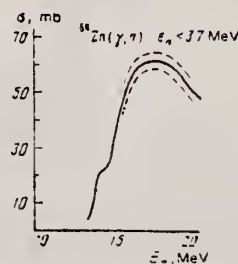


FIG. 6. Cross section of the reaction $^{64}\text{Zn}(\gamma, n)^{63}\text{Zn}$ for neutron emission with $\epsilon_n < 3.7$ MeV, obtained by subtracting the cross section for $\epsilon_n > 3.7$ MeV from the cross section for the emission of neutrons of all energies.

REF. Y. Cauchois, H. Ben Abdelaziz, R. Khérouf, C. Schloesing-Möller
J. Phys G7, 1539 (1981)

ELEM. SYM.	A	Z
Zn	64	30
REF. NO.		
81 Ca 2		hg

METHOD

REACTION	RESULT	EXCITATION ENERGY	SOURCE		DETECTOR		ANGLE
			TYPE	RANGE	TYPE	RANGE	
G.G	LET	0 (.992)	C	0 - 2	SCD-D		

.992 MeV

Abstract. Lifetimes of 49 excited states below 1.65 MeV have been measured in ^{24}Mg , ^{27}Al , ^{48}Ti , ^{58}Ni , ^{59}Co , $^{61,62}\text{Ni}$, $^{63,65}\text{Cu}$, $^{64,66,68}\text{Zn}$, ^{75}As , ^{103}Rh , $^{113,115}\text{In}$, $^{116,118,120}\text{Sn}$ and $^{121,123}\text{Sb}$ by means of nuclear resonance fluorescence experiments. The levels are excited by bremsstrahlung x-ray photons. The self-absorption technique applied to suitable cases provides nuclear absorption cross sections, widths and lifetimes from which the x-ray spectral distributions are also obtained. Scattering experiments are performed for all other cases in order to obtain widths and lifetimes from these x-ray photon curves. The Compton effect in the sample is taken into account. Self-absorption provides $g\Gamma_0$ from which Γ is deduced using adopted J^π and Γ_0/Γ values; scattering provides $u = g(\Gamma_0^2/\Gamma)W(\theta)$ from which Γ is also deduced with J , Γ_0/Γ and mixing ratios taken from the literature. Thanks to simultaneous determination of the x-ray spectra all the lifetimes as given by our programs with their statistical errors form an unusually coherent set of values.

NUCLEAR REACTIONS (γ , γ), bremsstrahlung excitation; natural isotopes: ^{24}Mg , ^{27}Al , ^{48}Ti , ^{58}Ni , ^{59}Co , $^{61,62}\text{Ni}$, $^{63,65}\text{Cu}$, $^{64,66,68}\text{Zn}$, ^{75}As , ^{103}Rh , $^{113,115}\text{In}$, $^{116,118,120}\text{Sn}$ and $^{121,123}\text{Sb}$; $E \approx 0.5\text{--}1.65$ MeV; measured $g\Gamma_0$ or $g(\Gamma_0^2/\Gamma)W(\theta)$; deduced $T_{1/2}$.

(OVER)

Tableau 3. Résultats des mesures des niveaux étudiés par diffusion.

Table 3. Results obtained using the diffusion method.

Isotope	Energie (keV)	J^π	J_0^π	Γ_0/Γ	δ	$u = g(\Gamma_0^2/\Gamma)W(\theta)$ (meV)	τ (ps) ce travail	τ_{ref} (ps)	Références †
²⁴ Mg	1368,59(4)	2 ⁺	0 ⁺	1	E2	1,08(13)	1,76(21)	1,98(4)	Endt et van der Leun (1978)
²⁷ Al	1014,45(3)	$\frac{3}{2}^+$	$\frac{3}{2}^+$	0,971	+ 0,351(12)	0,186(13)	2,20(16)	2,12(8)	Endt et van der Leun (1978)
⁴⁸ Ti	983,512(3)	2 ⁺	0 ⁺	1	E2	0,282(23)	6,74(55)	6,1(13)	Been (1978)
⁵⁸ Ni	1454,45(15)	2 ⁺	0 ⁺	1	E2	2,11(26)	0,90(11)	0,92(3)	Kocher et Auble (1976)
⁵⁹ Co	1099,224(25)	$\frac{3}{2}^-$	$\frac{7}{2}^-$	1	(E2)	0,069(8)	4,79(55)	3,17(58)	Kim (1976)
⁵⁹ Co	1458,8(3)	$\frac{1}{2}^-$	$\frac{3}{2}^-$	0,91	(E2)	0,68(8)	1,17(14)	1,52(16)	Kim (1976)
⁵⁹ Co	1480,9(3)	$\frac{3}{2}^-$	$\frac{5}{2}^-$	0,8	< 0,35 ^a	1,23(15)	0,254(31)	0,31(3)	Kim (1976)
⁶¹ Ni	1185,7(6)	$\frac{3}{2}^-$	$\frac{5}{2}^-$	0,77(8) ⁱ	[0,14]	1,88(49)	0,21(5)	0,16(3)	Andreev <i>et al</i> (1974)
⁶² Ni	1172,91(9)	2 ⁺	0 ⁺	1	E2	0,88(17)	2,15(42)	2,09(3)	Halbert (1979a)
⁶³ Cu	1327,00(7)	$\frac{7}{2}^-$	$\frac{5}{2}^-$	0,84	(E2)	1,04(14)	0,84(11)	0,88(4)	Auble (1979b)
⁶³ Cu	1412,05(4)	$\frac{3}{2}^-$	$\frac{5}{2}^-$	0,72	+ 0,61($\pm \frac{31}{8}$)	0,260(38)	1,90(28)	1,61(3)	Auble (1979b)
⁶⁴ Zn	991,54(7)	2 ⁺	0 ⁺	1	E2	0,640(54)	2,97(25)	2,60(13)	Halbert (1979b)
⁶⁵ Cu	1481,83(5)	$\frac{3}{2}^-$	$\frac{5}{2}^-$	0,85	(E2)	1,13(19)	0,79(13)	0,49(5)	Auble (1975a)
⁶⁶ Zn	1039,37(6)	2 ⁺	0 ⁺	1	E2	0,70(6)	2,71(23)	2,25(15)	Auble (1975b)
⁶⁸ Zn	1077,38(5)	2 ⁺	0 ⁺	1	E2	0,70(6)	2,71(23)	2,34(23)	Lewis (1975)
⁷⁵ As	572,5(10)	$\frac{3}{2}^-$	$\frac{5}{2}^-$	1 ^d	0,39 ^b	0,236(26)	4,14(46)	3,5(9)	Horen et Lewis (1975)
⁷⁵ As	823,0(10)	$\frac{3}{2}^-$	$\frac{5}{2}^-$	0,86 ^d	(E2)	0,214(22)	4,27(43)	3,5(3)	Robinson <i>et al</i> (1967)
⁷⁵ As	865,5(10)	$\frac{3}{2}^-$	$\frac{5}{2}^-$	0,83 ^d	— ^c	0,78(6)	0,863(68)	0,60(12)	Celliers <i>et al</i> (1977)
⁷⁵ As	1076,0(10)	$\frac{3}{2}^-$	$\frac{5}{2}^-$	0,94 ^d	0,38 ^d	1,97(13)	0,287(19)	0,32(7)	Celliers <i>et al</i> (1977)
⁷⁵ As	1128,5(10)	$\frac{3}{2}^-$	$\frac{5}{2}^-$	1	E1 ^d	0,224(24)	1,47(16)	—	
⁷⁵ As	1349,0(10)	$\frac{1}{2}^-$	$\frac{3}{2}^-$	0,67 ^d	0,20 ^d	1,61(29)	0,180(32)	0,12(3)	Wilson (1970)
⁷⁵ As	1370,0(10)	$\frac{1}{2}^-$	$\frac{3}{2}^-$	0,47 ^d	0,47 ^d	0,64(13)	0,218(44)	—	
¹⁰³ Rh	803,1(2)	$\frac{1}{2}^-$	$\frac{3}{2}^-$	0,70	M1	1,85(16)	0,174(15)	—	Harmatz (1979)
¹⁰³ Rh	1277,0(2)	$\frac{1}{2}^-$	$\frac{3}{2}^-$	0,75	— 0,62(30) ^e	0,81(9)	0,87(10)	1,3(9)	Harmatz (1979)
¹¹³ In	1177(1)	$\frac{1}{2}^-$	$\frac{3}{2}^-$	1	+ 0,5(2)	9,1(8)	0,086(8)	0,10(6)	Tuttle <i>et al</i> (1976)
¹¹³ In	1510(1)	$\frac{1}{2}^-$	$\frac{3}{2}^-$	0,935	— 0,5($\pm \frac{1}{2}$)	6,4(9)	0,071(10)	0,11($\pm \frac{4}{3}$)	Tuttle <i>et al</i> (1976)
¹¹⁵ In	1077,7(10)	$\frac{1}{2}^-$	$\frac{3}{2}^-$	0,81 ^j	(E2)	0,159(24)	1,61(24)	1,23(7)	Tuttle <i>et al</i> (1976)
¹¹⁵ In	1290,59(3)	$\frac{1}{2}^-$	$\frac{3}{2}^-$	0,98 ^j	(E2)	1,31(11)	0,66(6)	0,55(4)	Tuttle <i>et al</i> (1976)
¹¹⁵ In	1448,78(3)	$\frac{1}{2}^-$	$\frac{3}{2}^-$	0,86	— 8 ^f	0,90(11)	0,50(6)	0,52(20)	Tuttle <i>et al</i> (1976)
¹¹⁵ In	1486,1(1)	$\frac{1}{2}^-$	$\frac{3}{2}^-$	0,737	— 0,8 ^f	0,63(9)	0,63(9)	0,4(3)	Tuttle <i>et al</i> (1976)
¹¹⁵ In	1497,2(4)	($\frac{3}{2}^-$)	$\frac{5}{2}^-$	< 1	(E2)	1,33(16)	< 0,30(4)	—	
¹¹⁵ In	1607,8(15)	($\frac{3}{2}^-$)	$\frac{5}{2}^-$	$\ll 1$	(E2)	1,54(24)	$\leq 0,26(4)$	—	
¹¹⁶ Sn	1293,54(2)	2 ⁺	0 ⁺	1	E2	3,58(37)	0,53(6)	0,522(14)	Carlson <i>et al</i> (1975)
¹¹⁸ Sn	1229,64(4)	2 ⁺	0 ⁺	1	E2	2,75(28)	0,69(7)	0,67(2)	Carlson <i>et al</i> (1976)
¹²⁰ Sn	1171,6(2)	2 ⁺	0 ⁺	1	E2	1,83(16)	1,04(9)	0,91(2)	Kocher (1976)
¹²¹ Sb	1023,5(10)	$\frac{3}{2}^-$	$\frac{5}{2}^-$	1	[0,57] ^g	3,69(34)	0,228(21)	0,20(7) ^h	Tamura <i>et al</i> (1979)
¹²¹ Sb	1105,5(10)	$\frac{3}{2}^-$	$\frac{5}{2}^-$	0,4	—	0,47(4)	0,42(4)	—	
¹²¹ Sb	1142,5(10)	$\frac{3}{2}^-$	$\frac{5}{2}^-$	0,6	(E2)	0,85(8)	0,449(40)	0,41(8) ^h	Booth <i>et al</i> (1973)
¹²¹ Sb	1384,0(10)	$\frac{3}{2}^-$	$\frac{5}{2}^-$	1	[0,45] ^g	4,7(5)	0,092(10)	0,088(14) ^h	Booth <i>et al</i> (1973)
¹²³ Sb	1029,5(10)	$\frac{3}{2}^-$	$\frac{5}{2}^-$	1	[0,57] ^g	2,96(27)	0,272(25)	0,26(4) ^h	Booth <i>et al</i> (1973)
¹²³ Sb	1086,5(10)	$\frac{3}{2}^-$	$\frac{5}{2}^-$	1	[β] > 1,26 ^g	1,06(9)	0,67(6)	0,72(15) ^h	Booth <i>et al</i> (1973)

† Références pour les colonnes 3, 4, 5, 6 et 9 de chaque ligne, sauf indication appelée au bas de ce tableau. Pour les autres données se reporter au texte.

Remarque. Pour calculer β^2 quand nous ne disposons que de $B(E2)$, pour un mélange (E2) + (M1), nous déduisons $g\Gamma_0(E2) \propto B(E2)E_2^5$ en admettant $W(\theta) = 1$ et connaissant Γ_0/Γ , notre détermination de u donne une première approximation de $g\Gamma_0$ d'où une valeur de $\beta^2 = (g\Gamma_0(E2))/(g\Gamma_0 - g\Gamma_0(E2))$ qui permet d'améliorer $W(\theta)$ et $g\Gamma_0$ de proche en proche.

^a Swann (1971); ^b Robinson *et al* (1967); ^c $W(\theta) = 0,99$ calculé d'après la formule de Celliers *et al* (1977); ^d Abbonando *et al* (1978); ^e Sayer *et al* (1972); ^f Tuttle *et al* (1976); ^g d'après $B(E2)$ de Barnes *et al* (1966); ^h calculé d'après Booth *et al* (1973); ⁱ Williams *et al* (1975); ^j Dietrich *et al* (1970).

REF. W.R. Dodge, R.G. Leicht, E. Hayward, E. Wolyne
Phys. Rev. C24, 1952 (1981)

ELEM. SYM.	A	Z
Zn	64	30

METHOD

REF. NO.

81 Do 2

hg

REACTION	RESULT	EXCITATION ENERGY	SOURCE		DETECTOR		ANGLE
			TYPE	RANGE	TYPE	RANGE	
E, P	ABX	7-100	D	16-100	MAG-D		DST
E, A	ABX	4-100	D	16-100	MAG-D		DST

The (e,p) and (e, α) cross sections for ^{56}Fe , ^{59}Co , and ^{64}Zn have been measured in the electron energy range 16–100 MeV. They have been analyzed using the distorted-wave Born approximation E1 and E2 virtual photon spectra. The E1 and E2 components in the proton and α channels have been obtained.

VIRT PHOTON ANAL

NUCLEAR REACTIONS $^{56}\text{Fe}(e,p)$, $^{56}\text{Fe}(e,\alpha)$, $^{59}\text{Co}(e,p)$, $^{59}\text{Co}(e,\alpha)$, $^{64}\text{Zn}(e,p)$, and $^{64}\text{Zn}(e,\alpha)$; measured $\sigma(E_0, E_x, 34^\circ)$, $\sigma(E_0, E_x, 48^\circ)$, $\sigma(E_0, E_x, 62^\circ)$, $\sigma(E_0, E_x, 90^\circ)$, $\sigma(E_0, E_x, 118^\circ)$, $\sigma(E_0, E_x, 132^\circ)$; obtained $\sigma(e,p)$, $\sigma(e,\alpha)$; deduced $\sigma_{\text{E1}}^{\text{p}}(E)$, $\sigma_{\text{E2}}^{\text{p}}(E)$, $\sigma_{\text{E1}}^{\text{a}}(E)$, $\sigma_{\text{E2}}^{\text{a}}(E)$.

$^{13}\text{Y. -W.}$, Lui, P. Bogucki, J. D. Bronson, U. Garg, C. M. Rozsa, and D. H. Youngblood, Phys. Lett. 93B, 31 (1980).

$^{14}\text{S.}$ Costa, F. Ferrero, S. Ferroni, C. Molino and R. Malvano, Phys. Lett. 11, 324 (1964). ^{64}Co 2

TABLE III. Percentage of the E2 sum when only points up to 50 MeV ($E_0=50$ MeV) and when all measured points ($E_0=100$ MeV) are considered in the analysis. The bremsstrahlung cross section used is DBM. E2 sum: $0.22Z^2A^{-1/3} \mu\text{b/MeV}$.

Nucleus	Reaction	Without size effect		With size effect	
		$E_0=50$ MeV	$E_0=100$ MeV	$E_0=50$ MeV	$E_0=100$ MeV
^{56}Fe	(e, α)	9 ± 3	3 ± 1	11 ± 3	7 ± 1
	(e,p)	47 ± 30	8 ± 11	61 ± 32	37 ± 15
^{59}Co	(e, α)	7 ± 2	4 ± 1	8 ± 2	5 ± 1
	(e,p)	32 ± 22	4 ± 8	48 ± 24	28 ± 11
^{64}Zn	(e, α)	26 ± 6	12 ± 2	32 ± 6	25 ± 3
	(e,p)	29 ± 43	26 ± 15	56 ± 46	77 ± 21

TABLE IV. Percentage of the E1 and E2 sums in the α and proton channels. E1 sum: $60NZ/A$ MeV mb. E2 sum: $0.22Z^2A^{-1/3} \mu\text{b/MeV}$. Integrals to 100 MeV.

Nucleus	Reaction	E1		E2	
		Schiff	DMB	Schiff	DMB
^{56}Fe	(e, α)	5 ± 1	6 ± 1	10 ± 1	7 ± 1
	(e,p)	67 ± 20	82 ± 19	82 ± 14	37 ± 15
	(e, α)+(e,p)	72 ± 20	88 ± 19	92 ± 14	44 ± 15
^{59}Co	(e, α)	5 ± 1	7 ± 1	8 ± 1	5 ± 1
	(e,p)	52 ± 10	67 ± 12	63 ± 10	28 ± 11
	(e, α)+(e,p)	57 ± 10	74 ± 12	71 ± 10	33 ± 11
^{64}Zn	(e, α)	16 ± 4	18 ± 4	33 ± 3	25 ± 3
	(e,p)	129 ± 28	154 ± 30	137 ± 30	77 ± 21
	(e, α)+(e,p)	145 ± 28	172 ± 30	170 ± 20	102 ± 21

[over]

TABLE VI. $E1$ strength integrated up to 30 MeV.

Nucleus	α	$\int_0^{30} \sigma_{\gamma,x}(E) dE$ (MeV mb)		Total	Fraction of $E1$ sur
		p	n		
^{56}Fe	18 ± 3	256 ± 26	735^a	1009	1.21
^{59}Co	15 ± 2	211 ± 22	884^b	1110	1.26
^{64}Zn	66 ± 14	545 ± 75	616^b	1227	1.28

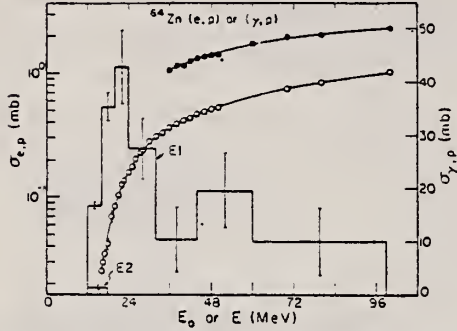
^aReference 13.^bReference 14.FIG. 5. The $\sigma_{e,p}(E_0)$ for ^{64}Zn . See caption of Fig. 3.

FIG. 3. The measured $\sigma_{e,p}(E_0)$ for ^{56}Fe as a function of total incident electron energy E_0 (open circles). The full circles represent the yield $Y_{e,p}(E_0)$ obtained when a 0.217 g/cm^2 tantalum foil was placed in the electron beam ahead of the target. The smooth curves are the best fits to the data and were obtained by combining the histograms representing the $E1$ and $E2$ (γ, p) cross sections (right-hand scale) in Eqs. (1) and (2) with the $E1$ and $E2$ DWBA virtual photon spectra and by making use of the DBM bremsstrahlung cross section. The size effect correction described in the text has been applied to the virtual photon spectra.

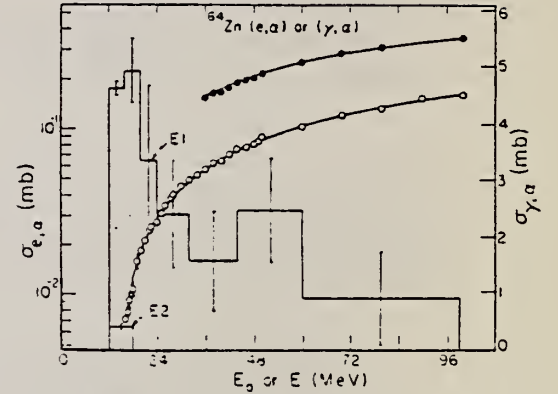
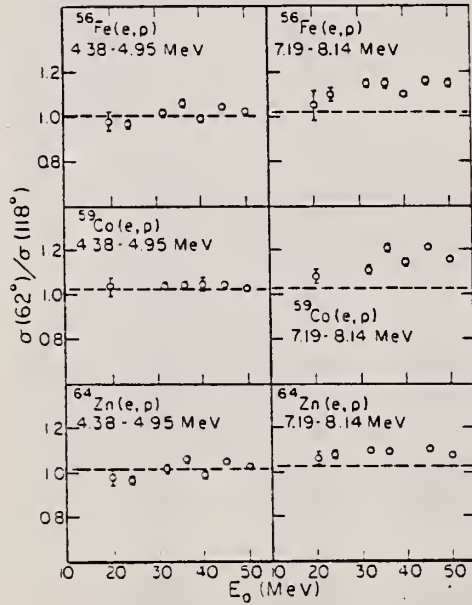
FIG. 3. The $\sigma_{e,a}(E_0)$ for ^{64}Zn . See caption of Fig. 3.

FIG. 9. The ratios of the number of protons observed in the indicated energy bite ΔT_p at 62° to the same number observed at 118° , $\sigma(62^\circ)/\sigma(118^\circ)$, as a function of incident electron energy.

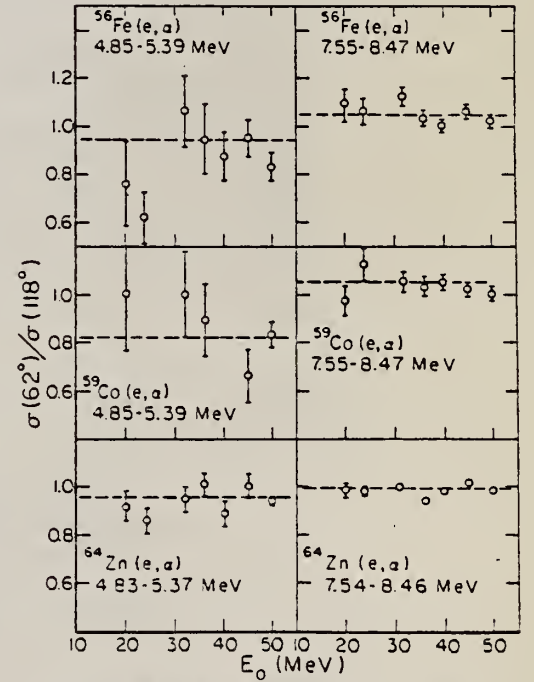


FIG. 10. The ratios of the number of α particles observed in the indicated energy bite ΔT_α at 62° to the same number observed at 118° , $\sigma(62^\circ)/\sigma(118^\circ)$, as a function of incident electron energy.

Z_N
 $A=66$

Z_N
 $A=66$

Z_N
 $A=66$

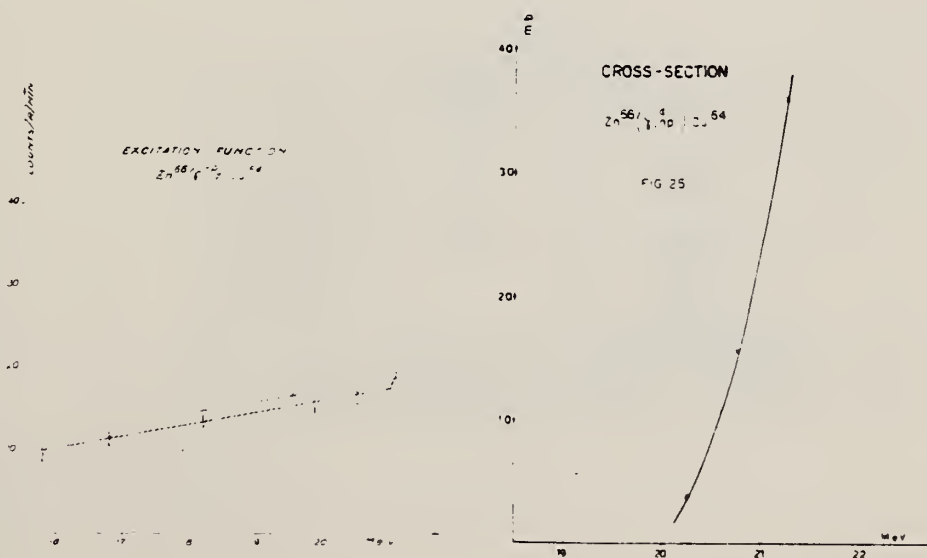
M.D. DeSouza Santos, J. Goldemberg, R.R. Pieroni, E. Silva,
O.A. Borello, S.S. Villaca, J.L. Lopes
Int. Conf. Peaceful Uses of Atomic Energy II (UN, NY) 169 (1955)

ELEM. SYM.	A	Z
Zn	66	30
REF. NO.		EGF
55 De 1		

METHOD Betatron; neutron, proton yield; radioactivity; r-chamber

REACTION	RESULT	EXCITATION ENERGY	SOURCE		DETECTOR		ANGLE
			TYPE	RANGE	TYPE	RANGE	
G, NP	ABX	19-23	C	19-23	ACT-I		4 PI

$$\sigma(\gamma, n)/\sigma(\gamma, np) = 1.6 \text{ at } 21 \text{ MeV}$$



REF. S.S. Villaca, J. Goldemberg
An. Acad. Brasil. Cienc. 27; 427 (1955)

ELEM. SYM.	A	Z
Zn	66	30

METHOD Betatron; ion chamber monitor

REF. NO.	NVB
55 Vi 1	

REACTION	RESULT	EXCITATION ENERGY	SOURCE		DETECTOR		ANGLE
			TYPE	RANGE	TYPE	RANGE	
G,D	ABX	20-22	C	20-22	ACT-I		4PI

INCLUDES G,NP

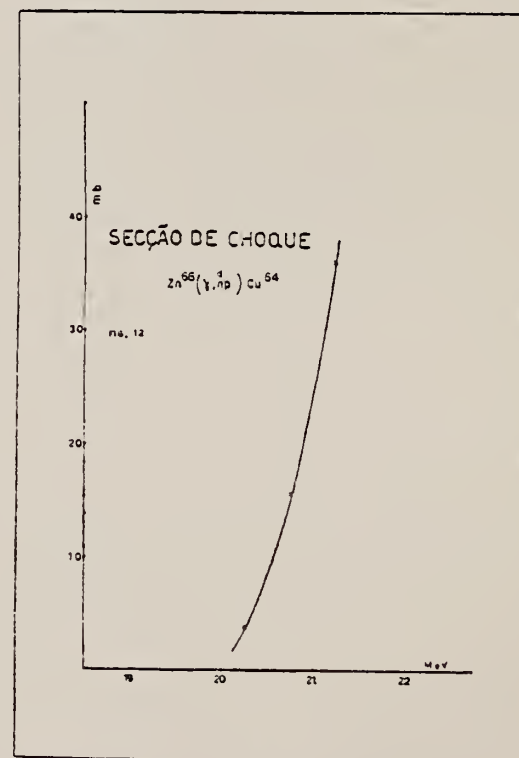


Fig. 12

ELEM. SYM.	A	Z
Zn	66	30
REF. NO.		57 81 1
METHOD		egf

REACTION	RESULT	EXCITATION ENERGY	SOURCE		DETECTOR		ANGLE
			TYPE	RANGE	TYPE	RANGE	
G, NP	ABX	22- 30	C	18- 32	ACT-I		4PI

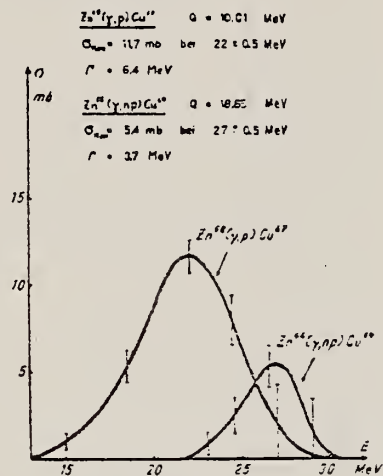


Fig. 1.
Wirkungsquerschnittsverlauf der Reaktionen $Zn^{66}(\gamma, np)Cu^{67}$ und $Zn^{66}(\gamma, p)Cu^{65}$.

Tabelle 1.
Zusammenstellung der gem. W. Q.

Reaktion	Q-Wert MeV	MeV barn	Verhältnis der Querschnitte
$Zn^{66}(\gamma, np)Cu^{67}$	13.65	0.02	$\frac{\sigma_{Zn^{66}(\gamma, p)}}{\sigma_{Zn^{66}(\gamma, np)}} = 3.6 \pm 0.5$
$Zn^{66}(\gamma, p)Cu^{65}$	10.01	0.08	$\frac{\sigma_{Zn^{66}(\gamma, np)}}{\sigma_{Zn^{66}(\gamma, p)}} = 0.25$
$Zn^{66}(\gamma, 2n)Zn^{64}$	20.82	0.08	$\frac{\sigma_{Zn^{66}(\gamma, p)}}{\sigma_{Zn^{66}(\gamma, 2n)}} = 4.5$
$Mo^{92}(\gamma, np)Nb^{90}$	19.5	0.02	$\frac{\sigma_{Mo^{92}(\gamma, p)}}{\sigma_{Mo^{92}(\gamma, np)}} = 4.5$
$Mo^{92}(\gamma, p)Nb^{91}$		0.09	
^{a)} σ_{max} : 5.3 mb bei $E_\gamma = 27 \pm 0.5$ MeV $\Gamma = 3.7$ MeV. ^{b)} σ_{max} : 11.5 mb bei $E_\gamma = 22 \pm 0.5$ MeV $\Gamma = 6.4$ MeV.			

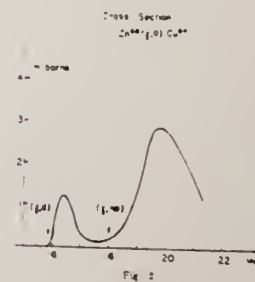
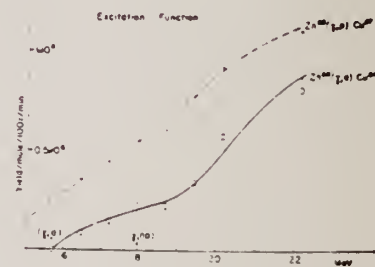
Ref. J. Goldemberg, L. Marquez
Nuclear Phys. 7, 202 (1958)

Elem. Sym.	A	Z
Zn	66	30

Method
activation; 22 MeV Betatron

Ref. No.	EH
58 Go 3	

Reaction	E or ΔE	E_0	Γ	$\int \sigma dE$	$J\pi$	Notes
$(\gamma, d) \uparrow$	16-22	~ 16.5				$\sigma_{\max} = \sim 1 \text{ mb.}$
(γ, np)		~ 19.8				$\sigma_{\max} = \sim 3 \text{ mb.}$



REF.

A. Hofmann, P. Stoll
 Helv. Phys. Acta 31, 591 (1958)

ELEM. SYM.	A	Z
Zn	66	30
REF. NO.		
58 Ho 1		egf

METHOD

REACTION	RESULT	EXCITATION ENERGY	SOURCE		DETECTOR		ANGLE
			TYPE	RANGE	TYPE	RANGE	
G, NP	ABX	21- 32	C	21- 32	ACT-I		4PI

(γ , np) yields include (γ , d).

Tabelle I

Reaktion	Q-Wert MeV	I.W.Q. $\bar{\sigma}$ MeV barn	σ_{\max} mb	E_{\max} MeV	Γ MeV
$\text{Ca}^{40}(\gamma, pn) \text{K}^{38}$	-24,3	0,005	2,4	30 ± 1	2,1
$\text{Zn}^{66}(\gamma, pn) \text{Cu}^{64}$	-18,36	0,03			
$\text{Zn}^{66}(\gamma, pn) \text{Cu}^{64}$	-18,65	0,031	7,2	28 ± 1	4
$\text{Zn}^{66}(\gamma, p) \text{Cu}^{67}$	-10,01	0,19	11,4	$22,7 \pm 1$	6
$\text{Se}^{80}(\gamma, pn) \text{As}^{78}$	-20,43	0,02			
$\text{Zn}^{64}(\gamma, 2n) \text{Zn}^{62}$	-20,82	0,08			
$\text{Mo}^{92}(\gamma, pn) \text{Nb}^{90}$	-19,5	0,02			
$\text{Sb}^{123}(\gamma, pn) \text{Sn}^{121}$	-18,2	0,0006			

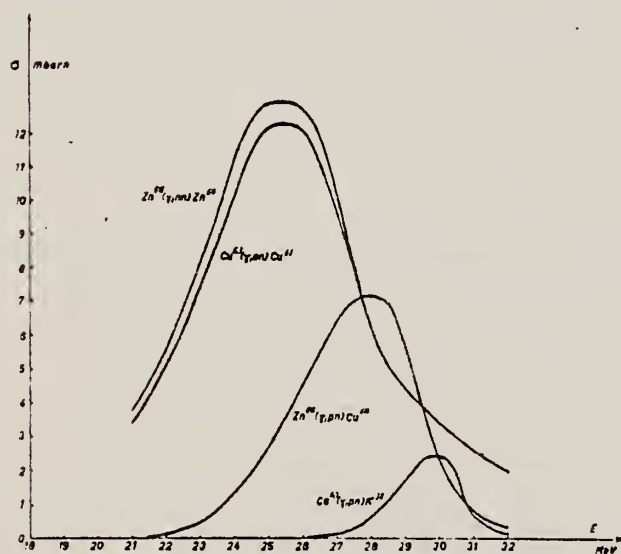


Fig. 1

Gemessene Anregungskurven folgender Reaktionen: $\text{Ca}^{40}(\gamma, pn) \text{K}^{38}$, $\text{Zn}^{66}(\gamma, pn) \text{Cu}^{64}$.
 Die Anregungskurve der $\text{Zn}^{66}(\gamma, nn) \text{Zn}^{64}$ -Reaktion wurde mit Hilfe der statistischen Theorie berechnet.

Der Anteil der (γ , d)-Reaktion ist in den entsprechenden (γ , pn)-Anregungskurven enthalten.

REF.

R. B. Begzhanov and A. A. Islamov
 J. Nucl. Phys. (USSR) 5, 483 (1967)
 Sov. J. Nucl. Phys. 5, 339 (1967)

ELEM. SYM.

A

Z

Zn

66

30

METHOD

REF. NO.

67 Be 5

HMG

REACTION	RESULT	EXCITATION ENERGY	SOURCE		DETECTOR		ANGLE
			TYPE	RANGE	TYPE	RANGE	
G.G	LFT	1.0	D	1.0	NAI-D		120

$$\tau = (20 \pm 6) \cdot 10^{-13} \text{ sec. } 1.064 \text{ MeV}$$

Y. Oka, T. Kato, K. Nomura, T. Saito, Hui-Tuh Tsai
Bull. Chem. Soc. Japan 41, 380 (1968)

ELEM. SYM.	A	Z
Zn	66	30
REF. NO.		
68 Ok 3		egf

METHOD

REACTION	RESULT	EXCITATION ENERGY	SOURCE		DETECTOR		ANGLE
			TYPE	RANGE	TYPE	RANGE	
G, NP	ABY	THR-20	C	20	ACT-I		4PI

TABLE 2. THE YIELDS OF SOME (γ , pn) REACTIONS
WITH 20 MeV BREMSSTRAHLUNG

Reaction	Half-life of product	Specific activity ^{a)} (μ Ci/mg)	Yield ($\text{mol} \cdot \text{l}^{-1} \cdot \text{R}^{-1}$)
$^{54}\text{Fe}(\gamma, \text{pn})^{54}\text{Mn}$	314 d	2.5×10^{-4}	3.6×10^2
$^{64}\text{Zn}(\gamma, \text{pn})^{64}\text{Cu}$	13 hr	7.2×10^{-3}	7.5×10^3
$^{104}\text{Pd}(\gamma, \text{pn})^{102}\text{Rh}$	210 d	1.1×10^{-4}	1.7×10^3

a) The value corrected at the end of 1 hr irradiation (9.4×10^6 R/min).

ELEM. SYM.	A	Z
Zn	66	30
REF. NO.		
68 Sh 5		egf

REACTION	RESULT	EXCITATION ENERGY	SOURCE		DETECTOR		ANGLE
			TYPE	RANGE	TYPE	RANGE	
G, G	NOX	7	D	7	SCD	1-7	DST
		(7.368)		(7.368)			

TABLE 2

Excitation energies of levels of ^{66}Zn populated by the transitions from the resonant level and reduced transition probabilities from the resonant level to the levels

$7=7.368 \text{ MEV}$

Excitation energy (keV)	Spin and parity	Gamma-ray energy (keV)	Relative intensity	Reduced transition probability (arbitrary units) ^{a)}
0	0 ⁺	7368	100	25.7
1039	2 ⁺	6326	≈ 0.3	≈ 0.1
1873	2 ⁺	5495	14.3	8.6
2373	0 ⁺	4995	≈ 0.4	≈ 0.3
3106	0	4262	8.6	10.5
3528	0	3840	1.6	2.8
3824	0	3544	1.6	3.6

^{a)} Reduced transition probability is defined as I_γ/E_γ^3 , where I_γ and E_γ denote the relative intensity and the gamma-ray energy, respectively.

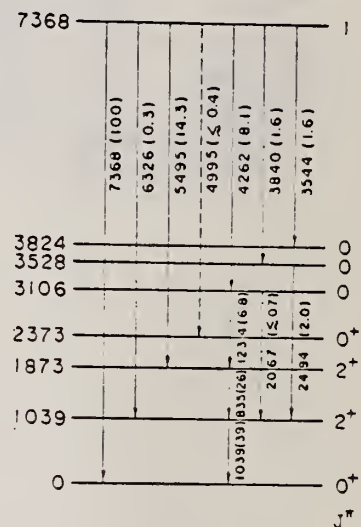


Fig. 10. Partial decay scheme for the 7368 keV level of ^{66}Zn . The transitions are labelled by energy in keV. The relative intensities are given in parentheses.

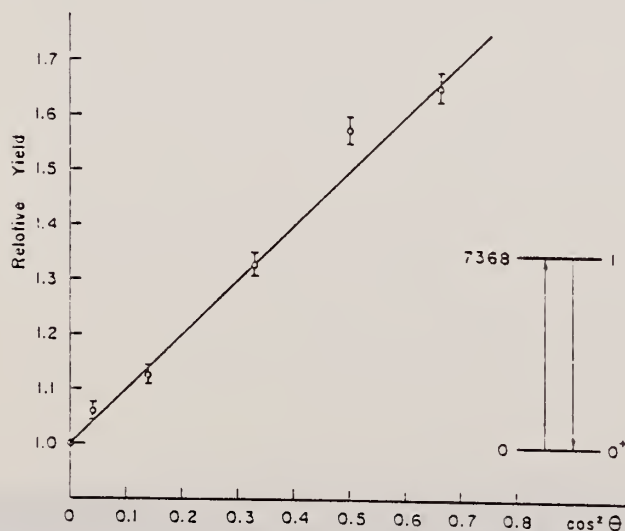


Fig. 5. Angular distribution of the elastically scattered 7368 keV gamma ray. The solid line indicates the theoretical line for a $0(1)1(1)0$ sequence, $1 + \cos^2 \theta$.

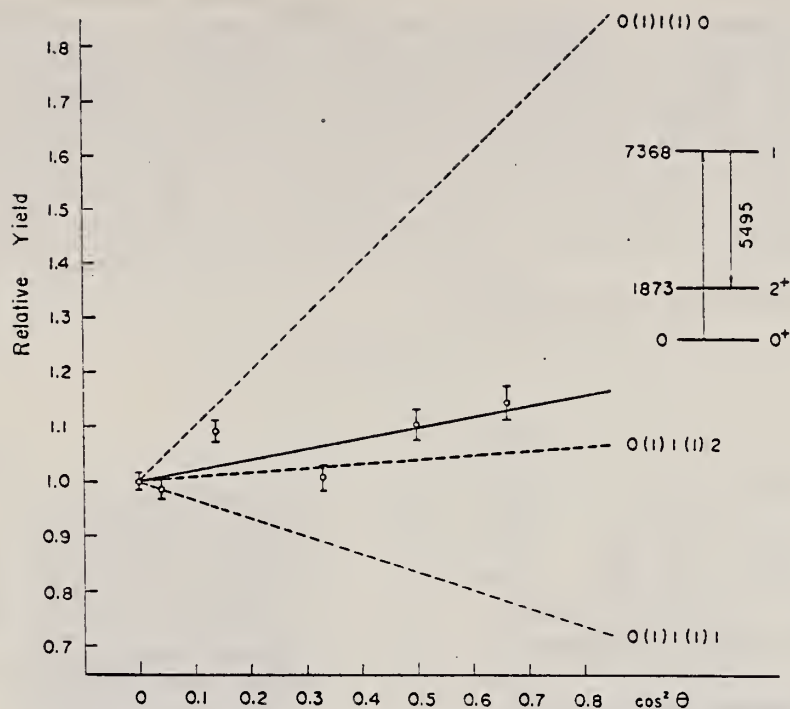


Fig. 6. Angular distribution of the inelastically scattered 5495 keV gamma ray. The solid line is obtained by a least-squares fit to the experimental points. The dashed lines indicate the theoretical lines for $0(1)1(1)0$, $0(1)1(1)1$ and $0(1)1(1)2$ sequences.

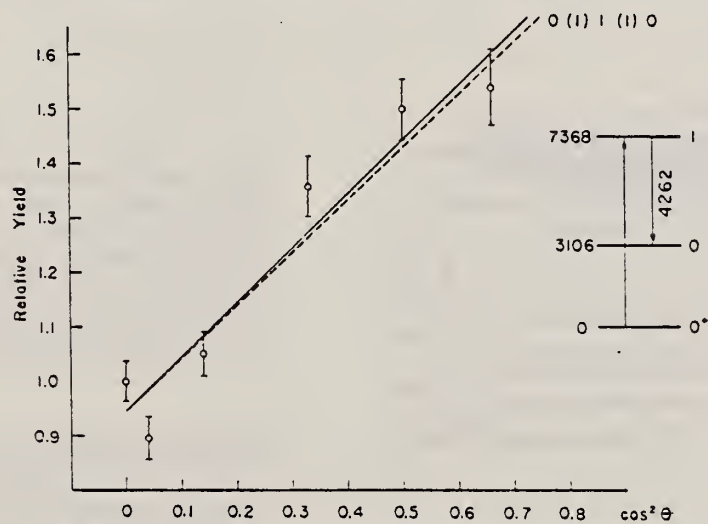


Fig. 7. Angular distribution of the inelastically scattered 4262 keV gamma ray. The solid line is obtained by a least-squares fit to the experimental points. The dashed line indicates the theoretical line for a $0(1)1(1)0$ sequence.

N. Shikazono and Y. Kwarasaki
J. Phys. Soc. Japan 27, 273 (1969)

ELEM. S.Y.M.		
Zn	66	30
REF. NO.		
69 Sh 1		egf

METHOD			SOURCE		DETECTOR		ANGLE
REACTION	RESULT	EXCITATION ENERGY	TYPE	RANGE	TYPE	RANGE	
G,G	LFT	7	D	7	SCD-D	7	135

$$\Gamma_0 = 0.22 \pm 0.02 \text{ eV}$$

$$7 = 7.368 \text{ MEV}$$

Separation from source line $8.5 \pm_{0.5}^{0.7} \text{ eV}$.

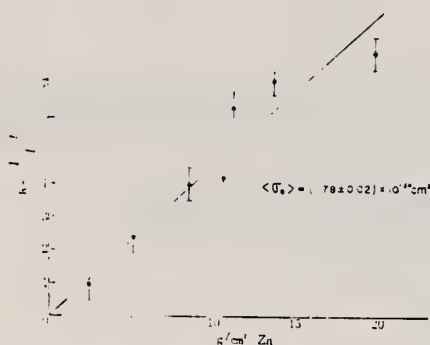


Fig. 3. Self-absorption ratio versus zinc absorber thickness. The solid line indicates the least-squares fit, corresponding the value of the effective absorption cross section to be 1.78 ± 0.02 barns.

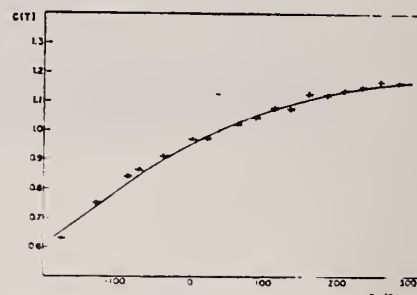


Fig. 4. Relative intensity of the scattered photons versus temperature of the scatterer. The intensity at 39°C is normalized to unity. The solid curve indicates a theoretical one calculated with best fit parameters; $\theta_{Dn} = 350^\circ \text{K}$, $\delta = 8.5 \text{ eV}$, $\Gamma_0 = 0.22 \text{ eV}$, where θ_{Dn} is the Debye temperature of zinc, δ the separation energy between source and target levels and Γ_0 the ground-state transition width.

REF. V.D. Afanas'ev, N.G. Afanas'ev, A. Yu. Buki, G.A. Savitskii,
V.M. Khvastunov, N.G. Shevchenko
Yad. Fiz. 12, 885 (1970)
Sov. J. Nucl. Phys. 12, 480 (1971)

ELEM. SYM.	A	Z
Zn	66	30

METHOD

REF. NO.

70 Af 1

hmg

REACTION	RESULT	EXCITATION ENERGY	SOURCE		DETECTOR		ANGLE
			TYPE	RANGE	TYPE	RANGE	
$E, E/$	FMF	0-3	D	150.225	MAG-D		DST

1.04, 2.8 MEV, B(EL)

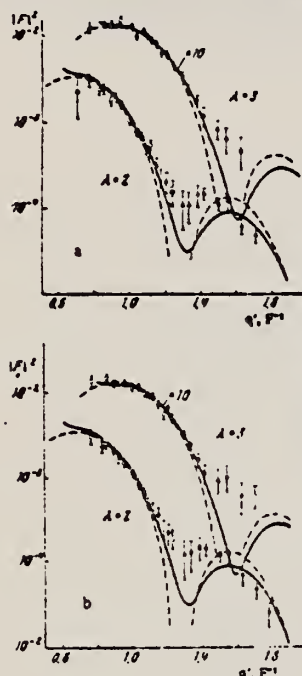


FIG. 2. Form factors of E_2 and E_3 transitions in Zn^{64} (a) and Zn^{66} (b). The solid curves pertain to the vibrational model with calculations in the high-energy approximation; the dashed curves pertain to Helm's model with calculations in the Born approximation. The experimental values and curves for E_3 transitions are enlarged 10-fold. Points: $\circ - E_0 = 150$ MeV, $\bullet - E_0 = 225$ MeV.

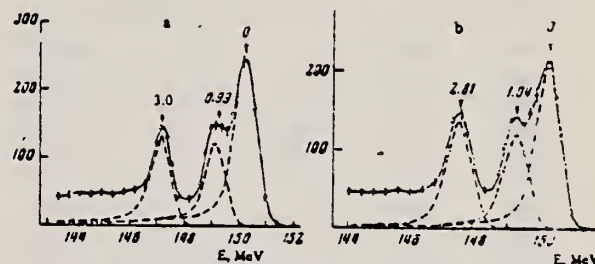


FIG. 1. Spectra of electrons scattered by (a) Zn^{64} and (b) Zn^{66} at 75° ($E_0 = 150$ MeV). Ordinates are given in arbitrary units.

Table I. Reduced probabilities and fitting parameters N_λ and B_λ of E_2 and E_3 transitions in Zn isotopes

Isotope	E, MeV	I^π	Vibrational model		Helm's model		Other results	
			$N_\lambda \cdot 10$	$H(E_\lambda)^\dagger$	$P_\lambda \cdot 10$	$H(E_\lambda)^\dagger$	$B(E_2)$ (experiment)	$B(E_2)$ (theory)
Zn^{64}	1.04	2^+	0.141 ± 0.005	1770 ± 140	0.546 ± 0.018	$1'00 \pm 70$	1100 [1], 1700 \pm 160 [4]	1800 [11], 1540 [12]
	3.3	3^-	0.070 ± 0.003	32300 ± 2300	0.489 ± 0.011	29100 ± 1500		
Zn^{66}	0.99	2^+	0.144 ± 0.005	1800 ± 150	0.557 ± 0.017	1650 ± 74	1100 [1], 1450 \pm 150 [4]	2000 [11]
	2.81	3^-	0.070 ± 0.003	33700 ± 2400	0.498 ± 0.013	29700 ± 1700		

Note. $B(E_\lambda)$ is given in units of $e^2 \cdot F^2$.

Table II. Parameters of the charge distribution in Zn isotopes for the Fermi model and the Gaussian uniform model

Isotope	Fermi model		Gaussian uniform model	
	c, F	L, F	R, F	B, F
Zn^{64}	4.265 ± 0.016	2.751 ± 0.017	4.500 ± 0.019	0.721 ± 0.015
Zn^{66}	4.291 ± 0.022	2.803 ± 0.027	4.504 ± 0.025	0.870 ± 0.014

METHOD

REF. NO.

72 Me 3

egf

REACTION	RESULT	EXCITATION ENERGY	SOURCE		DETECTOR		ANGLE
			TYPE	RANGE	TYPE	RANGE	
G,G	LFT	3-5	C	5	SCD-D		DST

J-PI

TABLE 1

Properties of the Zn levels observed in the bremsstrahlung experiments

Energy (keV)	Isotope	Spin	Parity	Γ_0/Γ	Γ_0 (meV)	Γ_0^{*+} (meV)
3346	(68)	1		(0.70) ^{a)}	42 \pm 7	9.9×10^{-4} (E1) 0.061 (M1)
3366	64	1 ^{b)}	+ ^{b)}	0.54 ^{c)}	8.2 \pm 1.3	0.012
3381	66	1	(-) ^{d)}	0.69 ^{e)}	16 \pm 3	0.022
3425	64	1 ^{b)}	+ ^{b)}	0.72 ^{c)}	6.9 \pm 1.6	0.009
3433	(66)	(1) ^{d,e)}	(-) ^{e)}	0.51 ^{e)}	8 \pm 3	1.7×10^{-4}
3704	64	1	(-) ^{f)}	(1.0) ^{f)}	18 \pm 3	3.2×10^{-4}
3717	(68)	(1)		(1.0) ^{f)}	8.5 \pm 2.2	1.5×10^{-4} (E1) 0.009 (M1)
3739	66	1	(-) ^{f)}	(1.0) ^{f)}	24 \pm 3	4.1×10^{-4}
4159	64	1	(-) ^{f)}	(0.54) ^{e)}	32 \pm 9	4.0×10^{-4}
4295	66	1 ^{b)}	(+) ^{b)}	0.60 ^{e)}	67 \pm 20	0.046
4339	(68)	(1)		(1.0) ^{f)}	38 \pm 10	4.2×10^{-4} (E1) 0.025 (M1)
4426	66	1	(-) ^{f)}	(1.0) ^{f)}	65 \pm 10	6.8×10^{-4}
4455	64	1 ^{b)}	+ ^{b)}	(1.0) ^{f,g)}	51 \pm 9	0.031
4462	66	1 ^{b)}	(+) ^{d,e)}	0.29 ^{e)}	28 \pm 21	0.017
4466	(68)	1		(1.0) ^{f)}	65 \pm 19	6.5×10^{-4} (E1) 0.040 (M1)
4503	(68)	(1)		(1.0) ^{f)}	38 \pm 13	3.6×10^{-4} (E1) 0.023 (M1)
4609	(66)	(1)		(1.0) ^{f)}	54 \pm 15	5.0×10^{-4} (E1) 0.030 (M1)
4664	(64)	(1)		(1.0) ^{f)}	11 \pm 4	1.0×10^{-4} (E1) 0.006 (M1)
4685	(66)	(1)		(1.0) ^{f)}	64 \pm 16	5.6×10^{-4} (E1) 0.034 (M1)
4806	(66)	1 ^{b)}	+ ^{e)}	0.81 ^{e)}	100 \pm 25	0.049

^{a)} Based on ref. ⁹⁾, see text.^{b)} Ref. ¹⁾.^{c)} Ref. ¹²⁾.^{d)} Ref. ²⁾.^{e)} Ref. ¹⁰⁾.^{f)} Assumed in the absence of evidence for branching.^{g)} Assuming that the branch to the 2_1^+ state, seen in the bremsstrahlung experiment, is the only branch to an excited state.^{h)} Refs. ^{11,12)} contradict each other with respect to this branching.ⁱ⁾ Ref. ¹⁰⁾ favors a (-) assignment. See text.

(over)

- 1) H. Verheul, Nucl. Data B2-3 (1967) 65
- 2) M. J. Martin and M. N. Rao, Nucl. Data B2-6 (1968) 43
- 3) F. R. Metzger, Annual progress report for 1967, AEC contract AT(30-1)-3525, Nucl. Sci. Abstr. 22-7661, 1968
- 4) F. R. Metzger, Annual progress report for 1968, AEC contract AT(30-1)-3525, Nucl. Sci. Abstr. 23-15431, 1969
- 5) F. R. Metzger, Phys. Rev. Lett. 18 (1967) 434; Phys. Rev. 171 (1968) 1257;
M. Berman and G. H. Beard, Phys. Rev. C2 (1970) 1506;
M. Schumacher, J. Weiss and H. Langhoff, Phys. Lett. 31B (1969) 61;
H. Langhoff, Phys. Rev. A3 (1971) 1
- 6) F. R. Metzger, Phys. Rev. 187 (1969) 1680, 1700; Nucl. Phys. A182 (1972) 213
- 7) F. R. Metzger, Nucl. Phys. A158 (1970) 88
- 8) R. P. Singh and M. L. Rustgi, Phys. Rev. C3 (1971) 1172
- 9) H. Ottmar, N. M. Ahmed, U. Fanger, D. Heck, W. Michaelis and H. Schmidt, Nucl. Phys. A164 (1971) 69
- 10) D. C. Camp and G. L. Meredith, Nucl. Phys. A166 (1971) 349
- 11) J. Konijn, R. van Lieshout, J. P. Deutsch and L. Grenacs, Nucl. Phys. A91 (1967) 439
- 12) L. G. Mann, K. G. Tirsell and S. D. Bloom, Nucl. Phys. A97 (1967) 425

H. Szichman
Z. Physik 259, 217 (1973)

Zn

66

30

METHOD

REF. NO.

73 Sz 2

egl

REACTION	RESULT	EXCITATION ENERGY	SOURCE		DETECTOR		ANGLE
			TYPE	RANGE	TYPE	RANGE	
G,G	LFT	8	D	8	SCD-D		DST

8 = 7.693Table 1. Reduced partial radiation widths of resonance levels in ^{66}Zn , ^{144}Sm and ^{120}Sn

Nucleus	Energy of transition (keV)	Energy of final state	Relative intensity Γ_j/Γ_0 (in percent)	Reduced widths ($\text{eV} \cdot \text{meV}^{-4} \times 10^3$)		Most likely characters	Derived spin and parity values J^π
				$K(E1)$	$K(M1)$		
^{66}Zn	7693	0	100 \pm 1	6 \pm 1	105 \pm 21	E1	0+
	6654	1039.2	42 \pm 1	4 \pm 1	68 \pm 14	E1	2+
	5819	1874	<2	<0.3	<5	E1 or M1	0, 1, 2
	5321	2372	<3	<0.6	<9	E1 or M1	0, 1, 2
	4930	2763	<2	<0.5	<8	E1 or M1	0, 1, 2
	4755	2938.1	24 \pm 2	7 \pm 2	106 \pm 23	E1	0+
	4587	3105.8	8 \pm 1	2.4 \pm 0.6	39 \pm 9	E1 or M1	0, 1, 2
	4480	3212.6	21 \pm 2	7 \pm 2	111 \pm 25	E1	0+
	4452	3240.6	7 \pm 2	2.3 \pm 0.8	38 \pm 13	E1 or M1	0, 1, 2
	4361	3331.7	13 \pm 2	5 \pm 1	75 \pm 19	E1	0, 2+
	4263	3430.0	25 \pm 3	9 \pm 2	154 \pm 36	E1	0, 2+
	4187	3506.3	8 \pm 2	3 \pm 1	52 \pm 17	E1 or M1	0, 1, 2
^{144}Sm	8995	0	100 \pm 1	15 \pm 3	412 \pm 82	E1	0+
	7333	1662.0	33 \pm 1	9 \pm 2	251 \pm 50	E1	2+
	6828	2167	3 \pm 1	10 \pm 4	28 \pm 11	E1 or M1	0, 1, 2
	6568	2426.5	21 \pm 1	8 \pm 2	222 \pm 44	E1	2+
	6514	2480.7	46 \pm 1	18 \pm 4	499 \pm 100	E1	0+
	6191	2804.1	12 \pm 1	6 \pm 1	164 \pm 33	E1	2+
^{120}Sn	7693	0	100 \pm 1.0	38 \pm 11	932 \pm 266	E1	0+
	6522	1171.4	7.3 \pm 0.5	5 \pm 1	112 \pm 32	E1	2+
	5520	2172.9	1.4 \pm 0.3	1.4 \pm 0.4	35 \pm 10	E1 or M1	0, 1, 2
	5337	2356.0	12.3 \pm 0.8	14 \pm 4	343 \pm 98	E1	2+

REF.

A.M. Goryachev, G.N. Zalesnyi, and B.A. Tulupov
 Izv. Akad. Nauk SSSR. Ser. Fiz. 39, 134 (1975)
 Bull. Acad. Sci. USSR Phys. Ser. 39, 116 (1975)

ELEM. SYM.	A	Z
Zn	66	30

METHOD

REF. NO.

75 Go 1

hmg

REACTION	RESULT	EXCITATION ENERGY	SOURCE		DETECTOR		ANGLE
			TYPE	RANGE	TYPE	RANGE	
G,XN	ABX	11- 25	C	9- 25	BF3-I		4PI

$\sigma(G,SN)$. Statistical theory used to obtain SN cross section from XN cross section.

Table 2

Nuclide	β_0	E_2 , MeV	E_1 , MeV	Nuclide	β_0	E_2 , MeV	E_1 , MeV
^{64}Zn	0.25	0.99	15	^{74}Ge	0.25	0.562	18
^{66}Zn	0.23	1.04	15	^{76}Se	0.33	0.559	18
^{68}Zn	0.2	1.08	18	^{78}Se	0.3	0.616	18
^{70}Ge	0.23	1.04	18	^{80}Se	0.25	0.654	18
^{72}Ge	0.25	0.835	18	^{82}Se	0.2	0.655	18
^{74}Ge	0.3	0.6	18				

Table 3

Nuclide	σ , mb	Nuclide	σ , mb	Nuclide	σ , mb
^{64}Zn	$397 \pm 19^*$	^{74}Ge	700 ± 37	^{74}Se	1021 ± 52
^{66}Zn	579 ± 27	^{76}Ge	872 ± 41	^{80}Se	1020 ± 50
^{68}Zn	718 ± 35	^{78}Ge	911 ± 43	^{82}Se	1067 ± 53
^{70}Ge	731 ± 37	^{80}Se	930 ± 50		

*Mean - square errors

Values given are for σ_0 (24.2 MeV).

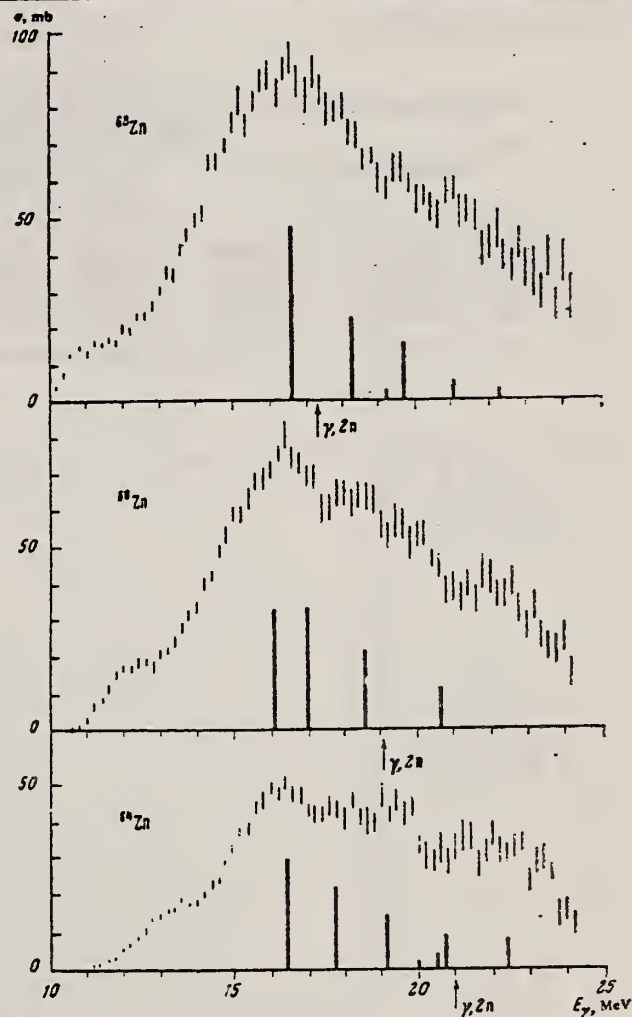


Fig. 1. Cross sections of photoneutron reactions on $^{64,66,68}\text{Zn}$. The dipole photoabsorption forces are taken from [6,7] (the solid black columns).

⁶M.G. Huber et al., Phys. Rev. 155, 1073 (1967)

⁷M.G. Huber et al., Z. Phys. 192, 223 (1966).

REF. R. Neuhausen, J. W. Lightbody, Jr., S. P. Fivozinsky,
and S. Penner
Nucl. Phys. A263, 249 (1976)

ELEM. SYM.	A	Z
Zn	66	30
REF. NO.		
76 Ne 1		egf

METHOD					
REACTION	RESULT	EXCITATION ENERGY	SOURCE		ANGLE
			TYPE	RANGE	
E, E/	ABX	1- 3	D	40-112	DST

2+, 3- STATES

TABLE 6
Reduced transition probabilities in single particle units, deformation parameters and deformation lengths ($R = 1.2 \text{ fm} \times A^{1/3}$)

	$B_1(E2)/B_1^{s.p.}(E2)$	β_2	$\beta_2 R$ (fm)	$B_1(E3)/B_1^{s.p.}(E3)$	β_3	$\beta_3 R$ (fm)
⁶⁴ Zn	20.4 ± 1.2	0.230 ± 0.007	1.10 ± 0.03	23.5 ± 4.0	0.224 ± 0.019	1.08 ± 0.09
⁶⁶ Zn	17.3 ± 1.3	0.212 ± 0.008	1.03 ± 0.04	23.4 ± 4.9	0.224 ± 0.023	1.09 ± 0.11
⁶⁸ Zn	13.5 ± 1.0	0.187 ± 0.007	0.92 ± 0.04	19.8 ± 4.3	0.206 ± 0.022	1.01 ± 0.11
⁷⁰ Zn	24.0 ± 2.2	0.249 ± 0.011	1.23 ± 0.06			

States: 1.039(2+), 2.83(3-) MeV.

METHOD					REF. NO.		
					77 Ne 3		hg
REACTION	RESULT	EXCITATION ENERGY	SOURCE		DETECTOR		ANGLE
			TYPE	RANGE	TYPE	RANGE	
E, E/	FMF	1-3	D	100-275	MAG-D		DST

Abstract: The inelastic electron scattering cross sections for the quadrupole transitions to the 2_1^+ and 2_2^+ states in the even Zn isotopes ^{64}Zn , ^{66}Zn and ^{68}Zn and for the hexadecapole transition to the 4_1^+ state in ^{64}Zn have been measured in a momentum transfer range up to $q = 2.2 \text{ fm}^{-1}$. In the framework of the vibrational model these states are considered as one- and two-quadrupole-phonon states. The measurements are characterized by high statistical accuracy and by an overall resolution of $\delta E/E_0 = 10^{-3}$ which permitted separation of almost all members of the two-phonon triplet. The measured cross sections are analyzed with phenomenological models as well as with a Fourier-Bessel expansion of the transition charge density. The latter analysis yields realistic error bands for the transition charge densities and model-independent values for the reduced transition probabilities and transition radii.

LEVELS 1.039, 1.873

NUCLEAR REACTIONS $^{64,66,68}\text{Zn}(e, e')$, $E = 100\text{--}275 \text{ MeV}$; measured $d\sigma/d\Omega(E, \theta)$.
 $^{64,66,68}\text{Zn}$ levels deduced transition charge density, $B_i(E\lambda)$ and transition charge radii $R_{i\mu}$.
 Enriched targets.

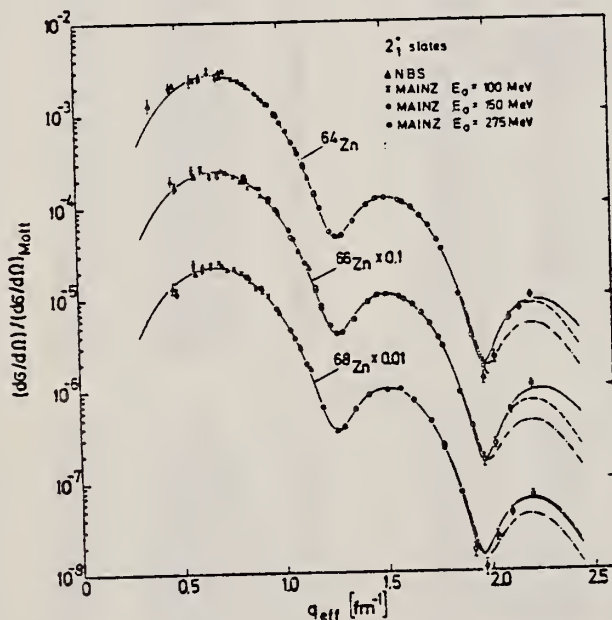


Fig. 3. Cross sections divided by the Mott cross section for the allowed transitions to the 2_1^+ state in ^{64}Zn , ^{66}Zn and ^{68}Zn versus the effective momentum transfer. The measured cross sections are transformed to a common incident energy $E_0 = 275 \text{ MeV}$. The curves represent best fit DWBA calculations with the Fourier-Bessel expansion of the transition charge density (solid line), the modified Tassie model (dashed line) and the Gaussian model (dashed-dotted line).

TABLE 3
Fitted parameters of the Gaussian model for the first 2_1^+ states in ^{64}Zn , ^{66}Zn and ^{68}Zn

	^{64}Zn $\epsilon = 0.992 \text{ MeV}$	^{66}Zn $\epsilon = 1.039 \text{ MeV}$	^{68}Zn $\epsilon = 1.077 \text{ MeV}$
$a \text{ (fm)}$	4.148 ± 0.004	4.154 ± 0.005	4.192 ± 0.005
$b \text{ (fm)}$	1.470 ± 0.005	1.478 ± 0.005	1.469 ± 0.006
$B_2(12) \text{ (fm}^4\text{)}$	1470 ± 15	1340 ± 15	1200 ± 15
χ^2/ν	3.95	5.43	3.12

TABLE 5

Reduced transition probabilities $B_\gamma(E2)$ and transition radii R_{tr} for the 2_1^+ states in ^{64}Zn , ^{66}Zn and ^{68}Zn

	^{64}Zn $\varepsilon = 0.992 \text{ MeV}$	^{66}Zn $\varepsilon = 1.039 \text{ MeV}$	^{68}Zn $\varepsilon = 1.077 \text{ MeV}$
$B_\gamma(E2) (\text{fm}^4)$			
(e. e.) ^{a)}	1620 ± 90	1410 ± 80	1320 ± 70
CE ^{b)}	1700 ± 150	1450 ± 130	1250 ± 110
$R_{tr} (\text{fm})$	5.44 ± 0.09	5.39 ± 0.09	5.47 ± 0.09
R_{tr}/R_m	1.38 ± 0.03	1.37 ± 0.03	1.38 ± 0.03

^{a)} Model independent analysis, this work.^{b)} Ref. ¹⁴⁾.

TABLE 8

Reduced transition probabilities $B_\gamma(E\lambda)$ and transition radii R_{tr} for the forbidden transition to the 2_2^+ states in ^{64}Zn , ^{66}Zn and ^{68}Zn and to the 4_1^+ state in ^{64}Zn

	^{64}Zn $\varepsilon = 1.800 \text{ MeV}$ $\lambda = 2$	^{66}Zn $\varepsilon = 1.873 \text{ MeV}$ $\lambda = 2$	^{68}Zn $\varepsilon = 1.883 \text{ MeV}$ $\lambda = 2$	^{64}Zn $\varepsilon = 2.305 \text{ MeV}$ $\lambda = 4$
$B_\gamma(E\lambda) (\text{fm}^{2\lambda})$	17.0 ± 1.2	4.5 ± 0.7	46 ± 7	$(3.4 \pm 1.0) \times 10^4$
$R_{tr} (\text{fm})$	4.6 ± 0.1	4.5 ± 0.1	5.9 ± 0.1	6.7 ± 0.3
R_{tr}/R_m	1.17 ± 0.03	1.14 ± 0.03	1.49 ± 0.03	1.70 ± 0.08
$R_{tr}^2(2_2^+)/R_{tr}^2(2_1^+)$	0.71 ± 0.03	0.69 ± 0.04	1.17 ± 0.06	

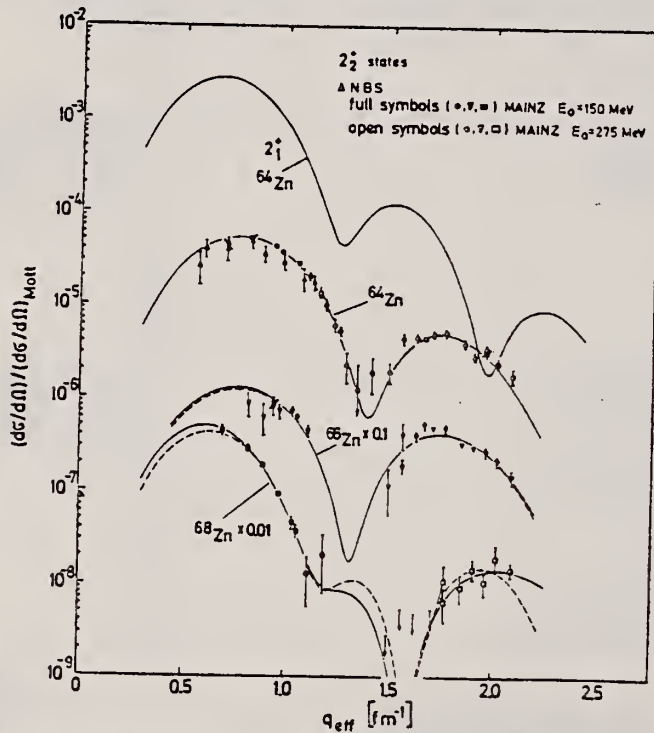


Fig. 8. Same as fig. 3, but for the forbidden transitions to the 2_2^+ states in ^{64}Zn , ^{66}Zn and ^{68}Zn , respectively. The curves represent best-fit DWBA calculations with the Fourier-Bessel expansion of the transition charge density (solid line) and the phenomenological model given in eq. (22) (dashed line). For comparison, the shape of the cross section for the allowed transition to the 2_1^+ state in ^{64}Zn is shown (uppermost curve).

METHOD					REF. NO.		77 Ne 3	hg
REACTION	RESULT	EXCITATION ENERGY	SOURCE		DETECTOR			
			TYPE	RANGE	TYPE	RANGE		

TABLE I

Compilation of the measured inelastic cross sections. The cross sections are multiplied by 10^4 , where the power x is given in cols. 4 and 8, respectively

E_0 (MeV)	θ (deg)	$10^4(d\sigma/d\Omega)$ (cm ² /sr)	x	E_0 (MeV)	θ (deg)	$10^4(d\sigma/d\Omega)$ (cm ² /sr)	x
⁶⁶ Zn; $\epsilon = 1.039$ MeV 2_1^+							
100.1	60.0	1.32 ± 0.16	29	275.1	42.0	1.47 ± 0.05	30
100.1	65.0	1.02 ± 0.11	29	275.1	47.0	2.41 ± 0.07	31
100.1	70.0	6.26 ± 0.56	30	275.2	47.0	2.58 ± 0.09	31
100.1	75.0	4.90 ± 0.36	30	275.1	50.0	7.81 ± 0.21	32
100.1	80.0	3.88 ± 0.22	30	275.1	52.5	5.35 ± 0.18	32
100.1	85.0	2.70 ± 0.14	30	275.3	55.0	7.19 ± 0.31	32
100.1	90.0	1.85 ± 0.08	30	275.1	58.0	7.63 ± 0.20	32
100.0	95.0	1.22 ± 0.05	30	275.1	60.0	7.70 ± 0.20	32
100.0	100.0	8.75 ± 0.29	31	275.1	62.0	6.76 ± 0.17	32
100.0	105.0	6.18 ± 0.19	31	275.2	65.0	5.13 ± 0.17	32
100.0	110.0	4.17 ± 0.13	31	275.1	65.0	5.29 ± 0.13	32
150.1	60.0	5.50 ± 0.16	30	275.1	66.0	4.54 ± 0.14	32
149.9	60.0	4.84 ± 0.12	30	275.1	68.0	3.50 ± 0.08	32
150.1	66.0	2.68 ± 0.08	30	275.1	70.0	2.54 ± 0.07	32
149.9	70.0	1.63 ± 0.04	30	275.1	70.0	2.43 ± 0.08	32
149.8	70.0	1.49 ± 0.04	30	275.1	72.0	1.66 ± 0.05	32
150.2	72.5	1.06 ± 0.03	30	275.1	74.0	1.04 ± 0.04	32
150.0	72.5	1.04 ± 0.03	30	275.3	75.0	7.88 ± 0.30	33
150.1	78.0	4.35 ± 0.11	31	275.1	79.0	1.97 ± 0.07	33
149.8	80.0	3.18 ± 0.08	31	275.1	82.0	7.11 ± 0.38	34
150.1	85.0	1.30 ± 0.03	31	275.1	85.0	2.52 ± 0.33	34
150.0	85.0	1.31 ± 0.04	31	275.1	88.0	3.27 ± 0.29	34
150.1	92.5	2.74 ± 0.08	32	275.1	92.0	6.20 ± 0.31	34
150.2	92.5	2.56 ± 0.10	32	275.1	98.0	8.55 ± 0.63	34
150.1	100.0	8.83 ± 0.35	33				
⁶⁶ Zn; $\epsilon = 1.873$ MeV 2_1^+							
150.1	60.0	2.2 ± 0.6	32	275.1	65.0	1.0 ± 0.2	33
150.1	66.0	1.0 ± 0.4	32	275.1	68.0	1.75 ± 0.12	33
149.9	70.0	1.15 ± 0.16	32	275.1	70.0	2.03 ± 0.14	33
149.8	70.0	1.03 ± 0.19	32	275.1	72.0	1.66 ± 0.10	33
150.2	72.5	7.9 ± 1.3	33	275.3	75.0	1.38 ± 0.10	33
150.1	78.0	5.72 ± 0.51	33	275.1	79.0	7.30 ± 0.43	34
149.8	80.0	4.39 ± 0.35	33	275.1	82.0	5.74 ± 0.36	34
150.1	85.0	2.38 ± 0.35	33	275.1	85.0	4.32 ± 0.37	34
275.1	62.0	7.4 ± 3.7	34	275.1	88.0	2.93 ± 0.33	34
275.2	65.0	2.1 ± 0.7	33	275.1	92.0	1.60 ± 0.27	34

REF. Y. Cauchois, H. Ben Abdelaziz, R. Khérouf, C. Schloesing-Möller
J. Phys. G7, 1539 (1981)

ELEM. SYM.	A	Z
Zn	66	30
REF. NO.		hg
81 Ca 2		

METHOD

REACTION	RESULT	EXCITATION ENERGY	SOURCE		DETECTOR		ANGLE
			TYPE	RANGE	TYPE	RANGE	
G,G	LFT	1	C	0 - 2	SCD-D		
		(1.040)					

1.040 MeV

Abstract. Lifetimes of 49 excited states below 1.65 MeV have been measured in ^{24}Mg , ^{27}Al , ^{48}Ti , ^{58}Ni , ^{59}Co , $^{61,62}\text{Ni}$, $^{63,65}\text{Cu}$, $^{64,66,68}\text{Zn}$, ^{75}As , ^{103}Rh , $^{113,115}\text{In}$, $^{116,118,120}\text{Sn}$ and $^{121,123}\text{Sb}$ by means of nuclear resonance fluorescence experiments. The levels are excited by bremsstrahlung x-ray photons. The self-absorption technique applied to suitable cases provides nuclear absorption cross sections, widths and lifetimes from which the x-ray spectral distributions are also obtained. Scattering experiments are performed for all other cases in order to obtain widths and lifetimes from these x-ray photon curves. The Compton effect in the sample is taken into account. Self-absorption provides $g\Gamma_0$ from which Γ is deduced using adopted J^π and Γ_0/Γ values; scattering provides $u = g(\Gamma_0^2/\Gamma)W(\theta)$ from which Γ is also deduced with J , Γ_0/Γ and mixing ratios taken from the literature. Thanks to simultaneous determination of the x-ray spectra all the lifetimes as given by our programs with their statistical errors form an unusually coherent set of values.

NUCLEAR REACTIONS (γ , γ), bremsstrahlung excitation: natural isotopes; ^{24}Mg , ^{27}Al , ^{48}Ti , ^{58}Ni , ^{59}Co , $^{61,62}\text{Ni}$, $^{63,65}\text{Cu}$, $^{64,66,68}\text{Zn}$, ^{75}As , ^{103}Rh , $^{113,115}\text{In}$, $^{116,118,120}\text{Sn}$ and $^{121,123}\text{Sb}$; $E \approx 0.5-1.65$ MeV; measured $g\Gamma_0$ or $g(\Gamma_0^2/\Gamma)W(\theta)$; deduced $T_{1/2}$.

(OVER)

Tableau 3. Resultats des mesures des niveaux étudiés par diffusion.

Table 3. Results obtained using the diffusion method.

Isotope	Energie (keV)	J^π	J_0^π	Γ_0/Γ	δ	$u = g(\Gamma_0^2/\Gamma)W(\theta)$ (meV)	τ (ps) ce travail	τ_{ref} (ps)	Références [†]
²⁴ Mg	1368.59(4)	2 ⁺	0 ⁺	1	E2	1,08(13)	1,76(21)	1,98(4)	Endt et van der Leun (1978)
²⁷ Al	1014.45(3)	$\frac{1}{2}^-$	$\frac{1}{2}^+$	0,971	+ 0,351(12)	0,186(13)	2,20(16)	2,12(8)	Endt et van der Leun (1978)
⁴⁸ Ti	983,512(3)	2 ⁺	0 ⁺	1	E2	0,282(23)	6,74(55)	6,1(13)	Been (1978)
⁵⁸ Ni	1454,45(15)	2 ⁺	0 ⁺	1	E2	2,11(26)	0,90(11)	0,92(3)	Kocher et Auble (1976)
⁵⁹ Co	1099,224(25)	$\frac{3}{2}^-$	$\frac{3}{2}^-$	1	(E2)	0,069(8)	4,79(55)	3,17(58)	Kim (1976)
⁵⁹ Co	1458,8(3)	$\frac{1}{2}^-$	$\frac{1}{2}^-$	0,91	(E2)	0,68(8)	1,17(14)	1,52(16)	Kim (1976)
⁵⁹ Co	1480,9(3)	$\frac{3}{2}^-$	$\frac{3}{2}^-$	0,8	< 0,35 ^a	1,23(15)	0,254(31)	0,31(3)	Kim (1976)
⁶¹ Ni	1185,7(6)	$\frac{3}{2}^-$	$\frac{3}{2}^-$	0,77(8) ⁱ	[0,14]	1,88(49)	0,21(5)	0,16(3)	Andreev et al (1974)
⁶² Ni	1172,91(9)	2 ⁺	0 ⁺	1	E2	0,88(17)	2,15(42)	2,09(3)	Halbert (1979a)
⁶³ Cu	1327,00(7)	$\frac{1}{2}^-$	$\frac{1}{2}^-$	0,84	(E2)	1,04(14)	0,84(11)	0,88(4)	Auble (1979b)
⁶³ Cu	1412,05(4)	$\frac{1}{2}^-$	$\frac{1}{2}^-$	0,72	+ 0,61 ⁱ $\begin{pmatrix} 2 \\ -8 \end{pmatrix}$	0,260(38)	1,90(28)	1,61(3)	Auble (1979b)
⁶⁴ Zn	991,54(7)	2 ⁺	0 ⁺	1	E2	0,640(54)	2,97(25)	2,60(13)	Halbert (1979b)
⁶⁵ Cu	1481,83(5)	$\frac{1}{2}^-$	$\frac{1}{2}^-$	0,85	(E2)	1,13(19)	0,79(13)	0,49(5)	Auble (1975a)
⁶⁶ Zn	1039,37(6)	2 ⁺	0 ⁺	1	E2	0,70(6)	2,71(23)	2,25(15)	Auble (1975b)
⁶⁶ Zn	1077,38(5)	2 ⁺	0 ⁺	1	E2	0,70(6)	2,71(23)	2,34(23)	Lewis (1975)
⁷⁵ As	572,5(10)	$\frac{1}{2}^-$	$\frac{1}{2}^-$	1 ^d	0,39 ^b	0,236(26)	4,14(46)	3,5(9)	Horen et Lewis (1975)
⁷⁵ As	823,0(10)	$\frac{1}{2}^-$	$\frac{1}{2}^-$	0,86 ^d	(E2)	0,214(22)	4,27(43)	3,5(3)	Robinson et al (1967)
⁷⁵ As	865,5(10)	$\frac{1}{2}^-$	$\frac{1}{2}^-$	0,83 ^d	— ^c	0,78(6)	0,863(68)	0,60(12)	Celliers et al (1977)
⁷⁵ As	1076,0(10)	$\frac{1}{2}^-$	$\frac{1}{2}^-$	0,94 ^d	0,38 ^d	1,97(13)	0,287(19)	0,32(7)	Celliers et al (1977)
⁷⁵ As	1128,5(10)	$\frac{1}{2}^-$	$\frac{1}{2}^-$	1	E1 ^d	0,224(24)	1,47(16)	—	
⁷⁵ As	1349,0(10)	$\frac{1}{2}^-$	$\frac{1}{2}^-$	0,67 ^d	0,20 ^d	1,61(29)	0,180(32)	0,12(3)	Wilson (1970)
⁷⁵ As	1370,0(10)	$\frac{1}{2}^-$	$\frac{1}{2}^-$	0,47 ^d	0,47 ^d	0,64(13)	0,218(44)	—	
¹⁰³ Rh	803,1(2)	$\frac{1}{2}^-$	$\frac{1}{2}^-$	0,70	M1	1,85(16)	0,174(15)	—	Harmatz (1979)
¹⁰³ Rh	1277,0(2)	$\frac{1}{2}^-$	$\frac{1}{2}^-$	0,75	- 0,62(30) ^e	0,81(9)	0,87(10)	1,3(9)	Harmatz (1979)
¹¹³ In	1177(1)	$\frac{1}{2}^-$	$\frac{1}{2}^-$	1	+ 0,5(2)	9,1(8)	0,086(8)	0,10(6)	Tuttle et al (1976)
¹¹³ In	1510(1)	$\frac{1}{2}^-$	$\frac{1}{2}^-$	0,935	- 0,5 ⁱ $\begin{pmatrix} 1 \\ -2 \end{pmatrix}$	6,4(9)	0,071(10)	0,11 ⁱ $\begin{pmatrix} 2 \\ -4 \end{pmatrix}$	Tuttle et al (1976)
¹¹⁵ In	1077,7(10)	$\frac{1}{2}^-$	$\frac{1}{2}^-$	0,81 ^j	(E2)	0,159(24)	1,61(24)	1,22(7)	Tuttle et al (1976)
¹¹⁵ In	1290,59(3)	$\frac{1}{2}^-$	$\frac{1}{2}^-$	0,98 ^j	(E2)	1,31(11)	0,66(6)	0,55(4)	Tuttle et al (1976)
¹¹⁵ In	1448,78(3)	$\frac{1}{2}^-$	$\frac{1}{2}^-$	0,86	- 8 ^f	0,90(11)	0,50(6)	0,52(20)	Tuttle et al (1976)
¹¹⁵ In	1486,1(1)	$\frac{1}{2}^-$	$\frac{1}{2}^-$	0,787	- 0,8 ^f	0,63(9)	0,63(9)	0,4(3)	Tuttle et al (1976)
¹¹⁵ In	1497,2(4)	$\frac{1}{2}^-$	$\frac{1}{2}^-$	< 1	(E2)	1,33(16)	< 0,30(4)	—	
¹¹⁵ In	1607,8(15)	$\frac{1}{2}^-$	$\frac{1}{2}^-$	< 1	(E2)	1,54(24)	≤ 0,26(4)	—	
¹¹⁶ Sn	1293,54(2)	2 ⁺	0 ⁺	1	E2	3,58(37)	0,53(6)	0,522(14)	Carlson et al (1975)
¹¹⁸ Sn	1229,64(4)	2 ⁺	0 ⁺	1	E2	2,75(28)	0,69(7)	0,67(2)	Carlson et al (1976)
¹²⁰ Sn	1171,6(2)	2 ⁺	0 ⁺	1	E2	1,83(16)	1,04(9)	0,91(2)	Kocher (1976)
¹²¹ Sb	1023,5(10)	$\frac{1}{2}^-$	$\frac{1}{2}^-$	1	[0,57] ^g	3,69(34)	0,228(21)	0,20(7) ^h	Tamura et al (1979)
¹²¹ Sb	1105,5(10)	$\frac{1}{2}^-$	$\frac{1}{2}^-$	0,4	—	0,47(4)	0,42(4)	—	
¹²¹ Sb	1142,5(10)	$\frac{1}{2}^-$	$\frac{1}{2}^-$	0,6	(E2)	0,85(8)	0,449(40)	0,41(8) ^h	Booth et al (1973)
¹²¹ Sb	1384,0(10)	$\frac{1}{2}^-$	$\frac{1}{2}^-$	1	[0,45] ^g	4,7(5)	0,092(10)	0,088(14) ^h	Booth et al (1973)
¹²³ Sb	1029,5(10)	$\frac{1}{2}^-$	$\frac{1}{2}^-$	1	[0,57] ^g	2,96(27)	0,272(25)	0,26(4) ^h	Booth et al (1973)
¹²³ Sb	1086,5(10)	$\frac{1}{2}^-$	$\frac{1}{2}^-$	1	[δ_1 > 1,26] ^g	1,06(9)	0,67(6)	0,72(15) ^h	Booth et al (1973)

[†] Références pour les colonnes 3, 4, 5, 6 et 9 de chaque ligne, sauf indication appelée au bas de ce tableau. Pour les autres données se reporter au texte.

Remarque. Pour calculer δ^2 quand nous ne disposons que de $B(E2)$, pour un mélange (E2)–(M1), nous déduisons $g\Gamma_0(E2) \propto B(E2)E_2^5$; en admettant $W(\theta)=1$ et connaissant Γ_0/Γ , notre détermination de u donne une première approximation de $g\Gamma_0$ d'où une valeur de $\delta^2 = (g\Gamma_0(E2))/(g\Gamma_0 - g\Gamma_0(E2))$ qui permet d'améliorer $W(\theta)$ et $g\Gamma_0$ de proche en proche.

^a Swann (1971); ^b Robinson et al (1967); ^c $W(\theta)=0,99$ calculé d'après la formule de Celliers et al (1977); ^d Abbondanno et al (1978); ^e Sayer et al (1972); ^f Tuttle et al (1976); ^g d'après $B(E2)$ de Barnes et al (1966); ^h calculé d'après Booth et al (1973); Williams et al (1975); ⁱ Dietrich et al (1970).

Z_N
 $A=67$

Z_N
 $A=67$

Z_N
 $A=67$

REF.

V.G. Ivanchenko and B.S. Ratner
 ZhETF Pis'ma 3, No. 11, 452-455, 1 June 1966
 JETP Letters 3, No. 11, 296 (1966)

ELEM. SYM.

A

Z

Zn

67

30

METHOD

30 MeV synchrotron

REF. NO.

66 Iv 1

JDM

REACTION	RESULT	EXCITATION ENERGY	SOURCE		DETECTOR		ANGLE
			TYPE	RANGE	TYPE	RANGE	
G,P	ABX	THR - 28	C	12 - 28	ACT-I		4PI

$$\int_{12}^{28} \sigma dE_{\gamma} = 118 \text{ MeV}\cdot\text{mb}$$

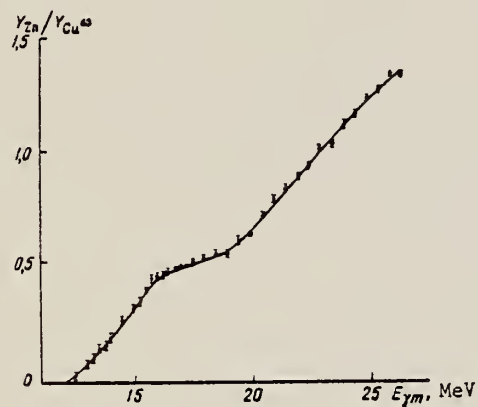


Fig. 1

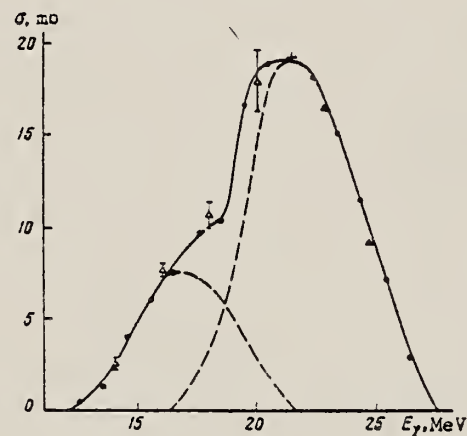


Fig. 2. Cross section of the reaction $\text{Zn}^{67}(\gamma p)\text{Cu}^{66}$ vs. E_{γ} .
 • -- cross section calculated with 1 MeV interval, Δ -- with 2 MeV interval. The dashed curves are drawn under the assumption that the form of the cross section for proton emission from the $1f_{7/2}$ shell (position of the maximum and half-width) is the same as in the case of the reaction $\text{Ni}^{62}(\gamma p)$ [6].

Z_N
 $A=68$

Z_N
 $A=68$

Z_N
 $A=68$

ELEM. SYM.	A	Z
Zn	68	30
REF. NO.		
57 El 1		egf

METHOD				REF. NO.	
				57 El 1	
REACTION	RESULT	EXCITATION ENERGY	SOURCE		ANGLE
			TYPE	RANGE	
G, P	ABX	13- 30	C	14- 32	4PI

Tabelle 1.
Zusammenstellung der gem. W. Q.

Reaktion	Q-Wert MeV	MeV barn	Verhältnis der Querschnitte
$Zn^{66}(\gamma, np)Cu^{64*}$	18,65	0,02	$\frac{\sigma Zn^{66}(\gamma, p)}{\sigma Zn^{66}(\gamma, np)} = 3,6 \pm 0,5$
$Zn^{66}(\gamma, p)Cu^{67*}^{**}$	10,01	0,08	
$Zn^{64}(\gamma, 2n)Zn^{62}$	20,82	0,08	$\frac{\sigma Zn^{64}(\gamma, np)}{\sigma Zn^{64}(\gamma, 2n)} = 0,25$
$Mo^{92}(\gamma, np)Nb^{90}$	19,5	0,02	
$Mo^{98}(\gamma, p)Nb^{97}$		0,09	$\frac{\sigma Mo^{98}(\gamma, p)}{\sigma Mo^{92}(\gamma, np)} = 4,5$
<p>*) σ_{max}: 5,3 mb bei $E_\gamma = 27 \pm 0,5$ MeV $\Gamma = 3,7$ MeV.</p> <p>**) σ_{max}: 11,5 mb bei $E_\gamma = 22 \pm 0,5$ MeV $\Gamma = 6,4$ MeV.</p>			

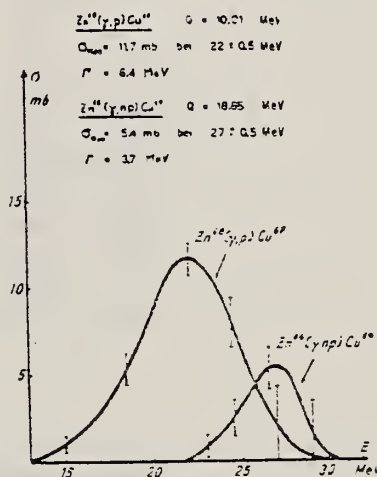


Fig. 1.
Wirkungsquerschnittsverlauf der Reaktionen $Zn^{66}(\gamma, np)Cu^{64}$ und $Zn^{66}(\gamma, p)Cu^{67}$.

REF.

A. Hofmann, P. Stoll
 Helv. Phys. Acta 31, 591 (1958)

ELEM. SYM.

A

Z

Zn

68

30

METHOD

REF. NO.

58 Ho 1

egf

REACTION	RESULT	EXCITATION ENERGY	SOURCE		DETECTOR		ANGLE
			TYPE	RANGE	TYPE	RANGE	
G,P	ABX	10- 32	G	15- 32	ACT-I		4PI

(γ ,np) yields include (γ ,d).

Tabelle I

Reaktion	Q-Wert MeV	I.W.Q. $\bar{\sigma}$ MeV barn	σ_{max} nb	E_{max} MeV	Γ MeV
Ca ⁴⁰ (γ , pn) K ³⁹	-24,3	0,005	2,4	30 \pm 1	2,1
Zn ⁶⁴ (γ , pn) Cu ⁶³	-18,36	0,03			
Zn ⁶⁸ (γ , pn) Cu ⁶⁴	-18,65	0,031	7,2	28 \pm 1	4
Zn ⁶⁸ (γ , p) Cu ⁶⁷	-10,01	0,19	11,4	22,7 \pm 1	6
Se ⁸⁰ (γ , pn) As ⁷⁸	-20,43	0,02			
Zn ⁶⁴ (γ , 2n) Zn ⁶²	-20,82	0,08			
Mo ⁹² (γ , pn) Nb ⁹⁰	-19,5	0,02			
Sb ¹²³ (γ , pn) Sn ¹²¹	-18,2	0,0006			

REACTION	RESULT	EXCITATION ENERGY	SOURCE		DETECTOR		ANGLE
			TYPE	RANGE	TYPE	RANGE	
G ₁ G	LFT	3-5	C	5	SCD-D		DST

J-PI

TABLE I
Properties of the Zn levels observed in the bremsstrahlung experiments

Energy (keV)	Isotope	Spin	Parity	Γ_0/Γ	Γ_0 (meV)	$\Gamma_0^{a,b}$ (meV)
3346	(68)	1		(0.70) ^a	42 \pm 7	9.9×10^{-4} (E1) 0.061 (M1)
3366	64	1 ^b	⁺ ^b	0.54 ^c	8.2 \pm 1.3	0.012
3381	66	1	(⁺) ^d	0.69 ^e	16 \pm 3	0.022
3425	64	1 ^b	⁺ ^b	0.72 ^c	6.9 \pm 1.6	0.009
3433	(66)	(1) ^{d,e}	(⁻) ^e	0.51 ^e	8 \pm 3	1.7×10^{-4}
3704	64	1	(⁻)	(1.0) ^f	18 \pm 3	3.2×10^{-4}
3717	(68)	(1)		(1.0) ^f	8.5 \pm 2.2	1.5×10^{-4} (E1) 0.009 (M1)
3739	66	1	(⁻)	(1.0) ^f	24 \pm 3	4.1×10^{-4}
4159	64	1	(⁻)	(0.54) ^a	32 \pm 9	4.0×10^{-4}
4295	66	1 ^b	(⁺) ^b	0.60 ^e	67 \pm 20	0.046
4339	(68)	(1)		(1.0) ^f	38 \pm 10	4.2×10^{-4} (E1) 0.025 (M1)
4426	66	1	(⁻)	(1.0) ^f	65 \pm 10	6.8×10^{-4}
4455	64	1 ^b	⁺ ^b	(1.0) ^{f,g}	51 \pm 9	0.031
4462	66	1 ^d	(⁺) ^{d,h}	0.29 ^e	28 \pm 21	0.017
4466	(68)	1		(1.0) ^f	65 \pm 19	6.5×10^{-4} (E1) 0.040 (M1)
4503	(68)	(1)		(1.0) ^f	38 \pm 13	3.6×10^{-4} (E1) 0.023 (M1)
4609	(66)	(1)		(1.0) ^f	54 \pm 15	5.0×10^{-4} (E1) 0.030 (M1)
4664	(64)	(1)		(1.0) ^f	11 \pm 4	1.0×10^{-4} (E1) 0.006 (M1)
4685	(66)	(1)		(1.0) ^f	64 \pm 16	5.6×10^{-4} (E1) 0.034 (M1)
4806	(66)	1 ^e	⁺ ^e	0.81 ^e	100 \pm 25	0.049

^a) Based on ref. ⁹), see text.^b) Ref. ¹).^c) Ref. ¹²).^d) Ref. ²).^e) Ref. ¹⁰).^f) Assumed in the absence of evidence for branching.^g) Assuming that the branch to the 2_1^+ state, seen in the bremsstrahlung experiment, is the only branch to an excited state.^h) Refs. ^{11,12}) contradict each other with respect to this branching.ⁱ) Ref. ¹⁰) favors a (⁻) assignment. See text.

(over)

- 1) H. Verheul, Nucl. Data B2-3 (1967) 65
- 2) M. J. Martin and M. N. Rao, Nucl. Data B2-6 (1968) 43
- 3) F. R. Metzger, Annual progress report for 1967, AEC contract AT(30-1)-3525, Nucl. Sci. Abstr. 22-7661, 1968
- 4) F. R. Metzger, Annual progress report for 1968, AEC contract AT(30-1)-3525, Nucl. Sci. Abstr. 23-15431, 1969
- 5) F. R. Metzger, Phys. Rev. Lett. 18 (1967) 434; Phys. Rev. 171 (1968) 1257;
M. Berman and G. B. Beard, Phys. Rev. C2 (1970) 1506;
M. Schumacher, J. Weiss and H. Langhoff, Phys. Lett. 31B (1969) 61;
H. Langhoff, Phys. Rev. A3 (1971) 1
- 6) F. R. Metzger, Phys. Rev. 187 (1969) 1680, 1700; Nucl. Phys. A182 (1972) 213
- 7) F. R. Metzger, Nucl. Phys. A158 (1970) 88
- 8) R. P. Singh and M. L. Rustgi, Phys. Rev. C3 (1971) 1172
- 9) H. Ottmar, N. M. Ahmed, U. Fanger, D. Heck, W. Michaelis and H. Schmidt, Nucl. Phys. A164 (1971) 69
- 10) D. C. Camp and G. L. Meredith, Nucl. Phys. A166 (1971) 349
- 11) J. Konijn, R. van Lieshout, J. P. Deutsch and L. Grenacs, Nucl. Phys. A91 (1967) 439
- 12) L. G. Mann, K. G. Tirsell and S. D. Bloom, Nucl. Phys. A97 (1967) 425

REF. A.S. Litvinenko, N.G. Shevchenko, N.G. Afanas'ev, V.D. Afanas'ev,
A.Yu. Buki, V.P. Likhachev, V.N. Polishchuk, G.A. Savitskii,
V.M. Khvastunov, A.A. Khomich, and I.I. Chkalov
Yad. Fiz. 18, 250 (1973)
Sov. J. Nucl. Phys. 18, 128 (1974)

ELEM. SYM.	A	Z
Zn	68	30

REF. NO.	
73 Li 5	hmg

REACTION	RESULT	EXCITATION ENERGY	SOURCE		DETECTOR		ANGLE
			TYPE	RANGE	TYPE	RANGE	
E, E/	FMF	1,3	D	225	MAG-D		DST
		(1.08, 2.8)					

LEVELS: 1.08, 2.8 MEV

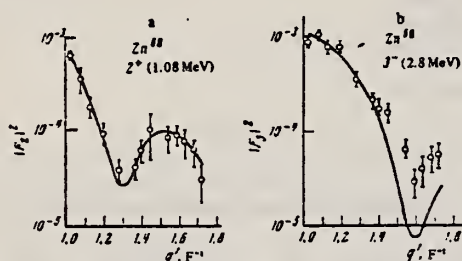


FIG. 4. Form factors of E2 transitions (a) and E3 transitions (b) in Zn^{68} . The solid curves are theoretical form-factor values fitted to the experimental points.

TABLE III. Reduced probabilities of radiative transitions $B(E\lambda)$ † for the nuclei $Zn^{66,68}$

Nucleus	J^π	$B(E\lambda) \dagger, e^2 F^2$	
		Our data	Data of Alkhazov et al. [16]
Zn^{66}	2^+	1077 ± 140	1100
	3^-	23500 ± 1700	
Zn^{68}	2^+	1800 ± 150	1450
	3^-	33900 ± 2400	

Note. For Zn^{66} our data from ref. 2 are given.

REF. B. S. Ishkhanov, I. M. Kapitonov, E. V. Lazutin,
I. M. Piskarev, O. P. Shevchenko
Yad. Fiz. 20, 433 (1974)
Sov. J. Nucl. Phys. 20, 233 (1975)

ELEM. SYM.	A	Z
Zn	68	30

METHOD

REF. NO.	
74 Is 3	hmg

REACTION	RESULT	EXCITATION ENERGY	SOURCE		DETECTOR		ANGLE
			TYPE	RANGE	TYPE	RANGE	
G, XN	ABX	10- 27	C	10- 27	BF3-I		4PI

SEP ISOTOPES

Total photoneutron cross sections have been obtained for ^{64}Zn and ^{66}Zn . The measurements were carried out from threshold to 27 MeV in 50-keV steps. A distinct structure is observed in the cross sections. The half-width of the curves is about 10 MeV. The integrated cross sections for ^{64}Zn and ^{66}Zn without taking into account multiple processes are 800 ± 80 and 1630 ± 160 MeV mb. The experimental data are compared with the predictions of the dynamic collective model and with the concept of isospin splitting of the giant resonance.

Target	Percentage content of various isotopes					Weight of target, g	Thresholds of photoneutron reactions (MeV) for the principal isotope of the target (^{64}Zn)		
	^{64}Zn	^{66}Zn	^{67}Zn	^{68}Zn	^{70}Zn		(γ, n)	($\gamma, 2n$)	(γ, np)
^{64}Zn	91.6	4.8	1.2	1.8	0.6	78	11.855	21.020	18.548
^{66}ZnO	3.3	7.9	1.6	86.8	0.4	67	10.203	17.255	19.099

¹⁴J.H.E. Mattauch et al.,
Nucl. Phys. 67, 54 (1965)

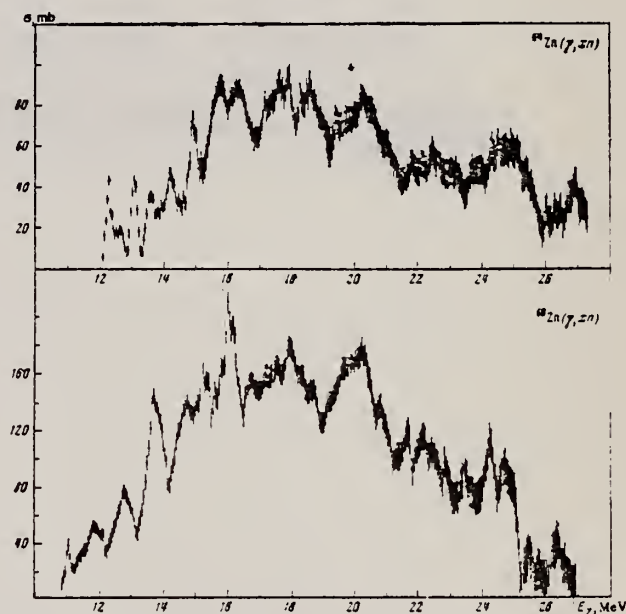


FIG. 1. Total photoneutron cross sections $\sigma(\gamma, xn)$ for ^{64}Zn (upper figure) and ^{66}Zn (lower figure).

REF.

A.M. Goryachev, G.N. Zalesnyi, and B.A. Tulupov
 Izv. Akad. Nauk SSSR. Ser. Fiz. 39, 134 (1975)
 Bull. Acad. Sci. USSR Phys. Ser. 39, 116 (1975)

ELEM. SYM.	A	Z
Zn	68	30

METHOD

REF. NO.

75 Go 1

hmg

REACTION	RESULT	EXCITATION ENERGY	SOURCE		DETECTOR		ANGLE
			TYPE	RANGE	TYPE	RANGE	
G, XN	ABX	10- 25	C	9- 25	BF3-I		4PI

$\sigma(G, SN)$. Statistical theory used to obtain SN cross section from XN cross section.

Table 2

Nuclide	β_0	E_2 , MeV	E_1 , MeV	Nuclide	β_0	E_2 , MeV	E_1 , MeV
^{64}Zn	0.25	0.99	18	^{76}Ge	0.25	0.562	18
^{66}Zn	0.23	1.04	18	^{78}Ge	0.33	0.559	18
^{68}Zn	0.2	1.03	18	^{80}Ge	0.3	0.616	18
^{70}Ge	0.23	1.04	18	^{82}Ge	0.25	0.654	18
^{72}Ge	0.25	0.835	18				
^{74}Ge	0.3	0.6	18				

Table 3

Nuclide	σ , mb	Nuclide	σ , mb	Nuclide	σ , mb
^{64}Zn	397 ± 19	^{76}Ge	760 ± 37	^{78}Ge	1021 ± 72
^{66}Zn	579 ± 27	^{78}Ge	872 ± 41	^{80}Ge	1029 ± 70
^{68}Zn	718 ± 35	^{80}Ge	911 ± 43	^{82}Ge	1067 ± 53
^{70}Ge	743 ± 37	^{82}Ge	930 ± 50		

*Mean - square errors

Values given are for σ_0 (24.2 MeV).

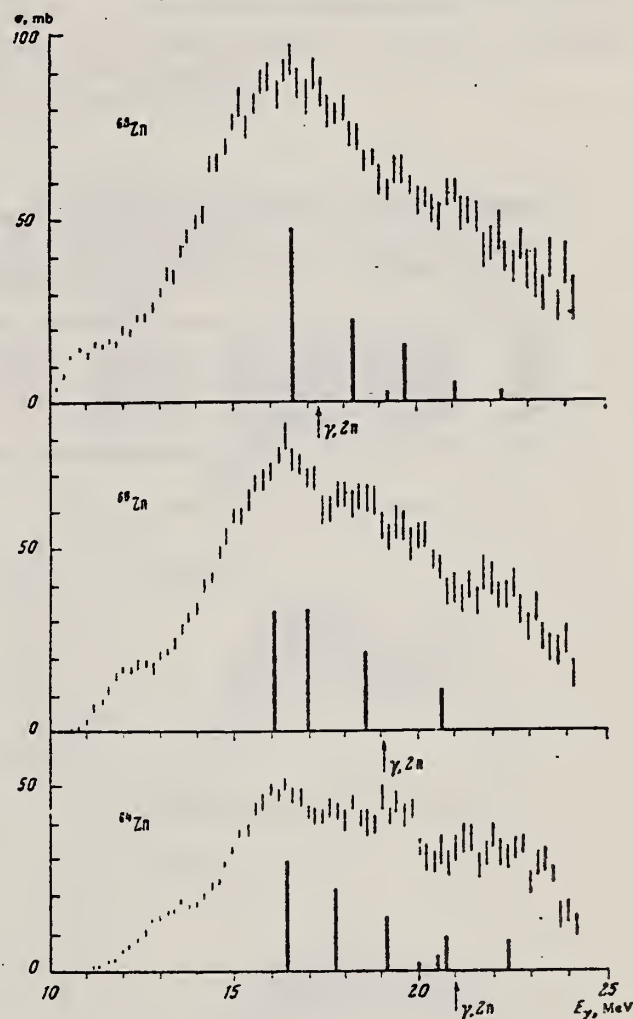


Fig. 1. Cross sections of photoneutron reactions on $^{64}, ^{66}, ^{68}\text{Zn}$. The dipole photoabsorption forces are taken from [6,7] (the solid black columns).

⁶M.G. Huber et al., Phys. Rev. 155, 1073 (1967).

⁷M.G. Huber et al., Z. Phys. 192, 223 (1966).

REF. R. Neuhausen, J. W. Lightbody, Jr., S. P. Fivozinsky,
and S. Penner
Nucl. Phys. A263, 249 (1976)

ELEM. SYM.	A	Z
Zn	68	30

METHOD	REF. NO.	
	76 Ne 1	egf

REACTION	RESULT	EXCITATION ENERGY	SOURCE		DETECTOR		ANGLE
			TYPE	RANGE	TYPE	RANGE	
E, E/	ABX	1- 3	D	40-112	MAG-D		DST

States: 1.077(2+), 2.75(3-) MeV.

2+, 3- STATES

TABLE 6

Reduced transition probabilities in single particle units, deformation parameters and deformation lengths ($R = 1.2 \text{ fm} \times A^{1/3}$)

	$B_{\uparrow}(E2)/B_{\uparrow}^{s.p.}(E2)$	β_2	$\beta_2 R$ (fm)	$B_{\uparrow}(E3)/B_{\uparrow}^{s.p.}(E3)$	β_3	$\beta_3 R$ (fm)
⁶⁴ Zn	20.4 ± 1.2	0.230 ± 0.007	1.10 ± 0.03	23.5 ± 4.0	0.224 ± 0.019	1.08 ± 0.09
⁶⁶ Zn	17.3 ± 1.3	0.212 ± 0.008	1.03 ± 0.04	23.4 ± 4.9	0.224 ± 0.023	1.09 ± 0.11
⁶⁸ Zn	13.5 ± 1.0	0.187 ± 0.007	0.92 ± 0.04	19.8 ± 4.3	0.206 ± 0.022	1.01 ± 0.11
⁷⁰ Zn	24.0 ± 2.2	0.249 ± 0.011	1.23 ± 0.06			

REACTION	RESULT	EXCITATION ENERGY	SOURCE		DETECTOR		ANGLE
			TYPE	RANGE	TYPE	RANGE	
G,P	ABX	10-800	C	75-800	ACT-I		4PI

The yields of (γ, p) reactions on ^{30}Si , ^{68}Zn and ^{130}Te have been measured as a function of the bremsstrahlung end-point energy, $E_{\gamma, \text{max}}$, in the energy range 75–800 MeV, using the activation method. Cross sections have been deduced and are compared to results obtained using a semi-empirical model.

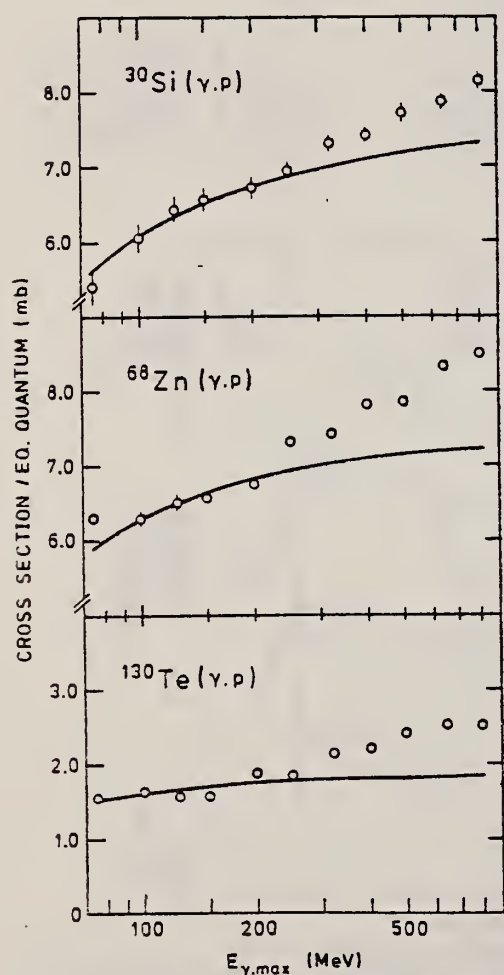


Fig. 1. Measured yields for the (γ, p) reactions in ^{30}Si , ^{68}Zn and ^{130}Te . The solid lines are the fitted yields due to the giant resonance and quasideuteron cross sections

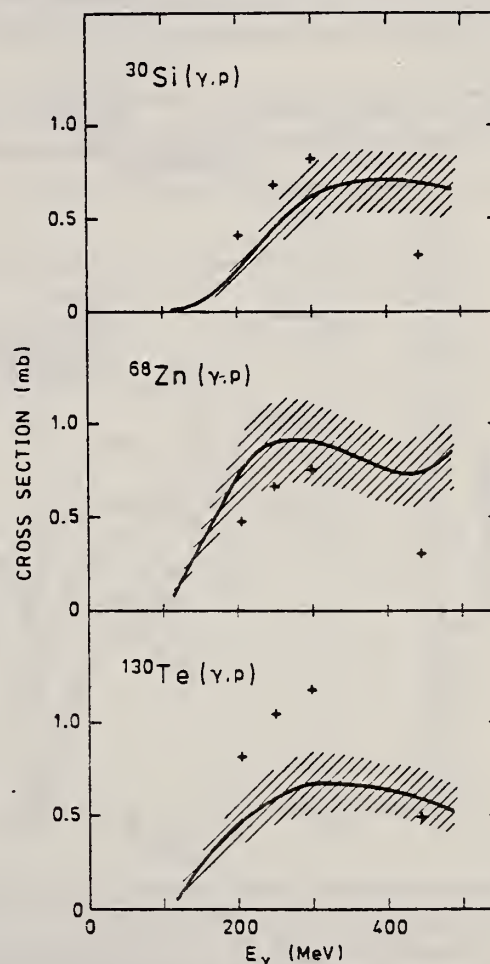


Fig. 2. The solid curves show the smoothed cross sections arising from photoproduction of mesons and the hatched areas indicate the estimated errors. + signs are values calculated using the semi-empirical formalism

ELEM. SYM.	A	Z
Zn	68	30
REF. NO.	77 Ne 3	
	hg	

REACTION	RESULT	EXCITATION ENERGY	SOURCE		DETECTOR		ANGLE
			TYPE	RANGE	TYPE	RANGE	
E, E/	FMF	1-3	D	100-275	MAG-D		DST

Abstract: The inelastic electron scattering cross sections for the quadrupole transitions to the 2_1^+ and 2_2^+ states in the even Zn isotopes ^{64}Zn , ^{66}Zn and ^{68}Zn and for the hexadecapole transition to the 4_1^+ state in ^{64}Zn have been measured in a momentum transfer range up to $q = 2.2 \text{ fm}^{-1}$. In the framework of the vibrational model these states are considered as one- and two-quadrupole-phonon states. The measurements are characterized by high statistical accuracy and by an overall resolution of $\delta E/E_0 = 10^{-3}$ which permitted separation of almost all members of the two-phonon triplet. The measured cross sections are analyzed with phenomenological models as well as with a Fourier-Bessel expansion of the transition charge density. The latter analysis yields realistic error bands for the transition charge densities and model-independent values for the reduced transition probabilities and transition radii.

LEVELS 1.077, 1.883

NUCLEAR REACTIONS $^{64,66,68}\text{Zn}(e, e')$, $E = 100\text{--}275 \text{ MeV}$; measured $d\sigma/d\Omega(E, \theta)$. $^{64,66,68}\text{Zn}$ levels deduced transition charge density, $B_1(E\lambda)$ and transition charge radii R_{tr} . Enriched targets.

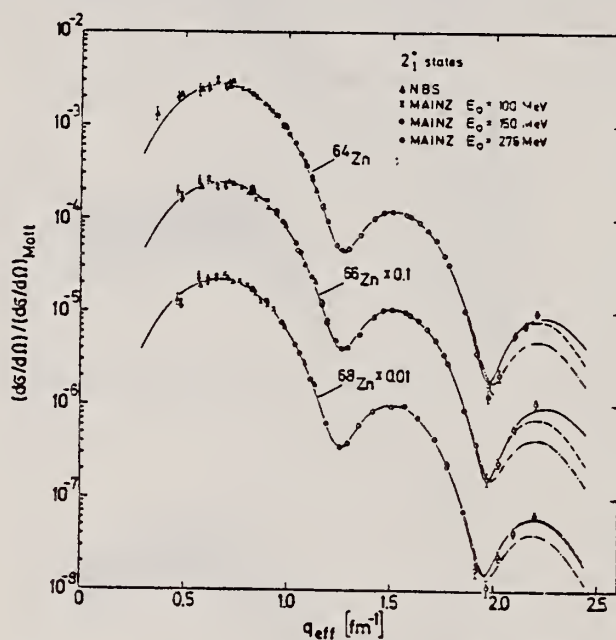


Fig. 3. Cross sections divided by the Mott cross section for the allowed transitions to the 2_1^+ state in ^{64}Zn , ^{66}Zn and ^{68}Zn versus the effective momentum transfer. The measured cross sections are transformed to a common incident energy $E_0 = 275 \text{ MeV}$. The curves represent best fit DWBA calculations with the Fourier-Bessel expansion of the transition charge density (solid line), the modified Tassie model (dashed line) and the Gaussian model (dashed-dotted line).

Table 3

	Fitted parameters of the Gaussian model for the first 2_1^+ states in ^{64}Zn , ^{66}Zn and ^{68}Zn	
	^{64}Zn $E = 0.992 \text{ MeV}$	^{66}Zn $E = 1.039 \text{ MeV}$
$a \text{ (fm)}$	4.148 ± 0.004	4.192 ± 0.005
$b \text{ (fm)}$	1.470 ± 0.005	1.469 ± 0.006
$B_1(E2) \text{ (fm}^4\text{)}$	1470 ± 15	1200 ± 15
χ^2/ν	3.95	5.43

TABLE 5

Reduced transition probabilities $B_1(E2)$ and transition radii R_{1r} for the 2_1^+ states in ^{64}Zn , ^{66}Zn and ^{68}Zn

	^{64}Zn $\epsilon = 0.992 \text{ MeV}$	^{66}Zn $\epsilon = 1.039 \text{ MeV}$	^{68}Zn $\epsilon = 1.077 \text{ MeV}$
$B_1(E2) (\text{fm}^4)$			
(e. e.) ^{a)}	1620 ± 90	1410 ± 80	1320 ± 70
CE ^{b)}	1700 ± 150	1450 ± 130	1250 ± 110
$R_{1r} (\text{fm})$	5.44 ± 0.09	5.39 ± 0.09	5.47 ± 0.09
R_{1r}/R_m	1.38 ± 0.03	1.37 ± 0.03	1.38 ± 0.03

^{a)} Model independent analysis, this work.^{b)} Ref. ¹⁶⁾.

TABLE 8

Reduced transition probabilities $B_1(E\lambda)$ and transition radii R_{1r} for the forbidden transition to the 2_1^+ states in ^{64}Zn , ^{66}Zn and ^{68}Zn and to the 4_1^+ state in ^{64}Zn

	^{64}Zn $\epsilon = 1.800 \text{ MeV}$ $\lambda = 2$	^{66}Zn $\epsilon = 1.873 \text{ MeV}$ $\lambda = 2$	^{68}Zn $\epsilon = 1.883 \text{ MeV}$ $\lambda = 2$	^{64}Zn $\epsilon = 2.305 \text{ MeV}$ $\lambda = 4$
$B_1(E\lambda) (\text{fm}^{2\lambda})$	17.0 ± 1.2	4.5 ± 0.7	46 ± 7	$(3.4 \pm 1.0) \times 10^4$
$R_{1r} (\text{fm})$	4.6 ± 0.1	4.5 ± 0.1	5.9 ± 0.1	6.7 ± 0.3
R_{1r}/R_m	1.17 ± 0.03	1.14 ± 0.03	1.49 ± 0.03	1.70 ± 0.08
$R_{1r}^2(2_1^+)/R_{1r}^2(2_1^+)$	0.71 ± 0.03	0.69 ± 0.04	1.17 ± 0.06	

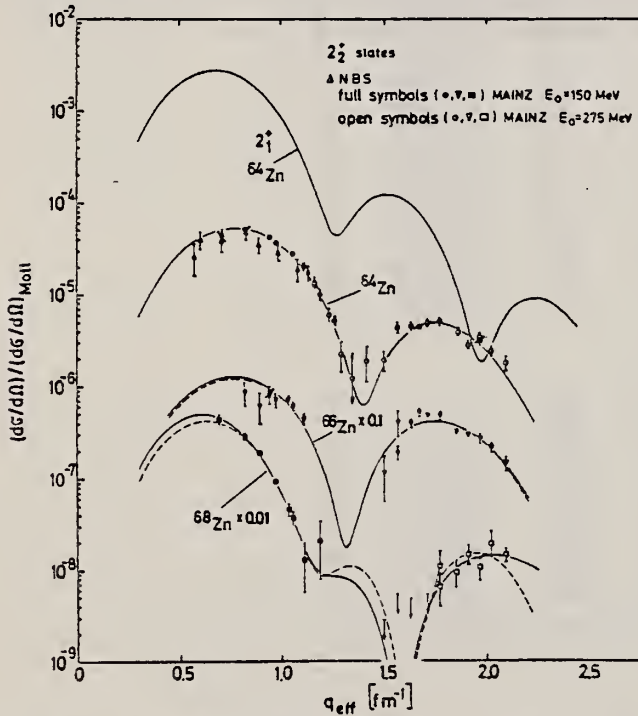


Fig. 8. Same as fig. 3, but for the forbidden transitions to the 2_1^+ states in ^{64}Zn , ^{66}Zn and ^{68}Zn , respectively. The curves represent best-fit DWBA calculations with the Fourier-Bessel expansion of the transition charge density (solid line) and the phenomenological model given in eq. (22) (dashed line). For comparison, the shape of the cross section for the allowed transition to the 2_1^+ state in ^{64}Zn is shown (uppermost curve).

ELEM. SYM.	A	Z
Zn	68	30
REF. NO.		
77 Ne 3		hg

METHOD					REF. NO.		
					77 Ne 3		hg
REACTION	RESULT	EXCITATION ENERGY	SOURCE		DETECTOR		ANGLE
			TYPE	RANGE	TYPE	RANGE	

TABLE I

Compilation of the measured inelastic cross sections. The cross sections are multiplied by 10^4 , where the power x is given in cols. 4 and 8, respectively

E_0 (MeV)	θ (deg)	$10^4(d\sigma/d\Omega)$ (cm ² /sr)	x	E_0 (MeV)	θ (deg)	$10^4(d\sigma/d\Omega)$ (cm ² /sr)	x
⁶⁸ Zn; $\epsilon = 1.077$ MeV 2_1^-							
100.1	60.0	1.28 ± 0.15	29	150.1	85.0	1.03 ± 0.03	31
100.1	65.0	8.52 ± 1.00	30	150.1	92.5	2.03 ± 0.06	32
100.1	70.0	6.69 ± 0.56	30	150.1	100.0	7.88 ± 0.34	33
100.1	75.0	5.49 ± 0.37	30	275.1	52.5	5.00 ± 0.17	32
100.1	80.0	3.36 ± 0.20	30	274.7	52.5	5.12 ± 0.17	32
100.1	85.0	2.68 ± 0.14	30	275.3	55.0	6.55 ± 0.29	32
100.1	90.0	1.86 ± 0.09	30	274.7	55.0	6.24 ± 0.18	32
100.1	95.0	1.18 ± 0.06	30	274.7	58.0	7.22 ± 0.19	32
100.0	100.0	7.79 ± 0.29	31	274.7	62.0	6.16 ± 0.16	32
100.0	105.0	5.51 ± 0.18	31	275.4	65.0	5.06 ± 0.14	32
100.0	110.0	3.85 ± 0.12	31	274.7	68.0	3.22 ± 0.09	32
150.1	50.0	1.26 ± 0.04	29	275.1	72.0	1.47 ± 0.04	32
150.0	60.0	4.14 ± 0.11	30	275.4	75.0	6.44 ± 0.23	33
150.1	60.0	4.49 ± 0.14	30	274.7	75.0	6.24 ± 0.18	33
150.1	66.0	2.23 ± 0.06	30	275.1	79.0	1.59 ± 0.07	33
150.0	72.5	8.71 ± 0.23	31	274.8	82.0	3.34 ± 0.49	34
150.2	72.5	8.79 ± 0.22	31	275.0	85.0	1.74 ± 0.35	34
150.1	78.0	3.64 ± 0.09	31	275.1	88.0	3.21 ± 0.40	34
149.8	80.0	2.68 ± 0.16	31	275.0	92.0	4.75 ± 0.40	34
150.0	85.0	1.01 ± 0.06	31	275.0	98.0	5.24 ± 0.40	34
⁶⁸ Zn; $\epsilon = 1.883$ MeV 2_2^-							
150.1	50.0	2.41 ± 0.25	31	275.4	65.0	< 2.8	34
150.1	60.0	7.42 ± 0.61	32	274.7	68.0	< 2.1	34
150.1	66.0	3.18 ± 0.20	32	275.1	72.0	< 1.8	34
150.0	72.5	1.02 ± 0.12	32	275.4	75.0	3.1 ± 1.3	34
150.2	72.5	1.01 ± 0.09	32	274.7	75.0	1.9 ± 0.8	34
150.1	78.0	3.45 ± 0.52	33	275.1	79.0	2.1 ± 0.7	34
149.8	80.0	2.45 ± 0.40	33	274.8	82.0	2.8 ± 0.7	34
150.1	85.0	5.9 ± 3.4	34	275.0	85.0	1.7 ± 0.5	34
150.1	92.5	6.2 ± 3.8	34	275.1	88.0	2.6 ± 0.8	34
274.7	62.0	< 1.8	34	275.0	92.0	1.6 ± 0.3	34

REF. Y. Cauchois, H. Ben Abdelaziz, R. Khérouf, C. Schloesing-Möller
J. Phys. G7, 1539 (1981)

ELEM. SYM.	A	Z
Zn	68	30
REF. NO.		
81 Ca 2		hg

METHOD

REACTION	RESULT	EXCITATION ENERGY	SOURCE		DETECTOR		ANGLE
			TYPE	RANGE	TYPE	RANGE	
G.G	LET	1	C	0 - 2	SCD-D		
		(1.077)					

1.077 MeV

Abstract. Lifetimes of 49 excited states below 1.65 MeV have been measured in ²⁴Mg, ²⁷Al, ⁴⁸Ti, ⁵⁸Ni, ⁵⁹Co, ^{61,62}Ni, ^{63,65}Cu, ^{64,66,68}Zn, ⁷⁵As, ¹⁰³Rh, ^{113,115}In, ^{116,118,120}Sn and ^{121,123}Sb by means of nuclear resonance fluorescence experiments. The levels are excited by bremsstrahlung x-ray photons. The self-absorption technique applied to suitable cases provides nuclear absorption cross sections, widths and lifetimes from which the x-ray spectral distributions are also obtained. Scattering experiments are performed for all other cases in order to obtain widths and lifetimes from these x-ray photon curves. The Compton effect in the sample is taken into account. Self-absorption provides $g\Gamma_0$ from which Γ is deduced using adopted J^π and Γ_0/Γ values; scattering provides $u = g(\Gamma_0^2/\Gamma)W(\theta)$ from which Γ is also deduced with J , Γ_0/Γ and mixing ratios taken from the literature. Thanks to simultaneous determination of the x-ray spectra all the lifetimes as given by our programs with their statistical errors form an unusually coherent set of values.

NUCLEAR REACTIONS (γ , γ), bremsstrahlung excitation; natural isotopes: ²⁴Mg, ²⁷Al, ⁴⁸Ti, ⁵⁸Ni, ⁵⁹Co, ^{61,62}Ni, ^{63,65}Cu, ^{64,66,68}Zn, ⁷⁵As, ¹⁰³Rh, ^{113,115}In, ^{116,118,120}Sn and ^{121,123}Sb; $E \approx 0.5-1.65$ MeV; measured $g\Gamma_0$ or $g(\Gamma_0^2/\Gamma)W(\theta)$; deduced $T_{1/2}$.

(OVER)

Tableau 3. Résultats des mesures des niveaux étudiés par diffusion.

Table 3. Results obtained using the diffusion method.

Isotope	Energie (keV)	J^π	J_0^π	Γ_0/Γ	δ	$u = g(\Gamma_0^2/\Gamma)W(\theta)$ (meV)	τ (ps) ce travail	τ_{ref} (ps)	Références †
²⁴ Mg	1368,59(4)	2 ⁺	0 ⁺	1	E2	1,08(13)	1,76(21)	1,98(4)	Endt et van der Leun (1978)
²⁷ Al	1014,45(3)	$\frac{1}{2}^+$	$\frac{1}{2}^+$	0,971	+ 0,351(12)	0,186(13)	2,20(16)	2,12(8)	Endt et van der Leun (1978)
⁴⁸ Ti	983,512(3)	2 ⁺	0 ⁺	1	E2	0,282(23)	6,74(55)	6,1(13)	Been (1978)
⁵⁸ Ni	1454,45(15)	2 ⁺	0 ⁺	1	E2	2,11(26)	0,90(11)	0,92(3)	Kocher et Auble (1976)
⁵⁹ Co	1099,224(25)	$\frac{3}{2}^-$	$\frac{3}{2}^-$	1	(E2)	0,069(8)	4,79(55)	3,17(58)	Kim (1976)
⁵⁹ Co	1458,8(3)	$\frac{3}{2}^-$	$\frac{3}{2}^-$	0,91	(E2)	0,68(8)	1,17(14)	1,52(16)	Kim (1976)
⁵⁹ Co	1480,9(3)	$\frac{3}{2}^-$	$\frac{3}{2}^-$	0,8	< 0,35 ^a	1,23(15)	0,254(31)	0,31(3)	Kim (1976)
⁶¹ Ni	1185,7(6)	$\frac{3}{2}^-$	$\frac{3}{2}^-$	0,77(8) ^a	[0,14]	1,88(49)	0,21(5)	0,16(3)	Andreev <i>et al</i> (1974)
⁶² Ni	1172,91(9)	2 ⁺	0 ⁺	1	E2	0,88(17)	2,15(42)	2,09(3)	Halbert (1979a)
⁶³ Cu	1327,00(7)	$\frac{3}{2}^-$	$\frac{3}{2}^-$	0,84	(E2)	1,04(14)	0,84(11)	0,88(4)	Auble (1979b)
⁶³ Cu	1412,05(4)	$\frac{3}{2}^-$	$\frac{3}{2}^-$	0,72	+ 0,61 $\left\{\begin{smallmatrix} -2 \\ -8 \end{smallmatrix}\right\}$	0,260(38)	1,90(28)	1,61(3)	Auble (1979b)
⁶⁴ Zn	991,54(7)	2 ⁺	0 ⁺	1	E2	0,640(54)	2,97(25)	2,60(13)	Halbert (1979b)
⁶⁵ Cu	1481,83(5)	$\frac{3}{2}^-$	$\frac{3}{2}^-$	0,85	(E2)	1,13(19)	0,79(13)	0,49(5)	Auble (1975a)
⁶⁶ Zn	1039,37(6)	2 ⁺	0 ⁺	1	E2	0,70(6)	2,71(23)	2,25(15)	Auble (1975b)
⁶⁸ Zn	1077,38(5)	2 ⁺	0 ⁺	1	E2	0,70(6)	2,71(23)	2,34(23)	Lewis (1975)
⁷⁵ As	572,5(10)	$\frac{1}{2}^-$	$\frac{1}{2}^-$	1 ^d	0,39 ^b	0,236(26)	4,14(46)	3,5(9)	Horn et Lewis (1975)
⁷⁵ As	823,0(10)	$\frac{1}{2}^-$	$\frac{1}{2}^-$	0,86 ^d	(E2)	0,214(22)	4,27(43)	3,5(3)	Robinson <i>et al</i> (1967)
⁷⁵ As	865,5(10)	$\frac{1}{2}^-$	$\frac{1}{2}^-$	0,83 ^d	— ^c	0,78(6)	0,863(68)	0,60(12)	Celliers <i>et al</i> (1977)
⁷⁵ As	1076,0(10)	$\frac{1}{2}^-$	$\frac{1}{2}^-$	0,94 ^d	0,38 ^d	1,97(13)	0,287(19)	0,32(7)	Celliers <i>et al</i> (1977)
⁷⁵ As	1128,5(10)	$\frac{3}{2}^+$	$\frac{3}{2}^+$	1	E1 ^d	0,224(24)	1,47(16)	—	—
⁷⁵ As	1349,0(10)	$\frac{3}{2}^-$	$\frac{3}{2}^-$	0,67 ^d	0,20 ^d	1,61(29)	0,180(32)	0,12(3)	Wilson (1970)
⁷⁵ As	1370,0(10)	$\frac{3}{2}^-$	$\frac{3}{2}^-$	0,47 ^d	0,47 ^d	0,64(13)	0,218(44)	—	—
¹⁰³ Rh	803,1(2)	$\frac{1}{2}^-$	$\frac{1}{2}^-$	0,70	M1	1,85(16)	0,174(15)	—	Harmatz (1979)
¹⁰³ Rh	1277,0(2)	$\frac{1}{2}^-$	$\frac{1}{2}^-$	0,75	-0,62(30) ^e	0,31(9)	0,87(10)	1,3(9)	Harmatz (1979)
¹¹³ In	1177(1)	$\frac{1}{2}^+$	$\frac{1}{2}^+$	1	+ 0,5(2)	9,1(8)	0,086(8)	0,10(6)	Tuttle <i>et al</i> (1976)
¹¹³ In	1510(1)	$\frac{1}{2}^+$	$\frac{1}{2}^+$	0,935	-0,5 $\left\{\begin{smallmatrix} -2 \\ -1 \end{smallmatrix}\right\}$	6,4(9)	0,071(10)	0,11 $\left\{\begin{smallmatrix} -4 \\ -2 \end{smallmatrix}\right\}$	Tuttle <i>et al</i> (1976)
¹¹⁵ In	1077,7(10)	$\frac{1}{2}^+$	$\frac{1}{2}^+$	0,81 ^j	(E2)	0,159(24)	1,61(24)	1,23(7)	Tuttle <i>et al</i> (1976)
¹¹⁵ In	1290,59(3)	$\frac{1}{2}^+$	$\frac{1}{2}^+$	0,98 ^j	(E2)	1,31(11)	0,66(6)	0,55(4)	Tuttle <i>et al</i> (1976)
¹¹⁵ In	1448,78(3)	$\frac{1}{2}^+$	$\frac{1}{2}^+$	0,86	-8 ⁱ	0,90(11)	0,50(6)	0,52(20)	Tuttle <i>et al</i> (1976)
¹¹⁵ In	1486,1(1)	$\frac{1}{2}^+$	$\frac{1}{2}^+$	0,787	-0,8 ^f	0,63(9)	0,63(9)	0,4(3)	Tuttle <i>et al</i> (1976)
¹¹⁵ In	1497,2(4)	$\frac{1}{2}^+$	$\frac{1}{2}^+$	< 1	(E2)	1,33(16)	< 0,30(4)	—	—
¹¹⁵ In	1607,7(15)	$\frac{1}{2}^+$	$\frac{1}{2}^+$	< 1	(E2)	1,54(24)	< 0,26(4)	—	—
¹¹⁶ Sn	1293,54(2)	2 ⁺	0 ⁺	1	E2	3,58(37)	0,53(6)	0,522(14)	Carlson <i>et al</i> (1975)
¹¹⁸ Sn	1229,64(4)	2 ⁺	0 ⁺	1	E2	2,75(28)	0,69(7)	0,67(2)	Carlson <i>et al</i> (1976)
¹²⁰ Sn	1171,6(2)	2 ⁺	0 ⁺	1	E2	1,83(16)	1,04(9)	0,91(2)	Kocher (1976)
¹²¹ Sb	1023,5(10)	$\frac{1}{2}^-$	$\frac{1}{2}^-$	1	[0,57] ^g	3,69(34)	0,228(21)	0,20(7) ^h	Tamura <i>et al</i> (1979)
¹²¹ Sb	1105,5(10)	$\frac{1}{2}^-$	$\frac{1}{2}^-$	0,4	—	0,47(4)	0,42(4)	—	—
¹²¹ Sb	1142,5(10)	$\frac{1}{2}^-$	$\frac{1}{2}^-$	0,6	(E2)	0,85(8)	0,449(40)	0,41(8) ^h	Booth <i>et al</i> (1973)
¹²¹ Sb	1384,0(10)	$\frac{1}{2}^-$	$\frac{1}{2}^-$	1	[0,45] ^g	4,7(5)	0,092(10)	0,088(14) ^h	Booth <i>et al</i> (1973)
¹²³ Sb	1029,5(10)	$\frac{1}{2}^-$	$\frac{1}{2}^-$	1	[0,57] ^g	2,96(27)	0,272(25)	0,26(4) ^h	Booth <i>et al</i> (1973)
¹²³ Sb	1086,5(10)	$\frac{1}{2}^-$	$\frac{1}{2}^-$	1	[δ] > 1,26 ^g	1,06(9)	0,67(6)	0,72(15) ^h	Booth <i>et al</i> (1973)

† Références pour les colonnes 3, 4, 5, 6 et 9 de chaque ligne, sauf indication appelée au bas de ce tableau. Pour les autres données se reporter au texte.

Remarque. Pour calculer δ^2 quand nous ne disposons que de $B(E2)$, pour un mélange $(E2) + (M1)$, nous déduisons $g\Gamma_0(E2) \propto B(E2)E_1^4$; en admettant $W(\theta) = 1$ et connaissant Γ_0/Γ , notre détermination de u donne une première approximation de $g\Gamma_0$ d'où une valeur de $\delta^2 = (g\Gamma_0(E2))/(g\Gamma_0 - g\Gamma_0(E2))$ qui permet d'améliorer $W(\theta)$ et $g\Gamma_0$ de proche en proche.

^a Swann (1971); ^b Robinson *et al* (1967); ^c $W(\theta) = 0,99$ calculé d'après la formule de Celliers *et al* (1977); ^d Abbondanno *et al* (1978); ^e Sayer *et al* (1972); ^f Tuttle *et al* (1976); ^g d'après $B(E2)$ de Barnes *et al* (1966); ^h calculé d'après Booth *et al* (1973); ⁱ Williams *et al* (1975); ^j Dietrich *et al* (1970).

Z_N
 $A=70$

Z_N
 $A=70$

Z_N
 $A=70$

ELEM. SYM.	A	Z
Zn	70	30
REF. NO.		egf
76 Ne 1		

REACTION	RESULT	EXCITATION ENERGY	SOURCE		DETECTOR		ANGLE
			TYPE	RANGE	TYPE	RANGE	
E, E/	ABX	1- 2	D	40-112	MAG-D		DST

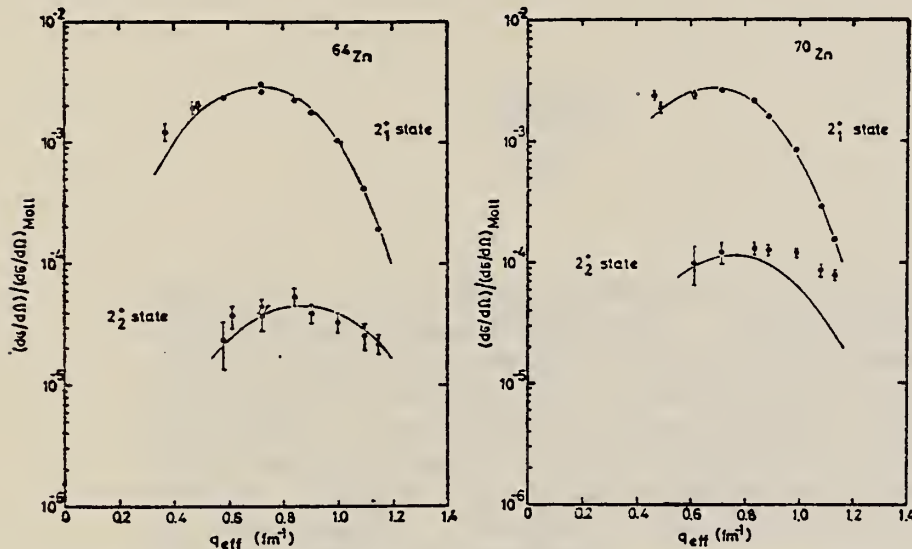
2+, 2+ STATES

Fig. 2. Cross sections divided by the Mott cross section for the excitation of the first and second 2^+ states in ^{64}Zn and ^{70}Zn , respectively, versus the effective momentum transfer. The cross sections measured at different values of the incident energy E were transformed to the common energy $E_0 = 120$ MeV. The curves are the best fit of the anharmonic vibrator model.

States: .884(2+), 1.76(2+) MeV.

TABLE 6

Reduced transition probabilities in single particle units, deformation parameters and deformation lengths ($R = 1.2 \text{ fm} \times A^{1/3}$)

	$B_{\uparrow}(E2)/B_{\uparrow}^{s.p.}(E2)$	β_2	$\beta_2 R$ (fm)	$B_{\uparrow}(E3)/B_{\uparrow}^{s.p.}(E3)$	β_3	$\beta_3 R$ (fm)
^{64}Zn	20.4 ± 1.2	0.230 ± 0.007	1.10 ± 0.03	23.5 ± 4.0	0.224 ± 0.019	1.08 ± 0.09
^{66}Zn	17.3 ± 1.3	0.212 ± 0.008	1.03 ± 0.04	23.4 ± 4.9	0.224 ± 0.023	1.09 ± 0.11
^{68}Zn	13.5 ± 1.0	0.187 ± 0.007	0.92 ± 0.04	19.8 ± 4.3	0.206 ± 0.022	1.01 ± 0.11
^{70}Zn	24.0 ± 2.2	0.249 ± 0.011	1.23 ± 0.06			

¹⁹ A.K. Sen Gupta and D.M. Van Patter, Nucl. Phys. **50** (1964) 17.

TABLE 7

The 2_1^+ and 2_2^+ state AVM fitting parameters for ^{64}Zn and ^{70}Zn

	$(\hbar/2\sqrt{BC})^{\dagger}$	c_{tr} (fm)	z_{tr} (fm)	a	$Q(2_1^+)(\text{AVM})$ (b)	BR(AVM)	BR(other) ^{a)}	$B(E2; 0_1^+ \rightarrow 2_1^+)$
^{64}Zn	0.109 ± 0.004	4.47 ± 0.08	0.53 ± 0.06	0.165 ± 0.005	-0.124 ± 0.012	456 ± 70	159 ± 12	8 ± 2
^{70}Zn	0.122 ± 0.006	4.29 ± 0.08	0.71 ± 0.05	0.25 ± 0.02	-0.233 ± 0.022	$72(\pm 1\%)$		50 ± 13

[†] Derived 2_1^+ state static quadrupole moments, 2_2^+ state branching ratios, and $B(E2; 0_1^+ \rightarrow 2_2^+)$ are given.
^{a)} Ref. ¹⁹).

GALLIUM

A=31

Gallium is a bluish-white metallic solid that becomes a liquid at near room temperature. It was discovered in 1875 by the French chemist, Lecoq de Boisbaudran, by spectroscopic examination of concentrates from a Pyrenean zinc blend. The position of the emission lines corresponded to those predicted for "eka-aluminum" a missing element between aluminum and indium in Mendelēyev's periodic scheme of the elements. He named it gallium from the Latin *gallia* in honor of his fatherland.

GA

METHOD

REF. NO.

64 Ba 4

egf

REACTION	RESULT	EXCITATION ENERGY	SOURCE		DETECTOR		ANGLE
			TYPE	RANGE	TYPE	RANGE	
G,XN	ABX	10-27	C	10-27	BF3-I		4PI

65 BA3 SAME DATA

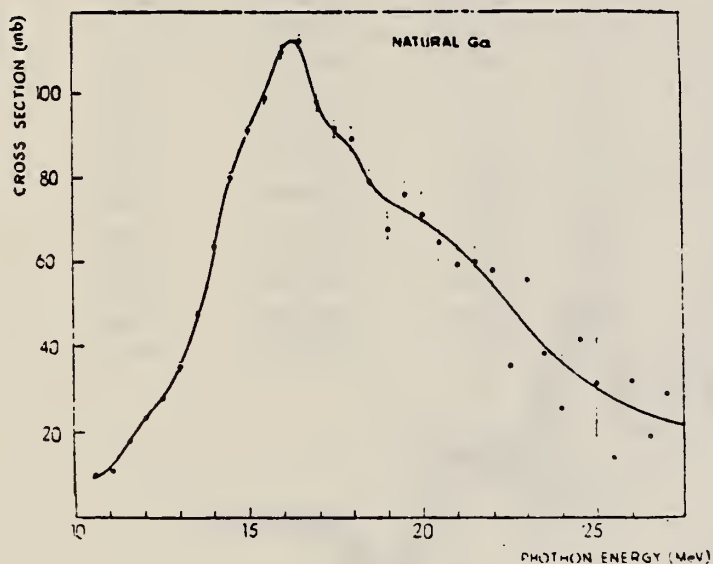


FIG. 4. — $\sigma(\gamma, Tn)$ for Ga of natural isotopic abundance.

ELEM. SIM.	A	L
Ga		31
REF. NO.	64 Ba 5	
	egf	

METHOD			SOURCE		DETECTOR		ANGLE
REACTION	RESULT	EXCITATION ENERGY	TYPE	RANGE	TYPE	RANGE	
G,XN	ABX	11-26	C	11-26	BF3-I		4PI

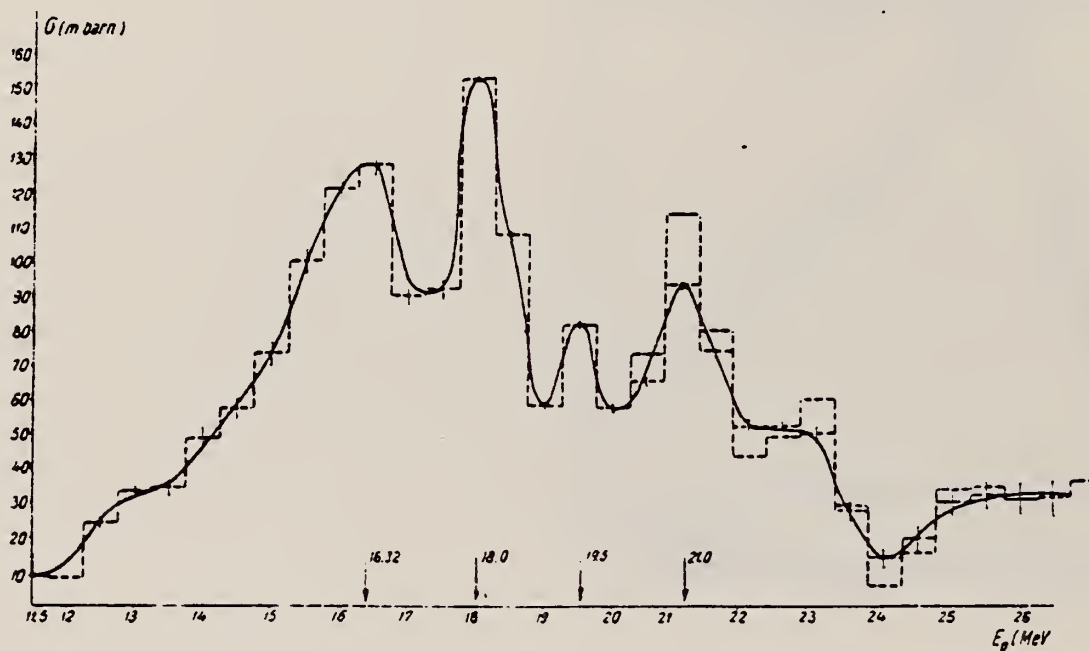


Fig. 3

1700

REF. NO.

Synchrotron; $C^{12}(\gamma, n)$ monitor

64 Co 2

JOC

REACTION	RESULT	EXCITATION ENERGY	SOURCE		DETECTOR		ANGLE
			TYPE	RANGE	TYPE	RANGE	
G, XN	ABY	THR - 80	C	80	BFD-1		4 PI

Table 1

Element	Yield (360°) eV cm ² mol MeV	60 NZ/A (mb MeV)	Σ 0	Σ 0	Σ / Σ 0 0	E_m (MeV)	σ_m (mb)
^{24}Cr	83×10^{-5}	777	1.21	2.1	0.58	18.5	97
^{25}Mn	106×10^{-5}	813	1.52	2.33	0.65	18.5	114
^{26}Fe	68×10^{-5}	802	0.83	1.46	0.60	17.5	75
^{27}Co	69×10^{-5}	878	1.08	1.32	0.59	17.5	92
^{28}Ni	44×10^{-5}	879	0.55	1.07	0.51	18.5	56
^{29}Cu	95×10^{-5}	947	1.06	1.99	0.53	17.5	98
^{30}Zn	88×10^{-5}	975	0.94	1.63	0.56	17.5	86
^{31}Ga	130×10^{-5}	1034	1.29	2.18	0.59	17.5	151
^{32}Ge	139×10^{-5}	1064	1.35	2.29	0.59	17.5	158
^{33}As	137×10^{-5}	1109	1.22	2.18	0.56	17.5	127

$$\Sigma = \int_0^{30} \sigma(\gamma, xn) dE$$

$$\frac{\Sigma}{60 \text{ NZ/A}}$$

Table 2

Element	maximum yield ($\times 10^{-5}$)	$\sigma_{-1}(\overline{\gamma n})$	$\sigma_{-1}(\overline{\gamma n}) \times \frac{3}{4\pi^2} \frac{Nc}{c^2} \left(\frac{A-1}{NZ} \right)^{1/2} A^{-1/2}$
^{6}C	4.0	3.54	2.13
^{8}O	5.2	4.95	1.92
^{11}Na	10.6	11.60	2.49
^{12}Mg	10.0	8.91	1.73
^{13}Al	15.9	13.92	2.30
^{14}Si	11.6	9.96	1.55
^{15}P	19.3	17.56	2.32
^{16}S	9.5	9.55	1.07
^{16}K	19.3	17.90	1.61
^{20}Ca	12.1	11.68	1.02
^{24}Cr	80	61.6	3.56
^{25}Mn	115	76.1	3.96
^{26}Fe	71	50.5	2.53
^{27}Co	94	63.5	2.94
^{28}Ni	46	34.2	1.59
^{29}Cu	102	72.3	2.96
^{30}Zn	93	65.7	2.68
^{31}Ga	140	93.6	3.31
^{32}Ge	150	101.5	3.36
^{33}As	151	99.8	3.12

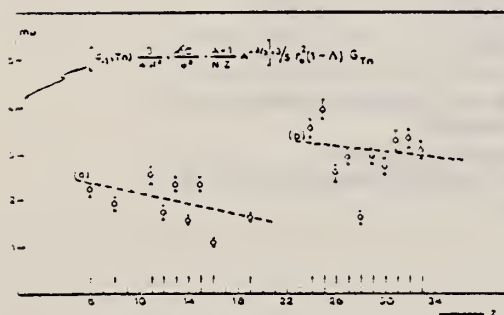


Fig. 2. Bremsstrahlung-weighted cross sections, $\sigma_{-1}(\overline{\gamma n})$, conveniently normalized, versus Z .

REF.

G. Baciú, G. C. Bonazzola, B. Minetti, C. Molino, L. Pasqualini
and G. Piragino
Nuclear Phys. 67, 178 (1965)

ELEM. SYM.

A

Z

Ga

31

METHOD

NBS Monitor

REF. NO.

65 Ba 3

EGF

[Page 1 of 2]

REACTION	RESULT	EXCITATION ENERGY	SOURCE		DETECTOR		ANGLE
			TYPE	RANGE	TYPE	RANGE	
G,XN	ABX	THR - 28	C	10-30	BF3-I		4PI

TABLE 2
Cross sections for Co, Ni, Cu and Ga

	E_m (MeV)	σ_m (mb)	$\int_0^x \sigma(E)dE$ (mb · MeV)	Ref.
Co ⁵⁸	16.9	130	750(24)	^{a)}
	16.75 19	110 103	709(25)	^{a)}
	17.5	68	725 ± 72(28)	^{a)}
	16.5 19	82 80	701 ± 91(29)	^{a)}
	16.5 19	72 74	657 ± 89(28)	this work
			537 ± 34(24)	this work
Ni			445 ± 48(24)	^{a)}
	16.5	50	340(24)	¹¹⁾
	16.5	46 ± 1	313 ± 48(28)	this work
Ni ⁵⁸			276 ± 25(24)	this work
	18.5	60	330(24)	¹²⁾
		30	180(24)	¹²⁾
	20.5	21	160(24)	¹²⁾
Ni ⁵⁸	19.0	32	220 ± 30(32)	¹⁴⁾
	16.5	85	440(± 20 %)(24)	^{b)}
Cu	19.5	120	870(20)	^{a)}
			904(27)	¹⁸⁾
	17.2	126	930(27)	¹⁸⁾
	17	90	450 ± 15(19.6)	¹⁷⁾
	16.75	71 ± 7	745 ± 74(28)	¹⁸⁾
	17.0	86 ± 2	733 ± 105(28)	this work
Ga			451 ± 18(20)	this work
	16.5	115 ± 3	947 ± 98(28)	this work

σ_m is the peak value of the cross section, E_m is the peak energy and $\int_0^x \sigma(E)dE$ is the integrated cross section. The upper limit of the integration is indicated in parentheses.

^{a)} Value obtained subtracting the (γ , 2n) reaction contribution from the $\sigma(\gamma, Tn)$.

^{b)} Value obtained by subtracting the Ni⁵⁸(γ , n)Ni⁵⁷ reaction contribution from the $\sigma(\gamma, Tn)$ for natural nickel corrected for the (γ , 2n) reaction contribution.

REF.

G. Baciú, G. C. Bonazzola, B. Minetti, C. Molino, L. Pasqualini
and G. Piragino
Nuclear Phys. 67, 178 (1965)

ELEM. STM.

Ga

31

METHOD

NBS Monitor

[Page 2 of 2]

REF. NO.

65 Ba 3

EGF

REACTION	RESULT	EXCITATION ENERGY	SOURCE		DETECTOR		ANGLE
			TYPE	RANGE	TYPE	RANGE	

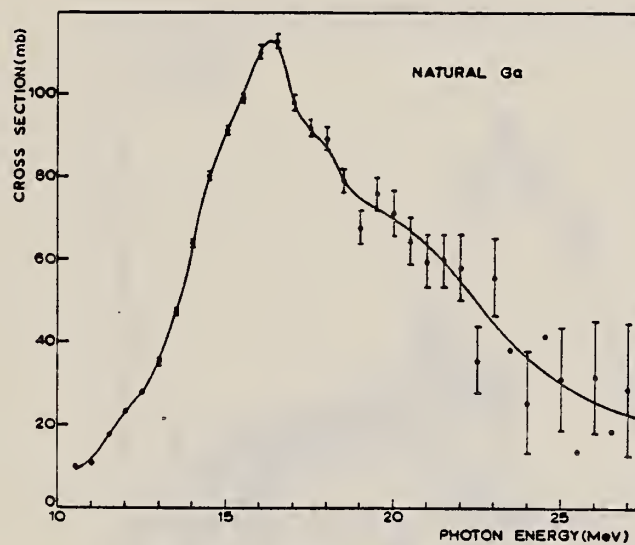


Fig. 4. The cross section $\sigma(\gamma, T_n)$ for natural gallium.

REF. P. Carlos, H. Beil, R. Bergere, J. Fagot, A. Lepretre,
A. Veyssiere, G. V. Solodukhov
Nucl. Phys. A258, 365 (1976)

ELEM. SYM.	A	Z
Ga		31

METHOD

REF. NO.	
76 Ca 1	egf

REACTION	RESULT	EXCITATION ENERGY	SOURCE		DETECTOR		ANGLE
			TYPE	RANGE	TYPE	RANGE	
G,N	ABX	9- 26	D	9- 26	MOD-I		4PI
G,2N	ABX	16- 26	D	9- 26	MOD-I		4PI

972+

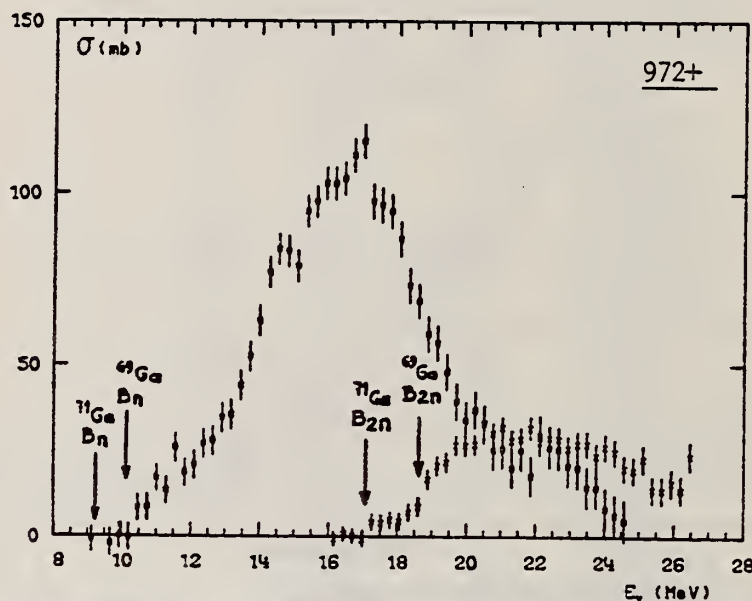


Fig. 2. Partial photoneutron cross sections [$\sigma(\gamma, n) + \sigma(\gamma, pn)$] and $\sigma(\gamma, 2n)$ for Ga. Arrows B_n and B_{2n} indicate theoretical threshold values for (γ, n) and $(\gamma, 2n)$ reactions respectively.

TABLE 3
Integrated photoneutron cross sections and comparison with sum rules

Nucleus	⁶⁴ Zn	⁶⁹ Ga ⁷¹ Ga	⁷⁰ Ge	⁷² Ge	⁷⁴ Ge	⁷⁶ Ge	⁷³ As	⁷⁴ Se	⁷⁶ Se	⁸⁰ Se	⁸² Se
E_M (MeV)	29	26.5	26.5	26.5	26.5	26.5	26.5	26.5	26.5	26.5	26.5
σ_{00} (MeV · b)	0.75	0.91	0.78	0.94	1.02	1.12	1.09	1.01	1.06	1.11	1.13
$\frac{\sigma_{00}A}{0.06NZ}$	0.78	0.87	0.75	0.88	0.94	1	0.98	0.90	0.92	0.94	0.95
$B_n - B_p$ (MeV)	4.2	$\begin{Bmatrix} 3.7 \\ 1.4 \end{Bmatrix}$	3	1	-0.8	-2.6	3.3	1.7	0.1	-1.5	-3
σ_{-10} (mb)	38	52	44	54	59	64	63	58	62	65	67
$\sigma_{-10}A^{-1}$ (mb)	0.15	0.18	0.15	0.18	0.19	0.20	0.20	0.18	0.19	0.19	0.19
σ_{-20} (mb · MeV ⁻¹)	2.0	3.1	2.5	3.2	3.6	3.9	3.7	3.4	3.8	3.9	4.2
$\sigma_{-20}A^{-1}$ (mb · MeV ⁻¹)	1.9	2.6	2.1	2.6	2.8	2.9	2.8	2.5	2.7	2.6	2.7

The notation used is defined in the text. The average experimental errors $\Delta\sigma_{00}/\sigma_{00}$, $\Delta\sigma_{-10}/\sigma_{-10}$ and $\Delta\sigma_{-20}/\sigma_{-20}$ are approximately 8 %.

GA
A=66

GA
A=66

GA
A=66

Method
Radioactivity

Ref. No.	JOC
59 Ga 1	

Reaction	E or ΔE	E_0	Γ	$\int \sigma dE$	$J\pi$	Notes
(d, γ)	3.5-4.5					At $E_d = 4.5$ MeV, $\sigma(d,\gamma) = 80 \mu b$.

TABLE I
Results for 4.5 MeV deuterons

Initial nucleus	Reaction	$\sigma_{exp} (\pm 15\%)$	σ_{theor}	σ_{tot} (direct capture)
^{66}Ga	d, γ	61 μb	48 μb	81 μb (assuming the measured σ to be totally accounted for by this process)
	d, p	85 mb	84 mb	
	d, n	$0.7 \cdot 10^{-3}$	$0.75 \cdot 10^{-3}$	
	d, α			
^{67}Ga	d, γ	80 μb	86 μb	192 μb
	d, n - d, p	180 mb	175 mb	
	d, γ			
	d, n - d, p	$0.5 \cdot 10^{-3}$	$0.49 \cdot 10^{-3}$	
^{68}Ga	d, γ	295 μb	215 μb	1230 μb
	d, p	75 mb	29 mb	
	d, γ			
	d, p	$3.9 \cdot 10^{-3}$	$7.4 \cdot 10^{-3}$	

* There is a misprint in eq. (5) of ref. 1), the right side of which should be divided by π . Eq. (6) of ref. 1) is correct.

Ref 1: Blair, Hintz & Van Patter - Phys. Rev. 96, 1023 (1954).

GA
A=69

GA
A=69

GA
A=69

REF.	S. Costa, F. Ferrero, S. Ferroni and R. Malvano Proc. Paris Conference 1034 (1964)	ELEM. SYM.	A	Z
		Ga	69	31
METHOD	100 MeV synchrotron	REF. NO.	64 Co 3	JDM

REACTION	RESULT	EXCITATION ENERGY	SOURCE		DETECTOR		ANGLE
			TYPE	RANGE	TYPE	RANGE	
G,N	AB	THR-80	C	10-80	BF3-I		4PI

TABLE

ELEMENT	Yield (36 MeV) $\left(\frac{n. cm^2}{mol. MeV} \times 10^8\right)$	\sum_0^{30}	\sum_0^{80}	$\sum_0^{30} / \sum_0^{80}$	σ_{-1} (mb)
²⁴ Cr	83	1.21	2.1	0.58	62
²⁵ Mn	108	1.52	2.33	0.65	76
²⁶ Fe	68	0.88	1.46	0.60	50
²⁷ Co	89	1.08	1.82	0.59	64
²⁸ Ni	44	0.55	1.07	0.51	34
²⁹ Cu	95	1.06	1.99	0.53	72
³⁰ Zn	88	0.94	1.68	0.56	66
³¹ Ga	130	1.29	2.18	0.59	94
³² Ge	139	1.35	2.29	0.59	101
³³ As	137	1.22	2.18	0.56	100

$\sum_a^b = \frac{A}{60 NZ} \int_a^b \sigma(E) dE$ is the integrated cross section measured in units of the classical dipole $60 NZ/A$ mb. MeV.

REF. W. J. Alston III, H. H. Wilson and E. C. Booth
Nucl. Phys. A116, 281 (1968)

ELEM. SYM.	A	Z
Ga	69	31

METHOD

REF. NO.

68 A1 1

egf

REACTION	RESULT	EXCITATION ENERGY	SOURCE		DETECTOR		ANGLE
			TYPE	RANGE	TYPE	RANGE	
G,G	LFT	0 - 1 (1.11)	C	4	SCD-D	0-3	130

Angle greater than 90° for all measurements.

SELF-ABSORPTION

TABLE I
Direct and absorption measurements of resonance fluorescence

Nucleus	E_r (MeV)	J_r	Γ_d/Γ	$gW\Gamma_0\Gamma_d/\Gamma$ (meV)	Error (%)	This work Γ_0 (meV)	Other work Γ_0
⁵⁵ Mn	0.000	$\frac{1}{2}^-$					
	1.527	($\frac{1}{2}^-$)	0.9	5.2 abs ^{a)}	25 40	8-12 8.0	
	1.884	?	0.82 ^{b)}	41 abs ^{a)}	25 10	50/ gW 55/ g	
	2.197	?	(0.8) ^{c)}	17 abs	25 20	21/ gW 17/ g	
	2.252	?	(0.9) ^{c)}	17 abs	25 20	19/ gW 13/ g	
	2.365	?	?	3.5	36	(2-6) Γ/Γ_0	
	2.564	?	(1.0)	50 abs ^{a)}	25 20	50/ gW 61/ g	
	2.751	?	?	6.7	42	6.7(Γ/Γ_0)/ gW	
	0.000	$\frac{3}{2}^-$					
	1.187	($\frac{3}{2}^-$)	(1.0)	6.8 abs	25 25 ^{a)}	7.5 12	0.33(E2) ^{d)}
⁶³ Co		($\frac{3}{2}^-$)	(1.0)	6.8 abs	25 25 ^{a)}	(5.4-6.5) 9.6	0.27(E2)
	0.000	$\frac{3}{2}^-$?	1.6	30	(1.1-1.7) Γ/Γ_0	
	1.414	$\frac{3}{2}^-$?	1.7	37	(1.7-2.5) Γ/Γ_0	0.1(E2) ^{e)}
⁶⁷ Ga	0.000	$\frac{3}{2}^-$					
	0.872	($\frac{3}{2}^-$)	0.95	1.1	35	0.8/ W	
⁷⁵ As	1.107	($\frac{3}{2}^-$)	0.95	8.0	20	8.4/ W	
	0.000	$\frac{3}{2}^-$					
	0.86	?	?	1.7	20	1.7 $\Gamma/gW\Gamma_0$	
⁸⁹ Y	1.07	?	?	2.6	30	2.6 $\Gamma/gW\Gamma_0$	
	1.35	?	?	3.6	20	3.6 $\Gamma/gW\Gamma_0$	
	0.000	$\frac{1}{2}^-$					
	1.51	$\frac{1}{2}^-$	(1.0)	52 ^{a)} abs ^{a)}	30 15	28 22	0.37(E2) ^{f)}

^{a)} Measured with NaI.

^{b)} Ref. ¹⁴⁾.

^{c)} Measured with a Ge(Li) detector to $\pm 10\%$.

^{d)} Ref. ¹³⁾.

^{e)} Ref. ¹⁴⁾.

^{f)} Ref. ¹²⁾.

- ¹³ D.G. Alkhazov, K.I. Erokhina and I.K. Lemberg, Izv.Akad.Nauk.SSSR(ser.fiz.) 28 (1964) 1667.
¹⁴ B.G. Harvey, J.R. Meriwether and A. Bussiere, Nucl. Phys. 70 (1965) 305.
²³ G.A. Peterson and J. Alster, Phys. Rev. 166 (1968) 136.
²⁴ N. Nath, M.A. Rothman, D.M. Van Patter and C.E. Mandeville, Nucl. Phys. 13 (1959) 74.

REF. H. Langhoff and L. Frevert
Nucl. Phys. A111, 225 (1968)

ELEM. SYM.	A	Z
Ga	69	31
REF. NO.		
68 La 1		EGF

METHOD			SOURCE		DETECTOR		ANGLE
REACTION	RESULT	EXCITATION ENERGY	TYPE	RANGE	TYPE	RANGE	
G,G	LFT	0-1	D	0-1	NAI-D	0-1	130

TABLE 1
Results of the resonance fluorescence investigation

E_γ (keV)	1337	1107	872	574
$\sigma_{\text{scatt}}^{\text{GeCl}_4}$ (mb)	<10	126 \pm 6	218 \pm 15	55 \pm 20
$\frac{\sigma_{\text{scatt}}^{\text{GeBr}_4}}{\sigma_{\text{scatt}}^{\text{GeCl}_4}}$		0.98 \pm 0.06	0.84 \pm 0.08	
$\frac{\sigma_{\text{scatt}}^{\text{GeCl}_4(\text{solid})}}{\sigma_{\text{scatt}}^{\text{GeCl}_4(\text{gas})}}$		0.042 \pm 0.015	0.17 \pm 0.04	
A_2		<0.07	<0.12	
$\epsilon(\%)$		26.8 \pm 2.5	28 \pm 5	
$\frac{g_1}{g_0} \Gamma$ (meV)		4.1 \pm 0.4	2.1 \pm 0.4	
$N(E_r)_{\text{exp}} (\text{eV}^{-1})$		(1.04 \pm 0.12) $\cdot 10^{-2}$	(2.3 \pm 0.5) $\cdot 10^{-2}$	
$N(E_r)_{\text{Ge atom}}^{(\text{eV}^{-1})}$		(1.6 \pm 0.2) $\cdot 10^{-2}$	2.7 $\cdot 10^{-2}$	3.8 $\cdot 10^{-2}$
$\frac{g_0}{g_1} \tau$ (psec)		(0.16 \pm 0.02)	(0.31 \pm 0.06)	(5 \pm 3)
$\frac{\Gamma_{\text{exp}}}{\Gamma_{\text{vibr}}(E_2)g_0} \frac{g_1}{g_0}$		10	16	8 \pm 4
$\frac{T(M1)_{\text{s.p.}}}{T_{\text{exp}}} \frac{g_0}{g_1}$		4.5	4	18

$\sigma_{\text{scatt}}^{\text{GeCl}_4}$ and $\sigma_{\text{scatt}}^{\text{GeBr}_4}$ are the cross sections for resonance scattering obtained with gaseous sources of GeCl_4 and GeBr_4 , respectively, $\sigma_{\text{scatt}}^{\text{solid}}$ the cross section with a solid source of GeCl_4 and A_2 the anisotropy in the angular distribution of the resonantly scattered radiation. The level width Γ and the lifetime τ are deduced from the observed self-absorption ϵ , g_1 and g_0 are the statistical factors of excited and ground state, respectively. $N(E_r)_{\text{exp}}$ the relative number of γ -quanta in the emission line which falls into an energy interval of 1 eV around the absorption line E_r and $N(E_r)_{\text{Ge}}$ the expected values for a gaseous source of Ge atoms. In lines 10 and 11, the experimental results for the line width Γ_{exp} and the transition probability T_{exp} are compared with predictions of a pure vibrational model $\Gamma(E_2)_{\text{vibr}}$ and the single-particle model omitting spin factors $T(M1)_{\text{s.p.}}$.

METHOD					REF. NO.	
					73 Ar 1	hmg
REACTION	RESULT	EXCITATION ENERGY	SOURCE		DETECTOR	
			TYPE	RANGE	TYPE	RANGE
G,G	LFT	0- 2	C	0- 2	SCD-D	

Absolute values come from normalizing to know total widths.
W is angular distribution factor to correct for difference
in unknown and standard distribution. Assumed = 1 to get
 Γ_0 values.

12 LEVELS

TABLE III. ^{68}Ga levels and results.

Level energy ^a (keV)	$J\pi$	E_γ This work (keV)	Γ_0/Γ^a	$g\bar{W}\Gamma_0\Gamma_0/\Gamma$ This work (meV)	Γ_0 Deduced (meV)
G.S.	$\frac{1}{2}^-$				
318.4(2)	$\frac{1}{2}^-^b$...	1.0	c	...
573.9(2)	$\frac{5}{2}^-^d$	574(1)	0.998(2)	0.053(6)	0.036(4)
871.7(2)	$\frac{3}{2}^-^e$	872(1)	0.948(5)	1.43(15)	1.51(15)
1027 ^b	$(\frac{1}{2})^-^f$...	0.20 ^b	<0.06	<0.5
1106.4(2)	$\frac{7}{2}^-^g$	1106(1)	0.964(2)	2.7(2)	2.8(2)
1336.2(2)	$\frac{7}{2}^-^b$	1337(1)	0.937(6)	0.70(4)	1.50(5)
1487.8(2)	$(\frac{1}{2})^+, (\frac{3}{2})^-^f$	1488(1)	0.51(5)	0.12(4)	0.23(8) g^{-1}
1525.7(2)	$(\frac{1}{2}, \frac{3}{2})^-^g$...	0.33(3)	<0.06	...
1723.5(4) ^h	$(\frac{3}{2})^-^g, f$	1723(2)	0.54(8)	0.32(10)	0.40(14)
1890.8(2)	$(\frac{1}{2}, \frac{3}{2})^-^g$	1892(2)	0.68(5)	10.3(6)	15.2(15) g^{-1}
1923.0(2)	0.093(9)	<0.4	...
2022.2(2)	$(\frac{1}{2} - \frac{1}{2})^-^g$	2024(2)	0.86(5)	2.9(2)	3.4(3) g^{-1}
2042.6(4)	$<\frac{1}{2}^-^g$	2045(2)	0.67(20)	2.1(2)	3.2(10) g^{-1}

^a Reference 8 unless otherwise marked.

^b Reference 7.

^c No data taken for this level. (See Sec. II in text).

^d References 7 and 8. M. M. Khodzhaev (Ref. 11) measured A_2 and A_4 coefficients in $(\gamma, \gamma\theta)$ experiments and deduced $\frac{1}{2}^-$ for this level. A reanalysis of his data indicates that the coefficients are also consistent with a $\frac{1}{2}^-$ assignment.

^e Reference 10.

^f Reference 9.

^g Reference 8.

^h This level was studied with electron energy $E_T < 2.04$ MeV to avoid population of the 2043-keV level with its 1724-keV decay to first excited state.

⁷ D. R. Velkley et al., Phys. Rev. 179, 1090 (1969).

⁸ W. H. Zoller et al., Nucl. Phys. A124, 15 (1969).

⁹ R. G. Couch et al., Phys. Rev. G2, 149 (1970).

¹⁰ S. Raman et al., Phys. Rev. G4, 744 (1970).

METHOD

REF. NO.

73 Mo 2

hmg

REACTION	RESULT	EXCITATION ENERGY	SOURCE		DETECTOR		ANGLE
			TYPE	RANGE	TYPE	RANGE	
G,G	LFT	6, 8	D	6, 8	SCD-D		DST

LEVELS 7.306, 6.874 MEV

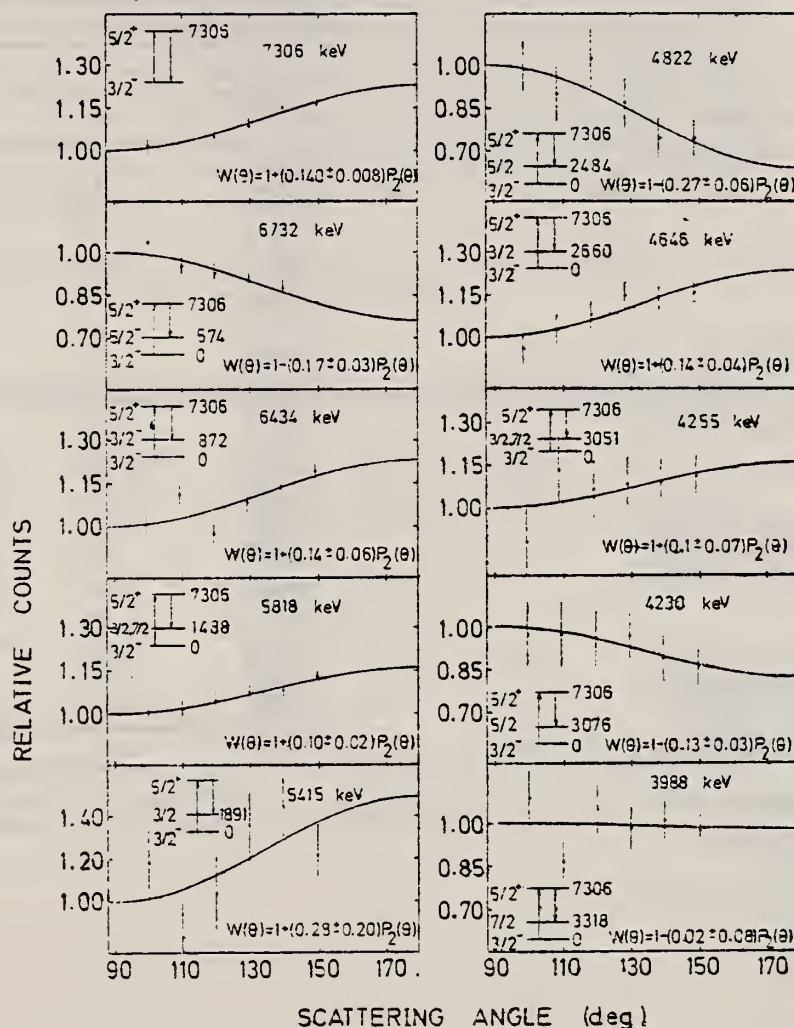


FIG. 4. Angular distributions of the elastic and inelastic transitions deexciting the 7306-keV level in ⁶⁹Ga as measured using a 20-cm³ Ge(Li) detector. The solid lines have the form $W(\theta) = 1 + A P_2(\cos \theta)$ and are least-square fits to the experimental distribution. In each case the corresponding γ - γ cascade is indicated.

(over)

Elastic and inelastic scattering of monochromatic photons were used for studying nuclear energy levels in ^{63}Ga ; the photons were produced by thermal neutron capture in copper and vanadium. The decay of one resonance at 7306 keV excited by the copper γ source and another resonance at 6874 keV excited by the vanadium γ source were studied in detail and 30 low-lying levels were observed from the ground state up to 3.4 MeV, 17 of which are believed to be new levels in ^{63}Ga . The angular distribution of some elastic and inelastic lines were measured and the following spin determinations were made (keV, J^π): 320, $\frac{1}{2}^-$, ($\frac{3}{2}^-$); 574, $\frac{5}{2}^-$; 872, $\frac{3}{2}^-$; 1488, $\frac{3}{2}^-$, $\frac{7}{2}^-$; 1525 ($\frac{1}{2}$, $\frac{3}{2}$); 1891, $\frac{3}{2}^-$; (1978), ($\frac{1}{2}$, $\frac{3}{2}$); 2457, $\frac{3}{2}$; 2484, $\frac{5}{2}$; (2565), ($\frac{1}{2}$, $\frac{3}{2}$); 2660, $\frac{5}{2}$; 3051, ($\frac{3}{2}$, $\frac{5}{2}$); 3076, $\frac{5}{2}$; 3318, ($\frac{3}{2}$); 6874, $\frac{1}{2}^{(u)}$ and 7306, $\frac{5}{2}^+$, where parentheses denote uncertain J^π assignments. The parity of the 7306-keV level was directly determined using a Compton polarimeter. The total radiative width of the 7306-keV level was measured and found to be $\Gamma = 0.105 \pm 0.020$ eV. For the 6874-keV level, a positive correlation coefficient was obtained, $\rho = 0.69$, between the (γ, γ') and (d, n) transition strengths leading to the same final states in ^{63}Ga . The levels of ^{63}Ga are compared with recent theoretical calculations.

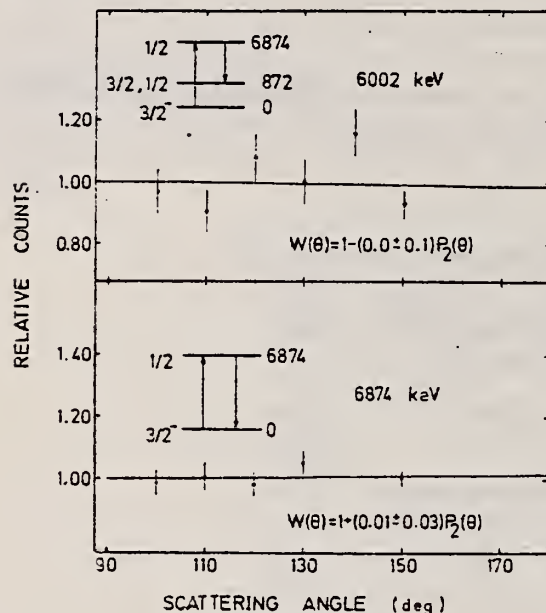


FIG. 5. Angular distribution of the elastic and one inelastic transition deexciting the 6874-keV level in ^{63}Ga as measured using a 30-cm³ Ge(Li) detector. See caption to Fig. 4.

TABLE II. γ energies of the scattered radiation from a Ga target using V γ rays. Intensities are normalized relative to the 6874-keV resonance line. Asterisks denote transitions believed to correspond to a possible resonance at 7310-keV resonance in ^{71}Ga . Daggers indicate unidentified transitions.

γ line energy (primaries) (± 4 keV)	Relative intensity ($\pm 20\%$)
7310*	20
6874	100
6554	205
6346*	37
6202*	11
6002	80
5349	20
4980	10
4896	25
4653†	20
4619†	20
4543†	12
4417	15
4309	10
4214	15

TABLE I. γ energies of the scattered radiation from a Ga target; the γ source was obtained from the Cu(n, γ) reaction. The branching ratios of the assumed primary transitions are given and are accurate to $\pm 15\%$. The γ energies of the low-energy spectrum are listed under secondaries. Daggers indicate unidentified transitions.

γ line energy (primaries) (keV)	Branching ratios (%)	γ line energy (secondaries) (keV)
7306 ± 2	52.0	2484 ± 4
6732 ± 2	3.6	2340 ± 4
6434 ± 2	3.0	1721 ± 3
5818 ± 2	6.0	1630 ± 3 †
5415 ± 3	0.8	1488 ± 2
5383 ± 3	0.1	1336 ± 2
5109 ± 3	0.5	1105 ± 2
4954 ± 3	1.3	915 ± 2
4880 ± 3	1.0	872 ± 2
4849 ± 2	1.9	574 ± 2
4822 ± 2	2.0	
4646 ± 2	4.2	
4541 ± 3	0.6	
4509 ± 3	2.0	
4460 ± 3	0.4	
4446 ± 4	0.3	
4342 ± 3	0.4	
4328 ± 2	1.2	
4255 ± 3	3.6	
4230 ± 4	3.4	
4102 ± 4	2.2	
4081 ± 6	2.2	
4024 ± 6	1.0	
3988 ± 6	4.1	

REF. K. Ramavataram, C. Rangacharyulu, I.M. Szöghy, R. Hilko,
C. St.-Pierre
Phys. Rev. C17, 1583 (1978)

ELEM. SYM.	A	Z
Ga	69	31

METHOD	REF. NO.	
	78 Ra 4	hg

REACTION	RESULT	EXCITATION ENERGY	SOURCE		DETECTOR		ANGLE
			TYPE	RANGE	TYPE	RANGE	
P, G0	LFT	9	D	3	SCD-D		55
		(9.85)		(3.250)			

Isobaric analog resonances in ^{69}Ga corresponding to the ground ($1/2^-$) and first excited ($9/2^+$) parent states of ^{69}Zn have been studied by the $^{69}\text{Zn}(p,\gamma)$ reaction. The γ decay of the ground state of ^{69}Zn is compared with the β decay of the parent isobaric analog state. The latter is a pure Gamow-Teller transition to the ground ($3/2^-$) and third ($3/2^-$) excited states, while both Gamow-Teller and Fermi matrix elements can contribute in the decay to the second excited ($1/2^-$) state of ^{69}Ga . The $M1$ decay widths obtained from the γ decay of the $J^\pi = 1/2^-$ isobaric analog state are in good agreement with the widths extracted from the $\log ft$ values in the first two of the three β -decay branches. However, the $M1$ decay width to the third excited state disagrees with the value deduced from the $\log ft$ value of the β decay of the ^{69}Zn g.s. to this state. In addition, the $M1$ transition strength of the $9/2^+$ (T_+) state to the $9/2^+$ (T_-) state in ^{69}Ga has been measured and is compared with the recently published systematic trends for the analog to antianalog transition in other f - p shell nuclei.

LEVEL 9.858 MEV

[NUCLEAR REACTIONS $^{69}\text{Zn}(p,\gamma)$, $E = 3.2\text{--}3.8$ MeV. ^{69}Ga deduced resonances,] measured E_γ and Γ_γ , $M1$ strength.

TABLE I. γ -decay properties of the IAR of the ($\frac{1}{2}^-$) ground state of ^{69}Zn at $E_p = 3.250$ MeV.

Transition	Assumed multipole order	Γ_γ (eV)	$B(M1)$ (μ_N^2)	$B(E2)$ ($e^2\text{fm}^4$)	$B(M1, \sigma)^a$ (μ_N^2)
IAR \rightarrow g.s. $\frac{1}{2}^- \rightarrow \frac{1}{2}^-$	M1	0.88 ± 0.20	0.080	...	0.085
IAR \rightarrow 0.318 $\frac{1}{2}^- \rightarrow \frac{1}{2}^-$	M1	<0.1	$<10^{-2}$...	$5 \times 10^{-6}^b$
IAR \rightarrow 0.372 $\frac{1}{2}^- \rightarrow \frac{1}{2}^-$	M1 E2	0.13 ± 0.11	0.09	14.9	0.01
IAR \rightarrow 1.525 $\frac{1}{2}^- \rightarrow (\frac{1}{2}, \frac{1}{2})$	M1 E2	0.52 ± 0.14	0.08
				16.0	

^a Value deduced from β decay of ^{69}Zn .

^b Value obtained assuming transition to be pure Gamow-Teller.

GA
A=71

GA
A=71

GA
A=71

60	71	31
Ga		
REF. NO.		
60 Ge 3		NVB

METHOD

Betatron; neutron threshold; ion chamber

REACTION	RESULT	EXCITATION ENERGY	SOURCE		DETECTOR		ANGLE
			TYPE	RANGE	TYPE	RANGE	
G,N	NØX	THR	C	THR	BF3-I		4 PI

THRESHOLD

TABLE I. Summary and comparison of neutron separation energies inferred from present threshold measurements with values predicted from mass data and reaction energies. All energies are expressed in the center-of-mass system in Mev.

Reaction	No. runs	Present results	Other results	Method	Reference
Ga ⁷¹ (γ,μ)Ga ⁷⁰	1	9.24 \pm 0.06	9.22 \pm 0.16	mass data Q(β^+)	n n

- Henry E. Duckworth, *Mass Spectroscopy* (Cambridge University Press, New York, 1958), p. 177.
- L. J. Lidoisky, *Revs. Modern Phys.* 29, 773 (1957).

REACTION	RESULT	EXCITATION ENERGY	SOURCE		DETECTOR		ANGLE
			TYPE	RANGE	TYPE	RANGE	
G, A	ABY	THR-20	C	20	ACT-I		4PI

TABLE 1. SUMMARY OF DATA ON (γ, α) REACTIONS WITH 20 MeV BREMSSTRAHLUNG

Nuclide		E_{th} (-Q, MeV)	Observed gamma-ray			Results obtained	
Parent (Natural abundance, %)	Product (Half-life)		Energy (MeV)	Branching ratio (%)	Type of multipole transition	$\mu\text{Ci}/\text{mg}^a$	Yield ($\text{mol}^{-1} \cdot \text{R}^{-1}$)
^{51}V (99.75)	^{47}Sc (3.4 d)	10.27	0.160	100	M1+E2	1.99×10^{-3}	2.8×10^3
^{63}Cu (30.9)	^{59}Co (99 min)	6.75	0.068	99	M1+E2	7.23×10^{-3}	9.7×10^3
^{71}Ga (39.6)	^{67}Cu (61 hr)	5.15	0.184	41	M1	2.70×10^{-3}	9.6×10^3
^{72}Ge (7.67)	^{68}Zn (14 hr)	5.89	0.435	100	M4	1.11×10^{-3}	5.0×10^3
^{81}Br (49.48)	^{77}As (39 hr)	6.46	0.246	2.81	M1+E2	1.97×10^{-4}	4.3×10^2
^{108}Ag (48.65)	^{104}Rh (36 hr)	3.28	$0.319 + 0.306$	24.8	M1+E2	8.29×10^{-4}	3.7×10^1
^{113}In (95.77)	^{109}Ag (7.6 d)	3.78	0.340	6	M1+E2	5.70×10^{-5}	4.3×10^1

a) The value corrected at the end of 1 hr irradiation ($9.4 \times 10^6 \text{ R/min}$).

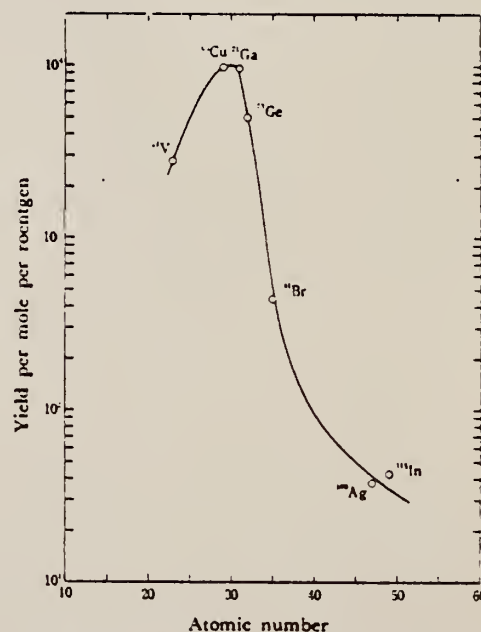


Fig. 1. The yield curve for (γ, α) reaction with 20 MeV bremsstrahlung.

METHOD

REF. NO.

73 Ar 1

hmg

REACTION	RESULT	EXCITATION ENERGY	SOURCE		DETECTOR		ANGLE
			TYPE	RANGE	TYPE	RANGE	
G.G	LFT	0- 2	C	0- 2	SCD-D		125

Absolute values come from normalizing to know total widths.
W is angular distribution factor to correct for difference in
unknown and standard distribution. Assumed = 1 to get Γ_0 values.

6 LEVELS

TABLE IV. ^{71}Ga levels and results.

Level energy (keV)	$J\pi^a$	E_γ This work (keV)	Γ_1/Γ^a	$gW\Gamma_1\Gamma_0/\Gamma$ This work (meV)	Γ_0 Deduced (meV)
g.s.	$\frac{1}{2}^-$				
389.87(5)	$\frac{1}{2}^-$...	1.0	<0.08	...
487.34(5)	$\frac{1}{2}^-$...	1.0	<0.03	...
511.55(5)	$\frac{1}{2}^-$...	0.91(6)	<0.08 ^b	...
910.3(1)	$\frac{3}{2}^-, (\frac{1}{2}^-)$	910(1)	1.0	0.57(5)	0.57(5) g^{-1}
964.7(1)	$\frac{1}{2}^-$	965(1)	0.78(3)	0.28(5)	0.24(4)
1107.4(2)	$\frac{1}{2}^-$...	0.022(3)
1109.3(5)	$(\frac{1}{2}^-)$	1109(1)	1.0	2.4(3)	4.8(6)
1395.2(4)	$(\frac{1}{2}^-, \frac{3}{2}^-)$	1395(1)	1.0	0.27(6)	0.27(6) g^{-1}
1476.1(2)	$\frac{1}{2}^-, \frac{1}{2}^-$...	0.24(2)	<0.08	...
1493.8(4)	$\frac{1}{2}^+$...	(0.0)	<0.08	...
1498.7(2)	$\frac{1}{2}^-, \frac{1}{2}^-$...	0.0	<0.08	...
1631.6(2)	$\frac{1}{2}^-, (\frac{1}{2}^-)$...	0.093(8)	<0.3	...
1702.1(8)	0.0	<0.3	...
1719.7(7)	$(\frac{1}{2}^-, \frac{1}{2}^-)$	1719(1)	0.43(10)	0.70(18)	1.6(6) g^{-1}
2064.6(2)	$\frac{1}{2}^-, \frac{1}{2}^-$	2064(1)	0.64(9)	1.8(2)	2.9(4) g^{-1}

^a From Ref. 12.

^b A small correction was made for the background 511-keV annihilation γ ray from environmental radiation.

¹² W.H. Zoller, W.B. Walters, and G.E. Gordon, Nucl Phys. A142, 177 (1970).

DEFINITIONS OF ABBREVIATIONS AND SYMBOLS

Note: In this list definitions are given for various photoneutron reactions in which the following symbols are used: N, NL, nN, SN and XN. Corresponding definitions apply for reactions involving other nuclear particles where the symbols N (neutron) is replaced by, e.g. P, D, T, HE, A etc. Where unknown reactions result in the production of a specific radionuclide, the chemical symbol and mass number is listed as the reaction product, e.g. a G,NA22 reaction in ^{59}Co .

A	alpha particle		response function. Contrast with D = discrete.
ANAL	analysis		
ABI	absolute integrated cross-section data	CCH	cloud chamber
ABX	absolute cross-section data	CF	compared with
ABY	absolute yield data. Often means cross-section per equivalent quantum is listed.	CHRGD	charged
		CMPT	Compton
		COIN COINC	coincidence, coincide
ACT	measurement of induced radio-activity of the target	COH	coherent
ASM	asymmetric, asymmetry	CK	Cerenkov
AVG	average	D	deuteron or discrete. When discrete, it is used to describe a photon source or a detector response function. Contrast with C = continuous.
BBL	bubble chamber		
BEL B(EL)	reduced electric radiative transition probability	DLTE	energy loss
BF3	BF ₃ neutron counter with moderator e.g., Halpern detector, long counter	DLTQ	momentum transfer
		DST	distribution
BML	reduced magnetic radiative transition probability, B(ML)	DT BAL	detailed balance
BREAKS	levels located by "breaks" in the yield curve	E	electron
BRKUP	breakup	E/ electron	inelastically scattered electron
BRMS	bremsstrahlung	E+	positron
BTW	between	EDST	energy distribution or spectrum
C	continuous. Used to describe a photon source or a detector	E/N	used only to indicate a coincidence experiment as in (E,E/N).

	N stands for any outgoing particle measured in coincidence with an inelastically scattered electron. Distinguish from eg., (E,N) which is used to represent an electron induced reaction when only the outgoing particle N is detected.	KE	kinetic energy
EMU	emulsions (photographic plates)	L	may be an integer or zero that always follows a reaction product symbol. This is used to indicate transitions to specific states in the residual nuclide. When the letter is used as in (G,NL) the cross section given is that for the sum of transitions to two or more specific final states.
EXCIT	excited	LFT	excited state lifetime
F	fission	LIM	limit
FMF	form factor	LV,LVS	level, levels
FM-1	inverse femtometers	LQD	liquid
FRAG	fragment	MAG	magnetic spectrometer
G	photon	MEAS	measurement(s)
G/	inelastically scattered photon	MGC	magnetic Compton spectrometer
G-WIDTH	gamma-ray transition width	MGP	magnetic pair spectrometer
HAD	hadrons, hadron production	MOD	moderated neutron detector <u>not</u> employing a BF ₃ counter, e.g. rhodium foil, Szilard-Chalmers reaction, ³ He, ⁶ Li reactions, GD loaded liquid scintillator, etc.
HE He3	³ He particle	MSP	mass spectrometer
INT	interaction, integral, intensity	MULT	multiple, multipole, multiplicity
INC	includes	MU-T	used only in combination with G to indicate a total photon absorption cross section measurement, i.e. (G,MU-T)
ION	ionization chamber	N	neutron (see also XN and SN). The notation (G,N) is used to indicate a reaction in which only a single neutron is emitted, i.e. the reaction that can, in many cases, be measured by observing the radioactive decay of the residual nuclide.
ISOB	isobaric		
ISM	isomer		
J	multiplicity of particle defined by following symbol e.g. (G,PJN) with remark J = 2,3,5,7		
JPI J-PI	spin and parity of a nuclear state		
K	second multiplicity index, e.g. (G,JPKN) with both J & K positive integers greater than 1		

nN	where n is any integer. (G,nN) indicates the sum over all reaction cross sections in which n neutrons are emitted.	SN	sum of neutron producing reactions, $\sigma(\gamma, SN) = \sigma(\gamma, N) + \sigma(\gamma, NP) + \sigma(\gamma, 2N) + \sigma(\gamma, 3N) + \text{etc.}$
NAI	NaI(Tl) spectrometer	SPC	photon or particle energy spectrum
NEUT	neutron(s)	SPK	spark chamber
NOX	no cross-section data	SPL	spallation
P	proton (see also XP)	STAT	statistical
PART	particle(s)	SYM	symetric, symmetry
PHOT	photon(s)	T	triton
PI	pion, usually written as PI^+ , PI^- , PI^0 to indicate charge	TEL	counter telescope
POL	polarized or polarization	THR	threshold for reaction or threshold detector, e.g., $^{29}\text{Si}(n,p)^{29}\text{Al}$.
Q-SQUAR	momentum transfer squared (q^2)	TOF	time-of-flight detector
RCL	recoil	TRK	tracks of particles or fragments observed in solid materials (glass, mylar, etc.)
REL	relative	TRNS	transition
RLI	relative integrated cross-section data	UKN UNK	unknown
RLX	relative cross-section data	VIB	vibrational
RSP	reaction spectrometer	VIR PHOT	virtual photon(s)
RLY	relative yield data	XN	all neutrons, total neutron yield, $\sigma(\gamma, XN) = \sigma(\gamma, N) + 2\sigma(\gamma, 2N) + 3\sigma(\gamma, 3N) + \sigma(\gamma, NP) + \text{etc.}$
SCTD	scattered	XP	all protons, total proton yield $\sigma(\gamma, XP) = \sigma(\gamma, P) + \sigma(\gamma, NP) + 2\sigma(\gamma, 2P) + \text{etc.}$
SCD	semiconductor (solid state) detector	XX XXX	reaction products defined in REMARKS
SCI	scintillator detector other than NaI, e.g., CsI, KI, organic (liquid or solid), stilbene, He	YLD	yield
SEP	separation		
SEP ISOTP	separated isotope used		
SIG	SIGMA (cross section)		

4PI	a 4π geometry was used or a method like radioactivity or a total absorption measurement		products was determined. The polarized particle is indicated in REMARKS.
999	energy defined in REMARKS	* or @	symbols used to indicate that the units associated with the numerals on one or both sides of the symbol in a specific column are not MeV. The units are defined in REMARKS.
\$	indicates the measurement involved beams or targets that were either polarized or aligned, or that the polarization of the reaction		

U.S. DEPT. OF COMM. BIBLIOGRAPHIC DATA SHEET (See instructions)	1. PUBLICATION OR REPORT NO.	2. Performing Organ. Report No.	3. Publication Date
4. TITLE AND SUBTITLE Photonuclear Data-Abstract Sheets 1955-1982			
5. AUTHOR(S) E.G. Fuller and Henry Gerstenberg			
6. PERFORMING ORGANIZATION (If joint or other than NBS, see instructions) NATIONAL BUREAU OF STANDARDS DEPARTMENT OF COMMERCE WASHINGTON, D.C. 20234		7. Contract/Grant No.	8. Type of Report & Period Covered
9. SPONSORING ORGANIZATION NAME AND COMPLETE ADDRESS (Street, City, State, ZIP)			
10. SUPPLEMENTARY NOTES <input type="checkbox"/> Document describes a computer program; SF-185, FIPS Software Summary, is attached.			
11. ABSTRACT (A 200-word or less factual summary of most significant information. If document includes a significant bibliography or literature survey, mention it here) These abstract sheets cover most classes of experimental photonuclear data leading to information of the electromagnetic matrix element between the ground and excited states of a given nucleus. This fifteen volume work contains nearly 7200 abstract sheets and covers 89 chemical elements from hydrogen through americium. It represents a twenty-seven year history of the study of electromagnetic interactions. The sheets are ordered by target element, target isotope, and by an assigned bibliographic reference code. Information is given on the type of measurement, excitation energies studied, source type and energies, detector type, and angular ranges covered in the measurement. For a given reference, the relevant figures and tables are mounted on a separate sheet for each nuclide studied.			
12. KEY WORDS (Six to twelve entries; alphabetical order; capitalize only proper names; and separate key words by semicolons) data-abstract sheets, elements, experimental, isotopes, nuclear physics, photonuclear reactions			
13. AVAILABILITY <input type="checkbox"/> Unlimited <input checked="" type="checkbox"/> For Official Distribution. Do Not Release to NTIS <input type="checkbox"/> Order From Superintendent of Documents, U.S. Government Printing Office, Washington, D.C. 20402. <input type="checkbox"/> Order From National Technical Information Service (NTIS), Springfield, VA. 22161			14. NO. OF PRINTED PAGES 15. Price

